The Dissertation Committee for Rubén Mario Salas Pereira
certifies that this is the approved version of the following dissertation:

Accelerated Corrosion Testing, Evaluation and Durability Design

of Bonded Post-Tensioned Concrete Tendons

Committee:

John E. Breen, Supervisor

Michael E. Kreger

James O. Jirsa

Harovel G. Wheat

Kevin J. Folliard

Accelerated Corrosion Testing, Evaluation and Durability Design of Bonded Post-Tensioned Concrete Tendons

by

Rubén Mario Salas Pereira, Lic, M.S.E.

Dissertation

Presented to the Faculty of the Graduate School of

The University of Texas at Austin

in Partial Fulfillment

of the Requirements

for the Degree of

Doctor of Philosophy

The University of Texas at Austin

August 2003

To Seidy

and

to my parents

Acknowledgements

I wish to express my deepest and sincere appreciation to Dr. John E. Breen for his encouragement and support in beginning these studies, and for his constant and inspiring guidance. It has been my distinct pleasure and proud privilege to have him as my supervising professor. I will treasure his advice and his lessons forever.

My sincere thanks are to all the committee members of this dissertation, Dr. Michael Kreger, Dr. James Jirsa, Dr. Harovel Wheat, and Dr. Kevin Folliard for their invaluable suggestions and constructive criticisms.

I would like to thank the graduate students that worked on TxDOT Project 1405 before I started, especially Jeff West and Andrea Schokker for their fine work that represents an important portion of this dissertation. I also wish to thank Andrea Kotys for her hard work, especially in the beam portion of the research project.

I wish to acknowledge the assistance of the administrative and technical staff of Ferguson Structural Engineering Laboratory especially Regina Forward, Hortensia Peoples, Mary Jo Moore, Blake Stasney and Mike Bell.

My sincere thanks are to the graduate and undergraduate students that worked with me during the project, especially to Juan José, Felipe, Art, Chris and Jeff.

v

Accelerated Corrosion Testing, Evaluation and Durability Design of Bonded Post-Tensioned Concrete Tendons

Publication No. _____

Rubén Mario Salas Pereira, Ph.D.

The University of Texas at Austin, 2003

Supervisor: John E. Breen

In the last few years, the effectiveness of cement grout in galvanized or polyethylene ducts, the most widely used corrosion protection system for multistrand bonded post-tensioned concrete tendons, has been under debate, due to significant tendon corrosion damage, several reported failures of individual tendons as well as a few collapses of non-typical structures. While experience in the USA has been generally good, some foreign experience has been less than satisfactory.

This dissertation is part of a comprehensive research program started in 1993, which has the objectives to examine the use of post-tensioning in bridge substructures, identify durability concerns and existing technology,   develop and carry out an experimental testing program, and conclude with durability design guidelines.

Three experimental programs were developed: A long term macrocell corrosion test series, to investigate corrosion protection for internal tendons in precast segmental construction; a long term beam corrosion test series, to examine the effects of post-tensioning on corrosion protection as affected by crack width; and, a long term column corrosion test series, to examine corrosion protection in vertical elements.

Preliminary design guidelines were developed previously in the overall study by the initial researchers, after an extensive literature review.

This dissertation scope includes continuation of exposure testing of the macrocell, beam and column specimens, performing comprehensive autopsies of selected specimens and updating the durability design guidelines based on the exposure testing and autopsy results.

After autopsies were performed, overall findings indicate negative durability effects due to the use of mixed reinforcement, small concrete covers, galvanized steel ducts, and industry standard or heat-shrink galvanized duct splices. The width of cracks was shown to have a direct negative effect on specimen performance. Grout voids were found to be detrimental to the durability of both galvanized ducts and strand. Relying on epoxy and galvanized bar coatings was also found inappropriate because of local attack. On the other hand, very positive effects were found with the use of high performance concrete, high post-tensioning levels, plastic ducts, and sound epoxy filling at the joints.

Table of Contents

xiii

List of Tables

List of Figures

xxxiii

xl

xlii

l

CHAPTER 1

Introduction

1.1 BACKGROUND

In the last few years, the effectiveness of cement grout in galvanized or polyethylene ducts, the most widely used corrosion protection system for internal and external multistrand post-tensioning for bridge superstructures has been under debate, due to significant tendon corrosion damages, several reported failures of individual tendons as well as a few collapses of non-typical structures.[1.1-1.5] While experience in the USA has been generally good,[1.6] some foreign experience has been less than satisfactory. A moratorium was established in the U.K. in 1992 for internal bonded post-tensioned structures (due to bridge failures including the well known collapse of the Ynys-y-Gwas Bridge in Wales), and is still in effect for "internal, grouted tendons with discontinuous (poorly sealed) ducts".[1.2,1.7] Germany has expressed a preference for the use of external prestressing.[1.8-1.9] The French Authorities have gone in the opposite direction considering the idea of forbidding external tendons injected with cement grouts[1.10]. Japan has expressed a preference for the use of fully external tendons using transparent sheath with grouting.[1.4] These are only a few examples of the general concern and show the need for comprehensive studies regarding the corrosion protection of bonded post-tensioning systems.

Recognizing the extent of the problem, in November 2001, engineers from many countries gathered at Ghent University,[1.11] Belgium, under the sponsorship of *fib* (federation internationale du béton) and IABSE (International Association for Bridge and Structural Engineering), to review the problems encountered and to discuss the available solutions. Other congresses and seminars have followed,

including the October 2002, first *fib* Congress "Concrete Structures in the 21st Century," in Osaka, Japan. However, many aspects still remain under discussion.

In United States, the very limited problems with tendon corrosion in precast segmental bridges[1.6, 1.12-1.17] include one external tendon failure found in 1999 in the Niles Channel Bridge, two tendon failures and eleven corroded tendons discovered during the year 2000 at the Mid-Bay Bridge, and, corroded and failed vertical tendons discovered in the same year in precast segmental columns of the high level approaches of the Sunshine Skyway Bridge. All of these bridges are located in the State of Florida. Additionally, grouting deficiencies were found in 2001 in the Sidney Lanier cable-stayed bridge in Georgia and in the Boston Central Artery bridges. No significant tendon corrosion problems have been reported in the states of California (with 3800 post-tensioned bridges), Georgia, Texas and Virginia, as reported by the American Segmental Bridge Association. [1.18]

The general concern after the unfortunate experiences world wide has lead many transportation agencies and technical societies to produce "emergency" documents and technical reports. These state of the art reports and specification documents are the response to knowledge and expertise to date, with regard to new material requirements, construction practices and monitoring techniques. However, it is clear, that more research is needed to reinforce or even to disprove some of these theories, since to date there is not a clear agreement on a consistent set of durability design, construction and monitoring guidelines. Some of the mentioned "emergency" documents include:

- **The Concrete Society (1996),** "Durable Bonded Post-Tensioned Concrete Bridges," The Concrete Society Technical Report TR47, United Kingdom, 1996.[1.22] Second edition to be published shortly as reported by Prof. G. Somerville.[1.23]

- **FIP (1996),** "Corrosion protection of Prestressing Steels," Fédération Internationale de la Précontrainte (FIP), London, 1996.[1.24]

- *fib* **(2000)**, "Corrugated Plastic Ducts for Internal Bonded Post-Tensioning," Fédération Internationale du béton (*fib*) Technical Report Bulletin No. 7, Lausanne, Switzerland, January, 2000.[1.25]

- *fib* **(2000),** "Grouting of tendons in prestressed concrete," Fédération Internationale du béton (*fib*) Technical Report Bulletin No. 20, Lausanne, Switzerland, July, 2000.[1.26]

- **JPCEA (2001),** "Manual for Maintenance of Prestressed Concrete Bridges," Japan, November 2000. As referenced in Hamada[1.27] and Kitazono.[1.28]

- **ASBI (2001),** "Interim Statement on Grouting Practices," Phoenix, Arizona, U.S.A., December 2000.[1.20]

- **JSCE (2001),** "Standard Specification for Maintenance of Concrete Structures," Japan, January 2001. As referenced by Hamada[1.27] and Kitazono.[1.28]

- **PTI (2001),** "Guide Specification for Grouting of Post-Tensioned Structures," Phoenix, Arizona, U.S.A. February 2001, First edition.[1.19]

- **ASBI (2002),** "2002 Grouting Certification Training Manual," Phoenix, Arizona, U.S.A., 2002.[1.21]

- **FLDOT (2002),** "New Directions for Florida Post-Tensioned Bridges," Tallahassee, Florida, U.S.A., February 2002.[1.16]

- **VSL (2002),** "Grouting of Post-Tensioning Tendons," VSL International Ltd. Lyssach, Switzerland, May 2002.[1.23]

- **Swiss Federal Roads Authority and the Swiss Federal Railways (2001)**, "Measures for providing durability of post-tensioning tendons in bridges," [1.29]

Corrosion protection for bonded internal tendons can be very effective. Within the elements, internal tendons can be well protected by the multilayer protection system; including a sound design taking away the surface water, surface treatments, high quality concrete, plastic or galvanized duct, sound cement grout, coatings and other internal barriers in the prestressing steel and good anchorage protection measures (for example, encapsulated systems). However, potential weak links exist, among others, when the high strength concrete has high permeability (due to mix design and construction or due to service/exposure conditions), and when the concrete has cracking (due to shrinkage or service loading). Additional weak links occur when ducts are not adequately spliced or adequately protected by impermeable concrete and so are prone to severe corrosion. In addition, voids, bleed water and cracks can be present in the Portland cement grout. Finally, the prestressing steel may not be adequately protected and handled during construction, including inadequate or total lack of temporary protection techniques.

One of the major problems that agencies face today is the difficulty of providing good monitoring and inspection techniques for bonded post-tensioned structures. Condition surveys are often limited to visual inspections for signs of cracking, spalling and rust staining.   This limited technique can often overlook the deterioration of prestressing steel and fail to detect the potential for very severe and sudden collapses, as demonstrated in the Ynys-y-Gwas Bridge failure.[1.2] Therefore, as stated by West[1.30] "…there is fear that figures reporting the incidence of corrosion in prestressed structures based on limited or visual inspections may be unconservative and produce a false sense of security." The same could happen even when using advanced techniques as borescopy, since in this case the analysis is limited to specific areas in selected bridge elements.

Grout voids or even corrosion of prestressing steel in many areas of the bridge element may still be overlooked.

As stated by Ganz[1.31] the design of the corrosion protection systems should take into account that most parts of the tendons are not accessible during the design life, and that in general individual components or the entire tendons, are not replaceable. Even if special details are provided to allow replaceability of the tendons during the design life, the replacement should be carried out only in "emergency" situations.

Stable grout mixes and better grouting procedures are now being implemented, in part after the important findings of Schockker et al.[1.32] at the Phil M. Ferguson Structural Engineering Laboratory (FSEL) at the University of Texas at Austin, in 1999. The American Segmental Bridge Institute (ASBI) in 2001 launched the Grouting Certification Training Program, which was first held in August 2001, at FSEL. This training program has been adopted by various Transportation Agencies throughout the United States as a requirement for grouting supervisors and inspectors.[1.18] Additionally, the Post-Tensioning Institute Committee on Grouting Specification, published in February 2001 the "Specification for Grouting of Post-Tensioned Structures."[1.19] The use of this guide and the new and better inspection procedures are expected to yield more durable structures.

Besides high performance grouts and better grouting practices, plastic ducts either polyethylene (PE) or polypropylene (PP) are being implemented as reported by *fib* technical report on "Corrugated Plastic Ducts for Internal Bonded-Post-Tensioning".[1.25] Yet, many durability aspects of bonded internal post-tensioning systems require further research and analysis.

1.2 RESEARCH OBJECTIVES AND SCOPE

1.2.1 Project Statement

The research presented in this dissertation is part of the University of Texas at Austin, Center for Transportation Research Project 0-1405: "Durability Design of Post-Tensioned Bridge Substructure Elements." The research is being performed at the Phil M. Ferguson Structural Engineering Laboratory and is sponsored by the Texas Department of Transportation and Federal Highway Administration. The title of Project 0-1405 involves two main aspects:

- Durability of Bridge Substructures, and
- Post-Tensioned Bridge Substructures.

The substructure emphasis is in response to the deteriorating condition of bridge substructures in some areas of Texas. While considerable research and design effort has been given to bridge deck design to prevent corrosion damage, substructures had historically been more overlooked. Often superstructure drainage details result in substructures having a high exposure to aggressive agents such as, deicing salts, also substructures are often in direct contact with salt water and damaging soils.

The second aspect of the research is post-tensioned substructures. Relatively few post-tensioned substructures have been used in the past. There are many possible applications in bridge substructures where post-tensioning can provide structural and economical benefits, and can possibly improve durability. Post-tensioning is now being used in Texas bridge substructures, and it is reasonable to expect the use of post-tensioning to increase in the future as precasting of substructure components becomes more prevalent and as foundation sizes increase. This is expected, even though some problems have been

encountered in post-tensioned bridges throughout the world as mentioned previously.

The problem that bridge engineers face is that there are few comprehensive durability design guidelines for post-tensioned concrete structures. Durability design guidelines should provide information on how to identify possible durability problems, how to improve durability using post-tensioning, and how to ensure that the post-tensioning system does not introduce new durability problems.

1.2.2 Project Objectives

The overall research objectives for TXDOT Project 0-1405 are as follows:

1. To examine the use of post-tensioning in bridge substructures,
2. To identify durability concerns for bridge substructures in Texas,
3. To identify existing technology to ensure durability or improve durability,
4. To develop experimental testing programs to evaluate protection measures for improving the durability of post-tensioned bridge substructures, and
5. To develop durability design guidelines and recommendations for post-tensioned bridge substructures.

A review of literature has indicated that while a few problems have been encountered in some bridges in Europe, Japan, and the U.S.A., damage has been limited to a very small percentage of post-tensioned bridges. In general, post-tensioning systems have been successfully used in bridge designs. However, as these bridges age and increase in cumulative exposure, more problems are being

noted. New practices and materials are required to guarantee the safety and design life of these structures.

The initial literature review performed by West [1.33] identified a substantial amount of relevant information that could be applied to the durability of post-tensioned bridge substructures. This existing information allowed the scope of the experimental portion of the project to be narrowed. The final objective represents the culmination of the project. All of the research findings are to be compiled into the practical format of comprehensive durability design guidelines.

1.2.3 Project Scope

The subject of durability is extremely broad, and as a result a broad scope of research was developed for TXDOT Project 0-1405. Based on the project proposal and an initial review of relevant literature performed by West[1.33], the project scope and necessary work plan were defined. The main components of TXDOT Project 0-1405 are:

1. Extensive Literature Review
2. Survey of Existing Bridge Substructures Inspection Reports (BRINSAP)
3. Long-Term Corrosion Tests with Large-Scale Post-Tensioned Beam and Column Elements
4. Investigation of Corrosion Protection (near joints) for Internal Prestressing Tendons in Precast Segmental Bridges
5. Development of Improved Grouts for Post-Tensioning
6. Development of recommendations and design guidelines for durable bonded post-tensioned bridge substructures

Components 1 and 2 (literature review and survey of Brinsap report) were performed initially by West[1.33], Schokker[1.34], Koester[1.35] and Larosche[1.36] and findings up to 1998 were published in references 1.33 and 1.34. The literature review process was continued by the author and is updated in this dissertation.

Component 3 was divided into Large Scale Column Corrosion Tests and Large Scale Beam Corrosion Tests. The column tests were started by Larosche[1.36] and West.[1.33] Column exposure testing began in July 1996. The beam tests were implemented in two phases: the first phase was implemented by West, [1.33] and exposure testing began in December 1997. The second phase was implemented by Schokker, [1.34] and exposure testing begun in December 1998. Comprehensive autopsies of around half of these specimens, at the end of their exposure testing period were performed by Kotys[1.37] and the author and are reported in this dissertation.

Component 4 (corrosion protection at joints of segmental bridges) was developed and implemented by Vignos[1.38] under TxDOT Project 0-1264. This testing program was transferred to TxDOT Project 0-1405 in 1995 for long-term testing. Although this aspect of the research was developed under Project 0-1264 to address corrosion concerns for precast segmental bridge superstructures, the concepts and variables are equally applicable to precast segmental substructures, and the testing program fits well within the scope of Project 0-1405. Half of the macrocell laboratory specimens were autopsied at four and a half years of exposure testing by West.[1.33] Final autopsies of the remaining specimens were performed by Kotys[1.37] and the author, and findings are reported in this dissertation.

Component 5 (Development of Improved Grouts for Post-Tensioning) was developed and implemented by Schokker[1.34] based on previous work published by Hamilton[1.39] and Koester[1.35]. The accelerated corrosion testing was performed

9

and conclusions were drawn and published.[1.32,1.34] Under this portion of the research, high-performance grouts for bonded post-tensioning were developed through a series of fresh property tests, accelerated corrosion tests, and large-scale field trials. These grouts have become widely used in practice.

Component 6 (Development of recommendations and design guidelines for durable bonded post-tensioned bridge substructures) refers to the most important implementation directed aspect of the research program. Interim design guidelines were developed and published by West and Schokker[1.40] based on research results up to 1999. Updated Guidelines based on final autopsy results from the macrocell, column and beam tests are included in this dissertation.

The project scope is outlined in Figure 1.1. This figure shows the cooperative effort performed by all graduate research assistants during the length of the project. In Figure 1.1 the years in brackets show the actual or expected publication dates for each Technical Report, published under TxDOT Project 0-1405. A more detailed description of the involvement of each graduate research assistant is shown in Table 1.1.

```
                    ┌─────────────────────────────┐
                    │  Investigating Corrosion    │
                    │    Protection Systems       │
                    └─────────────────────────────┘
```

| Literature Review - West, Koester, Larosche, Schokker Salas Kotys - 1405-1 (1999) 1405-8 (2003) | Evaluation of Improved Grouts for Post-Tensioning (Fresh properties and corrosion protection) Schokker Koester - 1405-2 (1999) | Segmental Joint Macrocell Specimen Corrosion Tests - West,Vignos Salas, Kotys - 1405-4 (1999) 1405-6 (2002) 1405-7 (2003) | Long Term Exposure Tests (corrosion) -- West, Schokker Larosche - 1405-3 (1999) |

| Beams - Salas Kotys - 1405-8 (2003) | Columns - Salas - 1405-8 (2003) |

Design Guidelines: West, Schokker (Interim Conclusions), 1405-5 (1999)
-
Salas, 1405-9 (2003)

Figure 1.1. TxDOT Project 0-1405 Scope, Researchers and

Technical Reports

Table 1.1 Major Project Tasks and Contributions of Graduate Students

Project Task	West (Ref. 1.33)	Schokker (Ref. 1.34)	Koester (Ref. 1.35)	Larosche (Ref. 1.36)	Vignos (Ref. 1.38)	Kotys (Ref. 1.37)	Salas (author)
Literature Review	X	X	X	X			X
Identification of Substructure PT Applications	X		X				
Identification of Protection Variables	X		X				
Survey of Existing Structures				X			
Testing Program Design							
Long Term Beam Exposure Tests	X						
Long Term Column Exposure Tests	X				X		
Segmental Macrocell Corrosion Tests					X		
Evaluation of Improved Grouts for PT		X	X				
Fabrication of Test Specimens							
Long Term Beam Exposure Tests	X	X					
Long Term Column Exposure Tests	X				X		
Segmental Macrocell Corrosion Tests					X		
Evaluation of Improved Grouts for PT		X	X				
Initial Exposure Testing							
Long Term Beam Exposure Tests	X	X					
Long Term Column Exposure Tests	X	X					
Segmental Macrocell Corrosion Tests	X				X		
Evaluation of Improved Grouts for PT		X	X				
Limited Specimen Autopsies							
Long Term Beam Exposure Tests		X					
Long Term Column Exposure Tests		X					
Segmental Macrocell Corrosion Tests	X						
Continuation of Exposure Testing							
Long Term Beam Exposure Tests						X	X
Long Term Column Exposure Tests						X	X
Segmental Macrocell Corrosion Tests							X
Final Autopsies							
Long Term Beam Exposure Tests						X	X
Long Term Column Corrosion Tests							X
Segmental Macrocell Corrosion Tests						X	X
Continuation of Exposure Testing							
Long Term Beam Exposure Tests						X	X
Preliminary Design Guidelines	X	X					
Design Guidelines update							X

1.2.4 Dissertation Scope

The author's involvement in Project 0-1405 started in August 2000, after exposure testing had begun in Components 3 and 4 above. This dissertation's scope includes the following:

1. Continuation of exposure testing of the remaining macrocell specimens,
2. Continuation of exposure testing of all beam and column specimens,
3. Performance of comprehensive autopsies of the remaining macrocell specimens, after eight years of aggressive exposure,
4. Performance of comprehensive autopsies and examinations of approximately half of Phase 1 and Phase 2 beams, after four and a half years, and three and a half years of exposure testing, respectively,
5. Performance of comprehensive autopsies and examinations of all column specimens after six and a half years of exposure testing, and
6. Updating of durability design guidelines based on exposure testing and autopsy results.

Figure 1.2 shows the project and dissertation (shaded area) schedule. As shown in this figure, approximately half of the beams from the large scale tests will undergo continuous exposure testing beyond the year 2003. The latter was decided after final macrocell corrosion tests results indicated longer exposure times to be desirable, as explained in detail in Chapter 4.

In Chapter 2 an overview of the history of bonded post-tensioning Systems and Structures is given, the main post-tensioning concepts, advantages, disadvantages, and durability aspects are summarized, and general background on durability protection techniques used to date is given. In Chapter 3, the

13

Segmental Macrocell Corrosion Test program and findings are explained. The Long-Term Beam Corrosion Test results are presented in Chapter 4. In Chapter 5 the Long-Term Column Corrosion Test results are summarized. In Chapter 6 the update on the Durability Design Guidelines based on the Interim Design Guidelines published previously under Project 0-1405[1.40] (as revised after the autopsy results of this series were analyzed) are presented. In Chapter 7 the program is summarized and conclusions on the Corrosion Testing, Evaluation and Durability Design of Bonded Post-Tensioned Tendons are presented.
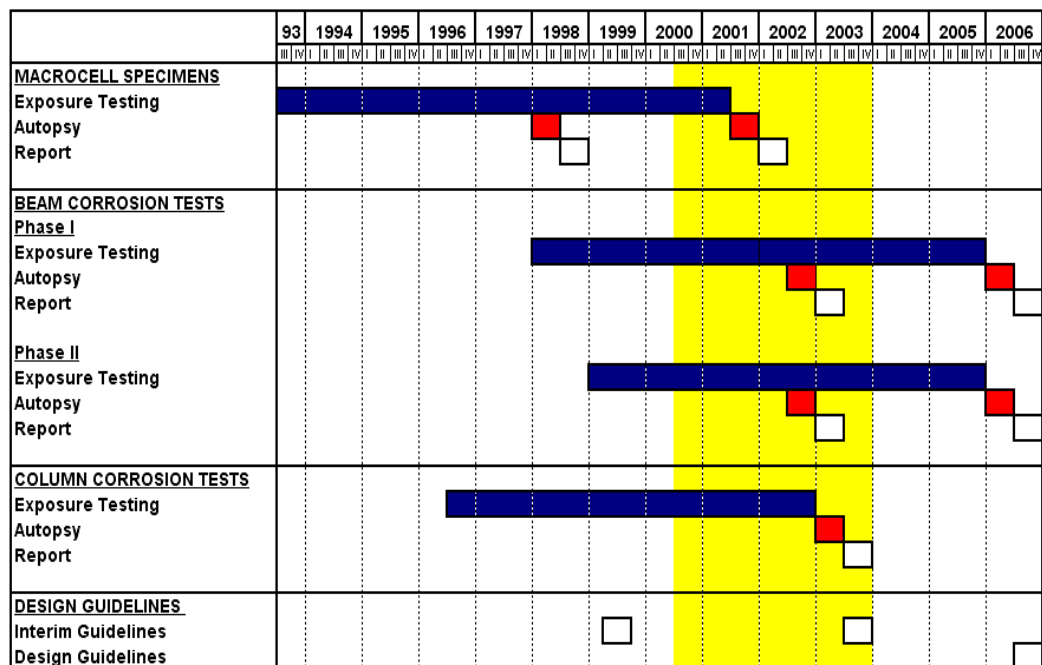
Figure 1.2. Project TxDOT 0-1405 (1993-2006) and Dissertation (2000-2003) Schedule

CHAPTER 2

Internal Bonded Post-Tensioning Systems

2.1 PRESTRESSED CONCRETE

2.1.1 Historical Development

Key events in the history of prestressed concrete structures started at the end of the 19th Century, with the concept of imposing preservice stresses on hardened concrete. However, the most important event in the development of this technique was recorded in 1933, when E. Freyssinet demonstrated the advantage of using higher strength concrete and high strength steel to minimize losses. Table 2.1 summarizes the key events as reported by Schupack.[2.1]

Table 2.1 Key Developments in Prestressed Concrete History[2.1]

Year	Author / researcher	Description
1888	P.H.Jackson	Concept of imposing preservice stresses on hardened concrete.
1907	M. Koenen	Identify losses due to classic shortening.
1908	G.R. Steiner	Recognized losses due to shrinkage.
1928	F.Dischinger	Loss of prestress compensated by retensioning.
1933	E.Freyssinet	Demonstrated advantage of using higher strength concrete and high strength steel to minimize losses.
1939	K.Wettstein E.Hoyer	Used high strength piano wire.
1943	J.M.Crom	Used high tensile drawn wire for tanks and pipe.
1944	G.Magnel	Identified the relaxation losses of work-hardened steels under constant strain.
1950	Reported by W.O. Everling.	Use of stress relieved wire 240 ksi (1.65 GPa) and strand 250 ksi (1.72 GPa) to provide user friendly steel.
1963	T.Cahill	Developed low-relaxation steel reducing loss from about 12 to 2.5%.

After these events, no other dramatic new concepts were reported through the end of the 20th Century, but continuous development has occurred and prestressing steel usage has been significantly increasing since the 1960's

After the second world war, as reported by Godart,[2.2] countries like France experienced the construction euphoria of widespread infrastructure reconstruction, during a period marked by cement and steel shortage. French viaducts were reconstructed with simply supported spans made up of prestressed beams, known as VIPP (Viaducts a travées Indépendantes a Poutres Précontraintes: Viaducts with simply supported spans made of prestressed beams). After an investigation by Trouillet in the year 2000 as reported by Godart, [2.2] fifteen out of a total of 720 VIPP built before 1966, had been demolished because of tendon corrosion.

In the USA, according to the National Bridge Inventory Database[2.3], there are approximately 600,000 bridges, of which half were built between 1950 and 1994. Based on Federal Highway Administration (FHWA) data reported by Yunovich, [2.3] approximately 18.5% of the total are prestressed concrete bridges. These include both post-tensioned and pretensioned technology.

The beginning of post-tensioned concrete bridges in the US started in Madison County, Tennessee, [2.4] where a concrete highway bridge was built and opened to traffic on October 28,1950. The bridge consisted of three-spans with a total length of 81 feet, using precast concrete blocks with mortar joints. This bridge was shortly followed by the Walnut Lane Bridge in Philadelphia, completed in the fall of 1950 and opened to traffic in February 1951. The construction of the Walnut Lane Bridge started in 1949, and therefore the beginning of post-tensioning in the US is often associated with this bridge. Three segmental I-girder bridges were constructed in western New York in 1950 and 1951. [2.5] By the end of 1952, there were prestressed concrete bridges in eight states and this grew to 17 states in 1954. By the year 1985, there were more than

60,000 prestressed concrete bridges in the United States.[2.4] The majority of these bridges used pretensioned units. The first precast post-tensioned segmental box girder bridge was the John F.Kennedy Memorial Causeway, built in 1971 in the coast of Texas. The Pine Valley Creek Bridge, built in the coastal mountains near San Diego, California in 1974 was the first U.S. cast-in place balanced cantilever bridge.[2.5]

In 1999, the use of bonded post-tensioning steel in bridges and earthwork comprised 22 percent (about 29,000 tons) of the total post-tensioning steel tonnage used in the US. Other uses include buildings, slabs-on-ground and miscellaneous.[2.5]

2.1.2 Basic Definitions

The current research refers to bonded internal post-tensioning systems. In general, prestressed concrete can be pretensioned or post-tensioned, depending on when the prestressing steel is tensioned. Table 2.2 gives the basic definitions and main differences among the different prestressing techniques.

In bridge post-tensioning applications, prestressing steels often consist of a bundle (tendon) of 7-wire prestressing strands of very high strength steel that are run through the ducts previously placed into the concrete element before casting. The end anchorage includes wedges to hold the tendons that run through an anchor head with tapered holes. Figure 2.1 shows a typical anchorage system. The wedges contain teeth that bite into the strand, and this makes corrosion protection of the end anchorage area critical. [2.6] Once the prestressing steel has been stressed to the desired level and adequately anchored, the ducts can be injected with cement grout, in which case the system is referred as bonded. In this case, the grout develops bond between the steel tendon and the duct and surrounding concrete and acts as a corrosion barrier.

Table 2.2 Basic Definitions (Adapted from 2.4)

Term	Definition
Prestressed Concrete	Technique of tensioning the steel reinforcement in a reinforced concrete structures so as to place the concrete in a state of compression to counteract the tensile stresses resulting from service loads. Prestressed concrete may be pretensioned or post-tensioned, depending on when the prestressing steel is tensioned.
Pretensioned Concrete	Pretensioned concrete is made by stressing the steel (normally wires or strand) between fixed points, usually the ends of a rigid casting bed, and then casting concrete around the steel. After the concrete has gained sufficient strength, the strands are released from their original anchorage, thereby applying compressive stress to the concrete.
Post-Tensioned Concrete	In post-tensioned concrete, the tendons are tensioned after the concrete has gained strength. This can be done by using tendons that have been encased in sheathing during manufacture. These covered tendons are cast in the concrete. Alternatively, ducts are cast in the concrete, normally using metal sheathing, through which the tendons are later threaded. When the concrete has achieved a predetermined strength, the tendons are stressed and anchored. Post-tensioned construction can be classified as bonded or unbonded.
Unbonded construction.	In unbonded construction, the tendons transfer stress to the structure only at the anchorages. Except for external tendons, unbonded construction is very rarely used in highway bridges because of the severity of the service environment and the uncontrolled crack width and reduction in capacity at the ultimate limit state.
Bonded construction	In bonded construction, grout is injected to fill the void between the tendon and the duct. This not only protects the tendon against corrosion but also increases the ultimate strength capacity of the component.
Internal Tendons	Tendons that are embedded in a member.
External Tendons	Tendons most frequently used in cellular sections and must be unbonded or partially bonded at intermediate deviators.
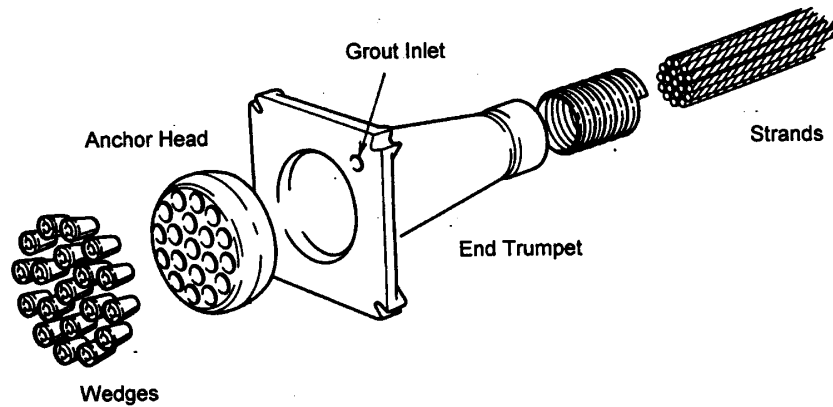
Figure 2.1 Post-Tensioning Anchorage Details
(from T.Y. Lin, and N.H. Burns, 1981) [2.6]

2.1.3 Advantages and Disadvantages of Internal and External Post-Tensioning

Prestressed concrete benefits include improved crack control (higher cracking moment, fewer cracks, smaller crack widths), reduced reinforcement congestion, continuity of reinforcement and efficient use of high strength steel and concrete. Additionally, post-tensioning will allow for a quick and efficient joining of precast elements and continuity between existing components and additions.[2.6]

Post-tensioning systems can be internal and external. Table 2.3 shows a comparison of these systems in terms of their advantages and disadvantages.

Table 2.3 Advantages and Disadvantages of Internal and External
Post-Tensioning (Adapted from References 2.2 and 2.7)

	Advantages	Disadvantages
Internal Post-Tensioning	- allow for possible reanchoring of the strands, losing only locally the prestress force in the event of failure of a section - tendons can follow well the moment diagram - low production costs - system reserves available	- concentration of vent hoses at the road surface (can be avoided) - design experience necessary - high requirements to quality, especially during grouting - grout characteristics are critical - expensive maintenance - very difficult to investigate and impossible to replace
External Post-Tensioning	- webs free of tendons - low weight - high quality - no vent hoses - tendons with high level-corrosion protection - restressable - strengthenable - theoretically replaceable - more easy to investigate	- can be damaged - exposed to atmospheric influences - reserve is missing due to no bond - full loading action on the anchorage - critical assembly operations - more expensive construction and demolition - more sensitive to fire - more easily attackable by vandals - with any failure the prestressing force disappears over the overall length of the tendon - the buckling and whipping generated by a sudden rupture create risks for the inspection staff and for the other tendons - design experience necessary

2.1.4   Mixed Post-Tensioning

There has been world wide debate with respect to the use of either internal or external post-tensioning.   After analyzing the advantages and disadvantages for each system, it appears obvious that in many cases the solution would be in the intermediate area. As noted by Jungwirth and Gehlen[2.7] a "mixed construction," which is use of a combination of internal and external tendons in a

section, is considered to have many advantages. These include among others: different loading cases during the construction and demolition phase can be handled more easily with internal post-tensioning tendons; residual load bearing capacity in case of failure of external tendons (for example: in case of fire or earthquakes); possibility of a subsequent strengthening with external tendons; and , better ductility with internal tendons in case of earthquakes.

After considering some decisions in Germany, Virlogeux [2.8] stated in 1999 that "… stopping internal prestressing, or limiting its application by some recommendations issued to protect against some exceptional problems, could create difficulties everywhere, especially when coming from Germany, which has the very well-deserved reputation of its use of prestressing. It would be against the facts: hundreds of thousands of structures have been built in prestressed concrete on the five continents, with very few problems."

Chaussin[2.9] stated in Ghent that "…it is a good thing, whenever it is possible, not to put all one's eggs in one basket and to combine internal and external tendons." He recommends that in internally prestressed members, a particular attention must be given to anchorage areas. The risk could be counteracted by placing in these zones enough non-prestressed mild reinforcing steel to withstand the action effects susceptible to occur even if cracks appear. In that case, crack formation would constitute an evident sign of distress for an experienced eye and the structure manager would have enough time to take appropriate actions. In externally prestressed structures, structures would have to be designed so the failure of one tendon does not seriously impair the proper functioning of the structure. The broken tendon should be easily inspected and replaced.   In this type of structure, it is advisable to incorporate, during the design phase, the potential for additional external tendons (anchor and deviation points) for strengthening purposes, either to respond to changes in service

conditions or to compensate the loss of part of the existing prestressing or to counteract an unexpected behavior of the structural concrete. It is understood that the additional cost of such measures if they are included in the design phase, would be a small fraction of the cost of installing them later during the structure's service life.

2.1.5 Applications of Bonded Post-Tensioning

Bonded post-tensioning is currently used in many bridge and building applications. In bridge applications, bonded post-tensioning is used in:

- Precast segmental balanced cantilever construction (cantilever tendons and continuity tendons) See Figure 2.2.
- Precast segmental span-by-span construction
- Post-tensioned AASHTO, bulb-T, and spliced girders
- Cast-in Place segmental balanced cantilever construction
- Cast-in-place bridges on falsework
- Transverse post-tensioning of superstructures (transverse top slab post-tensioning, transverse post-tensioning in diaphragms, vertical post-tensioning in diaphragms, transverse post-tensioning in deviator ribs of precast segments, vertical post-tensioning bars in webs,
- Post-tensioning of substructures, see Figure 2.3 and Figure 2.4 (hammerhead piers, straddle bents, cantilever piers, precast box piers, precast I-section pier columns, transverse confinement tendons at tops of piers)
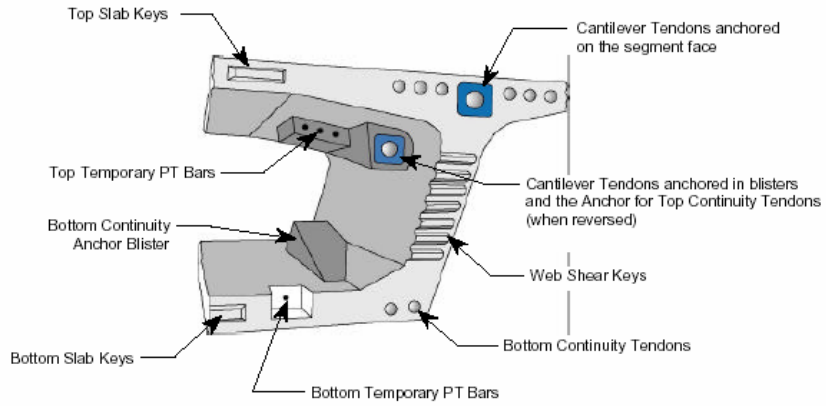
Figure 2.2 Typical Balanced Cantilever Segment [2.10]
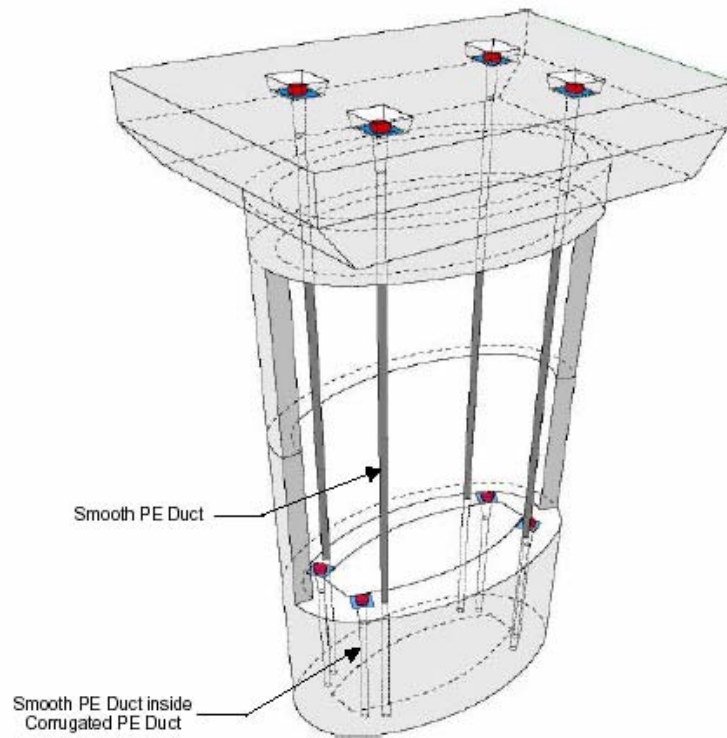
Figure 2.3 Vertical Post-Tensioning of the High-Level Approach Piers of the Sunshine Skyway Bridge, Florida [2.10]

23
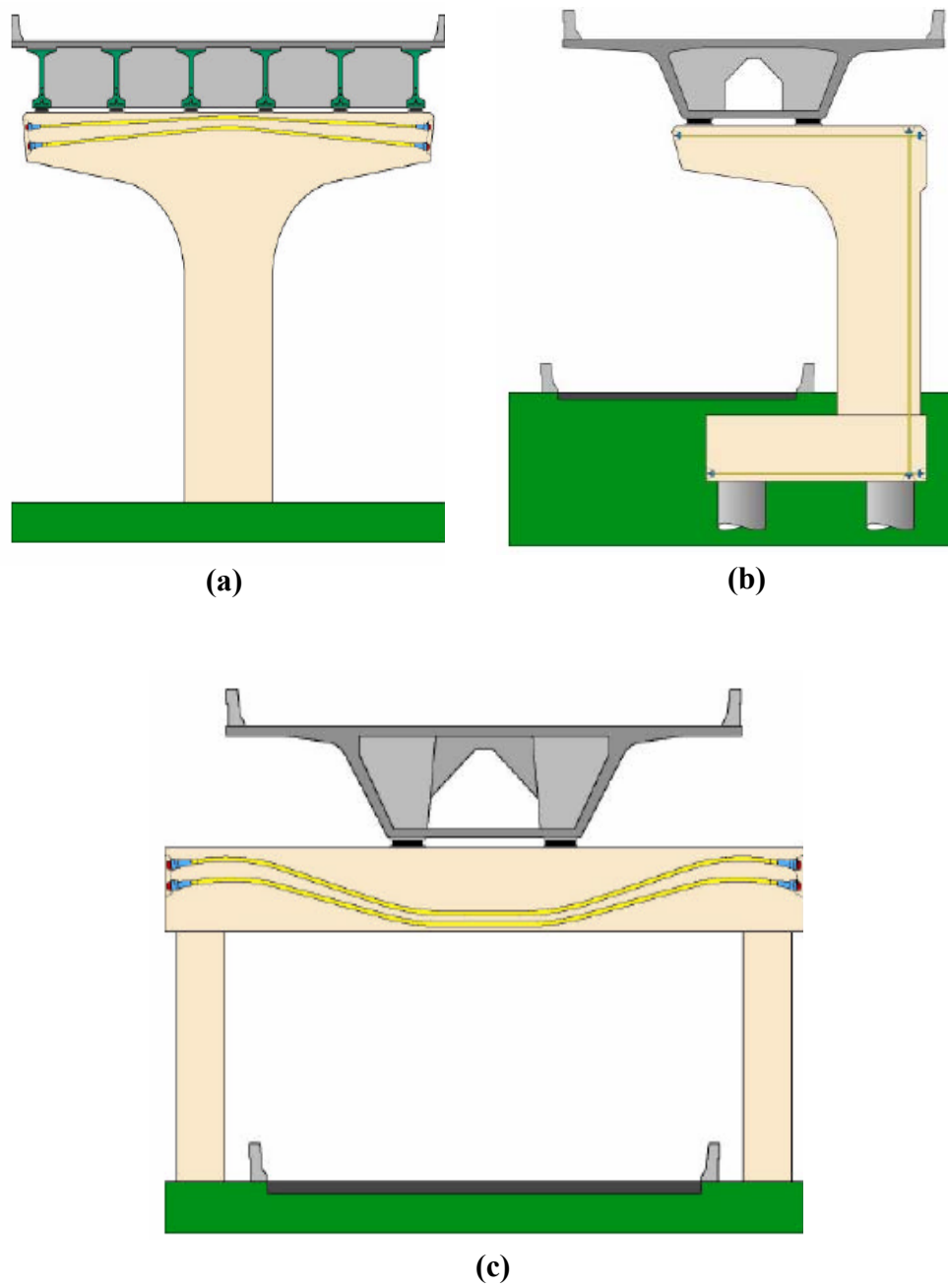
Figure 2.4 Post-Tensioning in (a) Hammerhead Piers,
(b) Cantilever Piers, and (c) Straddle Bents [2.10]

24

A detailed description of the above applications is included in Volume 1, Chapter 2, of the document "New Directions for Florida Post-Tensioned Bridges," published in 2002 by the Florida Department of Transportation. [2.10]

2.1.6 Mixed Reinforcement

AASHTO LRFD (Load and Resistance Factor Design) Bridge specification explicitly recognized the use of partial prestressing,[2.11 as referenced in 2.12] an unfortunate term. There are several conflicting definitions for partial prestressing in use in practice. It may refer to the level of stresses and what degree of tensile stress is permitted in the precompressed tensile zone under service load. AASHTO is using the term partial prestressed structures to refer to structural concrete members with a combination of high strength prestressing steel and non-prestressed mild steel reinforcement. Internationally the preferred term for this use is 'mixed reinforcement' a combination of active reinforcement (stressed in construction) and passive reinforcement (stressed by subsequent load condition). This more correct terminology will be used in this study. The relative amounts of prestressing steel and reinforcing bars may vary, and the level of prestress in the prestressing steel may be altered to suit specific design requirements. In most cases, members with mixed reinforcement are expected to crack under service load conditions (flexural cracks due to applied loads).[2.12]

As stated by West,[2.12] in the past practice in the United States prestressed concrete elements have always been required to meet the classic definition of full prestressing at service load levels where concrete stresses are kept within allowable limits and members are generally assumed to be uncracked (no flexural cracks due to applied loading). The design requirements for prestressed concrete were distinctly separate from those for reinforced concrete (non-prestressed) members, and are located in different chapters or sections of the codes. The fully

prestressed condition may not always lead to an optimum design. The limitation of concrete tensile stresses to below cracking can lead to large prestress requirements, resulting in very conservative design, excessive creep deflections (camber) and the requirement for staged prestressing as construction progresses. Some relief was given by allowing some levels of tensile stress in the precompressed tensile zones at service load levels.

Mixed reinforcement can provide a desirable design alternative to reinforced concrete and fully prestressed designs in many types of structures, including bridge substructures. The opposition to mixed reinforcement designs and the reluctance to recognize higher allowable tensile stresses at service level in design codes has primarily been related to concerns for increased cracking and its effect on corrosion. Mixed reinforcement structures will generally have more cracks than comparable fully prestressed structures but lesser cracking than non-prestressed structures. No explicit crack width limitations are placed on non-prestressed members. Due to the widely accepted notion that prestressing steel is more susceptible to corrosion, and that the consequences of corrosion in prestressed elements are more severe than in reinforced concrete, many engineers have felt that the benefits of mixed reinforced are outweighed by the increased corrosion risk. Little or no research has been performed to assess the effect of mixed reinforcement on corrosion. [2.12]

2.2 DURABILITY OF BONDED POST-TENSIONED CONCRETE STRUCTURES

As referenced by Kuesel [2.13], Hardy-Cross said that "The first requirement for a beautiful bridge is that it must stand up long enough for us to look at it." Kuesel continue saying that "…We should endeavor to design bridges that will be functional, enduring and – yes – beautiful. …. Design codes should require consideration of endurability – inspectability, maintainability, reliability and

resistance to water, corrosion, temperature cycles and neglect. …we should not be debating how much further we can reduce safety margins (for loads and strength), but rather how much we should increase safety margins (for wear and corrosion). … All around us we see the results of neglect of long-term problems, and yet we persist in concentrating our attention on short-term design. Least first cost is a short –term objective. Long useful life is a long term objective. We need them both."

Godart [2.2] indicates that "…Design defects are … mainly linked to construction defects or unsuitable techniques or to the use of low durability materials. The two principal construction defects responsible for corrosion are poor waterproofing and incomplete grouting of the prestressing ducts. In addition to these defects there is poor sealing of end anchorages, deck anchorages and transverse anchorages."

2.2.1 **Problems Encountered Around the World:** *The Ghent Workshop*

In November 2001, engineers from many countries gathered at Ghent University, under the sponsorship of *fib* and IABSE, to discuss the "Durability of Post-Tensioning Tendons." The findings are contain in the *fib*-IABSE Technical Report, Bulletin 15.[2.14] The problems reported from different countries lead to similar findings. Zivanovic et al. [2.15] succinctly summarized the conference findings with respect to the inventory and condition of post-tensioning bridges as follows:

a) Design Defects:
- Lack of waterproofing;
- Lack of sealing behind tendon anchorages;

- Construction resulting in a large number of unprepared construction joints, which could give rise to cracking due to restrained shrinkage;
- Use of unprotected transverse tendons in grooves in the deck;
- Use of sheaths made from bitumen-coated Kraft paper wrapped around the tendons which made grouting impossible;
- Low ratio of rebar/total steel, as low as zero for longitudinal construction joints along the length of the deck between the beams and slabs;
- Large numbers of tendons per span in older structures with deck anchorages increasing the number of points of possible water ingress;
- Use between 1950 and 1970 of prestressing steel which was susceptible to stress corrosion which gave rise to the possibility of brittle fracture;
- Lack of provision for drainage
- Leaking expansion joints;
- Insufficient concrete cover over the reinforcement, resulting in corrosion of the reinforcement and spalling of the concrete giving easier access to the prestressing tendons for aggressive agents.

b) Construction defects

The main defects leading to corrosion are poor waterproofing, incomplete grouting of the prestressing ducts and poor sealing of end anchorages.

Although concrete has generally performed well in older structures, there may be areas where poor workmanship has given rise to honeycombing or shrinkage cracking. The most common location are

the soffits of flanges where concreting has been made difficult by the congestion of ducts or where there has not been proper compaction, resulting in large areas where spalling may allow aggressive agents to penetrate.[2.15]

During the workshop, Godart[2.2] also mentioned that "…When …external tendons…are in a wet atmosphere, generally due to bad construction details (lack of ventilation, absence of waterproofing, non tight inspection access…), wire failures caused by corrosion occur and the durability of the tendons is lowered."

From Japan, Mutsuyoshi[2.16] reported that internal post-tensioned concrete structures with cement grouting have been forbidden by the Japan Highway Public Corporation, because bad quality of grouting after construction has been found in many bridges. Now, almost all new prestressed concrete structures are being constructed using fully external tendons using transparent sheath with grouting.

2.2.2 Experience in United States

Out of the total number of bridges in the USA, approximately 20% are prestressed concrete bridges; only 3% of these were classified, in 1998, as structural deficient (bridges that can no longer sustain the loads for which they were designed).[2.3]

A comprehensive survey performed in 1999 by the American Segmental Bridge Institute (ASBI), found that concrete segmental bridges were performing well with time. Based on inspection reports using Federal Highway Administration (FHWA) guidelines, all segmental bridges were rated as "fair" or better. Of the 131 bridges, 99 percent had superstructure ratings of "satisfactory" or better, 79 percent had superstructure ratings of "good" or better, and 31 percent had superstructure ratings of "very good" or better.[2.17]

29

The first segmental bridge constructed in the US, in 1971, the John F. Kennedy Memorial Causeway near Corpus Christi, Texas, was inspected extensively in a Federal Highway Administration study in 1988, and no indications of distress or corrosion of the prestressing tendons were found.[2.12] This bridge was constructed using match-cast epoxy joints, as required by designers, considering the hot, humid, seawater environment of the Gulf of Mexico.

Recently, some tendon failures and corrosion related problems have come to light, especially in the state of Florida.[2.5,2.10] In 1999, one of the external tendons in the Niles Channel Bridge built in 1983, failed due to corrosion at an expansion joint. A 9-inch movement of the tendon through one of the deviation saddles was noticed first. When the tendon was removed for replacement, a void in the grout and heavy pitting in the prestressing strands inside the anchor head were found. (See Figures 2.5 and 2.6). In 2000, eleven tendons out of a total of 846 were replaced in the Mid-Bay Bridge built in 1993. Ten of the eleven tendons that were replaced were located at expansion joints. (See Figures 2.7, 2.8 and 2.9) Also, in 2000, several corroded tendons were discovered in segmental piers of the Sunshine Skyway Bridge, built in 1986, where the corrosion resulted from seawater in ducts, permeable concrete anchorage protection at the top of piers and splitting of polyethylene ducts.[2.5] (See Figures 2.10 and 2.11)

*Figure 2.5 Plan View of Slipped Tendon at Deviation Saddle
Niles Channel Bridge [2.10]*
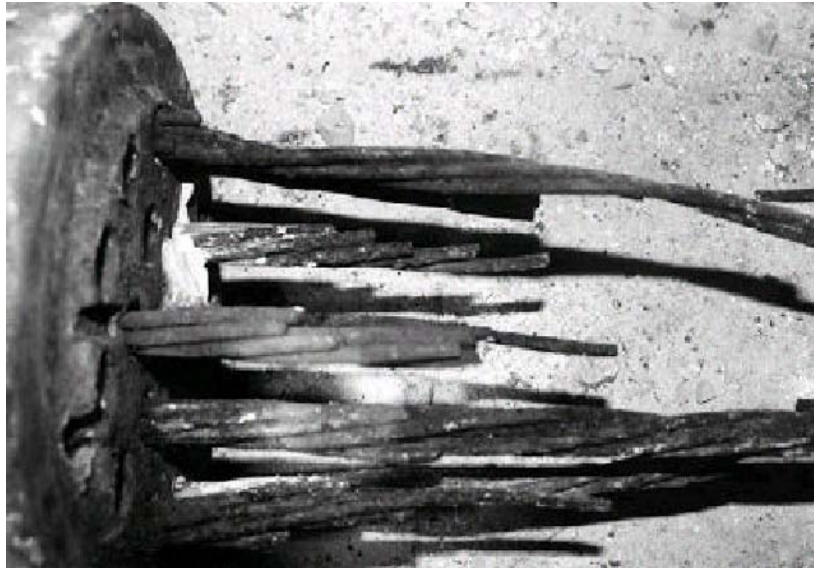
*Figure 2.6 Advanced Corrosion of Strands within Anchorage
Niles Channel Bridge [2.10]*

31

Figure 2.7 The Mid-Bay Bridge, Florida [2.10]

8/29/2000

Figure 2.8 Failure of Tendon 28-6 on the
Mid-Bay Bridge [2.10]

32

*Figure 2.9 Failure of Tendon 57-1 on the Mid-Bay Bridge-
At Expansion Joint Diaphragm-* [2.10]

*Figure 2.10 The Sunshine Skyway Bridge,
Tampa, Florida* [2.10]

***Figure 2.11 Tendon Corrosion inside the Sunshine Skyway Bridge Piers
(Refer to Figure 2.3) [2.10]***

In addition to the above, inspections in Florida bridges have revealed a large number of bleed water voids at anchorages, partially grouted tendons and ungrouted tendons, the same type of problems that were found in the Sidney Lanier Cable Stayed Bridge in Georgia and in the Boston Central Artery bridges.[2.5]

Freyermuth [2.5] has indicated that the major portion of the bridge tendon corrosion problems that have been observed in the U.S. have been identified with the following:[2.5]

1. An aggressive environment (northeast U.S. and Florida)

2. Areas with a low volume of post-tensioned construction

3. Contractors with no experience or expertise in post-tensioned construction

4. Grossly inadequate construction supervision

5. Design details without adequate provision for corrosion protection of tendons

6. Failures to respond to or correct construction problems

In particular, after analyzing the problems encountered in bridges located in the state of Florida, it appears that the tendon corrosion problems were due to:

1. Voids associated with accumulation of bleed water at tendons anchorages

2. Recharge of ungrouted tendon anchorages with salt water or surface drainage during construction.

3. Leakage through end anchorage protection details

4. Quality of the grout installation and grout materials

5. Splitting of polyethylene ducts

6. Deficiencies in implementation and inspection of grouting procedures.

The findings in Florida have lead to some immediate recommendations, with respect to the use of bonded post-tensioning systems:[2.18]

1. No precast concrete hollow column section should be specified below the waterline.

2. No PT tendons should be located in columns below the highest water splash zone elevation.

3. Grouting operation for vertical tendons should be carefully planned, tested and monitored. Stage and vacuum grouting should be specified in the upper section of tendons in combination with a pressurized sealed PT system and zero bleed grout.

35

4. Provide multiple levels of protection at anchorages, including permanent grout cap, epoxy material pour-back and polymer coating over the pour-back.

5. The impact of construction methods on the corrosion vulnerability of PT system should be thoroughly analyzed and designed for, especially for critical elements in aggressive corrosive environments.

6. PT redundancy system or practical replacement capabilities should be incorporated.

7. Corrosion detection methods should be included during the construction and service life of the structure.

After these important findings in Florida, many states are performing comprehensive investigations of their post-tensioned bridges, to determine the extent of the problem. These include among others the states of Texas, California, Virginia, and Georgia. [2.19]

In spite of the above, and as mentioned by Freyermuth,[2.5] the durability performance of prestressed and segmental post-tensioned bridges has been superior to all other types of construction. Recent improvements in grouting materials technology (ant-bleed –thixotropic - grouts), and training programs for grouting supervisors and inspectors are expected to yield significant results, reducing the incidence of corrosion problems in grouted tendons.

2.3 FACTORS AFFECTING THE DURABILITY OF BONDED POST-TENSIONED CONCRETE STRUCTURES

2.3.1 Exposure Conditions

There are four general environments where concrete structure durability may be a concern: coastal exposure, freezing exposure, and aggressive soils. These exposures may occur singly or in combination.

West[2.12] summarized and compiled information on these exposure conditions as follows:

2.3.1.1 Coastal Exposure

Coastal exposures are one of the most severe environments for concrete structures. This is particularly true for structural components located directly in the seawater, as in the case of bridge substructures. Seawater contains dissolved salts which affect the durability of concrete. The most prevalent salts in order of quantity are sodium, magnesium and potassium chlorides and magnesium, calcium and potassium sulfates. These salts provide sources of chlorides and sulfates which can lead to corrosion of reinforcement and sulfate attack on concrete. To a lesser extent, these salts also provide a source of alkalis which may lead to expansive alkali-aggregate reactions if reactive aggregates are present. There are four main exposure zones for a structure in a coastal exposure: atmospheric zone, splash zone, tidal zone and submerged zone.[2.12]

Corrosion of steel reinforcement requires oxygen and thus generally occurs only in zones which experience some amount of drying. Also, corrosion rates are highest when humidity is in the 90-95% range. The greatest risk of corrosion occurs in the splash and atmospheric zones for these reasons. Corrosion in the tidal zone is normally limited due to the shorter drying periods and slower

rate of oxygen diffusion through saturated concrete. The submerged zone of concrete has a low risk of corrosion due to lack of oxygen. [2.12]

Frost damage is most severe in concrete that is saturated, and therefore concrete within the tidal zone or immediately above the high tide level may experience the most significant damage. Freeze-thaw damage rarely occurs below the low tide level since the seawater would also have to freeze. [2.12]

Sulfate attack occurs primarily in zones where the concrete is submerged for some period, allowing greater sulfate concentrations. The greatest risk of sulfate attack normally occurs in the tidal zone and submerged zone. The same holds true for alkali-aggregate reactions due to alkalis in the seawater. [2.12]

The temperature range to which a structure is subjected also affects durability. Increases in temperature have an accelerating effect on many chemical reactions, including corrosion. The general rule of thumb is that a temperature increase of 10 degrees Celsius doubles the rate of reaction. Traditionally, seawater environments in cold climates, such as the North Sea, were viewed as the most severe exposure for structures. More recently, the accelerating effects of high temperatures have been recognized as equally or possible more severe than the combination of freezing temperatures and corrosive environments. [2.12]

2.3.1.2 Freezing Exposure

Environments where structures may be exposed to freezing temperatures may lead to freeze-thaw damage of concrete. A secondary effect is that the use of deicing chemicals in freezing exposures can exacerbate freeze-thaw damage and may lead to corrosion of steel reinforcement if the deicing agents contain chlorides. [2.12]

The severity of freeze-thaw damage of concrete is a function of the presence of moisture in the concrete and the number of times the moisture freezes

and thaws. Frost damage worsens when repeated cycles of freezing and thawing occur. Thus a moderate winter climate which experiences many freeze-thaw cycles can cause more frost damage than a severe winter climate that remains below freezing for long periods. [2.12]

2.3.1.3   Aggressive Soils

Chemical attack on concrete in the form of sulfate attack or alkali-aggregate reactions may occur in soils containing sulfates or alkalis. The presence of these aggressive agents must be accompanied by moisture for attack to occur (assuming the concrete is susceptible to either form of attack). Moisture provides the transport mechanism for sulfates and alkalis to penetrate concrete, and is also necessary for the deleterious reactions to occur.[2.12]

2.3.2   Concrete Durability

Concrete is typically the first level of protection for the reinforcement. Extensive research has been performed on the many subject areas pertaining to concrete durability.[2.6] Several aspects related to concrete durability are discussed in this section, but a detailed literature review on the subject can be found in West. [2.12]

2.3.2.1   Sulfate Attack

Sulfate attack is a fairly intricate process that causes cracking of the concrete. Sulfates react to the C_3A in concrete to form ettringite. The ettringite occupies a much larger volume in the concrete that then causes cracking due to expansive stresses. Sulfate attack can be controlled by utilizing cements with low C3A contents, such as Type V cements. Pozzolan addition has also been found to be helpful in preventing sulfate attack. (from various references in Schokker) [2.6]

2.3.2.2 Freezing and Thawing Damage

Saturated or nearly saturated concrete can be susceptible to freeze-thaw damage due to the expansion of water during freezing. Fortunately, this problem can be avoided by the addition of an air-entraining admixture. (from various references in Schokker) [2.6]

2.3.2.3 Alkali-Aggregate Reaction

Alkali-aggregate reactions are chemical reactions between alkalis and certain types of aggregates. The reactions may be alkali-silica or alkali-carbonate, depending on the type of aggregate. The alkali-silica reactions produce an alkali-silica gel that possesses expansive properties and can lead to cracking and deterioration of the concrete. The reaction of alkalis with carbonate aggregates is referred to as the dedolomitazation of the aggregate. The alkali-carbonate reaction products are prone to swelling in a manner similar to clays. [2.12]

2.3.2.4 Carbonation

Carbonation of concrete occurs when atmospheric carbon dioxide penetrates the concrete. In the presence of moisture, carbon dioxide will react with calcium hydroxide in the concrete to produce calcium carbonate.

The formation of calcium carbonate reduces the pH of the concrete to as low as 8, where the passive film is no longer stable allowing corrosion to begin.

The process of carbonation is slow in good quality concrete. The rate of carbon dioxide penetration is a function of the square-root of the exposure time. Factors affecting the rate of carbonation include the concrete permeability, cracking, the moisture content of the concrete and relative humidity. The presence of cracks will allow the carbonation front to reach the steel rapidly (a local scale). This may contribute to the formation of macrocell corrosion at the

crack. Carbonation will not occur in concrete that is saturated or very dry. The rate of carbonation is highest for relative humidity of 50% to 70%.

Carbonation may be slowed by specifying concrete with low permeability. Options include the use of low water-cement reactions, use of superplasticizers to reduce water demand, and the use of mineral admixtures. Compaction and proper curing are needed to ensure low permeability. Concrete surface treatments or sealers may slow penetration of carbon dioxide. (from various references in West) [2.12]

2.3.2.5 *Cracking*

The effect of cracking on the corrosion of reinforcing or prestressing steel is controversial. One viewpoint is that cracks reduce the service life of structures by permitting rapid penetration of carbonation and by providing a means of access of chloride ions, moisture, and oxygen to the reinforcing steel. Thus, cracks accelerate the onset of corrosion. [2.20]

The other viewpoint is that while cracks accelerate the onset of corrosion, that corrosion is localized. With time, chlorides and water penetrate even uncracked concrete and initiate more widespread corrosion. Consequently, after a few years of service for concrete with moderate to high permeability there is little difference between the amount of corrosion in cracked and uncracked concrete.[2.20]

With respect to cracking, Qing Li.[2.21] concluded that "…Load-induced cracking does affect the corrosion initiation of the reinforcement in structural concrete, … From the test results, it is almost certain that the corrosion initiates at the cracked sections of reinforced concrete structural members. How this localized corrosion propagates, leading to further longitudinal surface cracking, delamination, debonding , and the ultimate capacity reduction in terms of strength and stiffness of the structure, is of consequential importance to structures in

marine environment, where an ample supply of saltwater and oxygen is available. In particular, cyclic tides and/or waves pump saltwater in and out of the cracks, significantly exacerbating structural capacity deterioration. This intricate phenomenon has not been examined thoroughly thus far and needs considerable attention from the research community."

An in-depth analysis of cracking and corrosion is included in reference 2.12.

2.3.3   Grouts for Post-Tensioning

As summarized in West,[2.12] cement grout bonds the post-tensioning tendon to the surrounding concrete and provides corrosion protection for the tendon. Corrosion protection is in the form of a barrier to moisture and chloride penetration, and the presence of an alkaline environment for the tendon.

An optimum grout for post-tensioning combines desirable fresh properties with good corrosion protection. The fresh properties of the grout influence how well the grout fills the duct. The corrosion protection provided by the grout is rendered less effective if the duct is only partially or intermittently filled with grout. The presence of voids or discontinuous grouting may also permit movement of moisture and chlorides along the length of the tendon. Important grout fresh properties include: fluidity, bleed resistance, volume change, set time.

The fresh properties of grout can be controlled through water-cement ratio, the use of chemical and mineral admixtures, and by the type of cement. Admixtures include the use of anti-bleed agents sometimes referred to as thixotropic admixtures. This class of admixture gives the grout gel-like properties to minimize bleeding, while permitting the grout to become fluid when agitated (mixed, pumped, etc.).

Grouting techniques are critical. As reported by Hamada, et al.[2.22], at the
Ghent Workshop, " …it has been found in Japan … that serious deterioration has
occurred in prestressed bridges due to insufficient grouting."

2.3.3.1   Voids and Bleed Water

Voids can be formed in the post-tensioning duct from incomplete
grouting, trapped air pockets, or from the evaporation of bleed water pockets.
Top quality grout is of little benefit if poor grouting procedures result in large
void formations, which provide no protection to the strand and no transfer of
bond. Proper venting of the post-tensioning duct is critical for complete grouting.
The void between the tendon and the post-tensioining duct is a very complex
space. For instance, a parabolic shaped duct with a tensioned tendon may have a
number of small voids of varying shapes and sizes, and very stiff grout may not
fill the interstices [2.23 as referenced in 2.6]

Bleed lenses form as a result of the separation of water from the cement.
This sedimentation process is accentuated by the addition of seven –wire strand,
which acts as a "water-transport mechanism." [2.24 as referenced in 2.6] The spaces within
the individual twisted wires that form the strand are large enough to allow easy
passage of water but not cement. Ducts with vertical rises will typically cause
more bleed due to the increased pressure within the grout column. Intermediate
bleed water lenses may form in tall vertical ducts, leaving a void through the
cross-section of the duct exposing the tendon. Even in parabolic draped ducts,
any bleed water will tend to gather near the highest intermediate points, leaving
voids in the duct. [2.6]

Grouts containing anti-bleed admixture, or thixotropic grouts, can be bleed
resistant even when used in ducts with large vertical rises. [2.4 as referenced in 2.6] These

grouts are able to retain their water even under high pressures and can eliminate significant void formation when proper grouting procedures are followed. [2.6]

From the Florida experience, Pielstick[2.26] reported that "…the corrosion [of prestressing steel] resulted from the absence of grout due to accumulated bleed water at the anchorages leaving voids. The bleed water was either reabsorbed into the grout or evaporated. It appears that additional corrosion resulted when these voids were recharged with water and air leaking through at the anchorages. ….Multiple voids were …found near the anchorages which were then filled with grout by the vacuum injection method. This vacuum injection method removes as much air as possible and measures the air volume, then replaces the measured air volume with grout."

2.3.3.2 *Grout Cracking*

Grouts are injected after the concrete elements have been post-tensioned, and therefore there is no compression force in the hardened grout, making the grout matrix vulnerable to cracking.

The effect of grout cracking on prestressing steel corrosion has not received enough attention by researchers. Hamilton[2.27] reported after his series of accelerated corrosion tests, that "…the outline of the crack…is in line with the most intense area of corrosion. Away from the crack location the intensity of the pitting corrosion decreases. In some areas a greenish-white corrosion was noted which was still moist when the grout was removed. Usually within a day the corrosion product would dry and the remaining deposit would be red or black."

2.3.4 Corrosion of Steel Components in Post-Tensioning Systems

Corrosion of prestressing steel is generally of greater concern than corrosion of passive mild steel reinforcement because of the possibility that corrosion may cause a local reduction in cross section and failure of the steel.

The high stresses in the steel also render it more vulnerable to stress corrosion cracking and, where the loading is cyclic, to corrosion fatigue. [2.20]

Corrosion of prestressing reinforcement can be divided into three main types: conventional or electrolytic corrosion (rust, small pits, etc), stress corrosion, and hydrogen embrittlement corrosion. Conventional corrosion is by far the most widespread form.[2.2]

2.3.4.1 Corrosion Fundamentals

From Schokker[2.6], before considering the corrosion of prestressing steel in concrete, a general corrosion theory for metals must be understood. Corrosion of iron is an electrochemical process governed by Equations 2-1 and 2-2, commonly known as half-cell reactions:

$$\mathbf{Fe \rightarrow Fe^{2+} + 2e^-} \qquad \text{(anodic half-cell reaction)} \qquad (2\text{-}1)$$

$$\mathbf{2H_2O + O_2 + 4e^- \rightarrow 4OH^-} \quad \text{(cathodic half-cell reaction)} \qquad (2\text{-}2)$$
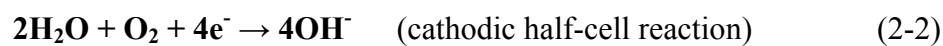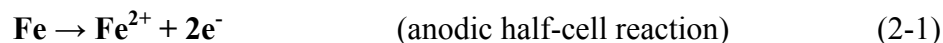
The anode (where electrochemical oxidation takes place) and the cathode (where reduction takes place) form on the metal surface. Iron is oxidized into ferrous ions at the anode as shown in Equation 2-1. The ferrous ions are converted to $2Fe(OH)_3$ (commonly known as rust) through a number of reactions. A summary of rust formation is shown in Equations 2-3 and 2-4. [2.28 as referenced in 2.6]

$$\mathbf{2Fe + 2H_2O + O_2 \rightarrow 2Fe^{2+} + 4OH^- \rightarrow 2Fe(OH)_2} \qquad (2\text{-}3)$$
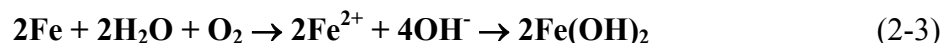
which can further react to give:

$$\mathbf{2Fe(OH)_2 + H_2O + \tfrac{1}{2}\,O_2 \rightarrow 2Fe(OH)_3} \qquad \text{(Rust)} \qquad (2\text{-}4)$$

The anodic and cathodic areas are regions of different electrochemical potential that develop due to two different metals (which therefore have different potentials) or a single metal with surface differences (metallurgical or local variations in electrolyte).[2.29 as referenced in 2.6] The anode and cathode locations can

change often and have an irregular pattern leading to a somewhat uniform corrosion or the locations can be more fixed and localized.

2.3.4.1.1 Passivity

Steel is an active-passive metal, and therefore its corrosion rate depends on potential as shown in Figure 2.12. Under typical conditions, steel in concrete is in a passive state and a passive protective film is found on the steel surface. Chlorides (and lowered pH) in the surrounding concrete have been shown to cause a breakdown of the passive film at potentials that should be well within the passive region[2.30 as referenced in 2.6.]
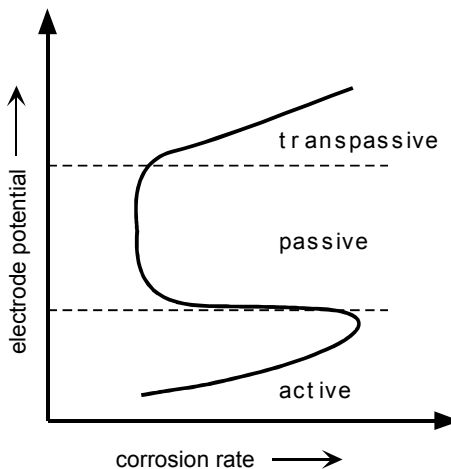
Figure 2.12 Passive-Active Behavior in Steel [2.6]

2.3.4.1.2 Corrosion of Steel in Concrete

In the case of corrosion of steel in concrete, the anodes and cathodes are formed on the steel surface with the cement paste pore solution acting as an electrolyte. Figure 2.13 shows the basic corrosion process for steel in concrete.

The rust product occupies a much larger volume than the products that go into its formation which can cause splitting tensile stresses in the concrete.[2.6]
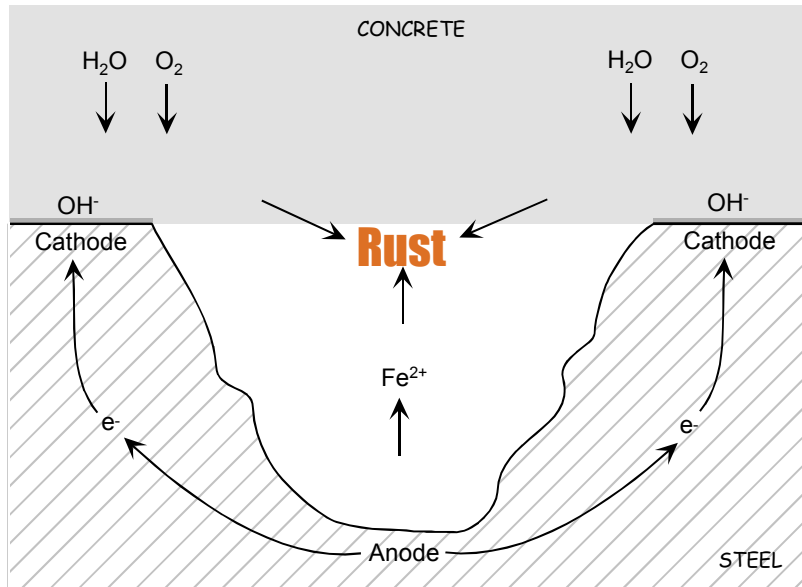
Figure 2.13 Corrosion of Steel in Concrete[2.6]

2.3.4.1.3 Half-Cell Potential Measurements

Electrical potential measurements are useful to monitor the corrosion of the steel embedded in the concrete. Electrical half-cell potential measurements are often used for this purpose. Because it is impossible to measure the absolute value of a half-cell potential, measurements must be made of two half-cell potentials with one used as a reference potential value. For convenience, the hydrogen half-cell reaction at standard state is arbitrarily defined as having a potential value of +0. Potentials may be reported in terms of the primary reference electrode, known as the Standard Hydrogen Electrode (SHE) or directly in terms of the secondary reference electrode used during half-cell potential

measurements. For half-cell potentials measured in concrete specimens, common secondary reference electrodes include the Copper-Copper Sulfate Electrode (CSE) and the Saturated Calomel Electrode (SCE). Table 2.4 gives the potential versus SHE for these reference electrodes.[2.28 as referenced in 2.6] Half-cell potentials throughout this document will be reported as millivolts versus SCE. In order to change these values to compare with results from the other common reference electrode, CSE, simply add +77 millivolts to the values.[2.6]

Table 2.4: Common Reference Electrode Potentials versus SHE

	Half-Cell Reaction	*Potential (V vs. SHE)*
Copper-Copper Sulfate (CSE)	$CuSO_4 + 2e^- = Cu + SO_4^{2-}$	+0.318
Saturated Calomel Electrode (SCE)	$Hg_2Cl_2 + 2e^- = 2Hg + 2Cl^-$	+0.241
Standard Hydrogen Electrode (SHE)	$2H + 2e^- = H_2$	+0.000

2.3.4.2 Chloride Induced Corosion

"Chloride attack has been found to be the severest factor in Japan and many prestressed concrete bridges have been found deteriorated due to this factor. Thus, it is supposed that chloride attack will be the most important factor in future durability of prestressed concrete bridges in Japan." [2.16]

"…The literature investigation revealed that almost all deterioration cases were caused by chloride induced corrosion." [2.22]

Chloride induced corrosion is the most common form of corrosion in reinforced concrete. This type of corrosion can be relatively quick and can localize to cause significant reductions in cross-sectional area. The rust product causes cracking and spalling as well as unsightly staining at the concrete surface.

48

The role of chlorides in depassivation has been much debated. The general consensus is that once the level of chlorides in the concrete at the steel exceeds a certain limit, the passive film either breaks down or is no longer able to protect the steel from corrosion. In general terms, the role of chlorides in depassivation may take one or a combination of the following forms:[2.12]

- chloride ions may disperse the passive film.
- chloride ions may make the film permeable to Fe2+ ions allowing the anodic reaction to occur even when the passive film is present.
- chloride ions may penetrate the passive film and anodic reactions with Cl- acting as a catalyst may occur.
- chloride ions may reduce the pH, making the passive film unstable.

Chloride thresholds for corrosion are controversial because corrosion is dependent on so many variables:[2.29 as referenced in 2.6]

- proportioning of concrete
- type and specific area of cement
- water-cement ratio
- sulfate content
- curing conditions, age, environment
- carbonation
- temperature and relative humidity
- condition of reinforcement

Chlorides may be present in the concrete from any of the concrete constituents. They may also penetrate the concrete from external sources, mostly commonly de-icing chemicals, which combine with the melted snow or ice and often run down the surface of the superstructure and substructure elements; and, seawater, from immersion or salt-water spray. [2.12, 2.6]

49

Three different analytical values have been used to designate the chloride content of fresh concrete, hardened concrete, or any of the concrete mixture ingredients: (a) total, (b) acid-soluble, and (c) water-soluble.[2.20] Work at Federal Highway Administration Laboratories and after field bridge deck studies in California and New York, demonstrated that for hardened concrete subject to externally applied chlorides, the corrosion threshold was 0.2 percent acid-soluble chlorides per weight of cement [2.20] (around 0.6 to 0.9 kg of Cl-/m^3 or 1.5 lb/yd^3). A detailed discussion on chloride threshold values is included in reference 2.12, pages 39-41.

To define the service life of a structure, based on chloride exposure, two concepts need to be defined. The initiation period (time to the onset of corrosion), and the propagation period.

The initiation period t_i defines the time it takes for chlorides to penetrate the concrete cover and accumulate at the location of the embedded steel in a sufficient quantity to break down the protective passive layer on the steel, initiating an active state of corrosion. The length of this period is a function of the concrete quality, depth of cover, exposure conditions (including the level of chloride at the surface and the temperature of the environment), and the threshold chloride concentration required to initiate corrosion. A simple approach used to predict the initiation period is to assume that ionic diffusion is the mechanism of chloride transport and to solve Fick's second law of diffusion. [2.31]

The propagation period t_p defines the time necessary for sufficient corrosion to occur to cause an unacceptable level of damage to the concrete structure or element under consideration. The length of this period depends not only on the rate of the corrosion process, but also on the definition of "unacceptable damage." This level of damage will vary depending on the requirements of the owner and the nature of the structure. [2.31]

2.3.4.2.1 Uniform Corrosion

Uniform corrosion is generalized corrosion over a large area. This type of corrosion may have a large amount of metal loss and cause cracking and staining over large areas. Since the damage is not localized, catastrophic failure is least likely for this type of corrosion than for the other types of corrosion found in prestressed concrete structures. [2.6]

2.3.4.2.2 Pitting Corrosion

Pitting corrosion is very common in reinforced concrete structures and can be quite destructive due to the concentrated pits of corrosion causing large reductions in cross-sectional area with a small amount of overall metal loss. The pitting process is a self-propagating process.[2.30] As the pits grow, the surface can be undercut resulting in a deceivingly large pit and making detection difficult even on bare steel. A schematic of the process for iron is shown in Figure 2.14. [2.6]

Figure 2.14 The Self-Propagating Process of Pitting Corrosion[2.6]

2.3.4.3 Hydrogen Embrittlement and Stress Corrosion Cracking

"...there are countries who do not permit the use of galvanized duct because of the fear that galvanizing could cause hydrogen embrittlement of the prestressing steel. Even though widely used there is no evidence known to the author [Ganz] where the use of galvanized duct would have caused damage to tendons made of cold drawn wire and 7-wire strand." [2.32]

"....its prestressing [of the Saint-Cloud Viaduct] is completely internal to the concrete. ....it was strengthened in 1979 by an additional external prestressing which is deviated in a vertical plane...In 1998, one of the additional tendons which were in the Northern side cell and which had a 300 m length broke in its middle...the prestressing wires were sensitive to the stress corrosion, and the majority of wires presented this type of cracking." [2.2]

As described by Schokker, [2.6] the combination of tensile stress and a corrosive environment can cause susceptibility in steel to certain types of environmentally induced cracking. The types of environmentally induced cracking most often associated with prestressing steel are stress-corrosion cracking and hydrogen embrittlement. Both types of corrosion may lead to brittle failures with minimal metal loss in the affected area. The most dangerous aspect of hydrogen embrittlement and stress-corrosion cracking failures is the potential for structural collapse without warning.

Jones[2.28 as referenced in 2.6] defines stress corrosion cracking (SCC) as brittle failure of an alloy in a corrosive environment at relatively low tensile stress. Hydrogen embrittlement (HE) is defined as brittle fracture caused by the absorption of atomic hydrogen into a metal alloy.

Schupack and Suarez[2.33 as referenced in 2.6] performed a survey in 1982 to investigate corrosion incidents in prestressed structures during the previous five years. The study indicated a small number of incidents with only 1/5 of these

reported as possible SCC / HE brittle failures. Most of these incidents were found in unbonded post-tensioned construction. The failures reported were within an isolated area in the structure and were not catastrophic collapses.

Stress corrosion cracking and hydrogen embrittlement both cause brittle fractures in a corrosive environment under tensile stress, but one difference is their behavior in the presence of cathodic protection. Cathodic protection can suppress stress corrosion cracking, but tends to enhance hydrogen embrittlement.[2.34, 2.28 as referenced in 2.6] For this reason, cathodic protection can be problematic for prestressed structures.

The effect of galvanizing on hydrogen embrittlement of prestressing wire is a topic of concern. The zinc coating on the galvanized wire reacts with the alkaline Portland cement in fresh concrete or grout and evolves hydrogen:[2.35 as referenced in 2.6]

$$Ca(OH)_2 + Zn + 2H_2O = Ca(Zn(OH)_4) + H_2 \qquad (2\text{-}5)$$
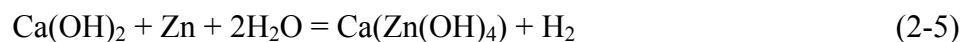
A study by Yamaoka, Hideyoshi and Kurachi[2.35 as referenced in 2.6] found indications that galvanization of prestressing steel helps protect the steel from hydrogen embrittlement.

2.3.4.4 *Steel Geometry and Crevice Corrosion*

As stated by Schokker,[2.6] the cross-section of prestressing strand makes it more susceptible to corrosion than traditional steel reinforcement. The strand is made up of a twisted bundle of seven individual wires, which give it a higher ratio of surface area to total cross-sectional area than we would find for a solid bar with the same diameter as the strand. The contact between the wires can also cause corrosion at the interfaces (crevice corrosion).

The geometric constraints of the crevice enhance the formation of chloride ion concentration cells. Once corrosion has initiated, it progresses similar to

pitting corrosion. Due to the geometry of the crevice, Fe2+ ions can not disperse easily, and chloride ions are drawn into the crevice by the positive charge accumulation.   The process becomes autocatalytic as the presence of chloride ions leads to formation of hydrochloric acid (HCl) and higher corrosion rates develop. [2.12]

2.3.5 Anchorage Sealing

Anchorage corrosion may lead to cracking and spalling of the concrete in the vicinity and even failure of the anchorage. Corrosion of the anchorage and strand stubs may also allow moisture entry into the duct and subsequent tendon corrosion.   Not all multistrand post-tensioning systems include an end cap. Anchorages are commonly recessed in a pocket at the end or edge of the concrete element. Corrosion protection for the anchorage normally consists of filling the anchorage recess or pocket with mortar or concrete.   The location of the anchorage within the structure can also play a role in the onset of corrosion and corrosion development. In many structures, the anchorages are located at the ends of structural elements below expansion joints, or at exterior member ends or slab edges. These locations are prone to concentrated exposure with moisture and chlorides, and often lead to severe anchorage corrosion damage. [2.12]

2.3.6 Precast Segmental Construction – Joint Performance

Dry joints or poorly sealed segmental joints have been shown to be extremely detrimental to the durability of post-tensioned structures, either with internal[2.36,2.37] or external post-tensioning.[2.10]   Experiences in the United Kingdom[2.36,2.37] led to the ban in 1992 on the use of internal bonded post-tensioned structures with discontinuous (poorly sealed) ducts.

2.4 CORROSION PROTECTION OF BONDED POST-TENSIONED CONCRETE STRUCTURES

"...The objective of the corrosion protection must be to achieve a design life of the tendons which is comparable to that of the structure in which they are placed." [2.38]

"Without exceptions, and regardless of cost, improvements in grouting practice and improvements in the quality of global tendon corrosion protection details, must be implemented to provide full assurance of the long-term durability (100+ years) of post-tensioning tendons." [2.19]

Corrosion protection of bonded post-tensioned concrete structures can be achieved by the careful design of the multilayer protection system. As shown in Figure 2.15, protection measures include surface treatments on the concrete, the concrete itself, the duct, the grout and strand or bar coatings such as epoxy or galvanizing. Post-tensioning also provides the opportunity to electrically isolate the prestressing system from the rest of the structure.
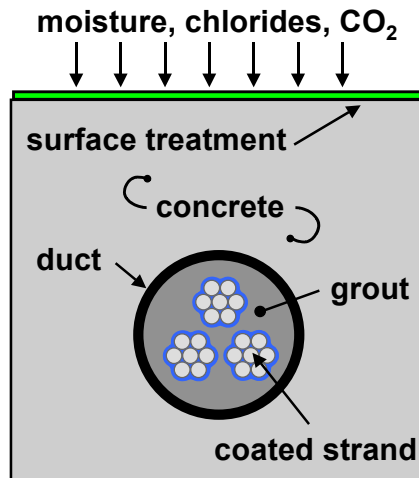
Figure 2.15 Multilayer Corrosion Protection For Bonded Post-Tensioned Systems[2.12]

As described by Matt[2.39] weak links could exist in every layer. In the first layer, water can penetrate through defective or inadequate design of non-structural elements such as waterproofing membranes, drainage systems, etc. and reach the concrete structure. In a second layer, water can be transported through the concrete cover by diffusion and capillary absorption. The rate is determined by the quality of the concrete (thickness, permeability, cracks, honey-combing, etc.) The third barrier/layer consists of the corrosion protection system of the post-tensioning tendons themselves. It can be impaired by open grouting vents, leaking ducts, cracked and porous pocket concrete as well as grout voids, etc. In the fourth layer the longitudinal water transport in an inclined tendon has to be considered in case the grouting may not be perfect. In the fifth layer, the prestressing steel can also corrode at locations remote from the point of ingress. Figure 2.16 shows the possible hazard scenarios in a typical box girder segment.

To ensure better corrosion protection of prestressing steel, Schupack[2.40] indicates that the following should be considered, particularly if the environment of use is aggressive or control of construction is doubtful:

- Designs should minimize concrete cracking, particularly in aggressive environments;
- High-quality, low – permeability concrete;
- Construction techniques should ensure specified concrete cover to all reinforcement;
- Tough plastic sheaths for post-tensioning;
- Improved grouting methods and materials (that is, nonbleeding grout);
- Use of electrically isolated tendons;
- New tough polymer coatings for strands and bars;
- Stainless steel-clad wires and bars;
- Stainless steel (now more than 10 times as expensive as A 416 strands);

- Low-carbon alloy bars with good stress-corrosion-cracking resistance;

- A more inherently corrosion-resistant steel; and,

- High-strength bars with subtle90

- deformations that can replace strand.
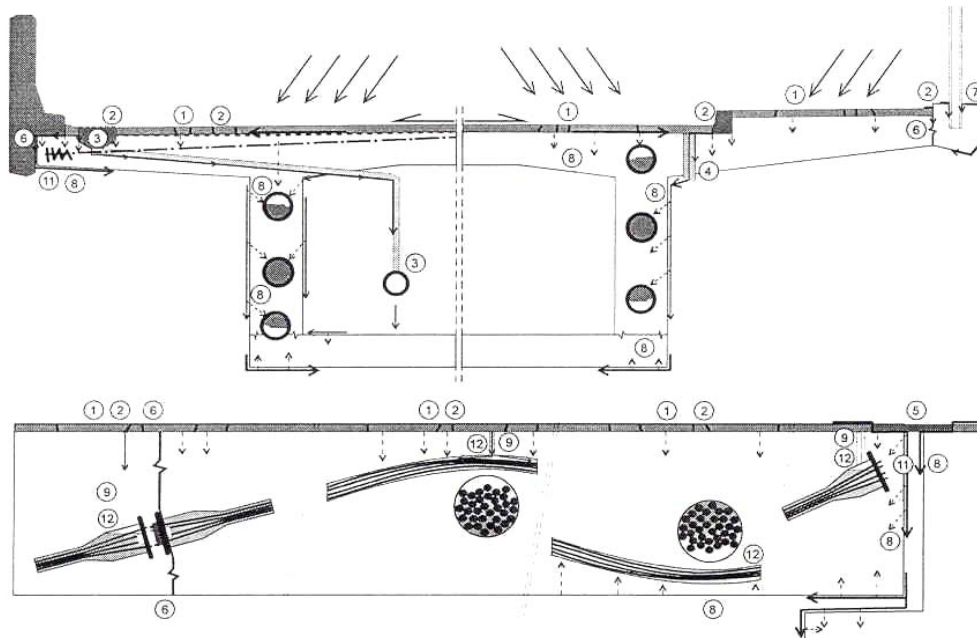
Hazard scenarios for prestressing steel in a typical box girder bridge: Indication of potentially "weak points" where water (possibly contaminated with chlorides) can gain access to the tendons and cause corrosion

Non-structural elements:
1. Defective wearing course (e.g. cracks)
2. Missing or defective waterproofing membrane incl. edge areas
3. Defective drainage intakes and pipes
4. Wrongly placed outlets for the drainage of wearing course and waterproofing
5. Leaking expansion joints
6. Cracked and leaking construction or element joints
7. Inserts (e.g. for electricity)

Corrosion protection system:
8. Defective concrete cover
9. Partly or fully open grouting in- and outlets (vents)
10. Leaking, damaged metallic ducts mechanically or by corrosion
11. Cracked and porous pocket concrete
12. Grout voids at tendon high points

Figure 2.16 Hazard Scenarios[2.39]

2.4.1 Structural Form

A detailed description of corrosion protection variables is included in West[2.12]. A summary of the most important aspects are included here as a reference.

2.4.1.1 Drainage

Since the most common cause of reinforcement corrosion is moisture-borne chlorides, whether as seawater or de-icing chemicals, adequate drainage is a critical factor in the selection of structural form. Adequate superstructure drainage must be provided, and must ensure chloride –laden water does not come in contact with the substructure. [2.12] Use of impermeable deck sealants or membranes should be considered.

2.4.1.2 Joints

A common source of substructure corrosion problems is moisture and chlorides dripping onto substructure components through leaking deck joints. Proper joint design and maintenance is required when severe conditions are encountered. [2.12]

2.4.1.3 Splashing

Substructure components adjacent to roadways where de-icing chemicals are used can be prone to corrosion damage due to splashing. Increasing the distance between the roadway and substructure may increase initial construction costs, but may reduce long term costs by avoiding this type of corrosion damage.[2.12]

2.4.1.4 Geometry

Other aspects of the structural geometry can influence durability. Decreasing the exposed surface by an efficient design and increasing concrete cover to safe limits can decrease the corrosion potential.

2.4.2 Structural Design Details

2.4.2.1 Cracking

Concrete cracking provides easy access for moisture and chlorides to reach the reinforcement. Although the significance of cracking on corrosion is often debated, cracking should be avoided or minimized where possible. [2.12]

2.4.2.2 Reinforcement Detailing

Reinforcement detailing not only affects cracking in the structure, it also can influence construction. Congested reinforcement details make concrete placement difficult and can lead to poor compaction and voids. [2.12]

2.4.3 Surface Treatments

Concrete surface treatments work to improve corrosion protection by preventing moisture and chlorides from entering the concrete. Surface treatments include waterproof membranes and surface polymer impregnation. In the latter, the exposed surface of the concrete is impregnated with polymer that fills the voids and cracks in the concrete, providing a barrier with very low permeability. Various overlays may be used to provide a low permeability barrier over existing concrete. Options include polymer concrete overlays, latex-modified concrete overlays and overlays with low permeability Portland cement concrete.[2.12]

2.4.4   Concrete as Corrosion Protection

Concrete acts as a physical barrier to moisture and chlorides, and provides the alkaline environment necessary for formation of the passive film on the surface of steel. [2.12]

2.4.4.1   Concrete Permeability

The permeability of concrete controls the rate at which moisture, oxygen and carbon dioxide penetrates the concrete. Because the penetration of moisture provides the transport mechanism for chlorides and other aggressive substances, lowering the concrete permeability increases the length of time before aggressive agents reach the steel, and thus improves corrosion protection. The permeability of concrete is affected by four general factors:[2.41 and 2.42 as referenced in 2.12] pore structure of the cement paste, aggregate, voids in the concrete, and, cracking of the concrete.

A detailed description of each factor is included in Reference 2.12.   The discussion includes the used and effects of low water/cementitios material ratio and the use of supplementary cementitious materials.

High Performance Concrete (HCP) as used in the text, refers to low permeability concrete with improved strength f'c=10000 psi, w/c = 0.29, 25% replacement by fly ash, and superplasticizer to reach a slump of 8 inches.

2.4.4.2   Cover Thickness

The thickness of concrete cover over the reinforcement plays a significant role in corrosion protection. Increased clear cover provides improved protection for the steel, particularly if low permeability concrete is used. The penetration of chlorides over time can be approximated by a square-root time law.[2.43 as referenced in 2.12] This means if the concrete cover thickness is doubled, it will take

approximately four times as long for chlorides to penetrate to the depth of the reinforcement.[2.12]

2.4.4.3   Corrosion Inhibitors

Many types of corrosion inhibitors are on the market today. They are intended to slow the corrosion process of steel in concrete without adversely affecting other properties and are typically included as an admixture in the fresh concrete. Corrosion inhibitors can be divided into three basic types by the method in which they slow the corrosion process:[244 and 245 as referenced in 2.6]

Anodic Inhibitors (Passive System)

Anodic inhibitors react with the steel to form a protective film, and proper dosage depends on the amount of chlorides penetrating the concrete.   If the amount of chlorides is too high for the dosage of corrosion inhibitor, then all of the anodic sites are not eliminated and corrosion continues at a rate greater or equal to that of untreated concrete.   The popular corrosion inhibitor, Calcium Nitrite, is an anodic inhibitor.

Cathodic Inhibitors (Active System)

Cathodic inhibitors form a barrier around the cathodic site to reduce chloride ingress. These inhibitors tend to be less efficient than anodic inhibitors. Silica fume is an example of a cathodic inhibitor.

Mixed Inhibitors (Passive-Active System)

Mixed inhibitors combine the inhibiting traits of both the anodic and cathodic type inhibitors.

2.4.5   High Performance Grouts

As West[2.12] has stated, the selection of suitable grout proportions and admixtures requires careful consideration of the grout fresh properties and

corrosion protection. The effects of various admixtures and grout proportions on fresh properties and corrosion protection have been studied by several researchers. [2.27,2.46] Schokker[2.6] performed an extensive research study to develop two optimized grouts for post-tensioned. The study was part of the research project related to this dissertation.

Additional information on mix proportioning and guide specifications for grouts for post-tensioning is provided by the PTI "Guide Specification for Grouting of Post-Tensioned Structures," [2.47] the fib report "Grouting of Tendons in Prestressed Concrete," [2.48] and the VSL report "Grouting of Post-Tensioning Tendons,"[2.49]

As a response for the need of better grout mixes, new prepacked grouts are available with thixotropic properties. One of these grouts is in the form of a plastic gel when at rest, and is instantly fluidized when it is shaken. This grout uses a w/c = 0.35, and two liquid additives: a stabilizer that retards hydration of the cement and fluidizes it, and also reduces shrinkage; and, a set activator that also acts as a thixotropic agent.[2.50]

In an effort to provide a more consistent grout material, the Florida Department of Transportation is requiring that pre-bagged resistant grouts be used. The ASBI and PTI have recommended anti-bleed or low bleed grouts meeting a series of performance requirements. These grouts reduce the size and number of voids due to bleed water, but anchorages should still be probed or visually inspected when the grout has set.[2.26]

2.4.6 Ducts for Post-Tensioning

Typically galvanized corrugated metal ducts have been used in Post-Tensioning applications. However, as a consequence of the corrosion concern, specific corrugated plastic duct systems for bonded post-tensioning have been

62

introduced on the market, since the 1990's. [2.38] To date, it is not considered necessary that plastic ducting is always required to provide an extra barrier. [2.53]

Plastic duct systems, when combined with suitable accessories such as connection details and anchorage caps, provide a complete encapsulation of the post-tensioning tendon. Considering that not all plastic ducts are suitable for post-tensioning applications, *fib* has taken the initiative some years ago, and has prepared a technical report for the testing and approval of plastic duct systems for use in post-tensioning.[2.51]

To avoid excessive wobble of the tendons, excessive friction losses during stressing, and leakage of grout during injection, more "robust" ducts of durable polyethylene are being introduced. [2.51,2.32]

Some of these plastic duct systems have now been used with excellent experience. Plastic duct systems had been specified exclusively in the UK since 1996, and are now being specified also in Florida, and in Switzerland for the general application in aggressive environment. Experience has shown that plastic ducts made of polypropylene (PP) perform better in warm climates than those made of polyethylene. It has also been found that the plastic ducts need to be protected from large local transverse loads at supports near the tendon profile high points by the provision of sufficiently rigid half shells. [2.38]

Changes in the material requirements for the High-Density Polyethylene (HDPE) duct systems have been suggested for all external post-tensioning systems. Robust plastic ducts have been recommended for internal tendons meeting the requirements of the fib Technical Report[2.51] as referenced in the PTI Guide Specification for Grouting of Post-Tensioned Structures[2.47]. [2.26]

2.4.7 Coatings on Prestressing Steel

2.4.7.1 Metallically coated prestressing steels

As indicated by Ganz [2.38] zinc coated prestressing steel is rarely used for post-tensioning. Zinc provides a sacrificial protection of the prestressing steel. The durability of the protection by zinc depends primarily on the consumption rate of zinc in the actual environment, and the available thickness of the zinc layer. Zinc coating is relatively insensitive to local damage and the prestressing steel remains protected even if the zinc coating is locally damaged. Galvanized prestressing steels have been standardized in the French standard NF A35035. It is understood that a European standard and a ISO standard are being prepared on galvanized prestressing steels.

2.4.7.2 Non Metallic Coatings for Prestressing Steels

From Ganz, [2.38] the most commonly used non-metallic coating is epoxy resin. Experience has shown that epoxy coated strand needs to have the interstices between wires completely filled with epoxy to avoid migration of water / humidity along the strand. [2.38] Further issues in ongoing discussions are on the effect of local defects in the coating in an aggressive environment such as under chloride attack. It has been reported that local defects may lead to accelerated pitting corrosion at these locations. The thickness of coating needs to be carefully controlled for reliable anchorage by wedges. [2.32]

Other non-metallic coatings have been developed including resins with delayed curing (After-Bond), tar epoxy resins, and others. However, experience is still limited for applications in pretensioning and post-tensioning. [2.38]

While there is no dispute that epoxy coating will extend the time to corrosion damage, compared with uncoated steel, the long-term performance remains somewhat uncertain. Not all the factors affecting corrosion performance

64

are understood, and there are many examples of good performance, as well as examples of premature corrosion damage. The dominant factors affecting performance are the number and size of defects in the coating and the long-term adhesion of the coating to the steel.[2.54]

2.4.8   Prestressing Steel – Other Prestressing Materials

Fiber-reinforcement polymer (FRP), stainless steel, stainless-clad steel, and MMFX steel bars comprise the new generation of concrete reinforcing materials being used for durable construction. [2.55]

With respect to FRP reinforcement, Clemena states that: "…Until we learn more …, I would consider the corrosion –resistant metallic reinforcing bar the superior reinforcing material, for at least the next decade." [2.56]

Ganz [2.38] states that: "…It has been proposed to replace prestressing steels with non-corrosive fiber reinforced plastic materials. It is the author's [Ganz] opinion that these materials still have to go through a long development until they can provide performance and reliability for post-tensioning applications comparable with well protected prestressing steel.

Gaubinger[2.57] states that: "…a common use [of CFRP tendons] is presently prevented by two main facts: high costs of manufacturing and the development of a suitable anchorage.

2.4.9   Anchorage Protection

As described by West[2.12], "the post-tensioning anchorages and end stubs of the strands must be carefully protected. Although anchorage corrosion may lead to failure of the anchorage, bond between the tendon and concrete will prevent a complete loss of prestress   Multistrand anchorage systems may be fitted with a sealed end cap to protect strand ends. The cap is grouted or filled with corrosion inhibiting grease. Not all multistrand post-tensioning systems include

an end cap. Anchorages are commonly recessed in a pocket at the end or edge of the concrete element. Corrosion protection for the anchorage normally consists of filling the anchorage recess or pocket with mortar or concrete. Common practice is to coat the anchorage and pocket surfaces with an epoxy bonding agent prior to filling the anchorage pocket with a non-shrink mortar.

The location of the anchorage within the structure can also play a role in corrosion protection and corrosion damage. In many structures, the anchorages are located at the ends of structural elements below expansion joints, or at exterior member ends or slab edges. The location of post-tensioning anchorages is often dictated by the method of construction. In instances where the anchorage can not be located away from a possible source of aggressive agents, the anchorage must be detailed to provide multiple layers of corrosion protection. The Concrete Society (U.K.) Technical Report No. 47 on bonded post-tensioned bridges[2.37 as referenced in 2.12] provides suggestions for anchorage protection details. The report discusses two approaches for anchorage protection. The first is to provide an anchorage that is not encased in mortar or concrete after stressing. Exposed anchorage hardware is protected by end caps and waterproof membrane, and has the advantage that the anchorage can be readily inspected for corrosion damage. The second approach provides a higher level of corrosion protection at the expense of inspectability by recessing the anchorage in a filled pocket. Details of multilevel corrosion protection for this form of buried anchorage are shown in Figure 2.17. The details of the member end can also be designed to minimize contact with moisture and chlorides draining through expansion joints, as shown in Figure 2.18. The member end is detailed to prevent water from dripping onto the anchorage region. An abutment gallery is provided to allow inspectors to gain access to the anchorage."

66
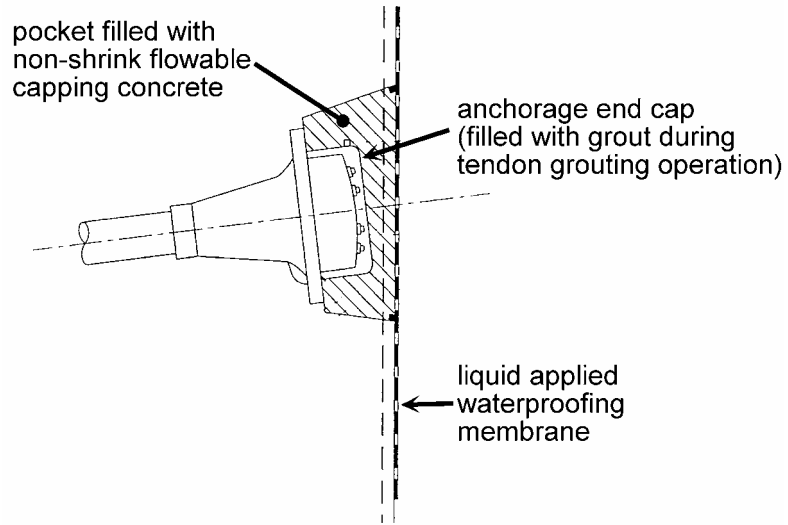
Figure 2.17 -Multi-Layer Corrosion Protection for Buried Post-Tensioning Anchorages [2.37 as referenced in 2.12]
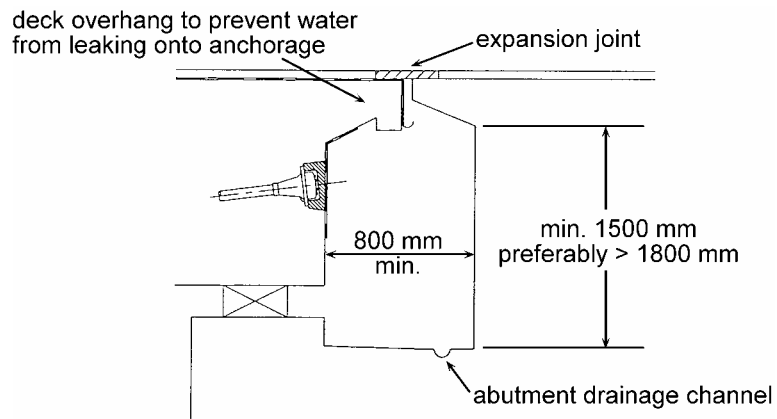
Figure 2.18 - Member End Details for Anchorage Corrosion Protection[2.37 as referenced in 2.12]

2.4.10 Encapsulated and Electrically Isolated Systems

In a Electrically Isolated Tendon (EIT), the prestressing steel is entirely isolated not only by a robust plastic duct, but also at the anchorages. In this way, the EIT system is used to protect tendons from the effects of stray currents which could cause hydrogen embrittlement and pitting corrosion to the prestressing steel. [2.38, 2.58]

Up to now, about 100 bridges have successfully been constructed using robust plastic ducts of which in over 20 bridges electrically isolated tendons have been installed. [2.58]

2.4.11 Precast Segmental Construction – Joint Detail

As stated by Moreton[2.52] "The U.K. "moratorium" is still in effect for "internal, grouted tendons with discontinuous (poorly sealed) ducts. This is broadly interpreted (or misinterpreted) to mean that only external tendons are allowed for precast segmental construction in the United Kingdom. This is not so. The concern of the Highways Agency is for the integrity of the ducts through the precast joints – that they should be completely sealed – and they require this via a performance specification."

Most countries consider epoxy resin to provide sufficient protection to post-tensioning tendons crossing joints between precast segments. However, the UK has specified full encapsulation for the tendons by plastic in these joints.[2.32]

In response to this problem, a new commercial coupler device is now available to connect plastic prestressing ducts used with match-cast joints in precast segmental construction[.250] The new coupler is suppose to yield good results in precast segmental construction. However, testing is still required. To this respect, Raiss[2.59] has stated that: " Pending further experience with this system, it may be prudent to assume that some percentage of the internal tendons

is lost (say 5-10%)." However, this could be still unconservative until new research is done.

2.4.12 Temporary Corrosion Protection

Without further protection measures, grouting should be done within one to about 4 weeks in aggressive and benign climatic conditions, respectively. If grouting needs to be delayed beyond the above proposed intervals, particular methods need to be provided for post-tensioning tendons. [2.38]

While the use of Rust-Ban 310 is still under investigation (by EMPA – Swiss Federal Laboratory for Materials and Testing and ASTRA – Swiss Federal Highways Administration) it seems that it provides good temporary protection. The solution is applied at the factory of the strand supplier and sufficient time needs to be permitted to let the solution dry on the tendon.[2.60]

In case unprotected tendons were installed and grouting cannot be achieved within the accepted time frame, the tendons can be protected by blowing dry air through the duct. [2.60]

2.4.13 Inspection Practices

The American Segmental Bridge Institute (ASBI) has developed a three-day training program for the Certification of grouting technicians. This program has been developed to train the Inspectors in theory and field procedures to achieve a properly grouted structures. [2.19] The training manual contain updated and detail information on grouting materials, procedures and specifications.

2.4.14 Monitoring

Various techniques are being used to monitor the condition of existing post-tensioned bridges. However, they are not totally satisfactory, all of them having some limitations.[2.15]

Some non-destructive testing (NDT) and methods that could be used include:[2.15]

- georadar
- potential mapping
- impact-echo
- remanent magnetism
- radiography
- reflectometry
- ultrasonic
- acoustic

In addition, the use of electrically isolated tendons have proved successful.[2.15]

CHAPTER 3

Macrocell Corrosion Tests

Post-tensioned segmental bridge design and construction has recently received much attention, due to a few reported tendon failures and the collapse of a few small bridges (see Section 2.2). Still, it has been shown that the durability performance of segmental post-tensioned bridges has been superior to all other types of construction. [3.1]

Recognizing that post-tensioned segmental construction has many advantages with respect to other bridge systems, it is clear that more research is needed to identify weak links, and counteract their negative effects. Structures should safely achieve their design service life and allow for safe monitoring and inspecting.

One of the most important aspects to be studied refers to segment joint sealing and waterproofing. Current guide specifications[3.2] require the use of match-cast epoxy joints whenever internal tendons are used. Epoxy joints were introduced to enhance force transfer across the segmental joint and to seal the joint against moisture ingress. Epoxy joints have been recognized as an absolute requirement for durability when internal tendons are used.

Plastic ducts have also been recognized as the preferred material for post-tensioning, when structures are exposed to very severe environment, as was described in Section 2.3.

As outlined in Chapter 1, an experimental research study using Macrocell Corrosion Tests was initiated in 1993 at the Ferguson Structural Engineering Laboratory. The main purpose of the study was to investigate the corrosion protection of internal tendons at segmental joints. As part of the program, half of

71

the laboratory specimens were autopsied in 1999, and were reported by West.[3.3] This chapter documents the final results, after the second half of the specimens were autopsied by the author after eight years of very aggressive exposure.

3.1 EXPERIMENTAL PROGRAM

The test method used in this series was originally developed and implemented by Rene Vignos[3.4] and later reported by West[3.3]. It is repeated with minor changes herein. The basic objectives for development of the testing program were as follows:

- The test method should provide meaningful comparisons in a reasonable amount of time.
- The test method should accommodate the desired variables in a realistic manner.
- The test method should allow measurement of both macrocell and microcell corrosion.
- The test method should be as standardized as possible to allow comparisons with past and future testing, and provide reproducible results.

Vignos patterned the test method after ASTM G109 - "Standard Test Method for Determining the Effects of Chemical Admixtures on the Corrosion of Embedded Steel Reinforcement in Concrete Exposed to Chloride Environments."[3.5] The standard macrocell corrosion specimens were modified to examine prestressing tendons in grouted ducts and simulate segmental joints. A full description of the development of the testing program and details of the experiment setup are provided in Reference 3.4. A summary of the general characteristics of the test specimens, variables and measurements is included in the following sections. Exposure testing was initiated by Vignos in August 1993.

3.1.1 Test Specimen

The specimens used in this program are patterned after the standard ASTM G109[3.5] macrocell specimen developed to evaluate the effect of concrete admixtures on the corrosion of mild steel reinforcement. The standard ASTM G109 specimen consisted of a single concrete block with two layers of mild steel reinforcement. During macrocell corrosion, the top layer of steel acts as the anode and the bottom layer acts as the cathode. Several modifications were made to the ASTM G109 specimens to evaluate corrosion protection for internal tendons in segmental bridge construction. These included the introduction of a transverse joint in the concrete block to allow the effect of the segmental joint type to be evaluated, the use of a grouted prestressing strand in the top layer (anode) in place of one of the mild steel reinforcement layers, and the addition of longitudinal compressive stress on the specimen to simulate prestress in the structure. The specimen revised configuration is shown in Figure 3.1.

Each specimen consists of two match-cast segments. Continuity between the segments is provided by a 0.5 inch diameter, seven-wire prestressing strand inside a grouted duct, representing a typical bonded internal tendon in segmental bridge construction. The duct is cast into each of the match-cast segments and is not continuous across the joint. Due to the small specimen size, the strand can not be post-tensioned effectively. To simulate precompression across the joint due to post-tensioning, the pairs of match-cast segments were stressed together using external loading frames.

73
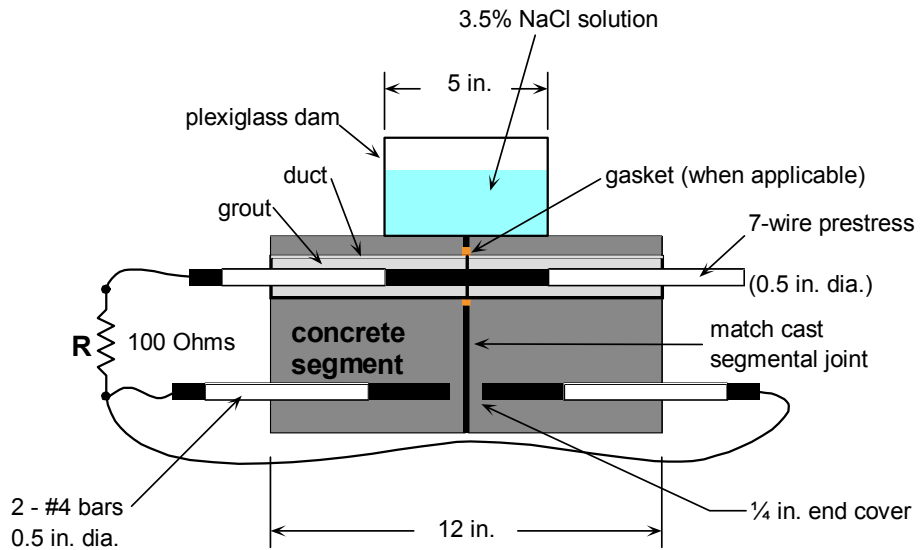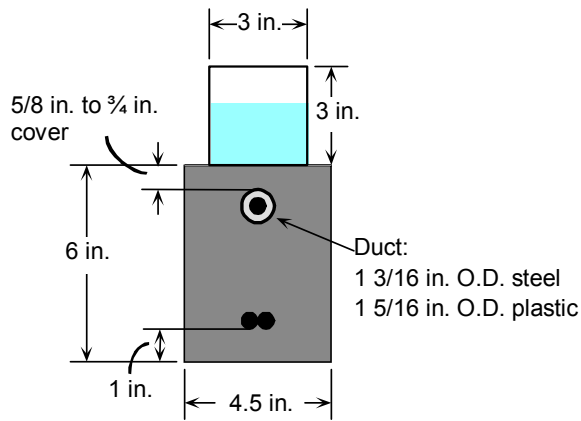
Figure 3.1 Macrocell Specimen Details [3.8]

Similar to ASTM G109, two 0.5 in. (#4) mild steel bars were used as the cathode. These bars would represent non-prestressed reinforcement within the

segment. The use of two bars increases the ratio of cathode area to anode area, accelerating macrocell corrosion. The cathode bars were discontinuous across the transverse joint, consistent with precast segmental construction. The end cover for the cathode bars at the segmental joint was 0.25 in. Following ASTM G109, the exposed length of the anode and cathode were limited to 5 in. by painting the strand and the mild steel bars with epoxy paint as shown in Figure 3.2.

Electrical contact must exist between the anode and cathode for macrocell corrosion to develop. This contact is achieved in the test specimen by wiring the protruding ends of the anode and cathode steel together, as shown in Figure 3.1. Zinc ground clamps are used to connect the wire to the steel. A 100-Ohm resistor is placed in the wire connection between the anode and cathode, as shown in Fig. 3.1, to allow assessment of the corrosion current by measuring the voltage drop across the resistor $(I_{corr} = V_{meas}/R)$.

Strand Detail (Anode)

0.5 in. dia. 7-wire strand

epoxy paint

exposed

1 in. | 5 in. | 5 in. | 6 in.

Bar Detail (Cathode)

0.5 in. (#4) bar

epoxy paint   exposed

1 in. | 5 in. | 2.5 in.
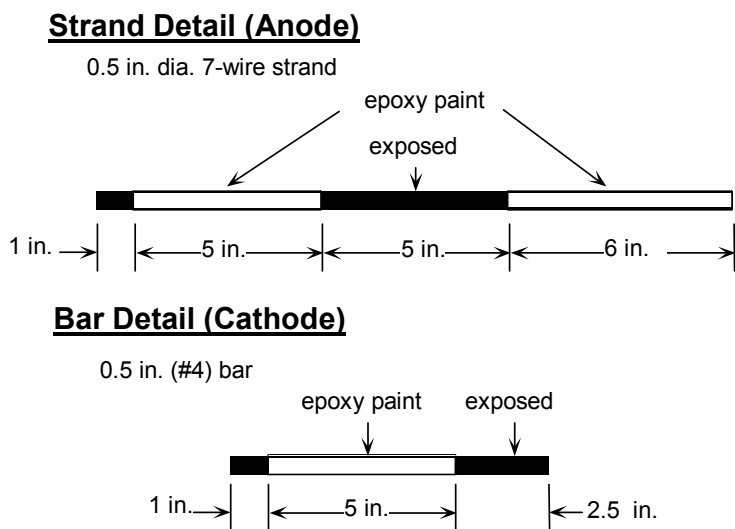
Figure 3.2 Anode and Cathode Bar Details [3.8]

75

Exposure conditions for the specimens consist of a 4-week cycle of 2 weeks dry and 2 weeks wet. During the wet period of the cycle, a portion of the top surface of the specimen is ponded with 3.5% NaCl solution, as shown in Figure 3.1. At the end of the wet period, the NaCl solution is removed from the Plexiglas dam using a wet/dry vacuum.

The specimen was chosen as an extreme aggressive environment to indicate relative effects of variables and is not representative of actual exposure and cover conditions.

3.1.2 Variables

A broad scope of protection variables was selected for investigation in this program. These variables cover four components of precast concrete segmental bridges related to corrosion of internal tendons. Included are; joint type, duct type, joint precompression and grout type.

3.1.2.1 Joint Type

Precast segmental joints are either dry or wet. Wet joints include mortar joints, concrete joints but most frequently epoxy joints. Dry joints and epoxy joints require match casting, and are the most common segmental joints used in North America. When match-cast epoxy joints are used, the entire face of the segment is coated with a thin layer of epoxy immediately before each segment is placed in the bridge. The segments are held in firm contact with temporary post-tensioning while the epoxy cures and the prestressing tendons are placed and stressed. In some situations, a small gasket is used around each duct opening to prevent epoxy from entering the duct when the segment is placed and initially stressed. If a gasket is not used, the duct is swabbed out immediately after initial stressing to prevent epoxy from blocking the duct.

To address typical North American practice, dry joints and epoxy joints, with and without gaskets, were selected for investigation in this testing program. All joint types were match-cast. The AASHTO Guide Specification for Segmental Bridges[3.6] does not permit the use of dry joints with internal tendons. However, dry joints were included as a worst case scenario for comparison purposes. At the time of initiation of the study, influential designers were requesting that they be allowed to use internal tendons with dry joints. It was agreed that the dry joint specimens be included to document actual behavior.

The epoxy-jointed specimens were assembled according to the standard practice. Both match cast faces were coated with epoxy and the segments were pushed together. The joint was precompressed at 50 psi for 48 hours after which the specimens were unloaded and re-loaded to the desired level of precompression (see Section 3.1.2.3). In the epoxy/gasket joint, a foam gasket was glued to the face of one segment around the duct opening prior to application of the epoxy. Details of the foam gasket are shown in Figure 3.3. In the epoxy joint without a gasket, the duct was swabbed out immediately after stressing to prevent the epoxy from blocking the duct.
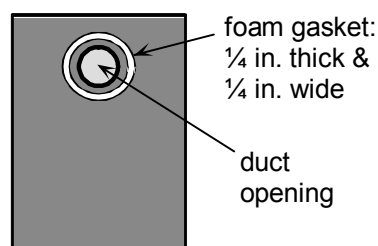
Figure 3.3 Gasket Details [3.8]

3.1.2.2 Duct Type

Two duct types were investigated; standard galvanized steel duct and plastic duct. Due to size limitations, PVC pipe was used for the plastic duct.

3.1.2.3 Joint Precompression

The joint precompression refers to the level of prestress provided by the internal and/or external tendons in the bridge. Three levels of precompression were selected; 5 psi, 50 psi and $3\sqrt{f_c}$ psi. The lowest level of 5 psi could represent the level of precompression encountered in a precast segmental column under self weight. The precompression of 50 psi is based on the *AASHTO Guide Specifications*.[3.6] The highest precompression value of $3\sqrt{f_c}$ psi. corresponds to 190 psi for this testing program.

3.1.2.4 Grout Type

Three cement grout types were selected for evaluation; normal grout (plain cement grout, no admixtures, w/c = 0.40), grout with silica fume (13% cement replacement by weight, w/c = 0.32, superplasticizer added) and grout with a commercial calcium nitrite corrosion inhibitor (w/c = 0.40). Grout mix proportions are provided in Section 3.1.3.

3.1.2.5 Specimen Types

A total of nineteen specimen types were selected to address all of the variables. Each specimen type was duplicated for a total of thirty-eight specimens. The notation used in the specimen designations is described in Table 3.1. Details of the specimen types and corresponding designations are listed in Table 3.2.

Table 3.1 Specimen Notation

Joint Type	Duct Type	Joint Precompression	Grout type
DJ: Dry Joint	**S**: Galvanized Steel	**L**: Low, 5 psi	**NG**: Normal Grout
SE: Standard Epoxy		**M**: Medium, 50 psi	**SF**: Silica Fume Added
EG:Epoxy with Gasket	**P**: Plastic	**H**: High, 190 psi (3√f'c)	**CI**: Corrosion Inhibitor
Example: DJ – S – L – NG			

Table 3.2 Specimen Types and Variables [3.8]

Specimen No.	Name	Duct Type	Joint Precompression	Grout Type
Dry Joints:				
1,2	DJ-S-L-NG	Steel	5 psi	Normal
7,8	DJ-S-M-NG	Steel	50 psi	Normal
11,12	DJ-S-H-NG	Steel	190 psi	Normal
31,32	DJ-P-L-NG	Plastic	5 psi	Normal
33,34	DJ-P-M-NG	Plastic	50 psi	Normal
3,4	DJ-S-L-CI	Steel	5 psi	Corrosion Inhibitor
9,10	DJ-S-M-CI	Steel	50 psi	Corrosion Inhibitor
Standard Epoxy Joints:				
15,16	SE-S-L-NG	Steel	5 psi	Normal
21,22	SE-S-M-NG	Steel	50 psi	Normal
27,28	SE-S-H-NG	Steel	190 psi	Normal
35,36	SE-P-L-NG	Plastic	5 psi	Normal
37,38	SE-P-M-NG	Plastic	50 psi	Normal
17,18	SE-S-L-CI	Steel	5 psi	Corrosion Inhibitor
23,24	SE-S-M-CI	Steel	50 psi	Corrosion Inhibitor
29,30	SE-S-H-CI	Steel	190 psi	Corrosion Inhibitor
19,20	SE-S-L-SF	Steel	5 psi	Silica Fume
Epoxy/Gasket Joints:				
5,6	EG-S-L-NG	Steel	5 psi	Normal
25,26	EG-S-M-NG	Steel	50 psi	Normal
13,14	EG-S-H-NG	Steel	190 psi	Normal

3.1.3 Materials

Details of the materials used in this testing program are summarized in Table 3.3. All materials and proportions were selected to match segmental bridge usage as closely as possible. Concrete was batched using a six cubic foot mixer in the laboratory. Grouts were batched in five gallon buckets using a paddle mixer mounted to a drill press. Complete details of specimen construction are provided in Reference 3.4.

<div align="center">

Table 3.3 Material Details [3.8]

</div>

Item	Description		
Segment Concrete	• w/c = 0.44, f'c =5000 psi • batch proportions:	Coarse Aggregate Fine Aggregate	383 lb (3/4 in. max.) 300 lb
		Type I/II Cement	150 lb
		Water	66 lb
	• cylinder strengths:	7-day 28-day	4493 psi 5145 psi
Normal Grout	• w/c = 0.40 • batch proportions:	Type I/II Cement Water	28.8 lb 11.6 lb
Corrosion Inhibitor Grout	• w/c = 0.40 • corrosion inhibitor: • batch proportions:	calcium nitrite Type I/II Cement Water Corrosion Inhibitor	28.8 lb 11.6 lb 187 ml
Silica Fume Grout	• w/c = 0.32 • silica fume: • superplasticizer: • batch proportions:	Sikacrete 950DP WRDA-19 Type I/II Cement Water Silica Fume Superplasticizer	21.7 lb 8.0 lb 3.26 lb 88.5 ml
Prestressing Strand	• 0.5 in. diameter seven wire strand • Grade 270 (270 ksi), low relaxation		
Mild Steel Reinforcement	• 0.5 in. diameter bars (#4) • ASTM A615, Grade 60 (60 ksi)		
Steel Duct	• Corrugated, semi-rigid, galvanized steel duct for post-tensioning • 1-3/16 in. outside diameter		
Plastic Duct	• ASTM D1785 PVC pipe • 1-5/16 in. outside diameter, 1 in. inside diameter		
Segment Epoxy	• B-73 Mid-Range two-part span epoxy		

3.1.4   Measurements during Exposure Testing

Two forms of regular measurements were taken to evaluate macrocell and microcell corrosion in the test specimens. Macrocell corrosion current can be measured directly as described in Section 3.1.1. In addition, the probability of macrocell corrosion can be estimated using half-cell potential measurements. Microcell corrosion cannot be measured directly. However, significant half-cell potential readings in the absence of measured macrocell corrosion current would indicate a high probability for microcell corrosion.

3.1.4.1   Macrocell Corrosion Current Measurements

The nature of the macrocell specimen allows direct measurement of the macrocell corrosion current. Macrocell corrosion currents provide three forms of information:

- The time at which corrosion began can be determined from regular measurements during testing.
- Corrosion rate or severity can be calculated from corrosion current measurements.
- The polarity of the corrosion current indicates which steel is corroding (prestressing strand or mild steel reinforcing bars).

The corrosion current is determined by measuring the voltage drop across a resistor placed between the anode and cathode steel, as shown in Figure 3.4. The corrosion current, I_{corr}, is calculated dividing the measured voltage drop by the known resistance (Ohm's Law). Each specimen is connected to a data acquisition system, allowing voltages (currents) for all specimens to be measured simultaneously. Corrosion currents are measured at one week intervals.

$$I_{corr} = \frac{V}{R}$$
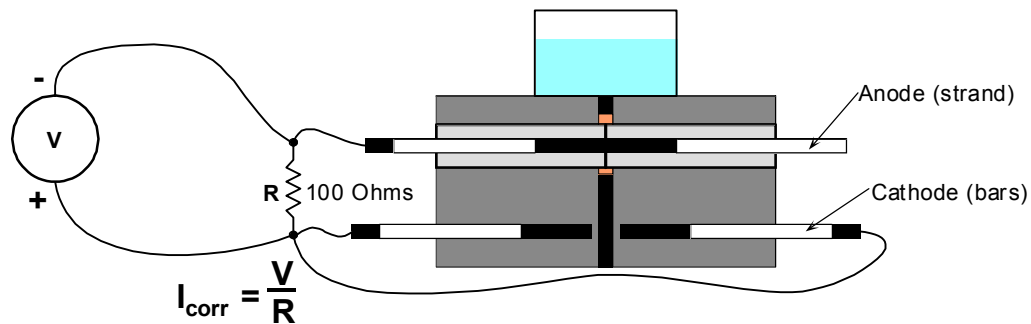
Figure 3.4 Macrocell Corrosion Current Measurement [3.8]

During corrosion, the electrons liberated at the anode travel through the electrical connection provided by the wire and resistor to the cathode. Since current moves in the direction opposite to electron flow, the current in the macrocell flows from the cathode to the anode. With the leads of the voltage measuring device attached as indicated in Figure 3.4, the measured voltage across the resistor will have a positive polarity if the anodic reaction is occurring on the prestressing strand. Thus, the polarity of the measured voltage allows the direction of the electron flow to be determined, indicating whether or not the expected corrosion cell has developed.

3.1.4.2 Half-Cell Potential Readings

Half-cell potential readings also provide three forms of information regarding the condition of the specimen:

- The magnitude of half-cell potential readings indicate the probability of corrosion at a given location.

- The time at which corrosion initiation occurred can be determined from regular potential readings taken during testing.

- Significant half-cell potentials in the absence of macrocell corrosion currents suggest the occurrence of microcell corrosion.

Half-cell potential readings were taken every two weeks at the start of the wet period and the start of the dry period. All measurements are performed according to ASTM C876[3.7] using a saturated calomel electrode (SCE). Three half-cell potential measurements are made manually on each specimen, as shown in Figure 3.5. One measurement is taken with the Plexiglas dam filled with NaCl solution and the electrode immersed in the solution. Two measurements are taken directly on the surface of each segment with the dam empty. The surface of the concrete is damp for these readings. In all cases, electrical contact between the anode and cathode is interrupted to ensure that the half-cell potential reading is for the strand only.
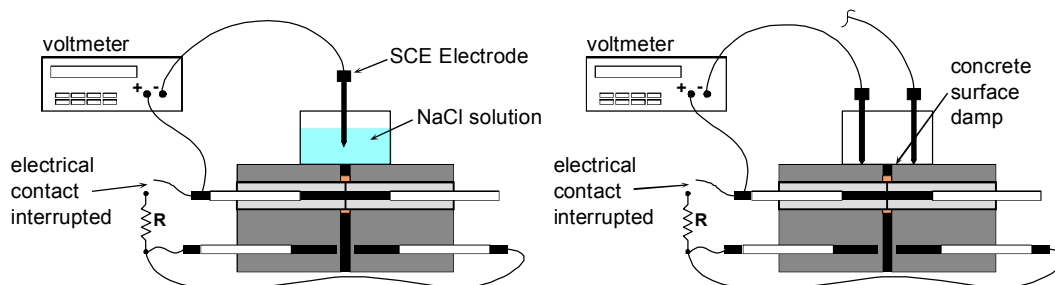
Figure 3.5 Half-Cell Potential Readings [3.8]

The numerical significance of the half-cell potential readings is shown in Table 3.4, as defined by ASTM C876. This standard was developed for half-cell potential readings of uncoated reinforcing steel in concrete, and therefore the values reported in Table 3.4 may not necessarily be appropriate for grouted prestressing strand in concrete. In general, half-cell potential readings are not an effective method for monitoring corrosion activity in bonded post-tensioned structures. In structures with galvanized steel ducts, the prestressing tendon will

be in contact with the duct in most cases and half-cell potentials taken on the prestressing tendon may in fact reflect the potential of the zinc on the galvanized steel duct. Because the potential of the zinc will be more negative than that of the tendon, this contact could lead to erroneous results and conclusions. In situations where the tendon is completely encapsulated in an impervious plastic duct system, half-cell potentials are not possible since the duct will act as a barrier to the ion flow necessary for half-cell potential readings.

In spite of these issues, half-cell potential readings were used effectively in the macrocell corrosion specimens in this testing program for two reasons. First, in all cases the prestressing tendon is not in contact with the galvanized duct. Second, for both galvanized ducts and plastic ducts the discontinuity in the duct at the segmental joint should allow ion movement and measurement of half-cell potentials. However, it is still possible that the presence of the duct, whether galvanized steel duct or plastic, may affect the magnitude of the half-cell potentials. Thus, it is important to consider both the magnitude and variation of the measured potentials over time.

Table 3.4 Interpretation of Half-Cell Potentials for Uncoated Reinforcing Steel [3.7]

Measured Potential (vs SCE)	Probability of Corrosion
More positive than −130 mV	less than 10% probability of corrosion
Between -130 mV and −280 mV	corrosion activity uncertain
More negative than −280 mV	greater than 90% probability of corrosion

3.2   EXPOSURE TEST RESULTS

Exposure testing was initiated on August 23, 1993.   Exposure testing continued without interruption until January 13, 1998, a period of four years and five months, (1603 days). At that time, one specimen from each pair of duplicates was removed for forensic examination and was reported in Reference 3.8. Exposure program and Half Cell readings continued for the remaining nineteen specimens, and they were interrupted only during the months of January 1998 to January 1999 (1603 to 1977 days), and July to December, 2000 (2523 to 2725 days) when the specimens remained in a dry condition.   Corrosion current readings were interrupted from January 8,1998 to January 13, 2000 (1598 to 2333 days after exposure testing was initiated) and from May 17,2000 to January 2001 (2458 to 2717 days).   Exposure testing ended on August 22, 2001, when the remaining specimens were removed for forensic examination, after a period of eight years (2920 days).   The exposure testing data indicated that at least ten specimens of the nineteen specimens had experienced corrosion, with measurable corrosion activity, while the other nine specimens showed low probability of corrosion or uncertain corrosion activity.

3.2.1   Macrocell Corrosion Current Results

Macrocell corrosion currents over time were plotted for all remaining specimens, after eight years of very aggressive exposure, grouped according to test variables, and are included in Appendix A. Figures 3.6 to 3.9 show examples of corrosion current plots comparing joint type, duct type, joint precompression and grout type, respectively. When examining these plots, the "polarity" of the current is important. As described in Section 3.1.4, the measured voltages and thus the corrosion currents are positive if the assumed macrocell corrosion mechanism (prestressing strand actively corroding) has developed.   Negative

85

corrosion currents indicate that a reversed corrosion cell has developed. That is, the prestressing strand is acting as the cathode, while the mild steel reinforcement bars are actively corroding.

Macrocell corrosion current plots for all dry joint specimens show active corrosion. Specimens DJ-S-L-NG-2, DJ-S-L-CI-2 and DJ-S-M-NG-2 show strand corrosion, while the remaining four specimens show reversed macrocell corrosion.

Seven out of nine epoxy joint specimens show stable corrosion currents close to zero, which suggests that the steel in these specimens had low or no corrosion. Only two epoxy joint specimens show a clear initiation of corrosion: specimen SE-S-M-CI-1 with strand corrosion, and specimen SE-S-H-CI-1 with reversed macrocell corrosion.

Epoxy Joint specimens with gaskets show a random behavior, with no corrosion, reversed macrocell corrosion and strand corrosion, in specimens EG-S-M-NG-1, EG-S-L-NG-1 and EG-S-H-NG-1, respectively. Table 3.5 shows the general results according to corrosion current activity and polarity.

Out of the 484 corrosion current data points for each specimen over 2902 days of exposure testing, a very few were considered outliers. These values clearly separated from the trend in an unpredictable and/or out of scale manner. They were clearly isolated from the rest of the data set. These data points would disproportionately affect the later calculations with regard to the time to initiation of corrosion, weighted average corrosion current, corrosion current density, and metal loss. A thorough examination of the data was made, finding outliers in the following specimens (number of outlier data in brackets): DJ-S-L-NG-2 (3), DJ-S-H-NG-2 (2),SE-S-L-NG-1 (5), SE-P-L-NG-1 (1), SE-S-M-CI-1(27), SE-S-M-NG-1 (4), and EG-S-H-NG-1 (14). These values were probably the product of

86

lost or bad connection between the strand and the cable system. These few outlier values have been excluded from Figures 3.6 to 3.9 and Figures A.1 to A.13.

In addition to the above, corrosion current data for specimen DJ-P-M-NG-2 was collected up to January 8, 1998, (1598 days after exposure testing was initiated). After this date, data values for this specimen were not consistent or coherent, and therefore, are not considered reliable.

Table 3.5 Corrosion Current Results Based on Corrosion Activity and Polarity

Zero currents (no corrosion)	Strand corrosion activity	Reversed macrocell corrosion
SE-P-L-NG-1	DJ-S-L-CI-2	DJ-S-M-CI-2
SE-S-L-CI-1	DJ-S-L-NG-2	DJ-P-M-NG-2
SE-S-L-SF-1	DJ-S-M-NG-2	DJ-P-L-NG-2
SE-S-L-NG-1	SE-S-M-CI-1	DJ-S-H-NG-2
SE-S-M-NG-1	-----------------	SE-S-H-CI-1
SE-P-M-NG-1	-----------------	EG-S-L-NG-1
SE-S-H-NG-1	-----------------	-----------------
EG-S-M-NG-1	-----------------	-----------------
EG-S-H-NG-1	-----------------	-----------------
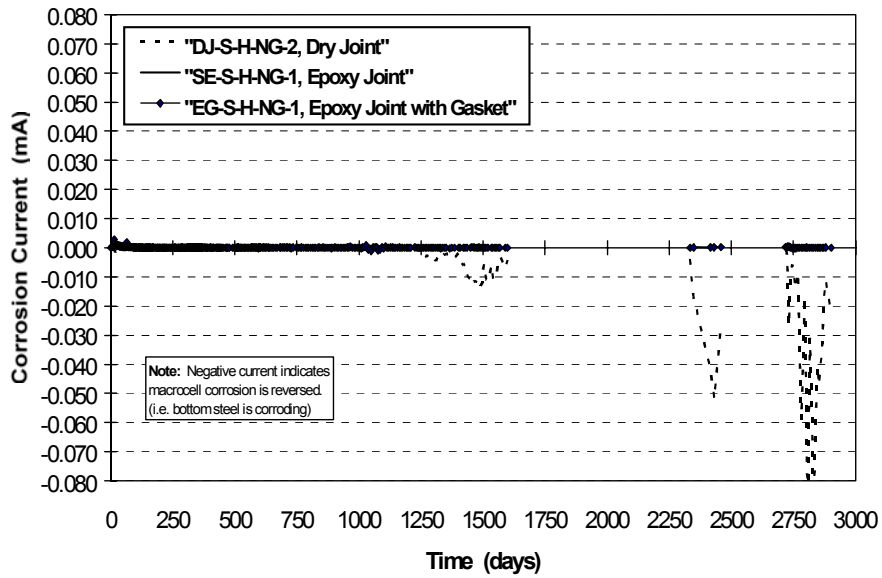
Figure 3.6 Macrocell Corrosion Current: Dry, Epoxy and Epoxy with Gasket Joint, Steel Duct, High Precompresion and Normal Grout
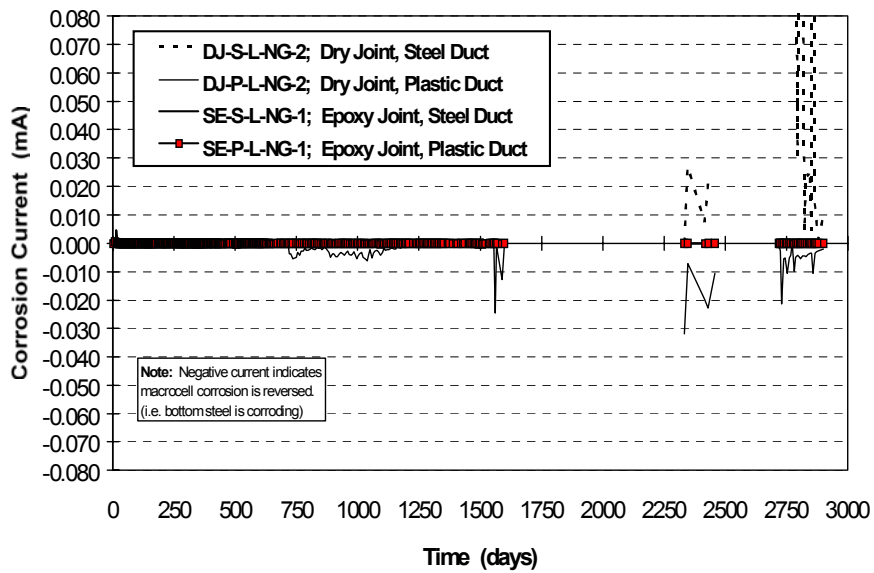
Figure 3.7 Macrocell Corrosion Current: Dry and Epoxy Joint, Steel and Plastic Duct, Low Precompresion and Normal Grout
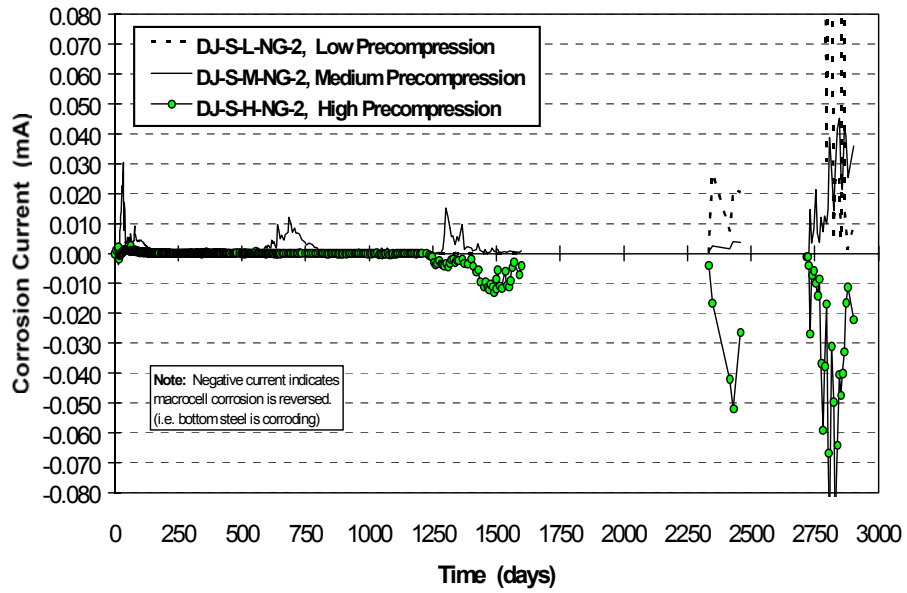
Figure 3.8 Macrocell Corrosion Current: Dry Joint, Steel Duct, Low, Medium and High Precompression and Normal Grout
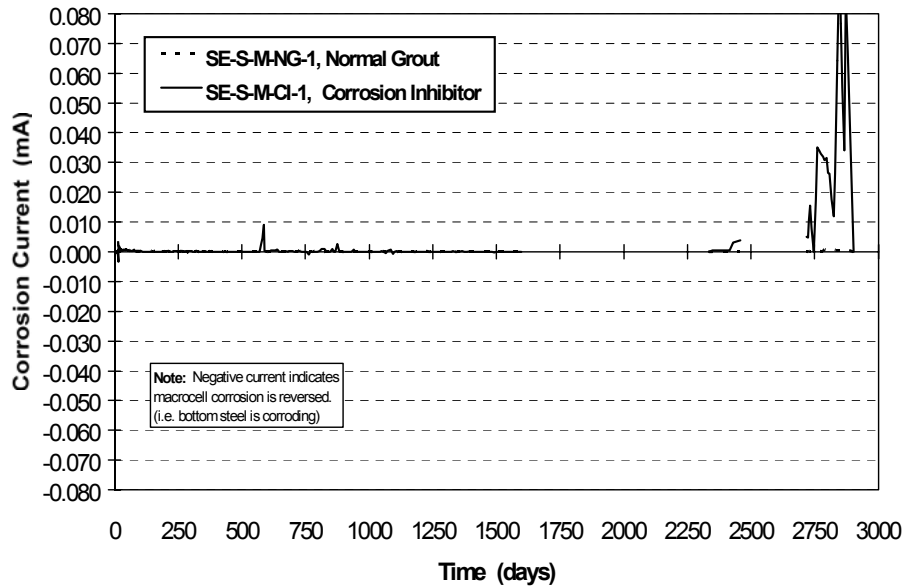
Figure 3.9 Macrocell Corrosion Current: Epoxy Joint, Steel Duct, Medium Precompresion and Different Grouts (Normal and Corrosion Inhibitor Added)

89

3.2.2 Half-Cell Potential Readings

Three half-cell potential readings were made on each specimen at the start of each of the dry and wet periods of the cycles, as explained in Section 3.1.4.2. When this data was examined for each specimen, little or no difference was observed between the three readings and thus only the half-cell potential readings immersed in the salt solution were plotted. The ASTM C876[3.7] guidelines of 130 mV and -280 mV (Table 3.4) are shown on each figure.

The half-cell potential measurements suggest a medium to high probability of corrosion for twelve specimens, including all dry joint specimens, three epoxy joint specimens (SE-S-M-NG-1, SE-S-M-CI-1, SE-S-H-CI-1), and two epoxy joint specimens with gasket (EG-S-L-NG-1, EG-S-H-NG-1).

As with the corrosion current plots, half cell potential readings over time were plotted for all nineteen specimens after eight years of very aggressive exposure, grouped according to test variables, and included in Appendix A. Figures 3.10 to 3.13 show examples of corrosion current plots comparing joint type, duct type, joint precompression and grout type, respectively. Figures A.14 to A.26 complement those presented herein. The specimens plotted in each figure correspond to the same specimens in Figure 3.6 through Figure 3.9, and Figure A.1 through A.13, respectively. Table 3.6 summarizes the general results based on half cell readings, according to ASTM C876.

Table 3.6 Half Cell Potential Results (Based on ASTM C876[3.7], See Table 3.4)

Less than 10% probability of corrosion	Between 10% to 90% probability of corrosion	More than 90% probability of corrosion
SE-P-L-NG-1	DJ-S-M-CI-2	DJ-S-L-NG-2
SE-S-L-CI-1	SE-S-M-NG-1	DJ-S-M-NG-2
SE-S-L-SF-1	EG-S-L-NG-1	DJ-S-H-NG-2
SE-S-L-NG-1	EG-S-H-NG-1	DJ-S-L-CI-2
SE-P-M-NG-1	------------------	DJ-P-L-NG-2
SE-S-H-NG-1	------------------	DJ-P-M-NG-2
EG-S-M-NG-1	------------------	SE-S-M-CI-1
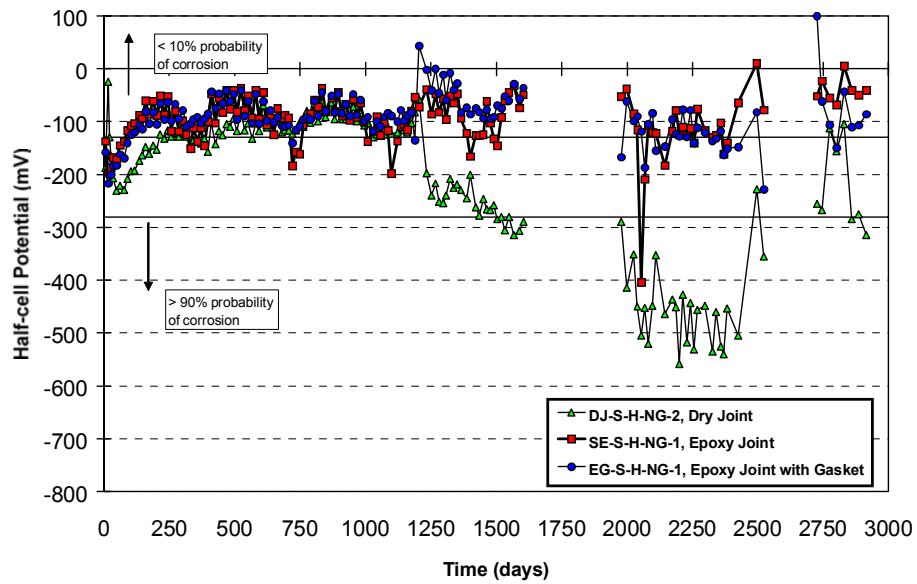
Figure 3.10 Half-Cell Potentials: Dry, Epoxy and Epoxy with Gasket Joints, Steel Duct, High Precompresion and Normal Grout
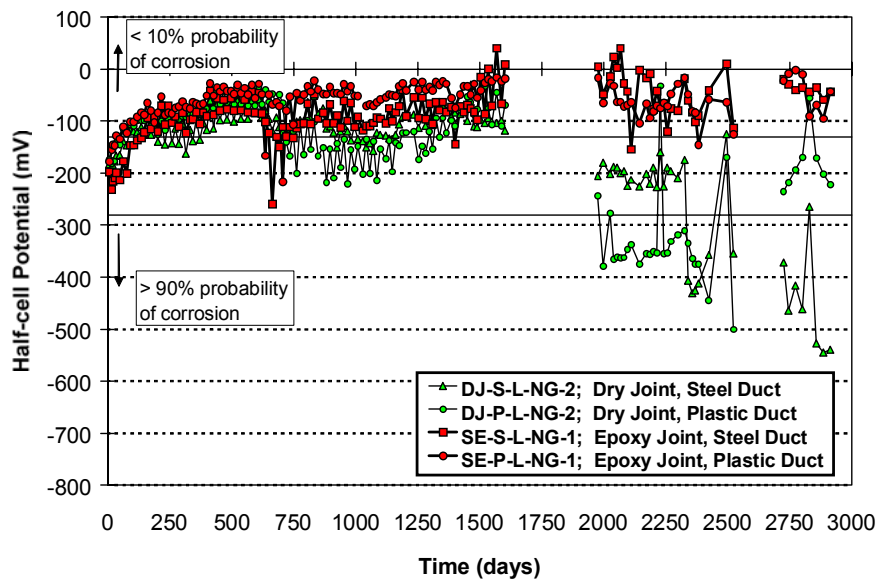
Figure 3.11 Half-Cell Potentials: Dry and Epoxy Joint, Plastic and Steel Duct, Low Precompression, and Normal Grout
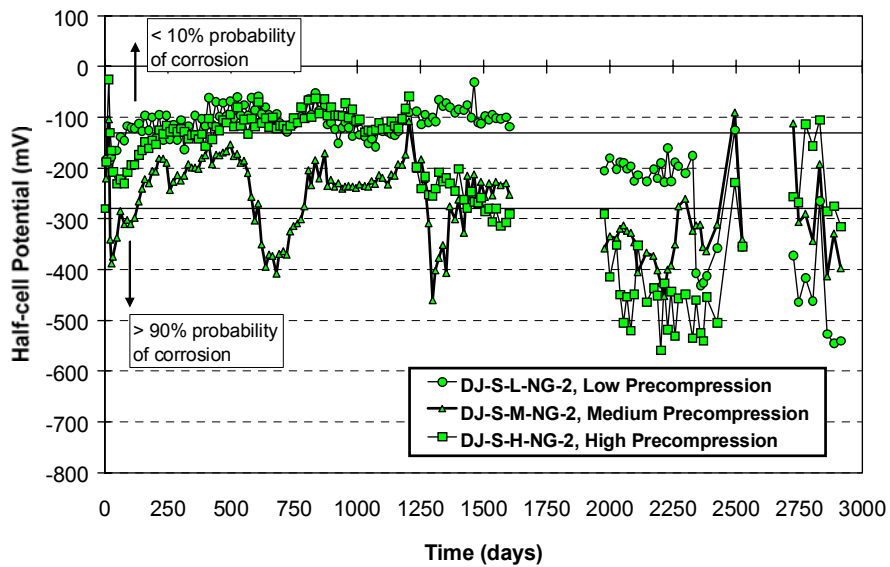
Figure 3.12 Half-Cell Potentials: Dry Joint, Steel Duct, Low, Medium and High Precompression, and Normal Grout
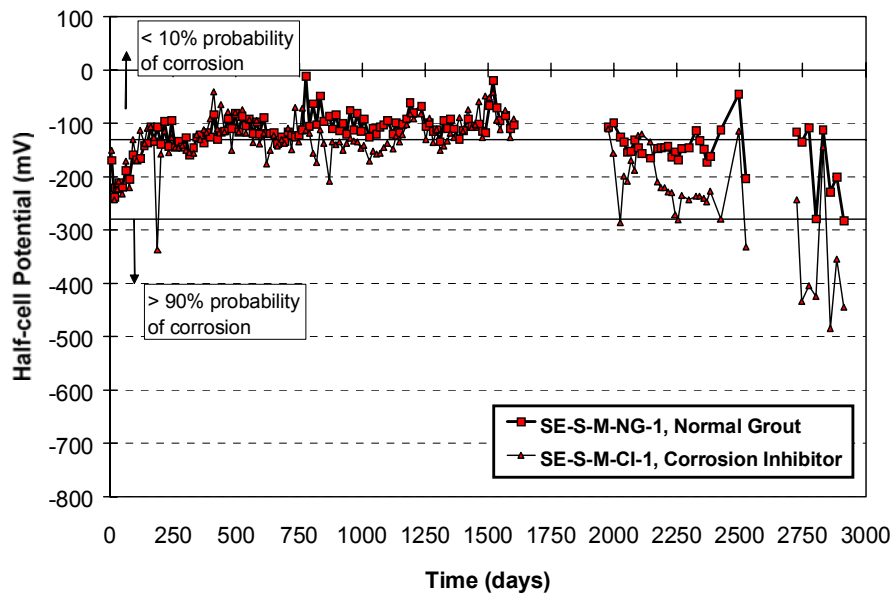
Figure 3.13 Half-Cell Potentials: Epoxy Joint, Steel Duct, Medium Precompression, and Different Grouts (Normal, and Corrosion Inhibitor Added)

3.2.3   Specimen Performance Reproducibility based on Half-Cell Potentials.

Half-Cell potentials were plotted for all nineteen specimens autopsied at eight years of very aggressive exposure with respect to their duplicates, autopsied at four and a half years. As it is observed in Figures 3.14, 3.15 and 3.16 for specimens DJ-S-H-NG, DJ-P-M-NG and SE-S-H-NG, respectively, a very good correlation existed among duplicated specimens, up to four and a half years of testing. These results confirmed that duplicated modified ASTM G109 macrocell specimens could be used at different dates of testing and be compared to obtain reliable partial and final results.   Half- Cell potential plots for specimens not shown herein are included in Appendix A, Figures A.27 to A.42.

93
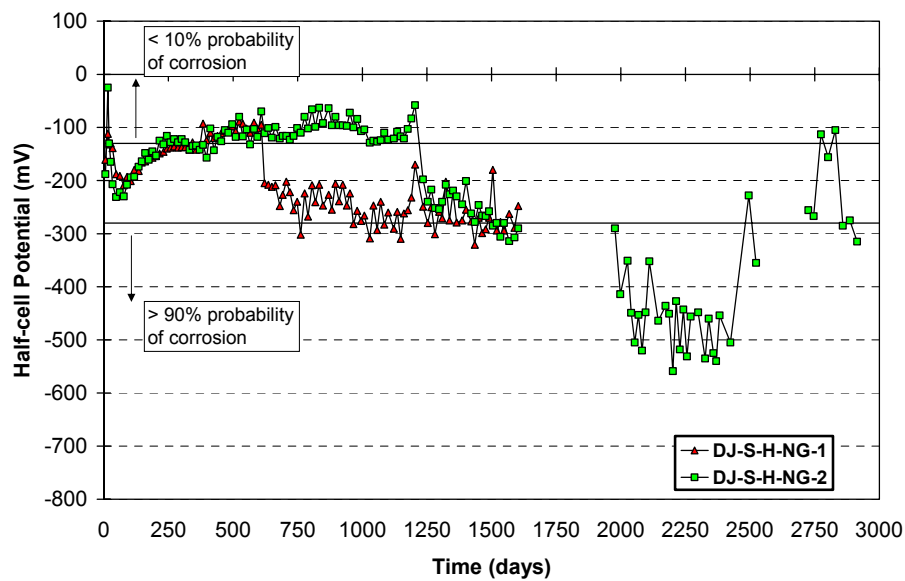
Figure 3.14 Half-Cell Potentials for Duplicated Specimens with
Dry Joint, Steel Duct, High Precompression and Normal Grout
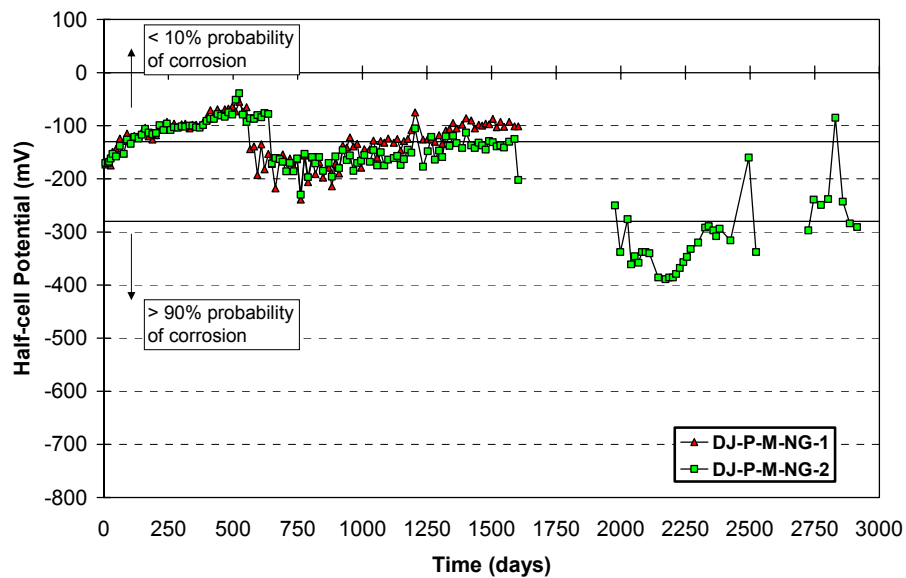
Figure 3.15 Half-Cell Potentials for Duplicated Specimens with
Dry Joint, Plastic Duct, Medium Precompression and Normal Grout

94
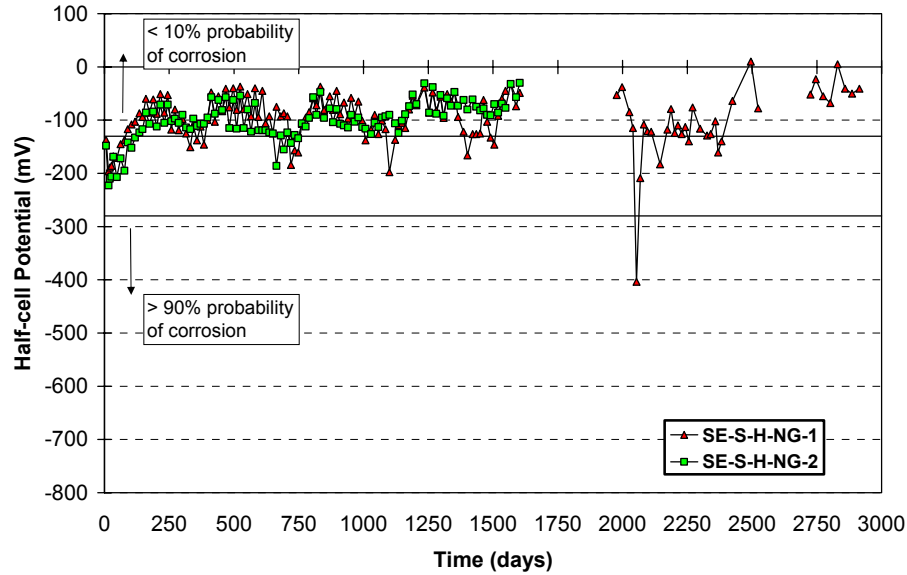
***Figure 3.16 Half-Cell Potentials for Duplicated Specimens with
Epoxy Joint, Steel Duct, High Precompression and Normal Grout***

3.2.4   Analysis and Discussion of Exposure Test Results

3.2.4.1   Time to Initiation of Corrosion

The relative length of exposure before corrosion initiation is detected may be used to compare the effectiveness of corrosion protection variables. For the purposes of this research program, the initiation of corrosion is defined as:

a)   a sudden and significant increase (in the order of 0.003 mA and above) in measured corrosion current, and/or

b)   half-cell potential measurements more negative than -280 mV, and/or

c)   a sudden and significant change (in the order of -100 mV) more negative in half-cell potential

Criterion (a) is evaluated by examining the plots of macrocell corrosion current over time for a significant increase in corrosion current. Criteria (b) is

95

based on the guidelines of ASTM C876,[3.7]as described in Section 3.1.4.2. However, the non-typical details of the macrocell specimens in this program may affect the reliability of the ASTM C876 guidelines, and corrosion may occur at potentials less negative than -280 mV. For this reason, Criterion (c) is included, where plots of half-cell potential over time are examined for a more negative significant change.

Based on corrosion current readings, ten specimens displayed some amount of increased corrosion activity or an initiation of corrosion, as described in Section 3.2.1, and shown in Figures 3.6 through Figure 3.9, and Figures A.1 through Figure A.13.   Half Cell potential readings include two additional specimens, for a total of twelve specimens showing increased corrosion activity, as described in Section 3.2.2, and shown in Figures 3.10 through 3.11, and Figures A.14 through A. 26.   Using these plots and the above definitions for corrosion initiation, the approximate time to the initiation of corrosion for these specimens are listed in Table 3.7.   The initiation of corrosion based on macrocell corrosion current was very clear for all specimens. The time to corrosion based on half-cell potentials was estimated using Criterion (b) for most specimens. In some cases, it was apparent that Criterion (c) better indicated the onset of corrosion. Examples include specimen DJ-S-M-CI-2, DJ-S-H-NG-2, DJ-P-M-NG-2, EG-S-L-NG-1, and EG-S-H-NG-1,

From Table 3.7, it is observed that most specimens show a good correlation between times to corrosion initiation based on macrocell current and half-cell potential. However, four specimens show different corrosion initiation times, these are: DJ-S-M-CI-2, SE-S-M-CI-1, SE-S-H-CI-1, EG-S-L-NG-1. For these specimens, Half Cell corrosion initiation dates correspond to the period when Corrosion Current readings were interrupted (period defined between 1598 days to 2333 days after exposure testing was initiated), as was indicated

96

previously in this chapter. However, as observed in the plots that have been referred to above and in Table 3.7, Corrosion Current readings at 2333 days did show any corrosion activity in those specimens. This suggests that analysis based on Corrosion Current readings failed to detect the corrosion initiation time based on the available data.

Table 3.7 Time to Initiation of Corrosion for Specimens Autopsied at Eight Years of Exposure

Specimen Name	Time to Corrosion		Comments
	Macrocell Current	Half-Cell Potentials	
DJ-S-L-NG-2	2347 days (128 days)	2340 days (129days)	- strand is corroding - very high corrosion currents after corrosion initiation.
DJ-S-M-NG-2	580 days (1110 days)	588 days (1110 days)	- strand is corroding - three distinct periods of corrosion activity
DJ-S-H-NG-2	1250 days (615 days)	1225 days (616 days)	- mild steel bars are corroding
DJ-P-L-NG-2	710 days (1250 days)	714 days (1225 days)	- mild steel bars corroding - two distinct periods of corrosion activity
DJ-P-M-NG-2	640 days (565 days)	644 days (560 days)	- data up to 1598 days
DJ-S-L-CI-2	2782 days (580 days)	2788 days (714 days)	- strand is corroding - corrosion current is very small
DJ-S-M-CI-2	2717 days (833 days)	2187 days (842 days)	- mild steel bars are corroding - corrosion current is very small - two distinct periods of corrosion activity based on HC potentials (after 2187 days and 2725 days)
SE-S-M-NG-1	NS (1330 days)	2802 days (1337 days)	- NS: No signs of corrosion initiation.
SE-S-M-CI-1	2431 days (NS)	2026 days (NS)	- strand is corroding
SE-S-H-CI-1	2347 days (NS)	2061 days (NS)	- mild steel bars are corroding - corrosion current is very small
EG-S-L-NG-1	2431 days (NS)	2096 days (NS)	- mild steel bars are corroding - corrosion current is very small
EG-S-H-NG-1	NS (NS)	1977 days (NS)	- NS: No signs of corrosion initiation.

LEGEND: **DJ**: Dry Joint; **SE**: Standard Epoxy Joint; **EG:** Epoxy with Gasket Joint; **S:** Galvanized Steel Duct; **P:** Plastic Duct; **L:** Low Precompression; **M:** Medium Precompression; **H:** High Precompression;

N: Normal Grout; **SF:** Silica Fume Added to Grout; **CI:** Corrosion Inhibitor in Grout

NOTE: Values in parenthesis are the corresponding times for the companion specimens after 4.4 years.

The length of time to corrosion for each of the twelve specimens showing activity do not suggest any trend between time to corrosion and levels of precompression, although conceptually, higher precompression may be expected to limit moisture and chloride ion penetration at the joint.

The presence of a corrosion inhibitor in grout appears to positively affect the time to corrosion, when comparing specimens DJ-S-L-NG-2 and DJ-S-M-NG-2 with specimens DJ-S-L-CI-2 and DJ-S-M-CI-2, respectively. However, this trend is contradicted when comparing specimen SE-S-M-NG-1 with specimen SE-S-M-CI-1.

Epoxy Joint specimen, SE-S-M-NG-1, shows a longer time for corrosion initiation when compared to Dry Joint specimen, DJ-S-M-NG-2. However, this trend is contradicted when comparing specimens SE-S-M-CI-1 and DJ-S-M-CI-2.

After carefully analyzing the reasons for the above contradictions with respect to the expected trends and results, it is deducted that this is due to the poor performance shown for specimen SE-S-M-CI-1. This conclusion suggests that an additional variable may be affecting this specimen, which is not fully understood based on nondestructive evaluations (Macrocell Currents and Half Cell Potentials). Total autopsy of this specimen is expected to reveal the cause.

3.2.4.2 General Behavior Over Exposure Time

3.2.4.2.1 Macrocell Current

Table 3.8 summarizes the general test results from Macrocell Current plots, when main test variables are compared after eight years of aggressive exposure.

Table 3.8 General Macrocell Current Results

Main Variable	Reference Plots	General Results
Joint Type	Figure 3.6 and Figures A.1, A.2, A.3, A.4	SE specimens show lower corrosion currents than EG specimens. EG specimens show less corrosion currents than DJ specimens. Exception: SE-S-M-CI-1.
Duct Type	Figure 3.7 and Figure A.5	DJ specimens with plastic duct clearly show lower corrosion currents (with reversed macrocell behavior) than DJ specimens with steel duct (active strand corrosion).
Joint Precompression	Figure 3.8 and Figures A.6, A.7, A.8, A.9	No clear trend is shown with respect to joint precompression.
Grout Type	Figure 3.9 and Figures A.10, A.11, A.12, A.13	Specimens with CI show in general less corrosion currents than NG specimens, with reversed macrocell behavior in most cases. Exception: SE-S-M-CI-1.

DJ: Dry Joint; SE: Epoxy Joint; EG: Epoxy Joint with Gasket; CI: Corrosion Inhibitor; NG: Normal Grout

3.2.4.2.2 Half-Cell Potentials

Table 3.9 summarizes the general test results from Half-Cell Potential Plots, when main test variables are compared after eight years of aggressive exposure.

Table 3.9 General Half-Cell Potential Results

Main Variable	Reference Plots	General Results
Joint Type	Figure 3.5 and Figures A.14, A.15, A.16, A.17	Epoxy Joint and Epoxy Joint with Gasket specimens show lower probability of strand corrosion than Dry Joint specimens. Exception: SE-S-M-CI-1.
Duct Type	Figure 3.6 and Figure A.18	Dry Joint and Epoxy Joint specimens with plastic duct (discontinuous at the joint) show lower probability of strand corrosion than similar specimens with steel duct.
Joint Precompression	Figure 3.7 and Figures A.19, A.20, A.21, A.22	Dry Joint specimen data indicate lower probability of strand corrosion with increasing levels of precompression. This trend is not observed in Epoxy Joint specimens due to behavior of specimen SE-S-M-CI-1. No clear trend is shown in Epoxy Joint with Gasket specimens with respect to joint precompression.
Grout Type	Figure 3.8 and Figures A.23, A.24, A.25, A.26	Dry Joint specimens with Corrosion Inhibitor show lower probability of strand corrosion with respect to specimens with Normal Grout. The contrary is found in Epoxy Joint specimens where higher probability of strand corrosion is shown in specimens with Corrosion Inhibitor than those with Normal Grout, these include specimen SE-S-M-CI-1 and specimen SE-S-H-CI-1.

3.2.4.3   *Corrosion Rate or Severity*

Corrosion severity is commonly evaluated in three ways using measured macrocell corrosion currents: weighted average corrosion current, corrosion current density and metal loss.

3.2.4.3.1 *Weighted Average Corrosion Current*

The weighted average corrosion current over the duration of testing, I_{wa}, was computed using the following expression:

$$I_{wa} = \frac{\sum I_{ai} T_i}{\sum T_i} \quad i = 1, n \qquad \textit{Eq. 3.1}$$

where,

$$I_{ai} \quad = \quad \text{average current in time interval i}$$

$$T_i \quad = \quad \text{duration of time interval i}$$

$$n \quad = \quad \text{number of measurements}$$

The effect of different time intervals between readings requires a weighted average. Table 3.12 gives weighted averages for the active specimens. ASTM G109[3.5] defines failure as an average corrosion current of 10 µA (0.010 mA). All specimens except specimen DJ-S-L-NG-2 are below this value.

3.2.4.3.2 Corrosion Current Density

The corrosion current density is the amount of corrosion current per unit surface area of the anode, calculated as the weighted average corrosion current divided by the total anode surface area.

$$\text{Corrosion Current Density} = \frac{I_{wa}}{A_{surf}} \quad (\mu A / cm^2) \qquad \textbf{\textit{Eq. 3.2}}$$

The anode surface area (A_{surf}) is taken as the total (nominal) surface area of the anode bar, assuming that corrosion is occurring over the entire exposed length of the anode. For this testing program, the non-typical macrocell specimens make estimation of the anode surface area very difficult. If the strand is the anodic site, the total surface area is computed as the sum of the surface areas of each of the seven wires of the strand. The presence of the duct and segmental joint raise further questions as to whether corrosion will occur over the exposed length of strand. For specimens in which the corrosion macrocell is

reversed the anode cross-sectional area is the area of the two reinforcing bars. However, chlorides may not have reached the entire bar length.

The uncertainty surrounding the computation of A_{surf} significantly affects the usefulness of calculated values of corrosion current density. For analysis purposes, the following values of A_{surf} were used:

For normal macrocell corrosion: (positive I_{wa})	use A_{surf} based on total surface are of 7 wires (5 in. exposed length)
For reversed macrocell corrosion: (negative I_{wa})	use A_{surf} based on surface area of two 0.5 in. (#4) bars (5 in. exposed length)

Guidelines have been proposed[3.9-3.11] to assess the rate of corrosion based on corrosion current densities, as shown in Table 3.10. Calculated values of corrosion current density are shown in Table 3.11. The computed corrosion current densities for all specimens are within the range of negligible corrosion, except for specimen DJ-S-L-NG-2 that falls in the range of moderate corrosion. However, because the corroded surface area is uncertain, overestimation of A_{surf} could produce unconservative results.

Table 3.10 Corrosion Severity Based on Current Density [3.9-3.11]

Corrosion Current Density	Corrosion Severity
Less than 0.1 $\mu A/cm^2$	Negligible
Between 0.1 and 0.2 $\mu A/cm^2$	Low (threshold for active deterioration mechanism)
Between 0.2 and 0.5 $\mu A/cm^2$	Moderate

3.2.4.3.3 Metal Loss

The amount of steel "consumed" by macrocell corrosion is directly related to the total amount of electrical charge, or number of electrons, exchanged between the anode and cathode. One amp of corrosion current consumes 1.04 grams of steel (iron) per hour.[3.12] The total amount of current passed, or charge flux, is computed by numerically integrating the macrocell corrosion current data over the duration of exposure. Although an absolute measurement of corrosion severity is difficult to obtain using metal loss (charge flux), a relative comparison of corrosion severity between specimens is possible. Calculated values of metal loss are listed in Table 3.11.

As mentioned in Section 3.3.3.1, ASTM G109[3.5] defines failure as an average macrocell corrosion current over the duration of testing of more than 10 μA. For an average corrosion current of 10 μA and the exposure duration of eight years, a metal loss of 729 milligrams (10^{-5} Amp. x 1.04 g/hour x 70080 h x 1000mg/g) would be expected. Only specimen DJ-S-L-NG-2 is above this value. Slightly below are specimens DJ-P-L-NG-2 and DJ-S-H-NG-2 with mild steel metal loss close to 465 mg corresponding to a weighted average corrosion current of approximately 6.4 μA; and, below are specimens DJ-S-M-NG-2 and SE-S-M-CI-1 with strand metal loss close to 190 mg corresponding to a weighted average corrosion current of approximately 2.6 μA. The other macrocell specimens are below 1 μA, with only very minor corrosion activity.

***Table 3.11 Calculated Weighted Average Current, Current Density and Metal
Loss for Active Specimens after Eight Years of Exposure***

	Specimen	Weighted Average Corrosion Current	Corrosion Current Density	Metal Loss
No.	Name	(µAmps)	(µA/cm^2)	(mg)
	DJ-S-L-NG-2	29.417	0.253	2135
	DJ-S-M-NG-2	2.572	0.022	187
	DJ-S-H-NG-2	-6.392	0.064	464
	DJ-S-L-CI-2	0.068	0.001	5
	DJ-S-M-CI-2	-0.422	0.004	31
	DJ-P-L-NG-2	-6.475	0.065	470
	SE-S-M-CI-1	2.664	0.023	193
	SE-S-H-CI-1	-0.266	0.003	19
	EG-S-L-NG-1	-0.211	0.002	15

Note: Negative average corrosion current indicates mild steel bars are corroding.
Specimen DJ-P-M-NG-2 due has been excluded. See discussion in Section 3.2.1.

3.2.4.3.4 Discussion: Corrosion Rate Calculations

The corrosion rate calculations for weighted average corrosion current, corrosion current density, and metal loss indicate that the corrosion activity is important for specimen DJ-S-L-NG-2, and moderately important for specimens DJ-S-M-NG-2, DJ-S-H-NG-2, DJ-P-L-NG and SE-S-M-CI-1. For all other specimens corrosion activity is considerably lower than what would be defined as failure.

The calculated corrosion rates using the three different methods are plotted in Figure 3.17 through Figure 3.19 where the relative performance of the nine specimens included in Table 3.11 is the same for all three cases. All three corrosion rate calculations are related to the charge flux or the number of electrons exchanged between the anode and cathode. The charge flux is calculated by integrating the corrosion current over time:

$$\text{Charge Flux} = \int I_{corr}\,dt \equiv \sum I_{ai} T_i \quad (i = 1, n) \quad \text{(Coulombs)} \qquad \textbf{\textit{Eq. 3.3}}$$

where, I_{corr} = instantaneous corrosion current

I_{ai} = average current in time interval i

T_i = duration of time interval i

n = number of measurements

The calculation of charge flux appears in the computation of weighted average corrosion current, current density and metal loss:

$$\text{Weighted Avg. Current, } I_{wa} = \frac{\int I_{corr}\,dt}{t_d} \equiv \frac{\sum I_{ai} T_i}{\sum T_i} \quad \text{(amps)}$$

$$\text{Current Density} = \frac{I_{wa}}{A_{surf}} \equiv \frac{\int I_{corr}\,dt}{t_d} \times \frac{1}{A_{surf}} \quad (\text{amps}/\text{cm}^2)$$

$$\text{Metal Loss} = \int I_{corr}\,dt \times \left(\frac{1\ \text{hr}}{3600\ \text{sec}} \times \frac{1.04\text{g}}{\text{amp} - \text{hr}} \times \frac{1000\text{mg}}{\text{g}} \right) (\text{mg})$$

where, t_d = duration of testing

A_{surf} = corroded surface area

In general, any one of the three forms of corrosion rate calculations would be appropriate for comparing the performance of the protection variables. Calculated metal loss will be used for discussion purposes in the remainder of this document.

The corrosion rate calculations provide a means for relative comparison of corrosion activity in the different specimens. However, it is difficult to use the calculated corrosion rates to obtain an absolute measure of corrosion severity. Corrosion current density can be used for this purpose if the area over which corrosion is occurring is known. The non-typical details of the segmental macrocells make estimation of the corroded surface area uncertain at best, and thus the use of corrosion current density to assign a corrosion severity using Table 3.10 is questionable for this testing program.

The effect of the different variables (other than joint type) is not clear based on the calculated corrosion rates (Figures 3.17 through Figure 3.19). However, data suggests that a higher level of precompression or protection to the strand (in the case of plastic ducts or corrosion inhibitor in grout), somewhat produces a higher tendency of reversed macrocell behavior, which may relate to lower strand corrosion.
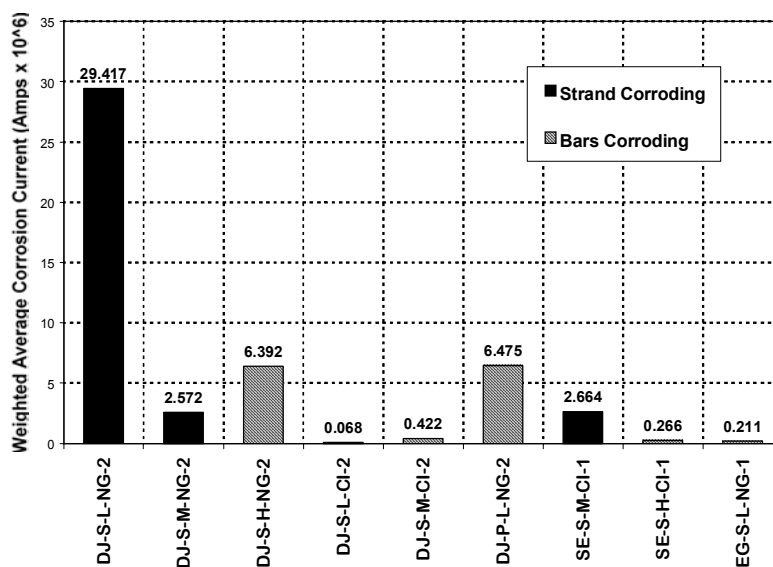
Figure 3.17 Calculated Weighted Average Corrosion Current for Active Specimens after Eight Years of Exposure
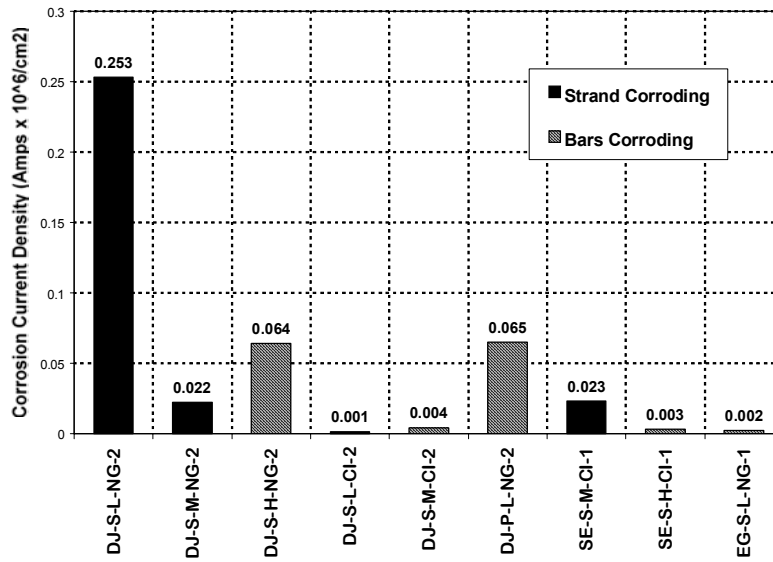
3.18 Calculated Corrosion Current Densities for Active Specimens after Eight Years of Exposure
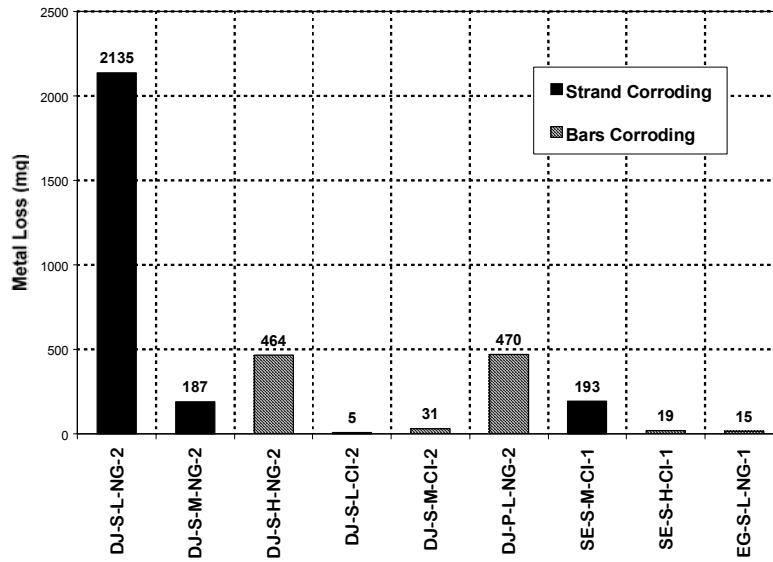
Figure 3.19 Calculated Metal loss for Active Specimens after Eight Years of Exposure

3.3 **FORENSIC EXAMINATION**

After 2920 days of exposure (taking place over eight years), the remaining 19 specimens out of the initial 38 were removed from testing for forensic examination or autopsy. The previous 19 specimens had been autopsied three and a half years before, at 1603 days of exposure. The objectives of the forensic examinations are as follows:

1. Obtain visual evaluation of corrosion damage on duct, strand and mild steel reinforcement.
2. Obtain visual evaluation of joint condition
3. Determine chloride ion penetration at locations adjacent to and away from the segmental joint.
4. Examine mechanisms of corrosion in segmental macrocell corrosion specimens

The notation scheme shown in Figure 3.20 was assigned for record keeping purposes. "Clamp end" refers to the end of the specimen where ground clamps were attached to complete the macrocell circuit. Segment B was cast first. Segment A was match –cast against Segment B. All specimens were numbered on Side C at the clamp end. This marking ensured that the orientation of all specimens was known throughout the forensic examination process. The notation scheme will be referred to throughout this chapter.

The following sections 3.3.1 through 3.3.3 have been repeated from Reference 3.8, with only minor changes, as they refer to the same procedure followed in the first autopsy, at four years and five months of aggressive exposure.

Side D

End B

Side C

Top View

End B

End A
Clamp End

22

Specimen
Number

Segment B

Segment A

Side C View
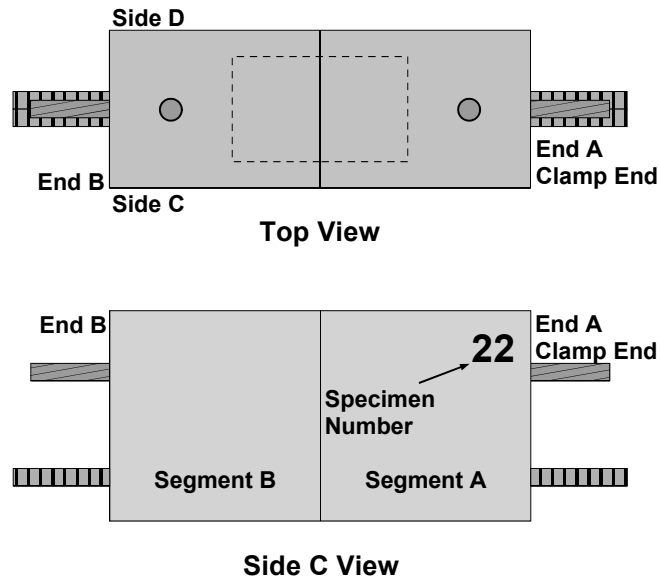
Figure 3.20 Specimen Labeling Scheme [3.8]

3.3.1   Procedure

3.3.1.1   Specimen Condition at End of Testing

The exterior surfaces of each specimen were examined for cracking and rust staining upon removal from testing. Duct ends were examined for grout voids and rust stains. The joint perimeter was examined for visible salt stains, joint epoxy and grout.

3.3.1.2   Concrete Powder Samples for Chloride Analysis

One of the objectives of the forensic examination was to determine the influence of the three joint types on the penetration of moisture and chlorides. It was expected that chloride contents could be higher in the vicinity of the joint, particularly for dry joint specimens. To examine the influence of joint type on chloride penetration, concrete powder samples were collected at multiple depths

and locations to determine chloride ion profiles adjacent to the joint and away from the joint. Sample locations are shown in Figure 3.21. Concrete powder samples were collected using a rotary hammer and following a procedure based on AASHTO T 260-94.[3.13] Two 1.5 g samples were collected at each depth. Samples were analyzed for acid soluble chlorides using a specific ion probe (CL Test System by James Instruments).

Plan View

Chloride Sample Depths at A and C

Chloride Sample Depths at B
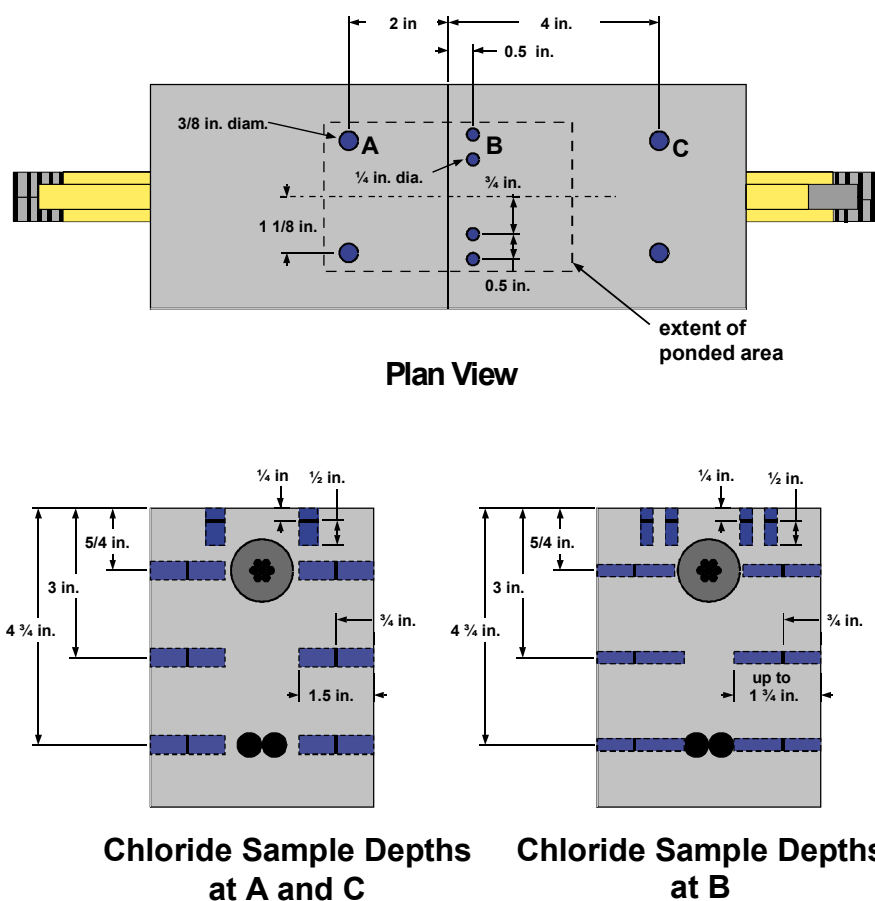
Figure 3.21 Chloride Sample Locations [3.8]

3.3.1.2.1 Location A

Samples at A were taken at a distance of 2 in. from the segmental joint using a 3/8 in. diameter drill bit. Two holes were drilled at each depth to later average the chloride content results. The first sample was taken on the top surface of the specimen. Initially, the holes were drilled to a depth of 0.25 in. The holes and bit were then cleaned, and the holes were drilled an additional depth of 0.5 in. An average depth of 0.5 in. was assumed for this sample. The remaining three samples at location A were obtained by drilling into the sides of the specimen. One hole was drilled into each side of the specimen at the desired depths. The holes were drilled to an initial depth of 0.75 in. so that the collected sample will be from concrete directly below the ponded area. Following cleaning, the holes were drilled an additional 0.5 to 0.75 in. to obtain the sample amount (total depth up to 1.5 in.).

3.3.1.2.2 Location B

Samples at B were collected at a distance of 0.5 in. from the segmental joint. Due to the close proximity of the joint, a smaller bit size of 0.25 in. was used for these samples. The procedure for obtaining the powder samples at location B was similar to that at location A with some minor modifications due to the smaller drill bit size. Four holes were required for the two samples on the top surface of the specimen, and the holes for the other samples were drilled slightly deeper (up to 1.75 in.) to obtain the necessary sample amount.

3.3.1.2.3 Location C

Samples at C were taken at a distance of 4 in. from the segmental joint. The procedure for collecting samples at C is identical to that for samples at A.

3.3.1.3 Longitudinal Saw Cuts

Four longitudinal saw cuts were made on each specimen to facilitate removal of the duct/strand unit and mild steel bars. Saw cuts were made to a depth of 1.5 in. at the level of the tendon and bars, as shown in Figure 3.22. These cuts are referred to as the strand cut line and bar cut line respectively. The specimen remained intact after cutting, but was easily opened using a hammer and chisel. Saw cuts were performed using a high torque circular saw fitted with a diamond dry-cut concrete blade as shown in Figure 3.23. Some cracked samples needed to be wrapped with duct tape to permit cutting of the specimen.
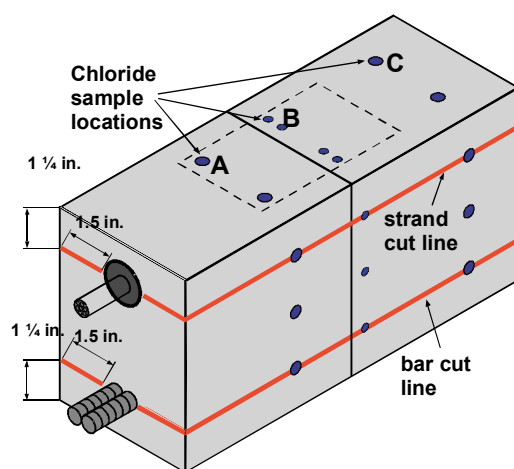
Figure 3.22 Longitudinal Saw Cuts [3.8]

3.3.1.4 Expose and Remove Duct and Strand

The duct was exposed by opening the specimen at the strand cut line, as shown in Figure 3.23. The duct and strand were then removed from the concrete as one unit. The concrete surrounding the duct was examined for voids, cracks, rust staining, salt collection and damage. After thorough examination, the duct was cut open by making two longitudinal cuts along the sides of the duct/strand

unit using a small air-driven grinder. The grout was examined for voids and cracks and indications of moisture and chloride ingress. If desired, grout samples were taken from the grout for chloride analysis at this time (see Section 3.3.1.5). The grout was then carefully removed, exposing the strand for examination. The extent and severity of corrosion on both the strand and duct was rated according to the corrosion rating scheme described in Section 3.3.3.
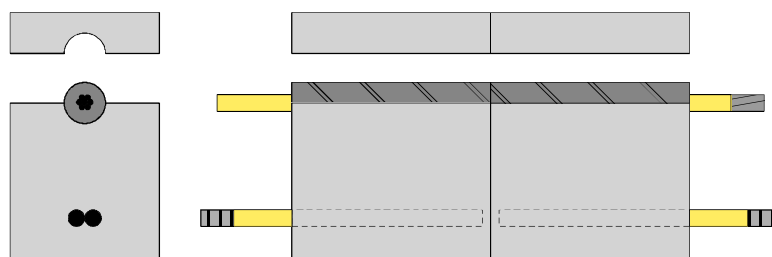
Figure 3.23 Specimen Opened to Expose Duct/Strand [3.8]

3.3.1.5   Grout Samples for Chloride Analysis

Grout samples were collected from selected specimens for chloride analysis. Samples were carefully removed from the strand at the location of the joint and at a distance of 2 in. from the joint. The grout pieces were crushed between two steel plates and ground into powder using a mortar and pestle. Grout powder samples were analyzed for acid soluble chlorides using a specific ion probe (CL Test System by James Instruments).

3.3.1.6   Expose and Remove Mild Steel

The mild steel bars were exposed by opening the specimen at the bar cut line, as shown in Figure 3.24. The bars were then removed from the concrete for examination.   The extent and severity of corrosion on the bars was rated

according to the corrosion rating scheme described in Section 4.3.2. The concrete surrounding the bars was examined for voids, rust staining, salt collection and any damage.
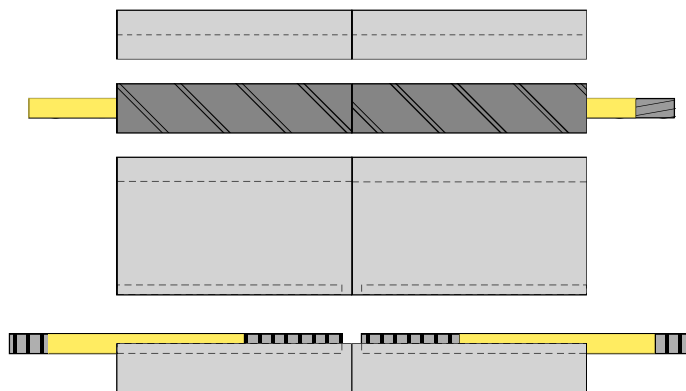
Figure 3.24 Specimen Opened to Expose Mild Steel Bars [3.8]

3.3.1.7   Examine Joint Condition

In the dry joint specimens, the specimen readily separated into its two segments after the duct/strand unit was removed (Section 3.3.1.4).   This separation allowed the condition of the joint face to be examined directly for cracking, rust staining, evidence of moisture and chloride penetration and general soundness of the joint.

The intention of the epoxy joint is to bond the two segments together. As a result, it was not possible to examine the joint in the same manner as the dry joint specimens. An indication of the epoxy joint condition was obtained by examining several sections through the joint, as shown in Figure 3.25. The saw cuts at the strand line and bar line (Section 3.3.1.3) revealed the epoxy joint condition at sections 1 and 3 in Figure 3.25. An addition longitudinal saw cut was made at the mid-height of the specimen to obtain a third section through the joint

(Joint Section 2 in the figure). The joint was also examined around the perimeter of the specimen. The joint sections were examined for indications of voids in the epoxy or the presence of moisture, salt or corrosion products.
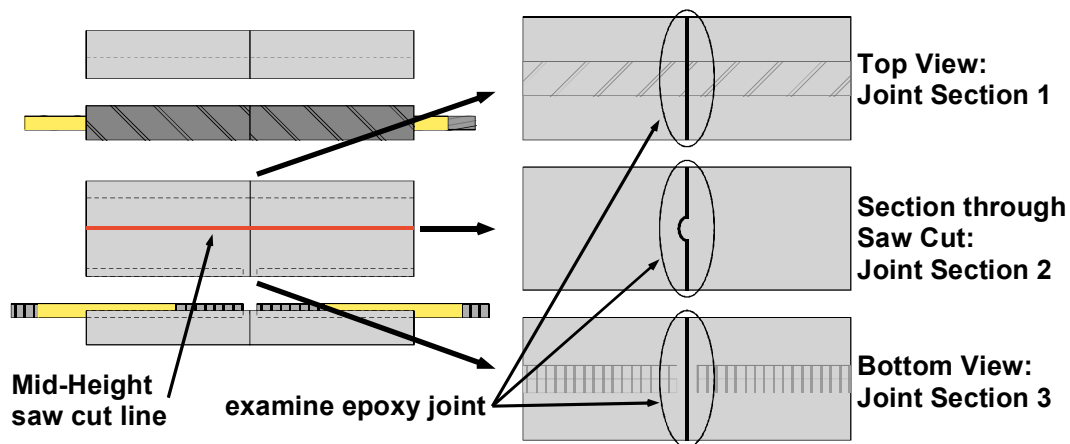
Figure 3.25 Examining Epoxy Joint Condition [3.8]

3.3.2 Autopsy Program

The remaining specimen from each duplicate pair of specimen types, was finally prepared for forensic examination.

Chloride samples were collected from ten of the nineteen specimens autopsied, in order to coincide with the specimen pair that was analyzed previously.   The ten specimens were selected out of the nineteen to provide a representative sample and address the major variables expected to influence chloride penetration.   The mid-height cut for epoxy-jointed specimens was performed on six of the twelve specimens with epoxy joints. Specimens selected were standard epoxy joints and epoxy/gasket joints at each of the three levels of joint precompression. Details of the nineteen specimens selected for autopsy are listed in Table 3.12.

Table 3.12 Specimens Selected for Forensic Examination

Specimen	Time to Corrosion	Corrosion Location	Chloride Samples	Mid-Height Cut
DJ-S-L-NG-2	2347 days	Strand	A, B, C	n/a
DJ-S-M-NG-2	580 days	Strand	A, B	n/a
DJ-S-H-NG-2	1250 days	Bars	A, B	n/a
DJ-P-L-NG-2	710 days	Bars	A, B	n/a
DJ-P-M-NG-2	640 days	Bars	None	n/a
DJ-S-L-CI-2	2782 days	Strand	A, B	n/a
DJ-S-M-CI-2	2717 days	Bars	A, B	n/a
SE-S-L-NG-1	n/a	n/a	A, B, C	Yes
SE-S-M-NG-1	n/a	n/a	A, B	Yes
SE-S-H-NG-1	n/a	n/a	A, B	Yes
SE-P-L-NG-1	n/a	n/a	None	No
SE-P-M-NG-1	n/a	n/a	None	No
SE-S-L-CI-1	n/a	n/a	None	No
SE-S-M-CI-1	2431 days	Strand	None	No
SE-S-H-CI-1	2347 days	Bars	None	No
SE-S-L-SF-1	n/a	n/a	None	No
EG-S-L-NG-1	2347 days	Bars	A, B	Yes
EG-S-M-NG-1	n/a	n/a	None	Yes
EG-S-H-NG-1	n/a	n/a	None	Yes

3.3.3 Evaluation and Rating of Corrosion Found During Forensic Examination

A generalized evaluation and rating system was developed to quantify the severity and extent of corrosion damage in the test specimens. The procedure is presented in a universal form with the intention of applying the same rating system to other situations. The length of strand, mild steel reinforcement or galvanized steel duct was subdivided into eight increments. At each increment, the steel was examined and a rating was assigned to describe the corrosion

severity within that increment. The ratings for the eight increments were summed to give a total corrosion rating for the element that could be compared for different specimens. By assigning a corrosion severity at eight locations, both the extent and severity of corrosion is considered.

The corrosion severity ratings are described below. The rating system is essentially the same for prestressing strand, mild steel reinforcement and galvanized duct, with some modifications to reflect unique corrosion aspects of each type of steel. In general, the evaluation system doubles the severity rating for each category of increasing corrosion damage.

3.3.3.1 Prestressing Strand

The strand was examined at eight intervals, as indicated in Figure 3.26. The interval sizes have been adjusted to provide four intervals in the unpainted region of the strand, and two intervals in each of the painted regions at both ends. Corrosion ratings were assigned to indicate the severity of corrosion on the outer six wires of the strand and on the center wire (after de-stranding) at each interval to address the possibility of different corrosion activity on the strand exterior and interstices between wires. The corrosion rating system for prestressing strand is described in Table 3.13. The total strand corrosion rating was calculated as follows:

$$\text{Strand Corrosion Rating} = \sum_{i=1}^{8} R_{outer,i} \times n_i + R_{center,i} \qquad \textit{Eq. 3.4}$$

where, $R_{outer,i}$ = outer wires corrosion rating, interval i

n_i = number of corroded outer wires, interval i

$R_{center,i}$ = center wire corrosion rating, interval i

i = interval, 1 to 8
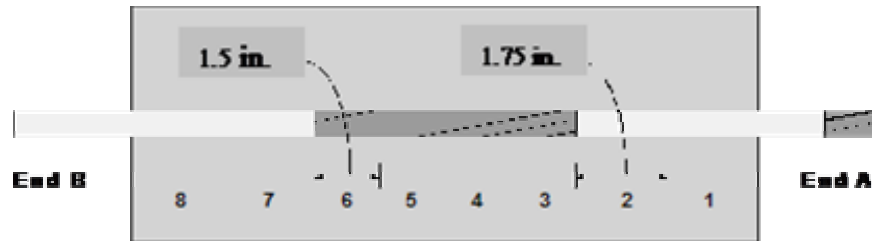
Figure 3.26 Intervals for Corrosion Ratings on Prestressing Strand

The corrosion rating system for prestressing strand was adapted from Poston[3.14] and Hamilton.[3.15] The use of a cleaning pad to assess corrosion severity was proposed by Sason[3.16] for classifying the degree of rusting on prestressing strand for new construction. The recommended cleaning pad is a 3M Scotch Brite Cleaning Pad. The pad is held by hand and rubbed longitudinally along the strand axis with a pressure similar to that used when cleaning pots and pans.   The classification of pitting severity was based on tensile tests performed on corroded prestressing strand.[3.17] The tests were used to assign a reduced tensile capacity of 97% GUTS to pitting damage at the level of P1. Moderate pitting (P2) was assigned a capacity of 90% GUTS, and severe pitting (P3) 77% GUTS.   In general, the presence of any pitting visible to the unaided eye is deemed cause for rejection in new construction.[3.16]

Table 3.13 Evaluation and Rating System for Corrosion Found on Prestressing Strand [3.8]

Code	Meaning	Description	Rating
NC	No Corrosion	No evidence of corrosion.	0
D	Discoloration	No evidence of corrosion, but some discoloration from original color.	1
L	Light	Surface corrosion on less than one half of the interval, no pitting. Surface corrosion can be removed using cleaning pad.	2
M	Moderate	Surface corrosion on more than one half of the interval, no pitting. **and/or** Corrosion can not be completely removed using cleaning pad.	4
P1	Mild Pitting	Broad shallow pits with a maximum pit depth not greater than 0.02 in.	8
P2	Moderate Pitting	Pitting where the maximum pit depth ranged between 0.02 and 0.04 in.	16
P3	Severe Pitting	Pitting where the maximum pit depth is greater than 0.04 in.	32

3.3.3.2 Mild Steel Reinforcement

The mild steel reinforcing bars were examined at eight intervals, as indicated in Figure 3.27 The interval sizes have been adjusted to provide four intervals in the unpainted region of the bars, and two intervals in the painted regions at both ends. Corrosion ratings were assigned to indicate the severity of corrosion on the top and bottom surfaces of each bar to reflect the possibility of different corrosion severity and extent. The corrosion rating system is described in Table 3.14. The total bar corrosion rating was calculated as follows:

$$\text{Bar Corrosion Rating} = \sum_{i=1}^{8} R_{Bar1Top,i} + R_{Bar1Bot,i} + R_{Bar2Top,i} + R_{Bar2Bot,i} \qquad \textbf{\textit{Eq. 3.5}}$$

where, $R_{Bar1Top,i}$ = Bar 1, top surface corrosion rating, interval i

$R_{Bar1Bot,i}$ = Bar 1, bottom surface corrosion rating, interval i

$R_{Bar2Top,i}$ = Bar 2, top surface corrosion rating, interval i

$R_{Bar2Bot,i}$ = Bar 2, bottom surface corrosion rating, interval i

i = interval, 1 to 8

Table 3.14 Evaluation and Rating System for Corrosion Found on Mild Steel Bars [3.8]

Code	Meaning	Description	Rating
NC	No Corrosion	No evidence of corrosion	0
D	Discoloration	No evidence of corrosion, but some discoloration from original color	1
L	Light	Surface corrosion on less than one half of the interval, no pitting. Surface corrosion can be removed using cleaning pad.	2
M	Moderate	Surface corrosion on more than one half of the interval, no pitting. **and/or** Corrosion can not be completely removed using cleaning pad.	4
P	Pitting	Pits visible to unaided eye.	8
AR	Area Reduction	Measurable reduction in bar cross-sectional area due to corrosion	R^2

R = Estimated cross-sectional area reduction in percent

Figure 3.27 Intervals for Corrosion Ratings on Mild Steel Bars

3.3.3.3 Galvanized Steel Duct

The galvanized steel duct was examined for eight equal intervals of 1.5 in., as indicated in Figure 3.28. At each location, corrosion ratings are assigned to indicate the severity of corrosion on the top and bottom surfaces of the inside and outside of each duct to reflect the possibility of different corrosion severity and extent. The corrosion rating system is described in Table 3.15. The total duct corrosion rating was calculated as follows:

$$\text{Duct Corrosion Rating} = \sum_{i=1}^{8} R_{TopOuter,i} + R_{BotOuter,i} + R_{TopInner,i} + R_{BotInner,i} \qquad \textbf{\textit{Eq. 3.6}}$$

where, $R_{TopOuter,i}$ = top outer surface corrosion rating, interval i

$R_{BotOuter,i}$ = bottom outer surface corrosion rating, interval i

$R_{TopInner,i}$ = top inner surface corrosion rating, interval i

$R_{BotInner,i}$ = bottom inner surface corrosion rating, interval i

i = interval, 1 to 8

121
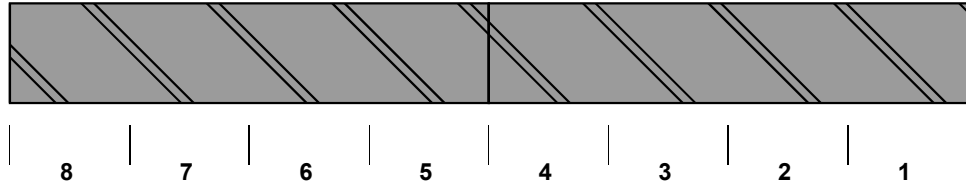
Figure 3.28 Intervals for Corrosion Ratings on Galvanized Duct[3.8]

Table 3.15 Evaluation and Rating System for Corrosion Found on
Post-tensioning Duct[3.8]

Code	Meaning	Description	Rating
NC	No Corrosion	No evidence of corrosion	0
D	Discoloration	No evidence of corrosion, but some discoloration from original color	1
L	Light	Surface corrosion on less than one half of the interval, no pitting.	2
M	Moderate	Surface corrosion on more than one half of the interval, no pitting.	4
S	Severe	Corrosion completely covers the interval. **and/or** Presence of pitting.	8
H	Hole Through Duct	Hole corroded through duct. Used in conjunction with ratings D, L, M and S.	$32 + A_h$

A_h =   Area of hole(s) in mm^2

3.3.4 Forensic Examination Results

3.3.4.1 *Detailed Visual Inspection*

A brief summary of the forensic examination results after eight years exposure is provided for each specimen in the following sections. The previous rating results from the autopsy performed at four years and five months are included in the individual tables, for comparison. The detailed description for the previous autopsy results is included in Reference 3.8.

3.3.4.1.1 Specimen DJ-S-L-NG-2 (Dry Joint, Steel Duct, Low Precompression, Normal Grout)

Duct corrosion produced a crack in the top of the concrete specimen extending its whole length, as shown in Figure 3.29. The crack had a maximum top width of 0.12 in., and extended the full depth of cover to the

Corrosion Rating:

Specimen	(1)	(2)
	4.4 yrs	8 yrs
Strand	26	612
Bars	12	54
Duct	528	15779

duct, and was clearly visible when the specimen was opened at the strand cut line. Rust staining was visible around the crack.

A 0.020 in. maximum width crack was also evident in the side, at the level of the strand.   Also, at one end of the specimen, three cracks were found extending from the duct perimeter to the outer limits of the specimen, corresponding to the cracks described above, in the top, and side directions. No cracks were found in the bottom of the specimen, below the location of the mild steel bars.

More than 50% of the duct had been consumed by corrosion, leaving a build up of corrosion products around the surface of the grout.   Corrosion

products were mixed with a white powder (that was analyzed with X-Ray Diffraction and was found to be Zinc Oxide and Zinc Hydroxide). At the remaining areas of the duct metal, severe uniform corrosion and pitting was found, as shown in Figure 3.29. The duct corrosion rating for this specimen was the maximum of all specimens examined.

Three shallow voids of around 0.016 in.^{2} each, were found in the grout surface, when extracting the remaining duct material. The voids appear to have resulted from insufficient grout fluidity rather than due to trapped air or bleed water collection. The grout was also cracked in the top, corresponding with the crack observed in the concrete cover.

The strand showed one of the highest corrosion rates when compared to the other 18 specimens. Uniform corrosion and pitting extended the complete length of the strand, including those sections where the epoxy paint had peeled off, which represented more than 50% of the painted area.

The mild steel showed moderate corrosion away from the joint, in the vicinity of the epoxy paint area, as shown in Figure 3.29. Additionally, light to moderate corrosion was found under the epoxy paint and in all those areas where the epoxy had peeled off, which represented around 15% to 20% of the epoxy area in the bars.

The match-cast dry joint was intact with no voids or cracks. Some grout infiltrated the joint during grouting. The entire face of the joint was covered with a white residue that may be salt or leaching.

Specimen condition prior to autopsy
(Top view) [Side view in detail]
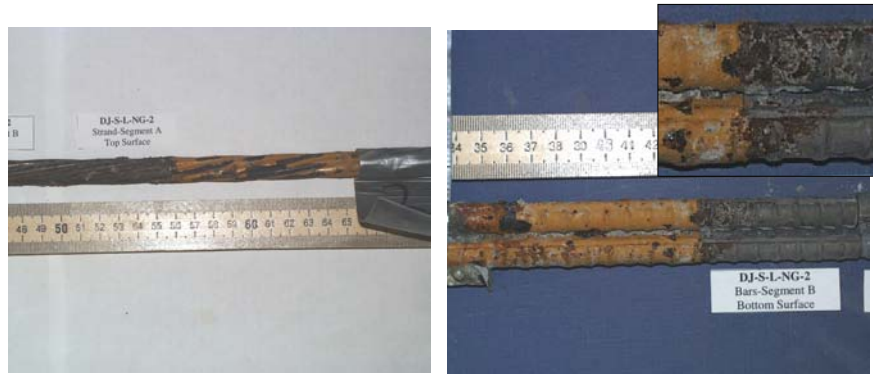
Duct

Strand

Mild Steel Bars

Figure 3.29 Concrete, Duct, Strand and Bar Condition for
Specimen DJ-S-L-NG-2

3.3.4.1.2 Specimen DJ-S-M-NG-2 (Dry Joint, Steel Duct, Medium
Precompression, Normal Grout)

Duct corrosion produced a 0.040 in. max. width crack at the top of the specimen, extending the whole length as shown in Figure 3.30. No cracks were found in the sides or bottom of the specimen.

Corrosion Rating:

Specimen	(1)	(2)
	4.4 yrs	8 yrs
Strand	43	780
Bars	12	44
Duct	325	3054

125

The crack extended the complete concrete cover depth, having a max width at the strand cut line of 0.080 in.

The duct was severely corroded at the top, with maximum corrosion occurring around the joint section and also at approximately 60 mm, on both sides, from the joint location. Corrosion products accumulated in thin layers. White powder was found in the duct, mixed with steel corrosion products, and was observed specially in the half duct below. Underneath the duct, a black stain of about 0.039 in.^{2} against the concrete surface was found, with moisture. Within a few minutes, this black stain rapidly changed color to a lighter dark rust color, after the duct was removed from the concrete and moisture was lost.

The most severe corrosion found in the duct corresponded to a large void in the grout of about 0.40 in.^{2}. The grout was covered with corrosion products from the duct metal.

The strand had moderate to severe corrosion in the top areas, where the epoxy paint had peeled off; and light corrosion in the exposed steel areas. On the bottom of the strand, moderate to severe corrosion was found at the epoxy paint areas, and very severe corrosion and pitting in the exposed steel area. The strand corrosion rating was the highest when compared to the other specimens.

Discoloration and light to moderate corrosion was found in the reinforcing bars, mainly underneath the epoxy paint, as shown in Figure 3.30. The epoxy paint seemed to have retained moisture, forcing the paint to peel off and triggering corrosion. Few small voids were found in the concrete surface underneath the reinforcing bars.

The entire face of the dry joint was covered with a white residue that may be salt or leaching.
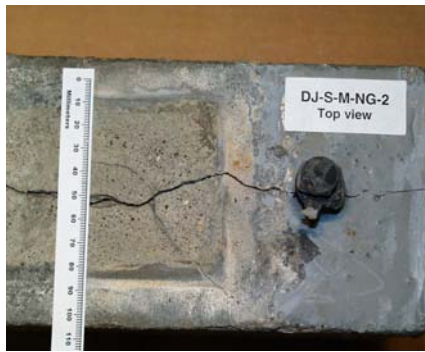
Specimen condition prior to autopsy (Top view)

Duct

Strand

Mild Steel Bars

Figure 3.30 Concrete, Duct, Strand and Bar Condition for Specimen DJ-S-M-NG-2

3.3.4.1.3 Specimen DJ-S-H-NG-2 (Dry Joint, Steel Duct, High Precompression, Normal Grout)

A 0.040 in. maximum width crack was evident at the top of the specimen, with a length of about 7 in., centered with respect to the joint location as shown in Figure 3.31. At the bottom of the specimen, there was another crack, extending one half of the specimen, with a maximum crack width in the order of 0.080 in. No cracks were visible in the sides of the specimen.

Corrosion Rating:

Specimen	(1)	(2)
	4.4 yrs	8 yrs
Strand	38	137
Bars	60	606
Duct	64	361

Severe uniform corrosion and pitting was found on the top and bottom of the galvanized steel duct, around the joint. Additionally, a black stain with moisture was found at approximately 2.35 in. from the joint in the top of the duct in Segment B. One hole of around 0.17 in.[2] was located in the duct at the joint and a 0.09 in.[2] hole was at approximately 1.2 in. from the joint, at the top of the duct in Segment A, corresponding to the location of a void in the grout. White stains (powder) and discoloration of the duct was evident in the bottom of the duct in Segments A and B.

Specimen condition prior to autopsy
(Bottom view)
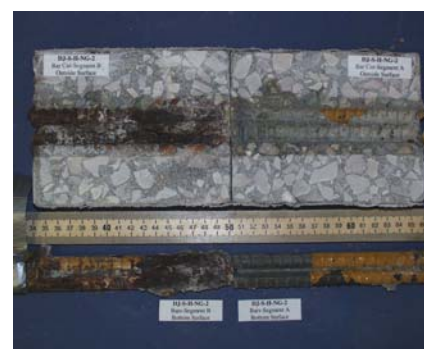
Duct

Strand

Mild Steel Bars

Figure 3.31 Concrete, Duct, Strand and Bar Condition for
Specimen DJ-S-H-NG-2

128

Moderate to severe corrosion was found on the strand in Segment A, in the areas where the epoxy had peeled off. Light to moderate corrosion was found on the unpainted areas.

Mild steel was severely corroded, with extensive pitting and severe volume decrease due to corrosion products, in Segment B. The bar corrosion produced a crack in the concrete cover in the bottom of the specimen. Mild steel in Segment A was only lightly corroded and discolored, especially in the areas where the epoxy paint had peeled off. See Figure 3.31. The mild steel corrosion rating was the highest when compared to the other specimens.

White dust covered the dry joint.

3.3.4.1.4 Specimen DJ-P-L-NG-2 (Dry Joint, Plastic Duct, Low Precompression, Normal Grout)

Corrosion Rating:

Specimen	(1)	(2)
	4.4 yrs	8 yrs
Strand	6	116
Bars	17	201
Duct	0	0

Corrosion in the reinforcing bars produced a 0.040 in. maximum width crack in Segment B, in the bottom of the specimen as shown in Figure 3.32. No cracks were found in the top or sides of the specimen.

White dust, corresponding to leaching or salt, was found in the inside surface of the concrete, at the duct/strand cut line, around the silicone holding the grouting ducts to the plastic duct. Also white dust was found at the joint section at the level of the plastic duct, where silicone was used to seal the duct joint.

A very deep void centered at 2 in. from the joint, in Segment A, was found in the top of the grout. Also shallow voids were found in the top of the grout at approximately 3 in. from the joint, in Segment B.

Light corrosion was found on the strand.

The mild steel had very severe corrosion and pitting in the exposed areas in Segment B, at the top and bottom of the bars. Severe corrosion and pitting was also observed in the same segment, in the areas where the epoxy paint had peeled off. The build-up of corrosion products was severe, causing the concrete cover to crack. At the adjoining segment, moderate corrosion was found at the bars, close to the joint section.

The dry joint was intact, with a white residue in the entire joint.

Specimen condition prior to autopsy (Top view)
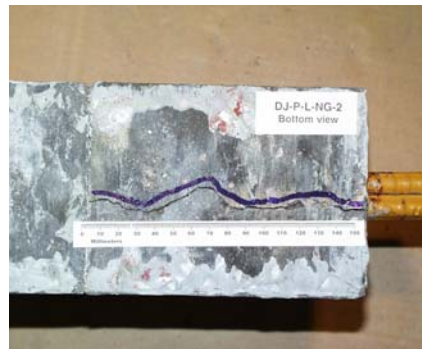
Specimen condition prior to autopsy (Bottom view of Segment B)

Duct and grout condition

Mild Steel Bars

Figure 3.32 Concrete, Duct, Strand and Bar Condition for Specimen DJ-P-L-NG-2

130

3.3.4.1.5 Specimen DJ-P-M-NG-2 (Dry Joint, Plastic Duct, Medium Precompression, Normal Grout)

Mild steel corrosion was responsible for a 0.020 in. maximum width crack at the bottom of the specimen in Segment A as shown in Figure 3.33. No cracks were visible at the top and sides of the specimen.

Corrosion Rating:

Specimen	(1)	(2)
	4.4 yrs	8 yrs
Strand	9	80
Bars	24	77
Duct	0	0

White residue was found in the inside concrete surface, at the duct/strand cut line, between the silicone used at the joint section and sides of the plastic duct and in the connection of the grouting duct and the plastic duct.

The dry joint was clean, with no signs of crystals or corrosion stains; however, little concrete discoloration was observed in the joint concrete surface in the top of the duct/strand level.

The plastic duct was intact, with no signs of damage.

Minor discoloration was observed at the outer wires of the strand, in the exposed surface area close to the joint section. The areas where the epoxy paint had peeled off, at both sides of the strand in Segments A and B, had light corrosion.

Moderate to severe corrosion was observed in the mild steel bars of Segment A, in the exposed areas close to the joint section. Additionally, light to moderate corrosion was found were the epoxy paint had peeled off. In Segment B, light corrosion was found were the epoxy paint had peeled off, and no corrosion was observed in the exposed steel areas, closer to the joint.

A few small voids (approx. 0.012 in.^{2}) were found in the grout surface, close to the joint section. Salt crystals were found inside the voids, in the interior concrete surface.

131

**Specimen condition prior to autopsy
(Bottom view, Segment A)**

Duct

Strand

Mild Steel Bars

*Figure 3.33 Concrete, Duct, Strand and Bar Condition for
Specimen DJ-P-M-NG-2*

3.3.4.1.6 Specimen DJ-S-L-CI-2 (Dry Joint, Plastic Duct, Low Precompression, Corrosion Inhibitor in Grout)

The top of the specimen had a 0.010 in. maximum width crack, extending a length of 4.75 in., centered in the specimen as shown in Figure 3.34. No cracks or signs of corrosion were observed in the sides or bottom of the specimen.

132

The galvanized steel duct had severe corrosion on the top surface, close to the joint section. The duct was consumed in approximately 0.72 in.[2] at the joint section and had another hole in the top on Segment A, within 0.75 in. to 2 in. from the dry joint. The duct also showed areas with white stains or products in the bottom sections against the concrete and in the top sections against the concrete around the grouting duct locations.

Corrosion Rating:

Specimen	(1)	(2)
	4.4 yrs	8 yrs
Strand	114	86
Bars	4	22
Duct	42	674

Specimen condition prior to autopsy
(Top view)

Duct

Strand

Mild Steel Bars

Figure 3.34 Concrete, Duct, Strand and Bar Condition for
Specimen DJ-S-L-CI-2

133

Duct corrosion produced a 0.010 in. crack in the concrete cover.

Some small 0.015-0.030 in.^{2} voids were observed in the top of the grout, underneath the galvanized steel duct. Salt crystals were found inside of the voids.

Minor discoloration and light corrosion was observed at the prestressing strand. Light corrosion was found on the exposed areas of the mild steel bars, next to the joint section in Segment B and at 20 mm from the joint section on Segment A. Light to moderate surface corrosion was observed were the epoxy paint had peeled off. The dry joint was clean, except for white stains – salt crystals or leaching – around the duct area.

3.3.4.1.7 Specimen DJ-S-M-CI-2 (Dry Joint, Plastic Duct, Medium Precompression, Corrosion Inhibitor in Grout)

A fine crack, 0.020 in. maximum width and 6 in. length, was visible in the top of the specimen, centered with respect to the dry joint section, as shown in Figure 3.35. No cracks or signs of corrosion were found at the sides or the bottom of the specimen.

Corrosion Rating:

Specimen	(1)	(2)
	4.4 yrs	8 yrs
Strand	24	54
Bars	20	27
Duct	151	346

At the duct/strand cut line, the concrete had several bubble holes under the duct, but there were no corrosion products inside the holes.

Moderate to severe corrosion was found in the galvanized steel duct, mixed with white deposits, corresponding to Zinc Oxide and Zinc Hydroxide, as examined by X-Ray Diffraction. The duct in Segment B had a small hole of approximately 0.030 in.^{2}, corresponding to a void in grout. Corrosion action was also responsible for a hole of an approximate area of 0.40 in.^{2} next to the joint section. The white residue was present in the top of the duct around the areas where the grouting vents were attached. At 0.6 in. from the joint in the bottom of

134

the duct in Segment B, there was a black spot of corrosion products with moisture.

**Condition prior to autopsy
(Top view)**

Duct

Strand

Mild Steel Bars
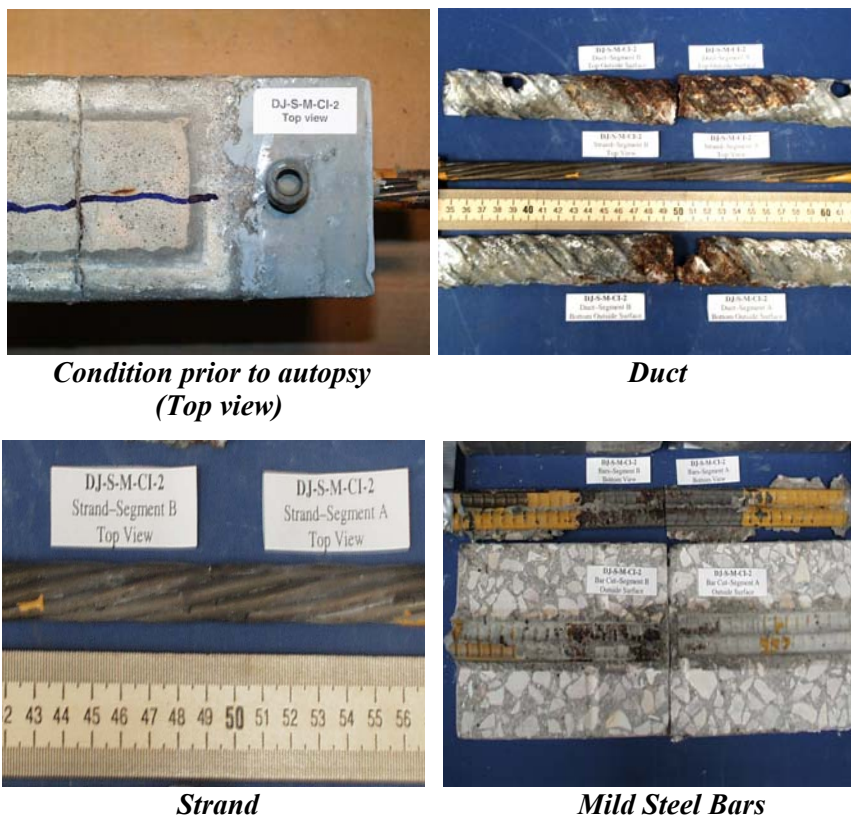
***Figure 3.35 Concrete, Duct, Strand and Bar Condition for
Specimen DJ-S-M-CI-2***

The grout had large voids across the top and bottom, with salt crystals deposited inside.

Discoloration was observed on the strand and corrosion was negligible.

The mild steel bars had moderate corrosion in the unpainted area of Segment B.   Discoloration was observed under the epoxy paint. In Segment A, light to moderate corrosion was found in the unpainted area of the bars close to the dry joint.

3.3.4.1.8 Specimen SE-S-L-NG-1 (Epoxy Joint, Steel Duct, Low Precompression, Normal Grout)

A hairline crack of about 3.5 in. in length was located in the top of the specimen, inside the ponded region, extending mainly in Segment B as shown in Figure 3.36. No cracks or corrosion stains were found in the sides or bottom of the specimen.

Corrosion Rating:

Specimen	(2)	(1)
	4.4 yrs	8 yrs
Strand	22	64
Bars	6	26
Duct	13	167

The duct halves did not meet at the joint, leaving a gap of approximately 0.12 in.

Severe corrosion covered most of the top of the duct in Segment B, as seen in Figure 3.36, and half the top of the duct in Segment A, extending from the joint face. Corrosion in Segment B produced a horizontal crack in the duct of approximately 1.5 in. that lead to another vertical crack of about 0.75 in. in length with a hole of 0.015 in^2. The bottom of the duct was covered mostly with a white residue (white powder) with only a few areas of light to moderate corrosion near the joint section.

A large void of an approximate length of 4 in. and width of 0.75 in. was found in the top of the duct, extending 2.5 in. into Segment B and 1.5 in. into Segment A. Another void of approximately 0.039 in.^{2} was found in the top of the grout in Segment B, with duct corrosion products inside.
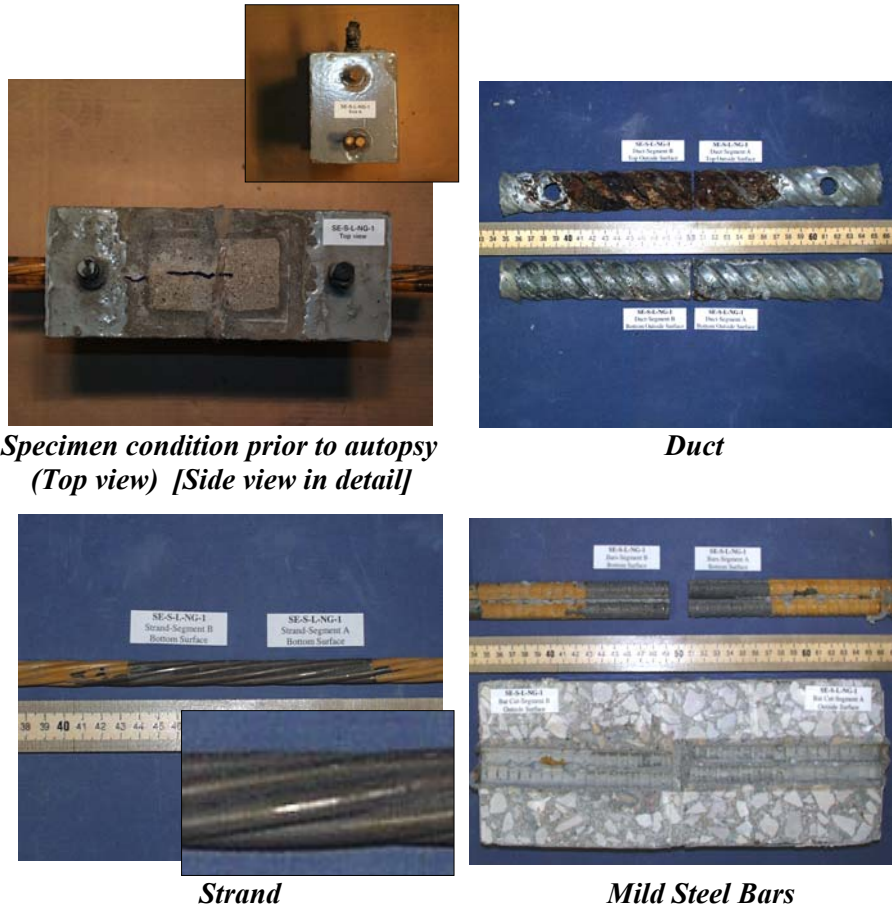
Specimen condition prior to autopsy
(Top view) [Side view in detail]

Duct

Strand

Mild Steel Bars

Figure 3.36 Concrete, Duct, Strand and Bar Condition for
Specimen SE-S-L-NG-1

Light to moderate corrosion was found on the strand in one of the outer wires, where the epoxy paint had peeled off, at 3 in. from the joint.   The other outer wires had discoloration in the unpainted areas and light surface corrosion in the areas were the epoxy paint had peeled off. The inner wire had light corrosion in its entire length.

137

The mild steel bars showed discoloration in the unpainted areas and light corrosion in the few areas where the epoxy paint had peeled off, as shown in Figure 3.36.

3.3.4.1.9 Specimen SE-S-M-NG-1 (Epoxy Joint, Steel Duct, Medium Precompression, Normal Grout)

The top of the specimen had a crack with an approximate maximum width of 0.016 in., extending a length of 6.3 in., centered with the joint as shown in Figure 3.37. No cracks were found on the sides or bottom of the specimen.

Corrosion Rating:

Specimen	(2)	(1)
	4.4 yrs	8 yrs
Strand	2	119
Bars	16	41
Duct	61	732

The epoxy at the joint did not cover the entire face. There were small holes in the epoxy in the top surface of the specimen. Epoxy bond on the lower part of the bar cut line broke along the joint.

At the duct/strand cut line, severe corrosion was found on the top of the galvanized steel duct, as shown on Figure 3.37. Corrosion produced several small holes through the duct in Segment B. In Segment A, one large longitudinal hole of about 0.55 in.^{2} was centered at approximately 23.6 in. from the joint. White powder was impregnated to the duct metal in various locations, especially in the bottom of the duct in Segment A and in the top of duct in Segments A and B, around the grout vent locations, as shown in Figure 3.37.

Moderate to severe corrosion was found on one of the outer wires of the strand of the unpainted section, in Segment B. The center wire has also moderately corroded at the same place. Light to moderate corrosion was found on the rest of the wires in that segment. Light corrosion and discoloration was found under the epoxy paint.

138

Specimen condition prior to autopsy
(Top view)
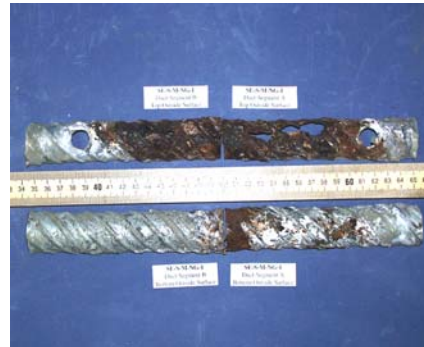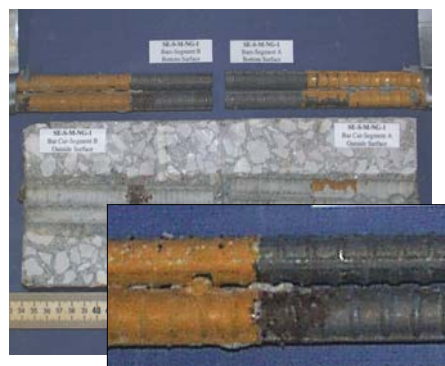
Duct

Strand

Mild Steel Bars

Figure 3.37 Concrete, Duct, Strand and Bar Condition for
Specimen SE-S-M-NG-1

Large amounts of corrosion were found on one of the bars in Segment B, under the epoxy paint, close to Face B. Severe corrosion was found on all areas were the epoxy paint had peeled off, being more severe and concentrated than seen on other specimens. Severe corrosion was found on the same bar, on Segment B, starting where the epoxy coating ends, and extending approximately 0.6 in.

3.3.4.1.10 Specimen SE-S-H-NG-1 (Epoxy Joint, Steel Duct, High Precompression, Normal Grout)

Corrosion Rating:

Specimen	(2)	(1)
	4.4 yrs	8 yrs
Strand	3	88
Bars	0	29
Duct	8	268

The specimen had a hairline crack in the top, with a length of 4.3 in., as seen in Figure 3.38. No cracks were found in the sides or bottom of the specimen.

The top of the galvanized metal duct had severe corrosion in two thirds of the total length of Segment B and one third of the length in Segment A, extending from the joint section. The most severe corrosion on both sides was found at approximately 2 in. from the joint.

Corrosion products in the duct were dark (black). Two holes, one of 0.18 in.^{2} and another of 0.016 in.^{2} were found centered at 2 in. from the joint in Segment B. The voids did not correspond to a large deep void in the grout located by the joint in the top of the grout in Segment A. White powder was found in the metal duct around the grout vent locations and by the joint section in the top of the duct in Segment A.

The strand had light corrosion in the areas were the epoxy paint had peeled off. In the unpainted areas, the outer wires were only discolored. The inner wire had light corrosion in its entire length.

Mild steel bars had discoloration in the unpainted areas and light corrosion where the epoxy paint had peeled off.

Specimen condition prior to autopsy (Top view)

Duct

Strand

Mild Steel Bars

Figure 3.38 Concrete, Duct, Strand and Bar Condition for Specimen SE-S-H-NG-1

3.3.4.1.11 Specimen SE-P-L-NG-1 (Epoxy Joint, Plastic Duct, Low Precompression, Normal Grout)

No cracks were found in the top, sides or bottom of the specimen.

The plastic duct was intact, with no signs of damage.

The top of the hardened grout had a large void in Segment A beginning 1 in. from

Corrosion Rating:

Specimen	(2)	(1)
	4.4 yrs	8 yrs
Strand	5	80
Bars	0	0
Duct	0	0

the joint section and extending 1.4 in.   The void was clean without salt deposits. In the Segment B side, the grout had a smaller void 0.8 in. from the joint extending 0.8 in. vertically with an approximate width of 0.080 in.   At the joint location there was a small circular void of 0.20 in. in diameter. The grout was smooth in the bottom surface.

Light corrosion was found at the sides of the strand, closer to Faces A and B, suggesting that some water may have seeped from the ends.   Around the joint and under the ponded region the outer wires of the strand were in excellent condition. The inner wire had light corrosion. Minor discoloration was found on the areas where the epoxy had peeled off.
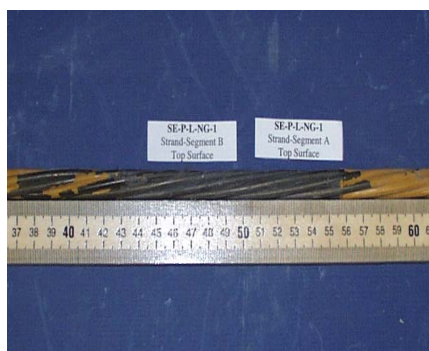
Specimen condition prior to autopsy (Top view)	*Duct*
Strand	*Mild Steel Bars*

Figure 3.39 Concrete, Duct, Strand and Bar Condition for Specimen SE-P-L-NG-1

No corrosion was found on the mild steel bars.

The epoxy segmental joint was intact around its perimeter, with no signs of moisture, salt or rust penetration at the strand and bar cut lines.

3.3.4.1.12 Specimen SE-P-M-NG-1 (Epoxy Joint, Plastic Duct, Medium Precompression, Normal Grout)

No cracks were found on the top, sides or bottom of the specimen as shown in Figure 3.40.

The plastic duct was intact, without any signs of deterioration.

Several large voids were found on the top surface of the grout. In most cases, the voids were less than 0.16 in. deep. The voids appear to have resulted from insufficient grout fluidity.

Corrosion Rating:

Specimen	(2)	(1)
	4.4 yrs	8 yrs
Strand	5	88
Bars	0	18
Duct	0	0

Discoloration and very light corrosion was found on the outer wires of the prestressing strand in the unpainted area. The inner wire showed light corrosion. In the areas with epoxy coating, the strand showed light corrosion, where the paint had peeled off.

Light corrosion occurred in the mild steel bars under the epoxy coating. No corrosion was found in the unpainted areas.
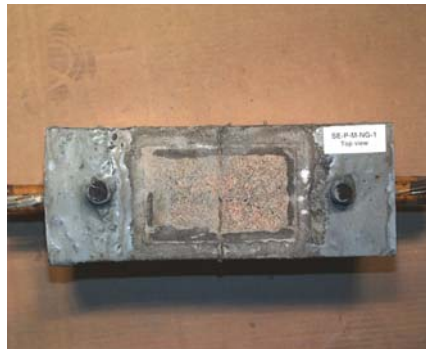
Specimen condition prior to autopsy

(Top view)
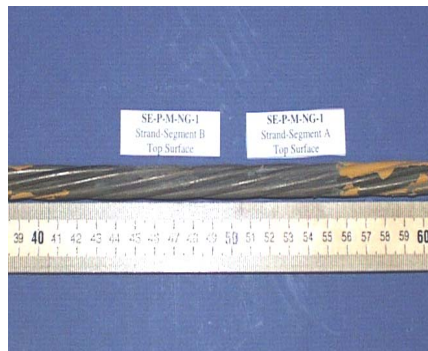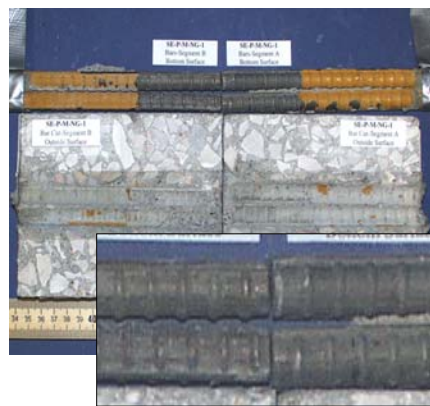
Duct

Strand

Mild Steel Bars

***Figure 3.40 Concrete, Duct, Strand and Bar Condition for
Specimen SE-P-M-NG-1***

***3.3.4.1.13 Specimen   SE-S-L-CI-1   (Epoxy   Joint,   Steel   Duct,   Low
Precompression, Corrosion Inhibitor in Grout)***

No cracks were found on the top, sides or bottom of the specimen as shown in Figure 3.41.

Severe corrosion was found on the top of the galvanized metal duct in Segment B, extending half of the segment from the joint section, and with the most severe corrosion at

Corrosion Rating:

Specimen	(2)	(1)
	4.4 yrs	8 yrs
Strand	24	95
Bars	0	28
Duct	85	126

144

1.75 in. from the joint. Also, moderate to severe corrosion was found on the top of the metal duct in Segment A, centered at 1.75 in. from the joint, as shown in Figure 3.41. White residue (powder) was found mixed with the dark corrosion products. The bottom of the duct showed no signs of corrosion products either in the form of dark or white residues.

Specimen condition prior to autopsy
(Top view)

Duct

Strand

Mild Steel Bars
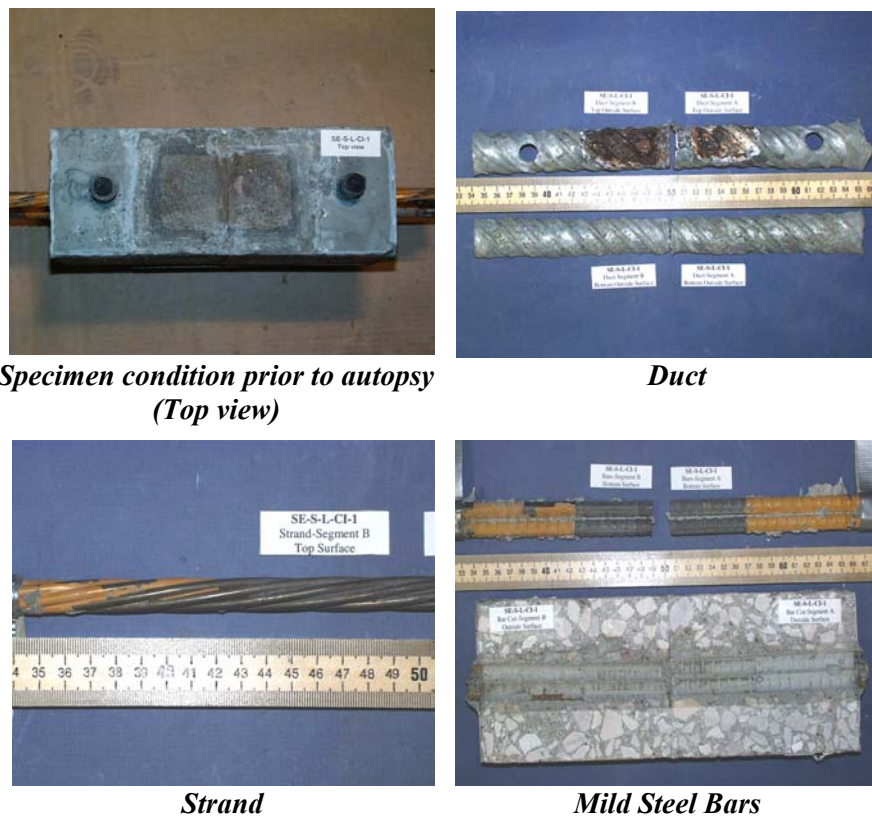
Figure 3.41 Concrete, Duct, Strand and Bar Condition for
Specimen SE-S-L-CI-1

Eleven small voids were found on the top of the grout surface, one of approximately 0.05 in.^{2} was deep enough to expose the strand. The voids appear to have resulted from insufficient grout fluidity.

Corrosion in the strand was very light in the unpainted areas and light in the areas where the epoxy paint had peeled off. The inner wire was more corroded than the outer wires, having light to moderate corrosion in its entire length.

3.3.4.1.14 Specimen SE-S-M-CI-1 (Epoxy Joint, Steel Duct, Medium Precompression, Corrosion Inhibitor in Grout)

The specimen had cracks in the top with a maximum width of 0.040 in. and extending a length of 7 in., centered in the ponded region as shown in Figure 3.42. No cracks were found in the sides and bottom of the specimen.

Corrosion Rating:

Specimen	(2)	(1)
	4.4 yrs	8 yrs
Strand	2	308
Bars	0	29
Duct	114	2445

The galvanized metal duct was severely corroded in its entirety. Holes accounted for 2.85 in.^{2}. The duct was practically consumed in the center section, under the ponded region. The sides had severe corrosion.

The strand showed very severe corrosion in the uncoated areas, especially on the bottom. Under the epoxy, the corrosion was severe and was worse in the top of the strand. The center wire had moderate to severe corrosion in its entirety.

The mild steel bars had only discoloration in the uncoated areas and light corrosion in the coated areas where the epoxy had peeled off.

The match-cast epoxy joint was incompletely filled in the top of the strand cut line, allowing water to penetrate to the duct. The joint had corrosion stains from the duct location up to the top of the specimen as shown in Figure 3.43.

146

Specimen condition prior to autopsy

Duct

(Top view)
Strand
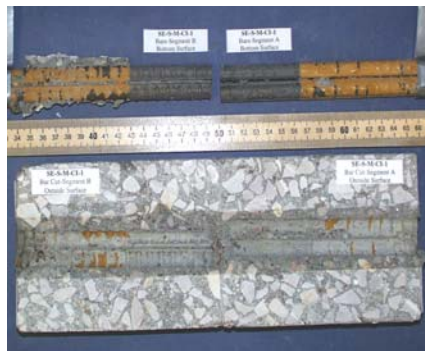
Mild Steel Bars

Figure 3.42 Concrete, Duct, Strand and Bar Condition for Specimen SE-S-M-CI-1

Figure 3.43 Incompletely filled Epoxy Joint (SE-S-M-CI-1)

147

3.3.4.1.15 Specimen SE-S-H-CI-1 (Epoxy Joint, Steel Duct, High Precompression, Corrosion Inhibitor in Grout)

The bottom of the specimen had one 0.010 in. maximum width crack extending two thirds of Segment B, from Face B, as shown in Figure 3.44. No cracks were found on the top and sides of the specimen.

Corrosion Rating:

Specimen	(2)	(1)
	4.4 yrs	8 yrs
Strand	3	78
Bars	1	132
Duct	10	44

After making the strand cut, the epoxy segmental joint came apart easily.

At the duct cut line, severe corrosion was found on the top of the duct in Segment A, centered at 1.75 in. from the joint section, as shown in Figure 3.44. Moderate corrosion and a heavy accumulation of white residue was found on the top of the duct, also centered at 1.75 in. from the epoxy segmental joint. No corrosion was found in the bottom of the duct.

Severe corrosion and pitting, and severe section loss, was found in the mild steel bars in Segment B, in the coated and uncoated areas. Light to moderate corrosion was found in the mild steel bars in the Segment A.

Strand corrosion was light in the outer wires with epoxy coat. In the uncoated areas, the wires showed only discoloration. The inner wire had light corrosion in its entirety.

148

Specimen condition prior to autopsy
(Bottom view)
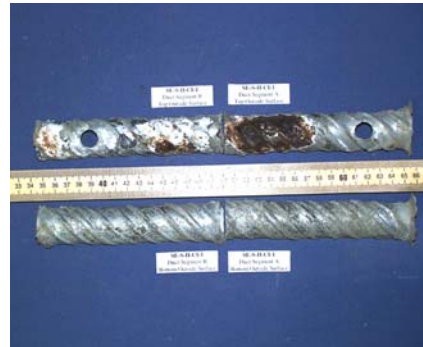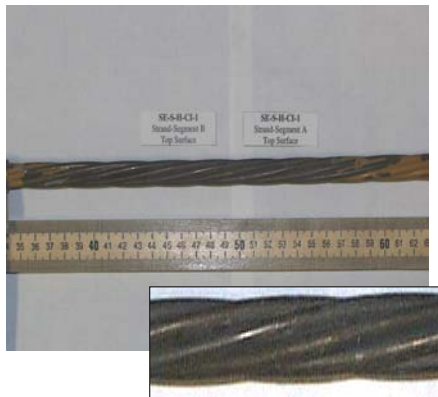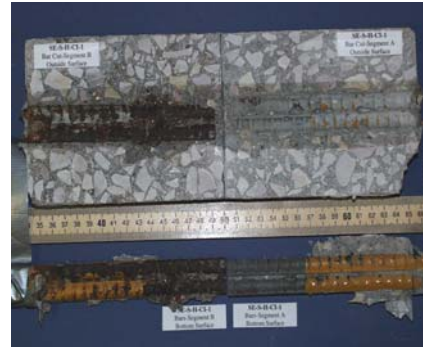
Duct

Strand

Mild Steel Bars

Figure 3.44 Concrete, Duct, Strand and Bar Condition for
Specimen SE-S-H-CI-1

3.3.4.1.16 Specimen SE-S-L-SF-1 (Epoxy Joint, Steel Duct, Low Precompression, Silica Fume added to Grout)

The concrete specimen had a crack in the top, with an approximately maximum width of 0.02 in. No cracks were visible in the sides or bottom of the specimen as shown in Figure 3.45.

The epoxy segmental joint separated easily after unloading the specimen, indicating lack of adequate bonding with the concrete surface. However, corrosion stains were found on the surface.

Corrosion Rating:

Specimen	(2)	(1)
	4.4 yrs	8 yrs
Strand	3	88
Bars	1	13
Duct	10	591

Severe corrosion was found in the top of the duct, between the location of the grout vents. The most severe corrosion was centered at 1.75 in. from the epoxy joint towards Face B. Centered at this location, a large hole of approximately 0.62 in.^{2} was found. Another small hole of approximately 0.0023 in.^{2} was found in Segment A next to the joint section and another of similar size at 1.20 in. from the joint. Moderate to light corrosion, mixed with white residue, was found in the bottom of the duct, mainly in Segment B, and centered at 1.20 in. from the joint.

The concrete surface against the bottom of the galvanized metal duct had several small round shallow voids.

The grout had a very porous structure, with many micro voids.

The strand had discoloration in the uncoated areas and light corrosion in the outer epoxy coated wires. The inner wire had light corrosion with a small area of moderate corrosion.

No corrosion was found on the mild steel bars in the uncoated areas. Discoloration and light corrosion was found in few areas where the epoxy coating had peeled off.

Specimen condition prior to autopsy
(Top view)

Duct

Strand

Mild Steel Bars

Figure 3.45 Concrete, Duct, Strand and Bar Condition for
Specimen SE-S-L-SF-1

3.3.4.1.17 Specimen EG-S-L-NG-1 (Epoxy Joint with Gasket, Steel Duct, Low Precompression, Normal Grout)

Corrosion in the galvanized metal duct produced a 0.020 in. maximum width longitudinal crack in the top of the specimen, 5.5 in. in length, and two additional hairline cracks of 1.2 in. and 2

Corrosion Rating:

Specimen	(2)	(1)
	4.4 yrs	8 yrs
Strand	2	88
Bars	0	25
Duct	54	1096

151

in. respectively in the top of Segment B at the border of the ponded region and extending to the sides, as shown in Figure 3.46.   No cracks were found in the sides or bottom of the specimen.
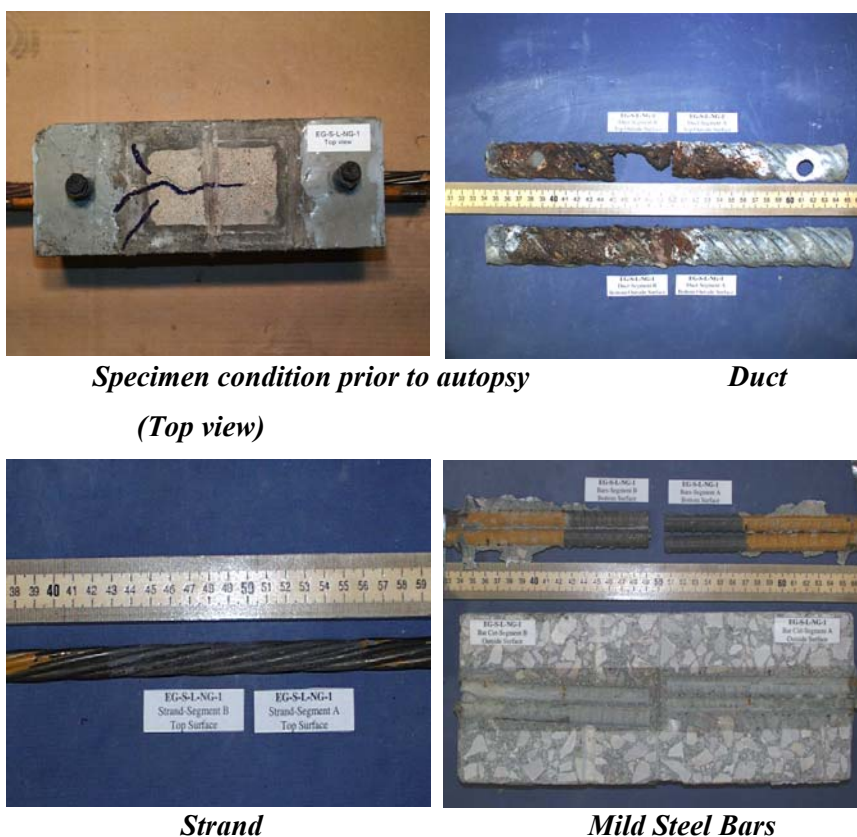
Specimen condition prior to autopsy   ***Duct***

(Top view)

Strand   ***Mild Steel Bars***

Figure 3.46 Concrete, Duct, Strand and Bar Condition for
Specimen EG-S-L-NG-1

The epoxy segmental joint was intact with no signs of moisture, salt or rust penetration. Examination of three sections through the joint showed it to be completely filled with epoxy and free from voids or cracks.

Severe corrosion was found in the top and bottom of the duct in segment B, and in half of the length in the top of the duct in Segment A, starting from the joint section.   The heaviest corrosion was found at 1.75 in. from the joint in

Segment B and at 1.40 in. from the joint in Segment A, corresponding to the holes found on each side of 1.33 in^2 and 0.030 in.^{2}, respectively. The corrosion products included black spots with moisture. No voids were found on the grout.

The outer wires of the strand had discoloration in the uncoated areas and light corrosion in those areas where the epoxy coating had peeled off. The inner wire had light corrosion in its entirety. Inside the duct, the strand was positioned at the bottom on Segment B and on the side on Segment A.

Discoloration was found on the mild steel bars in the unpainted area, and discoloration and light corrosion were the epoxy had peeled off. There was a small area of approximately 0.12 in.^{2} with moderate corrosion in the vicinity of Face B.

3.3.4.1.18 Specimen EG-S-M-NG-1 (Epoxy Joint with Gasket, Steel Duct, Medium Precompression, Normal Grout)

A 0.010 in. maximum width crack was at the top of the concrete specimen, extending 3 in. from the epoxy segmental joint towards face A as shown in Figure 3.48. No cracks or corrosion signs were found on the sides or bottom of the specimen.

Corrosion Rating:

Specimen	(2)	(1)
	4.4 yrs	8 yrs
Strand	23	90
Bars	0	31
Duct	237	198

The top portion of the specimen above the strand cut line separated at the joint during autopsy. The gasket appears to have prevented complete bonding of the segments. Around the gasket there were signs of moisture, salt and rust stains. The incomplete epoxy coverage is shown in Figure 3.47.

Severe corrosion was found on the top of the duct, mainly in Segment A, as shown in Figure 3.48. The corrosion products were black, dark green and typical dark orange, mixed with white residue. The most severe corrosion was

153

centered at 1.6 in. from the joint towards Face A.   Centered at this point there were three small holes of 0.040 in.[2] each in the duct.   Corrosion products were in the form of flakes or very thin layers.

Figure 3.47 Incomplete Epoxy Coverage in Epoxy/Gasket Joint (EG-S-M-NG-1)
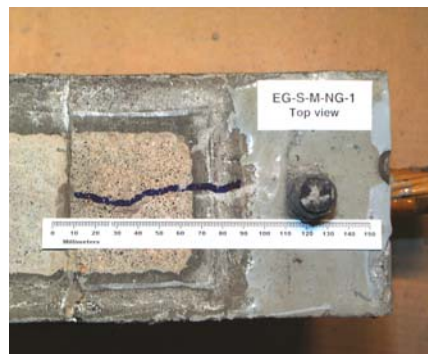
Specimen condition prior to autopsy (Top view)
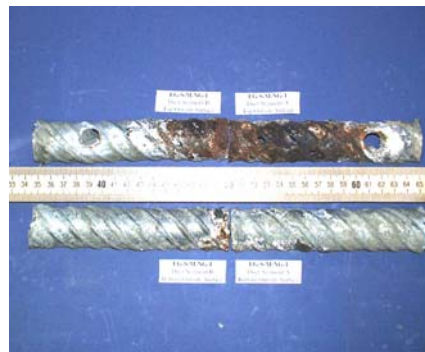
Duct

Strand

Mild Steel Bars

Figure 3.48 Concrete, Duct, Strand and Bar Condition for Specimen EG-S-M-NG-1

Discoloration was found on the outer wires of the strand, in the unpainted (uncoated) region. Light corrosion was found on the areas where the epoxy had peeled off. The inner wire had light corrosion.

Mild steel bars had minor discoloration under the ponded region (uncoated areas) and light corrosion in those areas where the epoxy coating had peeled off.

3.3.4.1.19 Specimen EG-S-H-NG-1 (Epoxy Join with Gasket, Steel Duct, High Precompression, Normal Grout)

No cracks were found on the top, sides or bottom of the specimen as shown in Figure 3.50.

Similar to specimen EG-S-M-NG-1, the side and bottom perimeter of the joint were intact and appeared to be filled with epoxy, but thin voids were visible at the joint on the top surface of

Corrosion Rating:

Specimen	(2)	(1)
	4.4 yrs	8 yrs
Strand	16	84
Bars	1	34
Duct	78	131

the specimen. Sections through the joint at the mid-height and bar and strand cut lines showed it to be completely filled with epoxy and free from voids or cracks. However, the gasket again appears to have prevented complete bonding of the segments immediately above the duct opening. Salt penetration and rust stains were visible on the joint as shown in Figure 3.49.   Similar results were obtained during autopsy performed at four and a half years of exposure, to the duplicate specimens EG-S-M-NG-2 and EG-S-H-NG-2[3.8].

The top of the duct had severe corrosion in Segments A and B, centered in each side at 1.60 in. from the epoxy joint with gasket, as shown in Figure 3.50. Holes in Segment A had 0.016 mm^2, same as the holes in Segment B. Corrosion products were very dark in color and there was one dark green spot close to the hole in Segment B.   The duct bottom had light to moderate corrosion

extending a few millimeters from the joint section at each side, as seen in Figure 3.50. White residue was present around all the corroded areas.

Figure 3.49 Incomplete Epoxy Coverage in Epoxy/Gasket Joint (EG-S-H-NG-1)

Specimen condition prior to autopsy (Top view)

Duct

Strand
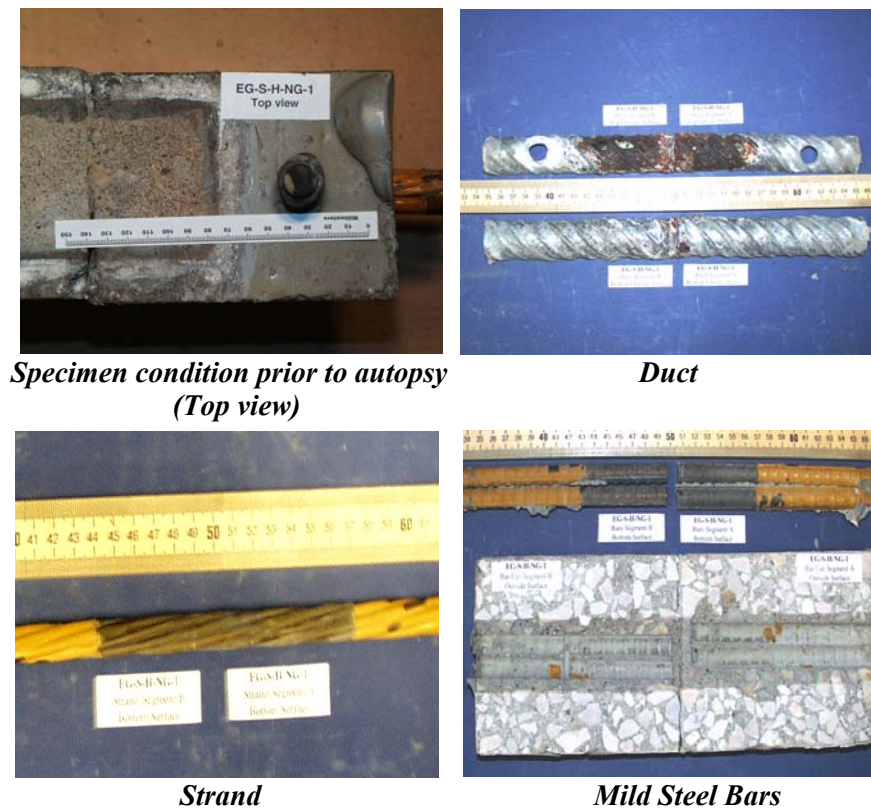
Mild Steel Bars

Figure 3.50 Concrete, Duct, Strand and Bar Condition for Specimen EG-S-H-NG-1

156

The strand had only discoloration in the unpainted section – for the outer and inner wires-, and light corrosion where the epoxy coating had peeled off.

Mild steel bars had discoloration and light corrosion in the unpainted areas and light corrosion where the epoxy coating had peeled off.

3.3.4.2   *Corrosion Rating Summary*

Strand, bar and duct corrosion ratings for all specimens are listed in Tables 3.17 and 3.18, and plotted in Figure 3.51 through Figure 3.53. Results from the autopsy performed at four and a half years of testing are included as a reference. Average, standard deviation and median values are listed at the bottom of the tables.

In order to put the corrosion ratings in perspective, a "Threshold of Concern" was assigned at the corrosion rating of 50 for the strands, bars and ducts. This threshold is used to indicate corrosion related deterioration deemed severe enough to warrant concern. In general, corrosion ratings greater than 50 corresponded to pitting corrosion for strands and bars, and holes in the galvanized steel duct caused by corrosion.

After four years and five months of exposure (Table 3.16), Specimen DJ-S-L-CI-1 had the most severe strand corrosion, with a strand corrosion rating of 114 compared to the average of 19.5 and median of 12. This was the only specimen with a strand corrosion rating greater than 50. Specimen DJ-S-H-NG-1 had the most severe mild steel reinforcement corrosion with a rating of 60 compared to the average of 9.1 and median of 1. This specimen was the only one with a bar corrosion rating greater than 50. Specimen DJ-S-L-NG-1 had the worst duct corrosion with a rating of 528 compared to the average of 122.9 and median of 79. In each case, the specimen with the largest corrosion rating was several times higher than the average and median values.

157

After eight years of aggressive exposure (Table 3.17), specimen DJ-S-M-NG-2 had the most severe strand corrosion with a corrosion rating of 780, followed by Specimen DJ-S-L-NG-2 with a corrosion rating of 612, both compared to the average of 164.8 and the median of 88. All specimens had strand corrosion ratings higher than the value of 50 that was chosen as the threshold of concern. Specimen SE-S-M-CI-1, in spite of being an epoxy jointed specimen, had high duct, strand and mild steel corrosion ratings of 305, 132 and 2445, respectively, when compared to the median values of 88, 29 and 268. Autopsy results for this specimen showed inadequate epoxy filling at the joint.

Table 3.16 Corrosion Ratings for Specimens Autopsied after 4.4 Years of Exposure[3.8]

Specimen Name	Corrosion Rating		
	Strand	Bars	Duct
DJ-S-L-NG-1	26	12	528
DJ-S-M-NG-1	43	12	325
DJ-S-H-NG-1	38	60	64
DJ-P-L-NG-1	6	17	0
DJ-P-M-NG-1	9	24	0
DJ-S-L-CI-1	114	4	42
DJ-S-M-CI-1	24	20	151
SE-S-L-NG-2	13	6	22
SE-S-M-NG-2	2	16	61
SE-S-H-NG-2	3	0	8
SE-P-L-NG-2	5	0	0
SE-P-M-NG-2	6	0	0
SE-S-L-CI-2	24	0	85
SE-S-M-CI-2	2	0	114
SE-S-H-CI-2	3	1	10
SE-S-L-SF-2	12	0	12
EG-S-L-NG-2	2	0	54
EG-S-M-NG-2	23	0	237
EG-S-H-NG-2	16	1	78
Average	19.5	9.1	94.3
Std. Dev.	25.3	14.3	132.6
Median	12	1	54

Specimen DJ-S-H-NG-2 had the most severe mild steel corrosion, with a corrosion rating of 606, followed by specimen DJ-P-L-NG-2, with a corrosion rating of 201. The average value and median values for mild steel corrosion were 75.6 and 29, respectively. Fourteen specimens out of the nineteen specimens had negligible bar corrosion, below the value of 50. Specimen DJ-S-L-NG-2 had the worst duct corrosion, with a corrosion rating of 15779 compared to the average value of 1369.1 and the median of 268. This specimen was followed by specimens DJ-S-M-NG-2 and SE-S-M-CI-1, with duct corrosion ratings of 3054 and 2445 respectively. These values show that duct corrosion was extremely severe in a number of specimens, which is in agreement with the extremely large destruction of galvanized duct observed during the autopsy process and reported in Section 3.3.4.

Table 3.17 Corrosion Ratings for Specimens Autopsied after 8 Years of Exposure

Specimen Name	Strand	Corrosion Rating Bars	Duct
DJ-S-L-NG-2	612	54	15,779
DJ-S-M-NG-2	780	44	3,054
DJ-S-H-NG-2	137	606	361
DJ-P-L-NG-2	116	201	0
DJ-P-M-NG-2	80	77	0
DJ-S-L-CI-2	86	22	674
DJ-S-M-CI-2	54	27	346
SE-S-L-NG-1	64	26	167
SE-S-M-NG-1	119	41	732
SE-S-H-NG-1	88	29	268
SE-P-L-NG-1	80	0	0
SE-P-M-NG-1	88	18	0
SE-S-L-CI-1	95	28	126
SE-S-M-CI-1	305	29	2,445
SE-S-H-CI-1	78	132	44
SE-S-L-SF-1	88	13	591
EG-S-L-NG-1	88	25	1,096
EG-S-M-NG-1	90	31	198
EG-S-H-NG-1	84	34	131
Average	164.8	75.6	1369.1
Std. Dev.	196.4	136.7	3587.3
Median	88	29	268
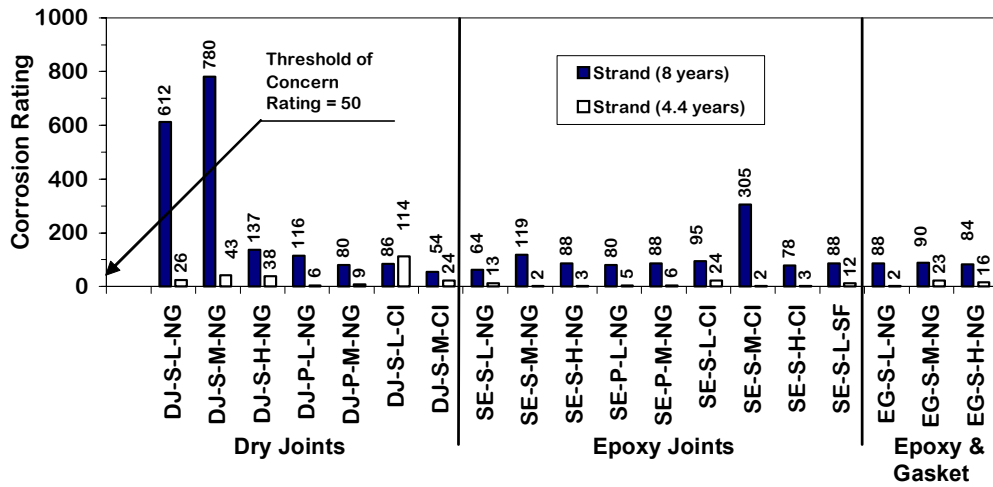
Figure 3.51 Strand Corrosion Ratings for All Specimens
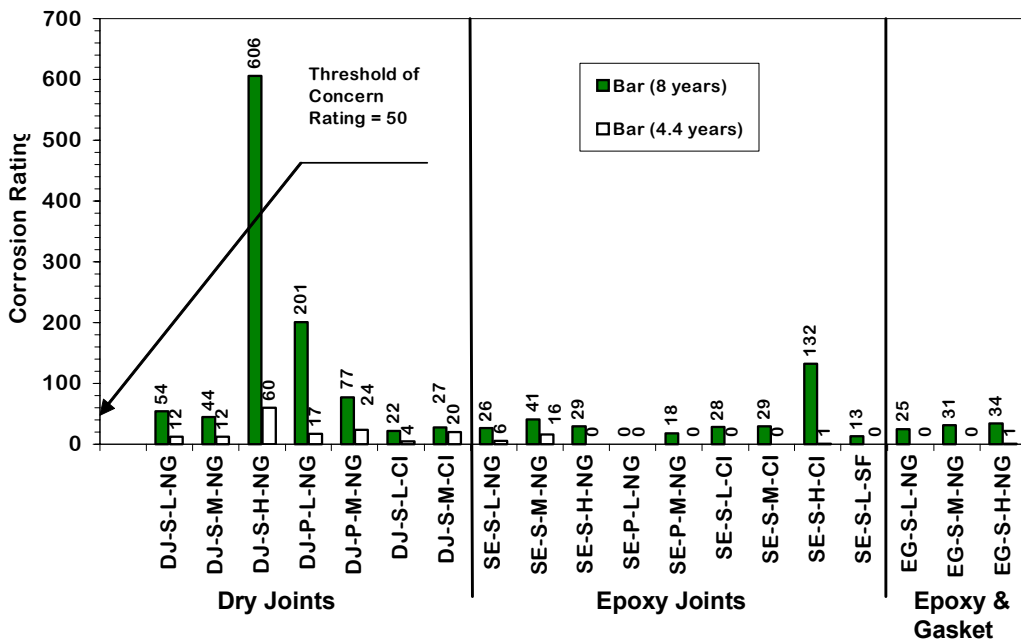
Figure 3.52 Mild Steel Bar Corrosion Ratings for All Specimens

160
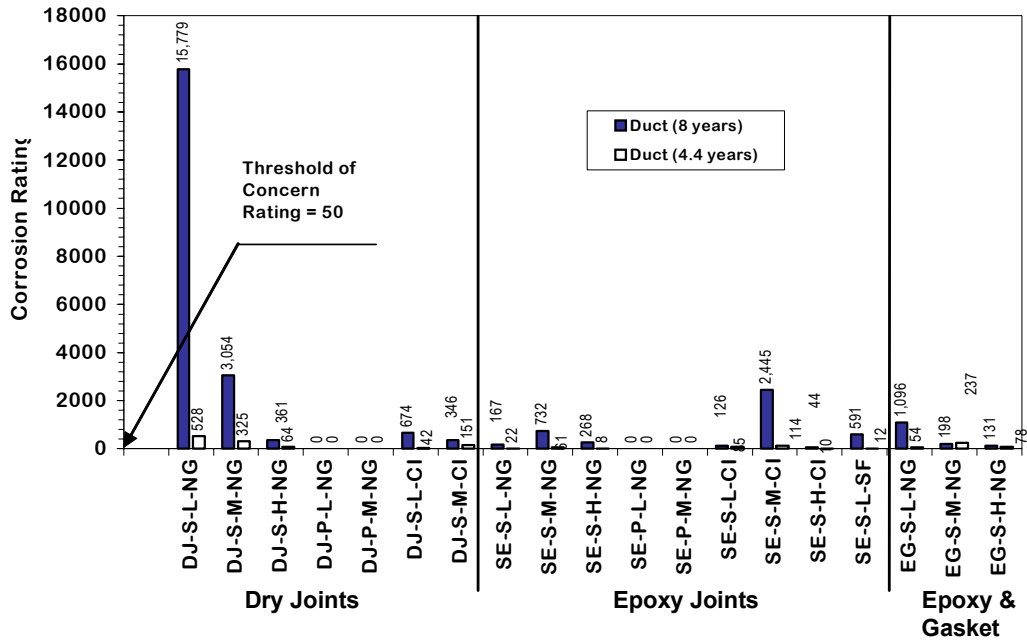
Figure 3.53 Duct Corrosion Ratings for All Specimens

3.3.4.3   Chloride Analysis

Concrete powder samples were collected from six dry joint specimens and four epoxy joint specimens for chloride analysis, following the procedure described in Section 3.3.1.2. In addition, samples were collected from the grout in these specimens for chloride analysis. Concrete chloride ion profiles for these 10 specimens are shown in Figure 3.54 through Figure 3.63. Values plotted in the figures are acid soluble chloride levels, expressed as a percentage of concrete weight. The chloride threshold for corrosion is indicated in the figures at 0.033%. This value, intended as a guide only, is based on the widely accepted chloride threshold value of 0.2% of the weight of cement.[3.18]   The same data has been rearranged in Figure 3.64 through Figure 3.67, to better compare the specimen chloride levels at the same depths.   Data for specimen DJ-S-L-NG-2, at 0.5 in.

from the joint, is not shown in the above mentioned figures, since the advanced cracking in the specimen did not allowed for the extraction of representative samples at the various depths.

Chloride Content analysis shows that in general under the area where the ponded region was located, there is a significant decrease in the level of chlorides with increasing depths, being more considerable in all four epoxy joint specimens analyzed, including the epoxy joint specimen with gasket.

Dry joint specimens showed significantly higher chloride contents adjacent to the joint in comparison to measurements away from the joint. This trend was also observed in the epoxy joint specimens but at a much lower scale, especially at higher depths.

Dry Joint specimens in the proximity of the joint showed chloride contents well above the corrosion threshold, over the depth of the specimen. At 2 in. from the joint, also under the ponded region, these specimens showed very high chloride contents, except for specimen DJ-S-L-CI-2 that showed low contents below the level of 3 in. At 4.25 in. from the joint, away from the ponded region, the dry joint specimen DJ-S-L-NG-2, showed very high corrosion levels at all depths.

Epoxy joint specimens showed a different pattern with respect to dry joint specimens. Under the ponded region these specimens showed very high chloride levels above the strand level, but below this depth, chloride levels were below the threshold value. Away from the joint, at 4.25 in., the chloride levels were negligible in specimen SE-S-L-NG-1, at all four depths analyzed.

The epoxy joint specimen with gasket, EG-S-L-NG-1, showed a very similar pattern in the proximity of the joint, as those epoxy joint specimens without gasket. However, at 2 in. away from the joint this specimen still showed

high chloride contents at a depth of 3 in., although below this depth the chloride content decreased considerably.

In general, no distinct trend was observed in all specimens with respect to different levels of precompression.

The chloride profile for specimens DJ-S-H-NG-2, DJ-P-L-NG-2, DJ-S-M-CI-2, and SE-S-H-NG-1   exhibit a discontinuity in the measurements at 2 in. away from the joint, as shown in Figures 3.55 through 3.57, 3.59 and 3.62. Chloride measurements decrease at mid-height of the specimen, and increase at the level of the mild steel bars. This discontinuity is also observed in specimen DJ-S-L-CI-2 adjacent to the joint, as shown in Figure 3.62.   After careful analysis of the possible reasons for this behavior, it was found that saltwater leakage from the ponded area ran down the exterior of the specimens to the bottom where it must have entered the concrete. For the epoxy joint specimen, the top surface and sides are sealed with epoxy according to ASTM G109[3.5] requirements, while the bottom is not. This mechanism is common in bridges, and the epoxy sealant on the top and sides would amplify the effect leading to increased chloride levels near the bottom surface. In dry joint specimens, the saltwater also penetrates the joint and deposits in the bottom area.
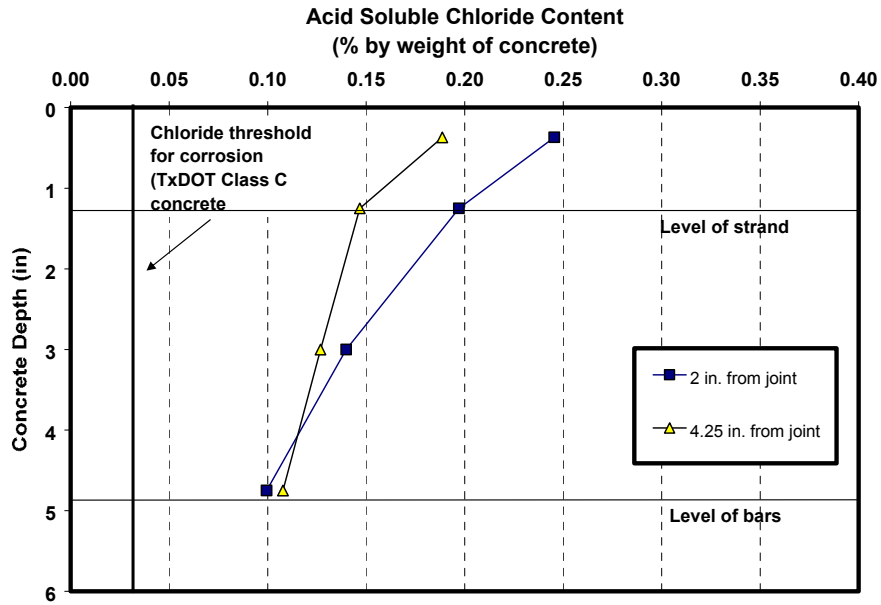
Figure 3.54 Concrete Chloride Ion Profiles for Specimen DJ-S-l-NG-2
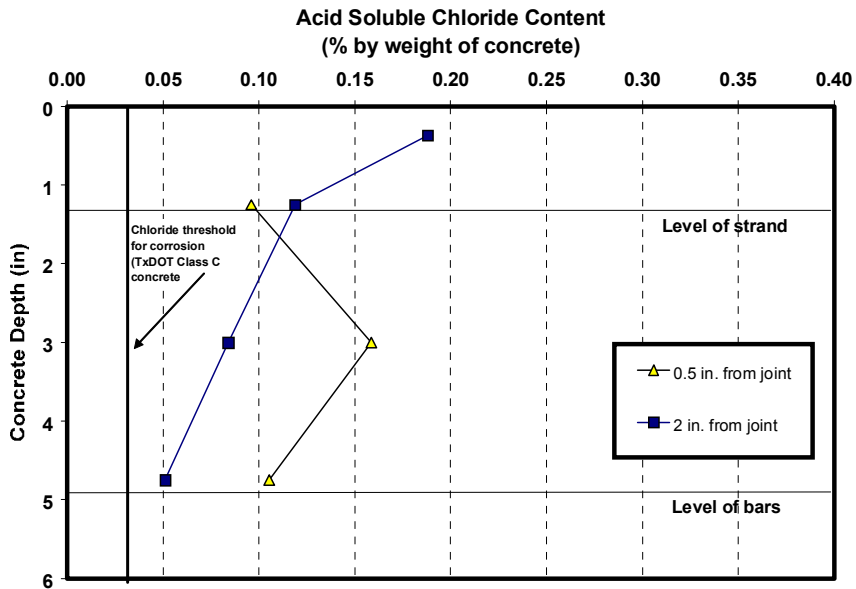
Figure 3.55 Concrete Chloride Ion Profiles for Specimen DJ-S-M-NG-2

164
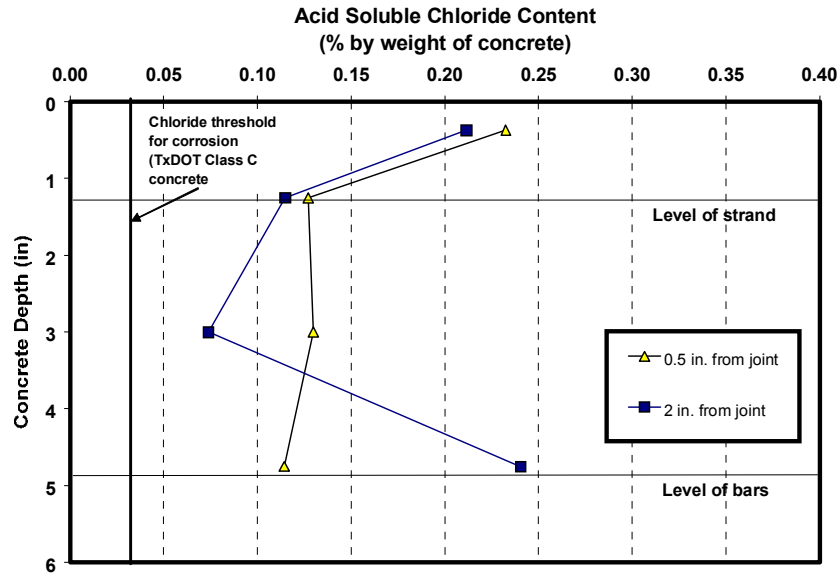
Figure 3.56 Concrete Chloride Ion Profiles for Specimen DJ-S-H-NG-2
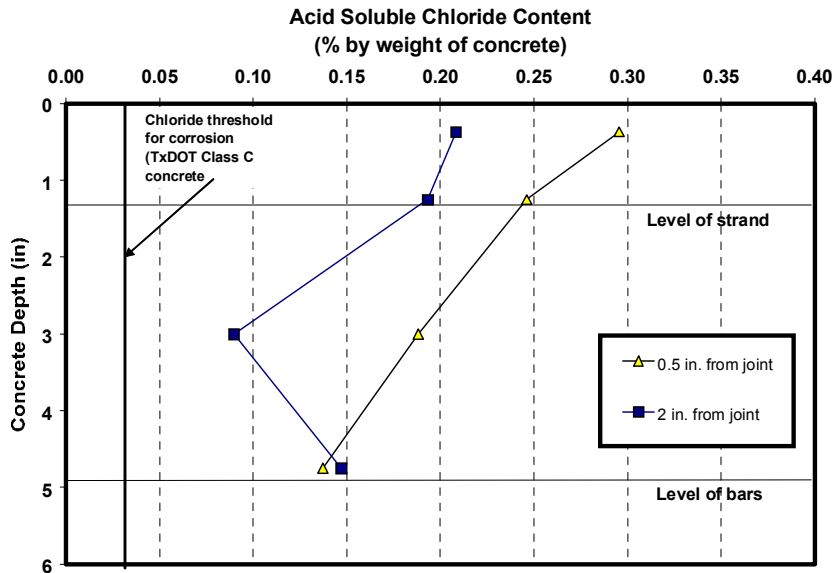
Figure 3.57 Concrete Chloride Ion Profiles for Specimen DJ-P-L-NG-2

165
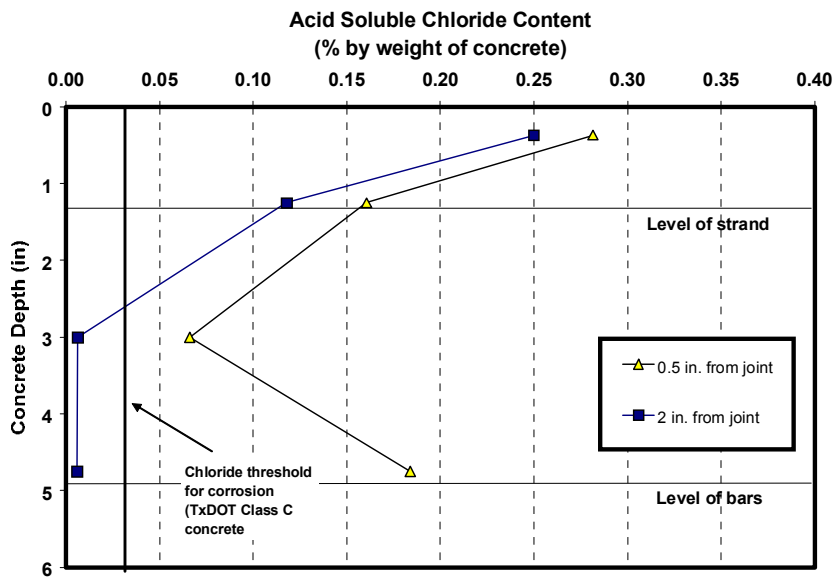
Figure 3.58 Concrete Chloride Ion Profiles for Specimen DJ-S-L-CI-2
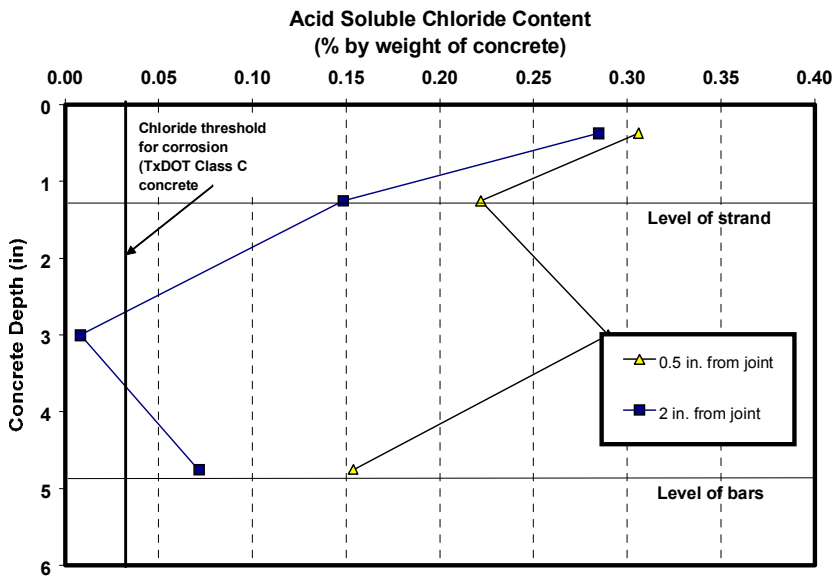
Figure 3.59 Concrete Chloride Ion Profiles for Specimen DJ-S-M-CI-2

166
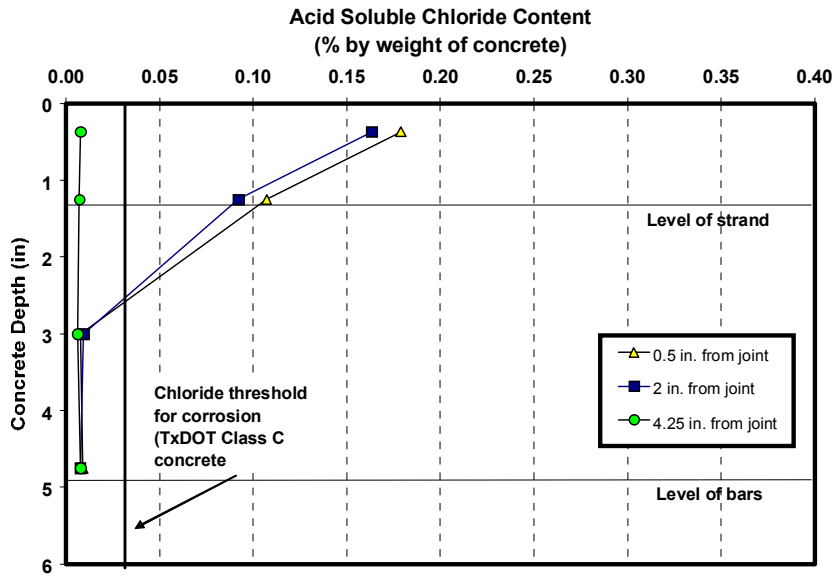
Figure 3.60 Concrete Chloride Ion Profiles for Specimen SE-S-L-NG-1
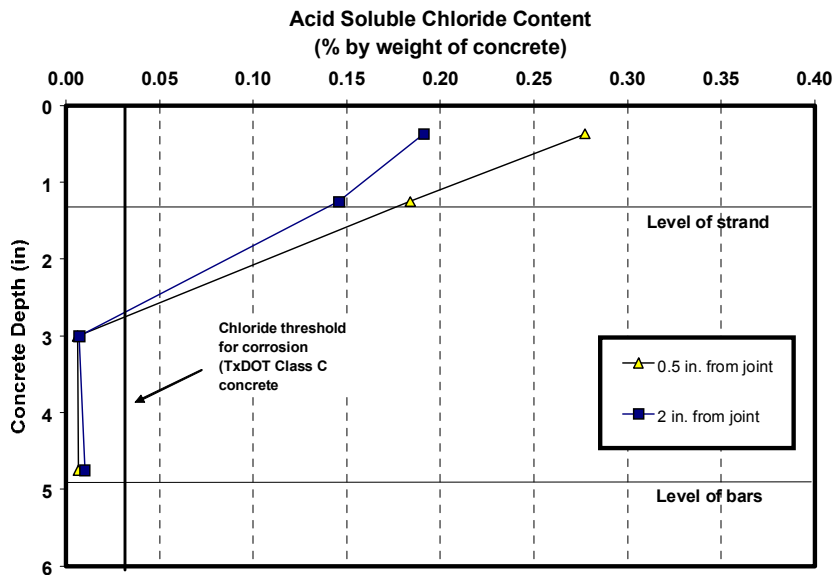
Figure 3.61 Concrete Chloride Ion Profiles for Specimen SE-S-M-NG-1

167
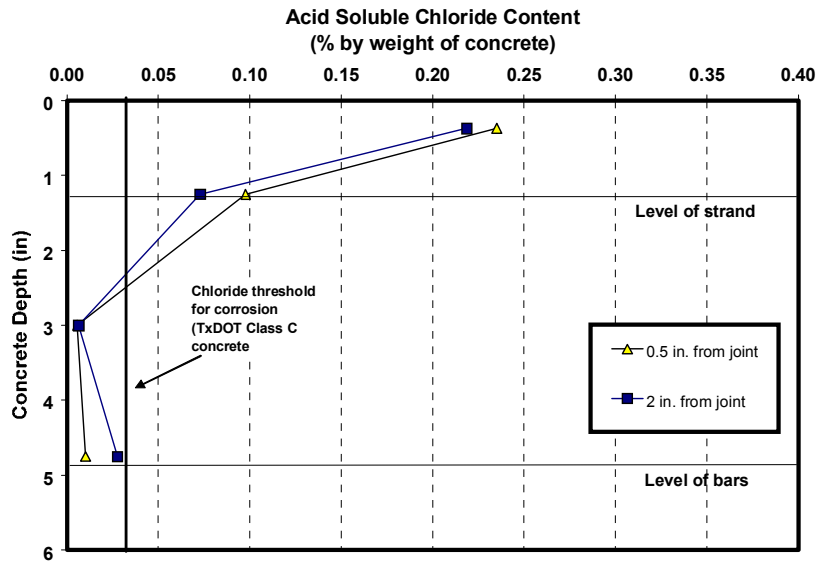
Figure 3.62 Concrete Chloride Ion Profiles for Specimen SE-S-H-NG-1
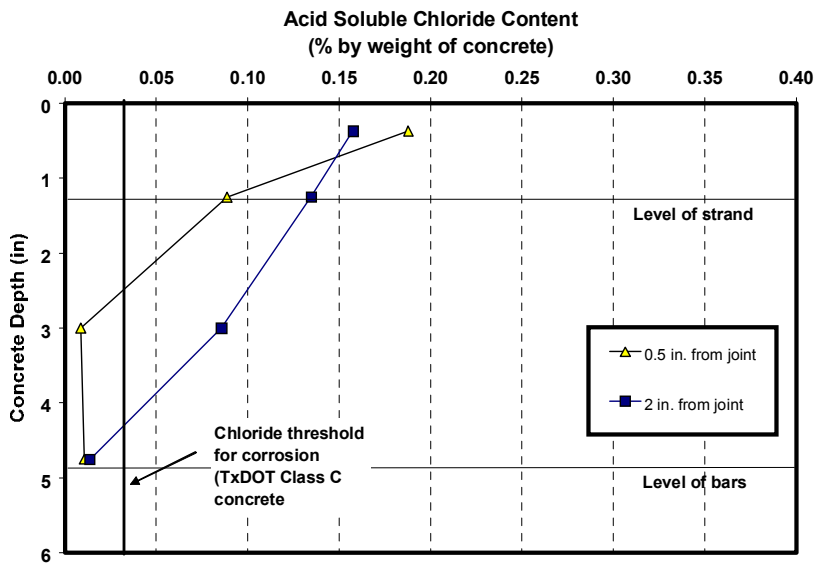
Figure 3.63 Concrete Chloride Ion Profiles for Specimen EG-S-L-NG-1

168
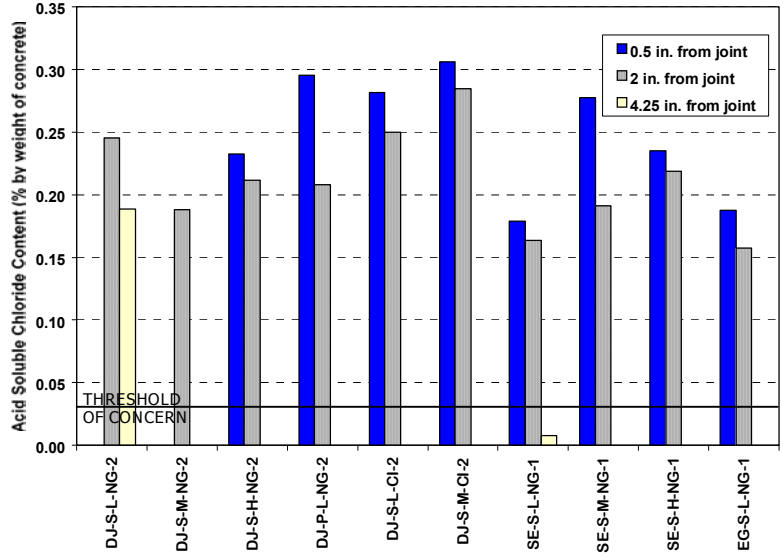
Figure 3.64 Acid Soluble Chloride Content at 0.5 in. depth
(Refer to Figure 3.17)
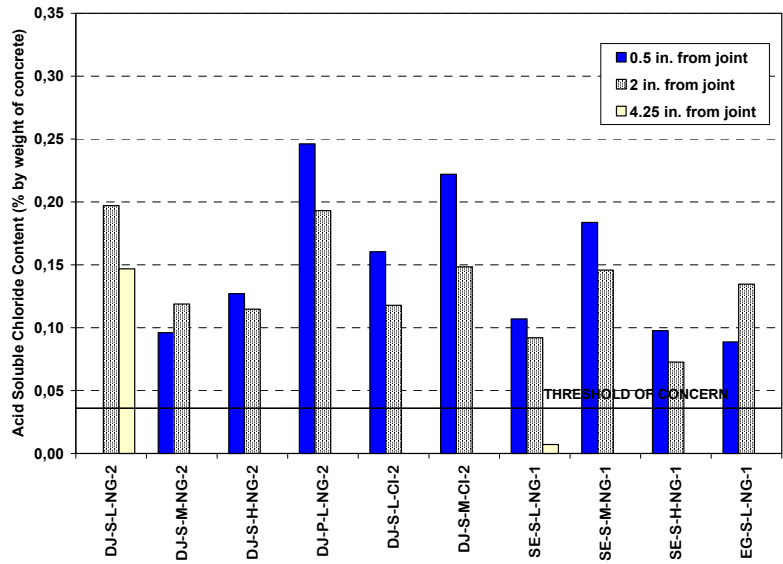
Figure 3.65 Acid Soluble Chloride Content at 1.25 in. depth
-Strand Level – (Refer to Figure 3.17)
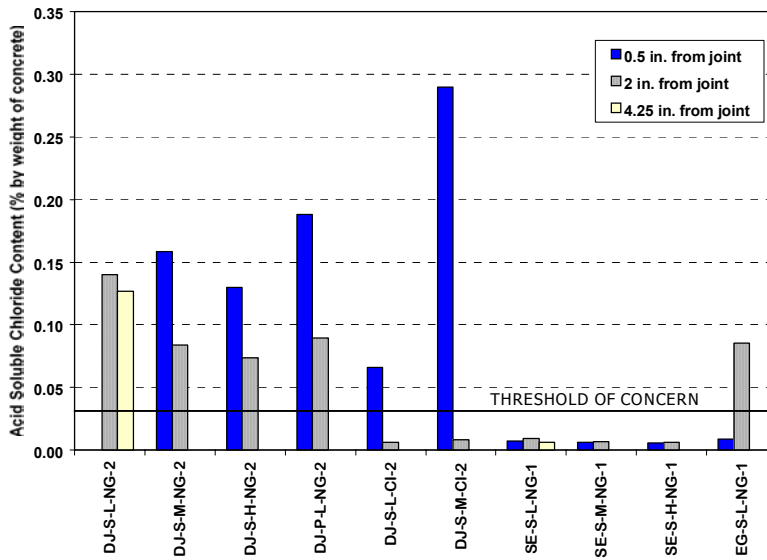
Figure 3.66 Acid Soluble Chloride Content at 3 in. depth
(Refer to Figure 3.17)
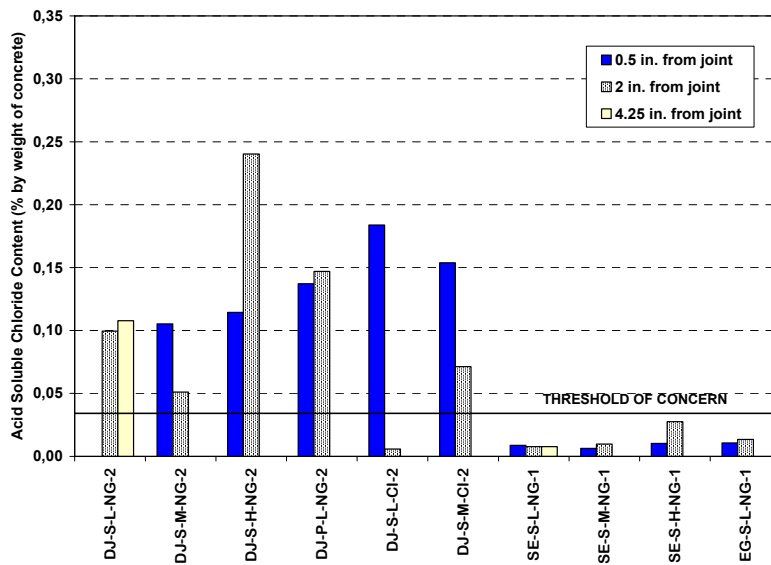
Figure 3.67 Acid Soluble Chloride Content at 4.75 in. depth
- Bar Level – (Refer to Figure 3.17)

170

The results of the chloride analysis on grout samples are shown in Figure 3.68. The values are plotted as acid soluble chlorides, as a percentage of the grout weight. The chloride threshold for corrosion in grout is taken as approximately 0.14%, assuming a chloride threshold of 0.2% by weight of cement and a water cement ratio of 0.44.

The results obtained from the analysis of the grout samples, are summarized as follows:

1. Dry Joint specimens show higher chloride contents at the joint section than at a distance of 2 in. from the joint. Specimen DJ-P-L-NG-2 is the only exception. However, this specimen had a large and deep void at approximately 2 in. from the joint where there was a salt deposit, as described in Section 3.3.4.1.4. The sample for this specimen was taken from this location, which may explain the inconsistency.

2. Dry Joint specimens with Corrosion Inhibitor show a dramatic decrease in the chloride content when comparing the sample taken at the joint with respect to the sample taken at 2 in.

3. Dry Joint specimens show in general higher chloride contents (in the order of 1.5 to 10 times higher) than the corresponding Epoxy Joint specimens.

4. Specimen DJ-S-M-CI-2 shows a very large chloride content at the joint, in the order of two times that for specimen DJ-S-M-NG-2. Since the chloride content was taken at the joint, no real influence of the grout type is expected. Since there are no other variables involved among these two specimens, the observed trend is unclear.

5. Epoxy Joint specimens show higher chloride content at 2 in. from the joint, corresponding with the most severe corrosion areas and voids in the metal duct. The only exception occurs with specimen SE-S-M-NG-1, where higher chloride content is shown at the joint. However, as it was reported in

Section 3.3.4.1.9, the epoxy in this specimen did not cover the entire face of the joint, leaving small gaps, which may have allowed saltwater to penetrate the joint.

6. Dry joint specimens with Steel Duct, and Normal Grout, show a distinct trend with respect to the level of precompression, having less chloride content with higher levels of precompression. The same trend is observed with Epoxy Joint specimens with Steel Duct, Normal Grout and Low and High Levels of Precompression. The only two exceptions are, specimen DJ-S-M-CI-2, which has higher chloride content than specimen DJ-S-L-CI-2; and, specimen SE-S-M-NG-1, which has higher chloride content than the other Epoxy Joint specimens. The last case is explained following the same reasoning as in 5. above.
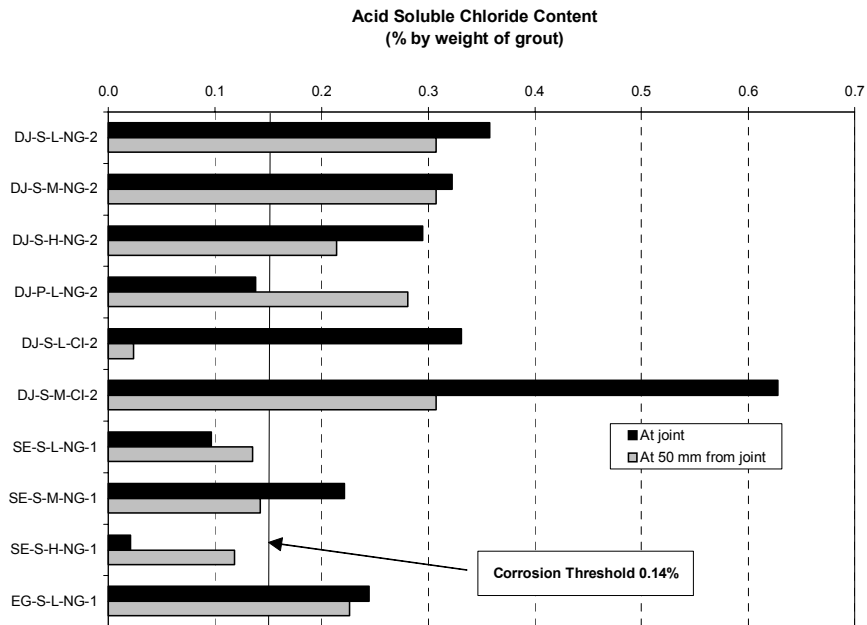
***Figure 3.68 Measured Chloride Contents in Post-tensioning Grout
after about Eight Years of Exposure***

172

3.4   ANALYSIS AND DISCUSSION OF RESULTS

After two forensic examinations, at four and a half years and at eight years of very aggressive exposure, the effect of all variables involved in this testing program can be analyzed and compared.   Findings and conclusions after the autopsy at four and a half years were described in detail in Reference 3.8.   This chapter includes the results after eight years of exposure, comparing them to results from the first forensic examination when appropriate.

3.4.1   Overall Performance

The use of a specimen based on ASTM G109[3.5] in this testing program, modified to examine prestressing tendons in grouted ducts and to simulate segmental ducts, was found to be an excellent method for analyzing relative specimen performance and for evaluating the adequacy of corrosion protection variables.   After eight years of aggressive exposure all specimens have shown strand and mild steel corrosion.   The galvanized steel ducts were severely damaged.

The relative performance of the specimens in this testing program was studied by looking at the corrosion ratings for the prestressing strands, ordered from lowest to highest. Figure 3.69 shows the results at four and a half years and at eight years of exposure.   As can be observed, important changes have occurred between the two autopsy dates. Major of these is the dramatic increase in strand corrosion between the two dates.

While at four and a half years specimen DJ-S-L-CI-1 had the highest strand corrosion rating, suggesting a very poor performance of the Corrosion Inhibitor added to the grout, the duplicated specimen DJ-S-L-CI-2 autopsied after eight years of exposure had a relatively good performance.   Specimen SE-S-M-CI-1 was the only corrosion inhibitor specimen showing a very high strand

173

corrosion rating after eight years. However, this specimen also had a faulty epoxy filling at the joint as illustrated in Figure 3.70. These results suggest that the corrosion inhibitor had a positive effect in limiting the corrosion rate after the onset of corrosion had started.

At the end of eight years of exposure all prestressing strands had experienced a corrosion rating above the value of 50, chosen as the threshold of concern. At four and a half years, only one specimen had exceeded that value.
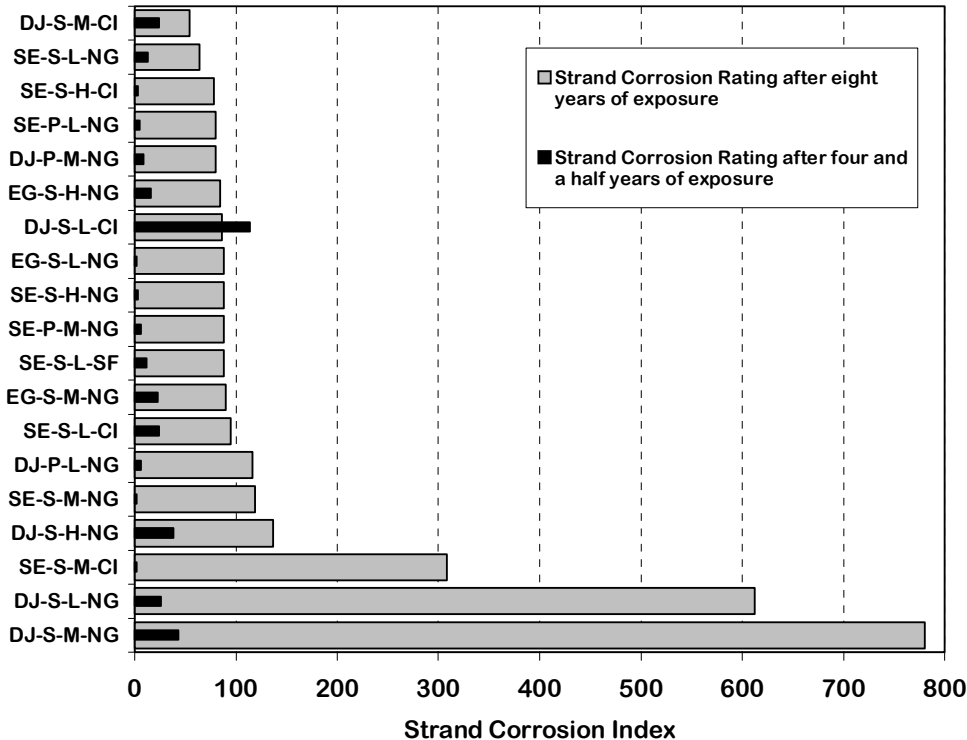
Figure 3.69 Comparison of Corrosion Ratings for Prestressing Strand (after Four Years and Five Months, and Eight Years of Exposure Testing)

174

***Figure 3.70 Top View of the Effect of a Faulty Epoxy Joint (SE-S-M-CI-1)
Compared to a Sound Epoxy Joint (SE-S-L-CI-1)***

The overall performance of the specimens is better compared by considering the total corrosion rating, obtained by summing the ratings for the strand, bars and duct, as shown in Figure 3.71 and Figure 3.72. Comparison between these two figures showed overall corrosion increased dramatically for most specimens between four and a half years and eight years of exposure. After eight years, the best performance was shown in the plastic duct specimens, while the dry joint specimens with steel ducts and normal grout showed the worst performance. The poor performance observed for specimen SE-S-M-CI-1 clearly shows the detrimental effect of faulty epoxy filling at the joint.
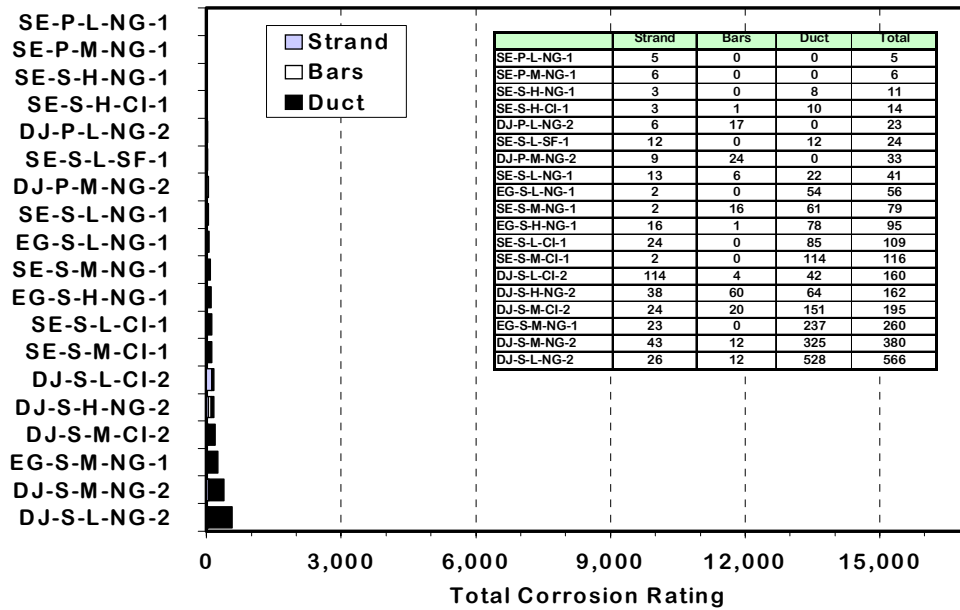
*Figure 3.71 Total Corrosion Rating Ordered According to Performance
(after Four Years and Five Months of Exposure)*

	Strand	Bars	Duct	Total
SE-P-L-NG-1	5	0	0	5
SE-P-M-NG-1	6	0	0	6
SE-S-H-NG-1	3	0	8	11
SE-S-H-CI-1	3	1	10	14
DJ-P-L-NG-2	6	17	0	23
SE-S-L-SF-1	12	0	12	24
DJ-P-M-NG-2	9	24	0	33
SE-S-L-NG-1	13	6	22	41
EG-S-L-NG-1	2	0	54	56
SE-S-M-NG-1	2	16	61	79
EG-S-H-NG-1	16	1	78	95
SE-S-L-CI-1	24	0	85	109
SE-S-M-CI-1	2	0	114	116
DJ-S-L-CI-2	114	4	42	160
DJ-S-H-NG-2	38	60	64	162
DJ-S-M-CI-2	24	20	151	195
EG-S-M-NG-1	23	0	237	260
DJ-S-M-NG-2	43	12	325	380
DJ-S-L-NG-2	26	12	528	566
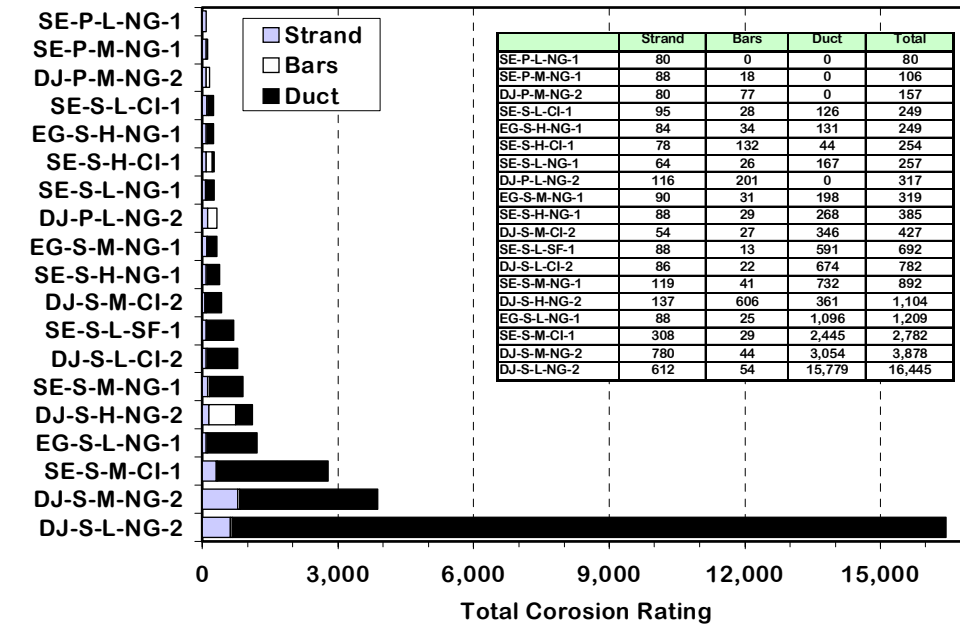
*Figure 3.72 Total Corrosion Rating Ordered According to Performance
(after Eight Years of Exposure)*

	Strand	Bars	Duct	Total
SE-P-L-NG-1	80	0	0	80
SE-P-M-NG-1	88	18	0	106
DJ-P-M-NG-2	80	77	0	157
SE-S-L-CI-1	95	28	126	249
EG-S-H-NG-1	84	34	131	249
SE-S-H-CI-1	78	132	44	254
SE-S-L-NG-1	64	26	167	257
DJ-P-L-NG-2	116	201	0	317
EG-S-M-NG-1	90	31	198	319
SE-S-H-NG-1	88	29	268	385
DJ-S-M-CI-2	54	27	346	427
SE-S-L-SF-1	88	13	591	692
DJ-S-L-CI-2	86	22	674	782
SE-S-M-NG-1	119	41	732	892
DJ-S-H-NG-2	137	606	361	1,104
EG-S-L-NG-1	88	25	1,096	1,209
SE-S-M-CI-1	308	29	2,445	2,782
DJ-S-M-NG-2	780	44	3,054	3,878
DJ-S-L-NG-2	612	54	15,779	16,445

176

3.4.2   Effect of Joint Type

After the eight-year forensic examination, it was determined that the joint type is the variable with the most significant effect on specimen performance. Significantly higher corrosion ratings for the strands, mild steel and galvanized ducts were obtained from dry joint specimens with steel ducts and normal grout. The only epoxy joint specimen showing high strand and duct ratings was the poorly applied epoxy joint specimen SE-S-M-CI-1. The effect of joint type on the measured and observed results is described below.

3.4.2.1   Galvanized Steel Duct Corrosion

Duct corrosion was highly influenced by joint type. Figure 3.73 shows typical corrosion found in galvanized steel ducts in each of four joint types. The specimens have been cut open at the level of the duct, and the photos show the top view of each duct and the corresponding corrosion stains and corrosion products attached to the concrete.   Duct corrosion in dry joint specimens was extremely severe, with a high percentage of metal loss and concrete cracking at the top of the specimen.   Duct corrosion in sound epoxy joint specimens was moderate to severe, with localized section loss extending approximately two inches at each side of the joint, below the ponded region. Cracking was also evident in some epoxy joint specimens when the corrosion had been extensive. Figure 3.73 also shows the damaging effect of the faulty epoxy joint on duct corrosion, corresponding to specimen SE-S-M-CI-1. Epoxy joints with gaskets performed similar to those without gasket, when the epoxy was able to fill the entire joint area during construction. However, as was emphasized, in some cases gaskets prevented the epoxy from adequately filling the joint area, allowing for moisture and chlorides to penetrate the joint.

Dry Joint   *Sound Epoxy joint*

Faulty Epoxy joint   *Epoxy/Gasket Joint*
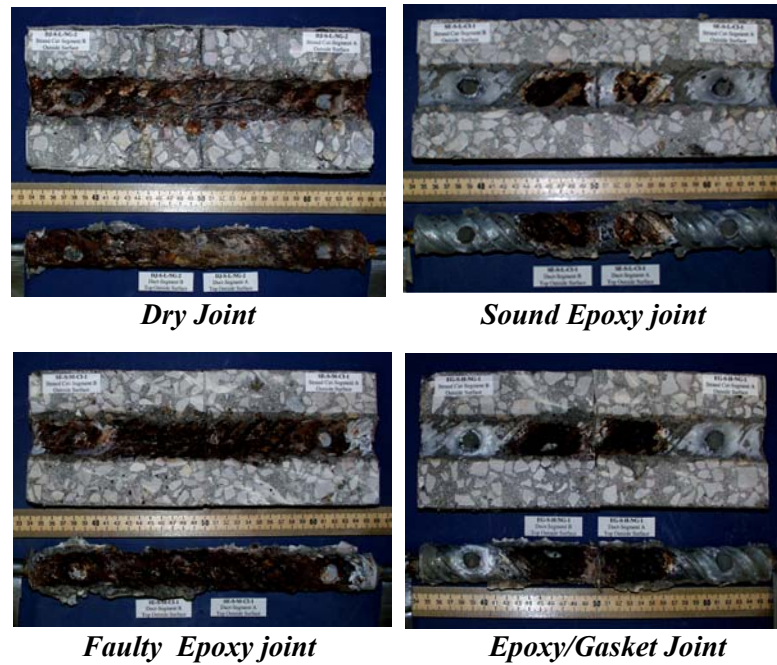
Figure 3.73 Galvanized Steel Duct Corrosion: Effect of Joint Type

The better performance of epoxy joint specimens with respect to dry joint specimens was clearly shown in Figure 3.51. In that figure, the following comparisons can be made: specimen DJ-S-L-NG-2 versus specimen SE-S-L-NG-1, specimen DJ-S-M-NG-2 versus SE-S-M-NG-1, specimen DJ-S-H-NG-2 versus SE-S-H-NG-1; and, specimen DJ-S-L-CI-2 versus SE-S-L-CI-1.

3.4.2.2 *Prestressing Strand Corrosion*

After eight years of exposure, corrosion above the corrosion rating of 50 chosen as the threshold of concern had occurred in all specimens. This means that most strands showed some degree of pitting and section loss. With respect to joint type there is a distinct difference in the strand corrosion. The highest strand corrosion ratings and therefore the largest deterioration was found on dry joint specimens with normal grout and low to medium precompression. These

specimens show very severe strand section loss. The corresponding epoxy joint specimens, with the same duct, precompression force and grout type, showed strand corrosion ratings on the order of eight to ten times smaller.   Other dry joint specimens, either with plastic ducts or with corrosion inhibitor added to the grout showed similar results to the corresponding epoxy joint specimens.   The only difference was observed in the faulty epoxy joint specimen SE-S-M-CI-1, which showed a much higher strand corrosion rating than the corresponding dry joint specimen. In this case, the faulty epoxy joint produced misleading results.

3.4.2.3   Mild Steel Reinforcement Corrosion

Four dry joint specimens (DJ-S-L-NG-2, DJ-S-H-NG-2, DJ-P-L-NG-2 and DJ-P-M-NG-2) and one epoxy joint specimen (SE-S-H-CI-1) showed mild steel corrosion ratings above the threshold value of 50, where there was pitting corrosion and section loss.   The largest mild steel bar deterioration was observed in specimen DJ-S-H-NG-2, whose bar corrosion rating was more than 20 times higher than the corresponding epoxy joint specimen, with same variables.   In general, dry joint specimens showed larger bar deterioration than epoxy joint specimens, except for specimens with improved grouts, where the results were practically the same in all cases.   Epoxy joint specimens with gaskets showed very similar results to those without gaskets in all three cases studied.

3.4.2.4   Chloride Penetration

Measured acid soluble chloride contents in the concrete adjacent to and at two inches from the joint were always higher for all dry joint specimens.   They were in all cases above the threshold value of 0.033% of concrete weight.   These dry joint specimens showed very high chloride contents across the entire face of the concrete adjacent to the joint, but lower chloride contents two inches inside.

179

Salt deposits were observed on the interior of the ducts in the dry joint specimens, clearly indicating that moisture and chlorides had penetrated through the joint.

Epoxy joint specimens had a very similar low chloride content at 0.5 in. and at 2 in. from the joint, suggesting a good performance of the joint. Below the depth of 3 in. (mid-height between the strand and mild steel bars) all epoxy joint specimens without gaskets showed negligible chloride contents. However, the faulty epoxy joint specimen SE-S-M-CI-1 had much higher chloride values for the reasons described previously.

Epoxy joint specimen with gasket EG-S-L-NG-1, showed a very similar pattern in the proximity of the joint as the epoxy joint specimens without gasket. However, at two inches away from the joint this specimen showed high chloride contents at a depth of three inches.

3.4.2.5 Grouting

Grout leaked into the joint region in two of the seven dry joint specimens autopsied at eight years of exposure. During the autopsy at four and a half years, five out of seven dry joint specimens were found with grout leakage through the joint. The extent of the leaks in both autopsies ranged from very minor around the duct opening to almost 80% of the joint face covered with grout. No leakage was found in the standard epoxy joint and epoxy/gasket joint specimens.

3.4.3 Effect of Duct Type

3.4.3.1 Duct Corrosion

Galvanized steel duct corrosion was severe in all seven dry joint specimens, producing longitudinal cracks in the top of the concrete specimen ranging from 0.010 in. to 0.12 in. in width. Dry joint specimens with normal grout and low to medium precompression showed very high steel duct

consumption by corrosion, up to 50% of the total duct area. The six epoxy joint specimens with steel ducts showed cracks in the top of the concrete specimens in all cases, but smaller than those in dry joint specimens, ranging from hairline cracks up to 0.020 in. cracks. The only exception was specimen SE-S-L-CI-1 with no concrete cracking. Specimen SE-S-M-CI-1 showed very severe duct corrosion, similar to specimen DJ-S-M-NG-1, due to the incomplete filling of the match-cast epoxy joint as explained in Section 4.4.1.14 and shown in Figure 3.70. In addition, two out of three Epoxy Joint specimens with gaskets and steel ducts, showed top cracks of 0.010 in. and 0.020 in. in width.

Plastic ducts performed extremely well in all four specimens tested. The two dry joint specimens with plastic ducts showed bottom cracks, below the mild steel, of 0.020 in. and 0.040 in. in width, while the two epoxy joint specimens with plastic ducts did not show any concrete cracking.

As was explained in Reference 3.8, the concrete cover in these specimens was substantially thinner than would be allowed by specifications. This condition contributed to the severe galvanized duct corrosion in such a short period of time. However, the test results indicate the potential corrosion problems when using galvanized ducts in aggressive exposures.   The relative performance of the galvanized and plastic ducts should not be affected by the thin cover. Plastic ducts performed extremely well in spite of the thin cover.

3.4.3.2   *Prestressing Strand Corrosion*

Strand corrosion ratings for dry joint specimens with steel ducts, normal grout and low to medium precompression showed much higher values, in the order of six to nine times, with respect to strand corrosion ratings in specimens with plastic ducts. This trend was not clearly shown in epoxy joint specimens, where strand ratings were much lower overall and were all in the same range.

Strand corrosion with plastic ducts ranged from no corrosion to light corrosion. In galvanized steel ducts, strand corrosion ranged from no corrosion to very severe uniform corrosion and pitting.

3.4.3.3 Reversed Macrocell

Dry Joint specimens with plastic ducts (DJ-P-L-NG-2 and DJ-P-M-NG-2) showed reversed macrocell behavior, while the corresponding specimens with steel duct (DJ-S-L-NG-2 and DJ-S-M-NG-2) showed strand corrosion activity, as it was indicated in Table 3.5. These results were confirmed after forensic examination where it was found that the mild steel bars in these plastic duct specimens were corroding as the primary corrosion area.

Corrosion currents did not indicate corrosion activity for epoxy joint specimens with either plastic ducts or steel ducts, except for specimens SE-S-M-CI-1 and SE-S-H-CI-1.

The results of dry joint specimens clearly show the superiority of plastic ducts in improving strand corrosion protection.

3.4.4 Effect of Joint Precompression

3.4.4.1 Strand and Mild Steel Corrosion

The results with regard to strand and mild steel corrosion did not show any distinct trend with respect to the three levels of joint precompression used in the testing program. The isolated result for dry joint specimen DJ-S-H-NG-2 with respect to specimens DJ-S-L-NG-2 and DJ-S-M-NG-2 in Figure 3.51 and Figure 3.52, indicates that at very high levels of precompression there is an increased level of protection of the strand and mild steel bars.   This result is not clearly shown for epoxy joint specimens with and without gaskets.

182

3.4.4.2 Duct Corrosion

Galvanized steel duct corrosion in dry joint specimens shows a clear trend with respect to the level of precompression. Figure 3.53 compares similar specimens where joint precompression is the only variable (DJ-S-L-NG-2, DJ-S-M-NG-2 and DJ-S-H-NG-2). For these specimens, a higher level of precompression (or prestress) results in significant corrosion rating reduction, and therefore, it improves significantly the duct corrosion protection. The same trend was observed during the autopsy performed at four and a half years of exposure, with the duplicate specimens.[3.8]

The improved duct corrosion protection with higher levels of precompression is also observed when comparing dry joint specimens with corrosion inhibitor added to the grout and when comparing epoxy joint specimens with gaskets.

Duct corrosion levels in epoxy joint specimens do not show any distinct trend with respect to the level of precompression.

Similar results are obtained from the use of a crack rating, defined as the length of the crack in the top of the concrete specimen multiplied by the maximum crack width. This seems a valid comparison since the concrete and clear cover are the same for all specimens. Crack ratings for all autopsied specimens with steel ducts have been plotted along with duct corrosion ratings in Figure 3.74. From these results, it can be seen that crack ratings are generally proportional to duct corrosion ratings.

183
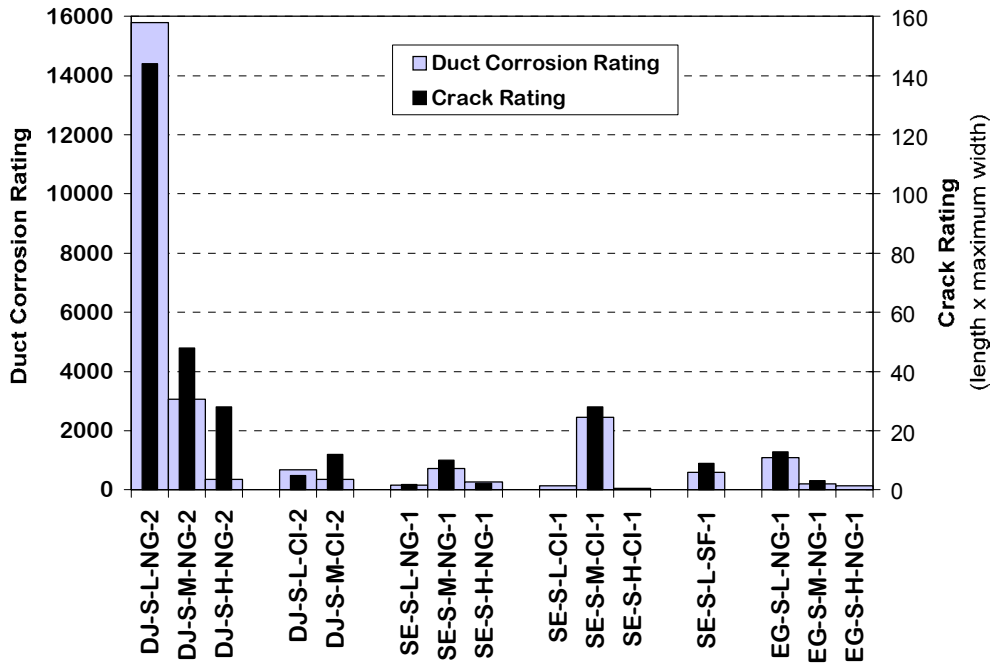
Figure 3.74. Effect of Joint Precompression on Duct Corrosion
(after Eight Years of Exposure Testing)

Proportionality between crack ratings and duct corrosion ratings shown in Figure 3.74 after eight years of exposure, was more evident than after four and a half years of exposure as shown in Figure 3.75.
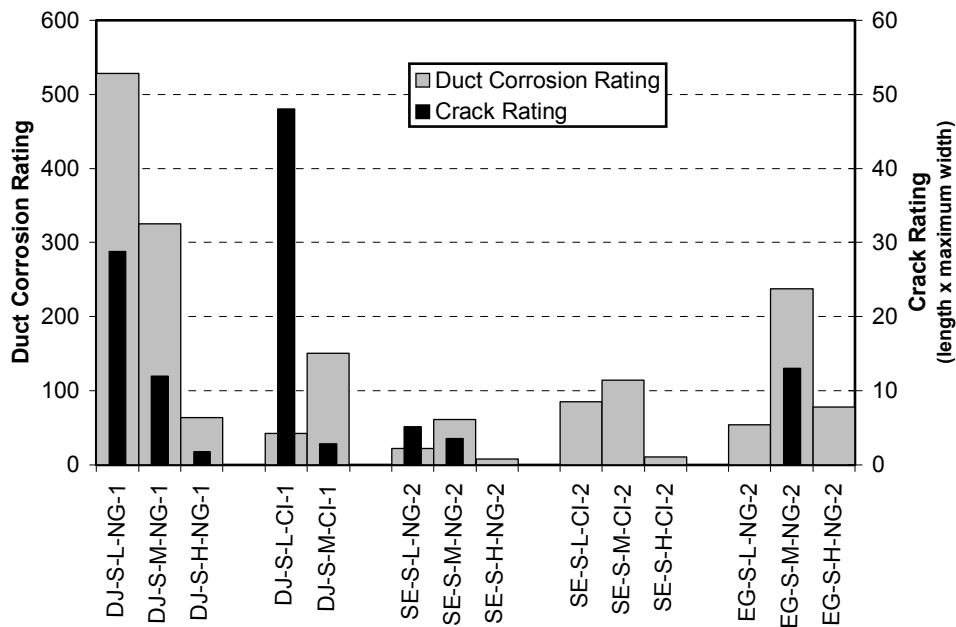
Figure 3.75 Effect of Joint Precompression on Duct Corrosion
(after Four Years of Exposure Testing)[3.8]

3.4.5   Effect of Grout Type

To examine the effect of grout type on strand corrosion severity, similar specimens with grout type as the only variable were grouped as shown in Table 3.18 and Figure 3.76.   From these, a clear trend is observed from dry joint specimens with and without corrosion inhibitor.   Specimens with Corrosion Inhibitor (Calcium Nitrite) added to the grout showed very low strand corrosion ratings when compared to those with normal grout. This trend was also observed from the results based on Macrocell currents and Half-Cell potentials, as included in Table 3.8 and Table 3.9, respectively.

185

Standard Epoxy Joint specimens had much lower corrosion values so that they did not show a distinct trend with the use of normal grout, corrosion inhibitor, silica fume, and low precompression. For these specimens light to moderate corrosion was found, without pitting. Similar results were obtained for standard epoxy joint specimens with high precompression. In this case there was light to negligible corrosion and discoloration. The only exception was found with specimen SE-S-M-CI-1 due to the faulty epoxy joint.

The above results suggest that calcium nitrite corrosion inhibitor was not detrimental with respect to the rate of corrosion. It may even be concluded that it was somewhat effective in counteracting the negative effects of chlorides in strand corrosion. These results contradict the earlier conclusions reached after four and a half years of exposure testing. However, as reported[3.8] these conclusions were based on very limited data available. They also contradict results obtained by Koester[3.19] who reported research performing anodic polarization tests on grouted prestressing strands to investigate the corrosion protection provided by various cement grouts. Koester concluded that calcium nitrite significantly reduced the time to corrosion in comparison to plain grout, and had no effect on corrosion rate after the initiation of corrosion. The calcium nitrite dosage used in that series was adjusted to account for the higher cement content in the grout, a factor that was not adjusted in the series reported herein.

Table 3.18 Effect of Grout Type – Strand Corrosion Ratings

Specimen	Strand Corrosion Rating	Comments
DJ-S-L-NG-2	612	Uniform corrosion extending complete length of strand and pitting.
DJ-S-L-CI-2	86	Light to moderate corrosion.
DJ-S-M-NG-2	780	Severe corrosion and pitting
DJ-S-M-CI-2	54	Light to negligible corrosion. Strand discoloration.
SE-S-L-NG-1	64	Light to moderate corrosion
SE-S-L-CI-1	95	Light to moderate corrosion
SE-S-L-SF-1	88	Light to moderate corrosion
SE-S-M-NG-1	119	Moderate to severe corrosion.
SE-S-M-CI-1	305	Moderate to severe corrosion.
SE-S-H-NG-1	88	Light to negligible corrosion. Strand discoloration.
SE-S-H-CI-1	78	Light to negligible corrosion. Strand discoloration.
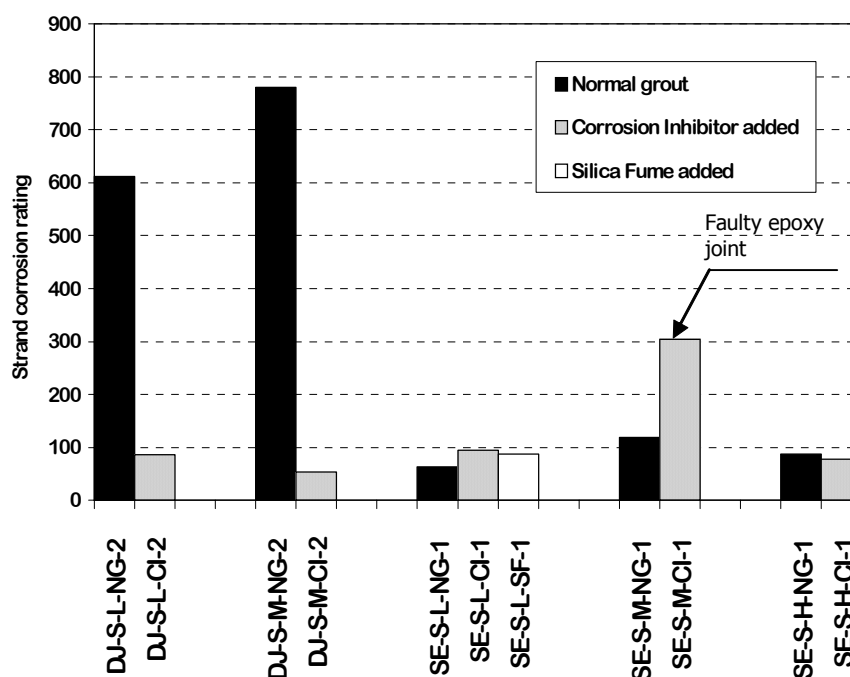
Figure 3.76 Effect of Grout Type – Strand Corrosion Rating

187

3.4.6   Grout Voids

Grout voids were found in seventeen out of the nineteen specimens autopsied at eight years of exposure. In nine specimens the shape of the voids suggests that they resulted from lack of grout fluidity.   In the remaining specimens the voids may be attributed to entrapped air, bleed water or incomplete filling. Typical voids are shown in Figure 3.77.

Void Caused by Entrapped Air, Bleed Water or Incomplete Filling
(from Reference 3.8)

Voids Caused by Lack of Grout Fluidity

Figure 3.77 Typical Grout Voids

In eleven cases the duct was corroded at the top of a grout void in different degrees as shown in Figure 3.78 for specimen DJ-S-M-NG-2. Similar findings were obtained in two specimens during the first autopsy at four an a half years, as shown in Figure 3.79.   The new findings reinforced the conclusion that the presence of a void in the grout may lead to more severe corrosion of the galvanized steel duct and define the area for a premature onset of corrosion.
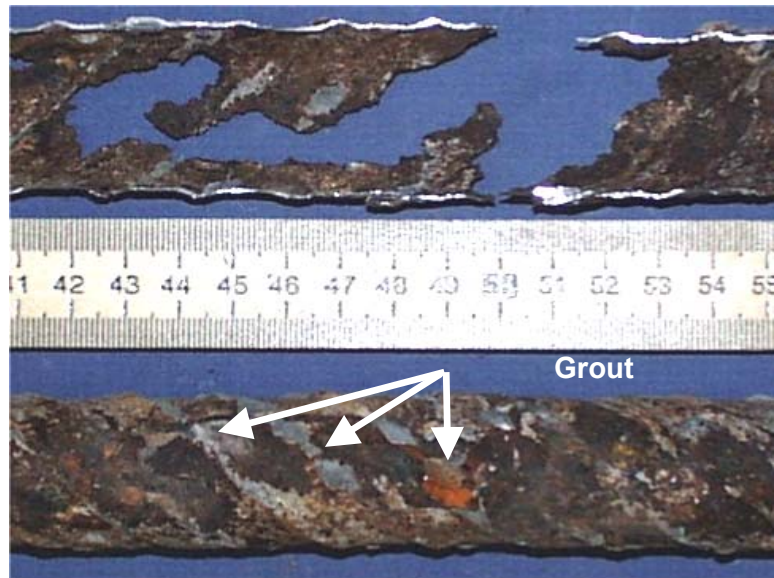
Figure 3.78 Hole in Duct Corresponding to Grout Void
(Specimen DJ-S-M-NG-2) (from Autopsy at Eight Years of Exposure Testing)
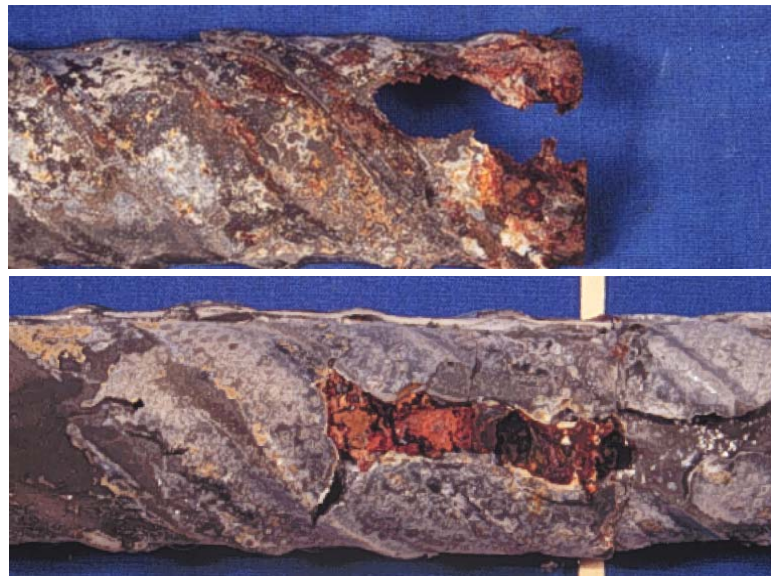
Figure 3.79 Hole in Duct Corresponding to Grout Void (Specimen DJ-S-M-NG-1) (from Autopsy at Four an a Half Years of Exposure Testing)[15]

3.4.7 Reversed Corrosion Macrocell

As shown in Table 3.5, six of the nineteen specimens were found to have reverse macrocell corrosion. This means that the mild steel bars were corroding (anodic reaction), instead of the prestressing strand. Four of these specimens were dry joint specimens, while the other two were specimens SE-S-M-CI-1 and EG-S-L-NG-1, both with epoxy joints. Specimen SE-S-M-CI-1 as discussed previously, had a very poor epoxy filling of the joint, which allowed water and chlorides to penetrate the joint. Specimen EG-S-L-NG-1 was found to have a sound epoxy joint.

As mentioned previously in reference 3.8, the development of a reversed macrocell in typical macrocell specimens is unlikely and is not addressed by ASTM G109.[3.5] The development of the reversed corrosion macrocell in this testing program was considered to be attributed to the transverse segmental joint. The use of a dry joint is particularly severe, as indicated by the experimental data. A possible mechanism is shown in Figure 3.80. The dry joint allows easy penetration of chlorides to the bottom layer of steel. The small end cover for the bottom bars, 0.25 in., provides little protection from lateral migration of the chlorides. The steel becomes quickly depassivated while the prestressing steel benefits from the additional protection provided by the grout and duct. It is assumed that the added protection is primarily due to the extra thickness of the grout over the strand in comparison to the end cover of the bars. Although the duct is discontinuous at the joint, it may also contribute to corrosion protection. These conditions are conducive to the formation of a reversed corrosion macrocell.

190
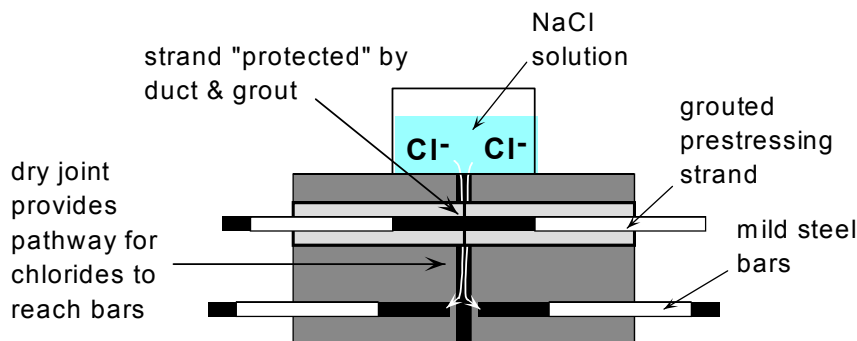
*Figure 3.80 Mechanism for Development of Reversed Macrocell
in Dry Joint Specimens or in Poor Epoxy Joint Specimens* [3.8]

The occurrence of a reversed macrocell was not clearly confirmed by forensic examination.   Only specimens DJ-S-H-NG-2 and DJ-P-L-NG-2 show a distinct behavior with very high mild steel corrosion and low prestressing strand corrosion.   However, specimens DJ-P-M-NG-2 and SE-S-H-CI-1 showed high mild steel and strand corrosion ratings at the same time.   Specimens DJ-S-M-CI-2 and EG-S-L-NG-1 showed low corrosion in both mild steel and strand. Chloride profiles (where available) indicated chloride levels in excess of the corrosion threshold in all specimens, except in specimens EG-S-L-NG-1.

3.4.8   Test Measurements

3.4.8.1   Comparison Between Half-Cell Potentials and Macrocell Corrosion Current

Similar results were obtained using Half – Cell Potentials and Macrocell Corrosion Currents when assessing strand corrosion in all macrocell specimens, as reported in Sections 3.1.4.1 and 3.1.4.2. Table 3.7 showed that most specimens had a good correlation between times to corrosion initiation, and Table 3.8 and Table 3.9 showed that conclusions with respect to the four main variables in the

191

testing program were basically the same. However, these methods were not able to detect corrosion in seven specimens in the case of Half-Cell Potentials, and nine specimens in the case of Corrosion Currents, all of which were found to have some degree of strand corrosion during forensic examination.

Figure 3.81 shows the comparison between Corrosion Currents and Half Cell Potentials for specimen DJ-S-M-NG-2 and specimen SE-S-M-CI-1. As can be observed, Half-Cell potentials (above 90% probability of corrosion as per ASTM C876[3.7]) showed very good correlation with corrosion currents, with regard to the onset of corrosion and corrosion activity.
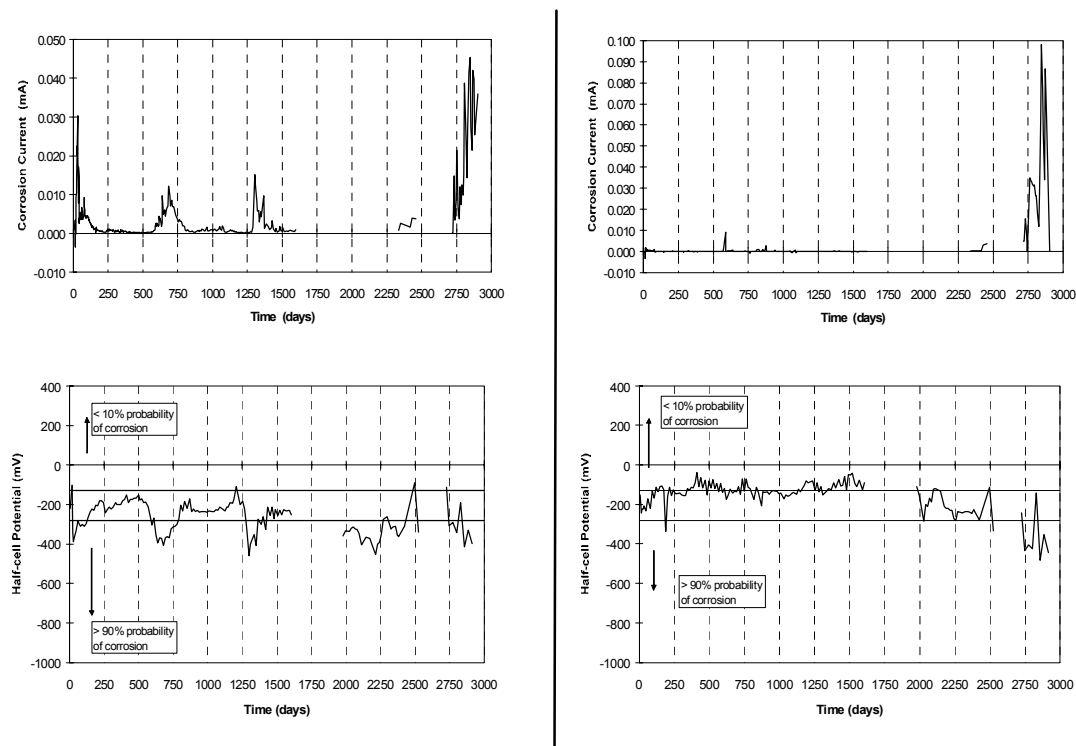
Figure 3.81 Comparison Between Corrosion Current and Half-Cell Potential Readings

Based on the above, half-cell potentials can readily be taken in in-service concrete structures to detect the onset of corrosion, while the corrosion current cannot be measured directly. However, it must be noted the particular conditions of in-service structures may differ considerably from those in the experimental specimens, which may affect the reliability of the readings. The prestressing strand in this testing program was not in contact with the metal duct. Thus, in typical situations half –cell potentials taken on the prestressing tendon may in fact reflect the very negative potential of the zinc on the galvanized steel duct, leading to erroneous conclusions. In the experimental specimens, it is possible that the discontinuity in the duct at the segmental joint facilitated ion flow through the grout, allowing half-cell potential readings from the prestressing strands to be taken.

3.4.8.2 *Comparison Between Macrocell Corrosion Current and Forensic Examination*

Metal loss values calculated in Section 3.2.4.3.3. and summarized in Table 3.11 were compared against the strand corrosion ratings presented in Section 3.3.4.2 and summarized in Table 3.17. Figures 3.82 and 3.83 show the results. As can be observed in these figures, there are many discrepancies. Computed metal loss calculations based on current measurements did not show major strand corrosion activity in many of the specimens, contrary to what was found during forensic examination. In addition, specimens with maximum values of calculated metal loss do not correspond to specimens with the maximum corrosion ratings observed.
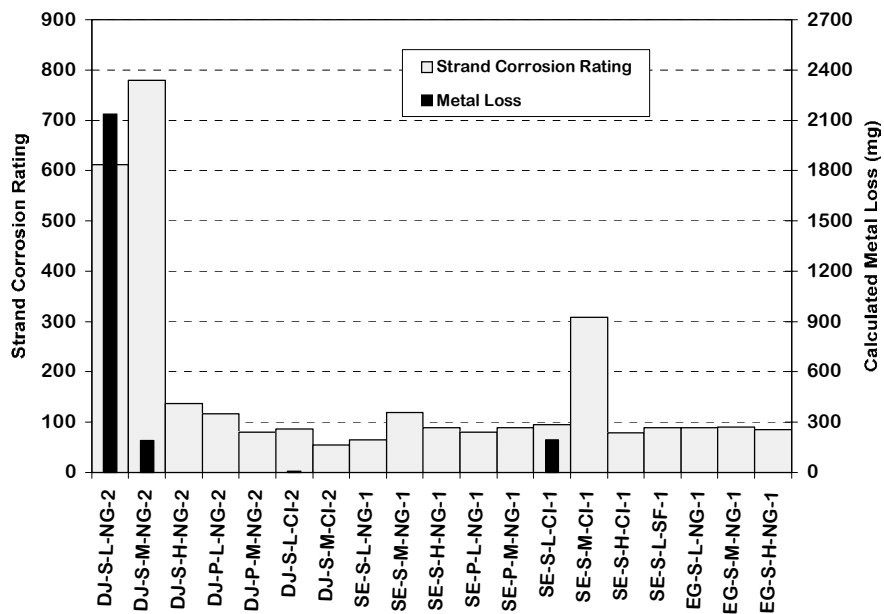
***Figure 3.82 Comparison of Corrosion Rating and Metal Loss for Prestressing
Strand***
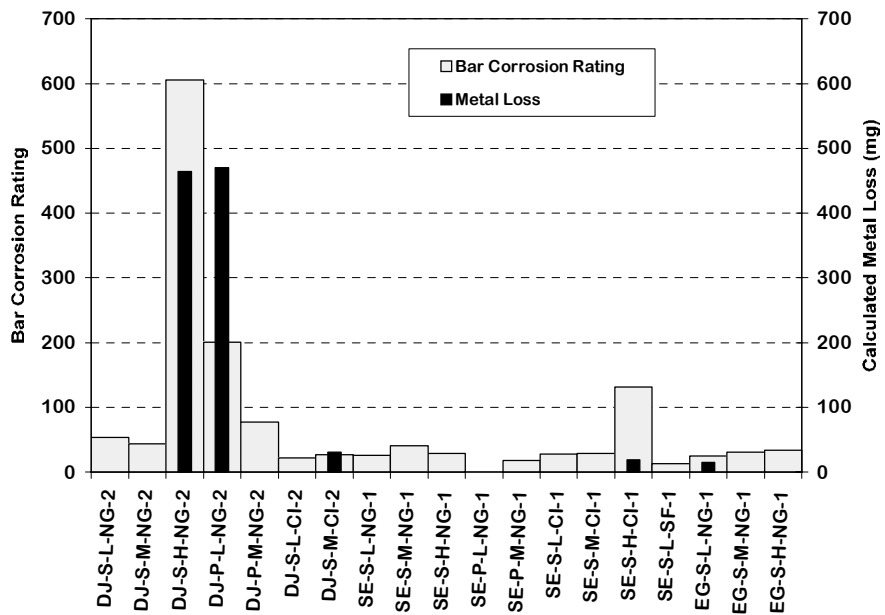
***Figure 3.83 Comparison of Corrosion Rating and Metal Loss for Mild Steel
Bars***

194

The above results comparing computed metal loss based on macrocell corrosion currents with the actual corrosion rating noted from the forensic examination results are similar to those obtained at four and a half years of exposure, and the same conclusions apply:

1. Some strand corrosion may be due to microcell corrosion activity or low corrosion currents that were not detected during exposure testing measurements.

2. The calculated metal loss procedure misses the fact that both layers of steel are corroding at the same time. Macrocell corrosion current would correctly indicate if either the mild steel bars or the prestressing strands were experiencing the more severe corrosion activity, but the other would be overlooked. The charge flux calculated from macrocell corrosion current would underestimate the actual corrosion severity or metal loss.

3. Since the driving force for macrocell corrosion is the potential difference between the two layers of steel (resulting from variations in chloride and moisture concentrations), this may disappear during a long-term test. The advanced moisture and chloride penetration may occur before corrosion can be initiated on the steel. This phenomenon may indicate an important limitation of the use of the metal loss calculation procedure in analyzing dry joint segmental construction with macrocell specimens.

3.5 SUMMARY AND CONCLUSIONS FROM MACROCELL CORROSION TESTS

Thirty eight macrocell specimens were used to investigate the corrosion protection of internal tendons at segmental joints. Half of the specimens were autopsied after around four and a half years of highly aggressive exposure and

preliminary conclusions were reported.[3.8] The variables analyzed during the testing program included: joint type (dry or epoxy), duct type (galvanized steel or plastic), grout type (3 grouts with differing additives) and level of joint compression (3 different levels).   The second half of the specimens was autopsied with over eight years of very aggressive exposure. Numerous conclusions can be drawn.

3.5.1   Overall Performance

- Superiority of plastic ducts was evident. Specimens with plastic duct had the best overall performance (quantified in terms of strand, mild steel and duct corrosion).

- Thin epoxy joints provided substantially improved corrosion protection when compared to dry joints. Incompletely filled epoxy joint performance was very similar to that of a dry joint.

- All galvanized steel duct specimens showed some degree of duct corrosion, from moderate uniform corrosion up to severe duct destruction.

- Post-tensioning strands were corroded in all specimens, from light uniform corrosion to moderate pitting.

- Mild steel bars were corroded in seventeen out of the nineteen specimens. One third of those had from moderate corrosion to severe pitting.

- In many instances, the epoxy coverage, provided on the strand and mild steel bars to limit the exposed length of the anode and cathode, failed to provide complete corrosion protection to these areas. Epoxy paint peeled off in many instances allowing for moisture and chloride ingress. Corrosion under the epoxy paint was in many cases comparable to the corrosion condition in the exposed lengths.   Among other effects, this affected the current density calculations.

- Metal loss calculations based on current density calculations failed to indicate the amount of corrosion in the specimens.

3.5.2 Assessing Corrosion Activity Using Half-Cell Potential Measurements

Half-Cell Potentials were taken at two week intervals at the start of the wet period and at the start of the dry period. All measurements were performed according to ASTM C876[3.7] using a saturated calomel electrode (SCE). In all cases the prestressing tendon was not in contact with the galvanized duct, and it was considered that the segmental joint allowed for ion movement. However, while HC-Potentials in dry joint specimens had good correlation with forensic examination results, they failed to detect corrosion activity in six out of nine epoxy joint specimens, and in one epoxy joint specimen with gasket.

With respect to testing variables, the following conclusions are drawn based on Half-Cell Potential Data:

- Epoxy joint specimens showed lower probability of strand corrosion than dry joint specimens.

- Macrocell specimens with plastic ducts (discontinuous) at the joint showed lower probability of strand corrosion than similar specimens with galvanized steel ducts.

- Dry joint specimen data indicated less probability of strand corrosion with increasing levels of joint precompression. This trend was not clearly shown in epoxy joint specimens.

- Dry Joint specimens with Corrosion Inhibitor (Calcium Nitrite) showed lower probability of strand corrosion with respect to specimens with Normal Grout.

3.5.3   Segmental Joints

To address typical North American practice, dry joints and epoxy joints, with and without gaskets, were selected for investigation in this testing program. All joint types were match-cast.   The AASHTO Guide Specifications for Segmental Bridges[3.6] does not permit the use of dry joints with internal tendons. However, dry joints were included as a worst case scenario for comparison purposes.   The thin epoxy-jointed specimens were assembled according to the standard practice.   In the epoxy/gasket joint, a foam gasket was glued to the face of one segment around the duct opening prior to application of the epoxy. Forensic examination after eight years of exposure included: seven specimens with dry joints, nine specimens with epoxy joints and three specimens with epoxy joints with gasket.   The conclusions are as follows:

- All galvanized steel ducts and prestressing strands in the nineteen specimens showed some degree of corrosion. The higher corrosion ratings were obtained from dry joint specimens with galvanized steel ducts and normal grout. Ducts in these specimens were extremely corroded, with corrosion centered at the joint, and with concrete cracking in the top of the specimen.   In general, dry joint specimens showed increased chloride penetration and increased corrosion of galvanized steel duct, prestressing strand and mild steel reinforcement.   These results show that dry joints do not provide adequate corrosion protection for internal tendons in aggressive environments.

- Sound epoxy joint specimens with galvanized steel ducts showed moderate to very severe duct corrosion centered away from the joint.   Clear cover for specimens was small (five eights to three quarters of an inch), significantly lower than would be allowed by specifications.   However, the test results indicate the potential corrosion problems when using galvanized ducts in

aggressive environments if chlorides penetrate the concrete cover away from the epoxy joint.

- Thin epoxy joints provided substantially improved corrosion protection when compared to dry joints. However, test results showed that poor epoxy filling at the joint is extremely detrimental to the performance of the duct, the prestressing strand and the mild steel reinforcement. Incompletely filled epoxy joint performance was very similar to that of a dry joint.

- Corrosion of mild steel in some epoxy joint specimens was found to be the result of an external source of moisture and chlorides rather than from penetration at the epoxy joint or through the concrete. This conclusion was reinforced with chloride levels measured at the joint and away from the joint. These findings reinforce the need to provide adequate clear cover over the ends of longitudinal bars in the segments, even if external post-tensioning is used.

- In some cases, the use of gaskets in epoxy jointed specimens prevented complete epoxy coverage of the joint. This condition could worsen under field conditions.

3.5.4 Ducts for Internal Post-Tensioning

Two duct types were investigated; standard galvanized steel duct and plastic duct. Due to size limitations, PVC pipe was used for the plastic duct. Test results indicated:

- Galvanized steel duct was corroded in all specimens. Severe corrosion and large duct destruction was observed in dry joint specimens. Such corrosion was often centered on the dry joint. Epoxy joint specimens showed moderate to severe duct corrosion. The corrosion was often centered away from the joint.

- Superiority of plastic ducts was evident. Strand encased in plastic ducts showed only light corrosion and discoloration. Specimens with plastic duct had the best overall performance (quantified in terms of strand, mild steel and duct corrosion).

- Concrete cover in specimens was lower than allowed by specifications. However, test results indicate that these are potential corrosion problems when using galvanized steel ducts in aggressive exposures if chlorides penetrate the cover. Plastic ducts performed well in spite of the small cover.

3.5.5 Joint Precompression

Due to the small specimen size, the strand could not be post-tensioned effectively. To simulate precompression across the joint due to post-tensioning, the pairs of match –cast segments were stressed together using external loading frames. Three levels of precompression were selected; 5 psi, 50 psi and $3\sqrt{f'c}$ psi. The lowest level of 5 psi could represent the level of precompression encountered in a precast segmental column under self weight. The precompression of 50 psi is based on AASHTO Guide Specifications.[3.6] The highest precompression value corresponded to 190 psi for this testing program. Eight out of the nineteen specimens (at eight years of exposure) had low precompression, seven medium precompression and four high precompression. Conclusions are as follows:

- Test results did not show a clear trend with respect to joint precompression when analyzing time to corrosion initiation and rate of corrosion in prestressing strands and mild steel bars. An isolated result for dry joint specimens with galvanized steel ducts and normal grout showed that at very high levels of precompression, there is an increased level of strand and mild steel protection. This result is not clearly shown for epoxy joint specimens with and without gasket.

- Galvanized steel duct corrosion in dry joint specimens also showed better performance with a higher level of precompression. However again, this result is not clearly shown in epoxy joint specimens. Precompression level is much important in dry joint specimens.

3.5.6   Grouts for Bonded Post-Tensioning

Three cement grout types were selected for evaluation; normal grout (plain cement grout, no admixtures, w/c = 0.40), grout with silica fume (13% cement replacement by weight, w/c = 0.32, superplasticizer added) and grout with a commercial calcium nitrite corrosion inhibitor (w/c = 0.40). The dosage of corrosion inhibitor used in this testing program was the same dosage normally used for concrete (aprox. 20 liters/m^3 concrete). The Calcium Nitrite dosage was not adjusted to account for the higher cement content in grout. The testing program for the nineteen remaining specimens at eight years of exposure included thirteen specimens with normal grout, five with corrosion inhibitor and one with silica fume. Conclusions are as follows:

- Dry joint Specimens with Corrosion Inhibitor (Calcium Nitrite) added to the grout showed a lower strand corrosion rating (less strand corrosion severity) at eight years of exposure, than specimens with normal grout (in the order of seven times smaller). This trend was not clearly shown in epoxy joint specimens. This result contradicts those obtained at four and a half years of exposure where the most severe corrosion of the prestressing tendon was found where calcium nitrite corrosion inhibitor was used.

- Epoxy joint specimens with silica fume, corrosion inhibitor and normal grout had very similar performances. No clear distinction was evident.

- Grout voids, due to entrapped air, bleed water, incomplete grout filling or lack of grout fluidity were detrimental not only to the prestressing strand, but also to the galvanized steel duct.

3.6 MEASURES FOR IMPLEMENTATION FROM MACROCELL RESULTS

Macrocell test results generated the following findings for immediate implementation to improve corrosion protection for precast segmental construction.

Joint Type

- Epoxy joints should always be used with internal prestressing tendons.
- Dry joints should be avoided with external prestressing tendons in aggressive exposures, to protect segment mild steel reinforcement at joints and to block entry of chlorides that might be transported to locations of flaws in external tendon sheaths or anchors.
- Stringent inspection and construction practices must be exercised to guarantee good epoxy filling at the joints and complete grouting.
- Gaskets in epoxy joints should be avoided since there is a potential for incomplete epoxy coverage of the joint. Preferred practice with epoxy joints is to utilize a thorough swabbing of tendon ducts immediately after initial segment placement and stressing to seal the duct edges at the joint. Tightness of the joint should be checked by air pressure testing. Carefully coupled ducts are an alternative as long as a positive seal is obtained.

<u>Duct type</u>

- Plastic ducts for post-tensioning should be used in all situations where aggressive exposure may occur.

<u>Grout type</u>

- Calcium Nitrite Corrosion inhibitor added to the grout had little effect on the onset of corrosion but did seem to enhance long-term strand corrosion protection.

(Page left blank intentionally)

CHAPTER 4

Large Scale Beam Corrosion Tests

The use of post-tensioning in flexural members can provide many advantages, as described in Chapter 2. The improvement in crack control and the precompression applied to the concrete suggest that moisture and chloride penetration would be reduced, impacting positively on durability. However, when post-tensioning systems are used, new durability concerns arise, since new hardware is incorporated within the elements.

The durability concern increases when mixed reinforcement (i.e., a combination of non-prestressed and prestressed reinforcement as the main flexural tension element) is used. Mixed reinforcement has received much attention in the last few years, since fully prestressed members may not always lead to an optimum design, from a strength and economic perspective.[4.1, 4.2] The limitation of concrete tensile stresses in fully prestressed members below cracking, can lead to large prestress requirements, resulting in very unconservative designs, excessive creep deflections and the requirement for stage prestressing as construction progresses. Mixed reinforcement may increase ductility in comparison to fully prestressed members, have less congestion than reinforced concrete elements, reduce creep and excessive camber, produce a more efficient design, and the reinforcement can be tailored to control deflections, cracking, and cracking moment.[4.2] Also, from recent research in Europe, it seems that a better fatigue resistance is also attained. However, all these benefits could be outweighed by the increased corrosion risk, since concrete is likely to crack under service load levels.

The large scale flexural elements in this research study are being used to evaluate the relative performance of several flexural concrete member protection variables, including:

1)   different levels of prestress and load, producing different crack widths and patterns

2)   different post-tensioning hardware: duct types, duct splices, strand types and anchorage systems

3)   different concrete and grout mixes

4)   different grout injection procedures

The beam research portion of the durability study concludes with recommendations for materials and implementation measures.

4.1   RESEARCH OBJECTIVES

The Large Scale Beam Corrosion Test program utilizes large-scale linear flexural elements, under long-term exposure testing. It has the following objectives:

1)   Determination of the effect of post-tensioning on durability (corrosion protection) through crack control, and

2)   Evaluation of the relative performance of a broad scope of corrosion protection variables for multistrand postensioning systems.

4.2   EXPERIMENTAL PROGRAM

Beam specimen exposure testing includes combination of structural loading with aggressive exposure, by means of cyclic wetting and drying with a 3.5% NaCl solution to promote accelerated corrosion. The effect of prestressing levels is investigated for a range of systems, from nonprestressed (reinforced concrete) to partially prestressed (mixed reinforcement) to fully prestressed.

206

Variables in the research program include the influence of crack width, type of concrete (normal and high performance concrete – refer to Section 2.4.4.1), prestressing strand coatings, duct splices, high performance grout, and encapsulated post-tensioning systems.

Two phases were implemented as part of the experimental program. Phase I was developed to investigate the influence of prestressing levels, cracking, high performance grout and post-tensioning duct splices. This phase was designed and implemented by West.[4.2] Phase II was developed to investigate high performance concrete (refer to Section 2.4.4.1), high performance grout, prestressing strand coatings and an encapsulated post-tensioning system. This phase was implemented by Schokker.[4.3] Both researchers, West and Schokker, built series of beam specimens and initiated exposure testing in the early part of the experimental program. Both phases used the same overall beam specimen design and loading.

Sections 4.2 through 4.3 include a summary of the work done by West and Schokker. For a detailed description of their experimental program and description of measurements during exposure testing, refer to References 4.2 and 4.3. CTR Research Report 1405-3[4.4] also contains a detailed summary of West's and Schokker's work.

Sections 4.4 through 4.10 include all exposure testing results and final autopsy results, conclusions and recommendations for the selected specimens. Exposure testing was performed as a cooperative effort by West and Schokker in the first stages, and Kotys [4.5] and the author in the final stages of the specimens selected for full autopsy. Full autopsies were performed by Kotys and the author. Approximately half of the specimens remain under exposure at the end of this reporting period, for future autopsy. These sections were written jointly between

Kotys and the author and were first published in Kotys' thesis. The sections are included here with few changes.

4.2.1 Test Specimen

4.2.1.1 Specimen Description

The specimens used in this experimental program are not patterned after a prototype structure. Linear rectangular flexural elements, as shown in Figure 4.1, were chosen for the following reasons:

- results can be applied to bent cap and beam elements directly and some results may be qualitatively applied to other elements such as pile caps.
- all desired variables can be readily incorporated into design
- ease of construction, handling and placement
- simplicity of controlling and maintaining loading

Figure 4.1 Linear Rectangular Beam Specimens (on Top of Reaction Beams)

The beams subjected to combined structural loading are tested outside the Ferguson Structural Engineering Laboratory and are exposed to cyclic wetting and drying with a 3.5% NaCl solution to provide and highly aggressive corrosive environment.

Specimen dimensions and details were selected to provide concrete covers, reinforcement sizes, post-tensioning hardware and crack widths of a similar order of magnitude as in practical applications, with consideration for handling and loading of the specimens. Prestressed specimens used a minimum of two tendons (multistrand) to represent applications typical of post-tensioned bridges.

The Type E multistrand anchorage hardware manufactured by VSL Corporation was selected because it is available in tendon configurations with as few as three strands. The 18" x 24" concrete section, accommodating up to eight strands in two tendons, was chosen to provide the most flexibility in the design of mixed reinforced sections. For practical reasons, a nominal beam length of 15
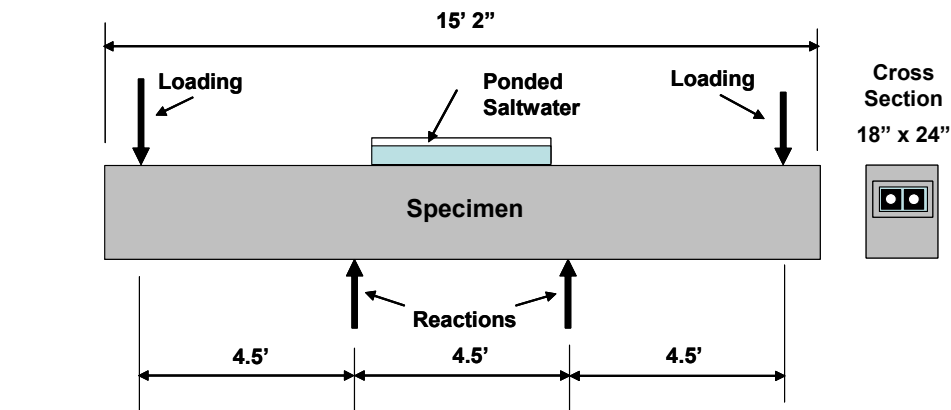
feet was chosen. Specimen dimensions are shown in Figure 4.2.

Figure 4.2 Specimen Dimensions

209

4.2.1.2 Specimen Design

4.2.1.2.1 Levels of Prestress

To examine a broad range of prestressing, section reinforcement was proportioned for the following prestressing levels:

- non-prestressed (Non-PS)

- mixed reinforcement with nominal prestress amount between 50% and 75% of total tensile force (2/3 PS). See definition in Section 2.1.6.

- 100% prestressed based on ultimate (nominal) strength (100 %U PS)

- 100% prestressed based on service load/allowable stress design (100%S PS)

The amount of prestress in percent, is defined as the tensile force component provided by prestressing steel at the nominal flexural capacity of the section. Only 100%S PS specimens would not be expected to crack under service loading. The selected specimen dimensions and requirement for two tendons dictated the use of 8 strands for the 100%S PS section, 6 strands for the 100%U PS section, and 4 strands for the 2/3 PS (mixed reinforcement) section.

4.2.1.2.2 Design Loading

Reinforcement was proportioned based on the total allowable service load moment (dead load plus live load) computed for the 100%S PS section. Assuming a ratio of dead load to live load of 1.5, the calculated permissible total service load moment was used to compute the dead and live load moments. The factored moment was then computed and used to proportion the reinforcement for the non-prestressed sections as well as the mixed reinforcement and the 100%U PS post-tensioned sections.

210

The 100%S PS section was design to meet the stress limits according to Clause 5.9.4 of AASHTO LRFD[4.6](Clause 18.4 of ACI 318[4.7]). The sections with eight post-tensioning strands in two tendons were analyzed with the following assumptions:

- Gross section properties, elastic stresses
- $f'_c = 5$ ksi
- $A_{ps} =$ eight 12.7 mm (0.5 in.) 7-wire prestressing strands, $f_{pu} = 270$ ksi
- $f_{pi} = 0.65 f_{pu}$
- Long term losses = 15% ($f_{pe} = 0.55 f_{pu}$)
- Maximum tendon eccentricity, e = 8 in. based on clear cover to duct of 2.5 in.
- Computation of the total allowable moment assumed that the governing stress in the concrete (tensile or compressive) is at least 75% of the corresponding allowable value. (i.e., either $0.75 f_{callow} \leq f_{cmax} \leq f_{callow}$ or $0.75 f_{tallow} \leq f_{tmax} \leq f_{tallow}$)
- Self weight of the beam could be neglected (self weight is very small in comparison to applied forces)

The section was analyzed for stresses in the concrete immediately after prestress transfer and under maximum applied loading.   Calculated stresses and moments are included in Reference 4.2.   The service load moment, with $f_t = 0.75 f_{tallow}$ governing, was calculated as 2750 k-in. To meet stress limits at the member ends a draped profile was chosen for the tendons. Figure 4.3 shows the tendon profile and the allowable limits for the steel center of gravity (cgs).
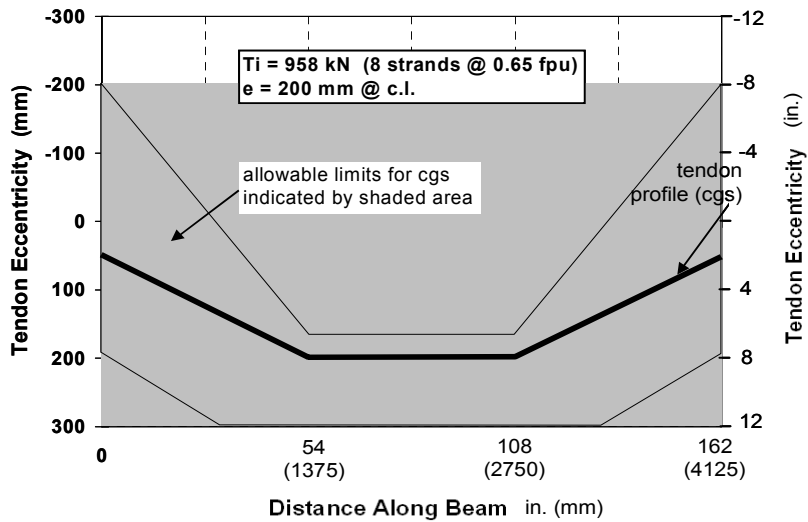
Figure 4.3 100%S PS Section Tendon Profile and Allowable Limits [4.3]

Based on the calculated service load moment, the dead and live load moments, factored moments and nominal moments were calculated as follows:

$M_{service}$ = 2750 k-in. (based on 100%S PS section)

M_D/M_L = 1.5   (assumed)

Therefore,

M_D = 1650 k-in.

M_L = 1100 k-in.

$M_{factored}$ = 4180 k-in.

$M_{nominal}$ = 4650 k-in. (for $\phi = 0.9$)

4.2.1.2.3 Section Reinforcement

The required nominal flexural capacity, M_n, was used for the strength design of the remaining sections. The 100%U PS section required the use of six strands. Mixed reinforced sections (50% to 75% prestress) required the use of four strands, for an effective prestress level of 66.7% (2/3 PS). Reference 4.2

212

describes in detail the procedure followed to select the appropriate amounts of reinforcement, based on AASHTO LRFD (1998) and ACI 318-95. Figure 4.4 shows the final reinforcement details for each section. Detailed construction drawings, from Reference 4.2, have been included in Appendix B. Table 4.1 includes a summary of Section Details.

Non-Prestressed

Compression Steel
2-#5's
Tension Steel:
6 - #6's and
2 - #4's

1.84 in.

2.38 in.   3.93 in.

2/3 Prestressed

Compression Steel
2-#5's
Tension Steel:
4 - #3's and
4 - #4's
Prestressing Steel:
4- 0.5in. dia. strands

5.4 in.

2.25 in. 1.5 in. 10.05 in.

100% Prestressed
Strength Design

Compression Steel
2-#5's
Tension Steel:
2 - #3's and
(not required by design)
Prestressing Steel:
6- 0.5in. dia. strands

5.4 in.

2.19 in.

100% Prestressed
Allowable Stress Design

Compression Steel
2-#5's
Tension Steel:
2 - #3's and
(not required by design)
Prestressing Steel:
8 - 0.5in. dia. strands

5.4 in.

2.19 in.

Figure 4.4 Section Reinforcement Details [4.2]

Table 4.1 Summary of Section Details [4.4]

Section	Prestressing Strands	Effective Prestress (after losses)	Mild Steel Bars (tension)	Nominal Capacity
Non-PS	None	n/a	6 #6 and 2 #4	4685 k-in
2/3 PS	4 – 0.5 in.	$0.6 \, f_{pu}$	4 #4 and 4 #3	4750 k-in
100%U PS	6 – 0.5 in.	$0.6 \, f_{pu}$	2 #3	4685 k-in
100%S PS	8 – 0-.5 in.	$0.55 \, f_{pu}$	2 #3	5935 k-in

213

Shear reinforcement was proportioned for the shear force corresponding to the development of the nominal flexural capacity of the sections.

Anchorage zone design and reinforcement was provided following Breen et al. recommendations. [4.8] Spirals used in the anchorage zone were based on the guidelines provided by the hardware supplier.   Details are included in Reference 4.2.

The post-tensioning system was draped with slope changes at third points. This profile was required to control stresses in the 100%S PS specimens and to ensure electrical contact among strands, since contact may influence corrosion behavior.

Type E anchorage system from VSL Corporation was used in all post-tensioned beams. 100%S PS Section used the Type E-4 with four strand capacity per tendon. 100%U PS and 2/3 PS used Type E-3 anchorage system with three strand capacity per tendon.   Anchorage and grout tube details are shown in the Appendix B drawings.

4.2.1.2.4 Analysis of Section Behavior

Each section was analyzed to determine its moment curvature behavior and applied moment vs. crack width behavior.   Surface crack widths were predicted using recommendations by Armstrong et al. [4.1] with the Gergely-Lutz expression. Details of these calculations are included in Reference 4.2. Figure 4.5 and Figure 4.6 show the computed moment-curvature and moment-crack width curves for the control Class C concrete.   Full details on Section Behavior are included in Reference 4.2, including long-term behavior.
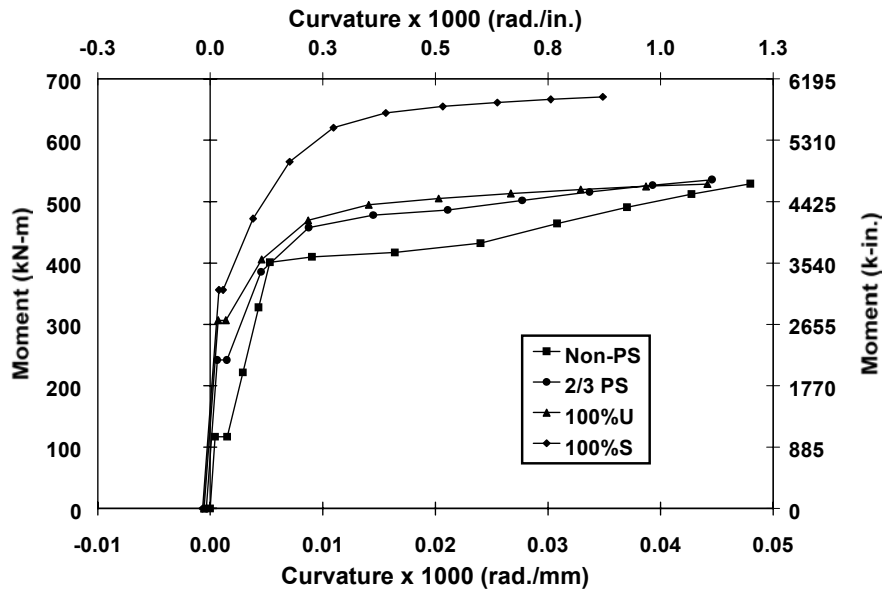
*Figure 4.5 Moment Curvature Behavior for All Sections
with Class C Concrete[4.2]*
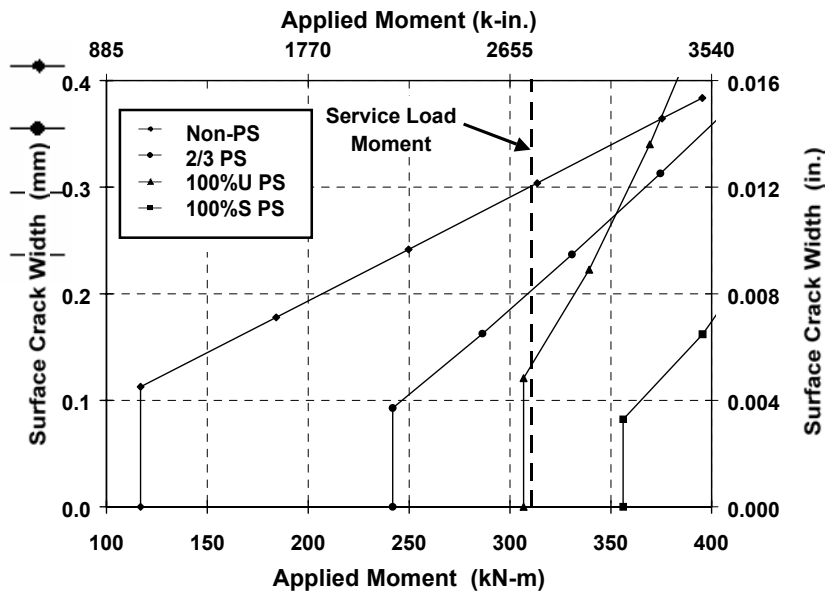
*Figure 4.6 Applied Moment- Estimated Crack Width Behavior for
All Sections with Class C Concrete [4.2]*

215

A long-term prestress loss (creep, shrinkage, relaxation) of 4.7% was calculated for the 100%S PS section. Prestress force losses of 5% and 4.3% were calculated for the 100%U PS and 2/3 PS sections, respectively, after four years of sustained loading, since these sections were cracked prior to and during sustained loading.

4.2.2 Variables

Beam Specimens were implemented in two phases, around a year apart. Phase I specimens included the following variables: level of prestress and crack width, one specimen with high performance grout, and the evaluation of duct splices. Phase II specimens include different concrete types, prestressing strand coatings and post-tensioning hardware protection, in addition to duct splice evaluation.

4.2.2.1 Control Variables

Typical TxDOT practice was considered to define the values of the variables for the control or reference specimens, as described in Table 4.2.

Table 4.2 Control Variables (Adapted from Reference 4.2)

Variable	Description
Concrete	Based on TxDOT Specification Item 421 TxDOT Class C concrete for bridge substructures Maximum w/c ratio = 0.533 (actual w/c will be closer to 0.45 based on slump requirements) Type I cement Slump = 4 in. Maximum coarse aggregate size = ¾ in. Retarder, Rheocrete 300 R Entrained air admixture 2 in. clear cover to main steel
Cement Grout	Based on TxDOT Specification Item 426.3.4a w/c ratio = 0.44 Type I cement Expanding admixture, Intraplast – N

Table 4.2 (Continued) Control Variables (Adapted from Reference 4.2)

Variable	Description
PT Duct	Rigid galvanized steel duct
Anchorage Protection	Based on TxDOT guidelines
	Type V State epoxy bonding compound
	Nonshrink grout patch (Euclid NS grout)

4.2.2.2   Phase I Variables

4.2.2.2.1 Levels of Prestresing, Loading and Cracking

Cracking was investigated using the three sections that would be expected to crack under service loads (Non-PS, 2/3 PS and 100% U). Crack widths for investigation were selected based on a survey of relevant literature and the moment-crack width behavior computed for each section.   Full description of crack width selection is presented in Reference 4.2. The selected crack widths and the corresponding loading and applicable sections are shown in Table 4.3. Some deviation would be expected from the planned crack widths due to the uncertain nature of cracking.

Table 4.3 Planned Crack Widths, Prestress Amounts and Loading [4.2]

Loading Case	Crack Widths	Applicable Sections	Loading
1.) Constant Service Load	uncracked	100%S PS	service load
	0.1 mm (0.004 in.)	100%U PS	service load
	0.2 mm (0.008 in.)	2/3 PS	service load
	0.3 mm (0.012 in.)	Non-PS	service load
2.) Very Small Crack	0.05 mm (0.002 in.)	2/3 PS & 100%U PS	as needed and hold
3.) Unloaded	Uncracked	Non-PS & 100%U PS	None
4.) Overload & Return to Service	as measured	Non-PS, 2/3 PS & 100%U PS	up to 1.33 x service load, then return to service load

4.2.2.2.2 Duct Splices for Galvanized Steel Duct

Two duct splices were studied: standard industry splice (IS) and heat shrink splice (HS). The first consisted of a 1 ft length of oversized duct with the ends drapped with duct tape. The second consisted of an 8 in. length of heat shrink tubing (original diameter of the tubing was 4 in.).   Splice damages were also studied consisting of poor or incomplete duct taping on IS splices, and a 1 in. cut made in the HS tubing in the middle section.   Figure 4.7 shows both duct splices used.

The following comparisons were studied:

1) Industry standard versus heat shrink

2) Industry standard versus unspliced

3)   Effect of damage for industry standard and heat shrink splices.

Industry Standard Splice   **Heat Shrink Splice**
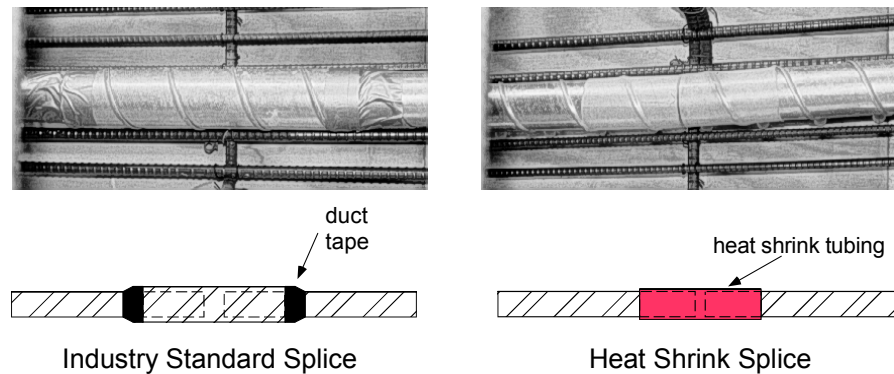
Figure 4.7 Duct Splices [4.2]

4.2.2.2.3 High Performance Fly Ash Grout

Fly ash grout was used in one beam specimen, with the following characteristics: w/c = 0.35, 30% cement replacement by weigh with Fly Ash, superplasticizer (4 milliliters per kilogram of cementitious material for fluidity).

4.2.2.3   Phase II Variables

4.2.2.3.1 Concrete Type

Two different concrete mixes were selected for comparison: TxDOT Class C Concrete with 25% Fly Ash and High Performance Concrete (refer to Section 2.4.4.1).

Fly Ash was used due to its increasing use in concrete.   For this experimental program, fly ash Class F was used due to availability from local ready-mix suppliers.   For the fly ash mix, the water cement ratio was 0.44 with 25% cement replacement by weight with fly ash, and no other significant changes to the standard Class C Concrete mix.

The high performance concrete mix selected had improved strength ($f'c$ = 10000 psi) and durability. The mix contained 25% cement replacement by fly ash (w/c = 0.29) with superplasticizer added on site to reach a slump of about 8 inches. Full details of the mix designs are included in Reference 4.3.

4.2.2.3.2 Prestressing strand types

Two types of prestressing strands, besides the normal uncoated strands, were chosen for comparison: epoxy-coated and galvanized. The strands were 0.5 in. diameter, 270 ksi, stress relieved.

The effect of damages to the epoxy coating was also studied. Figure 4.8 shows the location of intentional damage in one of the tendons. Damages consisted of ¼" x ¼" squares of epoxy removed at five selected locations. Damage locations were selected to coincide with likely crack locations and bends in the parabolic duct profile. In these areas, durability may be affected by chlorides penetrating the small gaps that may occur between the overlapping metal. One strand in the damaged tendon was repaired with an epoxy patch repair kit and the other strand was left damaged.
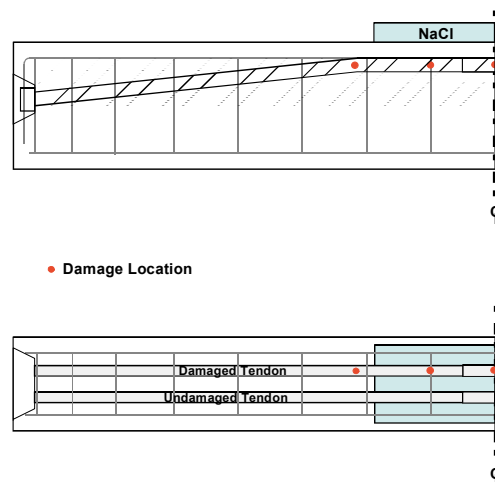
Figure 4.8 Locations of Intentional Damage to Epoxy-Coated Strand [4.3]

4.2.2.3.3 Duct Type and End Anchorage Protection

Polyethylene plastic ducts were used to compare with galvanized steel ducts. The VSLAB+™ system shown in Figure 4.9 was used, with an oval duct due to size limitations, to accommodate two strands. The system also allowed investigation of the end anchorage protection, since it provides an encapsulated system. The system is basically air and water tight.

The original intention was to evaluate an electrically isolated system, but such a system was not commercially available at the time of casting.
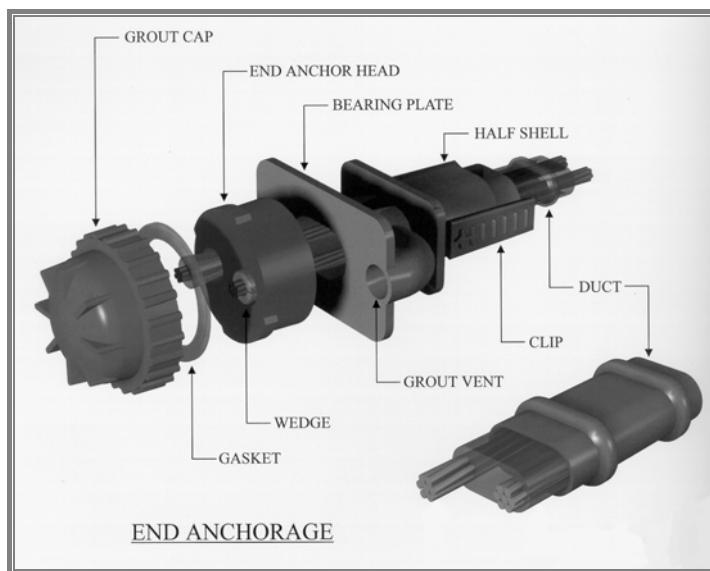
Figure 4.9 VSLAB+™ System[4.3]

4.2.2.3.4 High Performance Antibleed Grout and Poor Grouting Procedures

Under this project, antibleed grouts were studied by Schokker [4.3] and one mix was chosen for investigation in Phase II beams. The grout had a w/c ratio of 0.33 with 2% cement weight of antibleed admixture. The duct profile used in the

beams had only a small vertical rise, so bleed would not be a significant problem. The antibleed grout was chosen to compare its corrosion protection properties with the fly ash grout and TxDOT standard grout.

Poor grouting procedures were also investigated. One specimen was chosen, injecting grout with the standard method in one duct and using poor grouting procedures in the other duct (see Section 4.2.6).

4.2.3 Specimen Types

Twenty seven specimens were constructed in two phases. Phase I included sixteen specimens and Phase II had eleven specimens. Table 4.4 shows the specimen types and variables on each phase. Figures 4.10 and 4.11 show the description and labeling of all beam specimens, showing the location of the duct splices.

Table 4.4 Beam Specimen Types and Variables [4.2]

	Main Variable	Non-PS	2/3 PS	100% U	100% S
Phase I	Unloaded	1.1		3.1	
	Very Small Crack		2.1	3.2	
	Constant Service Load	1.2	2.2	3.3	4.1
	Constant Service Load (duplicate)	1.3	2.3	3.4	4.2
	Overload and Return to Service	1.4	2.4	3.5	
	High Performance Fly Ash Grout		2.11		
Phase II	Standard Concrete with 25% Fly Ash	1.5	2.5	3.6	
	High Performance Fly Ash Concrete	1.6	2.6	3.7	
	Epoxy Coated Strands		2.7		
	Galvanized Strands		2.8		
	Poor Grouting Procedures		2.9		
	High Performance Anti-Bleed Grout		2.10		
	Encapsulated System w/ Plastic Duct		2.12		

Non-Prestressed Beams

Beam 1.1: Unloaded

Beam 1.2: Service Load (cracked)
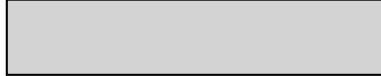
Beam 1.3: Service Load (cracked)

Beam 1.4: Overload & Return to Service

2/3 Prestressed Beams

Beam 2.1: Very Small Crack
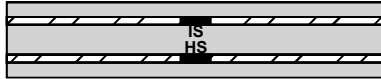
Beam 2.2: Service Load (cracked)
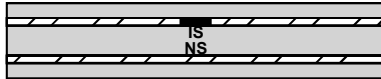
Beam 2.3: Service Load (cracked)
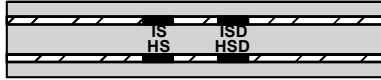
Beam 2.4: Overload & Return to Service
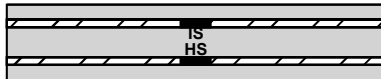
Beam 2.11: Service (Fly Ash Grout)
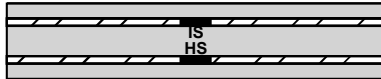
100%U Prestressed Beams

Beam 3.1: Unloaded
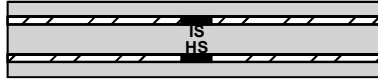
Beam 3.2: Very Small Crack
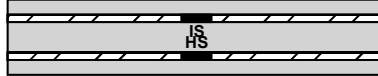
Beam 3.3: Service Load (cracked)
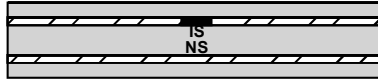
Beam 3.4: Service Load (cracked)
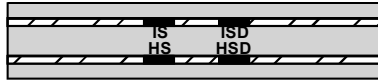
Beam 3.5: Overload & Return to Service
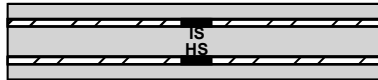
100%S Prestressed Beams

Beam 4.1: Service Load (uncracked)
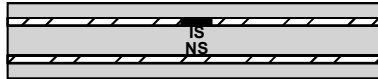
Beam 4.2: Service Load (uncracked)
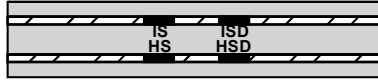
SPLICE DESCRIPTIONS:
IS - Industry Standard
HS - Heat Shrink
NS - No Splice
ISD - Industry Standard w/ Damage
HSD - Heat Shrink w/ Damage

Figure 4.10 Phase I Beam Specimens [4.2]

223

Non-Prestressed Beams

Beam 1.5: Fly Ash Concrete

Beam 1.6: High Performance Concrete

100%U Prestressed Beams

Beam 3.6: Fly Ash Concrete
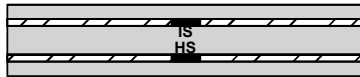
Beam 3.7: High Performance Concrete
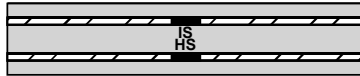
Splice Descriptions:
IS - Industry Standard
HS - Heat Shrink

2/3 Prestressed Beams

Beam 2.5: Fly Ash Concrete
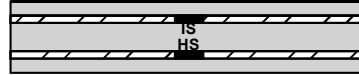
Beam 2.6: High Performance Concrete
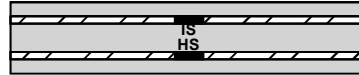
Beam 2.7: Epoxy Coated Strand
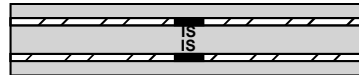
Beam 2.8: Galvanized Strand
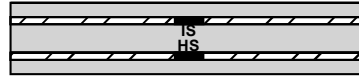
Beam 2.9: Poor Grouting Procedures
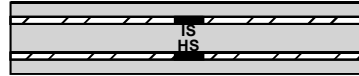
Beam 2.10: Anti-Bleed Grout
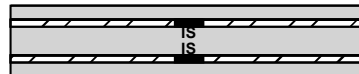
Beam 2.12: Enc. System / Plastic Duct
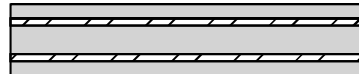
Figure 4.11 Phase II Beam Specimens [4.3]

4.2.4 Materials

Construction Materials for Phase I specimens are shown in Table 4.5. Phase II specimens used the same materials as in Phase I with the additions described previously in Section 4.2.2.3.

Table 4.5 Construction Material Details: Phase I Beam Specimens [4.2]

Item	Description

Texas DOT Class C Concrete for Bridge Substructures	• w/c = 0.53 maximum allowable
	• w/c = 0.45 actual based on required slump
	• f′c = 25 MPa (3600 psi) minimum allowable
	• batch proportions: (per 0.764 m³ (1 yd³))
	    Coarse Aggregate (19 mm)(0.75 in.) 851 kg 1877 lbs
	    Fine Aggregate 538 kg 1186 lbs
	    Type I/II Cement 256 kg 564 lbs
	    Water 115 kg 254 lbs
	    Set retarder 710 ml 24 oz
	    Entrained Air Admixture 118 ml 4 oz
	• cylinder strengths: 7-day 30.0 MPa 4345 psi
	  (average) 28-day 36.7 MPa 5320 psi
	    56-day 37.9 MPa 5490 psi

Reaction Beam Concrete	• w/c = 0.40
	• f′c = 42 MPa (6000 psi) design strength
	• batch proportions: (per 0.764 m³ (1 yd³))
	    Coarse Aggregate (19 mm)(0.75 in.) 848 kg 1869 lbs
	    Fine Aggregate 615 kg 1355 lbs
	    Type I/II Cement 234 kg 517 lbs
	    Water 95 kg 210 lbs
	    Set retarder 603 ml 20.4 oz
	• cylinder strengths: 3-day 28.7 MPa 4160 psi
	  (average) 28-day 36.7 MPa 5320 psi

Texas DOT Grout for Post-Tensioning	• w/c = 0.44
	• batch proportions: (per 0.028 m³ (1 ft³))
	    Type I Cement 37.4 kg 82.4 lbs
	    Water 16.4 kg 36.2 lbs
	    Expanding Admixture 0.37 kg 0.82 lbs
	    (Intraplast-N)
	• cube strengths: 7-day 22.2 MPa 3215 psi
	  (average) 28-day 28.8 MPa 4170 psi

High Performance Fly Ash Grout for Post-Tensioning	• w/c = 0.35
	• batch proportions: (per 0.028 m³ (1 ft³))
	    Type I Cement 28.9 kg 63.8 lbs
	    Class C Fly Ash 12.4 kg 27.4 lbs
	    Water 14.5 kg 31.9 lbs
	    Superplasticizer 165 ml 5.6 oz
	• cube strengths: 7-day 38.4 MPa 5560 psi
	  (average) 28-day 43.5 MPa 6310 psi

Prestressing Strand	• 12.7 mm (0.5 in.) diameter seven wire strand • Grade 270 (1860 MPa, 270 ksi), low relaxation • Supplier: Shinko Wire, Inc.
Mild Steel Reinforcement	• ASTM A615, Grade 60 (400 MPa, 60 ksi)

Table 4.5 (Continued) – Construction Material Details: Phase I Beam Specimens [4.2]

Item	Description
Steel Duct	• Corrugated, semi-rigid, galvanized steel duct • 54 mm (2-1/8 in.) outside diameter • Supplier: VSL Corporation, Inc.
PT Anchorage Hardware	• VSL Type E anchorage system • Supplier: VSL Corporation
Epoxy Bonding Agent	• Epoxy Adhesive Type V – General Epoxy Adhesive • Supplier: Industrial Coating Specialties Corp.
Non-Shrink Grout for Anchorage Protection	• Pre-bagged non-shrink grout mix • Trade Name: Euclid NS-Grout

Beam specimen concrete and reaction beam was sampled for strength testing using test cylinders. All cylinder strengths exceeded the minimum requirements for TxDOT Class C Concrete for Bridge Structures.

Grouts were samples according to PTI Specifications (1997). See details in Reference 4.2.

4.2.5 Experimental Set-Up

The experimental set-up used is shown in Figure 4.12. The applied loading consisted on two 50 kip loads. The exposure conditions consisted of a ponded region in the middle four feet of the beam specimens, to apply a wet-dry cycle with a 3.5% NaCl solution. The salt concentration was based on ASTM G109[4.9] recommendations. Specimens were oriented tension side up and paired with a reinforced concrete reaction beam. The ponded region was covered during exposure testing to avoid contamination.

Loading was applied through a system of post-tensioning bars and railroad springs (5% maximum force loss during first year).
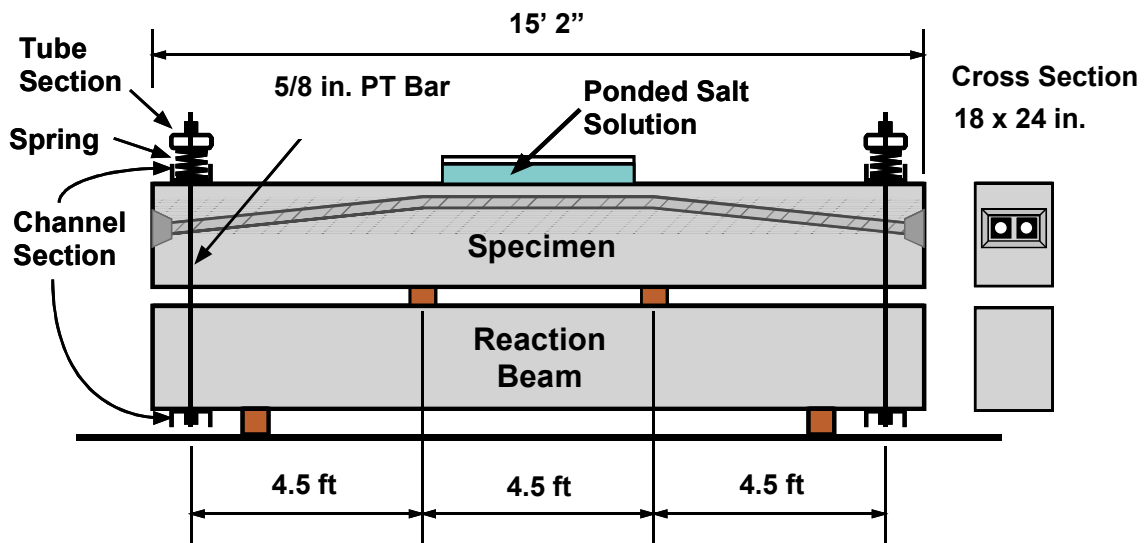
Figure 4.12 Test Setup [4.2]

Specimens were located in the paved area at the North end of the Ferguson Structural Engineering Laboratory, as shown in Figure 4.13.
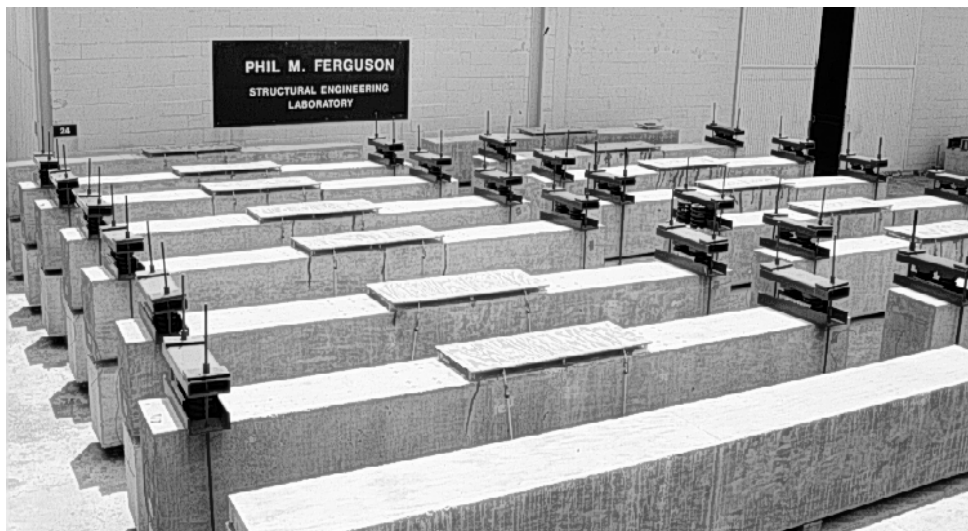
Figure 4.13.   Beam Test Setup at North End of Ferguson Laboratory [4.2]

227

4.2.6 Specimen Fabrication

All specimens were constructed at the Ferguson Structural Engineering Laboratory. Full description of the construction process is included in References 4.2 and 4.3. Figure 4.14 shows details of the construction process.
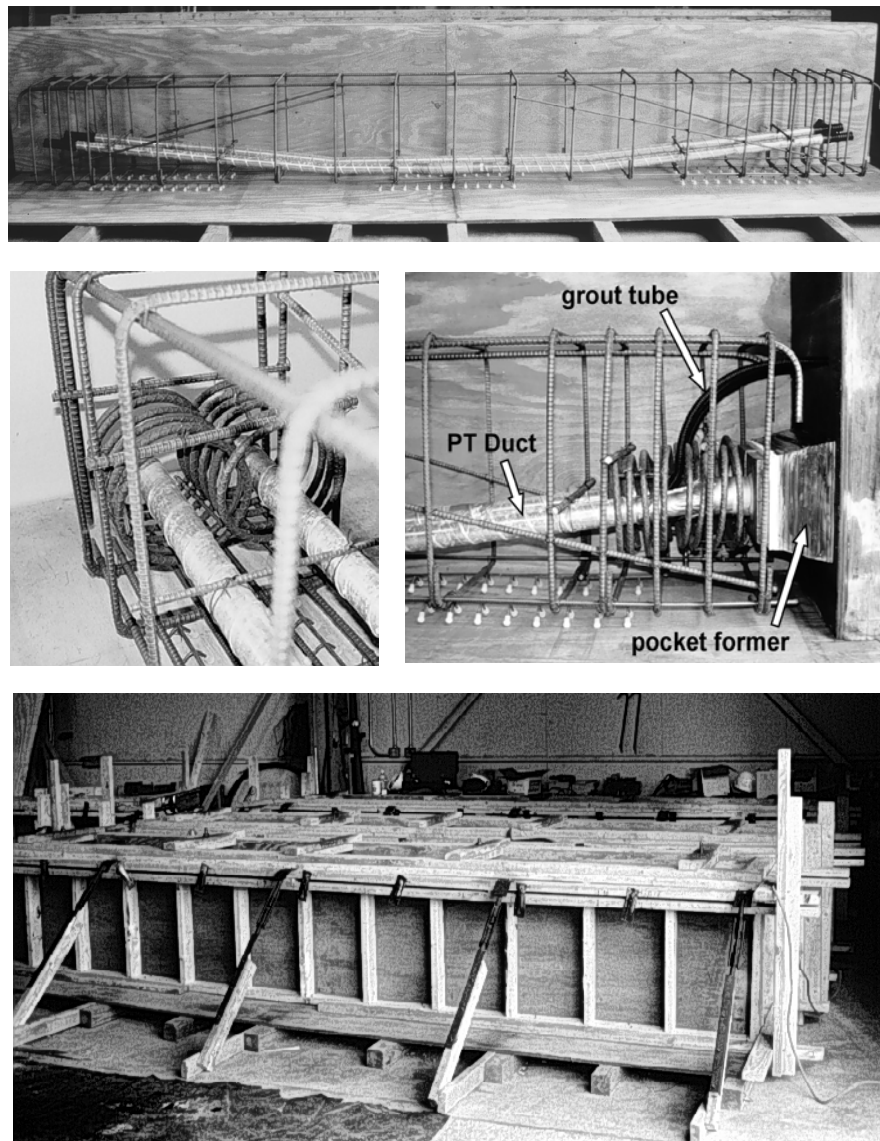
Figure 4.14. Reinforcing Cage, End Detail for PT Beam, and Formwork[4.2,4.3]

Post-Tensioning losses due to elastic shortening, friction and anchorage seating were considered in the design of each section type. Post-tensioning was applied in stages as shown in Figure 4.15. Several pull off tests were performed to determine necessary power seating forces to limit seating losses to tolerable levels.

Stage 1:
Tendon 1
to 1/3 T_j

1/3 T_j

Stage 2:
Tendon 2
to 2/3 T_j

2/3 T_j

Stage 3:
Tendon 1
from 1/3T_j
to T_j

T_j

Stage 4:
Tendon 2
from 2/3T_j
to T_j

T_j
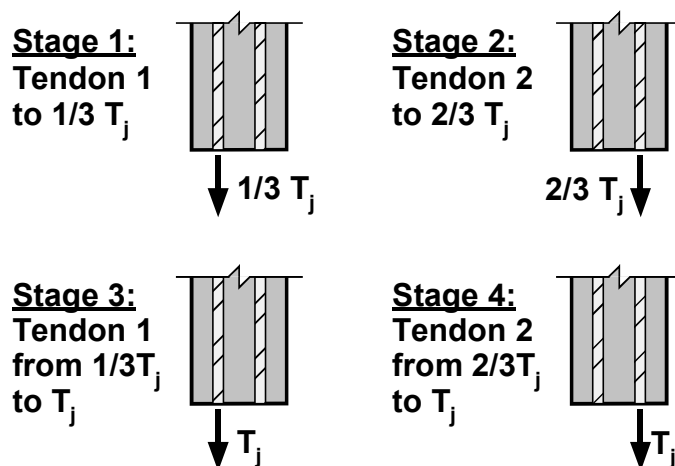
Figure 4.15 Staged Post-Tensioning Sequence [4.2]

Special wedges were used with the epoxy coated strands. These wedges were larger than standard wedges and proper anchor heads were fabricated to accommodate the wedges.

Grouting was performed following Post-Tensioning Institute recommendations. Vents were provided toward the end of the intermediate rise in the duct. Beam 2.9 had one tendon poorly grouted to compare against good practice procedures. As explain in Reference 4.3, for this tendon, the pump was turned off twice during pumping to allow possible pockets of air in the line. The pump was left off for approximately 10 minutes at one point during grouting to allow the grout already pumped into the tendon to reach a different consistency

than that of the grout in the pumping chamber that was continuously agitated. The far end grout tube was closed at the first appearance of grout instead of letting the grout flow to reach a continuous stream.

Anchorages were protected by filling the anchorage pockets with a nonshrink grout.

4.2.7 Specimen Loading

The specimens were loaded using two 120 kip hydraulic rams, one at each end of the beam. Figure 4.16 shows the loading hardware. The force in the post-tensioning bars was locked in by tightening the nuts. Load was maintained during exposure testing with the use of two railroad springs at each end. Loading was readjusted periodically to overcome losses. Detailed description of specimen load history is included in Reference 4.2.
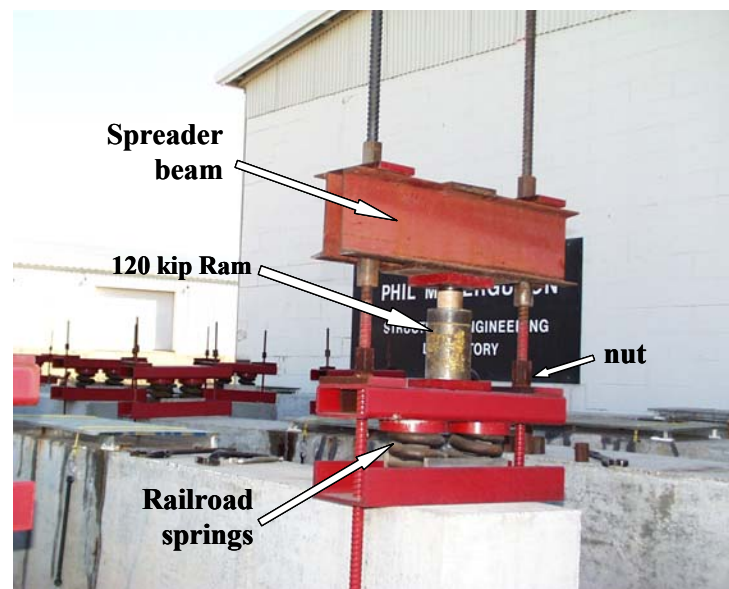
Figure 4.16 Beam Loading System

4.2.8 Block specimens

Concrete blocks were fabricated and cast simultaneously as the beam specimens, to monitor chloride penetration on beams during exposure testing. The use of these blocks avoids drilling in the test area of the actual beams to extract the powder samples for chloride analysis. Concrete block dimensions were 12 x 12 x 6 in., and were based on the AASHTO T 259-80 recommendations[4.10] for evaluating chloride ion permeability of concrete. Two blocks were cast during each pour, and were termed control block and ponded block. Each ponded block was fitted with a plexiglass ponded region that was filled with a 3.5% NaCl solution following the same exposure schedule as for the beam specimens. The control blocks were used to indicate the base level of chlorides in the concrete. Concrete blocks are shown in Figure 4.17
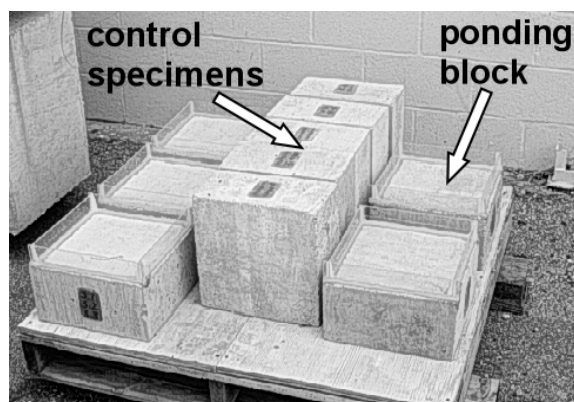
Figure 4.17 Concrete Blocks for Beam Chloride Analysis [4.2]

4.2.9 Beam Dripper System

Three specimens were selected to evaluate the effect of saltwater dripping in the anchorage area, at the top of the nonshrink grout: Specimen 2.7 (epoxy-coated strand), Specimen 2.9 (poorly grouted) and Specimen 2.12 (encapsulated system / plastic duct). The trickle saltwater system is shown in Figure 4.18.

Figure 4.18 Beam End Dripper System [4.3]

4.3   MEASUREMENTS DURING EXPOSURE TESTING

In an attempt to monitor the corrosion activity of the specimens during exposure testing, multiple non-destructive methods were used. All these methods have advantages and limitations that became more evident after full autopsies had been performed.   Non-destructive methods used in this series included: visual inspection, crack width measurements, half-cell potential readings, corrosion rate measurements and chloride penetration measurements.

4.3.1   Visual Inspection

During exposure testing, specimens were examined for any signs of distress, including changes in cracking, rust stains, and spalling.

4.3.2   Crack Width Measurements

Surface cracks were measured using a crack microscope and a crack comparator, where each crack crossed each one of the five reference lines drawn on the beam top (tension) side, as indicated in Figure 4.19.
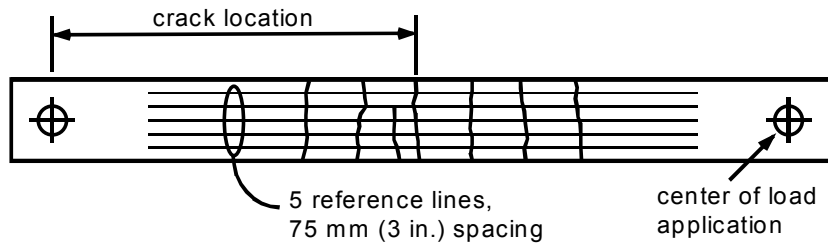
Figure 4.19 Crack Width Measurement Locations [4.2]

Cracks were measured after loading the specimens, at the beginning of exposure testing; and, at the end of testing for the selected specimens, immediately prior to full autopsies.

4.3.3   Half-Cell Readings

Half-cell potential measurements can provide two types of information:

- Probability of corrosion at a given location.

- Time for corrosion initiation.

Half-cell (HC) potentials were measured against a Saturated Calomel Electrode (SCE) at the end of the wet cycle.   Therefore, throughout this document, HC potentials are reported as millivolts versus SCE.   Other common reference electrodes and the potential of these electrodes versus the Standard Hydrogen Electrode (SHE) are shown in Table 4.6. A detailed description of the theory behind Half-Cell measurements is included in Reference 4.11.   Also, References 4.2 and 4.3 include a description of half-cell potential theory pertaining to this research program.

Half-Cell potential measurements require the use of a reference electrode, voltmeter and electrical connection to the reinforcement.   Ground clamps were used to attach a wire to the prestressing tendons before capping the anchorages. In addition, two ground wires were attached to the reinforcement cage, where

electrical continuous was found on the reinforcing cage, ducts and prestressing ducts.

Table 4.6 Common Reference Electrode Potentials versus SHE[4.11]

Reference Electrode	Half-Cell Reaction	Potential (V vs. SHE)
Copper-Copper Sulfate (CSE)	$CuSO_4 + 2e^- = Cu + SO_4^{2-}$	+0.318
Saturated Calomel Electrode (SCE)	$Hg_2Cl_2 = 2e^- = 2Hg + 2Cl^-$	+0.241
Standard Hydrogen Electrode (SHE)	$2H + 2e^- = H_2$	+0.000

HC potential measurements were taken every four weeks, and were based on ASTM C876 [4.12] guidelines. A grid was defined in the top of the specimens to serve as a guide for the readings. The grid spacing is 6 inches along the length of the beam. Figure 4.20 shows the example for non-prestressed beams and reading locations for other specimens.
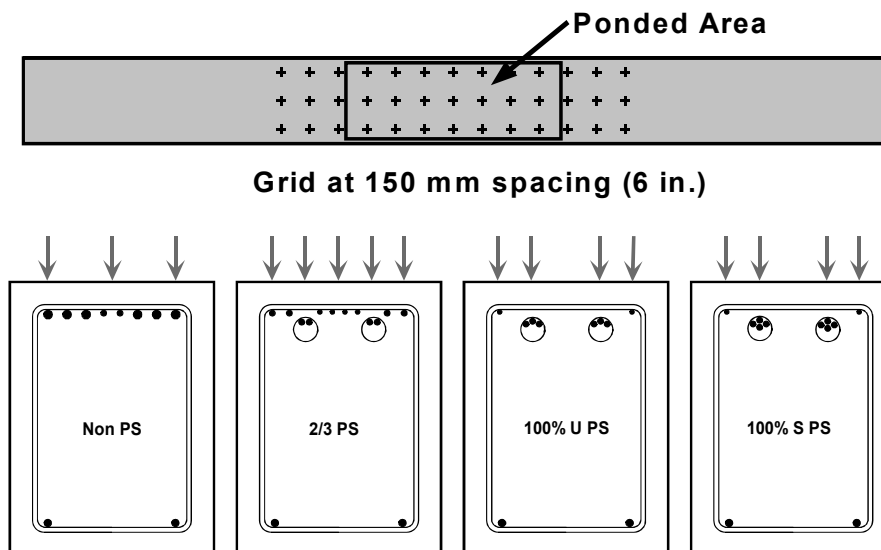
Figure 4.20 Grid for Half-Cell Potential Readings Non-Prestressed Beams and Half-Cell Reading Locations for other beams [4.2]

Table 4.7 shows the numerical significance of HC Potential readings. These values are reported for uncoated reinforcing steel and therefore they may not necessarily be appropriate for post-tensioned concrete. When galvanized steel ducts are used, half-cell potentials may reflect the potential of the zinc on the galvanized steel duct, which could lead to erroneous conclusions.

Table 4.7 Interpretation of Half-Cell Potentials for Uncoated Reinforcing Steel, Based on ASTM C876-91 [4.2]

Measured Potential (vs SCE)	Probability of Corrosion
more positive than –130 mV	less than 10% probability of corrosion
Between -130 mV and –280 mV	corrosion activity uncertain
more negative than –280 mV	greater than 90% probability of corrosion

During the first months of exposure testing, HC readings were taken before the saltwater solution was removed from the ponded area. It was later found that more accurate readings were obtained when taking the readings immediately after removal of the solution. Outside the ponded area, a wetting solution was used according to ASTM standards.

4.3.4 Corrosion Rate Readings

Full description of Corrosion Rate theory is included in Reference 4.2. The following description is an extract from that reference.

Polarization resistance is a useful technique for measuring instantaneous corrosion rates under laboratory and field conditions. Polarization measurements are rapid, highly sensitive, non-destructive and can be performed repeatedly. The theory states that within a small range of overvoltage (+/- 10 to 15 mV from the free corrosion potential), there is a linear relationship between applied current and electrode potential. The slope of the curve of ΔE versus $\Delta I_{applied}$ at the origin is

235

defined as the polarization resistance, R_p. The polarization resistance is inversely proportional to corrosion current, which in turn is directly proportional to corrosion rate. The computed corrosion rate can be compared to established guidelines to relate corrosion rate to corrosion damage. This method for corrosion rate measurements is often referred to as linear polarization or the polarization resistance method.[4.2]

The instantaneous corrosion current is related to the polarization resistance by the Stern-Geary equation shown below.[4.13,4.14]

$$i_{corr} = \frac{\beta_a \beta_c}{2.3(\beta_a + \beta_c)} \times \frac{1}{R_p}$$

Eq. 4.1

where

i_{corr} = corrosion current, mA

β_a = anodic Tafel constant, mV

β_c = cathodic Tafel constant, mV

R_p = polarization resistance, Ohms

The rate of corrosion in terms of corrosion current density, i, can be calculated by dividing the corrosion current, i_{corr}, by the area of polarized steel, A_p.

$$i = \frac{i_{corr}}{A_p}$$

Eq. 4.2

where

i_{corr} = corrosion current, mA

A_p = area of polarized steel, cm^2

i = corrosion current density, mA/cm^2

The computed corrosion rate, in terms of corrosion current density, can be compared to the established guidelines to relate corrosion rate to corrosion damage.

The polarization resistance, R_p, can be measured using several different techniques.[4.14,4.15] The two most common methods used for reinforced concrete are the three electrode procedure, and electrochemical impedance spectroscopy (sometimes referred to as AC impedance). Each method has advantages and disadvantages.[4.15] The three electrode method is most common due to its simplicity and low equipment cost.

The basic components of the equipment for the three electrode method are shown in Figure 4.21. The working electrode is the steel reinforcement for which the corrosion rate is to be measured. The counter electrode is used to apply the polarizing current to the steel. The reference electrode measures the free corrosion potential of the working electrode and the change in potential of the working electrode due to the applied current from the counter electrode. The process of measuring the polarization resistance begins with measuring the free corrosion potential or open-circuit potential of the tested area of steel reinforcement (working electrode). The working electrode is then polarized in uniform increments from the free corrosion potential and the associated current is measured. The polarization resistance is taken as the slope of the curve when ΔE versus $\Delta I_{applied}$ is plotted. This relationship is normally linear for a range of up to +/- 10 mV from the free corrosion potential.[4.13] When corrosion activity is low, small changes in applied current will produce a large change in potential and the polarization resistance will be large. When corrosion activity is high, large changes in applied current are needed to produce the desired potential increment, resulting in a low polarization resistance.

237

-322 mV | Potential
0.288 mA | Current

WE   CE   RE

WE - Working Electrode
CE - Counter Electrode
RE - Reference Electrode

polarizing
signal
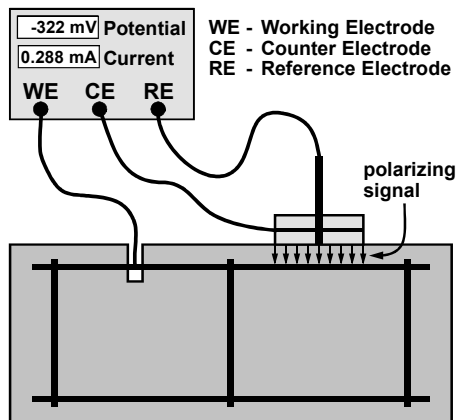
Figure 4.21 Polarization Resistance Apparatus (Schematic) [4.2]

Errors in Corosion Rate measurements based on Polarization Resistance include: Ohmic Electrolyte Resistance, uncertain polarized area, uncertain Tafel constants, use in prestressed concrete, erratic or very small polarization resistance. A detailed description of each source of error is included in Reference 4.2.

At the beginning of this experimental program there was no published work on using polarization resistance to monitor corrosion rates in pretensioned or post-tensioned concrete.   Some of the factors listed above may have a significant influence on the usefulness of the technique in prestressed concrete. In spite of these potential limitations, it was decided to use polarization resistance as an evaluation method in this testing program since qualitative information and comparisons may still be possible. Relative corrosion rate measurements can provide an indication of relative corrosion rates between specimens with different variables. For example, the relative effectiveness of different corrosion protection measures may be evaluated by comparing corrosion rates with those from "control" specimens. Also, regular measurements may indicate the onset of corrosion through increases in corrosion rate.

This program used two different types of equipment to take corrosion rate measurements: the CORRTEST PR-Monitor Model IN-4500 and the 3LP

Equipment. Both types of equipment use the three-electrode technique. Two corrosion rate measurements were taken on each beam, one at midspan and one at a 1 ft. (305 mm) offset from midspan. The polarization resistance technique requires a direct electrical connection to the steel for which the corrosion rate is being measured. This connection was provided by the ground wires attached to the mild steel reinforcement and prestressing tendons during construction. Corrosion rate measurements require the concrete to be initially dry. A wetting solution is used to moisten the concrete surface immediately prior to testing.

The PR-Monitor device uses a portable computer to control the corrosion rate measurement process. The PR-Monitor compensates for the concrete resistance and has a guard electrode to confine the polarization signal. The default polarization scan uses six steps of 5 mV, starting at -15 mV from the free corrosion potential and ending at +15 mV. The starting and ending potentials and voltage increment may be adjusted by the user in situations where the solution resistance is large in comparison to the polarization resistance. The increased potential range for the polarization scan can improve the accuracy of the measured polarization resistance when the solution resistance is high. At the end of the polarization scan, the concrete resistance or solution resistance is measured using AC impedance. A high frequency, low voltage AC signal is used to isolate the solution resistance. The computer performs a linear regression analysis on the polarization scan data and computes the total resistance, R_{tot}, as the slope of ΔE versus $\Delta I_{applied}$. The solution resistance, R_s, is subtracted from the total resistance to obtain the polarization resistance, R_p as shown below.

$$R_p = R_{tot} - R_s \qquad\qquad \textit{Eq. 4.3}$$

The corrosion current is calculated assuming a proportionality constant, B, of 26 mV, a typical value for actively corroding steel reinforcement in concrete.[4.16]

$$i_{corr} = \frac{B}{R_p}$$

Eq. 4.4

where,

$$B = \frac{\beta_a \beta_c}{2.3(\beta_a + \beta_c)}$$

Eq. 4.5

When all measurements and calculations are complete, the computer displays the free corrosion potential, polarization resistance, concrete resistance and corrosion rate in mils per year. This information and the polarization scan data are also written to an output file. The corrosion rate can be converted to current density by dividing the corrosion rate in mils per year by 0.4568.[4.17] The corrosion current density can also be calculated using the measured polarization resistance and assumed polarized area. (See Equations 4.1 and 4.2) The corrosion severity is assigned based on the ranges listed in Table 4.8.

Table 4.8 PR Monitor Corrosion Severity Based on Current Density [4.17]

Corrosion Current Density ($\mu A/cm^2$)	Corrosion Severity
Less than 0.1	Passive
Between 0.1 and 0.5	Low
Between 0.5 and 1.0	Moderate
Greater than 1.0	High

The 3LP Equipment was developed by Kenneth C. Clear, Inc., USA. A photograph of the equipment and setup is shown in Figure 4.22. The 3LP device is manually operated, and polarization scan data are recorded by hand. The counter electrode is rectangular and current confinement is not provided. The equipment measures the half-cell potential of the reinforcement (working electrode) and the applied polarization current. The polarization scan uses three

steps of 4 mV, starting at the free corrosion potential and ending at +12 mV. The concrete resistance is not measured by the 3LP device. The linear regression analysis on the polarization scan data must be performed using a hand calculator or computer to determine the total resistance, R_{tot}, as the slope of ΔE versus $\Delta I_{applied}$. No correction is made for the concrete resistance, and the polarization resistance, R_p, is simply taken as equal to the total resistance. The manufacturer recommends a proportionality constant, B, of 40.76 mV for calculating corrosion current. The manufacturer also provides guidance for relating corrosion current densities to expected corrosion damage. The SHRP Procedure Manual for Condition Evaluation of Bridges[4.18] indicates a proportionality constant, B, of 26 mV can be used with the 3LP device. The interpretation guidelines listed in Table 4.8 are appropriate for the 3LP device if B = 26 mV is used.[4.18]

Figure 4.22 3LP Equipment and Setup

4.3.5   Chloride Penetration Measurements

By regularly monitoring the penetration of chlorides into the concrete, it is possible to determine when chloride concentrations at the level of the steel reinforcement exceed the threshold for corrosion activity. Although this is not an

absolute measurement of corrosion activity, it can be used in conjunction with other data to estimate whether corrosion initiation had occurred. [4.2]

Chloride penetration is normally measured by collecting and testing samples from the concrete at varied depths. The most common method for obtaining samples is to use a rotary hammer (hammer drill). Holes are drilled in the concrete to the desired depth and the powder is collected for analysis. Samples were analyzed for acid-soluble chloride content using a specific ion probe (CL Test System by James Instruments).[4.2] Chloride sample and analysis procedure were based on AASHTO T260-94.[4.19]

Two samples were taken periodically from each concrete block at three depths: 0.5 in., 1 in., and 2 in. (bar level). The two powder samples per block were combined to give a representative sample at each depth. Several acid-soluble chloride tests were run and the results were averaged. Drill holes were filled with epoxy.[4.3]

At the end of testing, concrete samples for chloride content analysis were taken from beams scheduled for partial and full autopsy. Samples were taken at four locations from the beam transverse centerline: 2 in., 18 in., 26 in., and 32 in.; and, at three depths: 0.5 in., 1 in., and 2 in. In partial autopsy beams, 1.3 and 3.3 as described later, samples were not taken at the 2 in. depth so bars would not be damaged. For 100%U PS and 100%S PS beams, two samples were taken at each distance from the beam transverse centerline, since less reinforcement congestion allowed for drilling at these locations. Samples were combined, analyzed and results were averaged. Figures 4.23 and 4.24 shows the concrete sample locations.

242
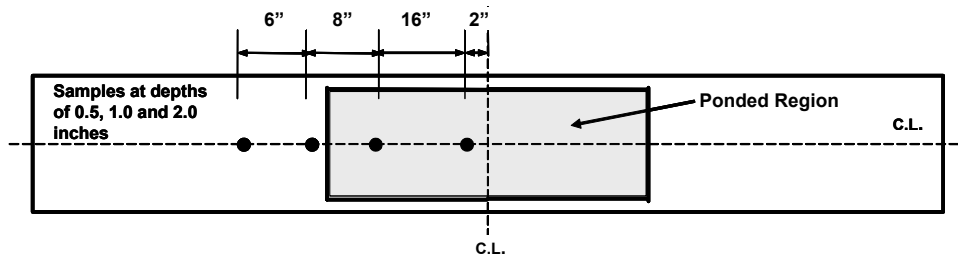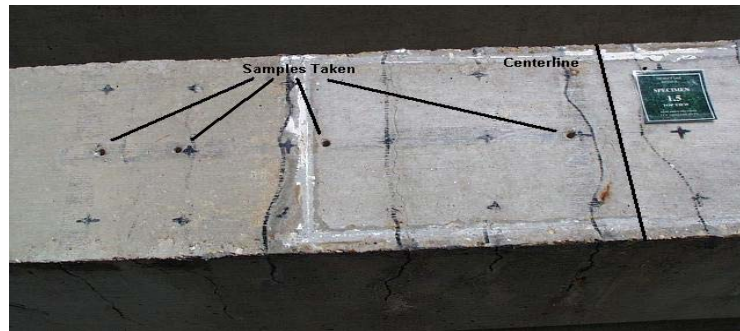
*Figure 4.23 Non-PS and 2/3 PS Beam Concrete Sample Locations
(Adapted from Reference 4.5)*
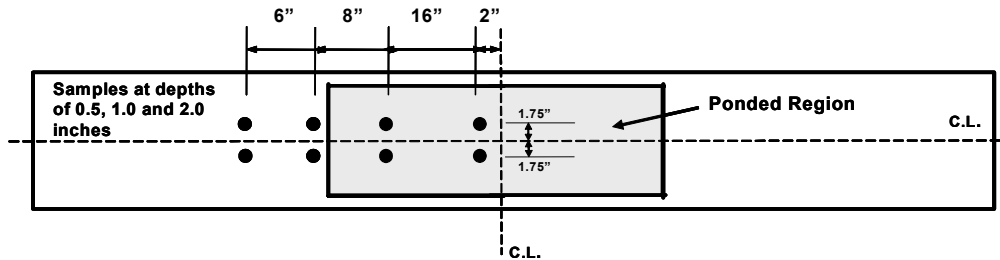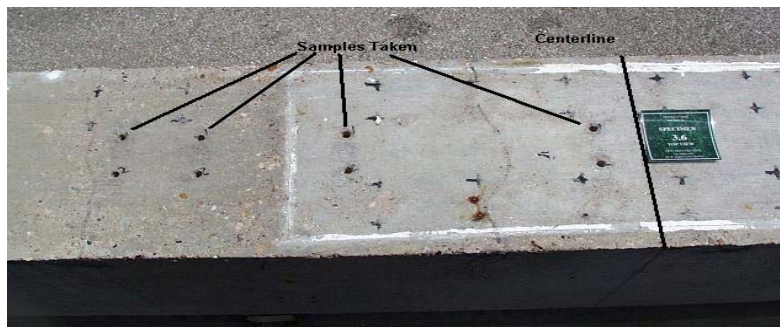
*Figure 4.24 100%U PS (and 100%S PS) Beam Concrete Sample Locations
(Adapted from Reference 4.5)*

243

The above sample locations allow for investigation of the following aspects:

- Vertical penetration of chlorides through concrete
- Horizontal propagation of chlorides through concrete
- Chloride content in ponded region versus non-ponded region
- Effect of surface cracking on chloride penetration.

4.3.6 Limited Autopsy

In order to correlate the half-cell potential readings with actual reinforcement condition, a limited autopsy was performed after 15 months of exposure testing by Schokker,[4.3] in Phase I beams 1.3, 3.3 and 3.4. Detailed description of limited autopsy procedure and findings are described in Reference 4.3

4.4 EXPOSURE TEST RESULTS

As described in Section 4.3, non-destructive testing to monitor corrosion activity in the specimens included: crack width measurements, half-cell potential readings, corrosion rate measurements, and chloride penetration and chloride content analysis. Results obtained during the exposure testing period are described herein.

4.4.1 Crack Width Measurements

Crack widths were measured at two dates: during initial loading and, at the end of testing for the selected partial and full autopsy beams. Measurements were taken using a microscope during initial loading and a crack comparator immediately before autopsy.

4.4.1.1 Crack Widths During Initial Loading

Crack patterns on the tension and side faces of all Phase I beams are shown in Figure 4.25. Load and reaction points are indicated in the figure. Only cracked specimens at service loading are shown. The measured crack data showed the following trends:[4.2]

- The number of cracks and extent of cracking was drastically reduced as the level of prestress increased.

- The extent of cracking along the beam was well predicted by the cracking moment for the three beam types. See Reference 4.2 for a detailed description of crack prediction and theory.

- Cracks commonly occurred at stirrup locations.

- The maximum surface crack widths were reduced as the level of prestress increased.

Non-PS: Service Load

1.2

2/3 PS: Very Small Crack (below Service)

2.1

Non-PS: Service Load

1.3

2/3 PS: Service Load

2.2

Non-PS: 25% Overload (Sustained Service)

1.4

2/3 PS: Service Load

2.3

100%U PS: 25% Overload (Sustained Service)

3.3

2/3 PS: 25% Overload (Sustained Service)

2.4

100%U PS: 33% Overload (Sustained Service)

3.4

2/3 PS: Service Load

2.11

100%U PS: 25% Overload (Sustained Service)

3.5

← Top surface (tension face)

← Side face
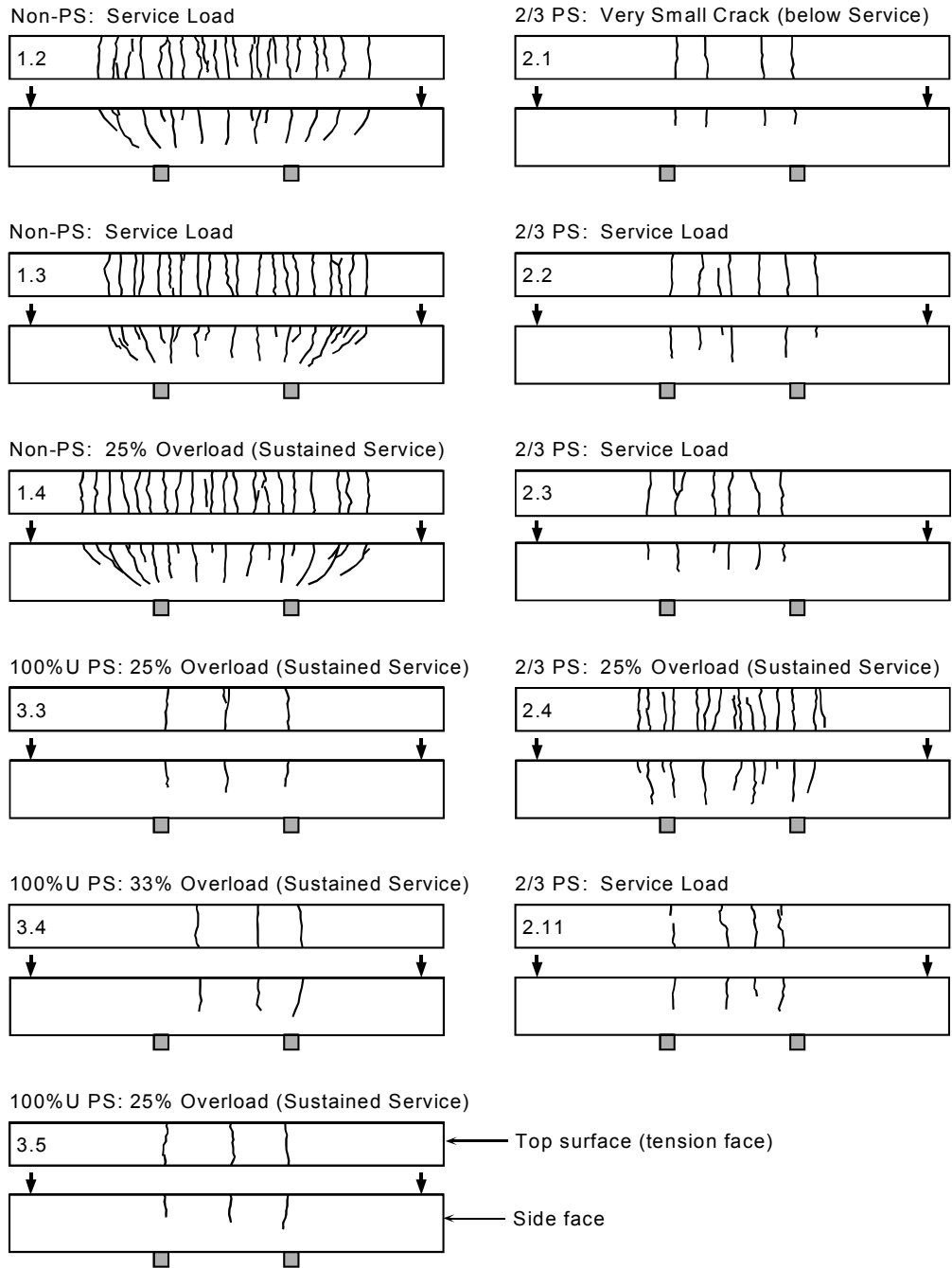
Figure 4.25 Phase I Beam Specimens Crack Patterns [4.2]

246

A comparison of the expected crack width versus moment curve for each of the three cracked section types is shown in Figure 4.26.
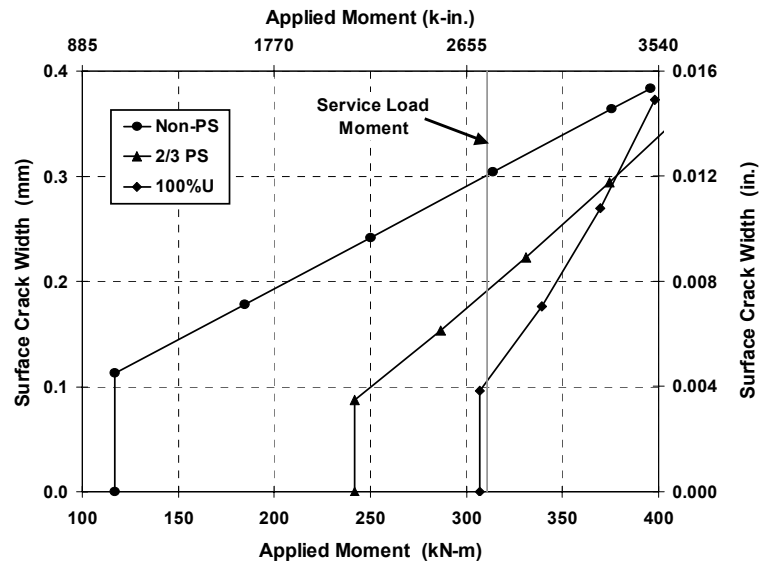
Figure 4.26 Calculated Cracking Behavior [4.3]

Figure 4.27 shows the measured maximum crack widths versus moment for each section type. The plots corresponding to the specimens with TxDOT standard concrete and control variables show excellent agreement with the estimated crack width values calculated prior to loading, using the Gergely-Lutz method with modifications for post-tensioned sections.[4.1] Plots of specimens with high performance concrete, high performance grout and epoxy-coated strand slightly deviated from the estimated crack width plots.[4.3]
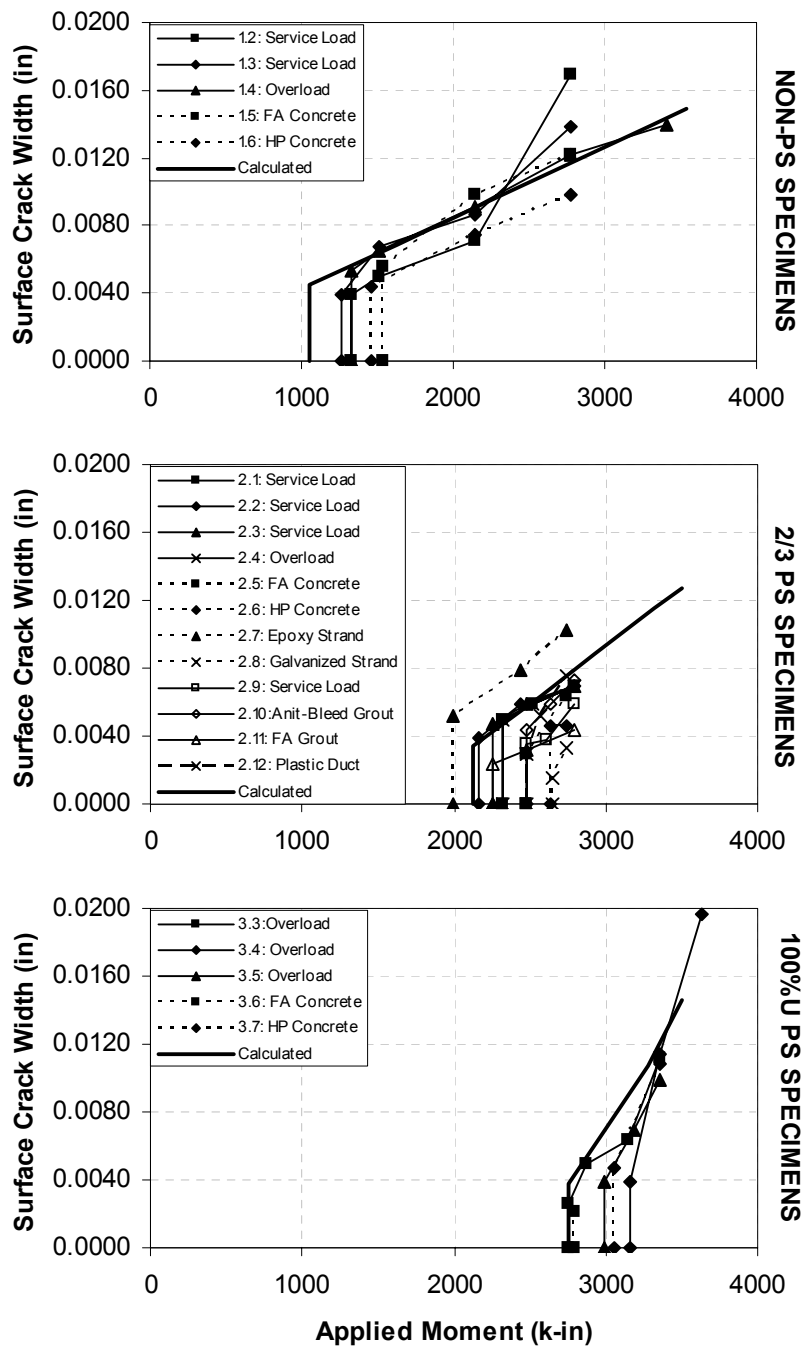
Figure 4.27 Measured Maximum Crack Widths [4.3]

248

4.4.1.2   Crack Widths at the End of Testing for Autopsy Beams

Transverse and longitudinal crack width measurements were taken from all autopsy beams immediately prior to concrete demolition and reinforcement removal.   Crack width measurements allowed:

- Determination of possible correlations between surface crack patterns and widths with any localized corrosion found during forensic examination

- Association of new surface cracking with corrosion products build-up.

Figures 4.28 show examples of each beam type from Phase II with final crack patterns and maximum and minimum crack width measurements at each crack location. Figures for all specimens are included in Appendix B. Similar figures from the initial crack width measurements can be found in Reference 4.2.
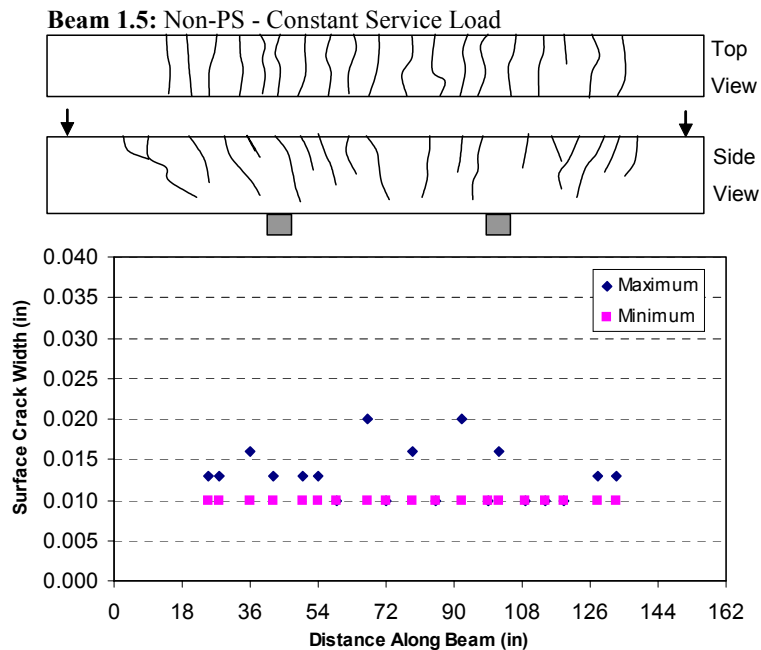
Figure 4.28   Non-PS Section – Crack Patterns and Measurements

249

Beam 2.5: 2/3 PS - Constant Service Load
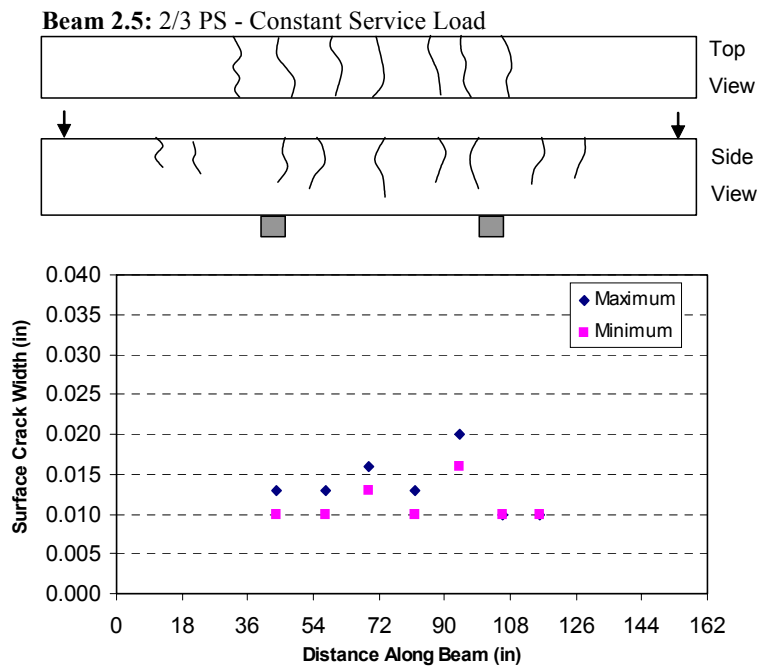
Figure 4.29   2/3 PS Section – Crack Patterns and Measurements

Beam 3.7: 100%U PS - Constant Service Load
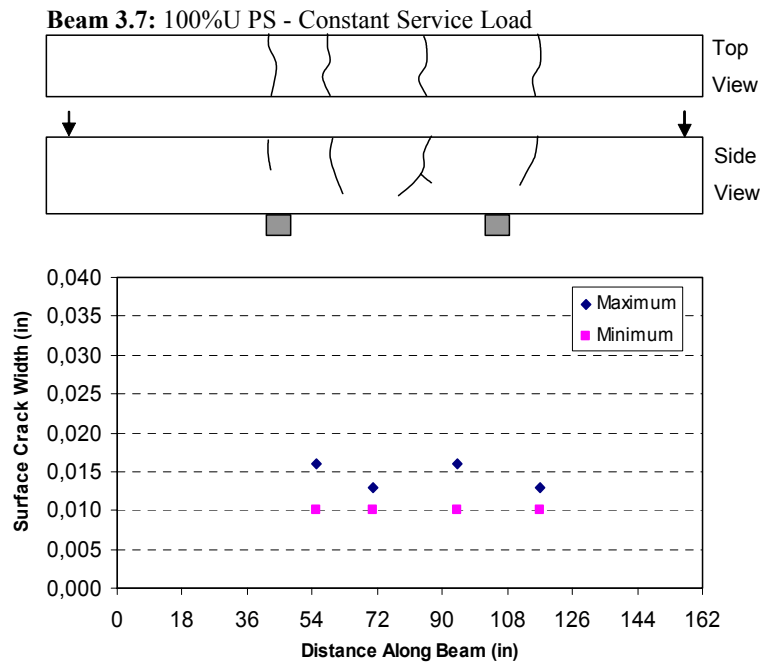
Figure 4.30   100%U PS Section – Crack Patterns and Measurements

It is observed that crack data did not exist for Specimen 3.2 and 4.2, since they remained uncracked under service load levels. The cracking of these specimens could be due to one of the previously mentioned reasons.

When comparing Figure 4.28 with Figure 4.27 for Specimen 1.5, it is observed an increase in crack width from initial to final testing. The maximum crack width for this specimen grew from 0.012 in. to 0.020 in. Similar comparisons can be made for Specimens 2.5 and 3.7 from Figures 4.27, 4.29 and 4.30. The crack width for Specimen 2.5 grew from 0.007 in. to 0.020 in. (about three times larger), while for Specimen 3.7 the maximum crack width grew from 0.010 in. to 0.016 in. Loading was kept constant during exposure period and therefore, it is concluded that additional crack opening was due to a combination of long term concrete deformations and, active reinforcement and duct corrosion.

Maximum measured crack widths and the average of the maximum crack widths from each crack for Phase I specimens are shown in Figure 4.31. From this figure, no difference is observed between the Non-PS and 2/3 PS beams, but shows a small decrease in the 100% PS Beams. The average maximum crack widths of the Phase I beams are almost identical, with Specimen 2.3 showing a slightly larger average maximum crack width. A slight trend of decreasing maximum crack width with increasing levels of prestress is observed.

Figure 4.32 shows the maximum measured crack width and the average of the maximum crack width from each crack for Phase II beams. No distinct trends are observed between the maximum crack widths and prestress levels, and between maximum crack widths and concrete type. However, the average maximum crack widths seem to show an increase with increasing prestress levels, even when differences may be considered very small.
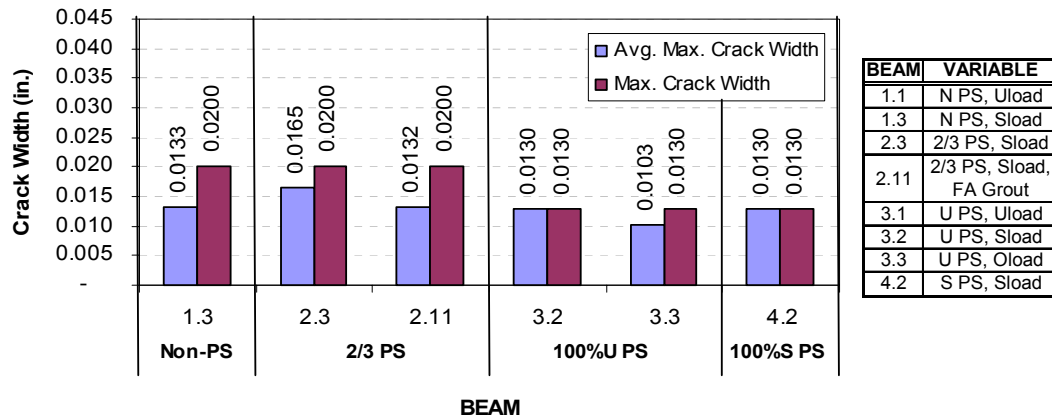
Figure 4.31 Crack Widths – Phase I Beams [4.5]
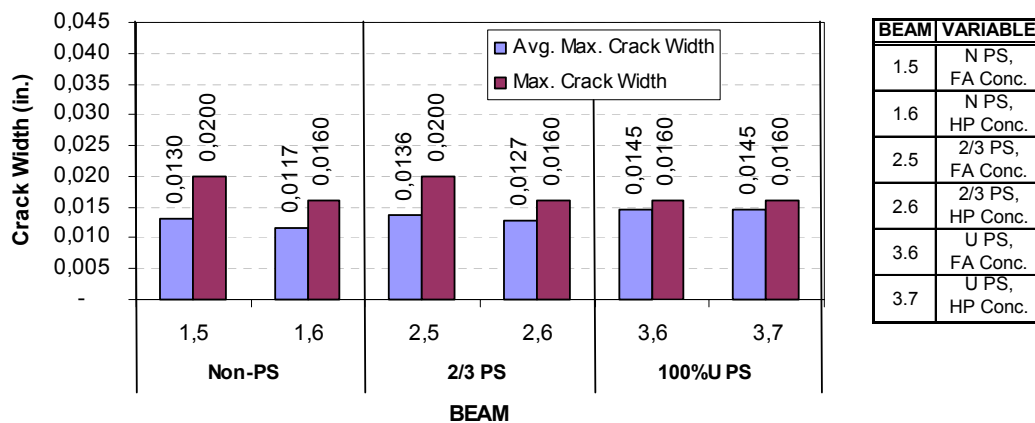
Figure 4.32 Crack Widths – Phase II Beams [4.5]

Wide longitudinal or splitting type cracks were found at the end of testing in Specimens 1.3, 2.3 and 2.11.   Section 4.6.2 includes a discussion on the importance of these cracks and their relation with corrosion found after forensic examination.

252

4.4.2   Half-Cell Potential Readings

Half-Cell potential readings were taken once every four weeks at the end of each wet cycle, as explain in Section 4.3.3.   The graphs presented in this section include readings from the beginning of the exposure testing period until the exposure testing ceased for the specimens chosen for forensic examination, corresponding to 1594 days for Phase I beams and 1235 days for Phase II beams. Due to these significantly different exposure durations, no attempt was made to compare data from both phases. Therefore, data from each phase will always be presented separately.

Potential plots correspond to the highest value for a specimen on a given reading date.   Average half-cell potentials and greatest negative potentials followed the same trend and therefore, only greatest negative potentials are shown. ASTM guidelines, as indicated in Table 4.7, are shown on the figures as a reference.

A seven month gap of half-cell plots can be observed on each graph. This gap represents a period in which readings were not taken due to changeover in personnel.

A negligible number of half-cell readings were found to not follow the trend of the rest of the plot. These outliers were clearly identified.   Due to their significant deviation from the trend, it was decided to replace the reading with an interpolation between the two adjacent readings.   These outliers are considered to be due to human error or to the unreliability of the equipment.   Over the course of exposure testing, complications commonly arose with the wiring system needed to take the readings. Although measures were taken to correct these problems, there was always some uncertainty of the accuracy of the readings. A description of the eleven data points considered as outliers in Phase I and the five data points in Phase II is included in Appendix B.

It is important to emphasize that half-cell potentials are only an indicator of corrosion activity, and a correlation with corrosion rate cannot be made. The ASTM C876 guidelines only indicate the probability of corrosion. Many factors can influence measured half-cell potentials, including concrete cover thickness, concrete resistivity, concrete moisture content, different metals and availability of oxygen. In some cases, these factors can lead to very negative half-cell potentials with little or no corrosion activity. For this reason it is important to consider the variation of half-cell potential measurements over an extended period of time in addition to the magnitude of the readings. [4.2]

The onset of corrosion can be determined based on the following:

- A sudden and significant change (more negative) in half-cell potentials, or
- Half-cell potential measurements more negative than -280 mV vs SCE.

When it is concluded that there is a high probability that corrosion activity is occurring within the member, it is difficult to determine which element (stirrups, rebars, ducts or prestressing strands) is corroding, since they are all electrically connected. This uncertainty can be resolved during forensic examination. [4.5]

4.4.2.1   Phase I Beam Specimens

Phase I beams started exposure testing in December 1997, and ended in May 2002 for the autopsy specimens, after 1594 days of testing. Figure 4.33 shows a plot of Phase I autopsy beams. At the end of testing, all specimens, except Specimen 3.1 (100%S PS, Unloaded), show high probability of corrosion activity, above 90%. Figures 4.34 through Figure 4.38 show the autopsy specimens separated according to the main variables. Half-cell potential plots for all specimens in Phase I can be found in Appendix B.
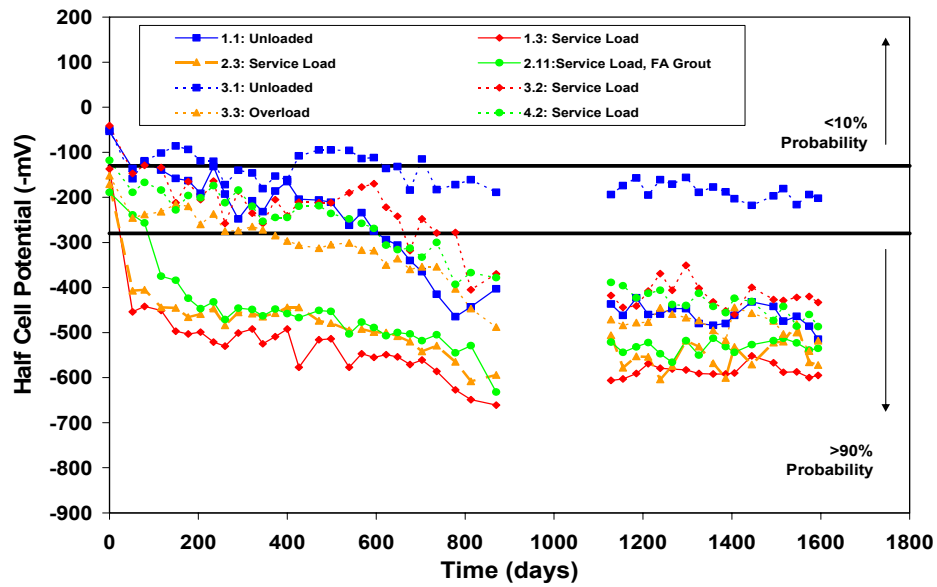
Figure 4.33 Half-Cell Potential Readings for Phase I Autopsy Beams

Figure 4.34 shows half-cell readings for the Non-PS beams in Phase I. The only variables on these specimens are the loading and cracking. The plot shows a decrease in the corrosion activity when the beam is unloaded and uncracked. The onset of corrosion shows also a significant difference, as would be expected, with an earlier possible initiation date for the loaded and cracked specimen. When analyzing this data, it has to be recognized that it is impractical to assume any structural member to be completely unloaded. Nevertheless, the negative effect of cracking is an important conclusion.

255
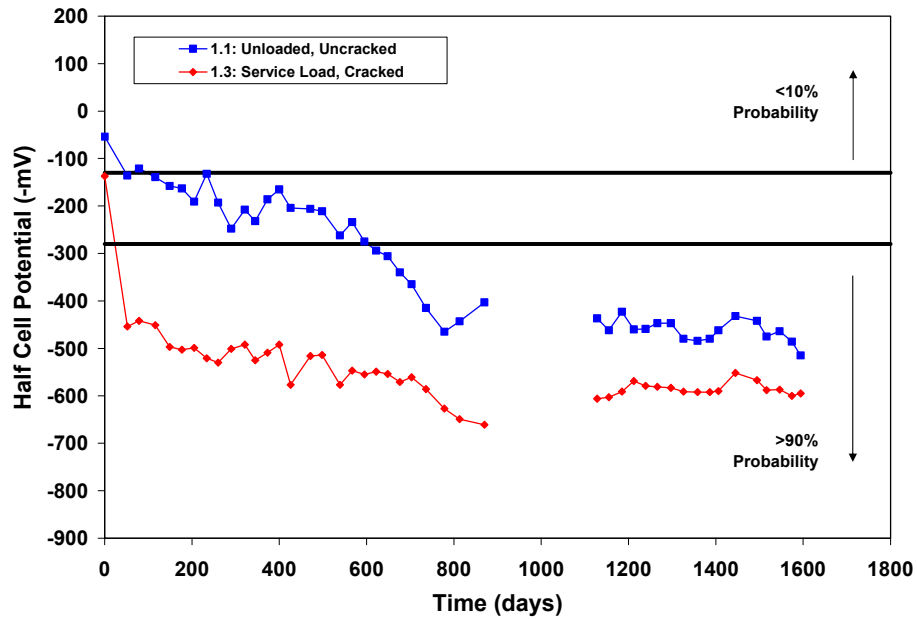
Figure 4.34 Half-Cell Potential Readings for Non-PS Specimens in Phase I Autopsy Beams

Figure 4.35 shows half-cell readings for mixed reinforcement beams in Phase I. Both specimens are identical except for the grout type. Based on this plot, it does not appear that the grout type has any effect on corrosion protection. However, care must be exercised when analyzing these results since readings could be reflecting the potential of the mild steel reinforcement and not the post-tensioning strands. If this is the case, it is reasonable to find both specimens with very similar potentials. The results will be confirmed after forensic examination.

256
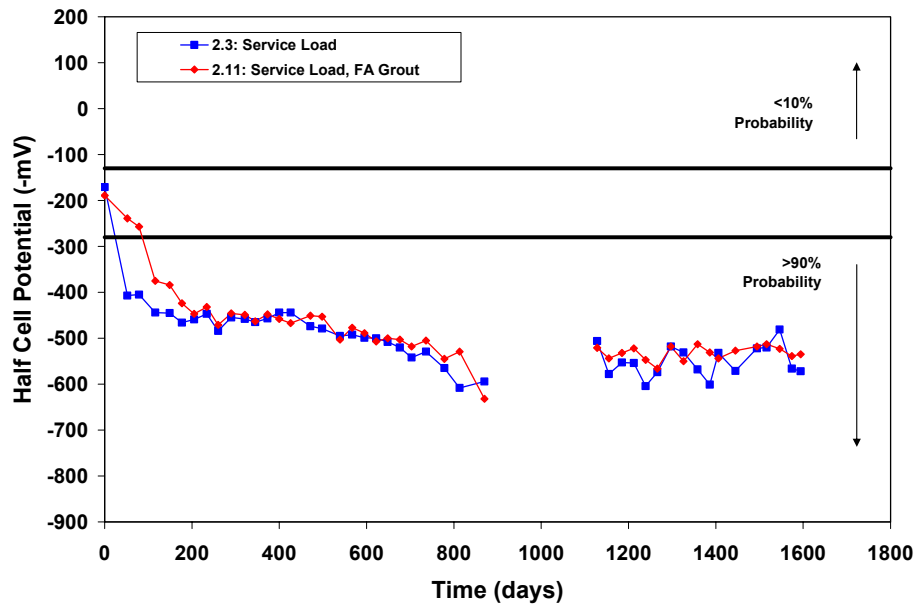
***Figure 4.35 Half-Cell Potential Readings for 2/3 PS Specimens in
Phase I Autopsy Beams***

Figure 4.36 shows half-cell readings for the 100%U PS beams in Phase I. Variables include applied load and cracking. There is a distinct trend showing a decrease in the performance of the specimens with increasing loading. The unloaded specimen had half-cell readings in the uncertain range, between 10% and 90% probability of corrosion, while loaded specimens exceeded the 90% probability line. Again, an increase in corrosion protection is observed when the specimen is uncracked through both time to initiation of corrosion and final potential readings. It should be noted that while Specimen 3.2 was uncracked at the beginning of testing, a fine crack at the end of testing was found on the specimen surface. The effect of this crack will be clearly determined after forensic examination.

257
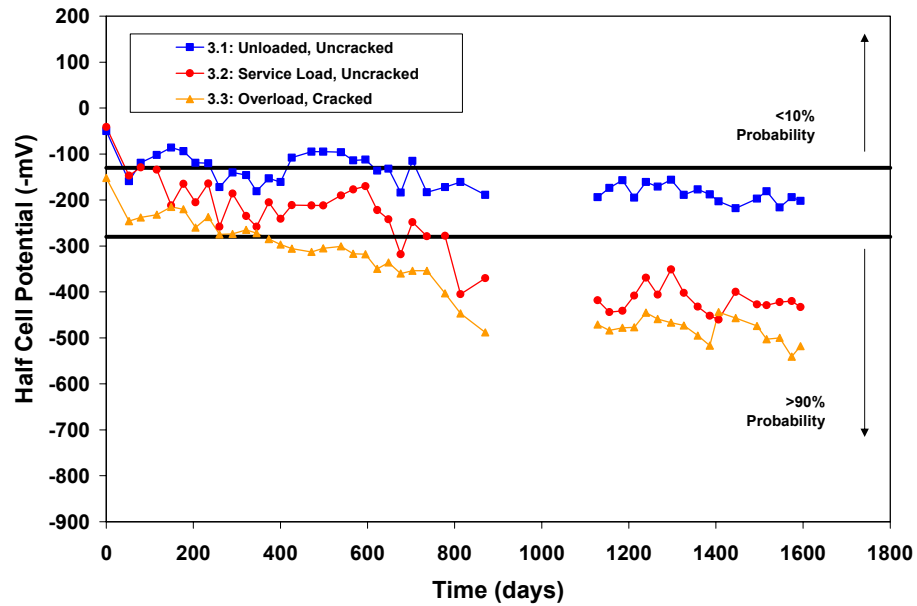
Figure 4.36 Half-Cell Potential Readings for 100%U PS Specimens in Phase I Autopsy Beams

Figure 4.37 shows half-cell readings for unloaded specimens in Phase I. The only variable is the level of prestress. A distinct trend is shown with higher probability of corrosion in the non-prestressed specimen with respect to the 100%U PS beam. The non prestressed beam shows potentials above the 90% probability of corrosion line, while the 100%U PS specimen is in the uncertain range, between the 10% and the 90%. Both specimens were uncracked during exposure testing. Therefore, the results could suggest the importance of concrete permeability and the effect of increased compressive stresses in post-tensioned specimens, since the only possible form of chloride ingress was through the concrete.

258
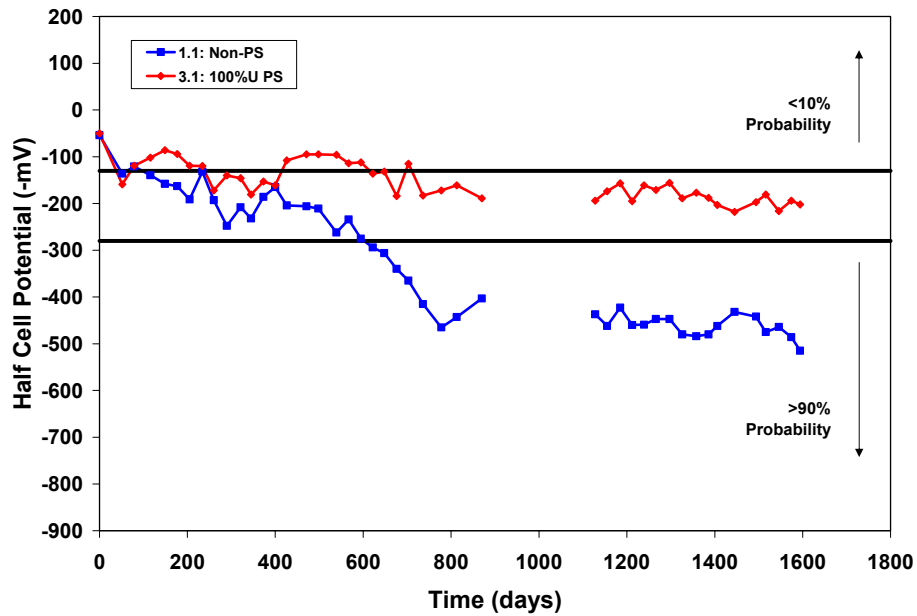
***Figure 4.37 Half-Cell Potential Readings for Unloaded Specimens in
Phase I Autopsy Beams***

`   Figure 4.38 shows half-cell potentials for beams subjected to service load
in Phase I. The only variable is the level of prestress. As in the previous case,
performance increases as the level of prestress increases. Mixed reinforced beams
show similar performance as Non-PS beams, with a distinct difference with
respect to 100% PS beams. Comparison among 100%U PS and 100%S PS shows
a slightly better performance of the 100%S PS. However, the difference is very
small to draw definite conclusions.
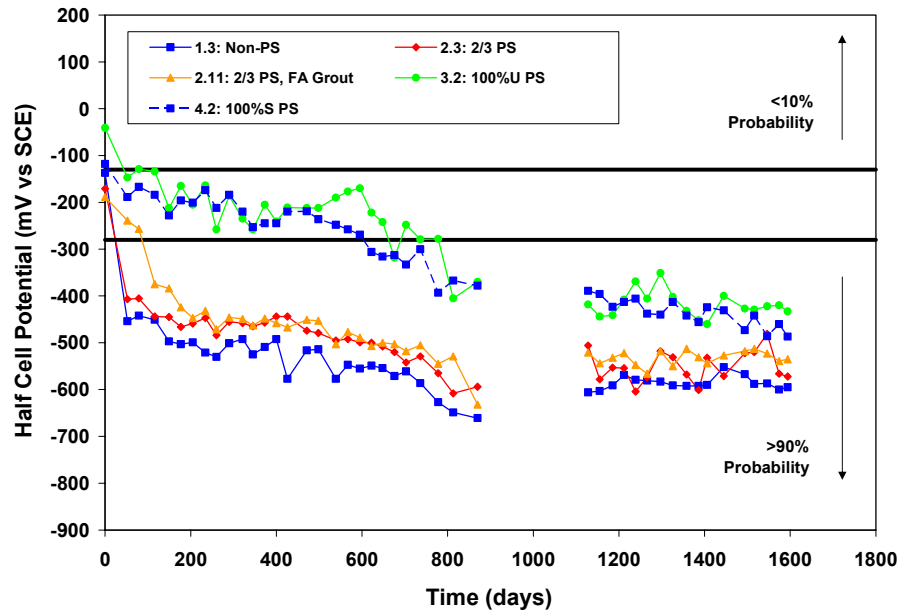
Figure 4.38 Half-Cell Potential Readings for Service Load Specimens in Phase I Autopsy Beams

Figure 4.39 shows the greatest negative half-cell potentials for all Phase I autopsy beams at the final reading date, corresponding to 1594 days of exposure. All specimens except Specimen 3.1 (100%U PS, Unloaded) show very negative potential readings, exceeding the value of -280 mV representing the 90% probability of corrosion. Non-prestressed and mixed reinforced (2/3 PS) beams show slightly greater negative potentials at the end of testing than 100% PS beams. Again, prestressing in the unloaded and uncracked Specimen 3.1 seems to play the major role in delaying chloride penetration and corrosion activity, when compared to Specimen 1.1.

Table 4.9 shows the time to initiation of corrosion activity for each Phase I autopsy beam. The onset of corrosion activity is defined as the date when a reading more negative than -280 mV is recorded, indicating a probability of corrosion greater than 90%.

260
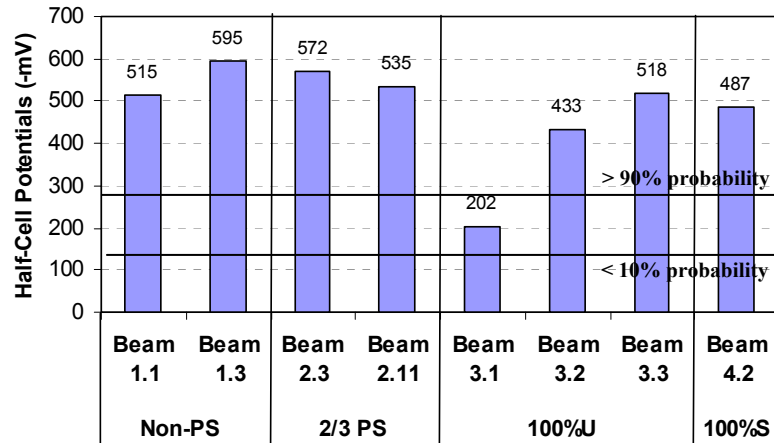
Figure 4.39 Greatest Negative Half-Cell Potential Reading at 1594 Days (End of Testing) for Phase I Autopsy Beams

Table 4.9 Time to Initiation of Corrosion for Phase I Autopsy Beams

Specimen	Description	Time to Corrosion (days)
1.1	Non-PS, Unloaded	622
1.3	Non-PS, Service Load	52
2.3	2/3 PS, Service Load	52
2.11	2/3 PS, Service Load, Fly Ash Grout	116
3.1	100% U PS, Unloaded	Never crosses threshold
3.2	100%U PS, Service Load	676
3.3	100% U PS Overload	373
4.1	100%S PS, Service Load	622

Figure 4.40 shows the half-cell potential contour maps for all Phase I specimens after 1594 days of exposure testing. Contour maps for the same beam specimens after 498 days are shown in Appendix B.

1.1 – Unloaded (uncracked)

1.2 – Service (cracked)

1.3 – Service (cracked)

1.4 – Overload (cracked)

2.1 – Very Small Cracks

2.2 – Service (cracked)

2.3 – Service (cracked)

2.4 – Overload (cracked)

2.11 – Service (cracked)

3.1 – Unloaded (uncracked)

3.2 – Service (uncracked)

3.3 – Overload (cracked)

3.4 – Overload (cracked)

3.5 – Overload (cracked)

4.1 – Service (uncracked)

4.2 – Service (uncracked)

■ < -580 V_{SCE}

■ -430 to -580 V_{SCE}

■ -280 to -430 V_{SCE}

□ -130 to -280 V_{SCE}

■ +20 to -130 V_{SCE}

Figure 4.40 Half-Cell Potential Contour Maps at 1594 Days for
All Phase I Beams

262

After half-cell potential readings had been analyzed from the Phase I specimen plots the following main conclusions are drawn:

- Probability of corrosion increases with increasing loading
- Probability of corrosion increases with increasing cracking
- Probability of corrosion decreases with increasing levels of prestress
- Performance of mixed reinforced (2/3 PS) specimens resemble more that of Non-Prestressed specimens, as opposed to 100% PS specimens
- No distinct difference is observed between the performance of 100%U PS and 100%S PS specimen.

4.4.2.2 Phase II Beam Specimens

Phase II beams started exposure testing in December 1998, and ended in May 2002 for the autopsy specimens, after 1235 days of testing.   Figure 4.41 shows a plot of Phase II autopsy beams.   At the end of testing, all specimens, show high probability of corrosion activity, above 90%.
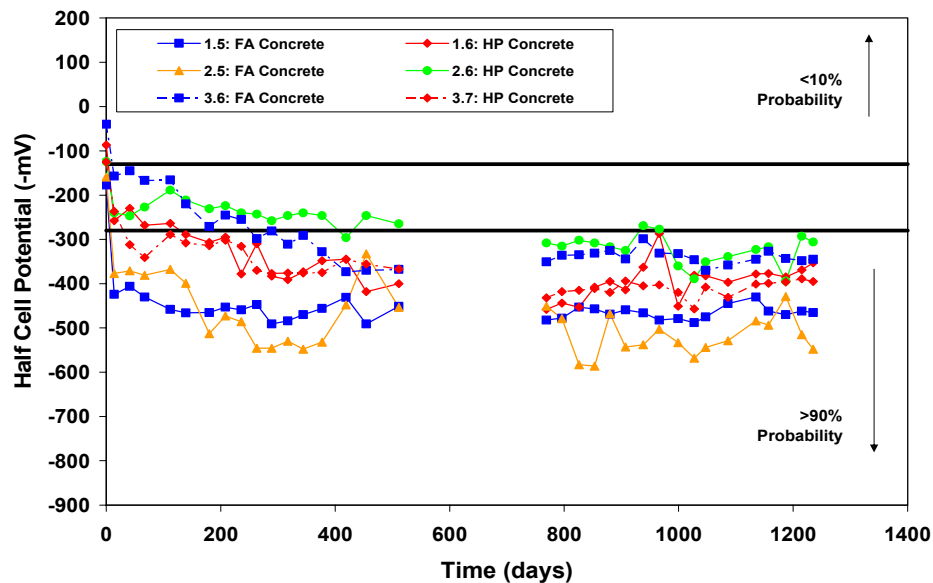
Figure 4.41 Half-Cell Potential Readings for Phase II Autopsy Beams

263

Figures 4.42 through Figure 4.46 show the autopsy specimens separated according to the main variables. Half-cell potential plots for all specimens in Phase II are included in Appendix B.

Figure 4.42 shows half-cell readings for the Non-PS beams in Phase II. The only variable being compared for these specimens is the concrete type. According to the time to initiation of corrosion and the potential readings throughout the exposure testing period, it appears that high performance concrete (as described in Section 2.4.4.1) performed better than the fly ash concrete. However, both appear to merge to the same potential range.
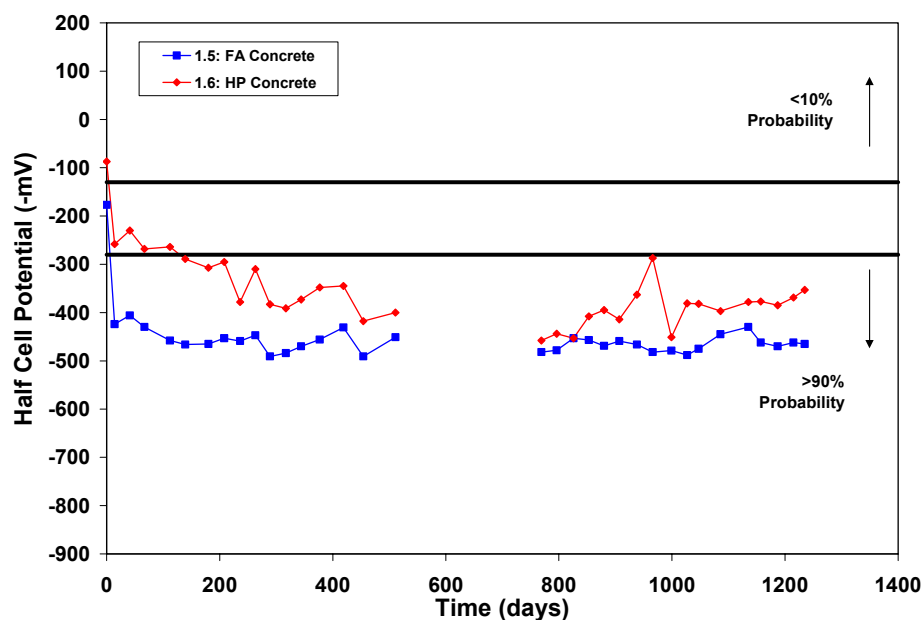
Figure 4.42 Half-Cell Potential Readings for Non-PS Specimens in Phase II Autopsy Beams

Figure 4.43 shows half-cell readings for the mixed reinforced beams (2/3 PS) in Phase II. As in the previous case, all the variables are the same, with the exception of concrete type. Based on the time to initiation of corrosion and

potential readings, the high performance concrete performed better than the fly ash concrete. These results show the positive effect of less permeable concrete, even when these specimens were cracked at service load levels.
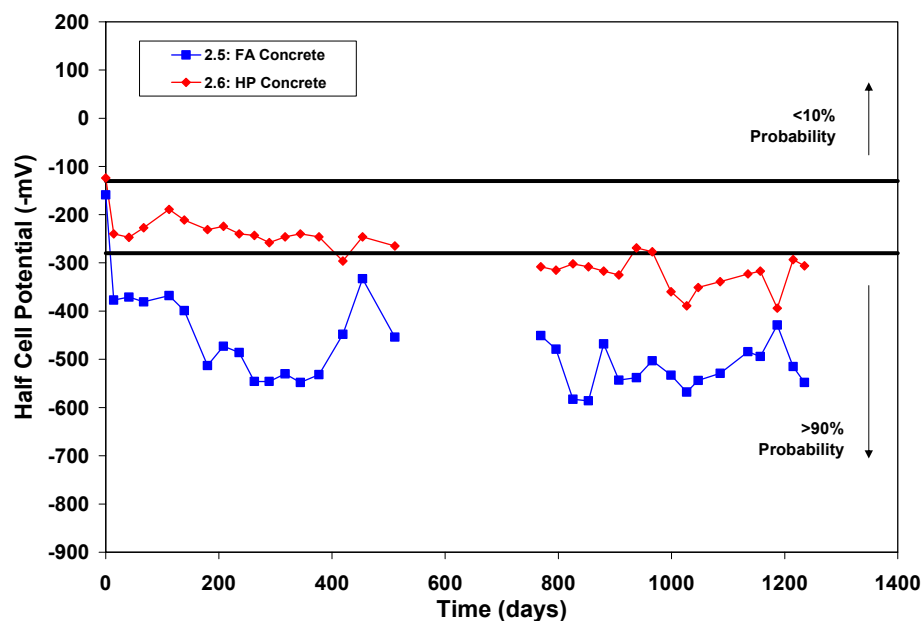
Figure 4.43 Half-Cell Potential Readings for 2/3 PS Specimens in Phase II Autopsy Beams

Figure 4.44 shows half-cell readings for the 100%U PS beams in Phase II. The only variable being compared among these specimens is concrete type. The plot shows that the fly ash performed slightly better than high performance concrete as defined in Section 2.4.4.1, in contrast to the previous plots. However, the half-cell potential difference between both curves is very small, and appears to be merging to the same potential range.
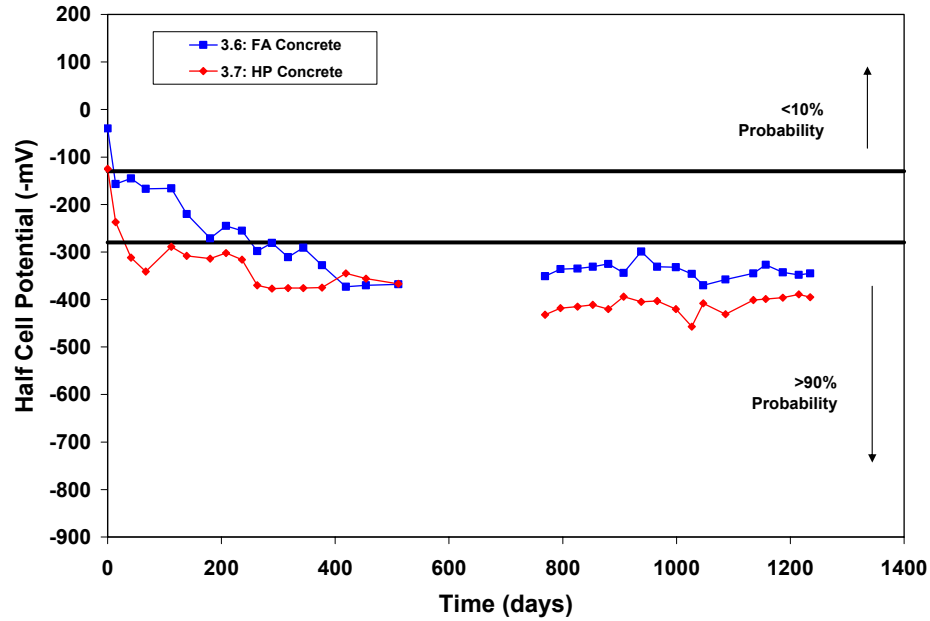
Figure 4.44 Half-Cell Potential Readings for 100%U PS Specimens in Phase II Autopsy Beams

Figure 4.45 shows half-cell potential readings of the fly ash concrete beams in Phase II. The three specimens differ only on the level of prestress. As observed from the plot, based on the time to initiation of corrosion and the half-cell potential values, the fully prestressed (100%U PS) beam performed better than the Non-PS and 2/3 PS beams. Both the simple reinforced and the mixed reinforced concrete specimens show the same corrosion initiation time, but the potential of the mixed reinforced beam becomes slightly more negative over the exposure period.
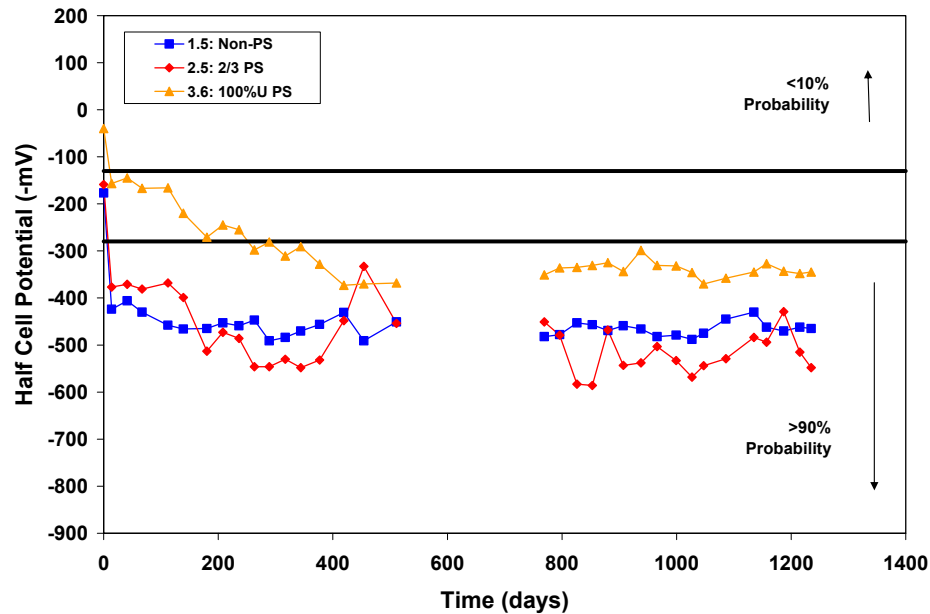
Figure 4.45 Half-Cell Potential Readings for Fly Ash Concrete Specimens in Phase II Autopsy Beams

Figure 4.46 shows half-cell potentials for the high performance concrete beams in Phase II. The only difference among the specimens is the level of prestress. As can be observed, it appears that the 2/3 PS beam performed better than both the 100%U PS and the Non-PS beams that performed very similar throughout the testing period. However, the final potentials are very similar for all three specimens.

When comparing Figures 4.45 and 4.46, it is observed that high performance concrete specimens performed slightly better than fly ash specimens. Both specimens have cement replacement by fly ash, but the high performance concrete as defined in Section 2.4.4.1, had a lower water-cement ratio.
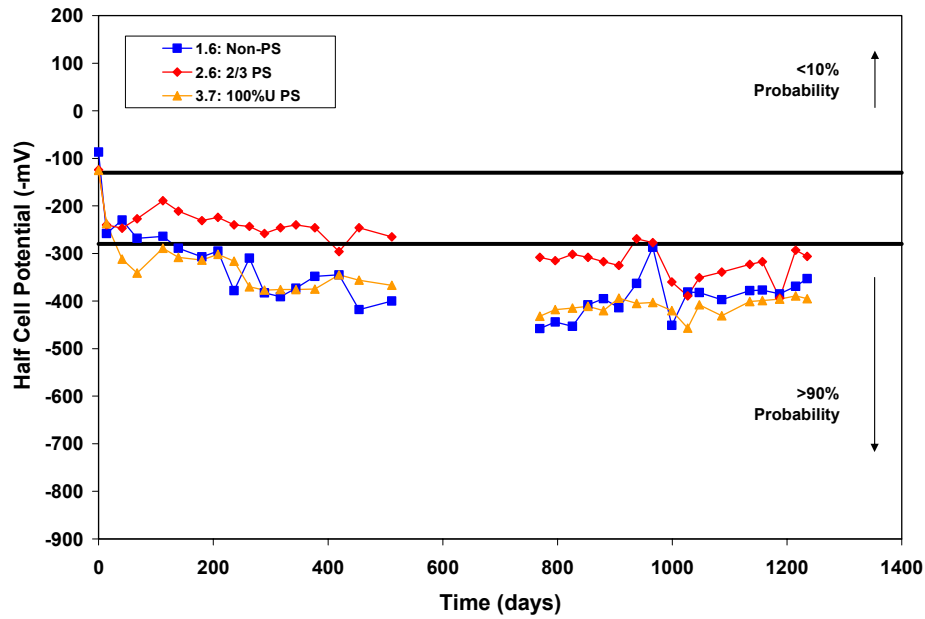
***Figure 4.46 Half-Cell Potential Readings for High Performance Concrete
Specimens in Phase II Autopsy Beams***

Figure 4.47 shows the greatest negative half-cell potentials for all Phase II
autopsy beams at the final reading date, corresponding to 1235 days of exposure.
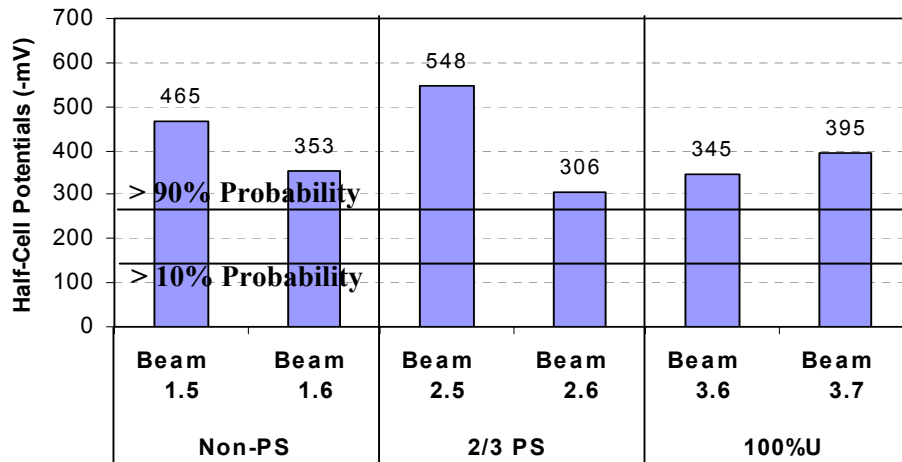
***Figure 4.47 Greatest Negative Half-Cell Potential Reading at 1235 Days
(End of Testing) for Phase II Autopsy Beams***

All specimens show very negative potentials and there is not a clear distinction among the Non-PS, 2/3 PS and 100%U PS specimens. Specimen 2.5 (mixed reinforced, fly ash concrete) show a slightly higher potential at the final date than the other specimens, but all were above the level of 90% probability of corrosion.

Table 4.10 shows the time to initiation of corrosion activity for each Phase II autopsy beam. The onset of corrosion activity is defined as the date when a reading more negative than -280 mV is recorded, indicating a probability of corrosion greater than 90%.

Table 4.10 Time to Initiation of Corrosion for Phase II Autopsy Beams

Specimen	Description	Time to Corrosion (days)
1.5	Non-PS, Fly Ash Concrete, Service Load	15
1.6	Non-PS, High Performance (HP) Concrete, Service Load	139
2.5	2/3 PS, Service Load, Fly Ash Concrete	14
2.6	2/3 PS, HP Concrete, Service Load	419
3.6	100% U PS, Unloaded, Fly Ash Concrete	263
3.7	100%U PS, HP Concrete, Service Load	41

Figure 4.48 shows the half-cell potential contours maps for all Phase II specimens after 1235 days of exposure testing. Contour maps at 139 days of testing are shown in Reference 4.4.

1.5 – Service (cracked)

2.9 – Service (cracked)

1.6 – Service (cracked)

2.10 – Service (uncracked)

2.5 – Service (cracked)

2.12 – Service (uncracked)

2.6 – Service (cracked)

3.6 – Service (cracked)

2.7 – Service (cracked)

3.7 – Service (cracked)

2.8 – Service (cracked)

■ < -580 V_{SCE}
■ -430 to -580 V_{SCE}
■ -280 to -430 V_{SCE}
□ -130 to -280 V_{SCE}
■ +20 to -130 V_{SCE}
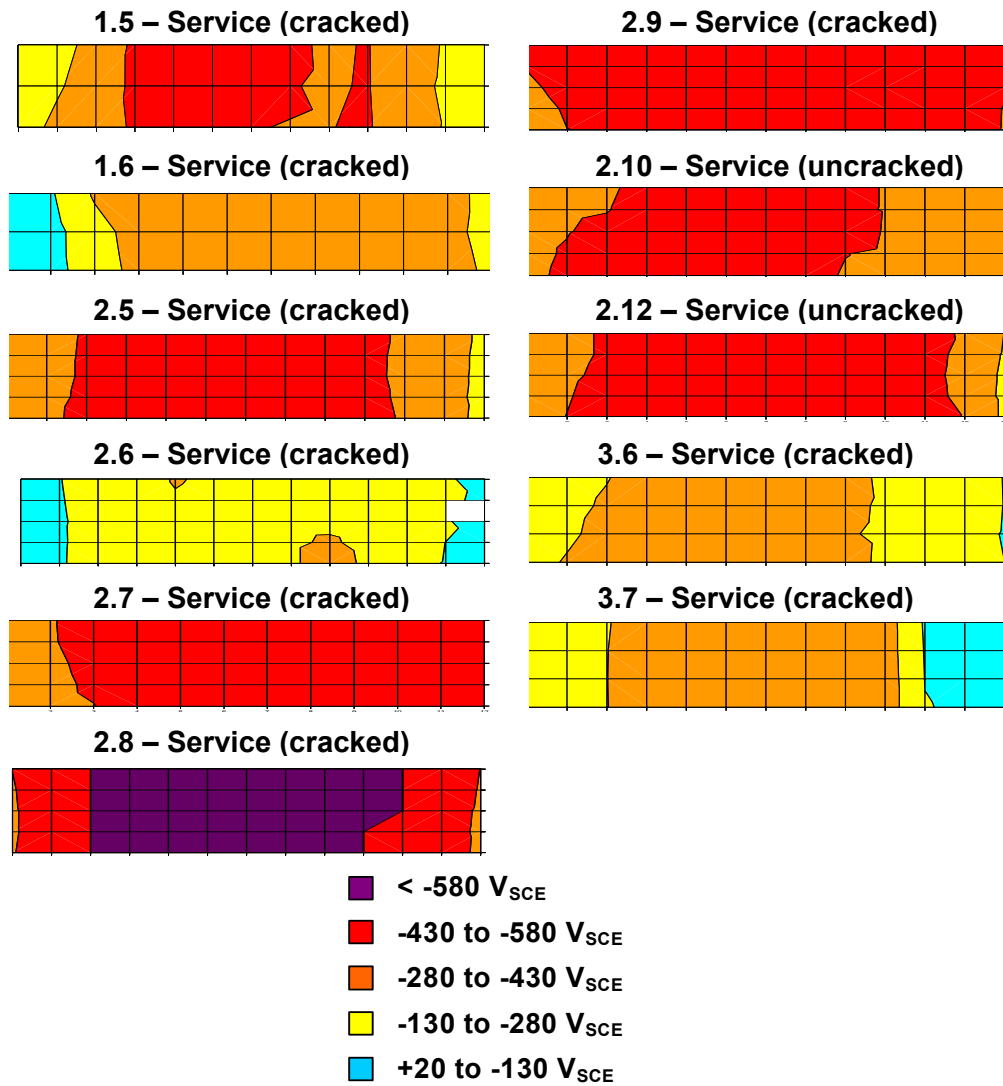
*Figure 4.48 Half-Cell Potential Contour Maps at 1235 Days for
All Phase II Beams*

After half-cell potential readings had been analyzed from the Phase II specimen plots the following main conclusions were drawn:

270

- Performance of mixed reinforced (2/3 PS) specimen is closer to that of a non-prestressed specimen than to a fully prestressed specimen.

- High Performance concrete as defined in Section 2.4.4.1, appears to perform slightly better than Class C concrete with cement replacement by Fly Ash. However, the difference is not significant.

- Phase II series lacked a control specimen with Class C concrete without fly ash. Therefore, the effect of fly ash concrete and high performance concrete could not be directly evaluated against common practice.

4.4.3   Corrosion Rate Measurements

The procedure and theory for the corrosion rate measurements is explained in Section 4.3.4. Four measurements were taking up to the forensic examination date. Two types of equipment were used: PR Monitor and 3LP. Phase I specimen measurements were taken at seven, twelve, fifteen and forty-seven months of exposure. Phase II specimen measurements were taken at 37 months of exposure. Difficulties with the measurement equipment did not permit taking of readings immediately prior to autopsy. The following discussion of corrosion rate results was reported in Reference 4.5.

4.4.3.1   Phase I Beam Measurements

Corrosion rate measurements of all the Phase I beams were performed after seven months of exposure testing using the PR Monitor equipment. Readings were taken midway (one week) through the dry portion of the exposure cycle. Corrosion rate measurements were performed after twelve months of exposure testing using the 3LP equipment. Readings were taken on day five of the two week dry portion of the exposure cycle. The next measurements were performed after fifteen months of exposure testing using both the PR Monitor and 3LP

equipment. Readings were taken sixteen days after the start of the dry portion of the exposure cycle (the dry period was extended beyond the normal two weeks because work was being performed on the beams). The final successful corrosion rate measurements of the Phase I beams were performed after 47 months of exposure testing using the 3LP equipment.

As recommended in the SHRP Procedure Manual for Condition Evaluation of Bridges,[4.18] a proportionality constant, B, of 26 mV was used in the calculation of the corrosion current when the 3LP equipment was used. This assumption was made so the interpretation guidelines in Table 4.8 (shown on each graph) could be used to rank the corrosion severity according to the measurements.

Corrosion rate readings, in terms of corrosion current density, for the Phase I autopsy beams are shown in Figures 4.49 and 4.50, and are listed in Table 4.11. Graphs of the corrosion rate readings of all the Phase I beams can be found in Appendix B.

Figure 4.49 is a graph of the maximum corrosion rate readings taken of the Phase I autopsy beams using the PR Monitor equipment. The graph shows a consistent trend that the corrosion rate decreased over time. This does not make practical sense. Therefore, further investigation of the corrosion rate readings will be made after the forensic examination to determine the reliability of the use of the PR Monitor equipment as a means of assessing corrosion rate. Through comparison of the three 100%U PS beams, both sets of readings show that the corrosion rate increases as the applied load, which corresponds to crack width increases.

272

The chart contains the following embedded tables and legend:

Current Density	Severity
< 0.1	Passive
0.1 to 0.5	Low
0.5 to 1.0	Moderate
> 1.0	Severe

BEAM	VARIABLE
1.1	N PS, Uload
1.3	N PS, Sload
2.3	2/3 PS, Sload
2.11	2/3 PS, Sload, FA Grout
3.1	U PS, Uload
3.2	U PS, Sload
3.3	U PS, Oload
4.2	S PS, Sload

Legend: PR Mon: 7 mon. / PR Mon: 15 mon.
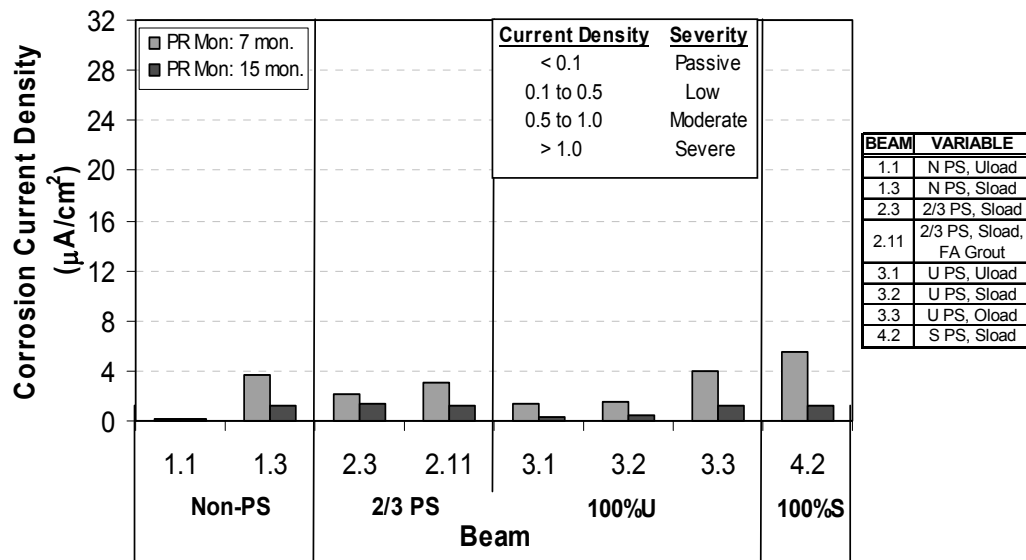
Figure 4.49 Maximum Corrosion Rate Readings Using PR Monitor for Phase I Autopsy Beams[4.5]

Figure 4.50 is a graph of all the maximum corrosion rate readings taken of the Phase I autopsy beams using the 3LP equipment. The graph shows a consistent trend that the corrosion rate increased over time, with the exception of Specimen 3.1. Again, comparison of the 100%U PS sections show increasing corrosion rates with increasing applied load. There is a significant increase from Specimen 3.2 (uncracked) to Specimen 3.3 (cracked).

Corrosion Current Density (μA/cm²)

Legend:
- □ 3LP: 12 mon.
- ▨ 3LP: 15 mon.
- ■ 3LP: 47 mon.

Current Density	Severity
< 0.1	Passive
0.1 to 0.5	Low
0.5 to 1.0	Moderate
> 1.0	Severe

BEAM	VARIABLE
1.1	N PS, Uload
1.3	N PS, Sload
2.3	2/3 PS, Sload
2.11	2/3 PS, Sload, FA Grout
3.1	U PS, Uload
3.2	U PS, Sload
3.3	U PS, Oload
4.2	S PS, Sload

Beam: 1.1, 1.3 (Non-PS); 2.3, 2.11 (2/3 PS); 3.1, 3.2, 3.3 (100%U); 4.2 (100%S)
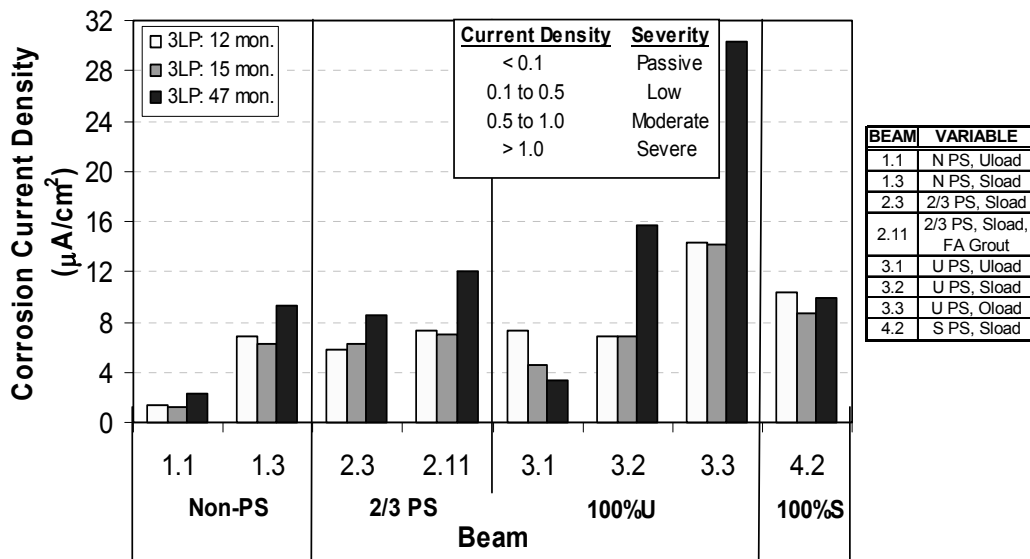
Figure 4.50 Maximum Corrosion Rate Readings Using 3LP for Phase I Autopsy Beams[4.5]

The corrosion severities determined in Table 4.11 are based on the last corrosion rate readings taken with the PR Monitor equipment. All readings taken with the 3LP equipment are extremely high, showing severe corrosion for all measurements. This indicates that, although they can be used to make relative comparisons and identify trends, readings using the 3LP are not reliable for determining actual corrosion rates and severities. For this reason, the corrosion severities assigned were based on the most recent reading taken with the PR Monitor.

Table 4.11 Phase I Autopsy Beam Corrosion Current Density Measurements[4.5]

Beam & Location	7 months PR Monitor $\mu A/cm^2$	12 months 3LP $\mu A/cm^2$	15 months PR Monitor $\mu A/cm^2$	3LP $\mu A/cm^2$	47 months 3LP $\mu A/cm^2$	Corrosion Severity at 15 Months
1.1: Offset	0.18	1.31	0.19	1.15	2.32	Low
Midspan	0.20	1.09	0.12	0.76	1.21	Low
1.3: Offset	3.70	6.83	1.29	6.29	9.27	Severe
Midspan	1.07	4.64	1.06	3.50	8.03	Severe
2.3: Offset	2.17	5.85	1.43	4.79	8.02	Severe
Midspan	1.53	4.93	0.47	6.32	8.52	Low
2.11: Offset	1.90	7.39	1.16	7.08	11.28	Severe
Midspan	3.09	6.61	1.26	6.70	12.07	Severe
3.1: Offset	1.29	7.06	0.31	4.62	3.03	Low
Midspan	1.34	7.37	0.14	4.44	3.30	Low
3.2: Offset	1.42	6.33	0.42	6.83	15.74	Low
Midspan	1.49	6.84	0.31	5.43	7.46	Low
3.3: Offset	0.99	7.50	0.45	6.56	5.62	Low
Midspan	3.92	14.27	1.21	14.14	30.32	Severe
4.2: Offset	4.95	10.31	1.21	8.75	9.43	Severe
Midspan	5.58	9.47	1.06	7.16	9.86	Severe

Differences Between 3LP and PR Monitor Corrosion Rates

The PR Monitor and 3LP equipment both use the three electrode technique for measuring polarization resistance. However, several differences exist between the two pieces of equipment. The 3LP equipment represents the first generation of polarization resistance equipment for measuring corrosion rates of steel in concrete. The PR Monitor reflects several advancements, including the use of a guard ring electrode to confine the polarizing signal of the counter electrode, and measurement of the concrete resistance to compensate for solution resistance. The possible effects of these differences are discussed in West.[4.2]

Figure 4.51 is a graph of maximum corrosion rate readings taken after 15 months of exposure. The purpose of this graph is to compare the two types of

equipment used for taking the readings over the duration of this experimental program. The 3LP corrosion rates measured after fifteen months of testing are significantly higher than the PR Monitor corrosion rates. Other research and field experience with various devices for corrosion rate measurement have consistently shown that the 3LP equipment indicates higher corrosion rates than other devices.[4.2] Although there is a large difference in the readings from the two types of equipment, the trends in corrosion activity are similar. This suggests that the large discrepancy in magnitude is likely due to inherent differences between the two devices. Although the magnitude measured by the 3LP equipment may not be reliable, it appears to be a good method for determining corrosion trends of individual specimens and comparing these trends among multiple specimens.
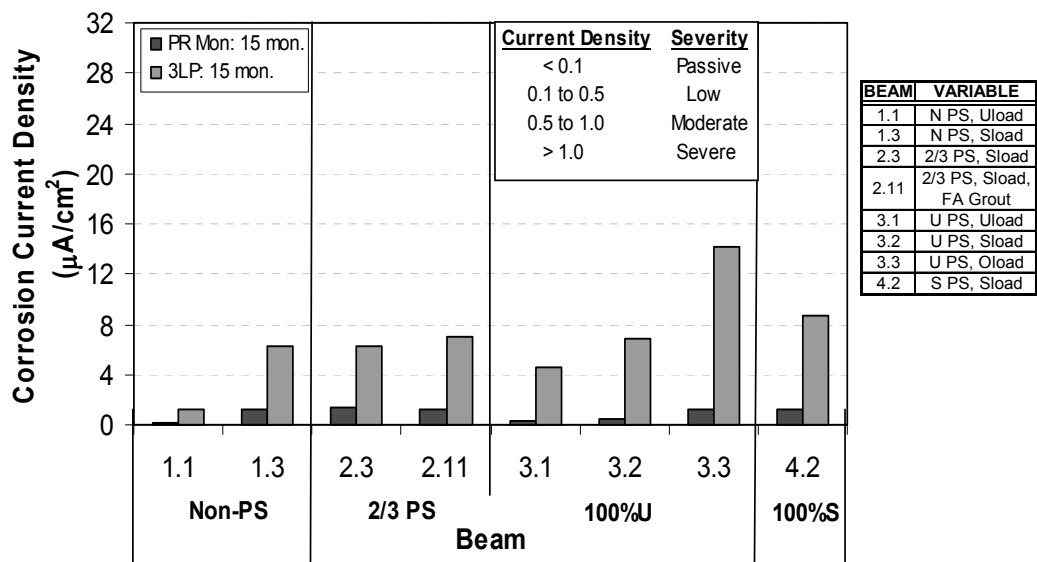
Figure 4.51 Comparison of Corrosion Rate Measurement Equipment[4.5]

4.4.3.2   Phase II Beam Measurements

Only one successful set of corrosion rate readings was obtained for the Phase II beams. They were performed after 35 months of exposure testing using the 3LP equipment. As with the measurements of the Phase I beams, a proportionality constant, B, of 26 mV was used in the corrosion current calculations. Corrosion rate readings, in terms of corrosion current density, for the Phase II autopsy beams are plotted in Figure 4.52 and listed in Table 4.12. A graph of the corrosion rate readings for all Phase II beams can be found in Appendix B.

Figure 4.52 shows higher corrosion rates in the 100%U PS than the 2/3 PS beams for both concrete types. Specimen 3.7 is significantly higher than all the other readings. The reason for this will be determined after the forensic examination. The readings do not show a consistently better concrete type. Since only one set of measurements was obtained, comparisons among readings over time or between equipment cannot be made for the Phase II specimens.
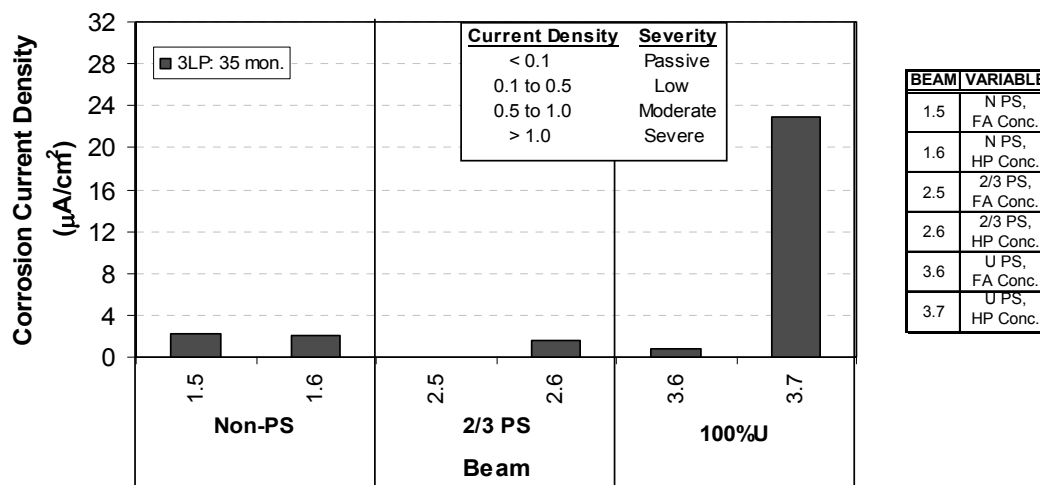
Figure 4.52 Corrosion Rate Readings Using 3LP for Phase II Autopsy Beams[4.5]

Because corrosion severities were only assigned according to readings taken with the PR Monitor, and no readings of the Phase II beams were taken using this equipment, corrosion severities could not be assigned to the Phase II beams in Table 4.12.

Table 4.12 Phase II Autopsy Beam Corrosion Current Density Measurements[4.5]

Beam & Location		35 months 3LP $\mu A/cm^2$
1.5:	Offset	2.17
	Midspan	2.01
1.6:	Offset	1.86
	Midspan	2.05
2.5:	Offset	0.06
	Midspan	0.07
2.6:	Offset	1.45
	Midspan	1.55
3.6:	Offset	no reading
	Midspan	0.78
3.7:	Offset	9.66
	Midspan	22.90

4.4.4 Chloride Content Analysis

Acid Soluble Chloride Analysis was performed as described in Section 4.3.5. Samples were taken at the following dates:

- From Phase I Concrete Blocks: Seven, fourteen, forty-one and fifty-four months of exposure testing.

- From Phase II Concrete Blocks: Twenty-nine and forty-two months of exposure testing.

- From Autopsy Beam Specimens: Immediately prior to forensic examination.

Chloride Threshold value is indicated in the figures at 0.033%. This value, intended as a guide only, is based on the widely accepted chloride threshold value of 0.2% of the weight of cement.[4.20]

4.4.4.1 *Phase I Concrete Block Specimens*

All Phase I specimens were constructed with Standard TxDOT Class C Concrete. However, concrete mixtures varied a little, which was the purpose of casting and testing the different block specimens. Figure 4.53 shows the acid soluble chloride content at different depths from the Phase I Ponded Block Specimens, representing only autopsy beams. The same results are presented in Table 4.13. Each block may have also represented non-autopsy beams, since various specimens were casted from the same batch of concrete. Appendix B includes the acid soluble chloride content graphs for all concrete blocks.

In addition to ponded blocks, control blocks were also constructed and analyzed for chloride content. Concrete blocks were maintained without saltwater ponding. As expected, control blocks showed negligible chloride content at all depths.

From the chloride content graphs for Phase I concrete ponded blocks it is concluded that:

- Chloride content decreases with depth.
- All the chloride contents at the bar level are below the threshold for corrosion, except for Specimen 1.1 and 1.3 after 54 months.
- Although all specimens were made of TxDOT Class C Concrete (same concrete mix), concrete in Beam 4.2 consistently shows the highest permeability, and that used in Beams 2.3 and 2.11 consistently shows the lowest permeability.
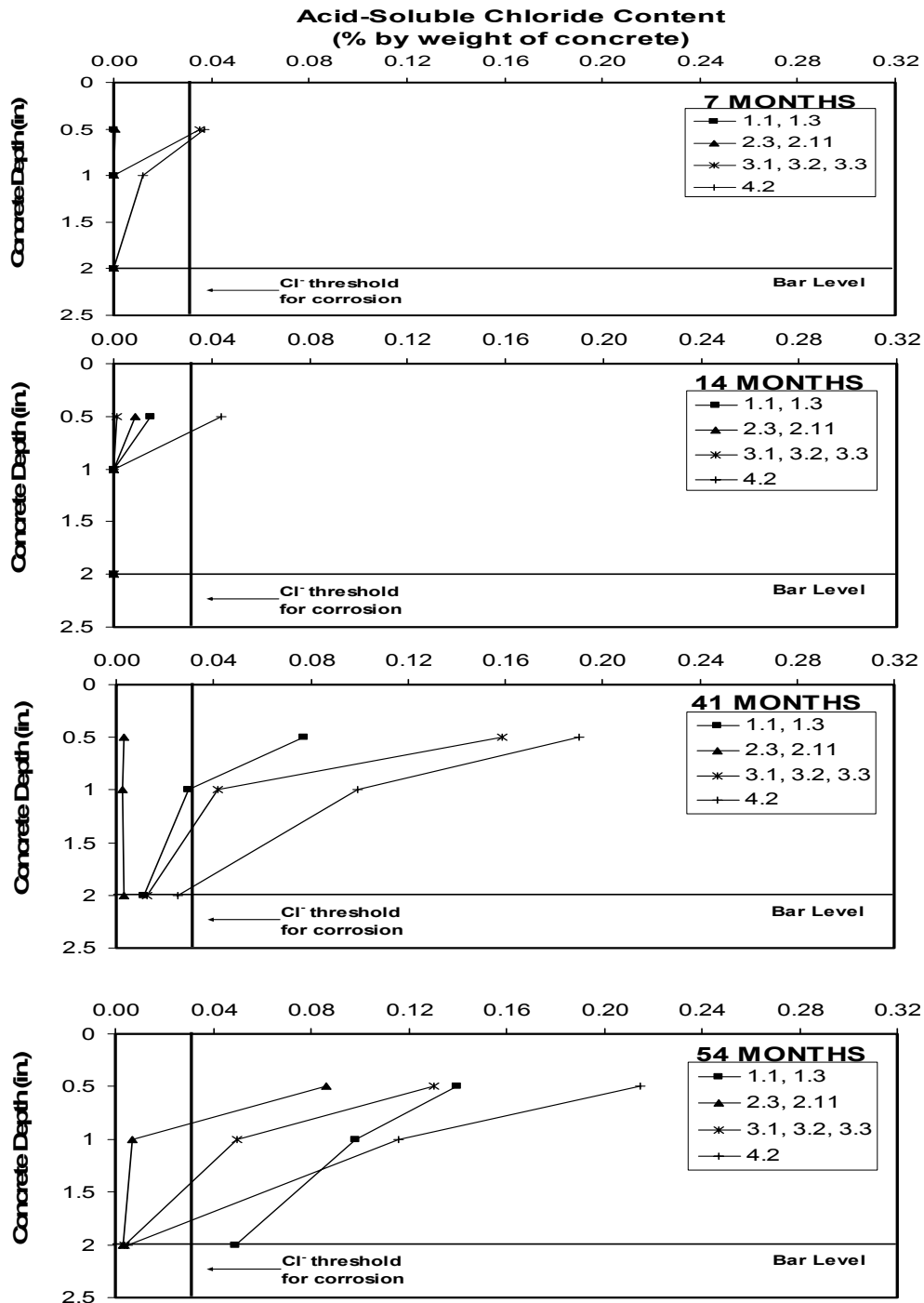
***Figure 4.53 Acid-Soluble Chloride Content for
Phase I Ponded Block Specimens[4.5]***

Table 4.13 Phase I Ponded Block Chloride Penetration Measurements[4.5]

Beams Represented	Depth (inches)	Acid Soluble Chloride Content (% by weight of concrete)			
		7 months	14 months	41 months	54 months
1.1, 1.3	0.5	0.0000	0.0152	0.0774	0.1399
	1.0	0.0000	0.0000	0.0300	0.0982
	2.0	0.0000	0.0000	0.0112	0.0490
2.3, 2.11	0.5	0.0000	0.0086	0.0029	0.0862
	1.0	0.0000	0.0000	0.0027	0.0068
	2.0	0.0000	0.0000	0.0035	0.0031
3.1, 3.2, 3.3	0.5	0.0004	0.0013	0.1586	0.1303
	1.0	0.0000	0.0000	0.0417	0.0501
	2.0	0.0000	0.0000	0.0125	0.0039
4.2	0.5	0.0004	0.0440	0.1904	0.2149
	1.0	0.0001	0.0000	0.0994	0.1162
	2.0	0.0000	0.0000	0.0250	0.0048

4.4.4.2   Phase II Concrete Block Specimens

Figure 4.54 shows the acid soluble chloride content for Phase II Ponded Block Specimens representing autopsy beams. The same information is presented in Table 4.14. For these series, concrete type is the main variable.   Again, as in the previous case, control blocks show negligible chloride content at all depths. Plots of the chloride content results for all the blocks can be found in Appendix B.

From these results it is found that:

- Acid-soluble chloride content progressively increases over time and decreases with depth, as expected.

- All chloride contents at one-inch and two-inch (bar level) depths are well below the threshold for corrosion and show little variation between the concrete types.

- Results at 0.5 inches after 29 and 42 months of exposure confirm that the high performance concrete was less permeable.

281

Acid Soluble Chloride Content
(% by weight of concrete)
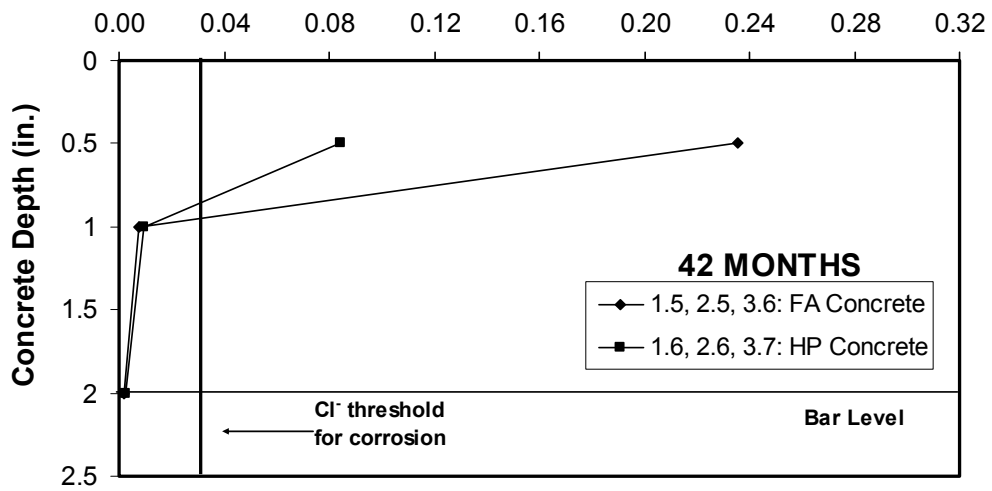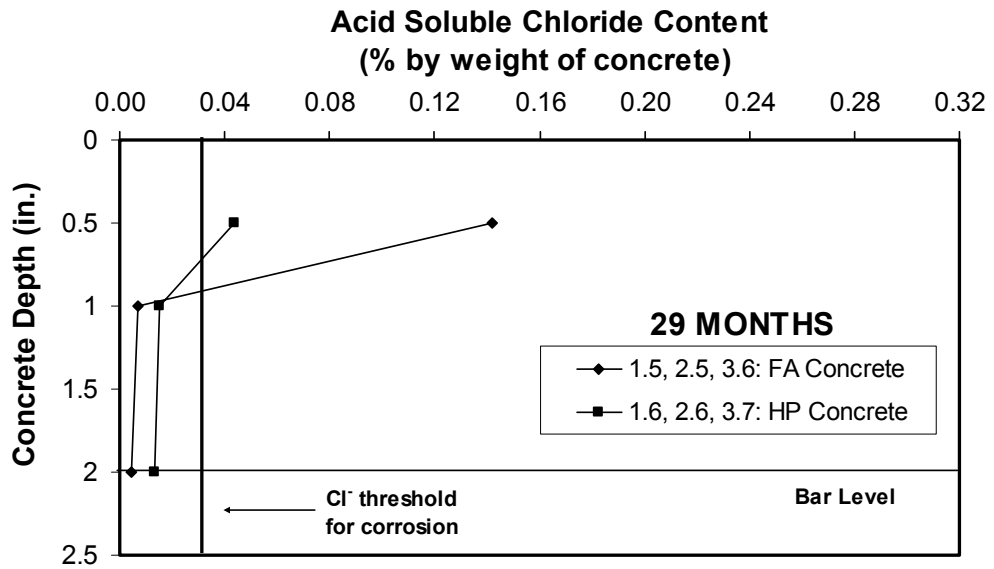
Figure 4.54 Acid-Soluble Chloride Content for
Phase II Ponded Block Specimens[4.5]

Table 4.14 Phase II Ponded Block Chloride Penetration Measurements[4.5]

Beams Represented	Depths (inches)	Acid-Soluble Chloride Content (% by weight of concrete)	
		29 months	42 months
1.5, 2.5, 3.6	0.5	0.1422	0.2359
	1.0	0.0072	0.0078
	2.0	0.0046	0.0017
1.6, 2.6, 3.7	0.5	0.0439	0.0846
	1.0	0.0151	0.0097
	2.0	0.0133	0.0025

4.4.4.3 Phase I Autopsy Beam Specimens

As described in Section 4.4.4.1, all Phase I beams were made of Standard TxDOT Class C Concrete. Figure 4.55 shows the beam and block chloride content plots at 1594 days (end of testing for autopsy beams), in the ponded region. Block chloride content is shown again for comparison. As shown on this graph, higher chloride content was found on the beams, in comparison to their corresponding blocks. The reason for this difference could be the result of cracking, which would allow ease of chloride ingress. This is clear in Specimen 1.3, since both concrete samples were taken at crack locations. The three-inch offset samples for Specimens 2.11 and 4.2 were also taken at crack locations, which would explain their high values at the bar level since the values from their blocks is essentially zero.

Figure 4.56 shows similar data for those samples taken outside the ponded region on the beams (at 27-inch and 32-inch offset). From this graph it is observed that most measurements at the bar level at both locations are at or below the threshold, with the exception of Specimen 1.3 whose 32-inch sample was taken at a crack location. Generally, chloride levels at the one-inch depth of the Non-PS and 2/3 PS beams are significantly higher at the 27-inch offset (immediately outside the ponded region) in comparison with those from the 32-

inch offset. This is not observed in the 100% PS beam, which suggest that the horizontal propagation of chlorides decreases with increasing levels of prestress.
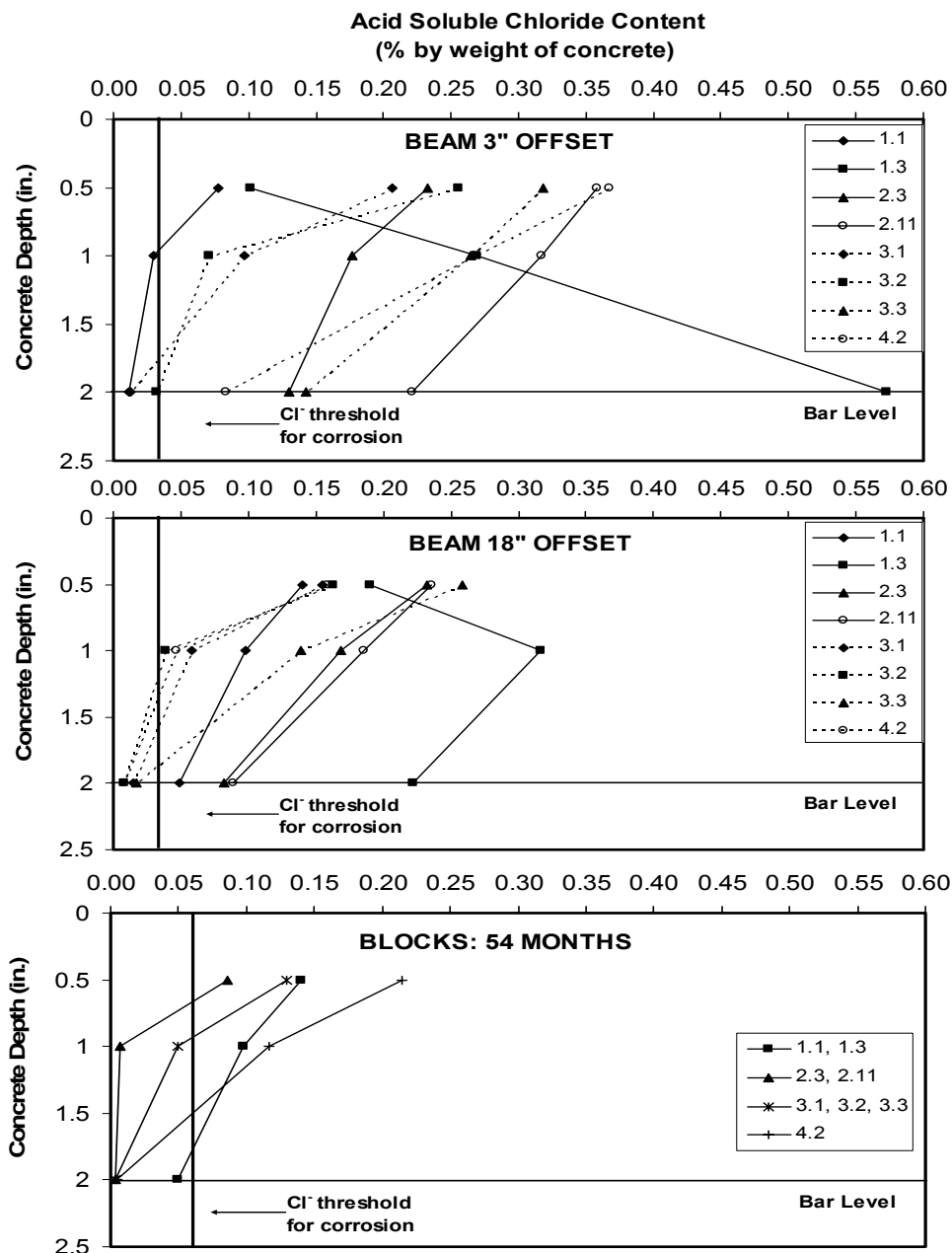
Figure 4.55 Beam and Block Chloride Penetration at 1594 Days for Phase I – Ponded Region on Beams[4.5]
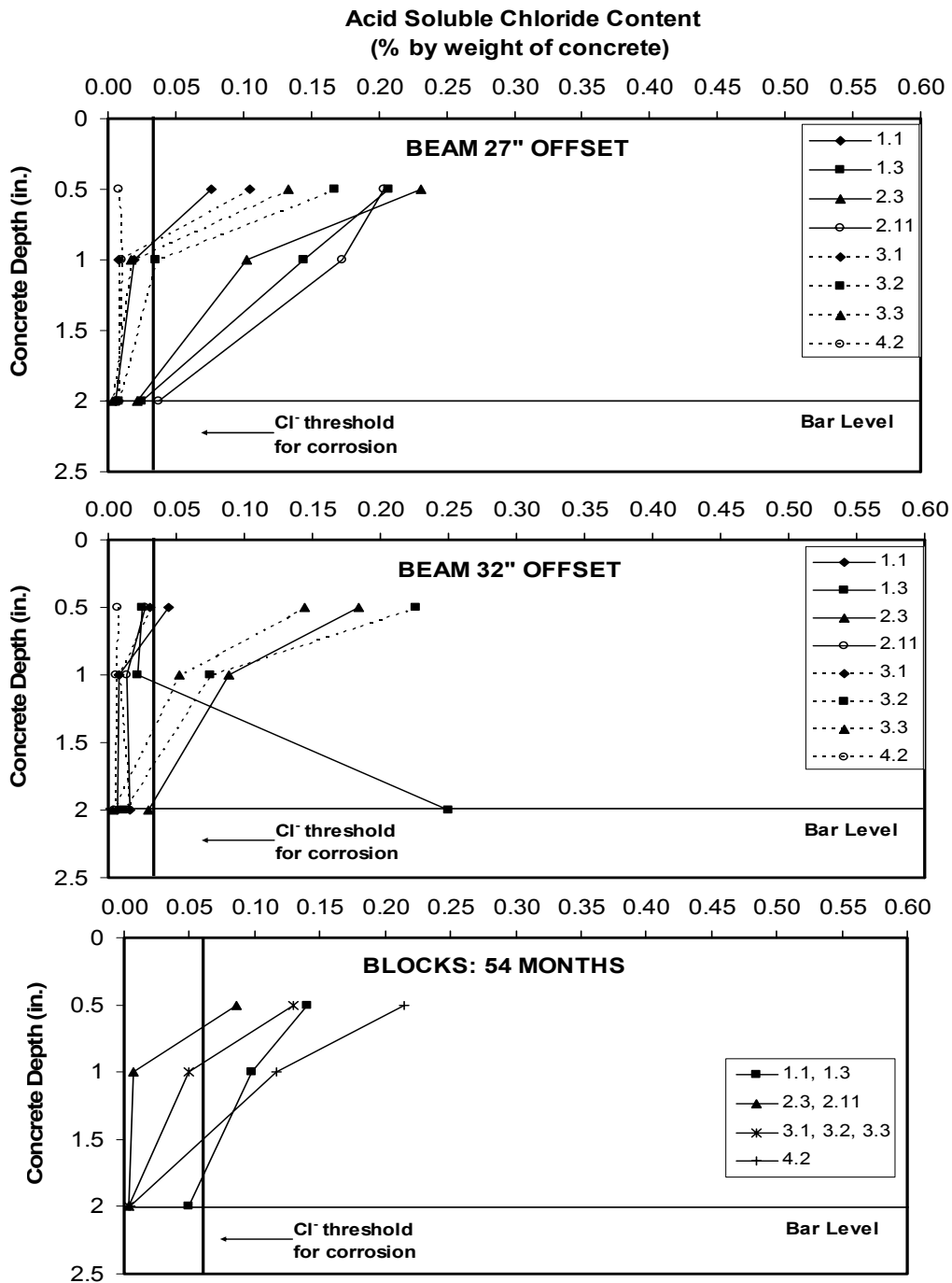
Figure 4.56 Beam and Block Chloride Penetration at 1594 Days for Phase I – Unponded Region on Beams[4.5]

285

Table 4.15 shows the results in a tabular form, for all Phase I autopsy beam acid-soluble chloride contents.

Table 4.15 Phase I Autopsy Beam Chloride Penetration Measurements[4.5]

Beam	Depth (inches)	Chloride Content (% by weight of concrete)			
		3" Offset	18" Offset	27" Offset	32" Offset
1.1	0.5	0.0774	0.1399	0.0757	0.0448
	1.0	0.0300	0.0982	0.0199	0.0080
	2.0	0.112	0.0490	0.0058	0.0064
1.3	0.5	0.1020	0.1901	0.2070	0.0250
	1.0	0.2695	0.3169	0.1447	0.0219
	2.0	0.5729	0.2216	0.0250	0.2496
2.3	0.5	0.2326	0.2326	0.2306	0.1836
	1.0	0.1765	0.1689	0.1025	0.0883
	2.0	0.1299	0.0820	0.0214	0.0296
2.11	0.5	0.3583	0.2352	0.2038	0.0277
	1.0	0.3173	0.1852	0.1735	0.0138
	2.0	0.2213	0.0890	0.0373	0.0157
3.1	0.5	0.2064	0.1547	0.1047	0.0307
	1.0	0.0965	0.0583	0.0082	0.0079
	2.0	0.0120	0.0150	0.0076	0.0154
3.2	0.5	0.2557	0.1626	0.1676	0.2258
	1.0	0.0712	0.0384	0.0355	0.0746
	2.0	0.0317	0.0079	0.0084	0.0116
3.3	0.5	0.3182	0.2581	0.1330	0.1445
	1.0	0.2641	0.1389	0.0171	0.0520
	2.0	0.1424	0.0169	0.0030	0.0031
4.2	0.5	0.3675	0.1583	0.0082	0.0064
	1.0	0.2668	0.0464	0.0097	0.0054
	2.0	0.0837	0.0084	0.0064	0.0050

Figure 4.57 shows the chloride content results at the bar and top-of-duct level (at the two-inch depth from the concrete surface), after 1594 days of exposure.

Acid Soluble Chloride Content
(% by weight of concrete)
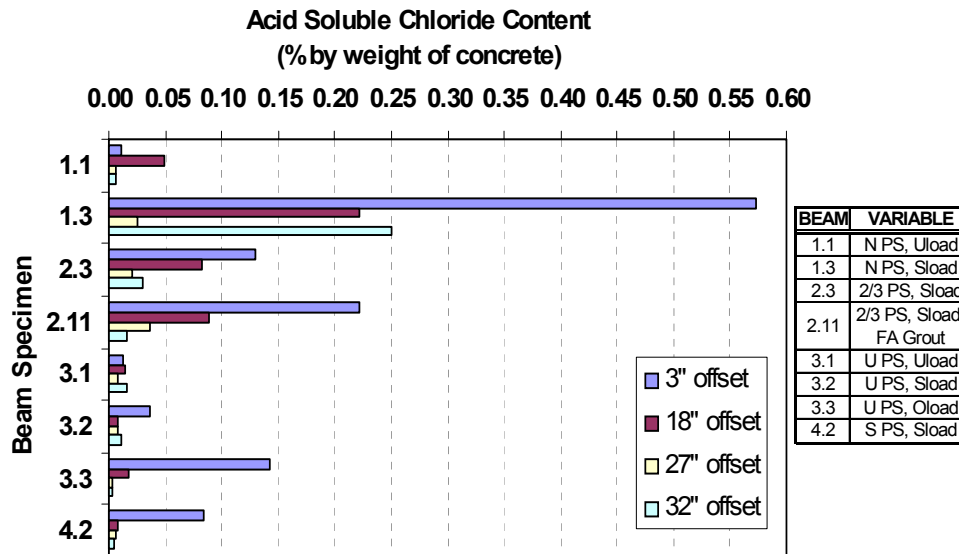
Figure 4.57 Acid-Soluble Chloride Content at Bar and
Top-of-Duct Level for Phase I Beams [4.5]

The following results are found:

- Chloride content in the ponded region is consistently higher at the bar level than outside the ponded region.

- Unloaded and uncracked specimens (1.3 and 3.1) show very low chloride contents at all locations.

- Measurements taken at crack locations give significantly larger chloride content values, as in the case of Specimens 1.3 and 2.3 at the three-inch offset.

- An increase in the level of prestress results in lower chloride contents due to fewer cracks and higher compressive stresses in the concrete.

- Minimal difference is observed in the performance of the 100%S and 100%U PS beams. The larger value from the 100%U PS beam at the three-inch offset location is due to the small crack at the sample locations.

287

4.4.4.4 Phase II Autopsy Beam Specimens

Concrete type is the only variable of interest when comparing Phase II autopsy beams, since all were loaded at the service load level. Figure 4.58 shows the beam and block chloride content plots at 1235 days (end of testing for autopsy beams), in the ponded region. Block chloride content is shown again for comparison. As can be observed, high performance concrete specimens consistently shows as the superior concrete type in both the beam and block specimens at 0.5 inch and one-inch depth. All samples from inside the ponded region at the bar level show negligible chloride contents, implying that both types of concrete are effective in limiting chloride penetration for this time period.

Figure 4.59 shows similar data for those samples taken outside the ponded region on the beams (at 27-inch and 32-inch offset). From this graph it is observed that most measurements taken outside the ponded region of the Phase II specimens show negligible chloride contents. The only notable measurements were found in the fly ash concrete specimens, supporting the above conclusion that high performance concrete as defined in Section 2.4.4.1 appears to be superior.

When comparing concrete block results with beam results, it is observed that inside the ponded region, chloride contents from the blocks are unconservative for beams 1.5 (Non-PS, Fly Ash Concrete) and 2.5 (2/3 PS, Fly Ash Concrete), at the one-inch depth, but very approximate at all depths for beams 1.6 (Non-PS, High Performance HP Concrete), 2.6 (2/3 PS, HP Concrete) and 3.7 (100%U PS, HP Concrete). In general, actual chloride contents at the two-inch depth were slightly higher than those measured from the concrete blocks.
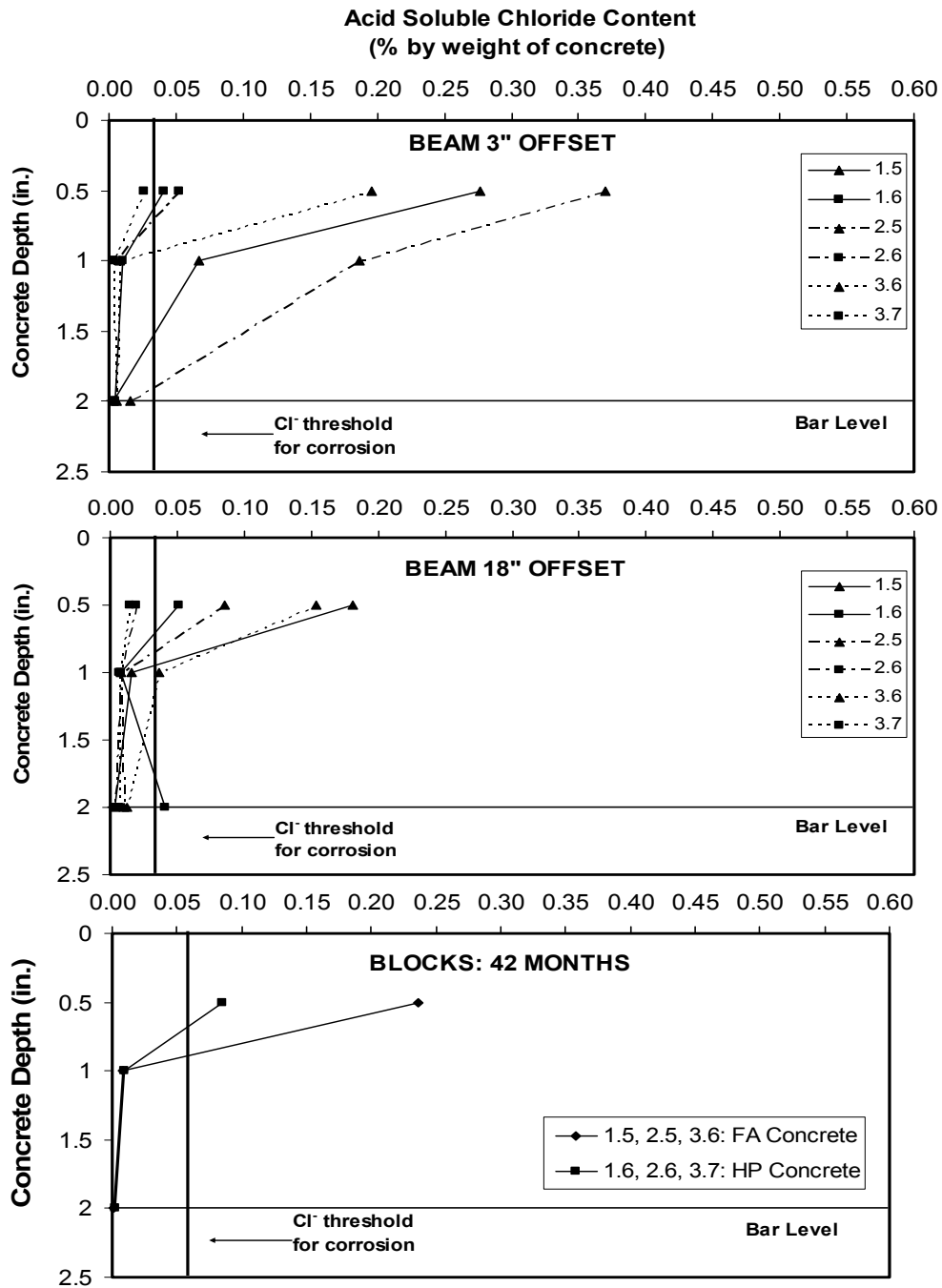
Figure 4.58 Beam and Block Chloride Penetration at 1235 Days for Phase II – Ponded Region on Beams[4.5]
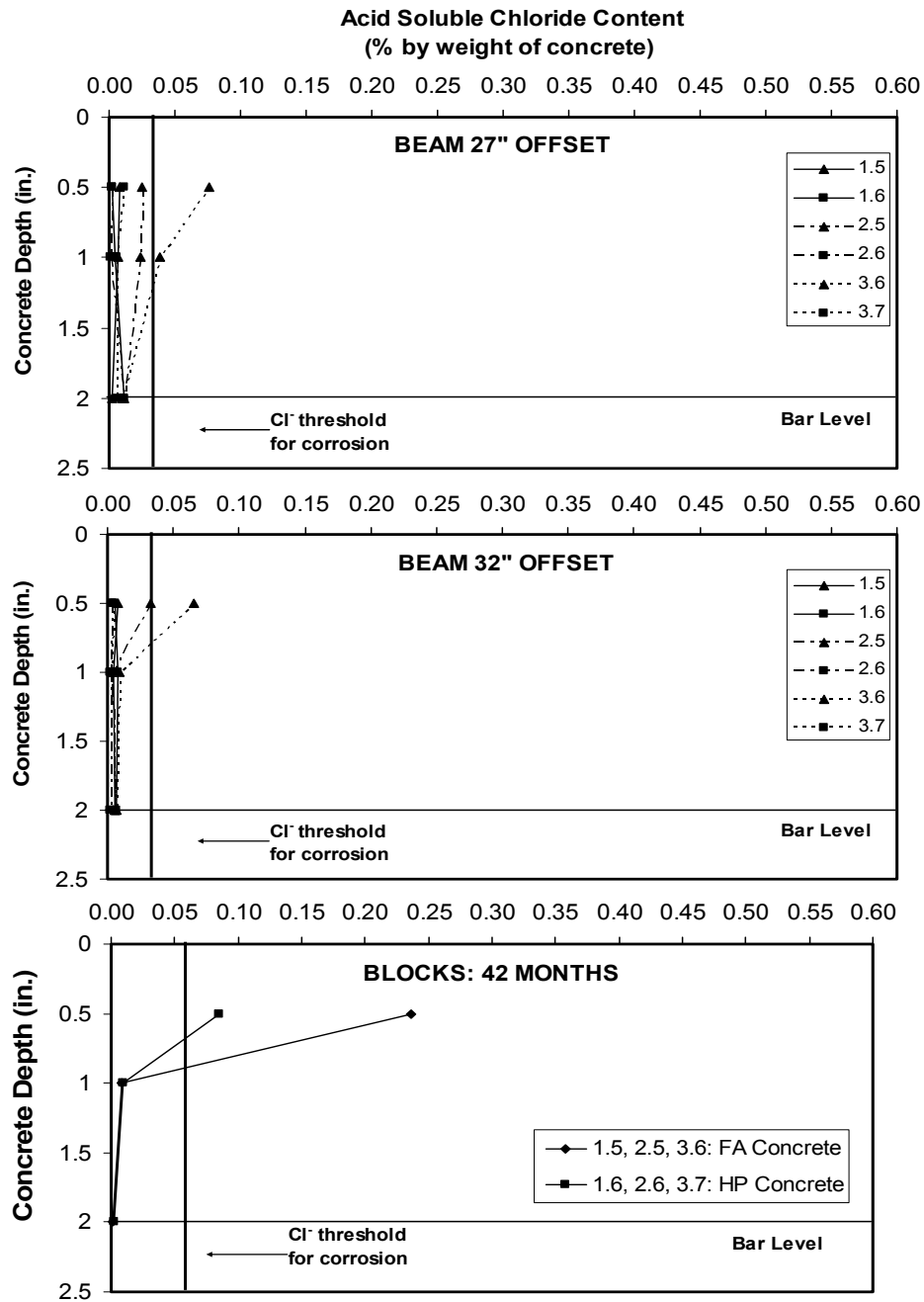
***Figure 4.59 Beam and Block Chloride Penetration at 1235 Days for
Phase II – Unponded Region on Beams[4.5]***

Table 4.16 shows the results from Figures 4.58 and 4.59 in a tabular form, for all Phase II autopsy beam acid-soluble chloride contents.

Table 4.16 Phase II Autopsy Beam Chloride Penetration Measurements[4.5]

Beam	Depth (inches)	Chloride Content (% by weight of concrete)			
		3" Offset	18" Offset	27" Offset	32" Offset
1.5	0.5	0.2770	0.1810	0.0076	0.0077
	1.0	0.0674	0.0163	0.0067	0.0043
	2.0	0.0034	0.0039	0.0021	0.0052
1.6	0.5	0.0410	0.0515	0.0019	00057
	1.0	0.0108	0.0082	0.0048	0.0076
	2.0	0.0046	0.0409	0.0111	0.0066
2.5	0.5	0.3700	0.0854	0.0250	0.0333
	1.0	0.1868	0.0077	0.0236	0.0039
	2.0	0.0156	0.0099	0.0109	0.0051
2.6	0.5	0.0525	0.0196	0.0018	0.0029
	1.0	0.0030	0.0076	0.0015	0.0019
	2.0	no reading	0.0033	0.0114	0.0021
3.6	0.5	0.1959	0.1540	0.0766	0.0652
	1.0	0.0081	0.0366	0.0381	0.0089
	2.0	0.0058	0.0120	0.0103	0.0070
3.7	0.5	0.0263	0.0144	0.0116	0.0045
	1.0	0.0035	0.0066	0.0057	0.0040
	2.0	0.0040	0.0064	0.0056	0.0051

Figure 4.60 shows the chloride content results at the bar and top-of-duct level (at the two-inch depth from the concrete surface), after 1235 days of exposure.

As observed from Figure 4.60, it is confirmed that acid-soluble chloride contents at the bar and top-of-duct level of the Phase II beams are very low, with respect to the chloride threshold value of 0.033%, meaning that the use of fly ash concrete and high performance concrete are effective in minimizing the penetration of chlorides through the concrete matrix.

Acid Soluble Chloride Content
(% by weight of concrete)

BEAM	VARIABLE
1.5	N PS, FA Conc.
1.6	N PS, HP Conc.
2.5	2/3 PS, FA Conc.
2.6	2/3 PS, HP Conc.
3.6	U PS, FA Conc.
3.7	U PS, HP Conc.

Legend: 3" offset, 18" offset, 27" offset, 32" offset
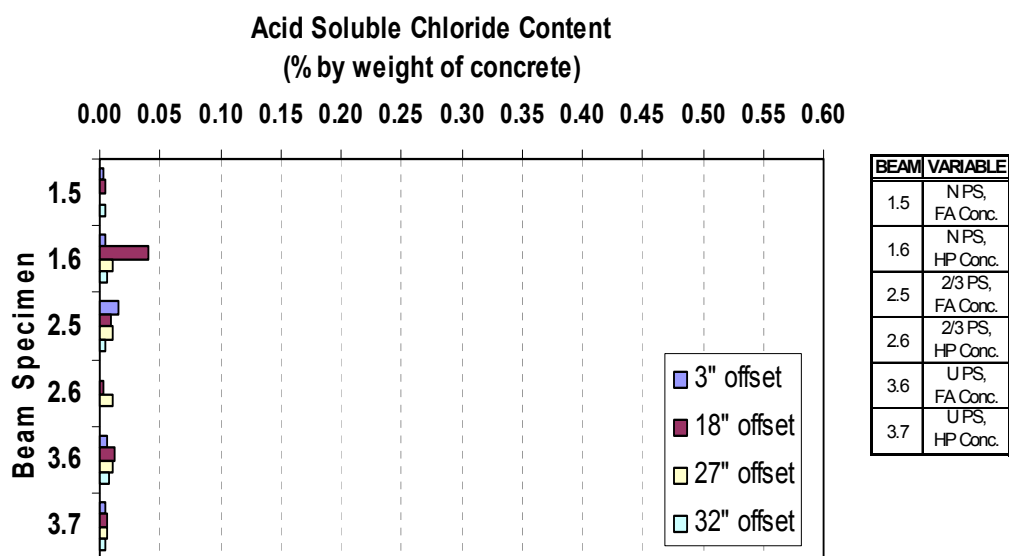
Figure 4.60 Acid-Soluble Chloride Content at Bar and Top-of-Duct Level for Phase II Beams [4.5]

4.5   FORENSIC EXAMINATION

After four and a half years of exposure testing for Phase I Beam Specimens and three and a half years for Phase II Beam Specimens, a detailed visual inspection on the exterior condition was performed on all 27 specimens, and exposure testing data were thoroughly analyzed. Based on this evaluation, it was decided to perform a forensic examination that included full and partial autopsies of approximately half of the beams. The forensic examination was performed according to the program objectives, which relate to the evaluation of the effect of post-tensioning on durability, and the evaluation of the relative performance of a large number of corrosion protection variables including prestress level and crack width, duct splices, grout type, concrete type, strand type, duct type, and end anchorage protection.

Specific forensic examination objectives were as follows:

1.   Obtain visual evaluation of the overall exterior condition of beam specimens.

2.   Determine chloride ion penetration through the concrete.

3.   Obtain visual evaluation of corrosion damage on duct, duct splice, strand and mild steel reinforcement.

4.   Determine chloride ion content in the grout.

5.   Determine most effective variables in corrosion protection.

4.5.1   Autopsy Procedure

4.5.1.1   Specimen Selection for Forensic Examination

Originally, all beam specimens were scheduled for full autopsy in May 2002. This date marked four and a half or three and a half years of exposure testing for Phase I and Phase II beams, respectively. However, results from the final segmental joint macrocell durability tests, as described in Chapter 3,

suggested that for a modest extension of the exposure testing program, it would be possible to obtain increased benefit from the full-size durability specimens. Half of the duplicated macrocell specimens were autopsied after four and a half years of very aggressive exposure. The remaining duplicates were autopsied after eight years of exposure. When the results from the longer exposure period were compared with the preliminary conclusions reported after four years of exposure testing, it was found that a number of significant changes had occurred. For example, while no corrosion had been found after four and a half years in epoxy jointed specimens, after eight years there was some corrosion (away from the joint) in epoxy jointed specimens and there was corrosion at one epoxy joint that was found to be incompletely filled with epoxy. More importantly, after eight years there was extremely large destruction of galvanized duct and clear indication of the superiority of the plastic duct, an aspect that was not so evident after the first autopsy. If all exposure testing had been halted after four and a half years in the macrocell series, a great deal of important information would have been missed.

For the above reason, it was decided to select approximately half of the beam specimens for autopsy in May 2002. Twelve out of the total of twenty seven specimens in Phase I and Phase II were selected for full autopsy, while two specimens were selected for partial autopsy. The remaining specimens were left under continuous exposure testing for future autopsy. Tables 4.17 and 4.18, and Figure 4.61 show the specimens selected for examination and the corresponding test variables. The autopsy specimen selection was made based on visual inspection, measurements taken during exposure testing and the necessity for comparison of the test variables.

Specimens 1.1 and 3.1 were selected for partial autopsy, since they would be needed for both the present and future autopsies because they were the only

uncracked and unloaded specimens. Thus, they served as control specimens for comparison. Since these beams were not loaded or cracked, a portion of the specimen could be removed while the remainder was returned to the exposure testing. The partial autopsy consisted of exposing and removing half of the mild steel/duct/strand section that was removed for each fully autopsied beam, leaving the other half for continued exposure testing.

Table 4.17 Phase I Beams Selected for Forensic Examination

Specimen	Prestress Level	Cracking (mm)	Applied Load	Concrete Type	Splice Type	Damage to Duct	Grout type	Strand	PT Anchorage
1.1	Non-PS	Uncracked	Unloaded	(1)	--	--	--	--	--
1.3	Non-PS	0.3	Constant Service	(1)	--	--	--	--	--
2.3	2/3 PS	0.2	Constant Service	(1)	(2)	(3)	(4)	(7)	(8)
2.11	2/3 PS	0.2	Constant Service	(1)	(2)	None	Fly Ash (5)	(7)	(8)
3.1	100% U PS	Uncracked	Unloaded	(1)	(2)	None	(4)	(7)	(9)
3.2	100% U PS	Uncracked	Constant Service	(1)	(2)	None	(4)	(7)	(9)
3.3	100% U PS	Cracked	124% - Return to Service	(1)	(6)	None	(4)	(7)	(9)
4.2	100% S PS	Uncracked	Constant Service	(1)	(2)	(3)	(4)	(7)	(10)

(1)   TxDOT Class C (0.45 w/c, cement Type I, retarder, air entrainment agent)
(2)   Industry Standard (IS) and Heat Shrink (HS)
(3)   IS with damage and HS with damage
(4)   TxDOT Class C (0.44 w/c, cement Type I, expanding admixture)
(5)   0.33 w/c, 30% Fly Ash replacement.
(6)   Industry Standard (IS)
(7)   7-wire 0.5 in. low relaxation (270 ksi) strand
(8)   VSL Type E5-3 (with third strand opening unused)
(9)   VSL Type E5-3
(10)   VSL Type E5-4

295

Table 4.18 Phase II Beams Selected for Forensic Examination

Specimen	Prestress Level	Cracking (mm)	Applied Load	Concrete Type	Splice Type	Damage to Duct	Grout type	Strand	PT Anchorage
1.5	Non-PS	0.3	Constant Service	(11)	--	--	--	--	--
1.6	Non-PS	0.3	Constant Service	(12)	--	--	--	--	--
2.5	2/3 PS	0.2	Constant Service	(11)	(13)	None	(14)	(15)	(16)
2.6	2/3 PS	0.2	Constant Service	(12)	(13)	None	(14)	(15)	(16)
3.6	100% U PS	0.1	Constant Service	(11)	(13)	None	(14)	(15)	(17)
3.7	100% U PS	0.1	Constant Service	(12)	(13)	None	(14)	(15)	(17)

(11)   TxDOT Class C with Fly Ash (0.44 w/c, with 25% Class F Fly Ash)
(12)   High Performance (0.29 w/c, 25% Fly Ash, superplasticizer)
(13)   Industry Standard Splice (IS) and Heat Shrink Splice (HS)
(14)   TxDOT Class C (0.44 w/c, cement Type I, expanding admixture)
(15)   7-wire 0.5 in. low relaxation (270 ksi) strand
(16)   VSL Type E5-3 (with third strand opening unused)
(17)   VSL Type E5-3

Figure 4.61 Selected Beams for Forensic Examination

4.5.1.2 Specimen Condition at End of Testing

The appearance of the specimens can indicate corrosion activity. The exterior surface of each beam specimen was examined for signs of additional cracking, rust staining and concrete spalling.

4.5.1.3 Crack Measurements

One of the main objectives of the forensic examination was to determine the influence of cracking on specimen performance and reinforcement corrosion (onset of corrosion and propagation) due to chloride and moisture ingress. Crack widths were measured at the beginning of exposure (after post-tensioning and first loading) and at the end of exposure. The crack width measurement procedure and the results are described in Section 4.3.2 and Section 4.4.1, respectively.

4.5.1.4 Concrete Powder Samples for Chloride Analysis

Concrete Powder Samples were collected from concrete block and beam specimens to assess the chloride penetration. Powder samples were tested for their acid soluble chloride content. The procedure for obtaining the samples is explained in Section 4.3.5 and the results of the chloride analysis are given in Section 4.4.4.

4.5.1.5 Saw Cuts and Concrete Removal

4.5.1.5.1 Full Autopsies

Analysis of duct, strand and mild steel was limited to a total length of 72 inches (42 inches from centerline to one side and 30 inches to the other side). Figure 4.62 shows a diagram of the section removed for investigation. The section included the entire 48-inch ponded region, and extended six inches outside the

297

ponded region on one side and 18 inches on the other side.   It was decided that this section would sufficiently provide the following information:

1. Reinforcement corrosion performance from the area in the ponded region

2. Possible horizontal penetration of chlorides through the concrete from the area immediately outside of the ponded region

3. A section of reinforcement not exposed to a corrosive environment for comparison
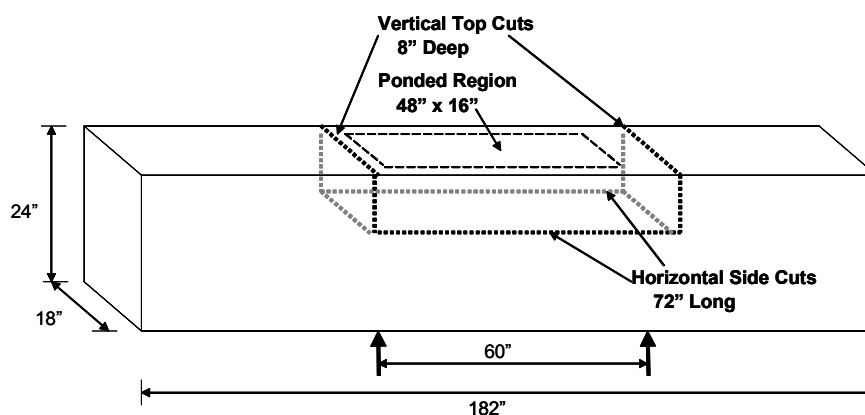
Figure 4.62 Beam Section Removed for Investigation[4.5]

The concrete saw with a 27-inch circular blade shown in Figure 4.63 was used to make all the cuts in the specimens. Two eight-inch deep vertical cuts were made on the top of the beam, and a horizontal cut was made on each side of the beam, below the duct line. These cuts separated the portion of the beam to be analyzed from the rest of the specimen, allowing the area of interest to be removed with a forklift.

Jack hammers and chipping hammers were used to carefully remove all existing concrete around post-tensioning ducts and mild steel reinforcement, as illustrated in Figure 4.64.

Figure 4.63 Concrete Saw Used in Autopsy

Figure 4.64 Concrete Removal to Expose Duct and Mild Steel

4.5.1.5.2 Partial Autopsies

The partial autopsy procedure consisted of exposing and removing half of the mild steel/duct/strand concrete section that was used for each fully autopsied beam, leaving the other half for continued exposure testing. Figure 4.65 shows one partial autopsied beam after the first half analysis portion has been removed, and the beam had the cut section epoxied to seal the surface and returned to exposure testing.
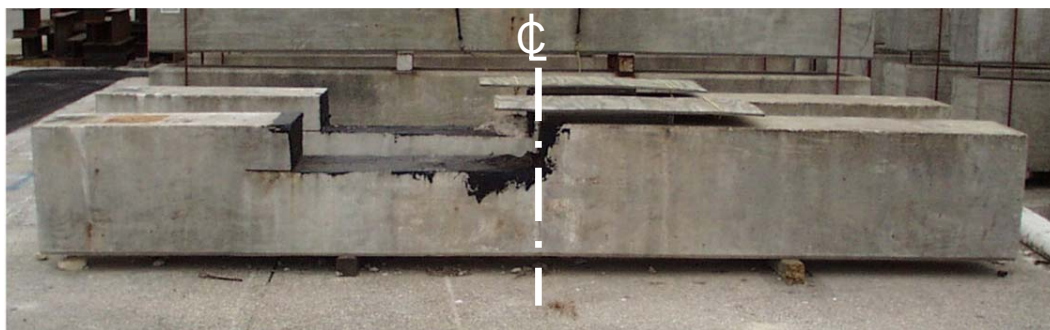
Figure 4.65 Partial Autopsied Beam

4.5.1.6 Exposure and Removal of Ducts

Metal or plastic duct was exposed after removing all concrete. The duct and strand were then removed from the concrete as one unit. Immediately after exposing the duct, the surface was examined for rust staining and color, salt collection and damage.

4.5.1.7 Splice Condition Examination

Splices (Heat-Shrink or Industry Standard) were examined after removing the duct/strand piece. Splices were thoroughly inspected for corrosion, salt deposits, zinc corrosion products and rust staining.

4.5.1.8 Duct Opening and Grout Condition Examination

After external splice examination, splices were cut open in half longitudinally, and the duct was also cut open by making two longitudinal cuts along the sides of the duct/strand using a small air grinder. The grout was examined for bleed water voids, incomplete duct filling and excessive porosity. Grout was also examined for cracking and any indication of moisture and chloride ingress. Since grout is injected after the stressing of post-tensioning steel, hardened grout is susceptible to service cracking due to deflections and vibrations.

4.5.1.9 Grout Samples for Chloride Analysis

Grout Samples were collected from every duct at six-inch intervals over the entire length of 72 in. The grout pieces were crushed between two steel plates and ground into powder using a mortar and pestle. Powder samples were analyzed for acid-soluble chlorides using a specific ion probe (CL Test System by James Instrument).

4.5.1.10 Grout Removal and Strand Exposure

After the desired grout samples were removed, the remainder of the grout was carefully removed, exposing the strand for examination. The extent and severity of corrosion on both the strand and duct was rated according to the corrosion rating scheme described in Section 4.5.2.

4.5.1.11 Mild Steel Exposure and Removal

The mild steel bars and stirrups were removed after ducts had been removed, using the jackhammers and chipping hammers. Analysis of longitudinal steel was limited to 72 in. corresponding to the same analysis length used for the post-tensioning ducts and strands. Stirrups were analyzed only in the top portion and two 3 in. legs at each side, as shown in Figure 4.66.

Figure 4.66 Mild Steel Reinforcement Cage

4.5.2   Evaluation and Corrosion Rating System Used During Forensic Examination

After all steel elements were exposed and removed, they were thoroughly examined and rated. The rating system selected for evaluation was the same used for the Macrocell Corrosion Tests, as described in Section 3.3.3. The procedure was created by West et al.[4.21] in a universal form with the intention of applying the same rating system to various situations.   For the beam corrosion tests, the length (72 inches) of longitudinal mild steel, duct and strand was subdivided into 36, two inch-intervals. At each interval, the steel was examined and a rating was assigned to describe the corrosion severity within that interval. By assigning a corrosion severity at 36 locations, both the extent and severity of corrosion are determined.

As described in West et al.[4.21] the rating system is essentially the same for prestressing strand, mild steel reinforcement and galvanized duct, with some modifications to reflect unique corrosion aspects of each type of steel. In general, the evaluation system doubles the severity rating for each category of increasing corrosion damage.

302

4.5.2.1 Mild Steel Reinforcement

The longitudinal mild steel was examined at 36, two inch intervals, as indicated in Figure 4.67. Corrosion ratings were assigned to indicate for each interval or segment, the corrosion severity on both the top and bottom bar surfaces. The same procedure was applied to the stirrups, except the interval division varied slightly. As with the longitudinal bars, the top portion of stirrups was divided into 7 two-inch intervals. Due to the dimensions of the section removed from each beam for forensic examination, there were 2 three-inch sections (legs) from the sides of the stirrup to be analyzed. (see Figure 4.67) Each three-inch leg was considered one interval, for a total of nine intervals per stirrup. One rating was assigned to the inside and outside surfaces of each leg.
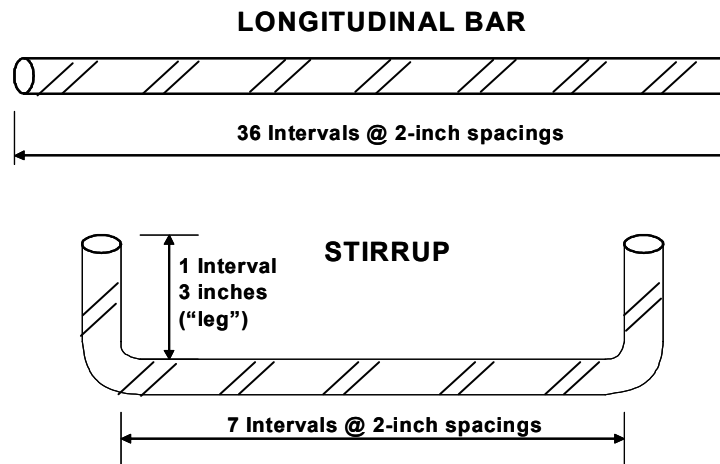
Figure 4.67 Intervals for Corrosion Rating on Mild Steel

The total bar corrosion rating was calculated as follows:

$$R_{Bar} = \sum_{i=1}^{36}(R_{Top\,i} + R_{Bot\,i}) \qquad\qquad \textbf{\textit{Eq. 4.6}}$$

$$Total\ Bar\ Corrosion\ Rating = \sum_{n=1}^{m} R_{Bar\ n} \qquad\qquad \textit{Eq. 4.7}$$

where,

$R_{Top\ i}$	=	corrosion rating on top bar surface, interval i
$R_{Bot\ i}$	=	corrosion rating on bottom bar surface, interval i
$R_{Bar\ n}$	=	total bar corrosion rating, bar n
i	=	interval, 1 to 36
n	=	bar number, 1 to m
m	=	total number of bars on each specimen (2 or 8)

The corrosion rating system is described in Table 4.19. Each beam design had a different number of mild steel bars (m), depending on the post-tensioning level. The Non-PS beams had 6#6 and 2#4 bars as the tensile steel reinforcement (m=8). The mixed reinforced beams (2/3 PS) had 4#3 and 4#4 bars (m=8). The 100% PS specimens, designed either with the strength design method or the allowable stress design method, had 2#3 mild steel bars (m=2). These bars were not required by design, but were included for construction purposes. The variation in number of longitudinal bars is accounted for in the analysis of the data.

The stirrups were also rated using Table 4.19. However, a different equation was used to calculate the total stirrup rating. As with the longitudinal mild steel, the ratings for the top and bottom bar surface of each interval were summed to give a total corrosion rating for the stirrup.

The total stirrup rating was calculated as follows:

$$R_{Stirrup} = \sum_{i=1}^{9} (R_{Top\ i} + R_{Bot\ i}) \qquad\qquad \textit{Eq.4.8}$$

$$Total\ Stirrup\ Corrosion\ Rating = \sum_{n=1}^{6} R_{Stirrup\ n} \qquad\qquad \textit{Eq. 4.9}$$

where, $R_{Top\ i}$ =   corrosion rating on top bar surface, interval i

$R_{Bot\ i}$ =   corrosion rating on bottom bar surface, interval i

$R_{Stirrup\ n}$ =   total stirrup corrosion rating, stirrup i

i   =   interval, 1 to 9

n   =   stirrup number, 1 to 6

Table 4.19 Evaluation and Rating System for Corrosion Found on
Mild Steel Bars [4.2]

Code	Meaning	Description	Rating
NC	No Corrosion	No evidence of corrosion	0
D	Discoloration	No evidence of corrosion, but some discoloration from original color	1
L	Light	Surface corrosion on less than one half of the interval, no pitting. Surface corrosion can be removed using cleaning pad.	2
M	Moderate	Surface corrosion on more than one half of the interval, no pitting. **and/or** Corrosion can not be completely removed using cleaning pad.	4
P	Pitting	Pits visible to unaided eye.	8
AR	Area Reduction	Measurable reduction in bar cross-sectional area due to corrosion	R^2

R = Estimated cross-sectional area reduction in percent

4.5.2.2 Galvanized Steel Duct/Duct Splice

The galvanized steel duct was examined at 36 two-inch intervals, and the duct splices at 6 two-inch intervals as indicated in Figure 4.68. At each location, a corrosion rating was assigned to indicate the severity of corrosion on the inside and outside surfaces of the top and bottom of each duct.
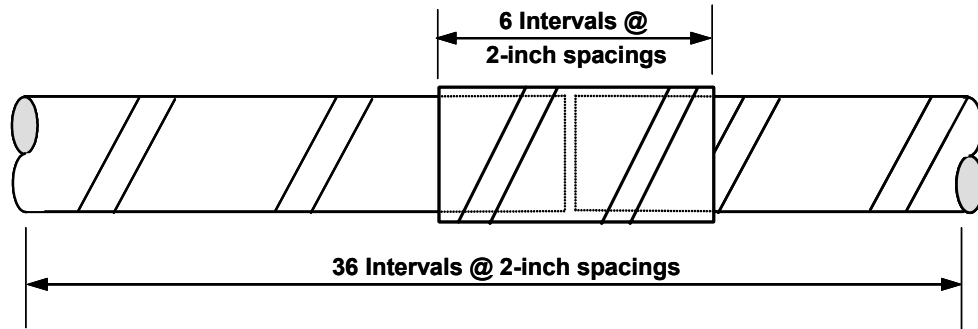
***Figure 4.68 Intervals for Corrosion Ratings on
Galvanized Steel Duct/Splice***

The corrosion rating system for the galvanized steel ducts and duct splices is described in Table 4.20.

The total duct corrosion rating was calculated as follows:

$$\text{Duct Corrosion Rating} = \sum_{i=1}^{36} R_{TopOuter,i} + R_{BotOuter,i} + R_{TopInner,i} + R_{BotInner,i} \quad \textbf{\textit{Eq. 4.10}}$$

where, $R_{TopOuter,i}$ = top outer surface corrosion rating, interval i

$R_{BotOuter,i}$ = bottom outer surface corrosion rating, interval i

$R_{TopInner,i}$ = top inner surface corrosion rating, interval i

$R_{BotInner,i}$ = bottom inner surface corrosion rating, interval i

i = interval, 1 to 36

Table 4.20 Evaluation and Rating System for Corrosion Found on Galvanized Steel Duct /Duct Splice [4.2]

Code	Meaning	Description	Rating
NC	No Corrosion	No evidence of corrosion	0
D	Discoloration	No evidence of corrosion, but some discoloration from original color	1
L	Light	Surface corrosion on less than one half of the interval, no pitting.	2
M	Moderate	Surface corrosion on more than one half of the interval, no pitting.	4
S	Severe	Corrosion completely covers the interval. **and/or** Presence of pitting.	8
H	Hole Through Duct	Hole corroded through duct. Used in conjunction with ratings D, L, M and S.	$32 + A_h$

A_h = Area of hole(s) in mm^2

4.5.2.3 Prestressing Strand

The strands were examined at 36 two-inch intervals, like the longitudinal mild steel bars. Corrosion ratings were assigned to indicate the severity of corrosion on the outer six wires of the strand and on the center wire (after de-stranding) at each interval. This was done to address the possibility of different corrosion activity on the strand exterior and interstices between wires. The corrosion rating system for prestressing strands is described in Table 4.21. The total strand corrosion rating was calculated as follows:

$$Strand\ Corrosion\ Rating = \sum_{i=1}^{36} R_{Outer,i} \times n_i + R_{Center,i} \qquad \textbf{\textit{Eq. 4.11}}$$

where, $R_{outer,i}$ = corrosion rating on outer wires, interval i

n_i = number of corroded outer wires, interval i

$R_{center,i}$= corrosion rating on center wire, interval i

i   = interval, 1 to 36

Table 4.21 Evaluation and Rating System for Corrosion Found on Prestressing Strand [4.2]

Code	Meaning	Description	Rating
NC	No Corrosion	No evidence of corrosion.	0
D	Discoloration	No evidence of corrosion, but some discoloration from original color.	1
L	Light	Surface corrosion on less than one half of the interval, no pitting. Surface corrosion can be removed using cleaning pad.	2
M	Moderate	Surface corrosion on more than one half of the interval, no pitting. **and/or** Corrosion can not be completely removed using cleaning pad.	4
P1	Mild Pitting	Broad shallow pits with a maximum pit depth not greater than 0.02 in.	8
P2	Moderate Pitting	Pitting where the maximum pit depth ranged between 0.02 and 0.04 in.	16
P3	Severe Pitting	Pitting where the maximum pit depth is greater than 0.04 in.	32

As reported by West et al.[4.21] the corrosion rating for prestressing strand was adapted from Poston[4.22] and Hamilton.[4.23] The use of a cleaning pad to assess corrosion severity was proposed by Sanson[4.24] for classifying the degree of rusting on prestressing strand for new construction. The recommended cleaning pad is a 3M Scotch Brite Cleaning Pad. The pad is held by hand and rubbed longitudinally along the strand axis with a pressure similar to that used when cleaning pots and pans. The classification of pitting severity was based on tensile

tests performed on corroded prestressing strand. The tests were used to assign a reduced tensile capacity of 97% GUTS to pitting damage at the level of P1. Moderate pitting (P2) was assigned a capacity of 90% GUTS, and severe pitting (P3) 77% GUTS. In general, the presence of any pitting visible to the unaided eye is deemed cause for rejection in new construction.

4.5.2.4 Duct Splices

All Industry Standard and Heat-Shrink duct splices were thoroughly inspected for corrosion, salt deposits, zinc corrosion products, rust staining and damage. Additionally, all Industry Standard duct splices were galvanized steel and were rated using the procedure in Section 4.5.2.2.

4.5.2.5 Grout

Since grout is injected after the stressing of post-tensioning steel, hardened grout is vulnerable to service cracking due to deflections and vibrations.

4.5.3 Forensic Examination Results for Phase I Beams

Forensic Examination for all autopsy specimens and the written description for each one, was performed by Kotys[4.5] and the author jointly, and therefore, the following discussion also appears in Reference 4.5.

4.5.3.1 Beam Specimen 1.1 - Non-PS, Unloaded.

At the end of exposure testing, rust stains were visible in the North side of the specimen, as shown in Figure 4.69. On the South side, only two small rust spots were visible. In most cases, corrosion stains were attributed to

Corrosion Rating:

Specimen	Generalized Rating	Localized Rating
Stirrups	101	295
Long. mild steel	1	8
Duct	NA	NA
Strand	NA	NA

corrosion of the bolster strips used to support the reinforcement during construction. This was evident due to the concrete spalling around the "feet" of many of the strips. The bolster strips were plastic tipped, but still corroded very early during testing, as reported by West.[4.2]   The spots of rust were aligned and at regular intervals.

<p align="center"><i>Lateral (North) view   Top view (from North side)</i></p>
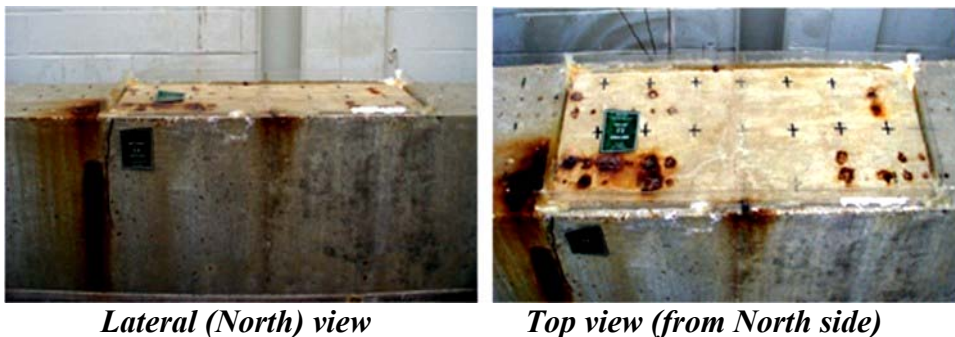
<p align="center"><i>Figure 4.69 Specimen 1.1 - Condition Prior to Autopsy</i></p>

A 0.03 in. maximum width crack extended from the Northeast corner of the ponded region down the side of the beam a distance of 11 inches. Hairline cracks were visible in the Northeast corner of the ponded region between the corroded bolster tips.

This specimen was partially autopsied as explained in Section 4.5.1.1, exposing and removing the mild steel bars only in a 42 inch length, west of the beam centerline.   The analysis length extended half of the ponded region (24 inches) and an additional foot and a half (18 inches) outside the ponded region.

After removing all mild steel bars in the autopsy region, severe corrosion was found in three out of eight longitudinal bars. The corrosion was very localized, at approximately 14 inches from the beam centerline. These localized corrosion areas coincided with the rust stains found previously on the top of the specimen in the Northeast corner of the ponded region. In Figure 4.70, the measurement tape indicates the localized corrosion at 28 inches from the left end

of the mild steel bar. This locations corresponds to 14 inches from the beam centerline.

Stirrups were placed at 12-inch spacings in all specimens. Therefore, four stirrups were included in the partial autopsy region. After a detailed visual inspection, severe localized corrosion was found in the stirrup located 14 inches from the beam centerline. (The actual location of the center stirrup was two inches from the beam centerline) The most severe corrosion was found in the north top corner of the stirrup, as shown in Figure 4.70. The stirrups located at 26 and 38 inches from the beam centerline had moderate to light corrosion in the top section, with no section loss. These stirrups were located outside the ponded region. The center stirrup, located 2 inches from the beam centerline, had only minor discoloration and light corrosion in localized areas.

Longitudinal bar   *Stirrup*
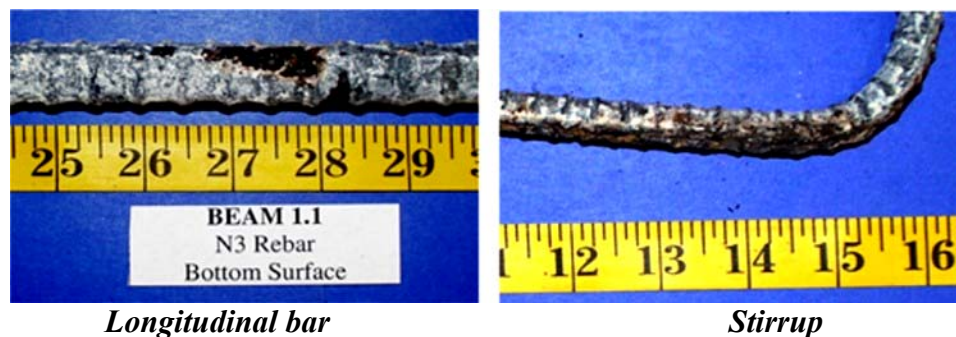
Figure 4.70 Specimen 1.1 - Mild Steel Bar and Stirrup

Figure 4.71 shows the longitudinal bar and stirrup corrosion rating graphs. Corrosion rating values for the east side of the beam were extrapolated from the west side, due to the partial autopsy procedure. This was done to compare results of the partial autopsy beams with those of the full autopsy beams. By doing so, it was assumed that the bars and stirrups to the east side of the beam centerline performed similarly to those west of the centerline.

311
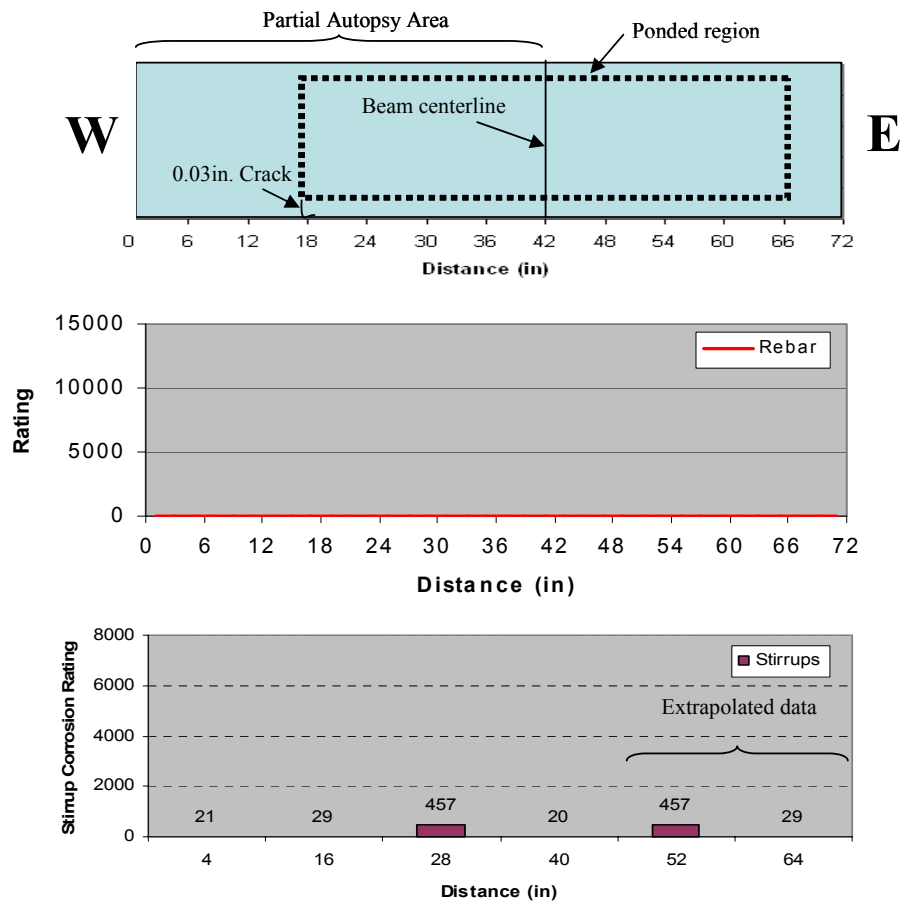
*Figure 4.71 Specimen 1.1. Crack Pattern and
Specimen Corrosion Rating Graphs*

4.5.3.2   Beam specimen 1.3 - Non-PS, Constant Service Load.

Specimen condition after testing included nine transverse cracks in the constant moment region (seven in the ponded region), with a maximum transverse crack width of 0.020 inches. Longitudinal cracks were also visible at

Corrosion Rating:

Specimen	Generalized Rating	Localized Rating
Stirrups	1231	770
Long. mild steel	91	261
Duct	NA	NA
Strand	NA	NA

4.5 inches from the sides of the beam, with a maximum crack width of 0.050 in.

Heavy rust stains and salt deposits were visible in the top of the cracks in localized areas, as shown in Figure 4.72.

Lateral (South) view   *Top view (from South side)*
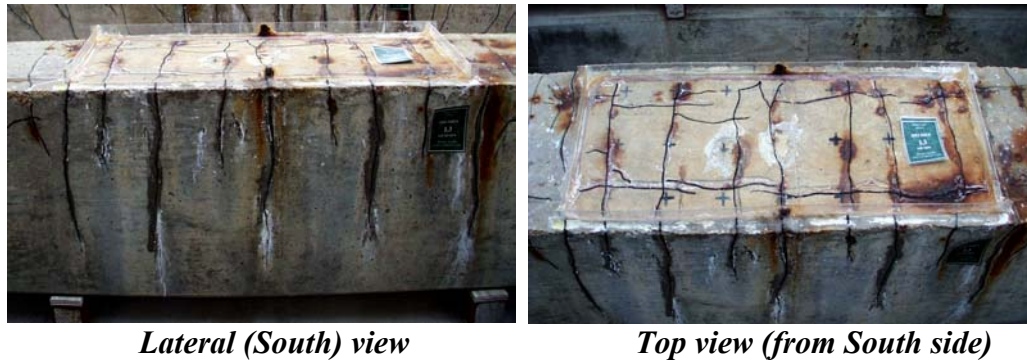
Figure 4.72 Specimen 1.3. Condition Prior to Autopsy

Very severe corrosion, pitting and section loss were observed for all longitudinal bars, corresponding with crack locations.   All the stirrups were also severely corroded, with large pits and section loss.   Crack locations coincided with the stirrup locations. Therefore, the stirrups were severely damaged, especially under the ponded region. Figure 4.73 shows examples of the typical longitudinal bar and stirrup corrosion in Specimen 1.3. Figure 4.74 shows the crack pattern in the top of the specimen after exposure and the rebar and stirrup corrosion ratings across the analyzed section.

Longitudinal Steel   *Stirrup*
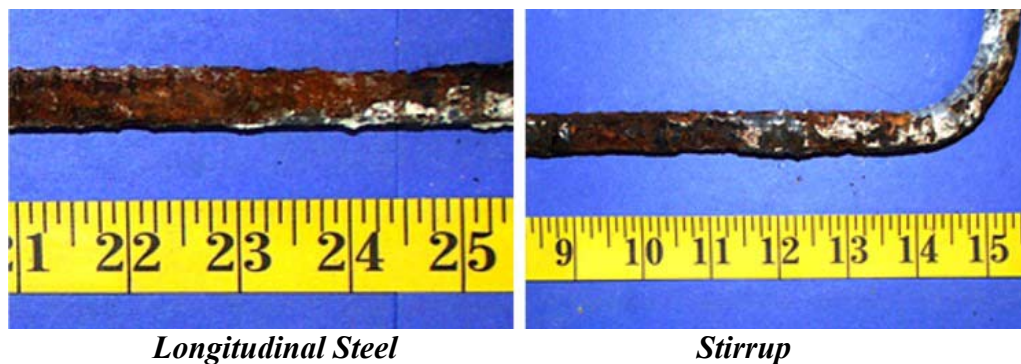
Figure 4.73 Specimen 1.3 Mild Steel Bar and Stirrup

Beam centerline   Ponded region

W   E
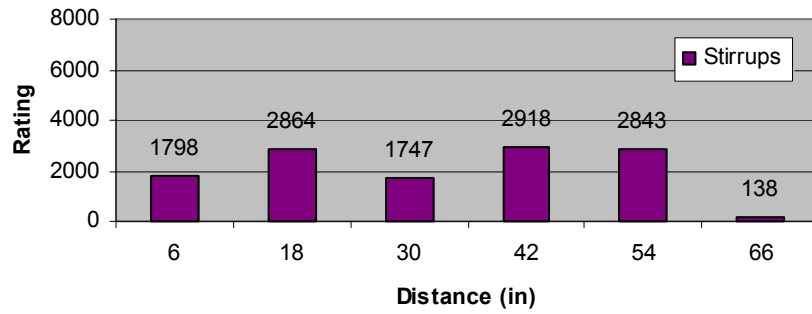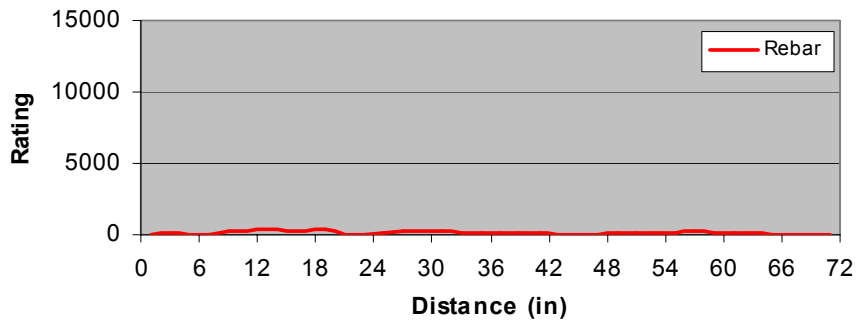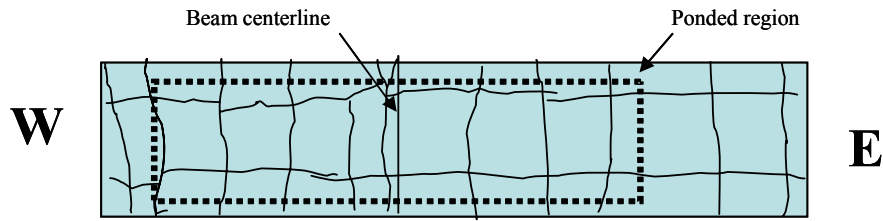
Figure 4.74 Specimen 1.3 Crack Pattern and
Specimen Corrosion Rating Graphs

4.5.3.3 Beam Specimen 2.3 – 2/3 PS, Service Load

Three main transverse cracks, with a maximum crack width of 0.02 inches, and two longitudinal cracks, with a maximum crack width of 0.05 inches, were found at the end of exposure. These cracks were located on the

Corrosion Rating:

Specimen	Generalized Rating	Localized Rating
Stirrups	1359	2236
Long. mild steel	467	6241
North Duct	4299	2107
South Duct	5069	6248
North Strands	96	20
South Strands	122	56

314

top of the specimen in the ponded region. Salt deposits and large rust stains were visible on the sides of the beam, as shown in Figure 4.75.

Very severe pitting and section loss was found on the mild steel bars in the northeast corner of the ponded region. (See Figure 4.77) The corrosion was located 24 inches from the beam centerline, which corresponded with the border of the ponded region. The stirrups were also severely corroded, as seen in Figure 5.16. It was found that severely corroded stirrups coincided with crack locations. (See graphs in Figure 4.78)

Lateral (South) View   *Top View (from South Side)*
Figure 4.75 Specimen 2.3 – Condition Prior to Autopsy

Extremely severe corrosion and area loss, corresponding to crack locations, was found in both post-tensioning ducts. (See Figure 4.77 and graphs in Figure 4.78) Corrosion was aggravated at locations where large grout voids existed, as shown in Figure 4.76. A large accumulation of corrosion products from the ducts was found attached to the grout.

Moderate localized corrosion and pitting in a few wires was found on the south strands. The north strands show only moderate to light uniform corrosion. As with the mild steel bars, stirrups and ducts, localized corrosion in the strands corresponded to crack locations in the ponded region.

315

The acid soluble chloride content in the grout reached a maximum value of 0.3% by weight of grout inside the south duct, and 0.18% inside the north duct. These values are much higher than the critical chloride threshold value of 0.033% by weight of grout (corresponding to 0.2% by weight of cement). Chloride samples were taken at 6-inch intervals within the forensic analysis length and chloride content plots were obtained, as observed in Figure 4.78.

Beam specimen 2.3 had four duct splices. The north duct had two industry standard splices, and the south duct had two heat-shrink splices. Figure 4.76 shows the condition of the duct splices at the end of exposure testing. Severe area loss and extremely severe corrosion were found on the oversized piece of both industry standard splices in the north duct. As shown in the photographs, moisture was able to enter the sides of the splice at the duct tape locations. This accelerated the corrosion by allowing corrosive attack from the inside of the splice as well as the outside. Voids in the grout at the splice locations also aggravated the corrosion in the galvanized steel pieces. The west duct splice on the north duct had been intentionally damaged during construction. The role the damage played with respect to the splice corrosion protection is not clear due to the effect of the other contributing factors, such as splice locations, crack locations, moisture ingress and chloride contents. The heat-shrink splices in the south duct also performed poorly. As can be seen from Figure 4.76, the east heat-shrink splice trapped moisture from the grout bleed water and accelerated the galvanized duct deterioration. The west side splice was intentionally damaged during construction, with a small cut (less than 1 inch) in the center. The generalized duct corrosion under the splice and the uniform rust stains on the inside of the heat-shrink splice indicate that the damage was not the main cause of duct corrosion. Nevertheless, the damage is considered as one of the duct deterioration contributing factors.

316
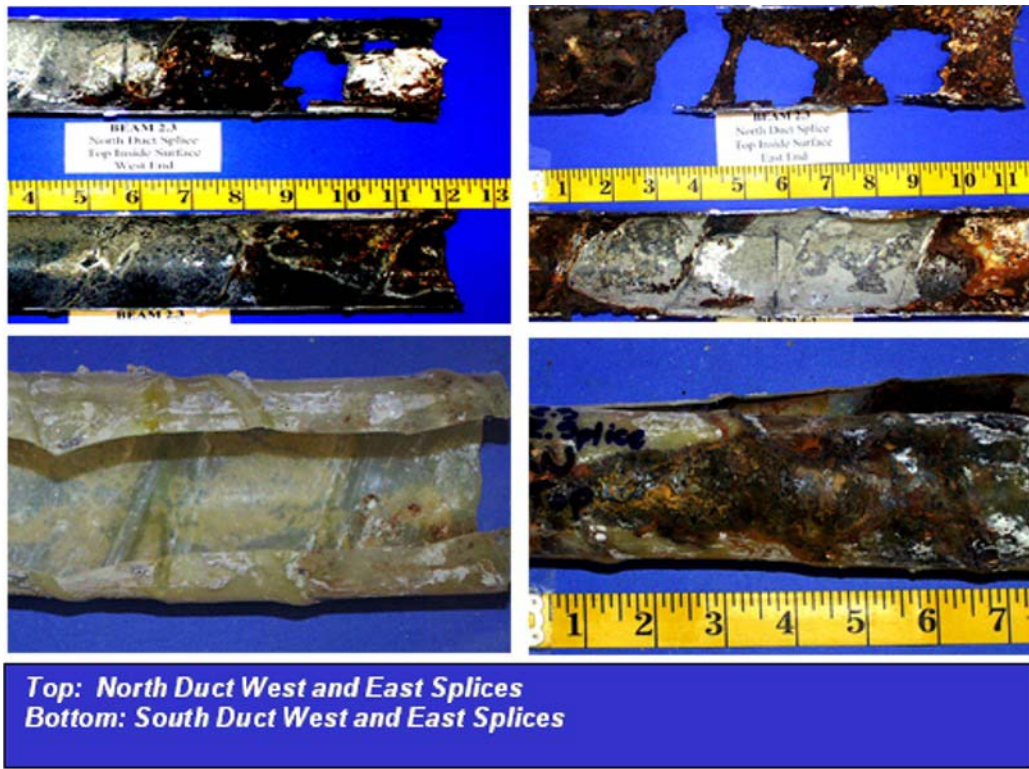
Figure 4.76   Specimen 2.3 – Duct Splices

317

Figure 4.77 Specimen 2.3 – Reinforcing Elements

318
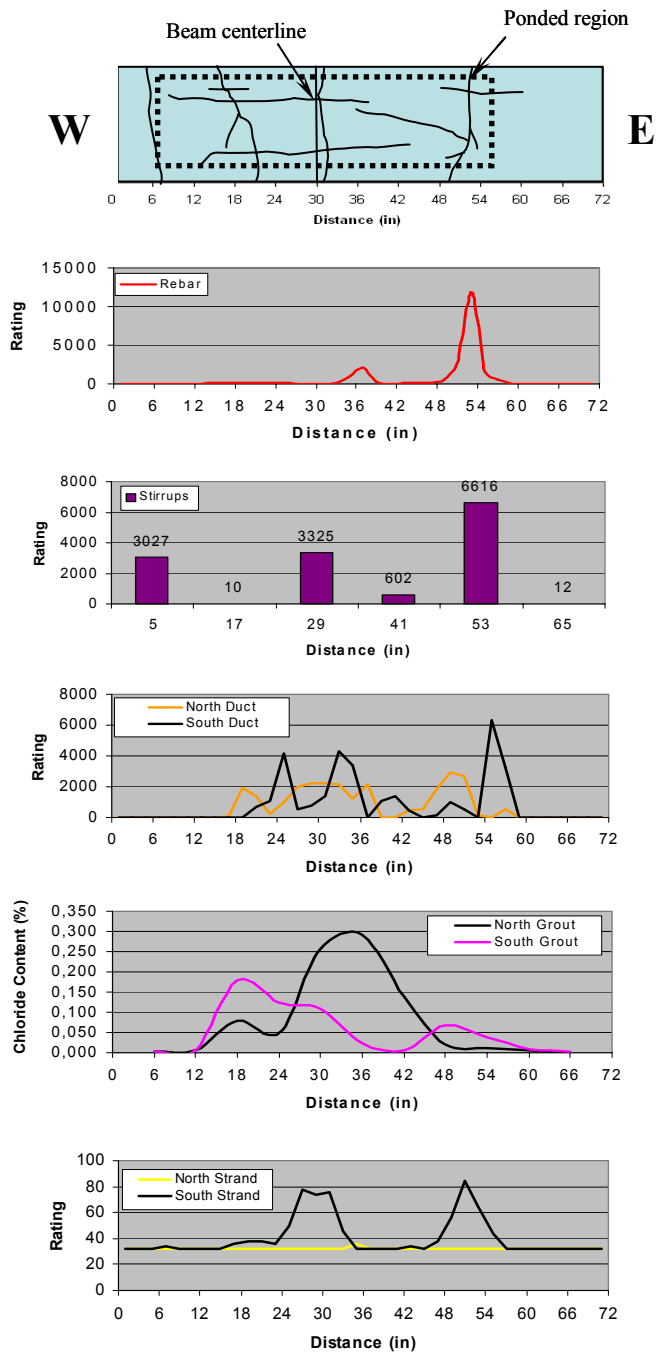
Figure 4.78 Specimen 2.3 – Crack Pattern and
Specimen Corrosion Rating Graphs

319

4.5.3.4   Beam Specimen 2.11 – 2/3 PS, Service Load, Fly Ash Grout

As shown in Figure 4.79, four main transverse cracks and several small longitudinal cracks were visible on the top of Specimen 2.11 in the constant moment region at the end of exposure. A maximum transverse crack width of 0.03 inches was found in the southwest area of the ponded region. The maximum longitudinal crack width was also 0.030 in. Heavy rust stains were visible on the top of the specimen in localized areas extending out of the cracks, as shown in Figure 4.79. The additional rust stains corresponded to the location of the "legs" of the bolster strips, used to support the reinforcement.

Corrosion Rating:

Specimen	Generalized Rating	Localized Rating
Stirrups	1923	2978
Long. mild steel	476	7757
North Duct	1504	2440
South Duct	1413	1673
North Strands	97	20
South Strands	92	26

A full autopsy of Specimen 2.11 was performed, providing a total length of 72 inches of the longitudinal bars, ducts, grout and strands and six stirrups to be analyzed. Thirty inches of the analysis length extended to the west of the centerline of the beam and the remaining 42 inches extended to the east.
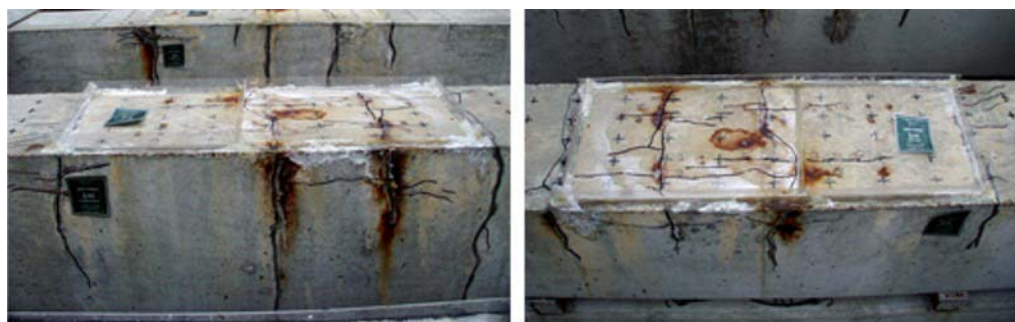
Lateral (North) View   *Top View (from South Side)*

Figure 4.79 Specimen 2.11 – Condition Prior to Autopsy

320

Very severe section loss and pitting was observed in all longitudinal mild steel bars corresponding to all crack locations. (See Figure 4.81) The most severe corrosion was found at the beam centerline crack. Similar results were found on the stirrups, where the beam centerline stirrup had extensive corrosion and section loss.

Figure 4.81 shows the severe corrosion and area loss found in the south duct. Extensive duct deterioration was mostly located to the west of the centerline. Zinc and steel corrosion products covered the remaining areas on the top of the duct. The bottom of the duct was found to be in better condition, with some areas of zinc and steel corrosion products. Corrosion on the north duct was less severe than on the south duct. It was also found to have a few areas of severe localized corrosion, section loss, and build up of zinc and steel corrosion products. The corrosion on the north duct was significant at the centerline of the beam, under the industry standard splice.

The south duct grout had several transverse cracks, with a maximum crack width of 0.060 inches. This crack coincided with the location of the heavy duct corrosion and area loss. Duct corrosion stains were found inside the grout cracks, where moisture had traveled down from the grout surface. (See Figure 4.81) The north duct grout had one large void due to bleed water that was 22 inches in length and 0.013 inches deep. Corrosion products were found attached to the grout in the void. This location corresponded with the splice location at the centerline of the beam. Three transverse cracks, with a maximum crack width of 0.010 inches, were found on the east side of the grout. The cracks coincided with the area where severe duct corrosion and duct area loss were found. The acid soluble chloride content in the grout reached a maximum value of 0.31% by weight of grout inside the north duct, and 0.033% inside the south duct. The content in the north duct was from the sample taken at the centerline of the beam,

under the industry standard splice. It was much higher than the critical chloride threshold value of 0.033% by weight of grout. Chloride samples were taken at 6-inch intervals within the forensic analysis length and chloride content plots were obtained, as observed in Figure 4.82.

Light to moderate corrosion was found on the outer wires of the strands in both ducts, with the center wires presenting a slight increase in corrosion severity.

Specimen 2.11 had two duct splices. The north duct had an industry standard splice, and the south duct had a heat-shrink splice. Both splices were located at the centerline of the beam. Figure 4.80 shows the condition of the duct splices at the end of exposure testing. The top of the north duct splice was found to be severely deteriorated. The heat-shrink splice showed severe signs of rust staining from the duct corrosion.
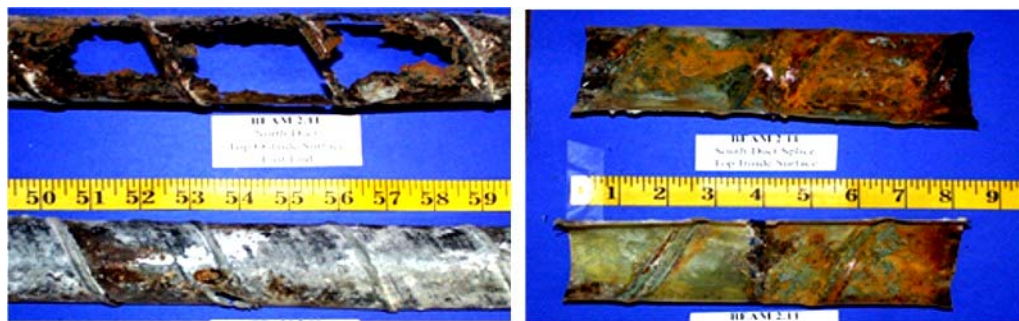
North Duct Splice   *South Duct Splice*

Figure 4.80 Specimen 2.11 – Duct Splices
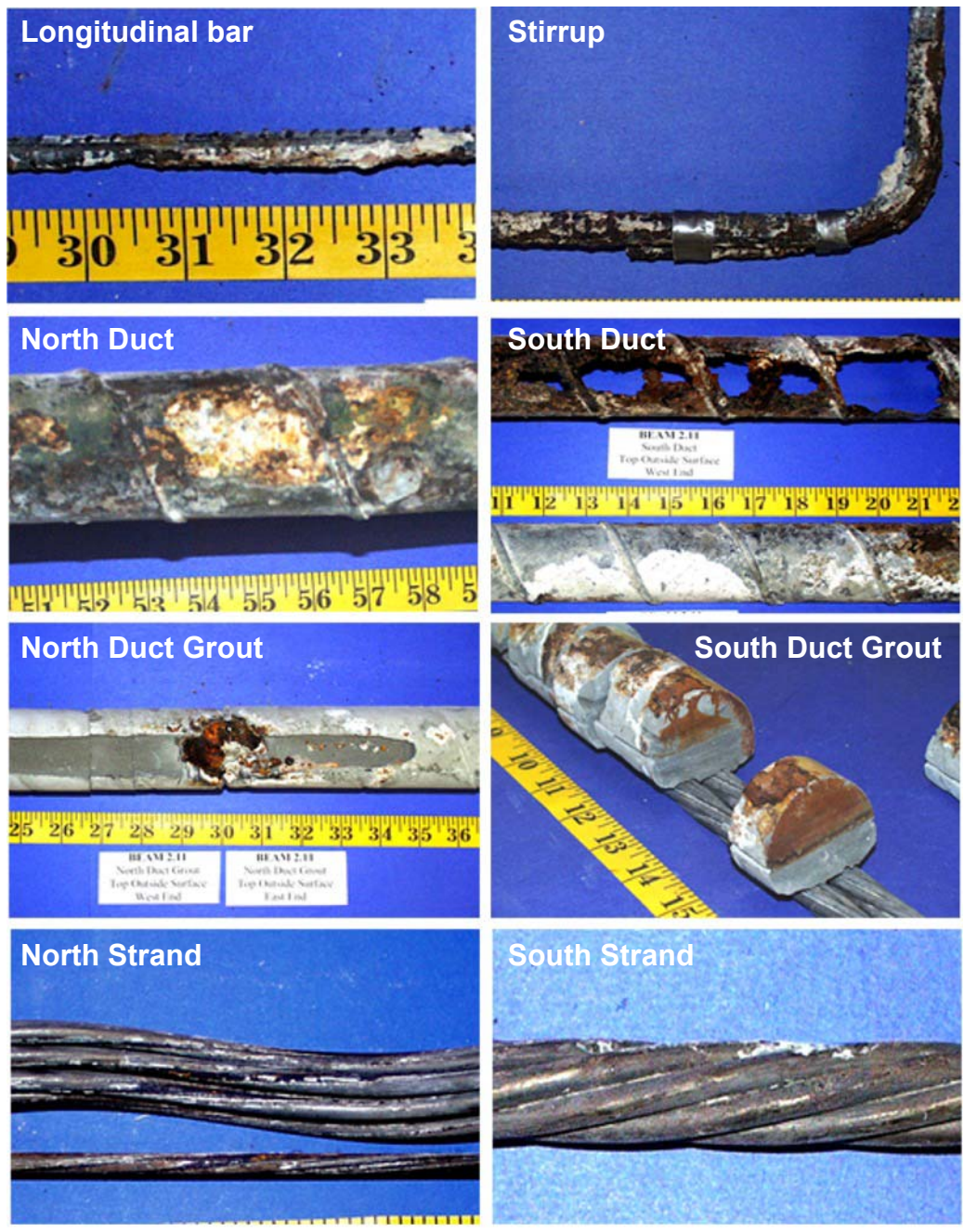
Figure 4.81 Specimen 2.11 – Reinforcing Elements
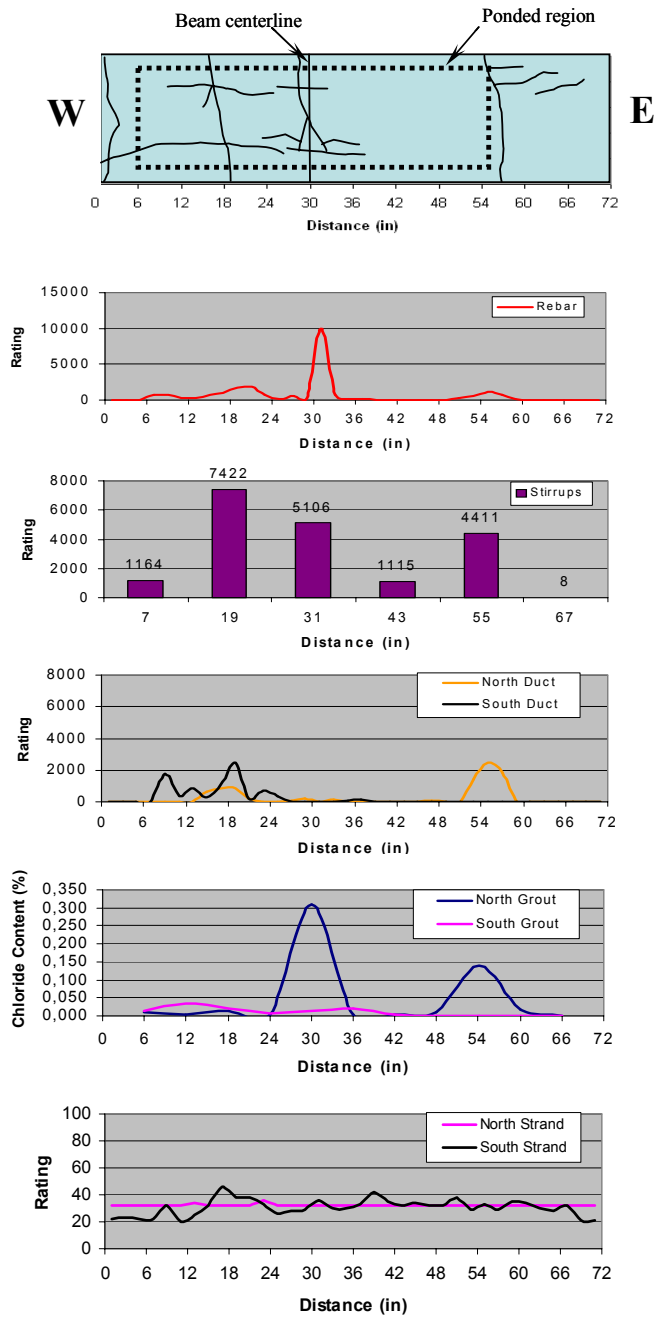
Figure 4.82 Specimen 2.11 – Crack Pattern and Specimen Corrosion Rating Graphs

324

4.5.3.5 Beam Specimen 3.1 – 100%U PS, Unloaded

As seen in Figure 4.83, a visual inspection of Specimen 3.1 at the end of exposure found that it remained uncracked. Any rust staining on Specimen 3.1 was due to the bolster strips.

This specimen was partially autopsied, as explained in Section

Corrosion Rating:

Specimen	Generalized Rating	Localized Rating
Stirrups	15	4
Long. mild steel	0	0
North Duct	0	0
South Duct	0	0
North Strands	119	20
South Strands	96	22

4.5.2.2. The analysis length included half of the ponded region (24 inches) and an additional foot and a half (18 inches) outside the ponded region. Forty-two inches of the mild steel bars, ducts, grout and strands west of the centerline were exposed and removed. The section autopsied only included three stirrups for analysis.

Lateral (North) View   *Top View (from North Side)*

Figure 4.83 Specimen 3.1 – Condition Prior to Autopsy

As shown in Figure 4.85, there was no corrosion found on either of the mild steel bars in Specimen 3.1.

Light uniform corrosion was found on the three stirrups included in the partial autopsy. The centerline stirrup was intended to be included in the partial

autopsy, but its actual location was outside of the section removed. This is why there is no analysis or rating for the centerline stirrup

There were no signs of corrosion on either of the ducts.

The grout in the north and south ducts showed multiple small voids over the entire length. Neither of the duct grouts had significantly large voids. The acid soluble chloride content in the north duct grout was negligible. The chloride content in the south duct grout was also negligible, except for the single measurement of 0.021% by weight of grout. The sample yielding this value was taken 36 inches to the west of the centerline. It was determined that this value was due to an error in the equipment and considered an outlier. Chloride samples were taken at 6-inch intervals within the forensic analysis length and chloride content plots were obtained, as shown in Figure 4.86.

Moderate uniform corrosion was found on the strands in the north duct, and light uniform corrosion was found on those located in the south duct. (See Figure 4.85)

Specimen 3.1 had two duct splices. The south duct had an industry standard splice and the north duct had a heat-shrink splice. Both splices were located at the centerline of the beam. Therefore, only half of each splice was included in the section autopsied. Figure 4.84 shows the condition of the duct splices at the end of exposure testing. No signs of corrosion were found on either splice.
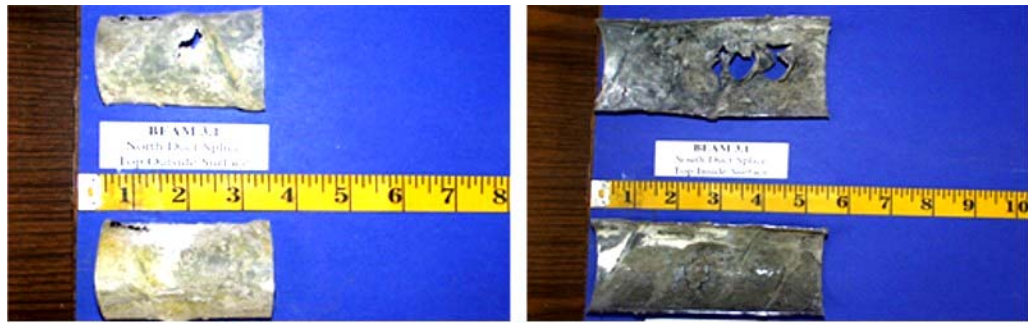
North Duct Splice   **South Duct Splice**

Figure 4.84 Specimen 3.1 – Duct Splices

Figure 4.86 shows the chloride content and corrosion rating graphs for each reinforcing element. Corrosion rating values for the east side of the beam were extrapolated from the west side, due to the partial autopsy procedure. This was done to compare results of the partial autopsy beam with those of the full autopsy beams. By doing so, it was assumed that the reinforcing elements to the east side of the beam centerline performed similarly to those west of the centerline.

327
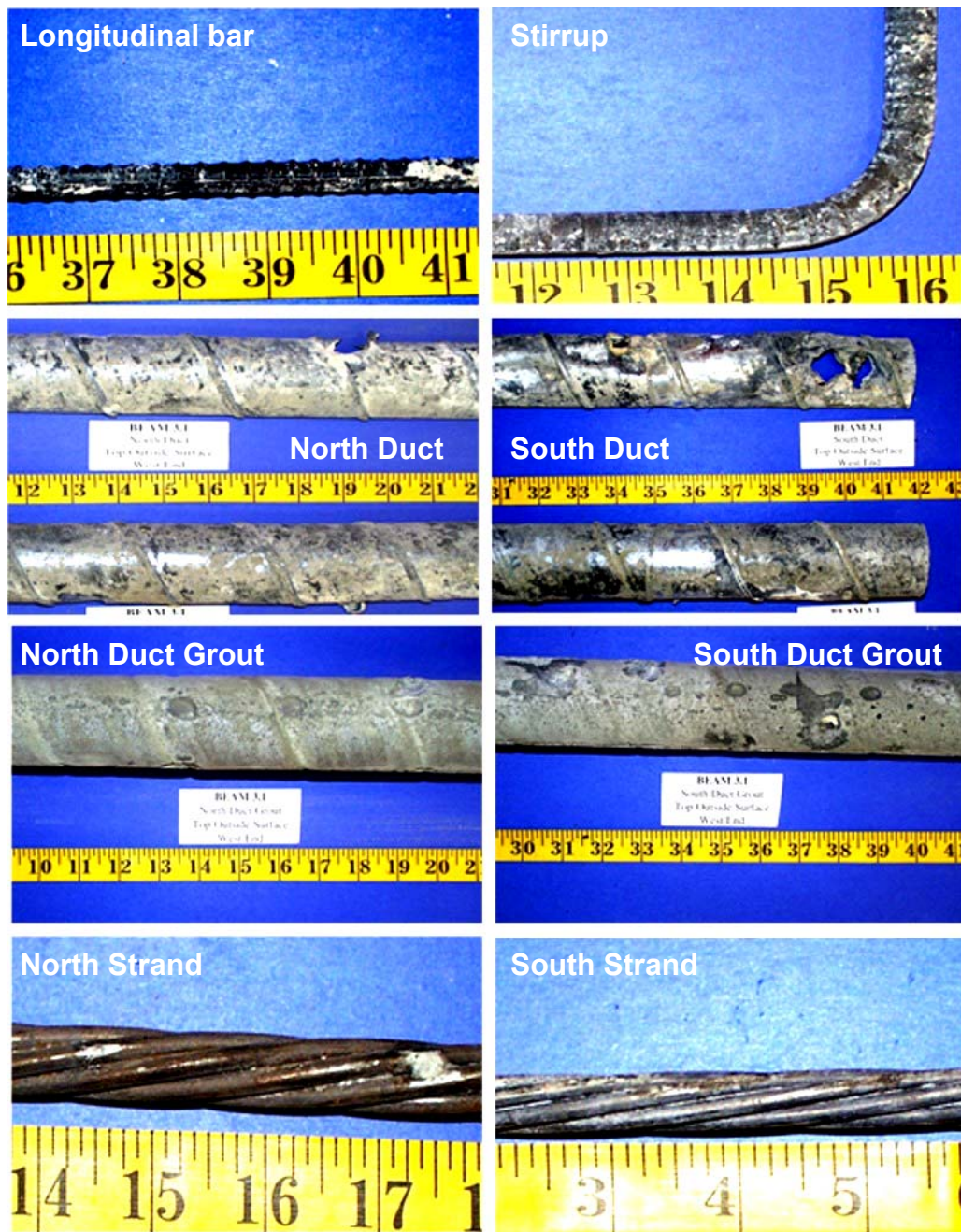
Figure 4.85 Specimen 3.1 – Reinforcing Elements

328
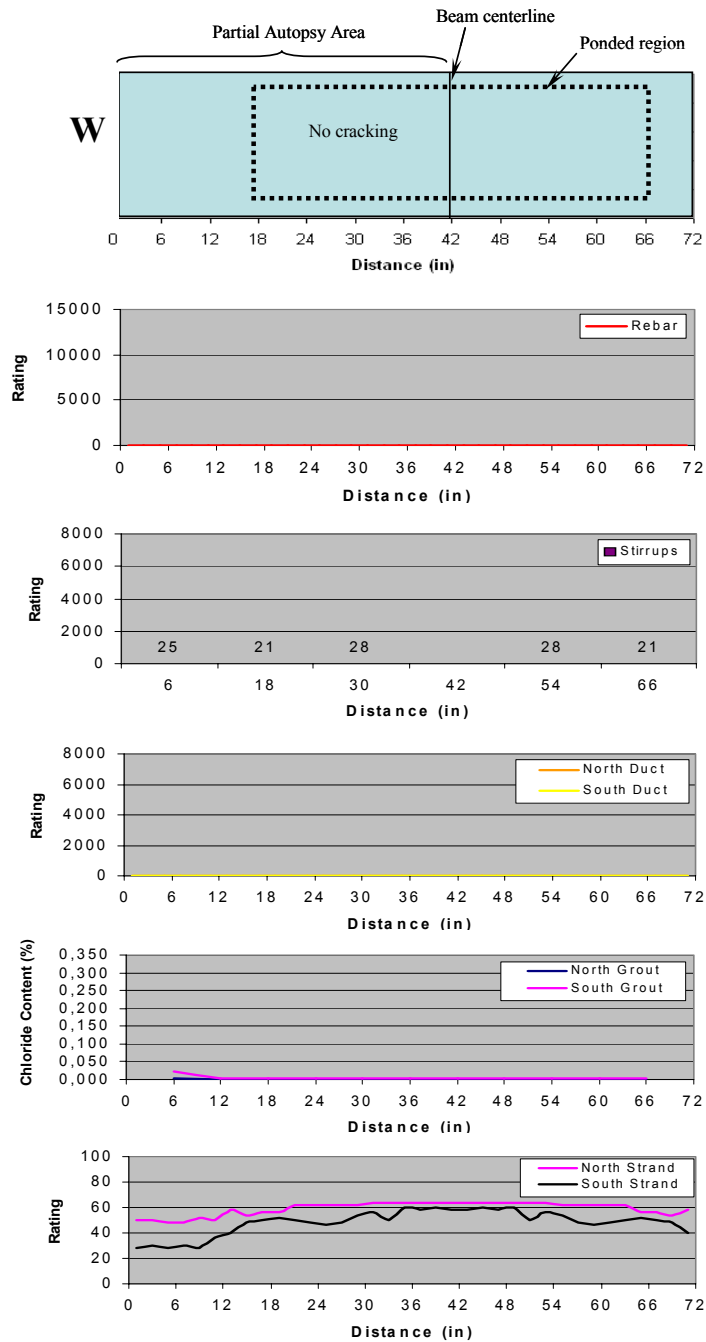
Figure 4.86 Specimen 3.1 – Crack Pattern and Specimen Corrosion Rating Graphs

329

4.5.3.6 Beam Specimen 3.2 – 100%U PS, Service Load

A visual inspection found that Specimen 3.2 had one transverse crack (See Figure 4.87) across the top of the beam at the end of exposure even though this specimen was designed to remain uncracked. The crack had a maximum width of 0.01 inches and was located 12 inches to the west of the centerline of the

Corrosion Rating:

Specimen	Generalized Rating	Localized Rating
Stirrups	95	462
Long. mild steel	1	4
North Duct	1	2
South Duct	0	2
North Strands	168	28
South Strands	168	28

beam. This location was directly above a stirrup. As seen in Figure 4.87, any rust staining was due to the bolster strips.

A full autopsy of Specimen 3.2 was performed, providing a total length of 72 inches of the longitudinal bars, ducts, grout and strands and six stirrups to be analyzed. (See Figure 4.90) Forty-two inches of the analysis length extended to the west of the centerline of the beam and the remaining 30 inches extended to the east.

Lateral (North) View   *Top View (from South Side)*

Figure 4.87 Specimen 3.2 – Condition Prior to Autopsy

The only corrosion found on the mild steel bars was a small localized area of light corrosion. It was located 10 inches to the east of the centerline.

Two localized areas of severe corrosion and area loss were found on the stirrups. These areas were found on the stirrups located 13 and 25 inches to the west of the centerline. The stirrup 13 inches to the west corresponds to the crack described above. The remaining stirrups showed light uniform corrosion.

The only corrosion found on the north duct was located under the heat-shrink splice at the centerline of the beam. It showed two very light spots of corrosion. The south duct showed no signs of corrosion. (See Figure 4.90)

The grout in the north duct showed multiple small voids over the entire length. The south duct grout had three large voids. A 14-inch long void was located at the centerline, as shown in Figure 4.90. Two six-inch long voids were found 24 inches to the east and to the west of the centerline. Figure 4.88 was included to illustrate the good grouting quality of both ducts in Specimen 3.2. The acid soluble chloride content in the north and south duct grout was negligible. Chloride samples were taken at 6-inch intervals within the forensic analysis length and chloride content plots were obtained, as shown in Figure 4.91.

Light uniform corrosion was found on all of the strands located in the north and south ducts.
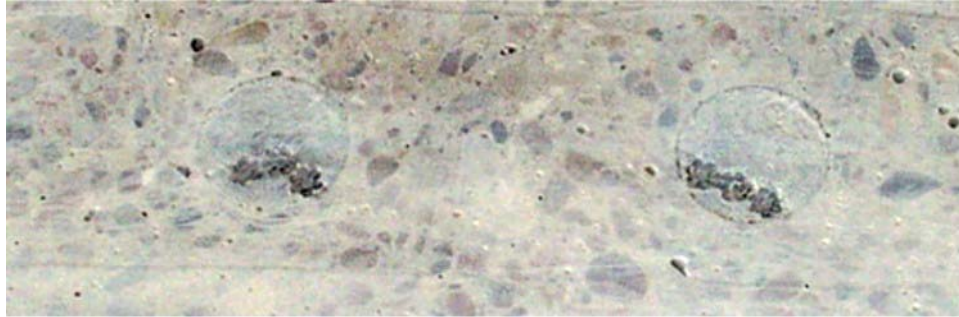
Figure 4.88 Specimen 3.2 – Grouted Duct

Specimen 3.2 had two duct splices. The south duct had an industry standard splice and the north duct had a heat-shrink spice. Both splices were located at the centerline of the beam. Figure 5.89 shows the condition of the duct splices at the end of exposure. Both splices showed no signs of corrosion, with only a minor salt stain on the industry standard splice.

*North Duct Splice*   *South Duct Splice*

Figure 4.89 Specimen 3.2 – Duct Splices
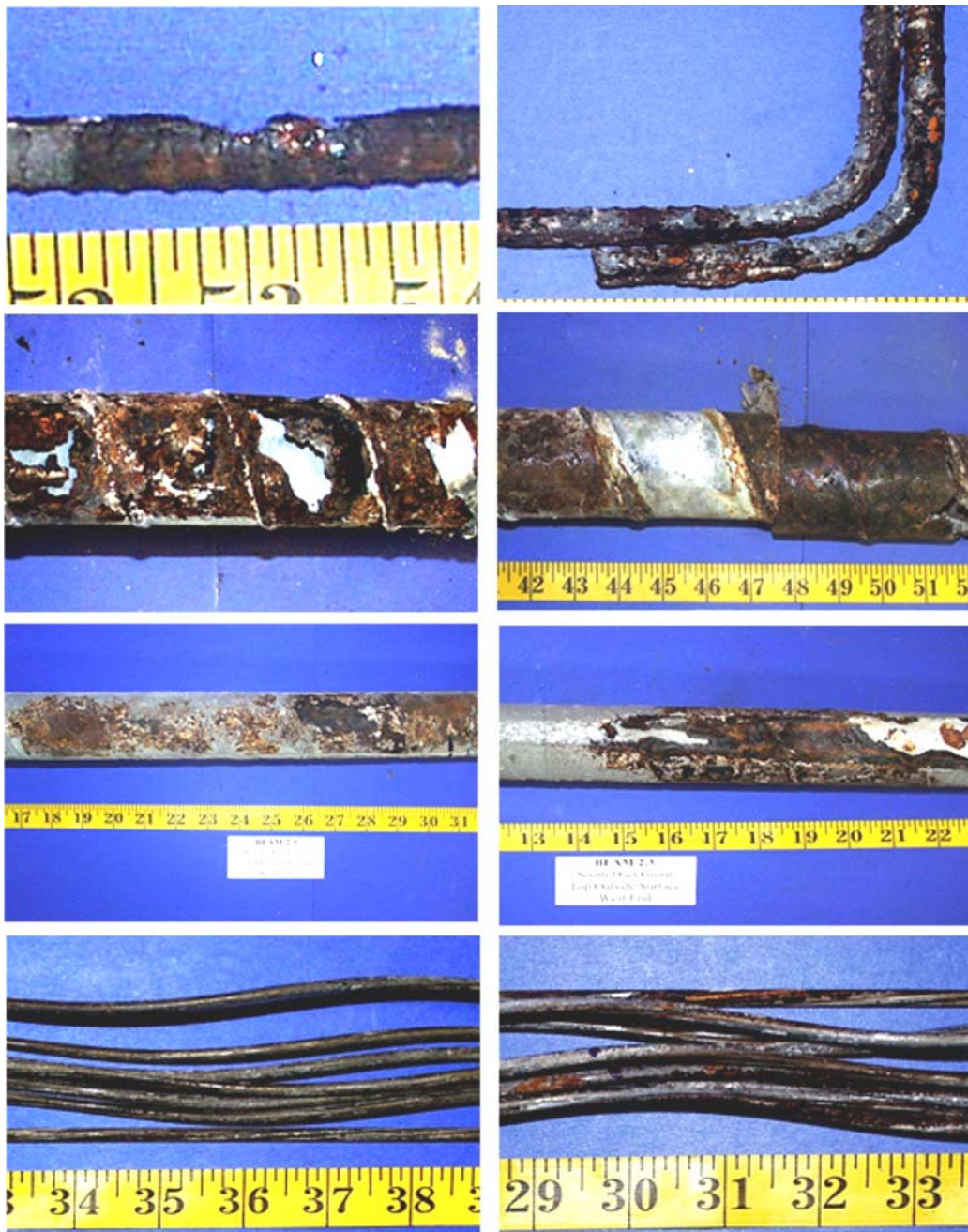
Figure 4.90 Specimen 3.2 – Reinforcing Elements
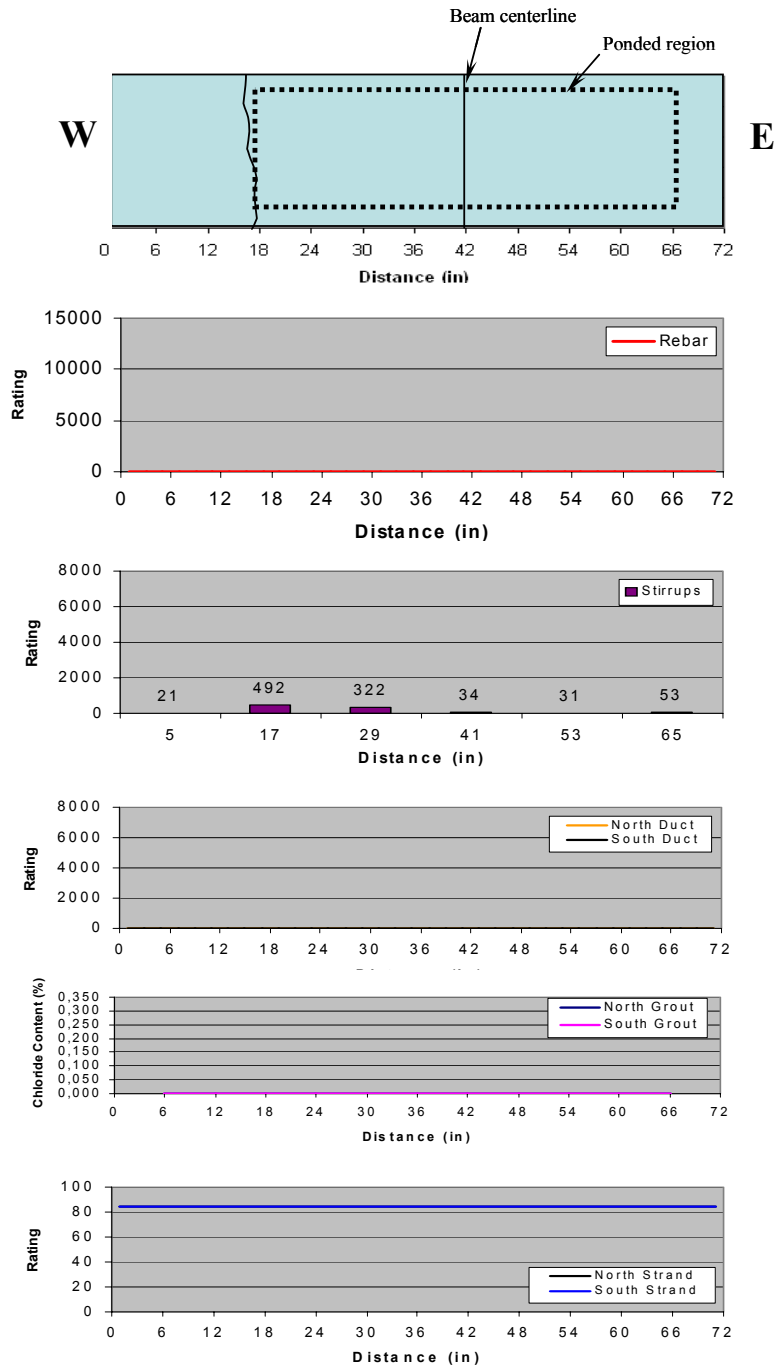
***Figure 4.91 Specimen 3.2 – Crack Pattern and Specimen
Corrosion Rating Graphs***

334

4.5.3.7   Beam Specimen 3.3 – 100%U PS, Overload

As shown in Figure 4.92, specimen 3.3 had three transverse cracks across the top of the beam at the end of exposure. The largest crack had a maximum width of 0.013 inches and was located at the centerline of the beam. This location was directly above a stirrup. The other two cracks had a

Corrosion Rating:

Specimen	Generalized Rating	Localized Rating
Stirrups	423	867
Long. mild steel	36	294
North Duct	429	924
South Duct	220	685
North Strands	161	64
South Strands	118	32

maximum width of 0.01 inches. They were located 24 inches to the east and west of the centerline. Both of these cracks also coincided with stirrup locations. As seen in Figure 4.92, there was minor rust staining around the cracks on the sides of the beam. A majority of the rust spots on the top were from the bolster strips.

A full autopsy of Specimen 3.3 was performed, providing a total length of 72 inches of the longitudinal bars, ducts, grout, and strands and six stirrups to be analyzed. Forty-two inches of the analysis length extended to the west of the centerline of the beam and the remaining 30 inches extended to the east. (See Figure 4.92)

Lateral (North) View   *Top View (from North Side)*

Figure 4.92 Specimen 3.3 – Condition Prior to Autopsy

Two areas with severe corrosion with area loss were found on one of the mild steel bars. They coincided with the stirrups located at the centerline and 24 inches to the west.

Severe uniform corrosion and section loss was found on the three stirrups located under the cracks described above. The remaining stirrups showed light uniform corrosion.

Severe corrosion and area loss corresponding to the three crack locations was found on the north duct. The south duct also showed signs of severe corrosion and area loss at the centerline, and moderate corrosion under the other two cracks. (See Figure 4.94) The remainder of the ducts showed no signs of corrosion.

The grout in the north duct had two voids located at the centerline and 24 inches to the east. Corrosion products from the duct were found coinciding with the three crack locations. Two voids were also present in the south duct grout. They were located 30 inches to the west and 14 inches to the east of the centerline. Neither of these voids coincided with any duct corrosion or crack locations. Corrosion products from the south duct were found coinciding with three crack locations. The acid soluble chloride content in the grout reached a maximum value of 0.0423% by weight of grout inside the north duct at the centerline. The maximum chloride content in the south duct grout was 0.0457% by weight of grout. This sample was located 24 inches to the east of the centerline, which is the same location as one of the cracks and severe duct corrosion. These values are higher than the critical chloride threshold value of 0.033% by weight of grout. Chloride samples were taken at 6-inch intervals within the forensic analysis length and chloride content plots were obtained, as shown in Figure 4.95.

336

Moderate to severe uniform corrosion was found on all three prestressing strands in the north duct. As shown in Figure 4.94, severe localized corrosion was found 24 inches to the west of the centerline, which again coincides with a crack location. Moderate to severe uniform corrosion was also found on all three prestressing strands in the south duct.

Specimen 3.3 had one duct splice. It was an industry standard splice located on the north duct at the centerline. Figure 4.93 shows the condition of the duct splice at the end of exposure testing. The top of the north duct splice was found to be severely corroded with significant section loss.

Figure 4.93 Specimen 3.3 – North Duct Splice

Figure 4.94 Specimen 3.3 – Reinforcing Elements

338

W **E**

Beam centerline

Ponded region

Previous limited autopsy area
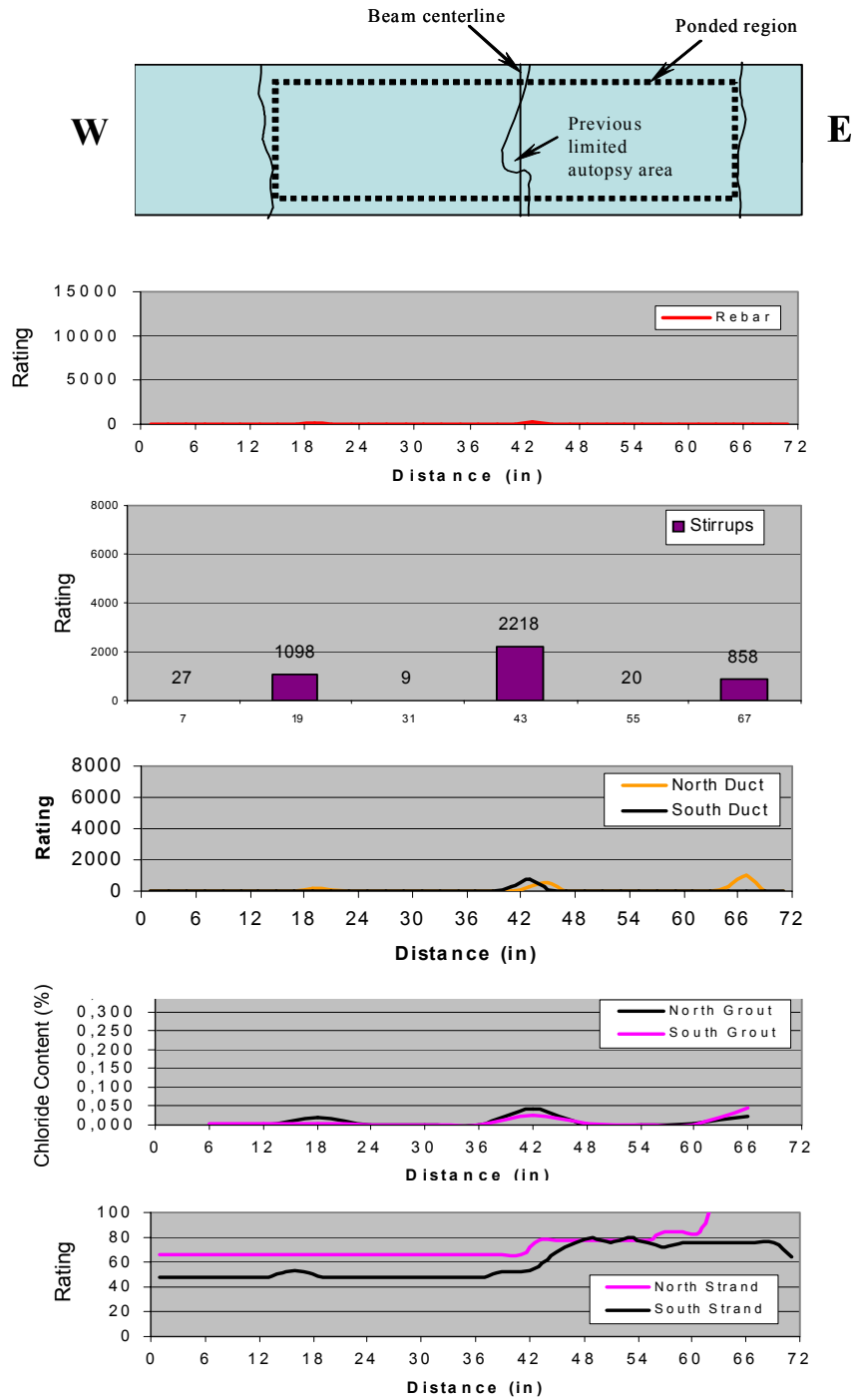
Figure 4.95 Specimen 3.3 – Crack Pattern and Specimen Corrosion Rating Graphs

339

4.5.3.8 Beam Specimen 4.2 – 100%S PS, Service Load

As shown in Figure 4.96, a visual inspection found that Specimen 4.2 had two transverse cracks across the top of the beam at the end of exposure. This specimen was designed to remain uncracked. The first crack had a maximum width of 0.013 inches and was located one inch to the west of

Corrosion Rating:

Specimen	Generalized Rating	Localized Rating
Stirrups	189	236
Long. mild steel	15	169
North Duct	7	8
South Duct	4	4
North Strands	96	22
South Strands	96	16

the centerline of the beam. This location was directly above a stirrup. The second crack had a maximum width of 0.01 inches. It was located 22 inches to the east of the centerline, also above a stirrup. As seen in Figure 4.96, there was no rust staining around the cracks. Any rust spots were again from the bolster strips.

A full autopsy of Specimen 4.2 was performed, providing a total length of 72 inches of the longitudinal bars, ducts, grout and strands and six stirrups to be analyzed. Thirty inches of the analysis length extended to the west of the centerline of the beam and the remaining 42 inches extended to the east. (See Figure 4.99)

Lateral (South) View   Top View (from East Side)

Figure 4.96 Specimen 4.2 – Condition Prior to Autopsy

Signs of corrosion were only found on one of the mild steel bars. It was severe localized corrosion with minor section loss at the centerline. (See Figure 4.98)

Severe localized corrosion and section loss were found on the two stirrups located under the cracks described before. The remaining stirrups showed light uniform corrosion with a few areas of moderate localized corrosion.

Severe corrosion corresponding to the maximum crack location at the centerline was found on the north duct. The south duct showed signs of light to moderate corrosion corresponding with the two cracks on the specimen. The remainder of the ducts showed no signs of corrosion. (See Figure 4.98)

The grout in the north duct had a large void approximately 12 inches long. It was located under the smaller crack to the east of the centerline. Corrosion stains from the duct were found a few inches to the east of the centerline. As seen in Figure 4.98, a large crack in the grout was also present at this location, showing rust stains on the face of the crack. Two large voids were present in the south duct grout. One began six inches to the west of the centerline, extending 18 inches. (See Figure 4.98) The second void was 14 inches in length and began 20 inches to the east. The acid soluble chloride content in the grout reached a maximum value of 0.0023% by weight of grout inside the north and south ducts. This value is much lower than the critical chloride threshold value of 0.033%. Chloride samples were taken at 6-inch intervals within the forensic analysis length and chloride content plots were obtained, as shown in Figure 4.99.

Light uniform corrosion was found on all of the strands located in the north and south ducts.

Specimen 4.2 had four duct splices. The south duct had two industry standard splices, one beginning 12 inches to the east of the centerline and the other 12 inches to the west. The north duct had two heat-shrink splices at the same

341

locations. Figure 4.97 shows the condition of the duct splices at the end of exposure testing. The only corrosion found on the industry standard splices was very light and located on the end of the splice. Both heat-shrink splices showed no signs of rust staining.
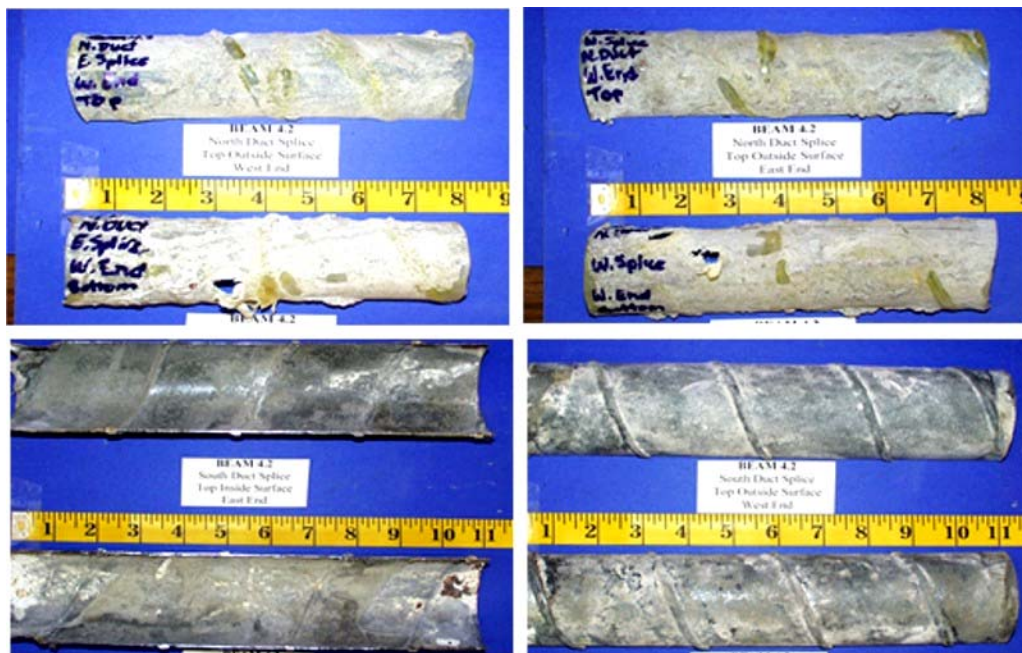
Figure 4.97 Specimen 4.2 – Duct Splices
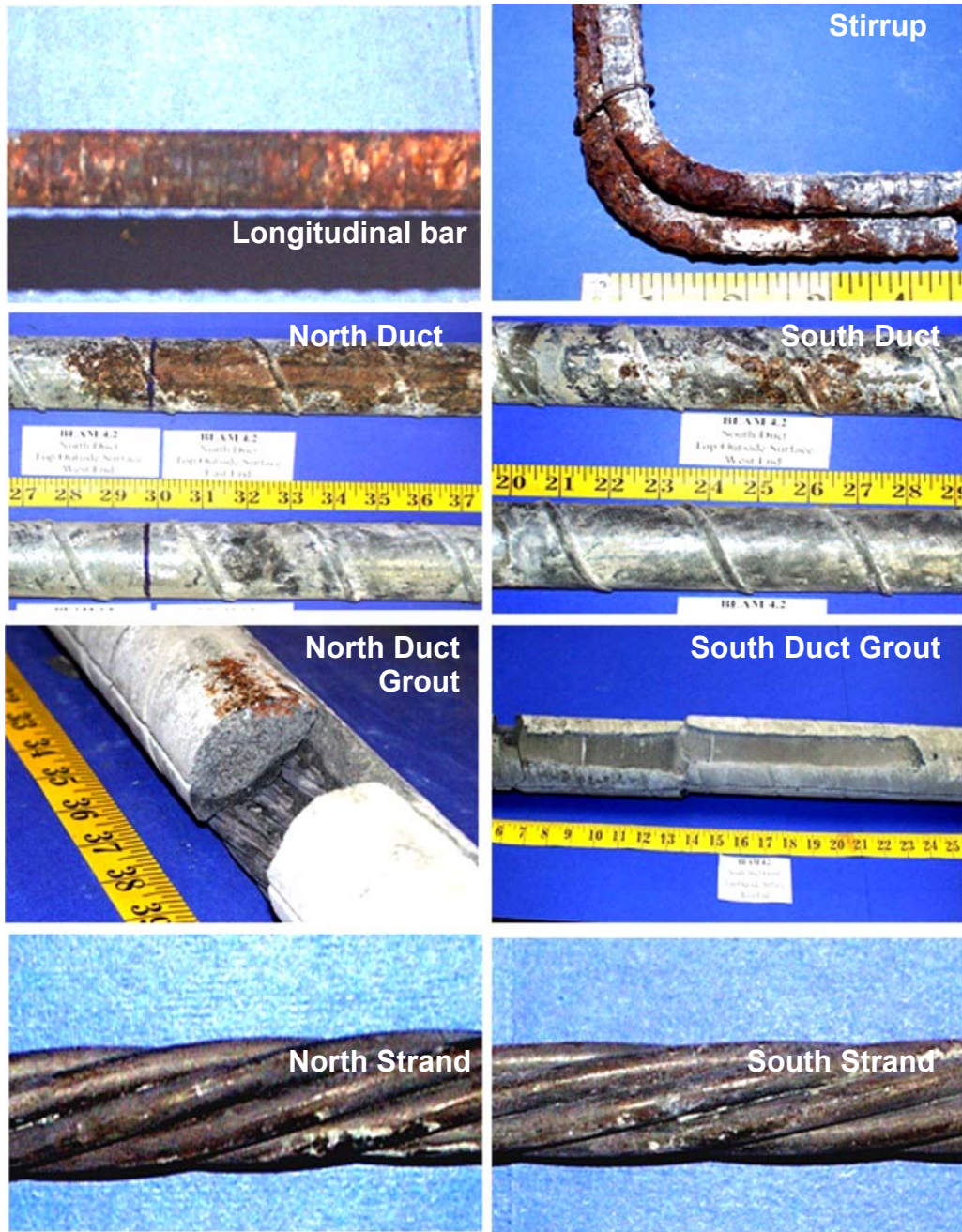
Figure 4.98 Specimen 4.2 – Reinforcing Elements

343

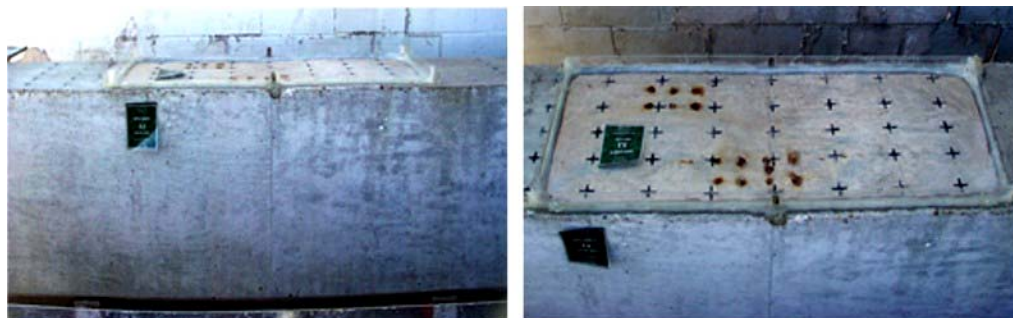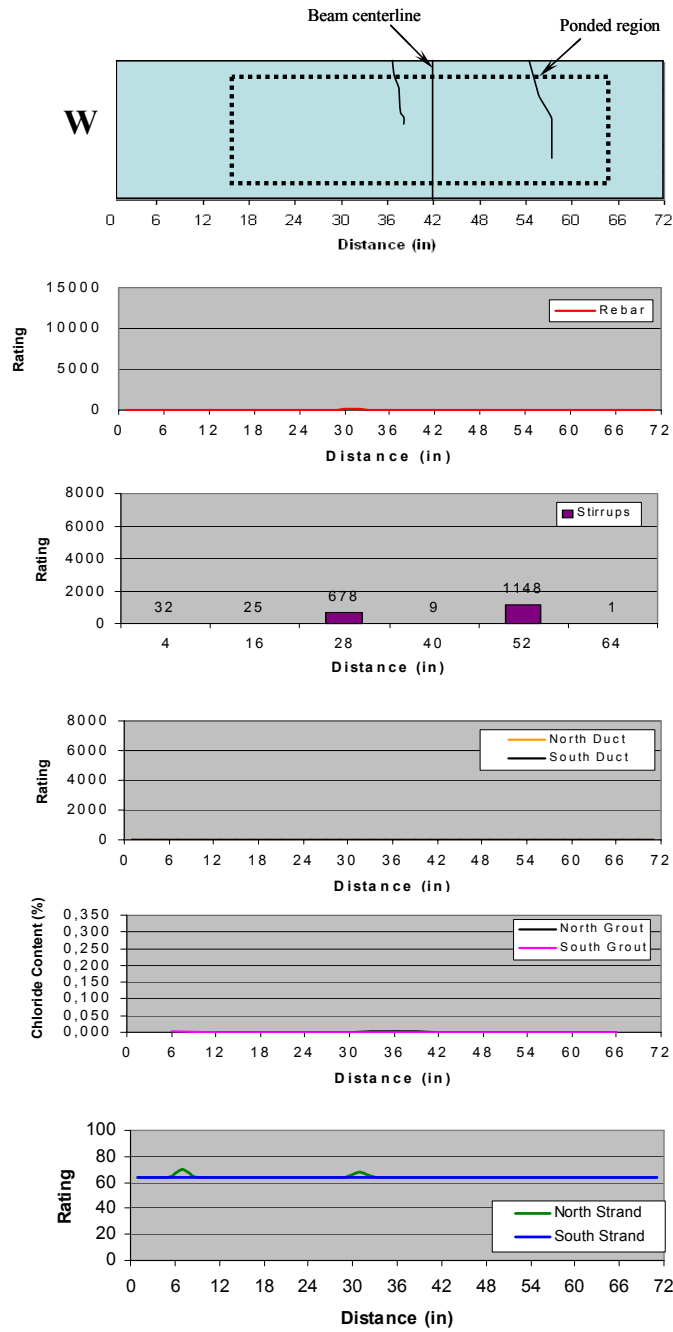*Figure 4.99 Specimen 4.2 – Crack Pattern and Specimen Corrosion Rating Graphs*

344

4.5.4 Forensic Examination Results for Phase II Beams

4.5.4.1 Beam Specimen 1.5 – Non-PS, Fly Ash Concrete

At the end of exposure, Specimen 1.5 had a large number of cracks on the top face and both sides. (See Figure 4.100) A majority of the cracks were confined to the constant maximum moment region. There was a large amount of rust staining, corresponding to the cracks, on both

Corrosion Rating:

Specimen	Generalized Rating	Localized Rating
Stirrups	224	296
Long. mild steel	6	8
North Duct	NA	NA
South Duct	NA	NA
North Strands	NA	NA
South Strands	NA	NA

sides of the specimen. Rust stains did not surround the cracks located outside the ponded region. Specimen 1.5 had a maximum crack width of 0.02 inches located 14 inches to the west and 11 inches to the east of the centerline.

Lateral (North) View   *Top View (from South Side)*

Figure 4.100 Specimen 1.5 – Condition Prior to Autopsy

345

Longitudinal Bar   *Stirrup*

Figure 4.101 Specimen 1.5 – Mild Steel Bar and Stirrup

A full autopsy of Specimen 1.5 was performed, providing a total length of 72 inches of the longitudinal bars and six stirrups to be analyzed. Forty-two inches of the analysis length extended to the west of the centerline of the beam and the remaining 30 inches extended to the east.

After removing all mild steel bars in the autopsy region, very mild corrosion was found on the eight longitudinal bars, with only a few locations showing moderate to severe corrosion. Five of the eight bars showed localized corrosion (See Figure 4.101) 14 inches to the west of the beam centerline. This location coincides with one of the maximum crack width locations.

The actual location of the centerline stirrup was offset one inch to the east of the centerline of the beam. After a detailed visual inspection, pitting and severe corrosion was found on the top portion of four out of the six stirrups. The two remaining stirrups also showed moderate to severe corrosion. All of the severely corroded stirrups were located inside the ponded region, with the exception of one, which was only one inch outside the ponded region. Figure 4.101 shows the longitudinal bar and stirrup corrosion rating graphs across the analysis length.
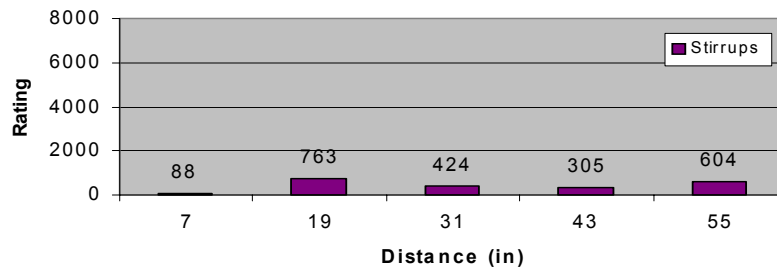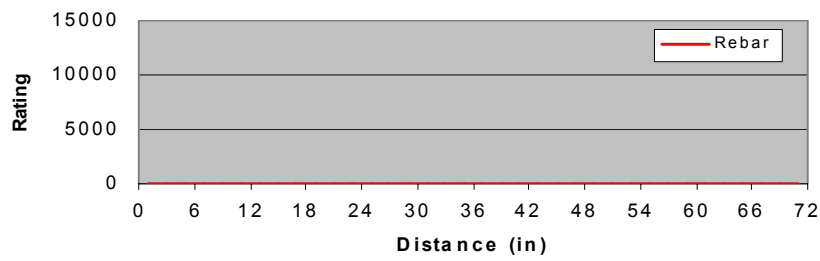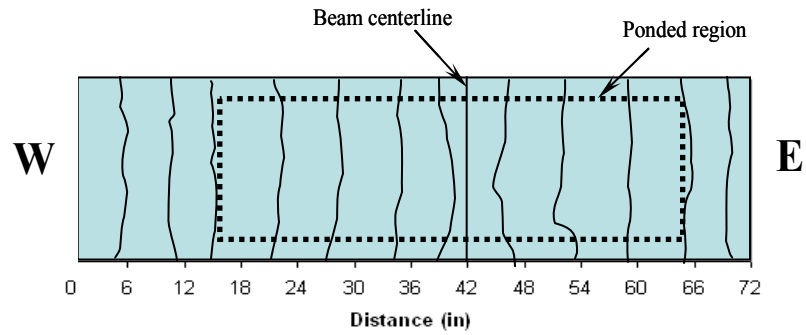
Figure 4.102 Specimen 1.5 – Crack Pattern and
Specimen Corrosion Rating Graphs

4.5.4.2 Beam Specimen 1.6 – Non-PS, High Performance Concrete

Specimen 1.6 had a large number of cracks on the top face and both sides at the end of exposure. (See Figure 4.103) A majority of the cracks were confined to the constant maximum moment region. There was minimal rust staining around a few of the cracks. Figure 4.103 shows moisture surrounding the cracks, indicating that the chlorides are traveling through the cracks. Specimen 1.6 had a maximum crack width of 0.016 inches on the crack located 13 inches to the west of the centerline.

Corrosion Rating:

Specimen	Generalized Rating	Localized Rating
Stirrups	92	361
Long. mild steel	7	15
North Duct	NA	NA
South Duct	NA	NA
North Strands	NA	NA
South Strands	NA	NA

Lateral (North) view   *Top view (from North side)*

Figure 4.103 Specimen 1.6 – Condition Prior to Autopsy
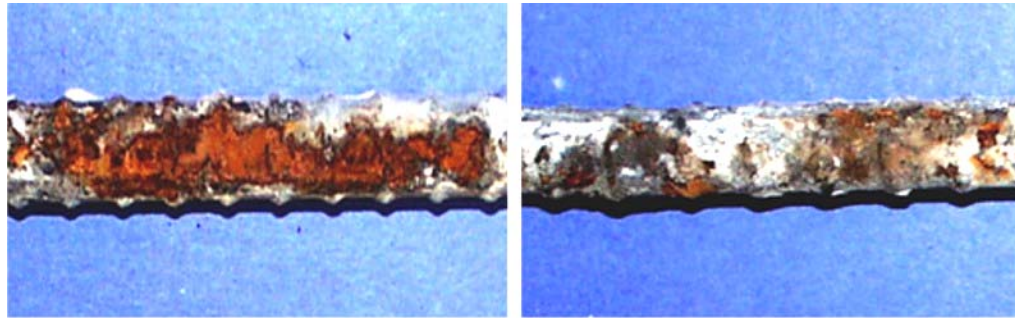
Longitudinal Bar   **Stirrup**

Figure 4.104 Specimen 1.6 – Mild Steel Bar and Stirrup

A full autopsy of Specimen 1.6 was performed, providing a total length of 72 inches of the longitudinal bars, ducts, grout and strands and six stirrups to be analyzed. Forty-two inches of the analysis length extended to the west of the centerline of the beam and the remaining 30 inches extended to the east.

After removing all mild steel bars in the autopsy region, spots of moderate to severe corrosion were found on all eight longitudinal bars. (See Figure 4.104) The most severe corrosion was found on all the bars in the same location as the maximum crack width. Other spots of corrosion on the bars were consistently located in the same areas, all of which coincided with crack locations.

The actual location of the centerline stirrup was offset one inch to the west of the centerline of the beam. After a detailed visual inspection, severe pitting and section loss were found on the top portion of the stirrup located 23 inches to the east of the centerline. Cracks were located two inches to each side of the stirrup. Pitting was also found on the stirrup located 25 inches to the west of the centerline, which was one inch from a crack. These two stirrups were included in the ponded region. The remaining stirrup showed light corrosion. Figure 4.105 shows a plot of the longitudinal bar and stirrup corrosion ratings across the analysis length.
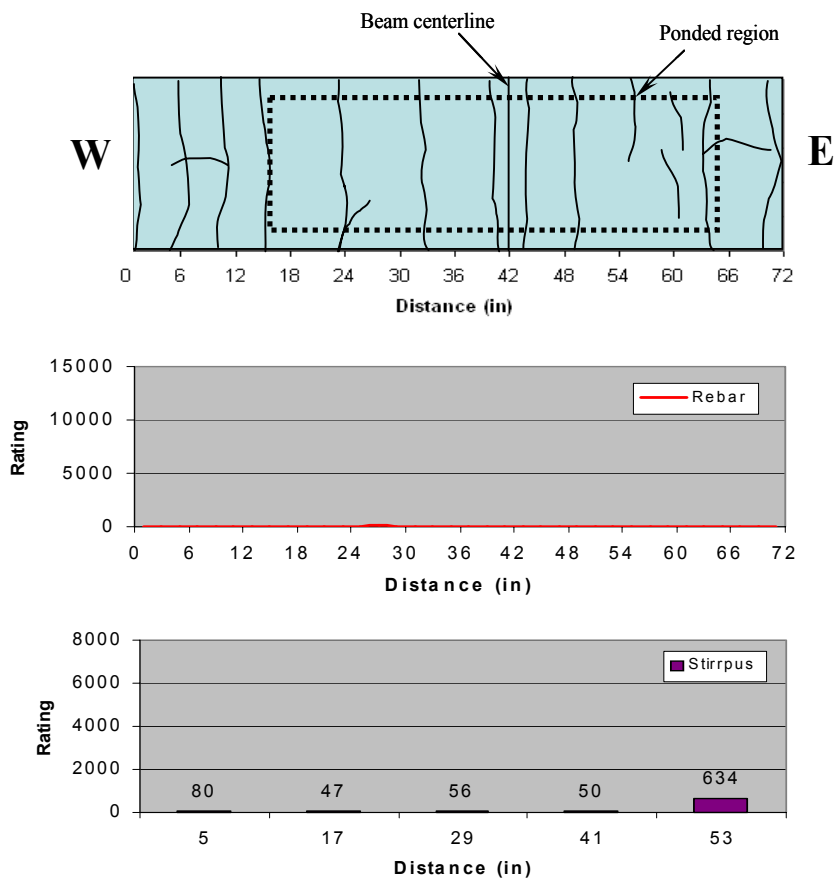
Figure 4.105 Specimen 1.6 – Crack Pattern and Specimen Corrosion Rating Graphs

350

4.5.4.3 Beam Specimen 2.5 – 2/3 PS, Fly Ash Concrete

As seen in Figure 4.106, Specimen 2.5 had five major transverse cracks at the end of exposure. Each of these cracks coincided with the stirrup locations. (See graphs in Figure 4.109) The maximum crack widths were 0.016 and 0.013 inches, located 13 inches to the east and 12 inches to the west of the beam centerline, respectively. Rust staining on the concrete was minimal for this specimen.

Corrosion Rating:

Specimen	Generalized Rating	Localized Rating
Stirrups	356	866
Long. mild steel	4	20
North Duct	21	8
South Duct	309	1776
North Strands	168	32
South Strands	168	28

A full autopsy of Specimen 2.5 was performed, providing a total length of 72 inches of the longitudinal bars, duct, grout and strands, and six stirrups for analysis. (See Figure 4.108) Forty-two inches of the analysis length extended to the west of the centerline of the beam and the remaining 30 inches extended to the east.
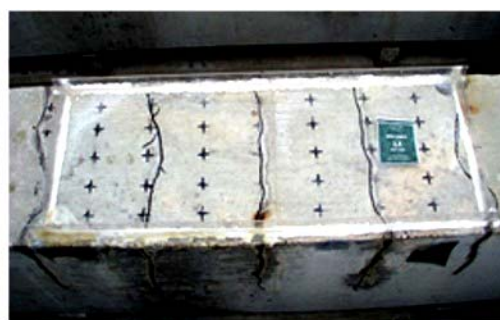
Lateral (North) view   *Top view (from South side)*

Figure 4.106 Specimen 2.5 – Condition Prior to Autopsy

Any corrosion found on the mild steel bars was moderate to severe and very localized. No bars had any section loss. Seven of the eight bars had localized corrosion that corresponded to the maximum crack width. Four of the eight bars

experienced moderate corrosion that corresponded to the second maximum crack width of 0.013 inches. No corrosion was found anywhere on any of the bars, except in these two previously described locations.

After a thorough visual inspection, severe uniform corrosion, pitting and section loss were found covering the stirrups located under the largest crack and at the centerline of the beam. The stirrup coinciding with the second largest crack was completely covered with uniform corrosion and pitting. The stirrup 20 inches to the east of the centerline did not show signs of uniform corrosion, but did have one large area of severe corrosion and section loss. This stirrup was also located beneath a crack. The remaining two stirrups showed few signs of corrosion.

Extremely severe corrosion and area loss, corresponding to the second maximum crack location, were found on the south duct. (See Figure 4.108 and graphs in Figure 4.109) Both ducts showed signs of light corrosion at the centerline.

The grout in both ducts showed large voids in the top due to bleed water. The void did not affect the north duct; however it appears to have contributed to the consumption of the south duct. A large accumulation of corrosion products from the south duct was found attached to the grout. (See Figure 4.108) The corrosion rating of the south duct and the chloride content of the south duct are significantly higher at the second maximum crack location. The acid soluble chloride content in the grout reached a maximum value of 0.0036% by weight of grout inside the south duct, and 0.0013% by weight of grout inside the north duct. These values are much lower than the critical chloride threshold value of 0.033% by weight of grout. Chloride samples were taken at 6-inch intervals within the forensic analysis length and chloride content plots were obtained, as shown in Figure 4.109.

Light uniform corrosion was found on all of the strands located in the north and south ducts.

Specimen 2.5 had two duct splices. The south duct had an industry standard splice, and the north duct had a heat-shrink splice. Both splices were located at the centerline of the beam. Figure 4.107 shows the condition of the duct splices at the end of exposure. Severe corrosion and minor section loss were found on the center half of the top of the oversized piece of the industry standard splice. The heat-shrink splice on the north duct showed signs of rust staining on one side. This is due to the lack of sufficient adhesion between the steel duct and splice, allowing moisture to be trapped under the splice.

Figure 4.107 Specimen 2.5 – Duct Splices
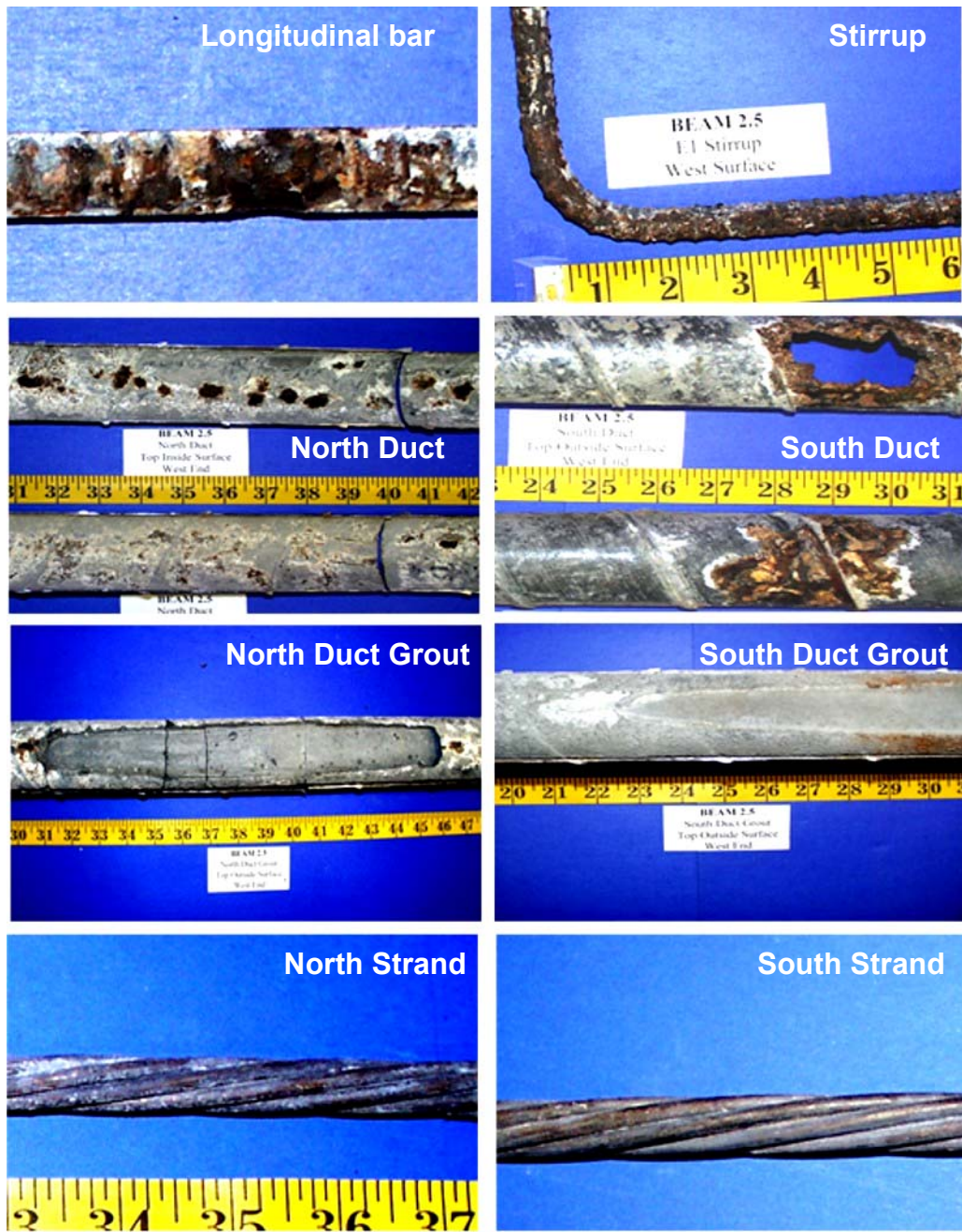
Figure 4.108 Specimen 2.5 – Reinforcing Elements

354
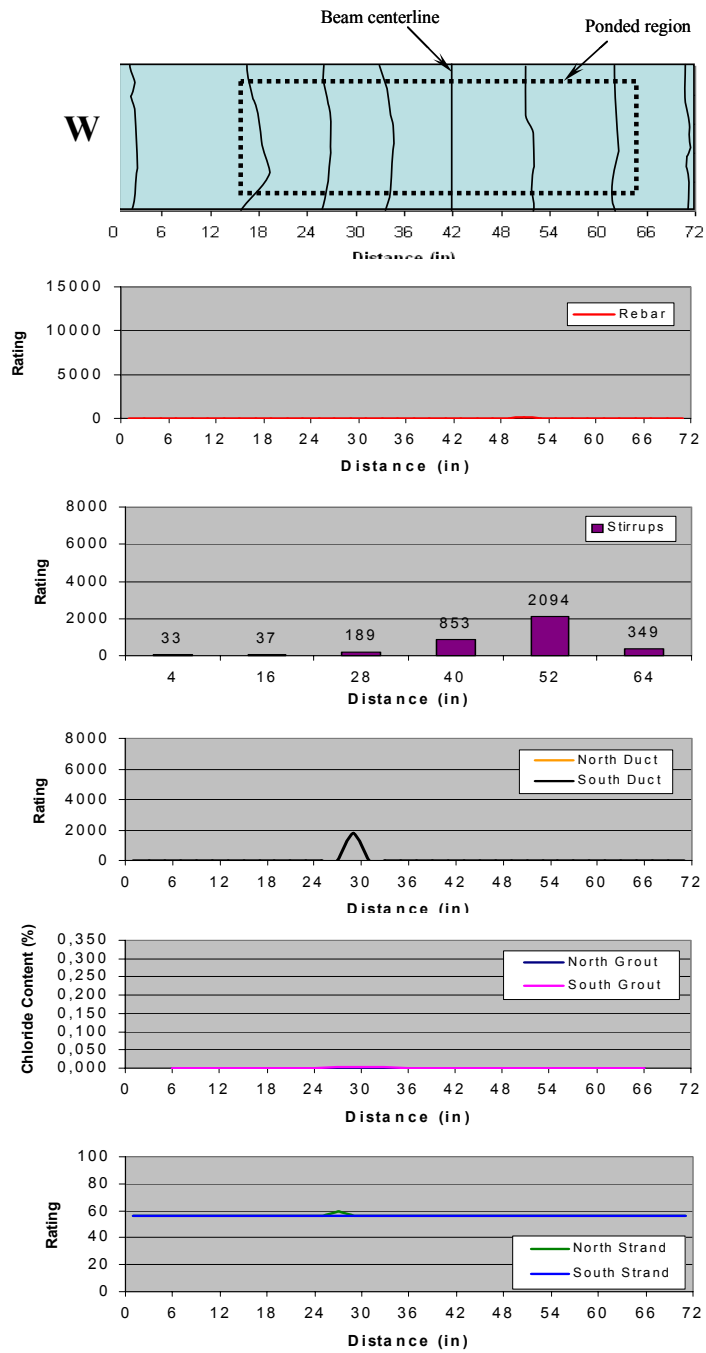
Figure 4.109 Specimen 2.5 Crack Pattern and Specimen Corrosion Rating Graphs

355

4.5.4.4 Beam Specimen 2.6 – 2/3 PS, High Performance Concrete

Figure 4.110 shows Specimen 2.6 as having five major cracks at the end of exposure. Each of these cracks coincided with the stirrup locations. (See graphs in Figure 4.113) The maximum crack width was 0.016 inches, located 26 inches to the east and 23 inches to the west of the beam centerline. As seen in Figure 4.110, rust staining on the concrete was present around a few of the cracks.

Corrosion Rating:

Specimen	Generalized Rating	Localized Rating
Stirrups	41	88
Long. mild steel	7	190
North Duct	2	4
South Duct	10	34
North Strands	95	16
South Strands	96	16

A full autopsy of Specimen 2.6 was performed, providing a total length of 72 inches of the longitudinal bars, duct, grout and strands, and six stirrups for analysis. Forty-two inches of the analysis length extended to the west of the centerline of the beam and the remaining 30 inches extended to the east. (See Figure 4.112)

Lateral (North) view   *Top view (from South side)*

Figure 4.110 Specimen 2.6 – Condition Prior to Autopsy

The only corrosion found on the mild steel bars was confined to one bar. It was severe corrosion with significant section loss. This area was located 22 inches to the west of the centerline. It was found to be due to its contact with cross bars that were present for construction purposes only.

The only significant corrosion found on the stirrups was present on those located 14 and two inches to the west of the centerline. These two stirrups had minor section loss in very localized areas. The remaining stirrups showed little signs of corrosion.

Few signs of corrosion were found on both ducts in Specimen 2.6. One area of localized corrosion was found 11 inches to the east of the centerline, as shown in Figure 4.112. The only corrosion found on the south duct was at the centerline, located under the industry standard splice. This area showed severe corrosion with minor area loss.

The grout in both ducts showed large voids in the top due to bleed water. The void in the north duct extended from about 22 to 32 inches west of the centerline, as shown in Figure 4.112. This void did not appear to affect the corrosion protection of the duct. The void in the south duct grout extended from 20 inches west of the centerline to 22 inches to the east, also pictured in Figure 4.112. It is likely that this void contributed to the corrosion of the south duct at the centerline, as it trapped the bleed water under the duct. The acid soluble chloride content in the grout reached a maximum value of 0.0016% by weight of grout inside the north duct, and 0.005% inside the south duct. These values are much lower than the critical chloride threshold value of 0.033% by weight of grout. Chloride samples were taken at 6-inch intervals within the forensic analysis length and chloride content plots were obtained, as shown in Figure 4.113.

Light uniform corrosion was found on all the strands located in the north and south ducts.

Specimen 2.6 had two duct splices. The south duct had an industry standard splice, and the north duct had a heat-shrink splice. Both splices were located at the centerline of the beam. Figure 4.111 shows the condition of the duct splices at the end of exposure testing. Severe corrosion and minor section loss was found on the center two inches of the top of the oversized piece of the industry standard splice. The heat-shrink splice, pictured with the north duct, showed minor signs of rust staining on the inside only.

Figure 4.111 Specimen 2.6 – Duct Splices

Figure 4.112 Specimen 2.6 – Reinforcing Elements
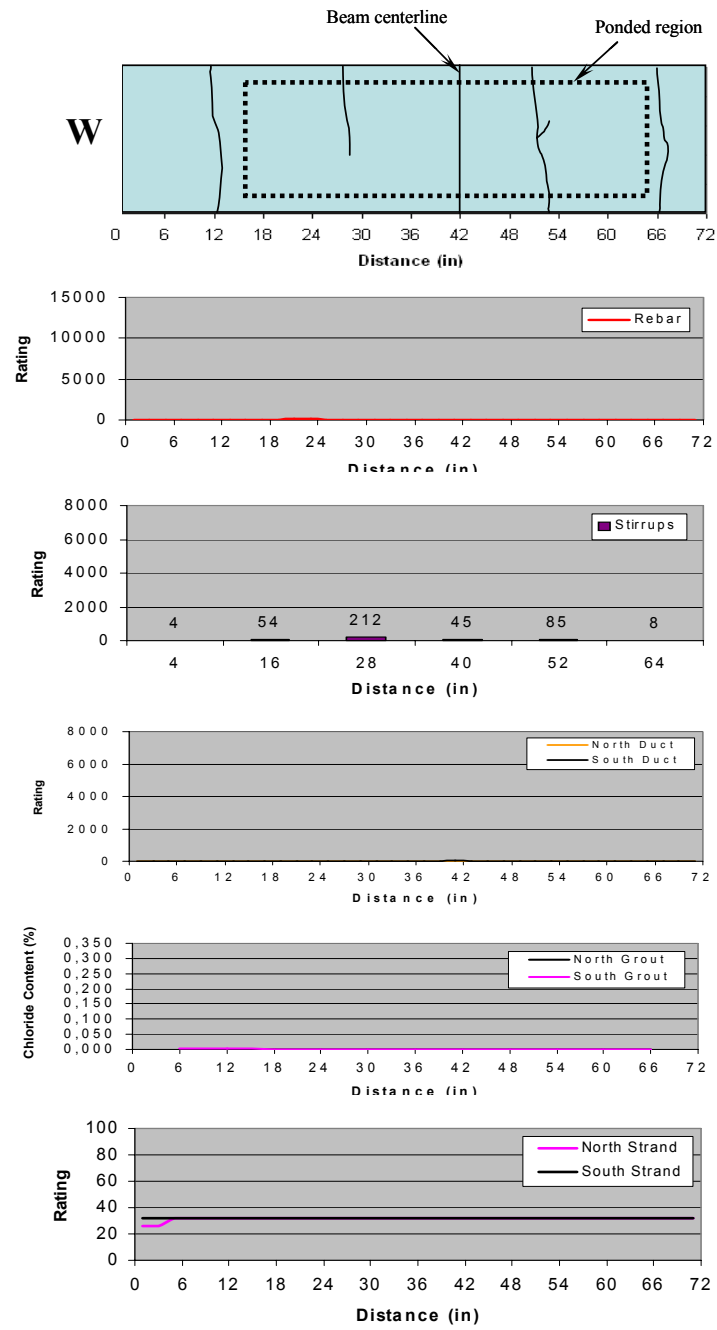
Figure 4.113 Specimen 2.6 – Crack Pattern and Specimen Corrosion Rating Graphs

360

4.5.4.5 Beam Specimen 3.6 – 100%U PS, Fly Ash Concrete

Specimen 3.6 had only two major transverse cracks across the top of the beam, as shown in Figure 4.114 The location of both of these cracks coincided with a stirrup. (See Figure 4.117) The maximum crack width was 0.016 inches, located 13 inches to the east. The second crack, located 11 inches to the west of the centerline, had a maximum width of 0.013 inches. As shown in Figure 4.114, rust staining around the cracks was minimal. A majority of the rust spots were again from the bolster strips.

Corrosion Rating:

Specimen	Generalized Rating	Localized Rating
Stirrups	78	245
Long. mild steel	4	4
North Duct	24	44
South Duct	6	8
North Strands	91	16
South Strands	96	16

A full autopsy of Specimen 3.6 was performed, providing a total length of 72 inches of the longitudinal bars, duct, grout and strands, and six stirrups for analysis. (See Figure 4.116) Forty-two inches of the analysis length extended to the west of the centerline of the beam and the remaining 30 inches extended to the east.
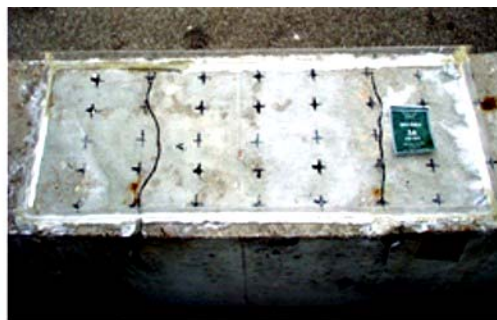
Lateral (North) view   *Top view (from South side)*

Figure 4.114 Specimen 3.6 – Condition Prior to Autopsy

The only corrosion found on the two mild steel bars was light to moderate, and coincided with the two cracks.

Uniform light to moderate corrosion was found on all the stirrups, except the two located directly under the cracks. These stirrups were severely corroded in many areas, with some section loss.

Corrosion in the north duct was found at the centerline and directly under the larger crack. The centerline corrosion was a result of the industry standard splice on the outside and the large void in the grout on the inside. There was minor area loss at the location, which was due to the alignment with the larger crack and the void in the grout. The only corrosion found on the south duct was moderate to severe corrosion with no area loss, located under the larger crack. (See Figure 4.116)

The grout in the north duct showed a large void in the top due to bleed water. The void extended from the centerline across the entire east side. The effect of the void in the corrosion of the duct is apparent in Figure 4.116. The corrosion on the north duct and the corrosion products on the north grout are confined to the area above the void. A few small voids were present on the south duct grout, with the most significant one located 13 inches to the east of the centerline. This location is again directly under the larger crack. The acid soluble chloride content in the north duct grout reached a maximum value of 0.0022% by weight of grout at the location under the larger crack. The grout in the south duct reached 0.0021%. These values are much lower than the critical chloride threshold value of 0.033% by weight of grout. Chloride samples were taken at 6-inch intervals within the forensic analysis length and chloride content plots were obtained, as shown in Figure 4.117.

Light uniform corrosion was found on all the strands located in the north and south ducts.

Specimen 3.6 had two duct splices. The north duct had an industry standard splice, and the south duct had a heat-shrink splice. Both splices were located at the centerline of the beam. Figure 4.115 shows the condition of the duct splices at the end of exposure. Minor corrosion and salt staining was found on the center of the oversized piece of the industry standard splice. The heat-shrink splice showed no signs of rust staining or corrosion.

Figure 4.115 Specimen 3.6 – Duct Splices
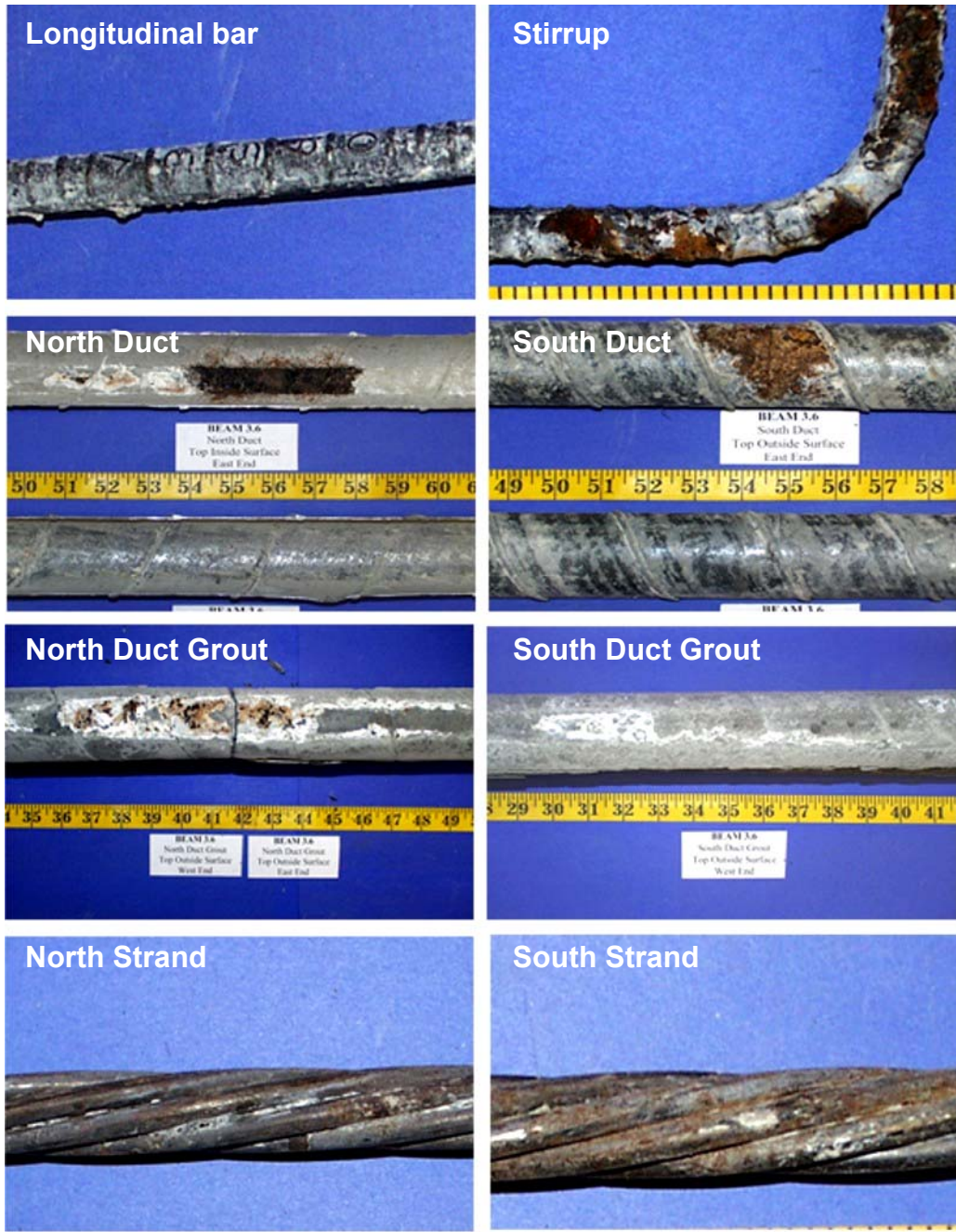
Figure 4.116 Specimen 3.6 – Reinforcing Elements
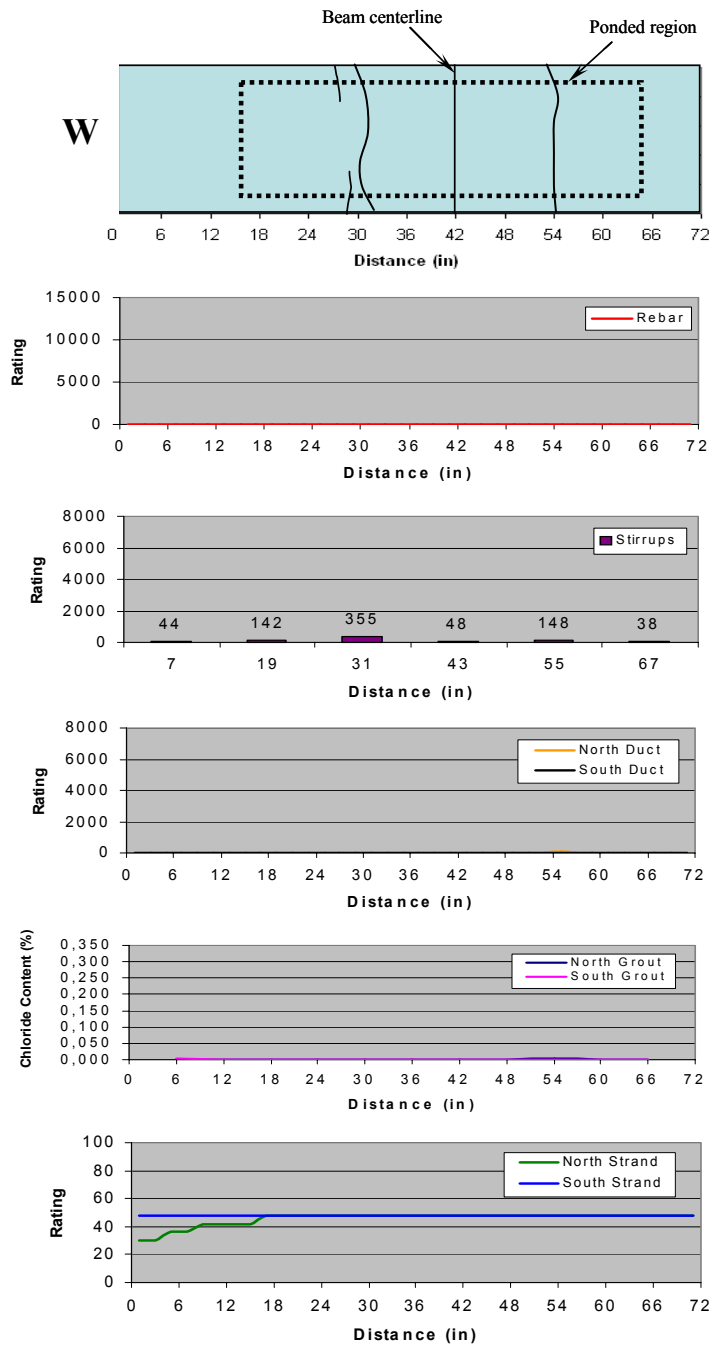
Figure 4.117 Specimen 3.6 – Crack Pattern and Specimen Corrosion Rating Graphs

365

4.5.4.6 Beam Specimen 3.7 – 100%U PS, High Performance Concrete

Specimen 3.7 had four major transverse cracks across the top of the beam, two of which were located outside the ponded region (See Figure 4.118) The maximum crack width was 0.04 inches, located outside the ponded region at 26 inches to the west of the centerline. The second largest crack,

Corrosion Rating:

Specimen	Generalized Rating	Localized Rating
Stirrups	27	16
Long. mild steel	0	2
North Duct	214	1164
South Duct	12	20
North Strands	168	28
South Strands	168	28

located 13 inches to the east of the centerline, had a maximum width of 0.016 inches. As seen in Figure 4.118, rust staining around the cracks was present on the sides of the beam.

A full autopsy of Specimen 3.7 was performed, providing a total length of 72 inches of the longitudinal bars, duct, grout and strands, and six stirrups for analysis. (See Figure 4.120) Forty-two inches of the analysis length extended to the west of the centerline of the beam and the remaining 30 inches extended to the east.
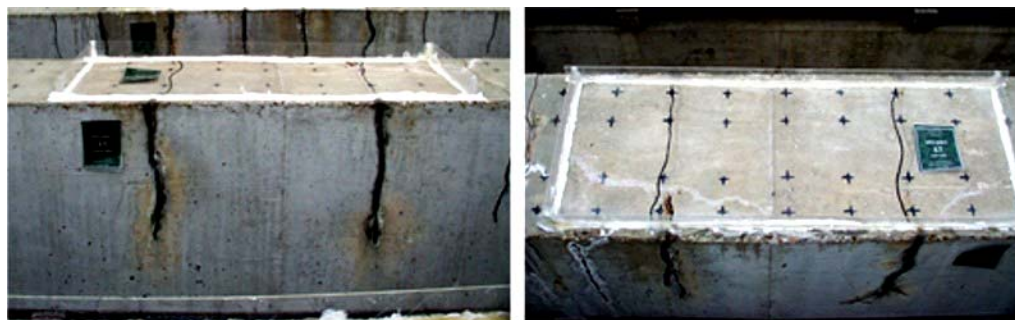
Lateral (North) view   *Top view (from South side)*

Figure 4.118 Specimen 3.7 – Condition Prior to Autopsy

No corrosion was found on the two mild steel bars in Specimen 3.7.

Moderate to severe uniform corrosion was found on the stirrups 10 inches to the west and 14 inches to the east. Both of these stirrups were located directly under cracks. The remaining stirrups showed light uniform corrosion.

A significant amount of area loss was found on the north duct, as shown in Figure 4.120. This location was very close to a 0.013-inch crack. There was severe corrosion and minor area loss at this same location on the south duct. (See Figure 4.120) These were the only significant areas of corrosion found on the ducts in Specimen 3.7.

The grout in the north duct showed a large void in the top due to bleed water. The void extended from 30 inches west of the centerline to six inches west. Corrosion products from the north duct at the location of area loss were found on the grout. (See Figure 4.120) A few small voids were present on the south duct grout, with the most significant one located under the location of minor area loss in the south duct. The acid soluble chloride content in the north duct grout reached a maximum value of 0.004% by weight of grout. A value of 0.0199% in the south duct was found in the region of the duct area loss. These values are much lower than the critical chloride threshold value of 0.033% by weight of grout. Chloride samples were taken at 6-inch intervals within the forensic analysis length and chloride content plots were obtained, as shown in Figure 4.121.

Light uniform corrosion was found on all the strands located in the north and south ducts.

Specimen 3.7 had two duct splices. The north duct had an industry standard splice, and the south duct had a heat-shrink splice. Both splices were located at the centerline of the beam. Figure 4.119 shows the condition of the duct splices at the end of exposure. The only corrosion found on the industry standard splice was located under the duct tape. The heat-shrink splice showed no signs of rust staining or corrosion.

Figure 4.119 Specimen 3.7 – Duct Splices
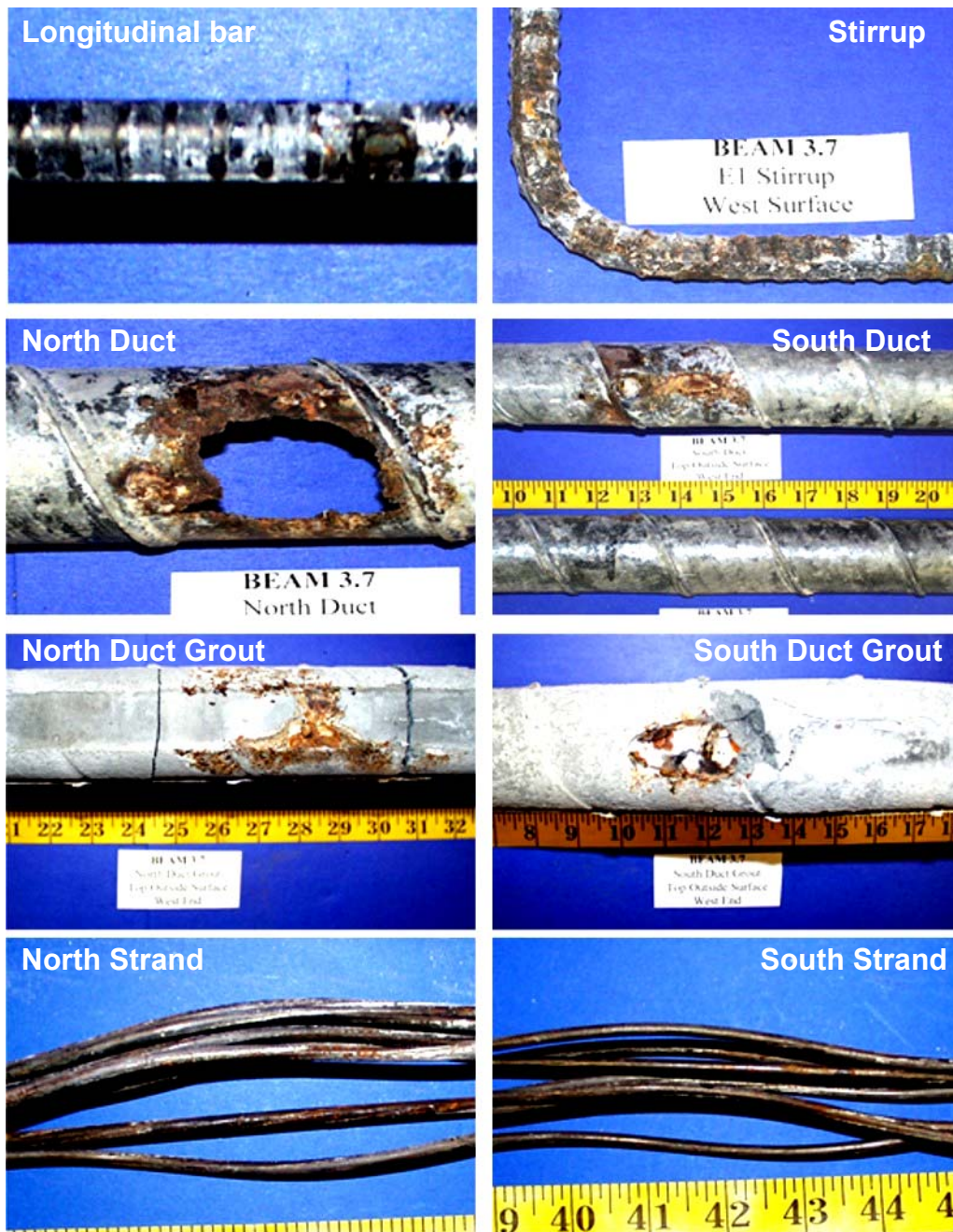
Figure 4.120 Specimen 3.7 – Reinforcing Elements
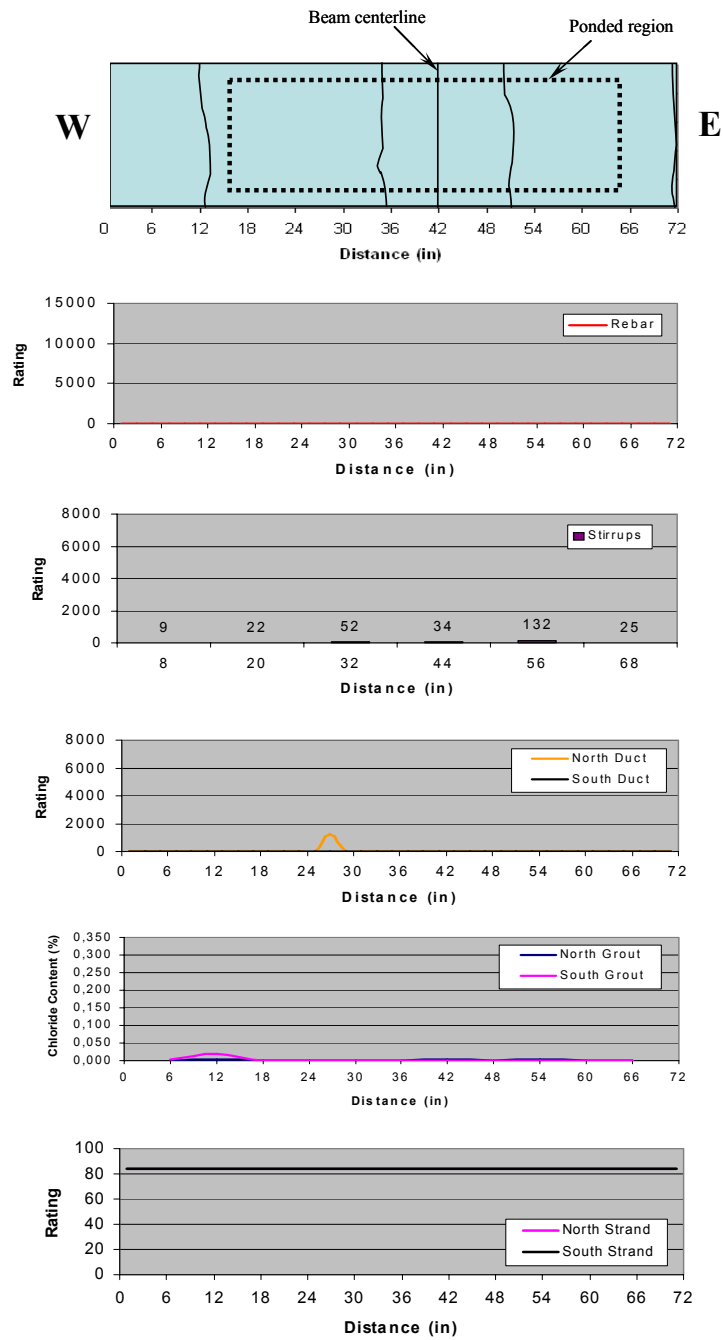
***Figure 4.121 Specimen 3.7 – Crack Pattern and
Specimen Corrosion Rating Graphs***

370

4.5.5   Corrosion Rating Summary

The extent of corrosion is analyzed by obtaining the "generalized" corrosion rating for stirrups, mild steel reinforcement, ducts and strands for all autopsy specimens. Generalized corrosion ratings are calculated by dividing the total corrosion rating by the total length of each element. The result is a rating per unit foot of each element.   For longitudinal reinforcing bars, since the number varied among specimens, the total rebar rating for each beam was divided by the total length of rebar being evaluated.   The same procedure was followed for strands, where the number of strands per duct in each type of prestressed specimen also varied.   In this case, the total strand rating for each duct was divided by the total length of prestressing strand being evaluated. The total length used for stirrups was 10.5 ft, for rebar 48 ft (for Non-PS and 2/3 PS beams) and 12 ft (for 100% PS beams), for ducts 6 ft, and for strands 12 ft (for 2/3 PS beams), 18 ft (for 100%U PS beams) and 24 ft (for 100%S PS beams).

The severity of corrosion is analyzed by obtaining the "localized" corrosion rating for all elements. Localized corrosion is of great interest in this research program since this is the type of corrosion that will ultimately result in failure of the structural element, or structure. Localized corrosion rating was taken as the maximum rating recorded for any 2-inch interval for each element.

4.5.5.1   Stirrup Corrosion Ratings

Figure 4.122 shows the generalized stirrup corrosion ratings for Phase I and Phase II beams.   The analysis of this figure shows that:

- Specimen performance increases as the level of prestress increases from 2/3 PS to 100% PS
- Performance of 2/3 prestress beams appears to be much more similar to that of the Non-PS beams, as opposed to that of the 100% PS beams

371

- Corrosion index increases as the loading, and thus transverse cracking increases
- High performance concrete specimens, as defined in Section 2.4.4.1, perform better than Class C Concrete specimens with Fly Ash
- Mixed reinforcing beams (2/3 PS) show the worst stirrup performance, even when comparing with non prestressed beams.
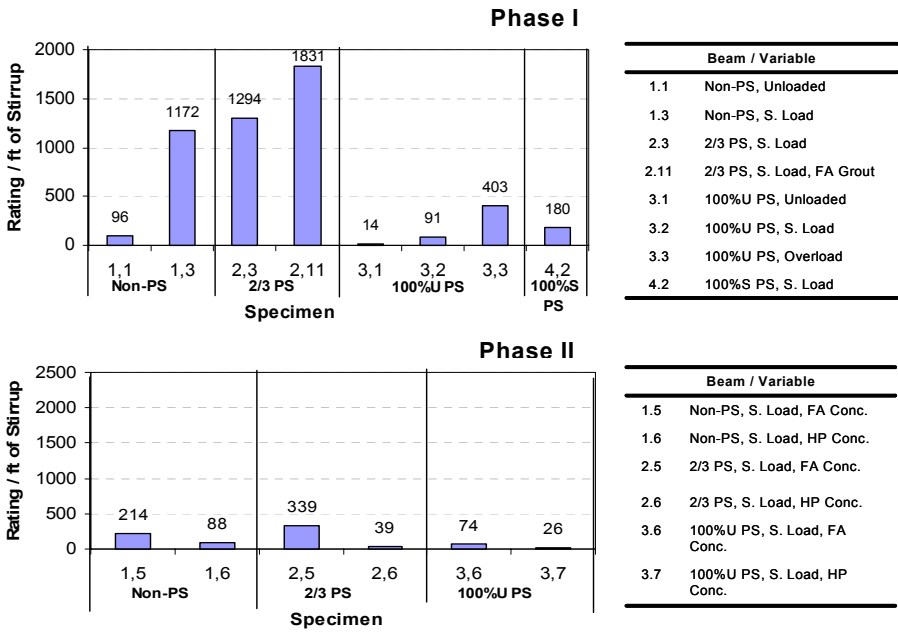
Figure 4.122 Generalized Stirrup Corrosion Ratings

Figure 4.123 shows the localized stirrup corrosion ratings for all autopsy beams.   Similar trends as found from the generalized corrosion ratings.   The increase in corrosion rating as the crack width increases is more apparent as the localized ratings significantly increase from Specimen 1.3 to Specimens 2.3 and 2.11.   Also, the corrosion rating increase from Specimen 3.1 (uncracked - unloaded) to Specimens 3.2 (service load) and 3.3 (overloaded) is significant.

Phase I

	Beam / Variable
1.1	Non-PS, Unloaded
1.3	Non-PS, S. Load
2.3	2/3 PS, S. Load
2.11	2/3 PS, S. Load, FA Grout
3.1	100%U PS, Unloaded
3.2	100%U PS, S. Load
3.3	100%U PS, Overload
4.2	100%S PS, S. Load

Phase II

	Beam / Variable
1.5	Non-PS, S. Load, FA Conc.
1.6	Non-PS, S. Load, HP Conc.
2.5	2/3 PS, S. Load, FA Conc.
2.6	2/3 PS, S. Load, HP Conc.
3.6	100%U PS, S. Load, FA Conc.
3.7	100%U PS, S. Load, HP Conc.
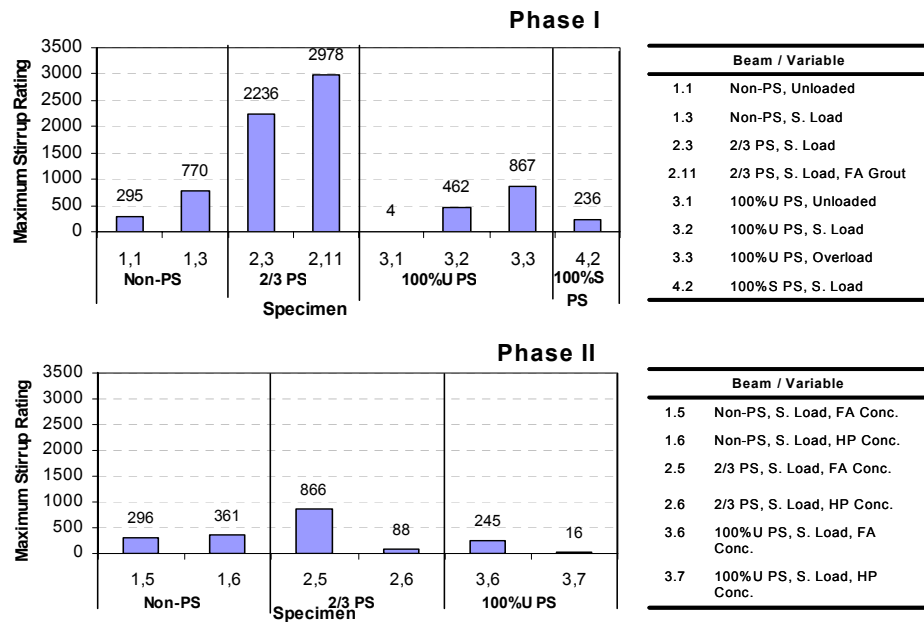
Figure 4.123 Localized Stirrup Corrosion Ratings

4.5.5.2   Rebar Corrosion Ratings

Figure 4.124 shows the generalized bar corrosion ratings for all autopsy beams. The plots show that:

- Mixed reinforced beams (2/3 PS) show extremely poor performance when compare with non prestressed and fully prestressed beams

- The negative effects of cracking clearly show when comparing non prestressed beams 1.1 (unloaded, uncracked) and 1.3 (Service load, cracked)

- All ratings for Phase II beams are very low, which is possible due to the use of fly ash concrete and high performance concrete. However, results cannot be compared against Phase I beams since there is a one year exposure testing difference.

Figure 4.125 shows the corresponding localized bar corrosion ratings. This figure shows the same trends as in Figue 4.124.

373

Phase I

	Beam / Variable
1.1	Non-PS, Unloaded
1.3	Non-PS, S. Load
2.3	2/3 PS, S. Load
2.11	2/3 PS, S. Load, FA Grout
3.1	100%U PS, Unloaded
3.2	100%U PS, S. Load
3.3	100%U PS, Overload
4.2	100%S PS, S. Load

Phase II

	Beam / Variable
1.5	Non-PS, S. Load, FA Conc.
1.6	Non-PS, S. Load, HP Conc.
2.5	2/3 PS, S. Load, FA Conc.
2.6	2/3 PS, S. Load, HP Conc.
3.6	100%U PS, S. Load, FA Conc.
3.7	100%U PS, S. Load, HP Conc.
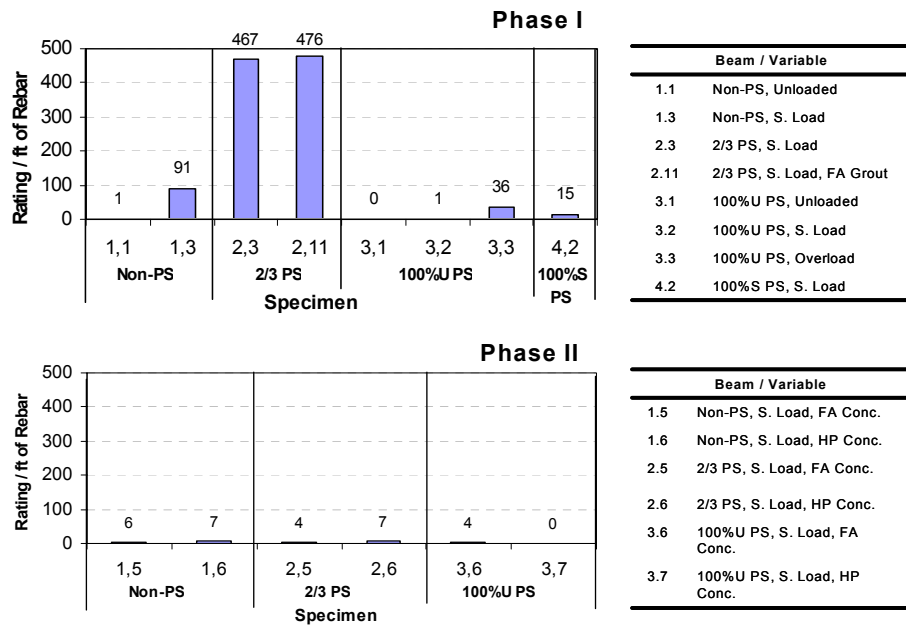
Figure 4.124 Generalized Bar Corrosion Rating

Phase I

	Beam / Variable
1.1	Non-PS, Unloaded
1.3	Non-PS, S. Load
2.3	2/3 PS, S. Load
2.11	2/3 PS, S. Load, FA Grout
3.1	100%U PS, Unloaded
3.2	100%U PS, S. Load
3.3	100%U PS, Overload
4.2	100%S PS, S. Load

Phase II

	Beam / Variable
1.5	Non-PS, S. Load, FA Conc.
1.6	Non-PS, S. Load, HP Conc.
2.5	2/3 PS, S. Load, FA Conc.
2.6	2/3 PS, S. Load, HP Conc.
3.6	100%U PS, S. Load, FA Conc.
3.7	100%U PS, S. Load, HP Conc.
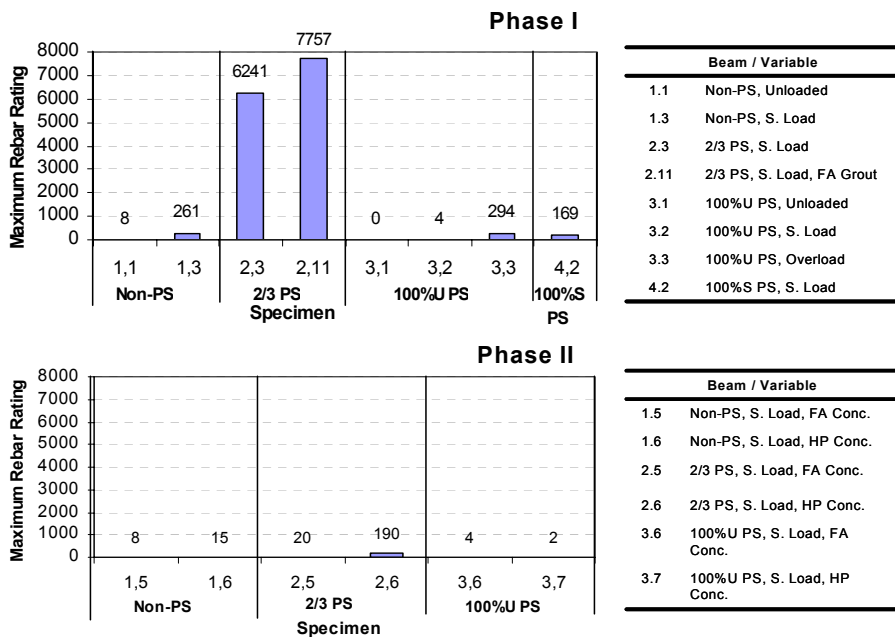
Figure 4.125 Localized Bar Corrosion Ratings

374

4.5.5.3 Galvanized Steel Duct Ratings

Figure 4.126 shows the generalized corrosion rating for all autopsy beams. The two ducts on each specimen are clearly indicated by D1 and D2. From this figure it can be concluded that:

- Phase I beams show a significantly worse performance of the 2/3 PS beams with respect to 100% PS beams

- The negative effect of cracking is observed when comparing Specimen 3.1 (uncracked, unloaded) and Specimen 3.3 (cracked, overloaded)

- Fly Ash added to the grout seems to provide better duct corrosion protection, when comparing Specimen 2.3 (2/3 PS, service load, normal grout) an Specimen 2.11 (2/3 PS, service load, fly ash grout)

- The large rating of Specimen 3.7 in the Phase II beams does not follow the trend of an increase in corrosion resistance with an increase of prestressing

- Phase II specimens do not show a distinct trend with respect to concrete types. Fly ash − class C concrete and high performance concrete appear to be performing well and in a similar manner.

Figure 4.127 shows the corresponding localized duct corrosion ratings for all autopsy specimens. The same trends are observed as in Figure 4.126.

Phase I

Rating / ft of Duct

Specimen	Rating
2.3 (D1)	4299
2.3 (D2)	5069
2.11 (D1)	1504
2.11 (D2)	1413
3.1 (D1)	0
3.1 (D2)	0
3.2 (D1)	1
3.2 (D2)	0
3.3 (D1)	429
3.3 (D2)	220
4.2 (D1)	7
4.2 (D2)	4

2/3 PS | 100%U PS | 100%S PS

Beam / Variable	
1.1	Non-PS, Unloaded
1.3	Non-PS, S. Load
2.3	2/3 PS, S. Load
2.11	2/3 PS, S. Load, FA Grout
3.1	100%U PS, Unloaded
3.2	100%U PS, S. Load
3.3	100%U PS, Overload
4.2	100%S PS, S. Load

Phase II

Rating / ft of Duct

Specimen	Rating
2.5 (D1)	21
2.5 (D2)	309
2.6 (D1)	2
2.6 (D2)	10
3.6 (D1)	24
3.6 (D2)	6
3.7 (D1)	214
3.7 (D2)	12

2/3 PS | 100%U PS

Beam / Variable	
1.5	Non-PS, S. Load, FA Conc.
1.6	Non-PS, S. Load, HP Conc.
2.5	2/3 PS, S. Load, FA Conc.
2.6	2/3 PS, S. Load, HP Conc.
3.6	100%U PS, S. Load, FA Conc.
3.7	100%U PS, S. Load, HP Conc.

Figure 4.126 Generalized Duct Corrosion Ratings

Phase I

Maximum Duct Rating

Specimen	Rating
2.3 (D1)	2107
2.3 (D2)	6248
2.11 (D1)	2440
2.11 (D2)	1673
3.1 (D1)	0
3.1 (D2)	0
3.2 (D1)	2
3.2 (D2)	2
3.3 (D1)	924
3.3 (D2)	685
4.2 (D1)	8
4.2 (D2)	4

2/3 PS | 100%U PS | 100%S PS

Beam / Variable	
1.1	Non-PS, Unloaded
1.3	Non-PS, S. Load
2.3	2/3 PS, S. Load
2.11	2/3 PS, S. Load, FA Grout
3.1	100%U PS, Unloaded
3.2	100%U PS, S. Load
3.3	100%U PS, Overload
4.2	100%S PS, S. Load

Phase II

Maximum Duct Rating

Specimen	Rating
2.5 (D1)	8
2.5 (D2)	1776
2.6 (D1)	4
2.6 (D2)	34
3.6 (D1)	44
3.6 (D2)	8
3.7 (D1)	1164
3.7 (D2)	20

2/3 PS | 100%U PS

Beam / Variable	
1.5	Non-PS, S. Load, FA Conc.
1.6	Non-PS, S. Load, HP Conc.
2.5	2/3 PS, S. Load, FA Conc.
2.6	2/3 PS, S. Load, HP Conc.
3.6	100%U PS, S. Load, FA Conc.
3.7	100%U PS, S. Load, HP Conc.

Figure 4.127 Localized Duct Corrosion Ratings

4.5.5.4 Prestressing Strand Ratings

Figure 4.128 shows the generalized strand corrosion ratings for all autopsy beams. Findings from this plot include:

- All strands appear to be performing similarly

- After visual inspection only minimal variation was found on the performance of the strands. Therefore, it appears that specimens require more exposure time to indicate differences and trends

- The difference between Specimen 2.3 (normal grout) and 2.11 (fly ash grout) indicates that the addition of fly ash to the grout does not have a large effect on the corrosion protection of the strand
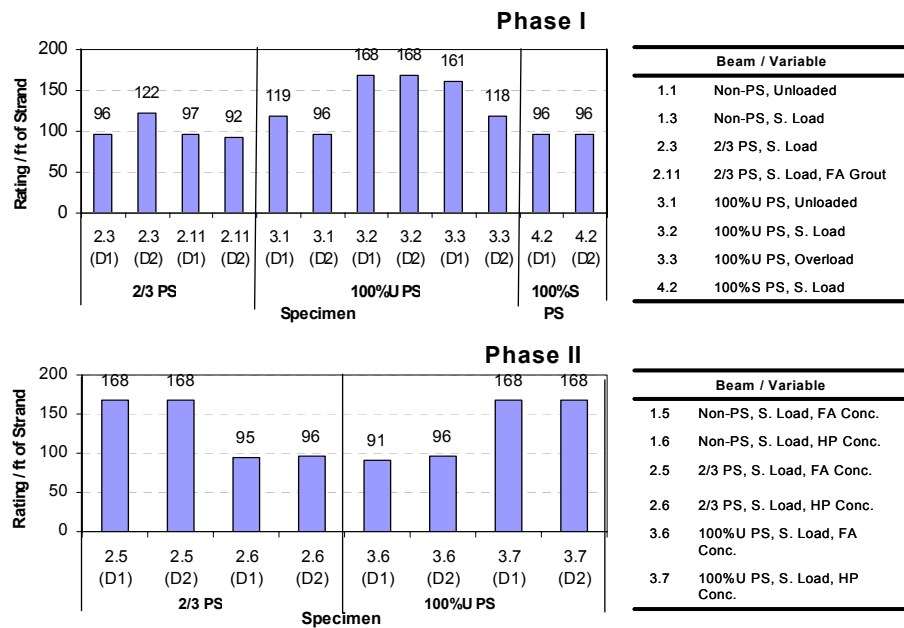
Figure 4.128 Generalized Strand Corrosion Ratings

Figure 4.129 shows the localized strand corrosion ratings.   Phase II beams show very similar results as those from Phase I.   However, Specimens 2.3 (D1) and 3.3 (D1) show larger ratings, corresponding with crack locations.
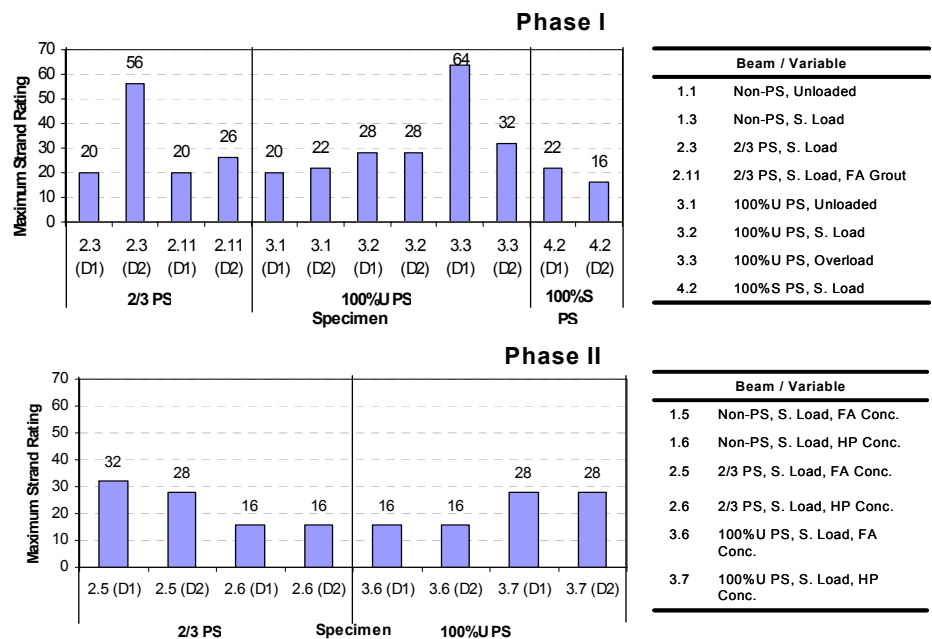
Figure 4.129 Localized Strand Corrosion Ratings

4.6   ANALYSIS AND DISCUSSION OF RESULTS

After four and a half years of exposure for phase I beams and three and a half years for phase II beams, the effect of many of the variables involved in this testing program can be analyzed and compared.

4.6.1   Overall Performance

The use of the large scale beam specimen was found to be a very good method for analyzing relative specimen performance and for evaluating the adequacy of corrosion protection variables, especially when considering different loading and prestressing levels.

378

After four and a half years in Phase I beams distinct differences are shown in stirrup, rebar and duct corrosion ratings among the autopsy specimens. Strand corrosion was found to be somewhat similar in all specimens, and therefore, it was clear the need for additional exposure testing for the remaining specimens. Similar results were obtained from Phase II beams.

The relative performance of the specimens in this testing program was studied by looking at the corrosion ratings for stirrups, rebar, ducts and strands, ordered from highest to lowest. Figure 4.130 and Figure 4.131 show the generalized stirrup corrosion ratings for phase I autopsy beams and phase II autopsy beams, respectively. Figure 4.132 and Figure 4.133 show the generalized rebar corrosion ratings for phase I and phase II, respectively. The corrosion rating system used for stirrups and rebar was the same, but the horizontal scale on the graphs is shown different to clearly indicate the relative performance of the specimens with respect to the element under analysis.
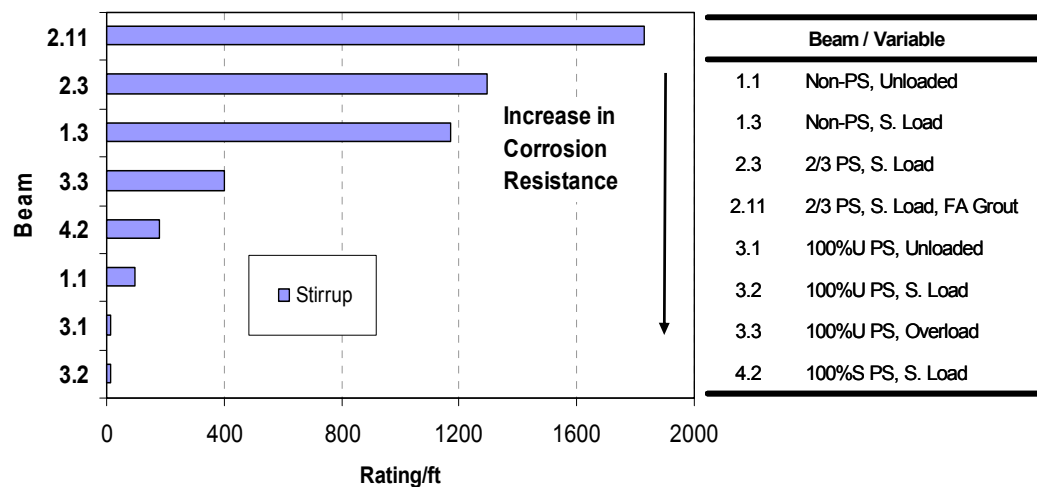
Figure 4.130 Generalized Stirrup Corrosion Ratings
for Phase I Autopsy Beams Ordered According to Performance

379
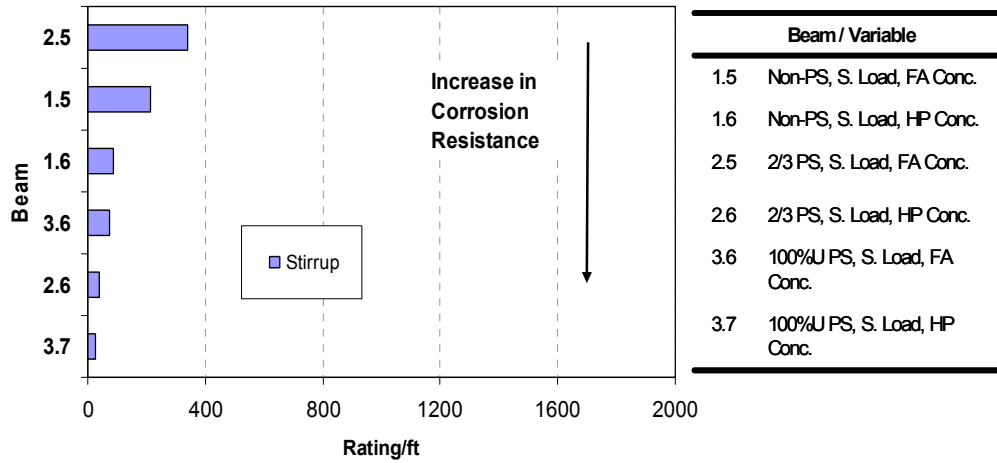
Figure 4.131 Generalized Stirrup Corrosion Ratings
for Phase II Autopsy Beams Ordered According to Performance
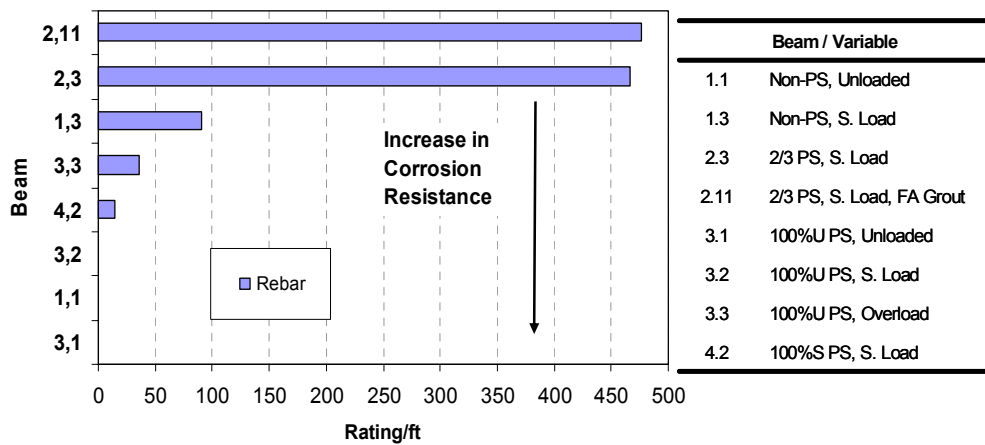
Figure 4.132 Generalized Rebar Corrosion Ratings
for Phase I Autopsy Beams Ordered According to Performance

380
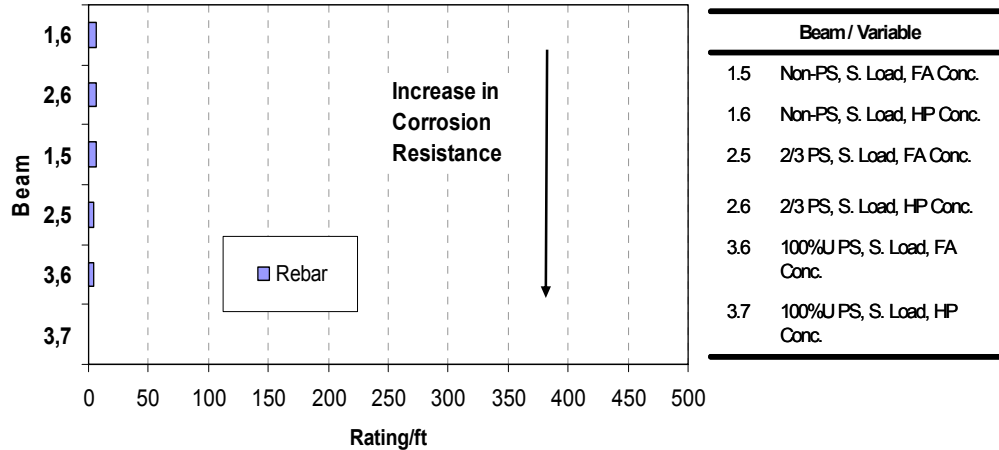
Figure 4.133 Generalized Rebar Corrosion Ratings
for Phase II Autopsy Beams Ordered According to Performance

As observed from these graphs, phase I specimens follow basically the same order according to performance for stirrup and rebar corrosion ratings. As shown, mixed reinforced (2/3 PS) beams show the worst corrosion resistance, followed by the loaded Non-PS beam, the 100% U PS and the 100%S PS beam. Unloaded specimens show the best overall performance. These results clearly indicate the negative effect of cracking on corrosion resistance. Except for the relative good performance of Specimen 1.3 (non prestressed, loaded), the graphs show a distinct trend with lower corrosion ratings for higher levels of prestress.

Relative performance of Phase II beams appears to show better corrosion protection in 100% PS beams with respect to mixed reinforced (2/3 PS) beams. There is not a clear distinction with respect to non-prestressed and prestressed members. Also, there is not a clear distinction among class C (with fly ash) concrete specimens and high performance concrete specimens.

The overall performance of the specimens is better compared by considering the total corrosion rating, obtained by summing the ratings for the rebar, duct and strand, as shown in Figure 4.134 and Figure 4.135.
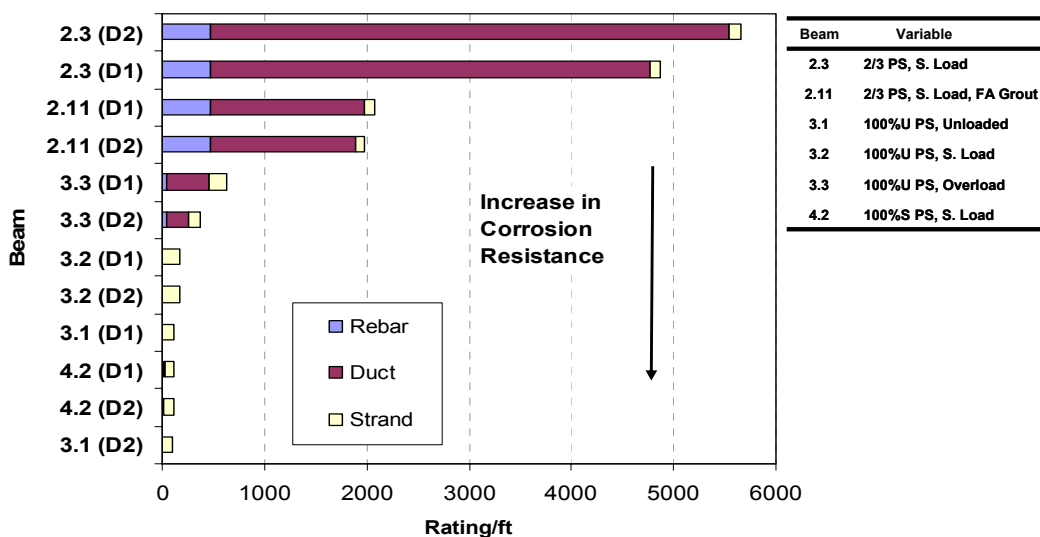
Figure 4.134 Generalized Corrosion Ratings for Phase I Autopsy Beams Ordered According to Performance

As observed from Figure 4.134, it shows a clear trend with respect to the level of prestress. As the level of prestress increases, the corrosion resistance increases. In this graphs, it is observed that the strand rating is very similar for all specimens, which suggest the need for a longer period of exposure testing, in order to obtain more conclusive results with respect to strand corrosion.

Figure 4.134 also shows that galvanized duct corrosion is a major problem, even when rebar and corrosion ratings cannot be compared because they are the result of different rating systems.

The uncracked and unloaded Specimen 3.1 shows the overall best performance as expected. This is a clear indication of the very negative effects of

cracking in the other specimens, and the positive effect of precompression force in the concrete.

Figure 4.135 does not show a clear trend with respect to concrete type and levels of prestress. By comparing Phase I and Phase II results, the need for longer periods of exposure testing appears evident and may reflect the relative better performance of specialty concretes (with fly ash) with respect to standard class C concrete specimens. Care must be exercised when making this conclusion, since phase II autopsy beams had around 23% less exposure time than phase I autopsy beams.
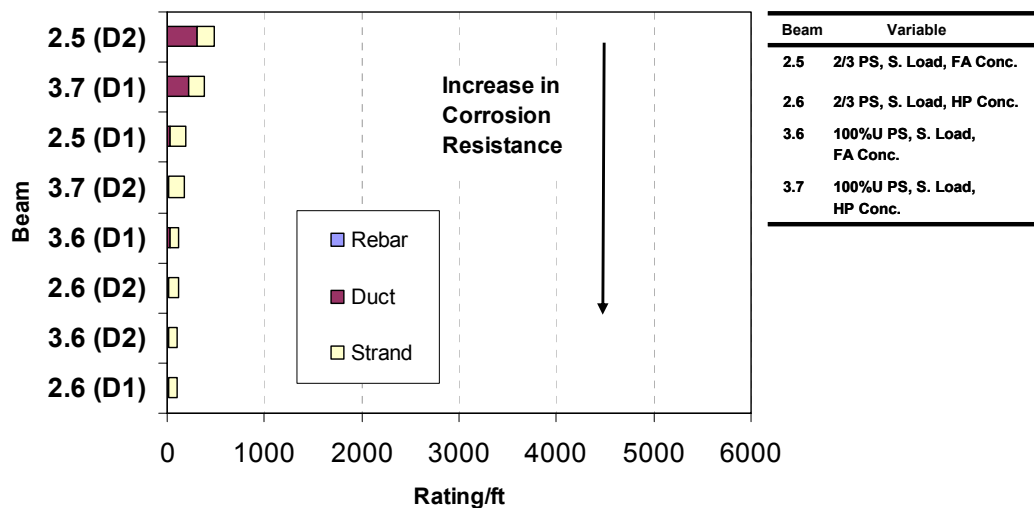
Figure 4.135 Generalized Corrosion Ratings for Phase II Autopsy Beams Ordered According to Performance

A summary table of results prepared by Kotys [4.5] is presented in Table 4.22. In this table, generalized and localized corrosion ratings from Section 4.5.5 are used to conclude on the relative performance of the testing variables.

383

Table 4.22 Summary of Forensic Examination Corrosion Rating Results[4.5]

Method of Comparison	Beams Compared	Variable Analyzed	Result
Gen. Stirrup	1.3, 2.3, 3.2, 4.2	Prestress	• Non and 2/3 PS much worse corrosion protection than 100%S and U PS
Loc. Stirrup	1.3, 2.3, 3.2, 4.2	Prestress	• 2/3 PS is much worse corrosion protection than all others, including Non-PS
Gen. and Loc. Duct	2.3, 3.2, 4.2	Prestress	• 2/3 PS the worst corrosion protection by a significant amount
Gen. and Loc. Strand	2.3, 3.2, 4.2	Prestress	• All corrosion protections about the same, with 100%U PS a little worse
Gen. Stirrup	1.5, 2.5, 3.6 1.6, 2.6, 3.7	Prestress	• 100%U PS consistently best corrosion protection • corrosion protection of Non and 2/3 PS similar, no consistent superiority
Gen. and Loc. Bar	1.5, 2.5, 3.6 1.6, 2.6, 3.7	Prestress	• 2/3 PS shows worst corrosion protection by a significant amount
Gen. and Loc. Duct	2.5, 3.6	Prestress	• 2/3 and 100%U PS corrosion protection similar, no consistent superior PS
Gen. and Loc. Strand	2.5, 3.6	Prestress	• 2/3 and 100%U PS corrosion protection similar, no consistent superior PS
Gen. Stirrup	1.1, 1.3 3.1, 3.2, 3.3	Load/Cracking	• Much worse corrosion protection when cracking is present • Corrosion protection decreases as loading increases
Loc. Stirrup	1.1, 1.3 3.1, 3.2, 3.3	Load/Cracking	• Much worse corrosion protection when cracking is present • Corrosion protection decreases as loading increases
Gen. and Loc. Bar	1.1, 1.3 3.1, 3.2, 3.3	Load/Cracking	• Cracked beams show a little worse corrosion protection
Gen. and Loc. Duct	3.1, 3.2, 3.3	Load/Cracking	• Much worse corrosion protection when cracking is present
Gen. and Loc. Stirrup	1.5, 1.6 2.5, 2.6 3.6, 3.7	Concrete Type	• HP concrete consistently better corrosion protection
Gen. and Loc. Bar	1.5, 1.6 2.5, 2.6 3.6, 3.7	Concrete Type	• All similar corrosion protection and all low ratings…both concretes provide good corrosion protection
Gen. and Loc. Duct	1.5, 1.6 2.5, 2.6 3.6, 3.7	Concrete Type	• All corrosion protections similar, no consistent superior concrete
Gen. and Loc. Strand	1.5, 1.6 2.5, 2.6 3.6, 3.7	Concrete Type	• All corrosion protections similar, no consistent superior concrete
Gen. Duct	2.3, 2.11	Grout Type	• Fly ash grout shows much better corrosion protection
Gen. and Loc. Strand	2.3, 2.11	Grout Type	• No difference in corrosion protection between grout types

4.6.2 Effect of Cracking

Cracking effects were investigated using the three sections that would be expected to crack under service loads (Non-PS, 2/3 PS and 100% U).   In addition, Specimen 4.2 (100%U PS) was found to be cracked at the end of the exposure period, and therefore, it is included in the comparisons.

Specimens 1.3 (Non-PS), 2.3 (2/3 PS) and 2.11 (2/3 PS) developed substantial longitudinal (splitting type) cracking during exposure. Non of the other autopsied specimens evidenced longitudinal cracking.   Since the longitudinal cracks were very wide and could provided additional paths for chloride penetration, they were considered in crack ratings.

4.6.2.1 Crack Density

Crack ratings for all autopsied specimens in Phase I have been plotted along with stirrup, rebar, duct and strand generalized corrosion ratings, in Figure 4.136 and Figure 4.137.   In a similar manner, crack ratings for all autopsied specimens in Phase II have been plotted along with generalized corrosion ratings in Figure 4.138 and Figure 4.139.   Crack ratings are defined as indicated in Equation 4.12.

$$\textit{Crack Rating for each Specimen} = \sum_{i=1}^{m} \left(\overline{w}_i \; x \; l_i \right) \qquad \textbf{\textit{Eq. 4.12}}$$

where, $\overline{w}_i$ = average crack width, for crack i

l_i = crack length at the end of testing, for crack i

m = number of longitudinal and transverse cracks on the specimen top surface, in the 72 inch-analysis length

i = crack under consideration

With the purpose of clearly showing the relationship between crack and corrosion ratings Figure 4.136 through Figure 4.139 have been plotted

maintaining the same crack rating scale, and selecting the adequate generalized corrosion rating scale depending on the level of corrosion found on each element. For Phase II beams, the generalized corrosion rating scale for stirrups, rebar and ducts has been changed to one fifth of that used in Phase I, since corrosion ratings in Phase II beams were much smaller. The generalized corrosion rating scale for Phase II beam strands was selected as half of that used in Phase I beams.

As observed from Figures 4.136 and 4.137, there seems to be a correlation in Phase I beams between stirrup, rebar and duct corrosion ratings and crack density (by means of a crack rating), with some deviations as in the case of rebar corrosion of Specimen 1.3 in Figure 4.136, and, duct corrosion in Specimens 2.11 and 4.2 in Figure 4.137. The proportionality is not shown for the strands, which do not show any distinct trend. It appears that the proportionality is better shown on those elements closer to the top surface of the specimens, and therefore, those receiving the effect of moisture and chlorides in a more direct means.

For Phase II autopsy beams, Figures 4.138 and 4.139 do not show any distinct correlation. These beams constructed with high performance concrete or fly ash concrete, had three years and a half of exposure testing at the time of autopsy, as opposed to Phase I beams that had four years and a half. It is not clear from these results if the non-proportionality observed is the result of the effect of the different concrete types or the shorter exposure testing period. It is anticipated that final autopsies of the remaining specimens in the beam series will yield more conclusive results after several additional years of exposure testing.
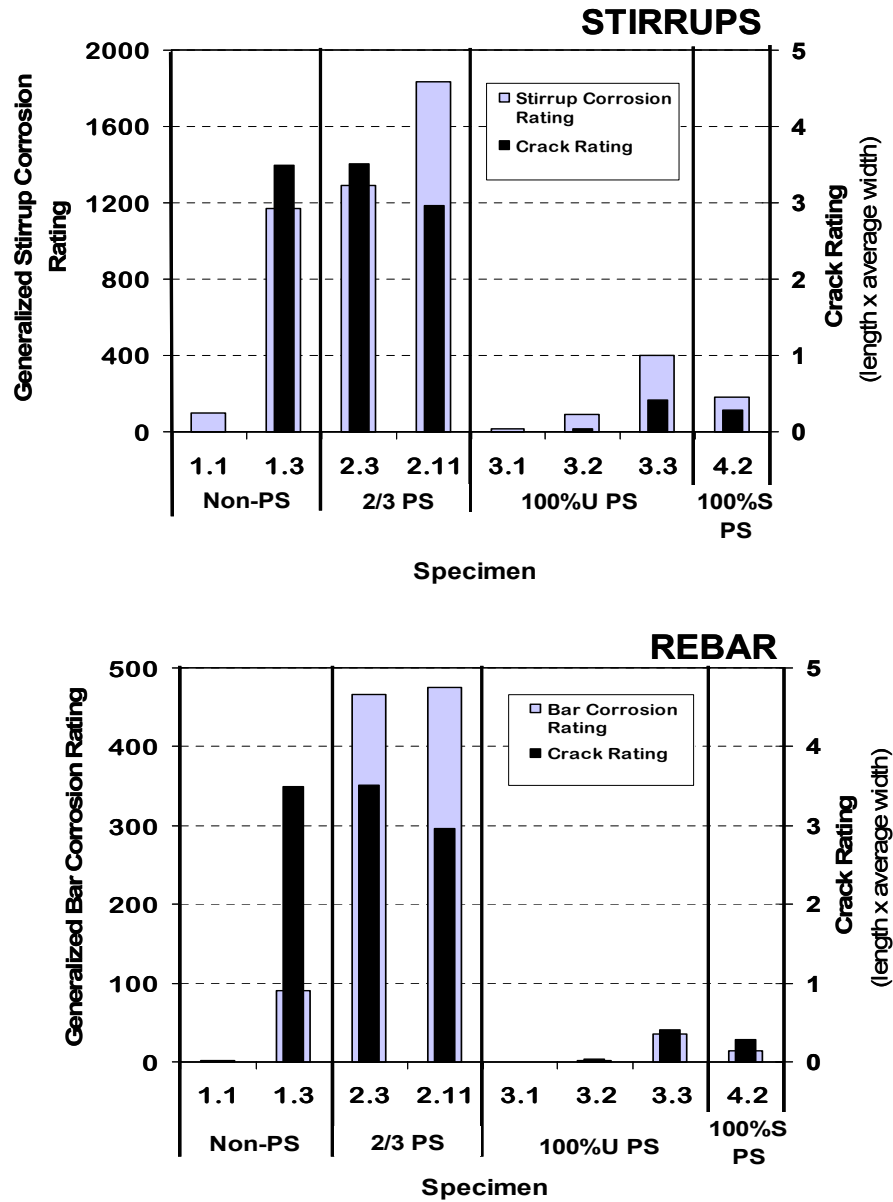
***Figure 4.136 Effect of Crack Density on Stirrup and Rebar Corrosion
for Phase I Autopsy Beams***

DUCTS
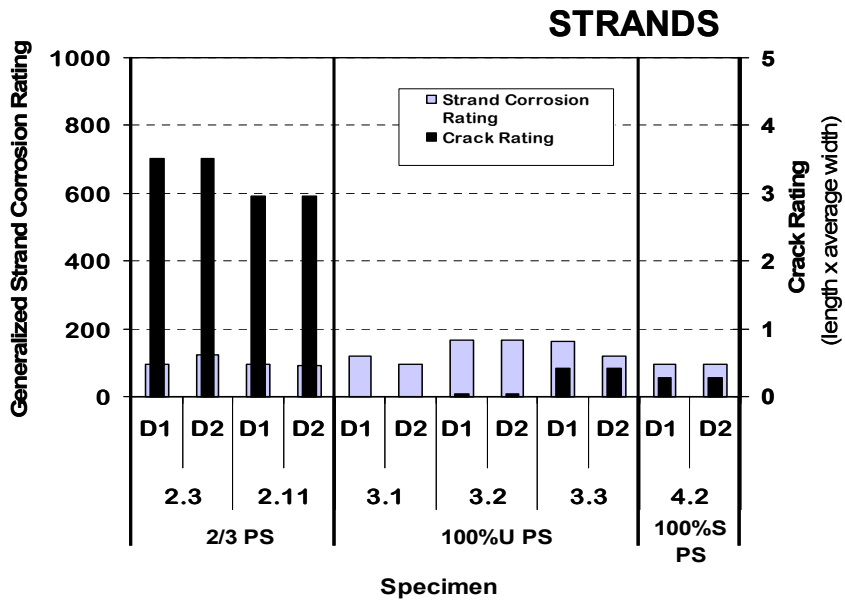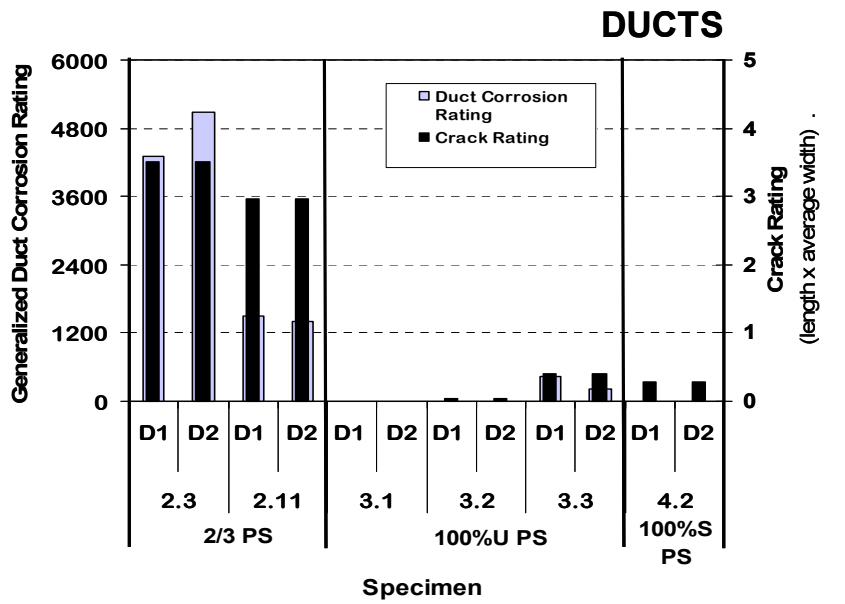
STRANDS

Figure 4.137 Effect of Crack Density on Duct and Strand Corrosion

for Phase I Autopsy Beams

388
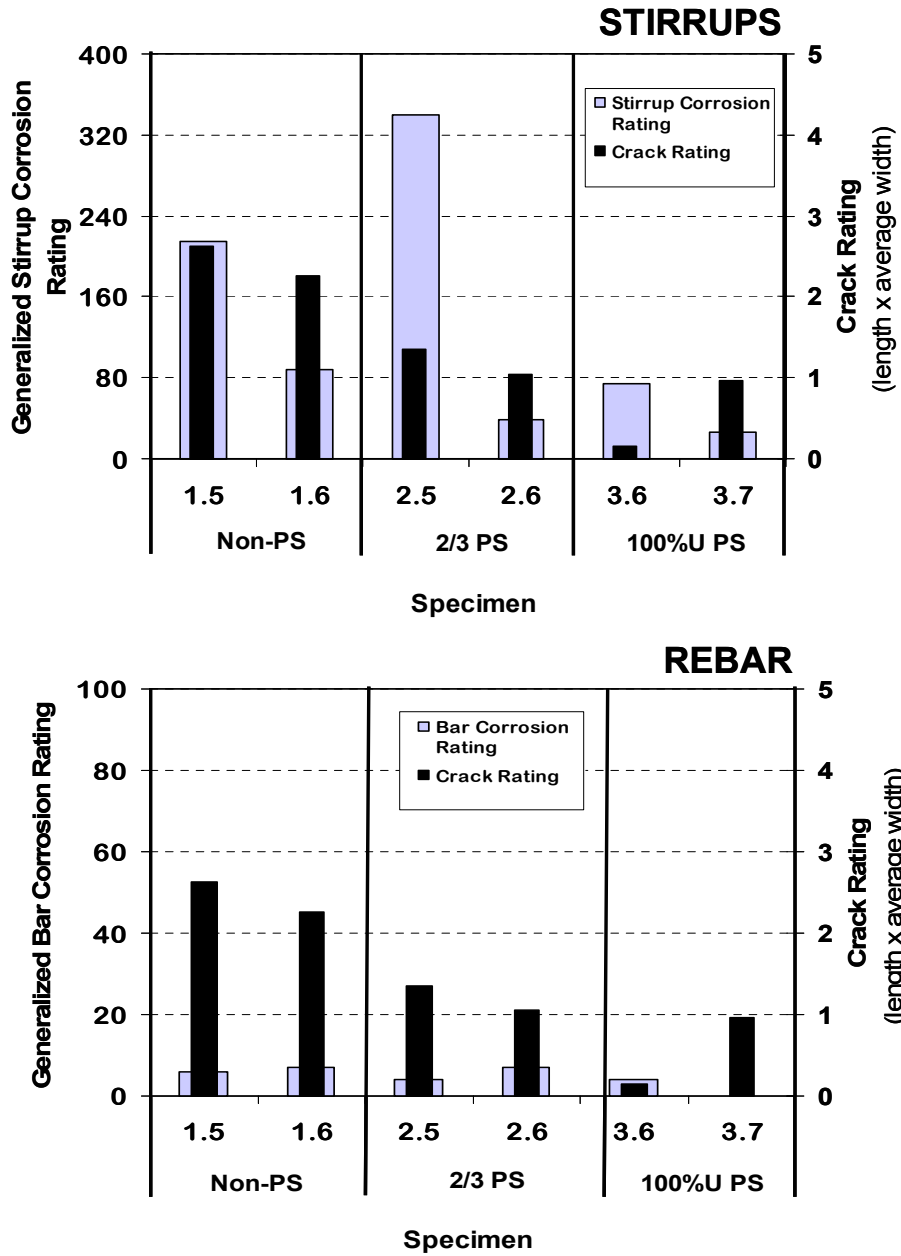
Figure 4.138 Effect of Crack Density on Stirrup and Rebar Corrosion for Phase II Autopsy Beams

389
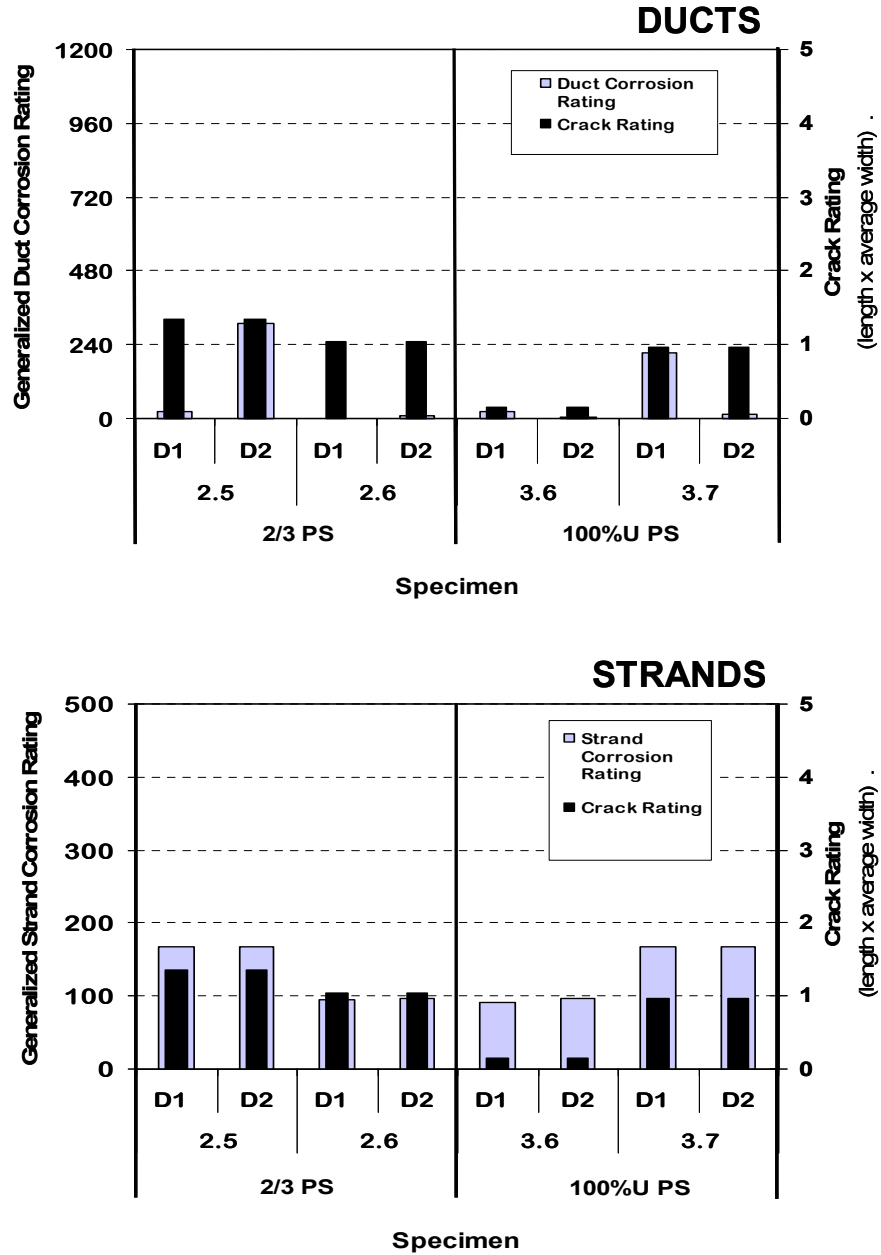
Figure 4.139 Effect of Crack Density on Duct and Strand Corrosion for Phase II Autopsy Beams

390

4.6.2.2   Crack Width

In discussing crack width it is assumed that transverse cracks (formed originally prior to exposure testing) are causes and longitudinal or splitting type cracking formed after substantial exposure due to corrosion products are effects. Thus, all correlations in this section are made with transverse crack widths only.

The effect of transverse crack width on stirrup, rebar, galvanized steel duct and strand corrosion is illustrated on Figure 4.140 and Figure 4.141 for Phase I beams, and on Figure 4.142 and Figure 4.143 for Phase II beams.   In these figures, the localized corrosion rating (maximum corrosion rating recorded for any 2-inch interval for each element) is plotted versus the maximum transverse crack width.   The scale used for the corrosion rating (y scale) has been adjusted for every element, to clearly show any proportionality among the variables.   The plots for Phase II beams use half of the corrosion rating scale in Phase I beam plots, except for the strand rating that uses half of the scale.

As observed from Figure 4.140 there is a distinct trend among localized corrosion rating and maximum crack width for post-tensioned specimens. Mixed reinforced (2/3 PS) beams with wider cracks show higher stirrup, rebar and duct corrosion ratings than 100% PS beams. The trend is not clearly observed for the Non-PS beams nor for the strands   However, from Section 4.5.5.4 it was shown that strands were all performing similarly, with only minimal variations, and therefore, it appears that specimens would require more exposure time to indicate distinct performance differences.

The performance of Specimen 1.3, as observed from Figure 4.140, shows a similar behavior to fully post-tensioned (100%U PS and 100%S PS beams). This conclusion differs from the trend observed for mixed reinforced specimens and from the expected results.   The reason for this difference it is not apparent.

Figures 4.140 and 4.141 show the excellent performance of uncracked specimens (see Specimens 1.1 and 3.1).
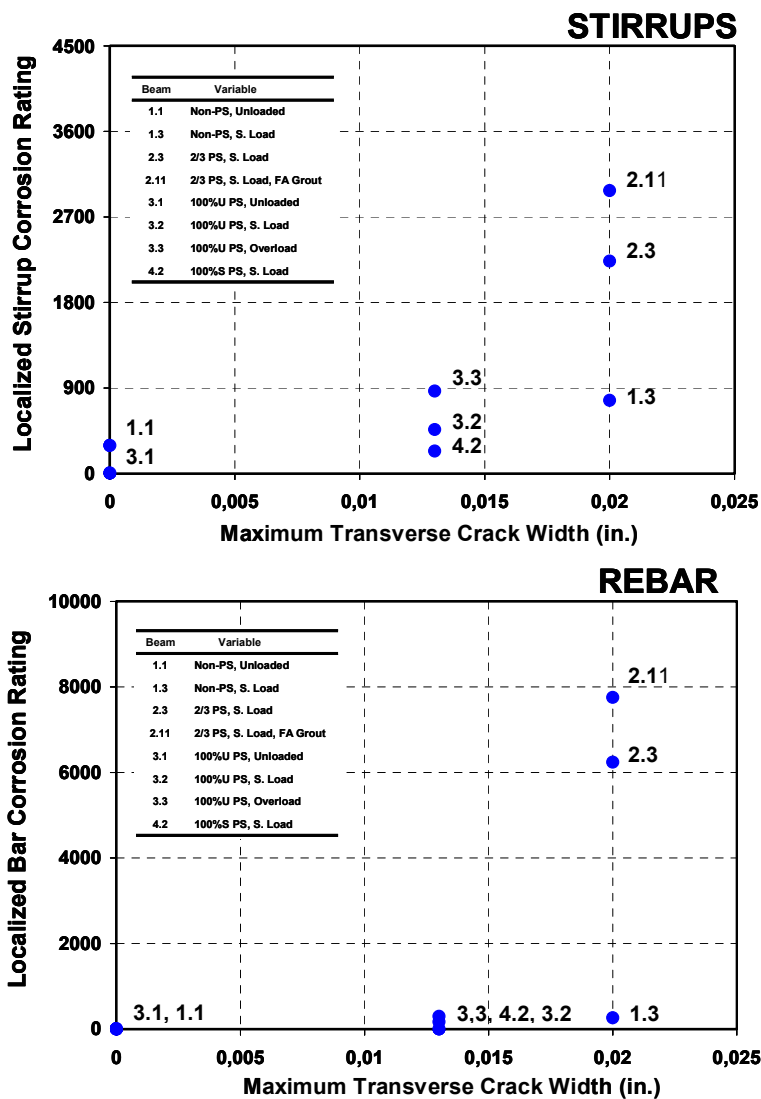
Figure 4.140 Localized Stirrup and Rebar Corrosion Rating versus Maximum Crack Width for Phase I Autopsy Specimens

DUCTS
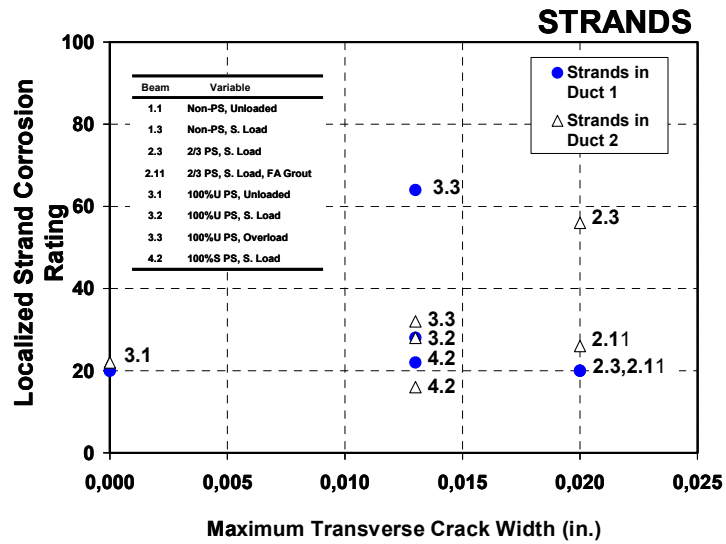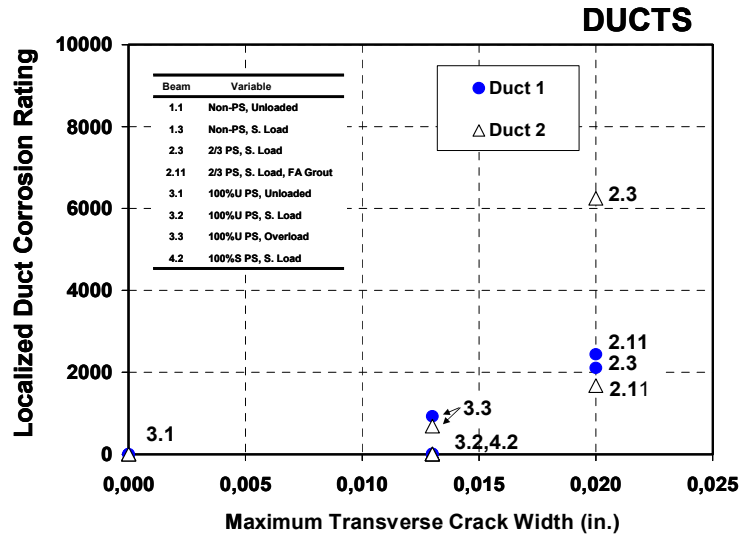
STRANDS

Figure 4.141 Localized Duct and Strand Corrosion Rating versus Maximum Crack Width for Phase I Autopsy Specimens

393
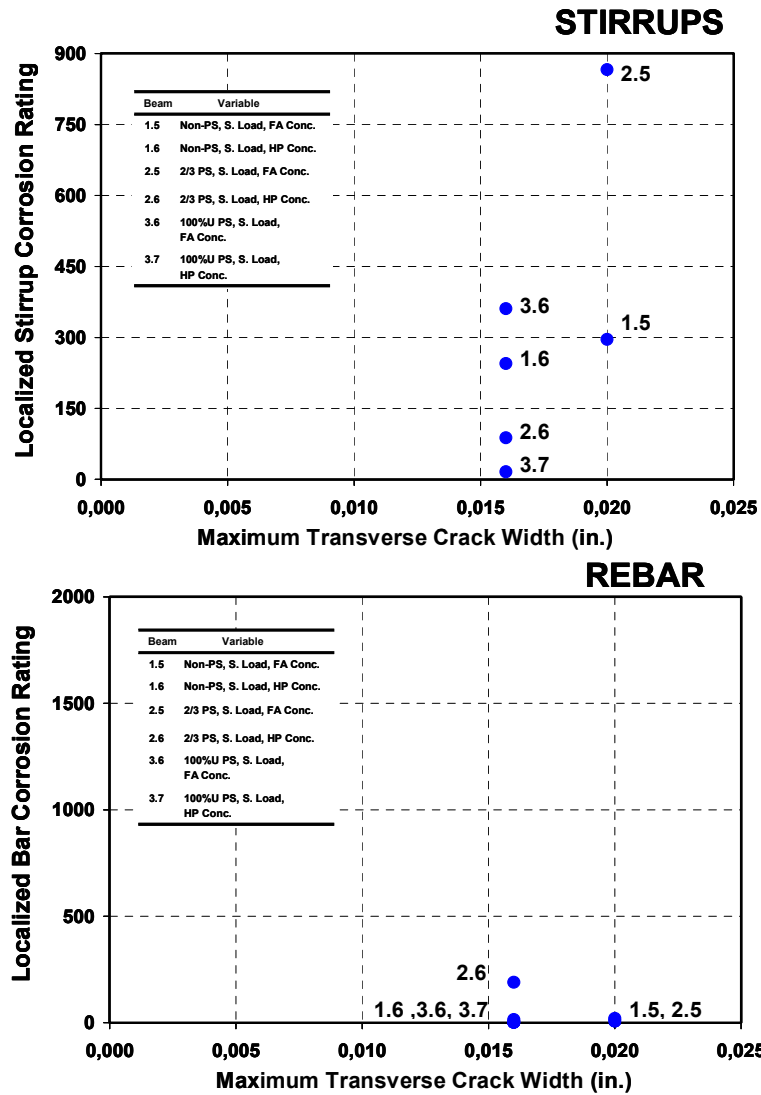
Figure 4.142 Localized Stirrup and Rebar Corrosion Rating versus Maximum Crack Width for Phase II Autopsy Specimens
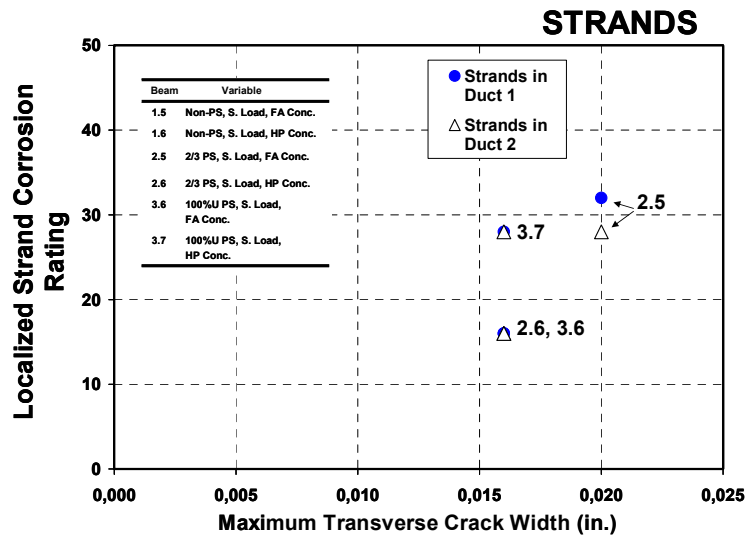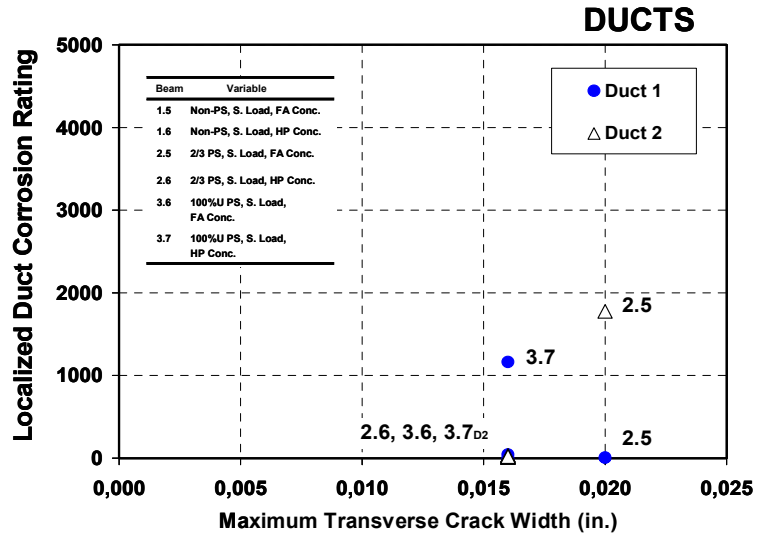
Figure 4.143 Localized Duct and Strand Corrosion Rating versus Maximum Crack Width for Phase II Autopsy Specimens

395

For Phase II specimens, Figure 4.142 and Figure 4.143 show a trend with respect to stirrup, and strand corrosion, and maximum crack width for fly ash concrete post-tensioned specimens. As the level of post-tensioning decreases, cracking and corrosion rating increase.   The trend is not clearly shown for rebar corrosion and for high performance concrete specimens.

In spite of the few deviations observed from the general trends, the above results confirm the negative effect of cracking and wide crack widths on corrosion of steel and post-tensioning system reinforcement.

4.6.2.3 Longitudinal Cracking

Longitudinal or splitting type cracks were found at the end of testing in Specimens 1.3, 2.3 and 2.11,   corresponding with those specimens with the maximum generalized stirrup, rebar and duct (in the case of post-tensioned specimens) corrosion ratings, as shown in Figures 4.122, 4.124 and 4.126, respectively. Longitudinal cracks are the result of very severe reinforcement or duct corrosion occurring within the concrete member.

Longitudinal cracks for Specimen 1.3, 2.3 and 2.11 corresponded with the location of the mild steel reinforcement, as shown in Figures 4.74, 4.78, 4.82, referring to the reinforcement location in Figure 4.4. Longitudinal cracks in Specimens 2.3 and 2.11 were also very close and along the location of the post-tensioning galvanized ducts.

Without any other methods of externally monitoring the condition of the concrete members, longitudinal or splitting cracks by themselves appear to be a definite sign of very severe corrosion deem enough to generate concern.

4.6.2.4 Loading Levels

The effect of loading on reinforcement corrosion is clearly shown in Figures 4.130 and 4.132 when comparing Specimens 1.1 and 1.3, and Specimens

396

3.2 and 3.3.   Also, when comparing Specimens 3.2 and 3.3 in Figure 4.134.   The results are also shown in Figure 4.136 through Figure 4.143. The corrosion rating (and therefore, corrosion extent and severity) increases when loading increases. An increase in loading is associated with an increase in cracking.

4.6.2.5   *Prestressing Levels*

The effect of prestressing levels is shown in Figures 4.130 and 4.132 for Phase I beam Specimens: 1.3, 2.3, 3.2 and 4.2. The corrosion severity decreases with increasing prestressing   levels. In particular, mixed reinforcing (2/3 PS) beams show the worst corrosion protection and perform similar to loaded Non-PS beams. An increase in prestressing level is associated with a decrease in crack density and maximum crack widths.

4.6.3   Effect of Concrete Type

Concrete type effects are determined from Phase II beam specimens. Figure 4.131 shows a distinct trend for stirrup corrosion, with higher corrosion ratings for Class C concrete specimens with fly ash, in comparison to the high performance concrete specimens.   The opposite trend is shown in Figure 4.133 for rebar corrosion ratings, but in this case all ratings are very close to each other, and therefore the trend is not clear.   Figure 4.135 shows a better performance of Specimen 2.6 (high performance concrete) when compared to Specimen 2.5 (Class C with Fly Ash concrete). However, the opposite results are obtained when comparing Specimens 3.6 and 3.7. See definition of high performance concrete used in Section 2.4.4.1.

It appears that concrete type will be better compared when the remaining beams are left under continuous exposure for additional testing time.

397

4.6.4 Effect of Splice Type

Two splice types were tested: Industry Standard splice (IS) and Heat Shrink splice (HS).   Figure 4.144 shows both types of splices and the corrosion and stains typically found.   As observed, the industry standard splice allows moisture to enter through the sides of the splice and get trapped between the duct and the splice due to inefficiency of duct tape.   This results in moisture and chlorides attacking the splice from both sides.

The heat-shrink splice also allows moisture to enter through the sides and get trapped due to insufficient adhesion between the splice and the duct.   It also traps bleed water from the grout.
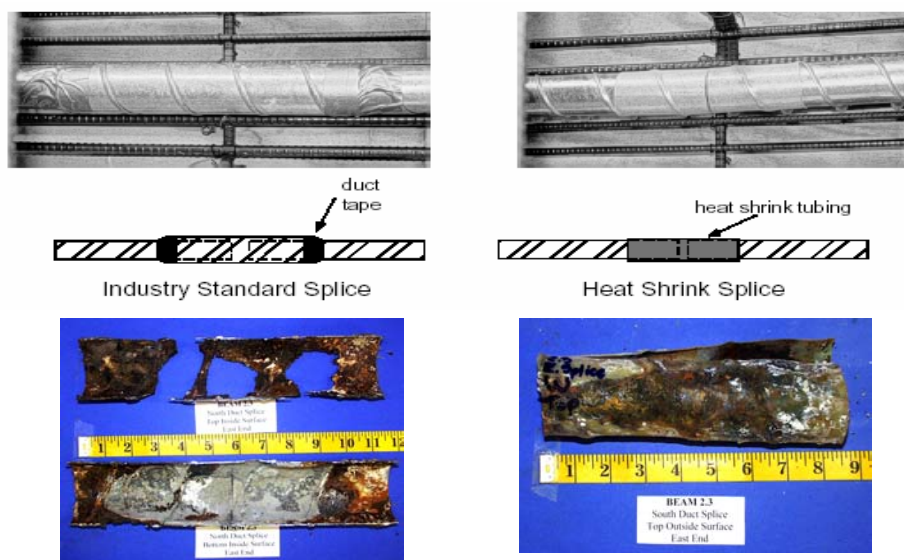
Figure 4.144 Duct Splice Performance

Neither the IS nor the HS splice appears to be a satisfactory duct splice with respect to corrosion protection of galvanized steel ducts.

4.6.5   Effect of Splice Damage

Since the basic undamaged splices were so ineffective, the intentional damage on the duct splices does not show a direct correlation with the severity of corrosion.

4.6.6   Effect of Grout Type

Strand corrosion ratings for Specimens 2.3 and 2.11 are all very low and close in value and therefore, there is not a distinct trend with respect to grout type (standard Class C versus fly ash grout).   The remaining specimens in this testing program are expected to yield more conclusive results with regard to the use of different types of grout, including anti-bleed grout.

4.6.7   Special Autopsy Findings

Since grout is injected after post-tensioning of the element, it is susceptible to cracking due to deflections from loading and vibrations. Cracking in the grout may serve as direct paths for moisture and chlorides to the strands.

Figure 4.145 shows the grout condition found during forensic examination for Specimen 2.11.   As shown in this figure, moisture and corrosion stains coming from the galvanized duct were present in many grout transverse slices. At the time of forensic examination, it appeared that only a short time would have been required for the moisture to get to the strand level.   Similar finding were also reported before by Hamilton. [4.26] However, this aspect in the multilayer strand corrosion protection concept has not received enough attention to date.

Figure 4.145 Effect of Grout Cracking

Bleed water voids were also found inside the ducts on a few specimens, even when they were supposed to have been grouted following correct procedures. Figure 4.146 shows the negative effects of a bleed water void. It was found that grout voids do not only affect the corrosion protection of the strands, but they also appear to be detrimental to the duct.

Figure 4.146 Bleed Water Void and Duct Corrosion

4.6.8   Exposure Testing Measurements versus Forensic Examination Results

Table 4.23 shows the summary of exposure test results with respect to the main test variables.   This table can be compared to Table 4.22, which shows the forensic examination results.

Table 4.23 Summary of Exposure Test Results[4.5]

Method of Comparison	Beams Compared	Variable Analyzed	Result
Half-Cell	1.1, 3.1	Prestress	• 2/3 PS worse than 100%U PS
Half-Cell	1.3, 2.3, 3.2, 4.2	Prestress	• Increase in corrosion protection with increase in PS • 2/3 PS corrosion protection much more similar to Non-PS than 100% PS • No significant difference between 100%U and 100%S PS
Half-Cell	1.5, 2.5, 3.6	Prestress	• Increase in corrosion protection with increase in PS • 2/3 PS corrosion protection almost identical to Non-PS
Half-Cell	1.6, 2.6, 3.7	Prestress	• All levels of PS similar (due to very large crack in 100%U PS beam)
Corr. Rate	1.5, 2.5, 3.6	Prestress	• Increase in corrosion protection with increase in PS
Cl⁻ Content	All Phase I Beams	Prestress	• Increase in horizontal chloride penetration with decrease in PS • Increase in corrosion protection with increase in PS
Half-Cell	1.1, 1.3	Load/Cracking	• Decrease in corrosion protection with increase in loading
Half-Cell	3.1, 3.2, 3.3	Load/Cracking	• Decrease in corrosion protection with increase in loading • Significant decrease in corrosion protection with cracking present
Corr. Rate	3.1, 3.2, 3.3	Load/Cracking	• Decrease in corrosion protection with increase in loading and cracking
Cl⁻ Content	1.3, 2.11, 4.2	Load/Cracking	• Significantly higher chloride content at bar level when samples taken at crack location
Half-Cell	1.5, 1.6 2.5, 2.6	Concrete Type	• HP concrete corrosion protection better than FA
Half-Cell	3.6, 3.7	Concrete Type	• FA concrete corrosion protection better than HP (this HP beam is the one with a very large crack)
Half-Cell	All Phase II Beams	Concrete Type	• HP concrete corrosion protection better than FA
Corr. Rate	1.5, 1.6 2.5, 2.6 3.6, 3.7	Concrete Type	• No significant difference in corrosion protection of HP and FA concrete
Cl⁻ Content	Blocks	Concrete Type	• HP concrete corrosion protection better than FA
Cl⁻ Content	1.5, 1.6 2.5, 2.6 3.6, 3.7	Concrete Type	• HP concrete better at preventing chloride penetration • Both concrete types minimize chloride penetration to bar level
Half-Cell	2.3, 2.11	Grout Type	• No difference in corrosion protection between normal and FA grout

Legend:

PHASE I BEAMS: 1.1 Non-PS, Unloaded; **1.3** Non-PS, S. Load; **2.3** 2/3 PS, S.Load; **2.11** 2/3 PS, S. Load;

3.1 100% U PS, Unloaded, **3.2** 100% U PS, S. Load; **3.3** 100% U PS, Overload; **4.2** 100%S PS, S. Load

PHASE II BEAMS: 1.5 Non-PS, S. Load, FA Conc.; **1.6** Non-PS, S. Load, HP Conc.; **2.5** 2/3 PS, S. Load, FA Conc.;

2.6 2/3 PS, S. Load, HP Conc.; **3.6** 100%U PS, S. Load, FA Conc.; **3.7** 100%U PS, S. Load, HP Conc.

4.6.8.1 Half-Cell Potential Readings versus Forensic Examination Results

Half-cell potential readings have been ordered according to specimen performance in Figures 4.147 through Figure 4.150, including readings at the time to initiation of corrosion and at the end of testing for all autopsied specimens.
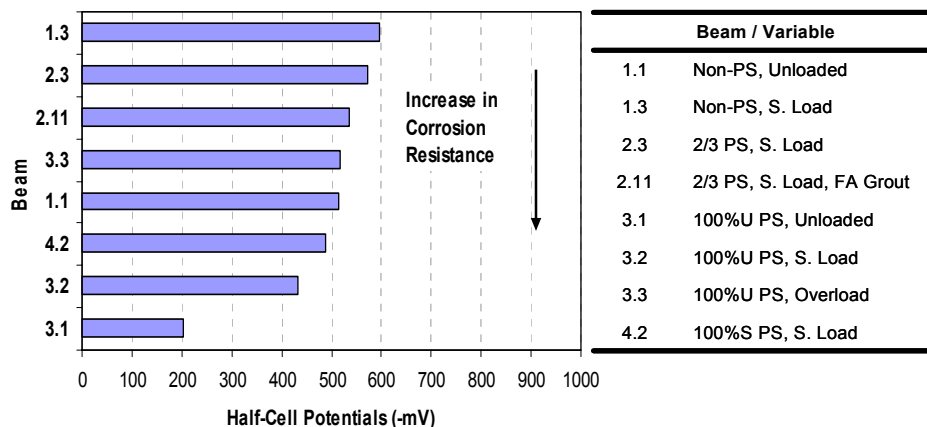
Figure 4.147 Half-Cell Potential at 1594 Days (End of Testing) for Phase I Autopsy Beams
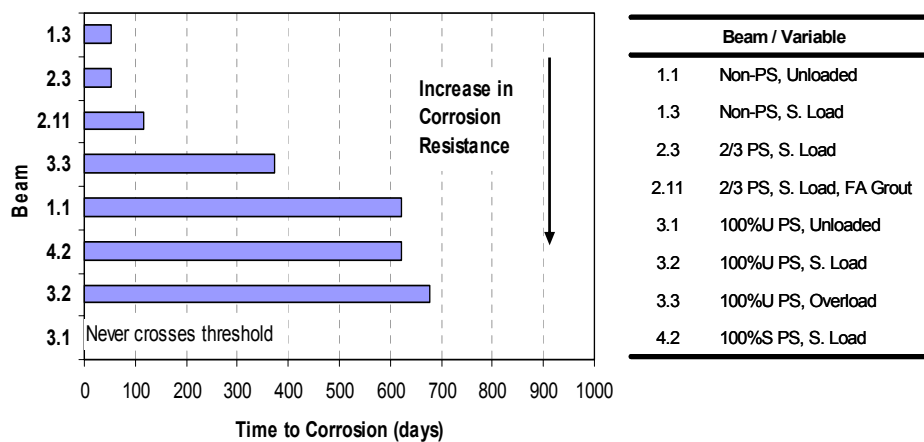
Figure 4.148 Time to Initiation of Corrosion for Phase I Autopsy Beams

402

The half-cell potentials show an excellent inverse correlation in specimen performance between the negative potential and the time to corrosion.
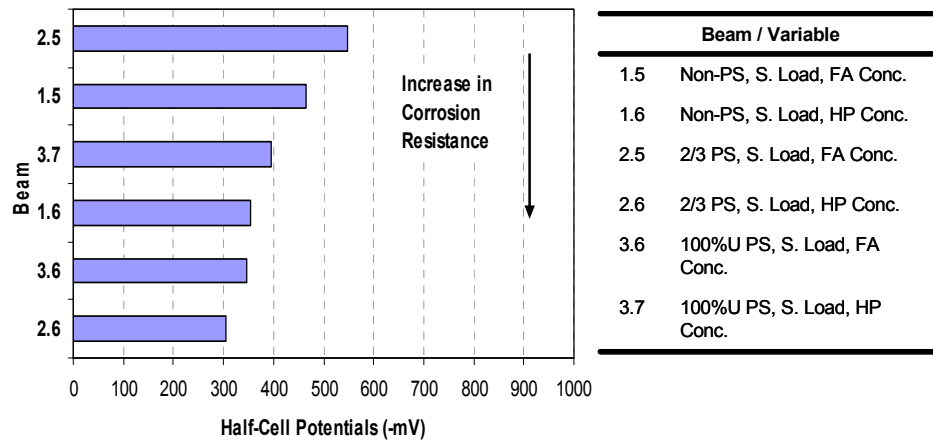
**Figure 4.149 Half-Cell Potential at 1594 days (end of testing)
for Phase II Autopsy Beams**
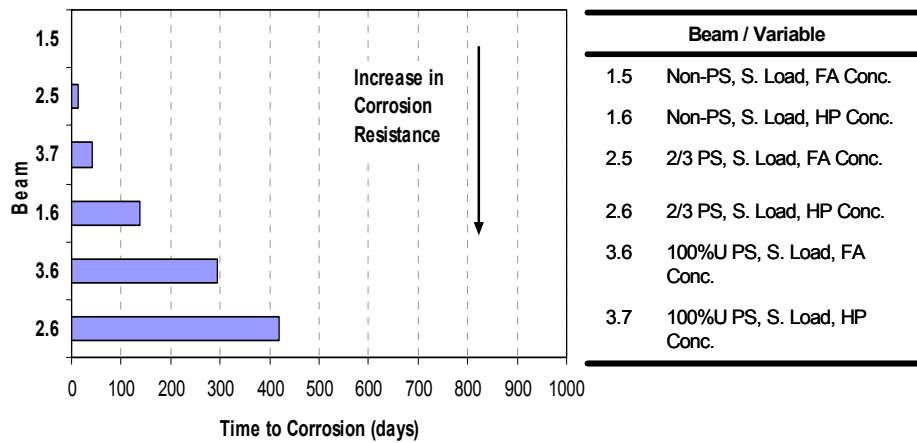
**Figure 4.150 Time to Initiation of Corrosion
for Phase II Autopsy Beams**

403

Half-cell potential readings at the end of testing versus forensic examination results are directly compared in Figure 4.151 through Figure 4.154. In these figures, the same scales used in Section 4.6.2 for stirrup, rebar, duct and strand corrosion ratings have been maintained for consistency and clarity.

With the Phase I beams shown in Figure 4.151 and 4.152, it can be seen that there is not a clear cut correlation between the half-cell readings and forensic examination results. The loaded Non-PS and 2/3 PS beams (1.3, 2.3, 2.11) show very fine correlation. However, the other specimens generally show quite poor correlation. Some very high negative potential readings occurred in specimens that evidenced very small amounts of actual corrosion (1.1, 3.1, 3.2).

With the Phase II beams, shown in Figures 4.153 and 4.154 there is little relationship between the half-cell potential and the corrosion rating for most specimens other than stirrups, but this is due to the actual corrosion ratings for bars, ducts and strands being very low and close in values.
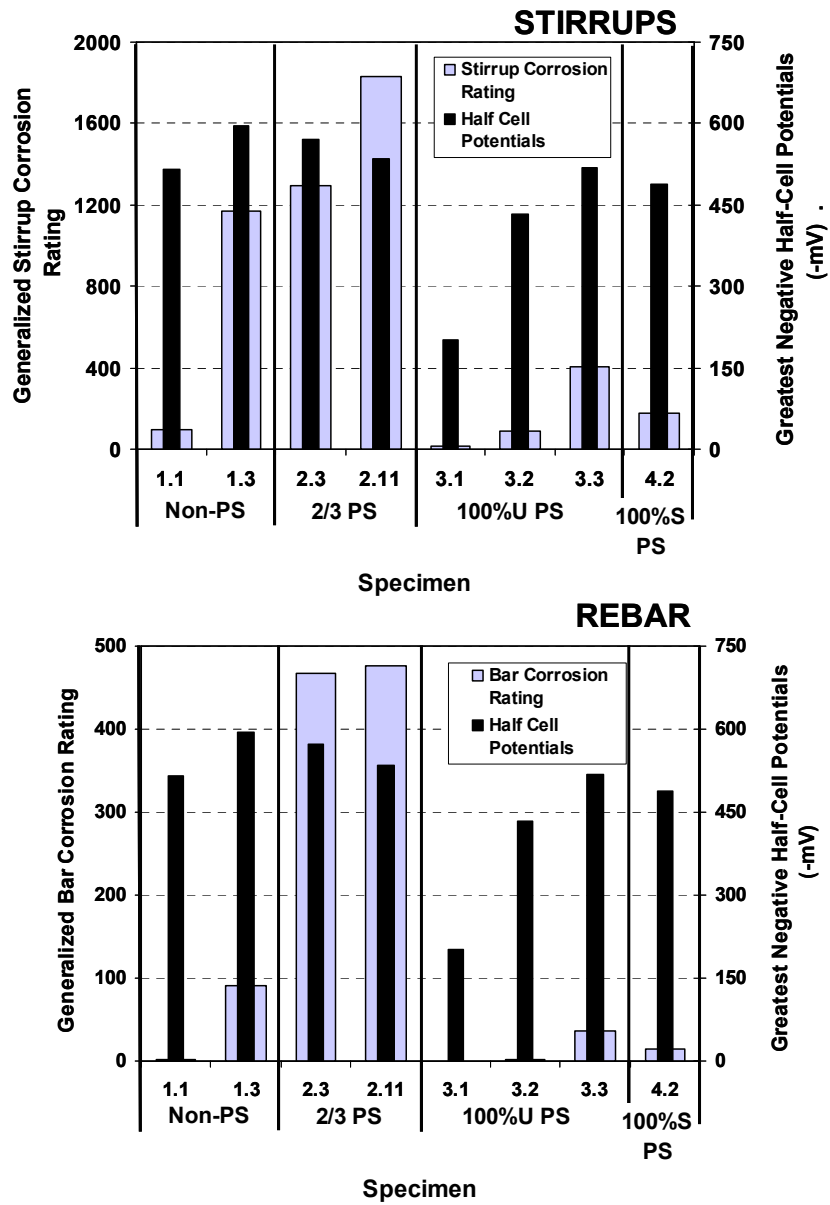
Figure 4.151 Half-Cell Readings at the End of Testing vs.
Stirrup and Rebar Corrosion Ratings for Phase I Autopsy Specimens
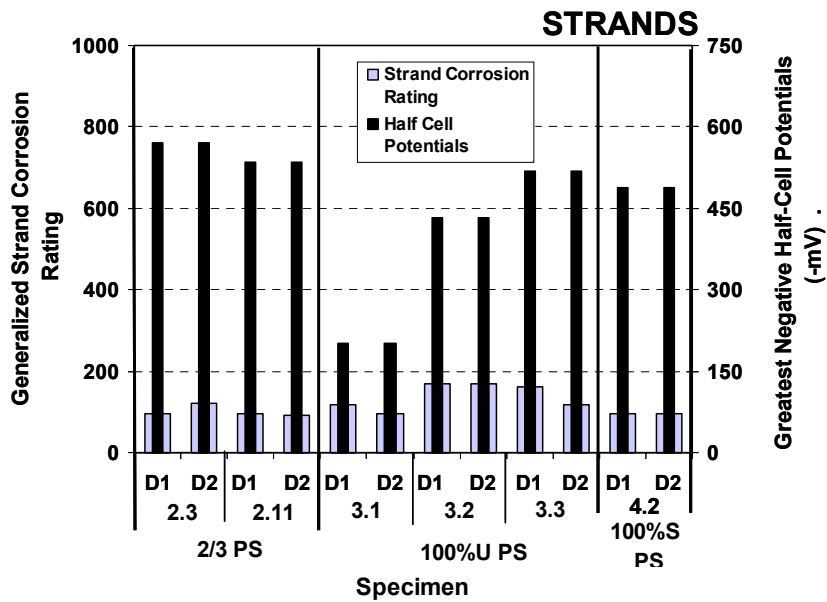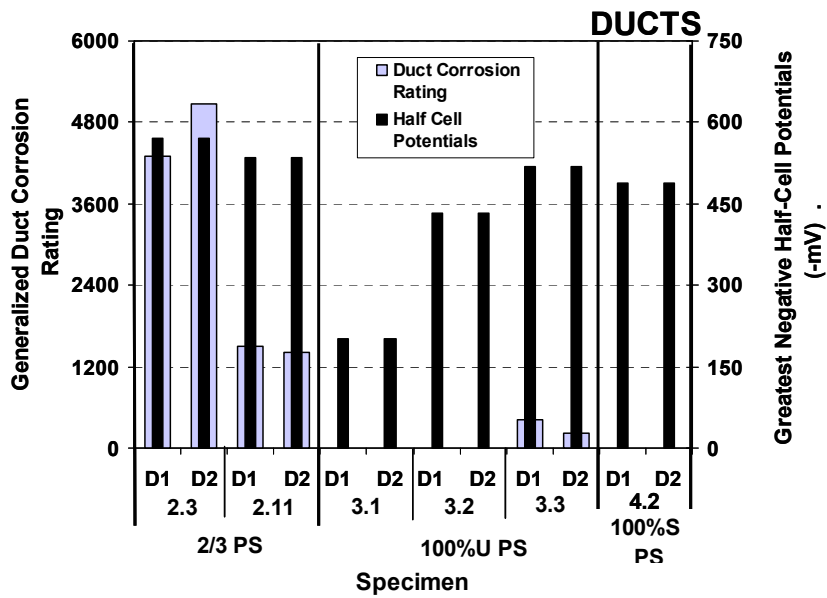
*Figure 4.152 Half-Cell Readings at the End of Testing vs.
Duct and Strand Corrosion Ratings for Phase I Autopsy Specimens*

406
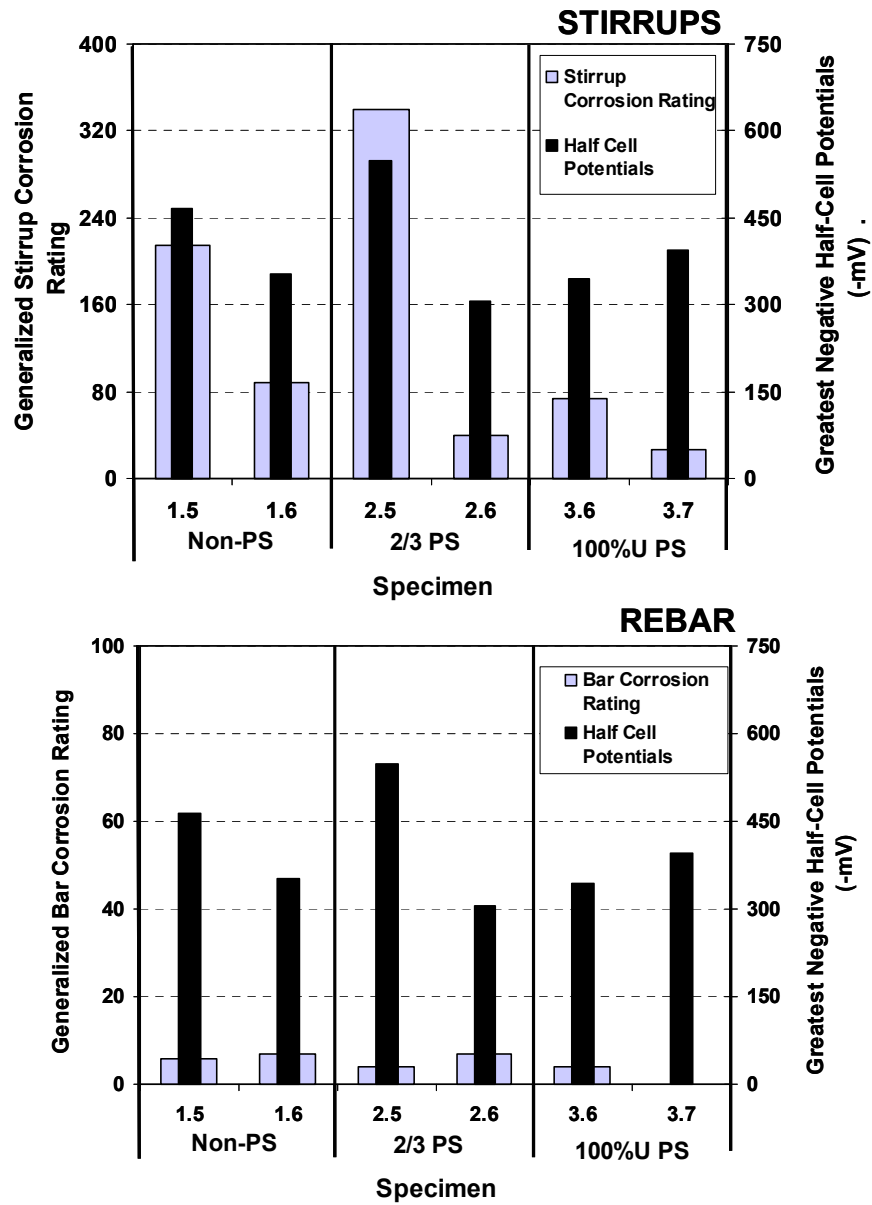
Figure 4.153 Half-Cell Readings at the End of Testing vs.
Stirrup and Rebar Corrosion Ratings for Phase II Autopsy Specimens
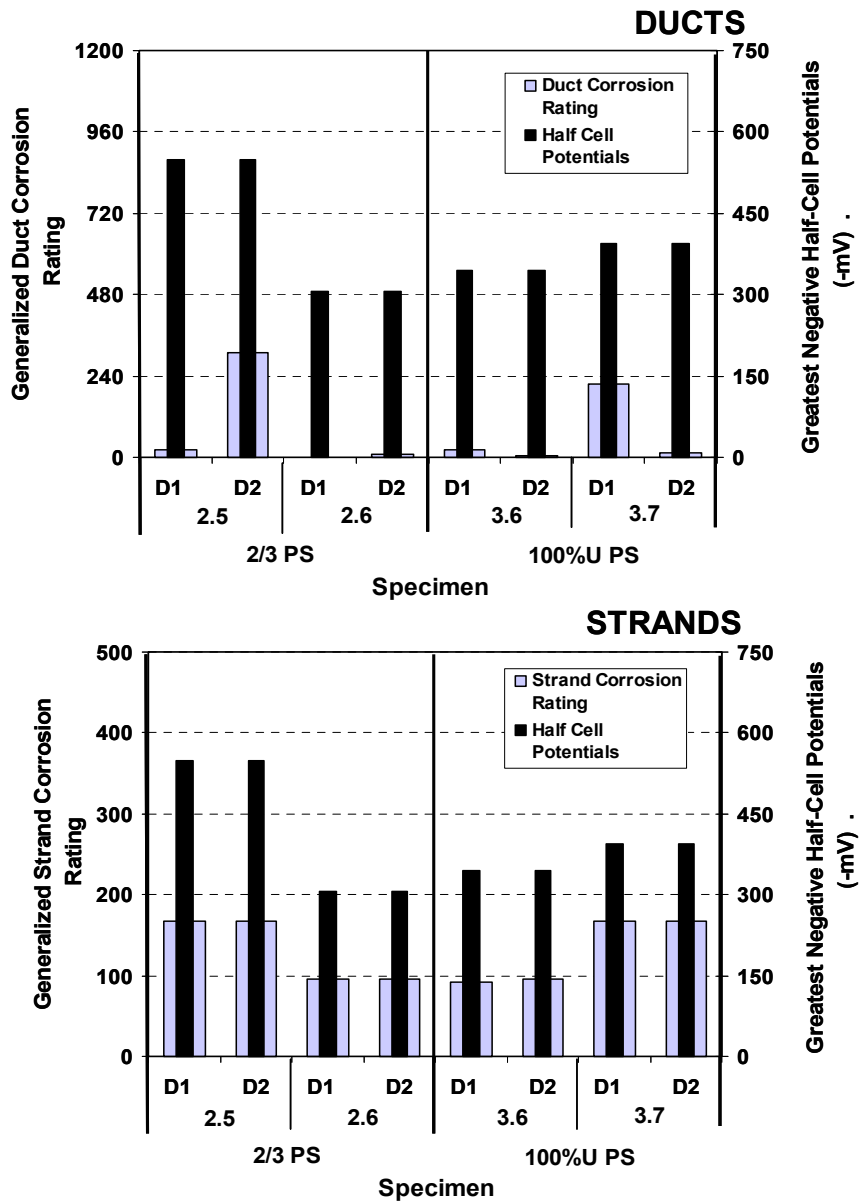
Figure 4.154 Half-Cell Readings at the End of Testing vs.
Duct and Strand Corrosion Ratings for Phase II Autopsy Specimens

4.6.9 Corrosion Rate Measurements versus Forensic Examination Results

Final corrosion rate measurements taken from Phase I and Phase II autopsy beams are shown in Figure 4.155 and Figure 4.156, respectively, ordered according to performance. As will be shown in Figures 4.157 through 4.160, these corrosion rate indicators are highly misleading. For example, the worst corrosion performance was generally Specimens 1.3, 2.3 and 2.11. These specimens are not as critical in the corrosion rate measurements as more lightly corroded specimens 3.2 and 3.3.
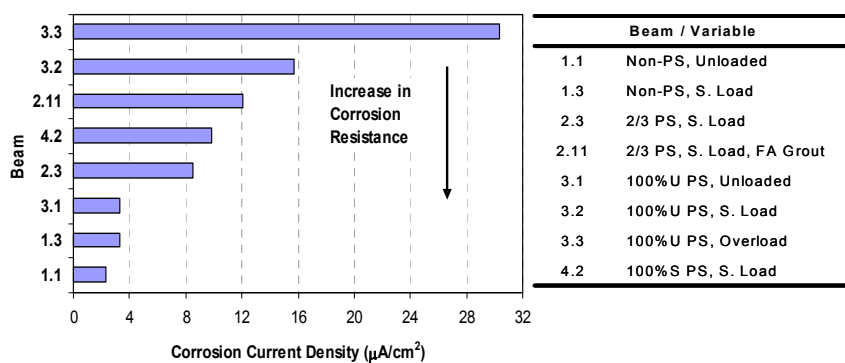
Figure 4.155 Final Corrosion Rate Measurements Using 3LP Equipment for Phase I Autopsy Beams
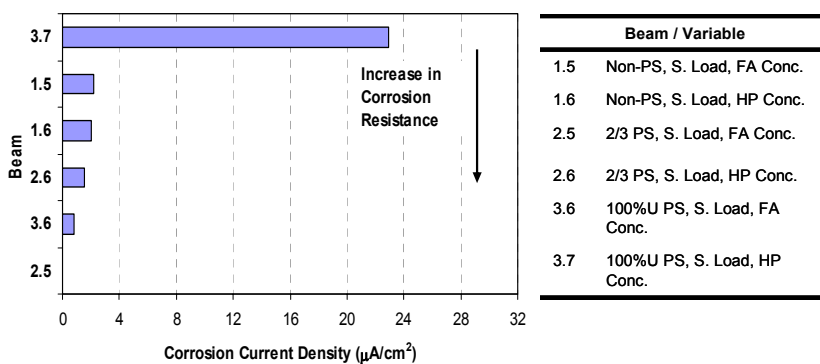
Figure 4.156 Final Corrosion Rate Measurements Using 3LP Equipment for Phase II Autopsy Beams

409

Corrosion rate measurements versus forensic examination results are directly compared in Figure 4.157 through Figure 4.160.
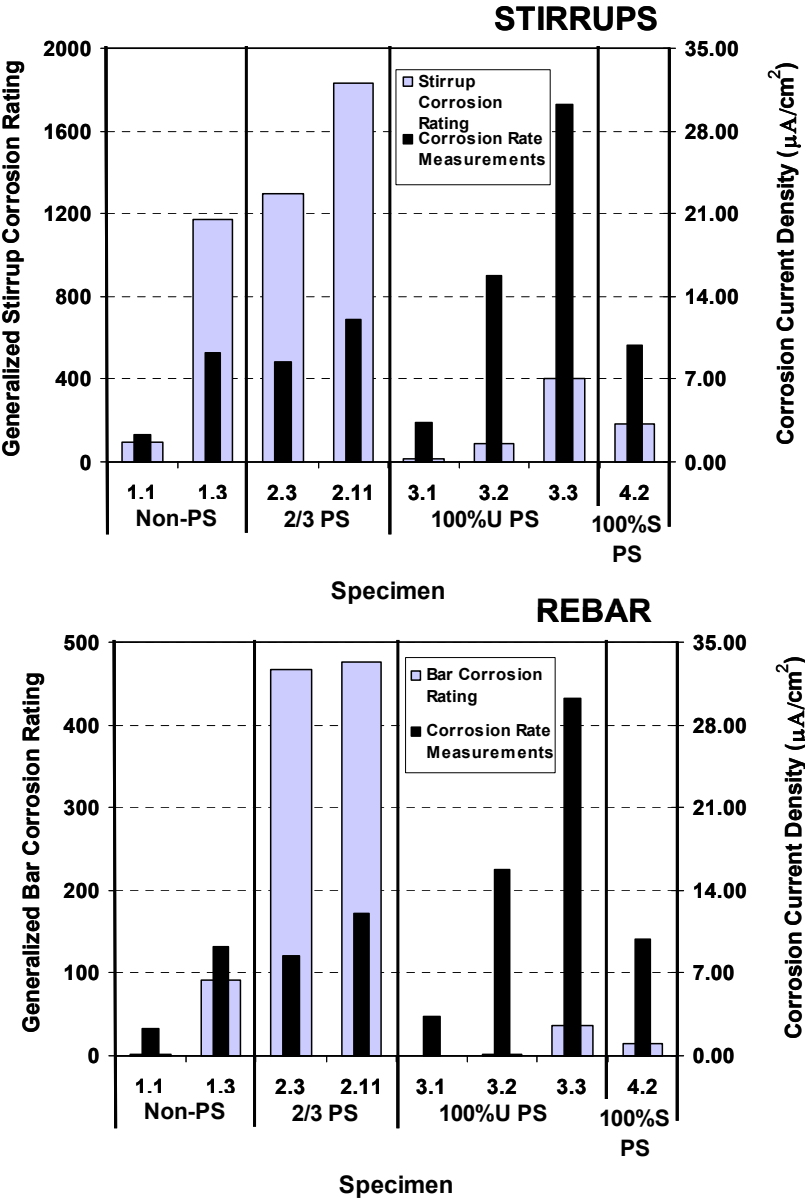
Figure 4.157 Corrosion Rate Measurements (using 3LP equipment) after 47 Months of Exposure vs. Stirrup and Rebar Corrosion Ratings for Phase I Autopsy Specimens
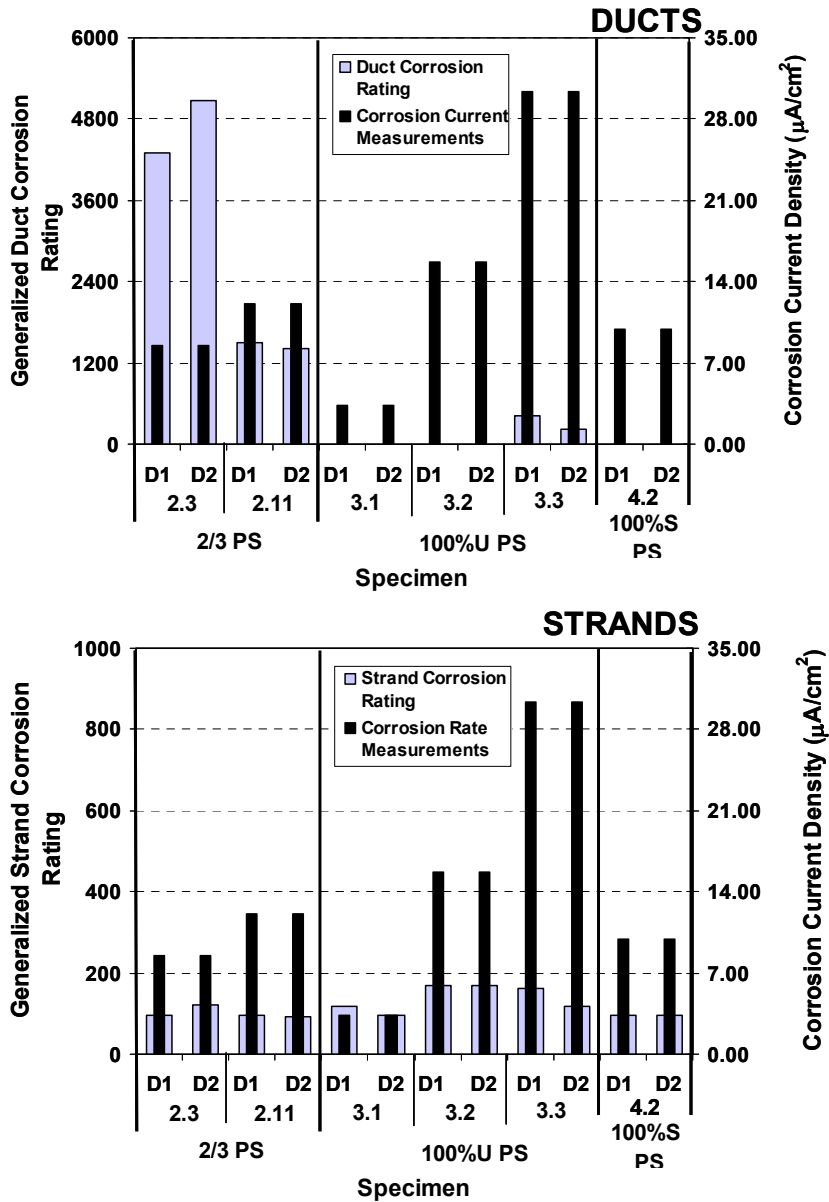
Figure 4.158 Corrosion Rate Measurements (using 3LP equipment) after 47 Months of Exposure vs. Duct and Strand Corrosion Ratings for Phase I Autopsy Specimens

411
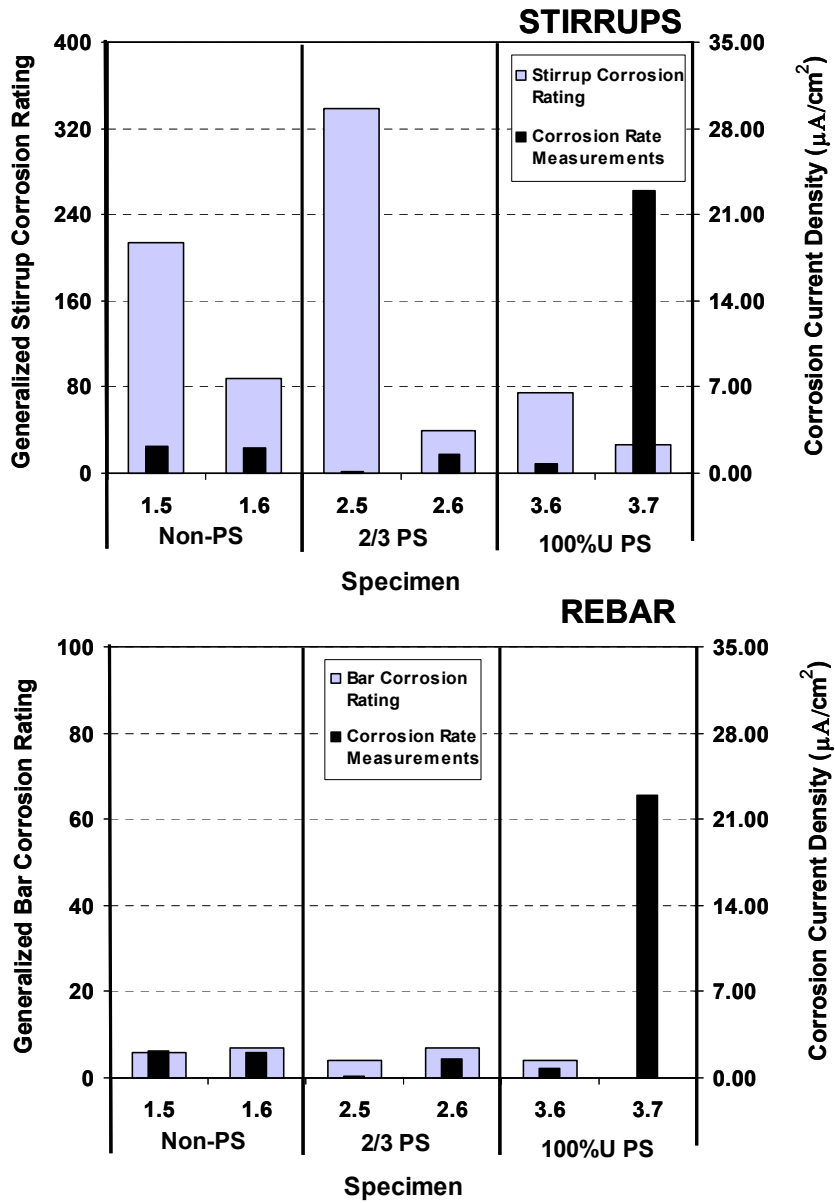
Figure 4.159 Corrosion Rate Measurements (using 3LP equipment) after 35 Months of Exposure vs.Stirrup and Rebar Corrosion Ratings for Phase II Autopsy Specimens

412
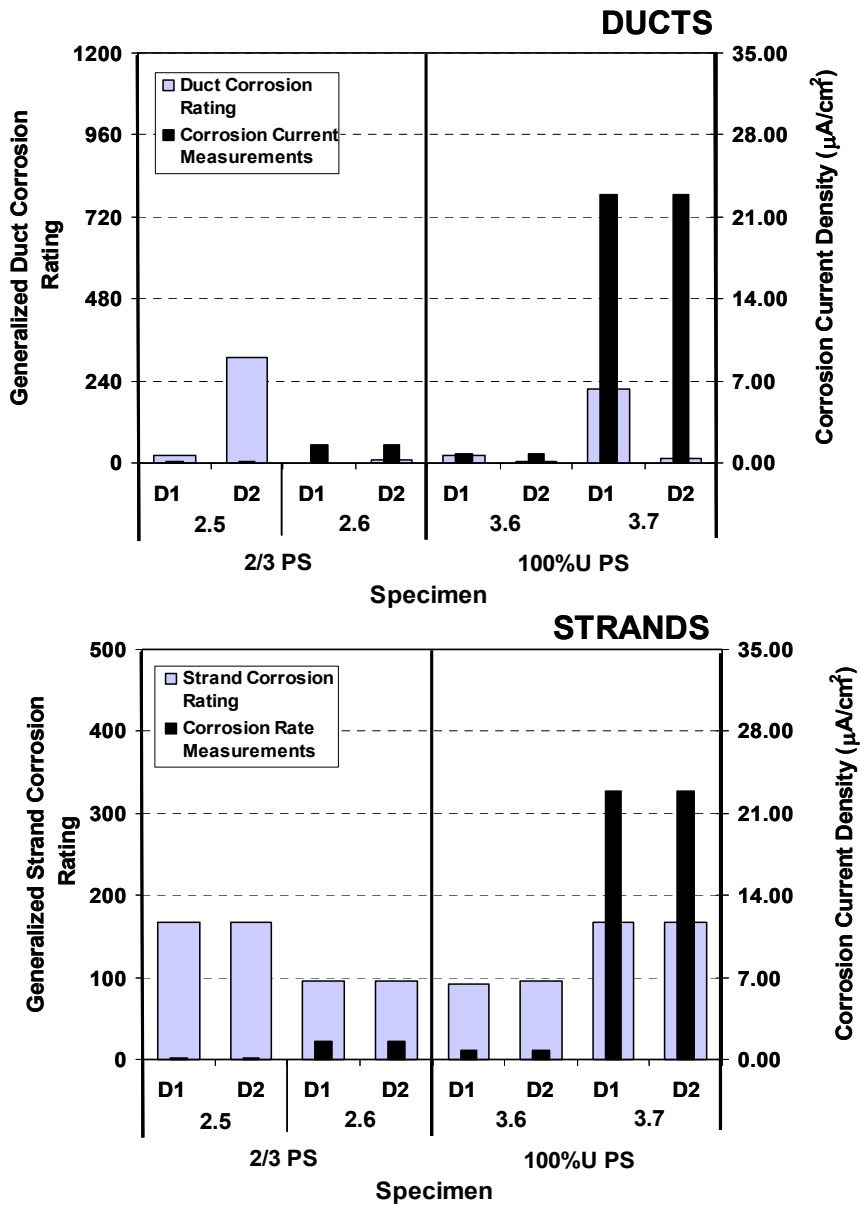
Figure 4.160 Corrosion Rate Measurements (using 3LP equipment) after 35 Months of Exposure vs. Duct and Strand Corrosion Ratings for Phase II Autopsy Specimens

413

Figures 4.157 through Figure 4.160 show very poor or inexistent correlation among corrosion rate readings and stirrup, rebar, duct and strand corrosion ratings.

4.6.10 Chloride Penetration versus Forensic Examination Results

Chloride penetration plots for samples taken within the ponded region (3-inch and 18-inch offset from centerline of beam), are shown in Figure 4.161 and Figure 4.162 for Phase I beams.   In these graphs, the chloride content for the ponded blocks is compare to the chloride content for the beam specimens. As shown in these figures, the negative effect of cracking is evidenced since the ponded blocks were uncracked.   While the chloride content in the beam specimens is very high, except in the case of Specimen 1.1, the corresponding chloride content in the ponded blocks is very low.
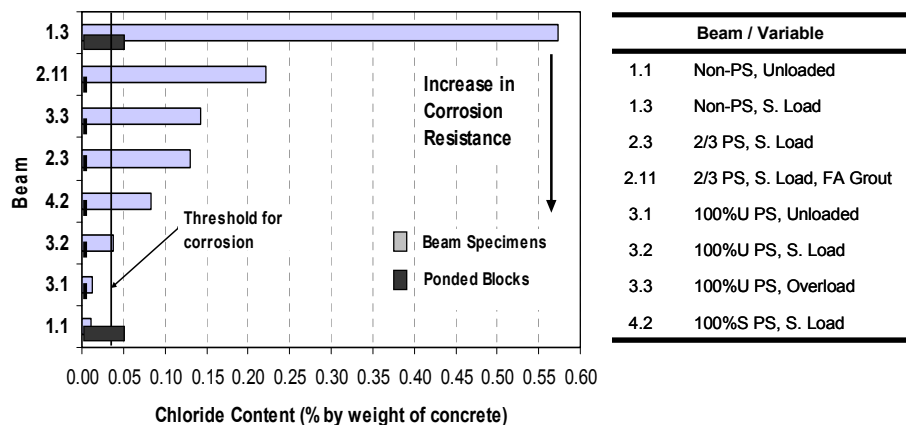
Figure 4.161 Beam Chloride Content at Bar Level – 3 in. Offset for Phase I Autopsy Beams

	Beam / Variable
1.1	Non-PS, Unloaded
1.3	Non-PS, S. Load
2.3	2/3 PS, S. Load
2.11	2/3 PS, S. Load, FA Grout
3.1	100%U PS, Unloaded
3.2	100%U PS, S. Load
3.3	100%U PS, Overload
4.2	100%S PS, S. Load
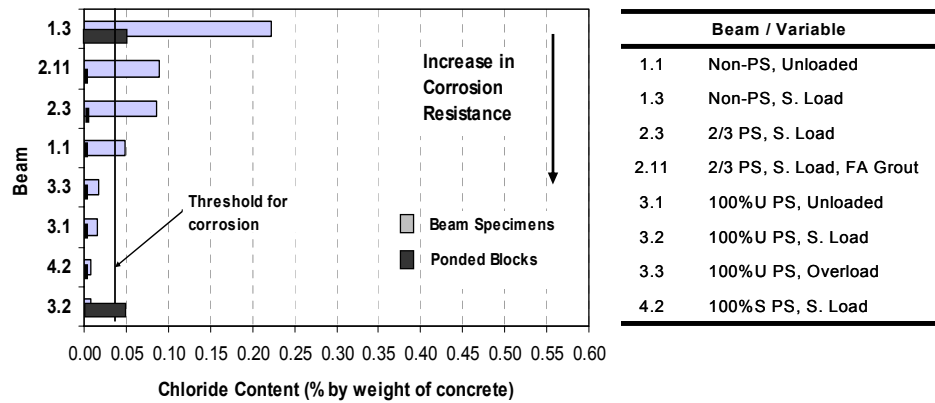
Figure 4.162 Beam Chloride Content at Bar Level – 18 in. Offset for Phase I Autopsy Beams

Figure 4.163 and Figure 4.164 show the chloride penetration results for Phase II beams. Again, the chloride content for the blocks is shown. In this case, chloride contents were in all cases below the threshold of concern. However, it should be recognized that the chloride samples in the beams were taken at the location shown (3 in. or 18 in. offset), and therefore, they may not correspond to crack locations. Nevertheless, samples from the beam specimens showed in general higher chloride contents than those from the ponded blocks, which reflect again the negative effect of cracking on chloride penetration.

Figures 4.165 through Figure 4.168 show the comparison of acid-soluble chloride content at the bar level taken at three inches from the beam centerline versus stirrup, rebar, duct and strand corrosion ratings.

Overall, the chloride content measurements showed good correlation with stirrup, rebar and stand corrosion ratings in Phase I specimens, except for Specimen 1.3 that showed very high chloride content, and for Specimens 2.3 and 2.11 that showed lower chloride contents. However, chloride contents did not correlate well with duct corrosion ratings in all specimens. For Phase II beams there was no relationship between the chloride content at 3 in. offset and the

415

actual corrosion ratings for most specimens, but this was due to the chloride contents for stirrups, bars, ducts and strands being very low.   One of the reasons for these low chloride values was that samples were taken at specific distances from the beam centerline, and they may not have corresponded to crack locations.
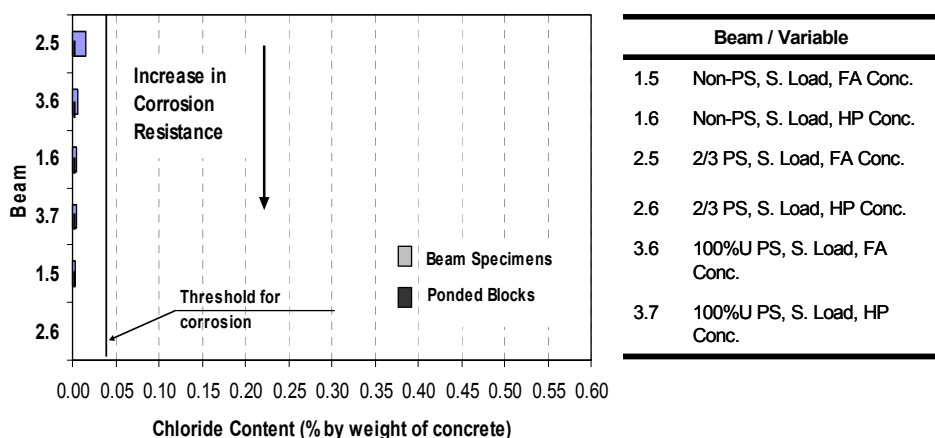
Figure 4.163 Beam Chloride Content at Bar Level – 3 in. Offset for Phase II Autopsy Beams
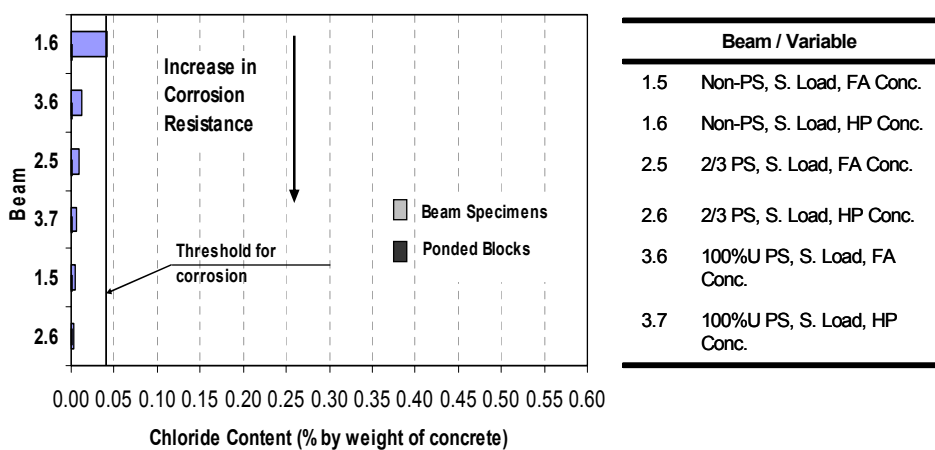
Figure 4.164 Beam Chloride Content at Bar Level – 18 in. Offset for Phase II Autopsy Beams
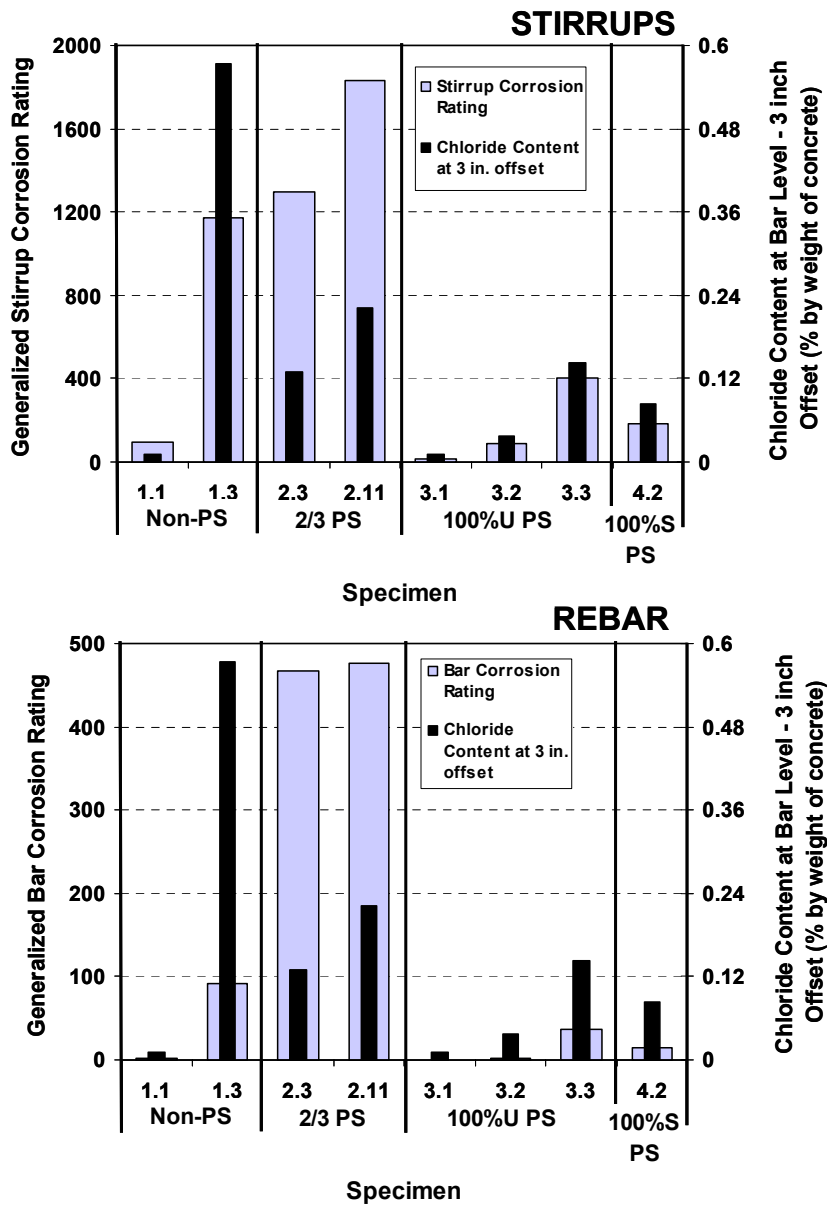
***Figure 4.165 Acid-Soluble Chloride Content versus vs. Stirrup and Rebar
Corrosion Ratings for Phase I Autopsy Specimens***

417
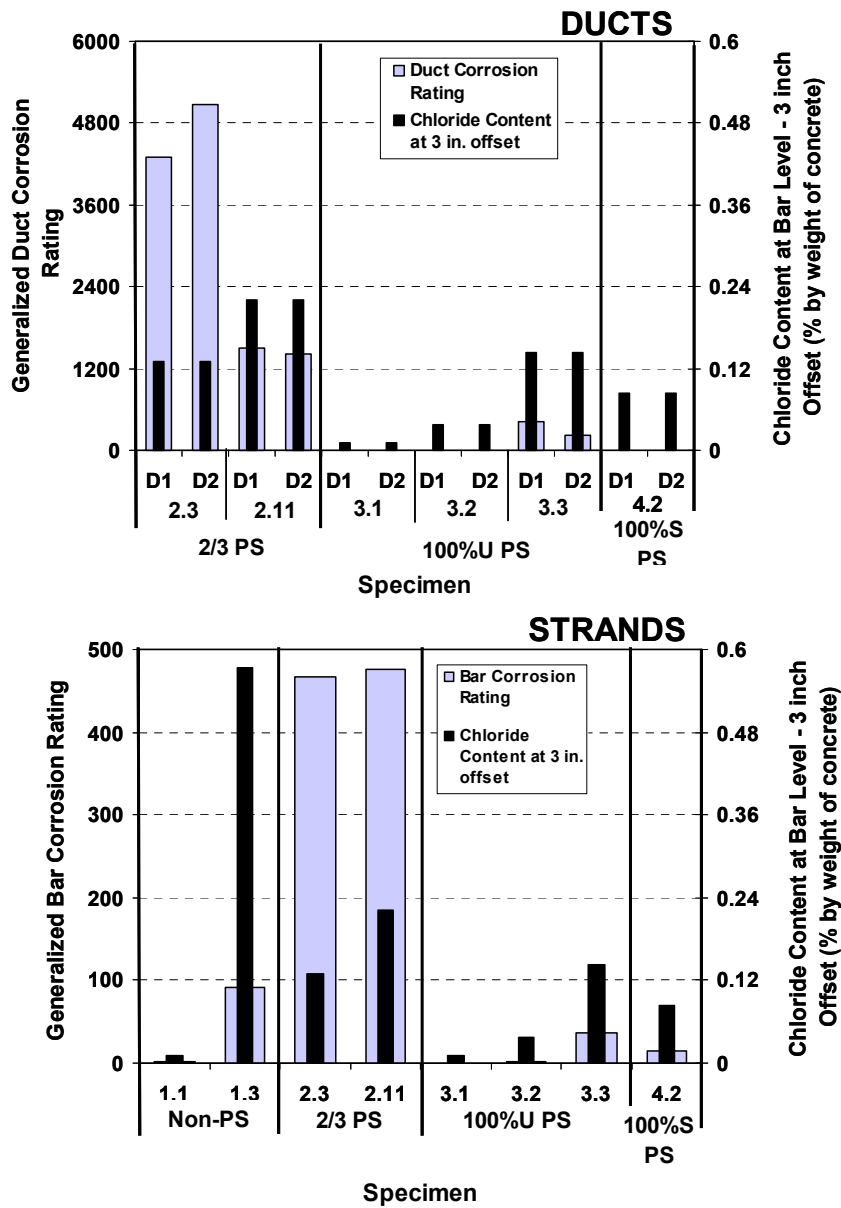
Figure 4.166 Acid-Soluble Chloride Content versus vs. Duct and Strand Corrosion Ratings for Phase I Autopsy Specimens
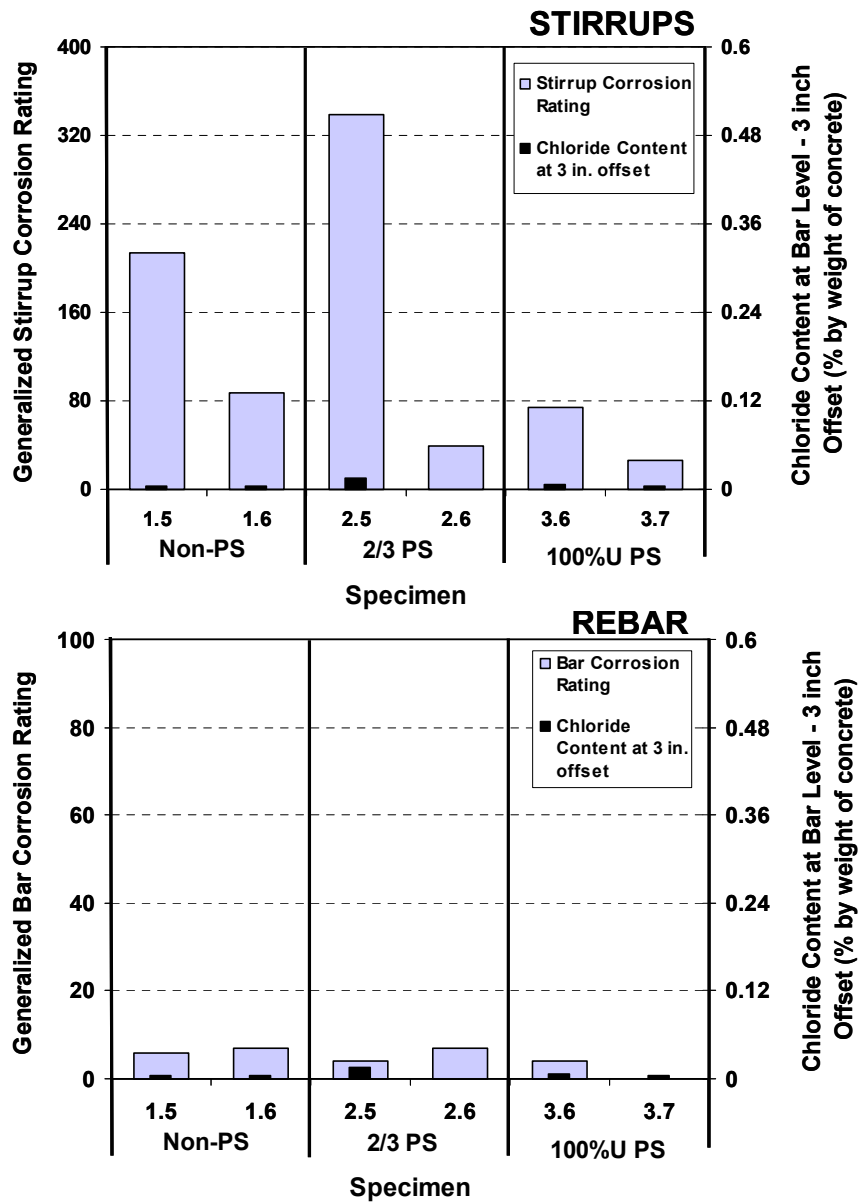
***Figure 4.167 Acid-Soluble Chloride Content versus vs. Stitrup and Rebar
Corrosion Ratings for Phase II Autopsy Specimens***

419
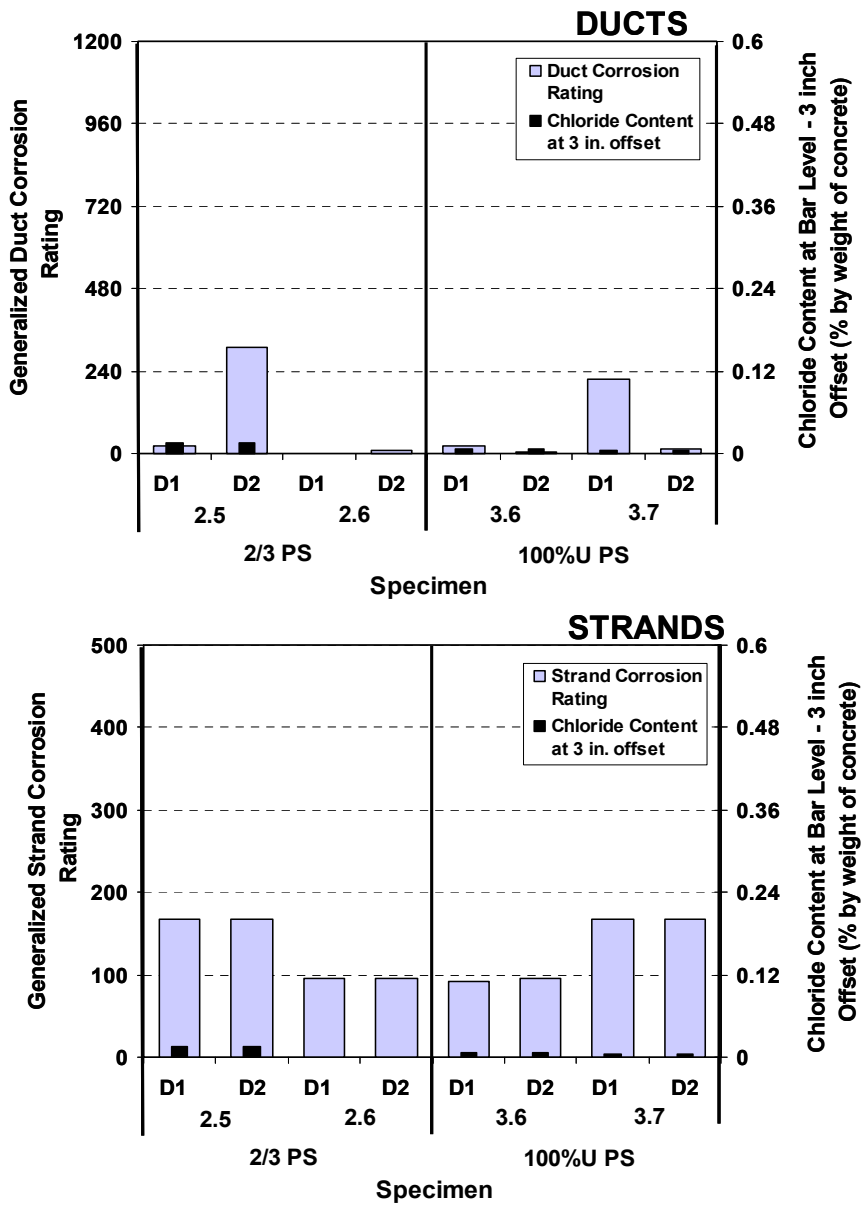
Figure 4.168 Acid-Soluble Chloride Content versus vs. Duct and Strand Corrosion Ratings for Phase II Autopsy Specimens

4.6.11 Final Full Autopsies

Exposure testing will continue for nearly half of the laboratory specimens, for several years, until signs of corrosion based on exposure testing results and visual inspection, are deemed enough to decide on final autopsy.   Table 4.24 shows the specimens to be compared and the main variables to be analyzed.

Table 4.24 Main Variables to be Analyzed During Final (Future) Autopsy of Beam Specimens

Beams to be compared	Variable to be analyzed
1.1, 1.2, 1.4 3.1, 3.5	loading / cracking
1.4, 2.4, 3.5, 4.1 2.1, 4.1 1.2, 2.1, 4.1 1.1, 3.1	level of prestress / cracking
1.9, 2.12	Duct type
3.4; 3.4, 3.5	splice damage
3.4, 3.5; 2.2; 2.8; 2.9; 3.1	splice type
2.9, 2.10	grout type / poor grouting procedure
2.7, 2.8, 2.9	strand type / strand coating damage
2.7, 2.9, 212	anchorage system / encapsulated system

4.7   SUMMARY AND CONCLUSIONS

Twelve out of the twenty-seven large scale beam specimens were fully autopsied to evaluate the effect of post-tensioning on durability and to evaluate the relative performance of a large number of corrosion protection variables. Two additional specimens were partially autopsied. Full autopsies for the remaining specimens will be performed at a future date. Beams were fabricated in two phases in order to begin exposure testing on a portion of the specimens while the remaining specimens were being fabricated. In Phase I (16 beams), which started exposure testing in December 1997, researchers investigated the effect of prestress level and crack width and also included one of the high performance grout specimens. In Phase II (11 beams), which started exposure testing in December 1998, researchers investigated duct splices, grout type, concrete type, strand type, duct type, and end anchorage protection. After the first full autopsy performed at four and a half years for six Phase I beams, and three and a half years for six Phase II beams, and partial autopsies performed to two Phase I beams, preliminary conclusions were drawn.

4.7.1   Overall Performance

The variables selected for evaluation in this beam testing program fall into four main categories: level of prestress and crack width, concrete type, prestressing strand coatings and post-tensioning hardware protection. In addition, different post-tensioning duct splices were also evaluated. After the initial autopsies of the fourteen beams, the use of large scale beam specimens was found to be a very good method for determining the effect of most of these variables. Prestressing strand coatings and post-tensioned hardware protection will be evaluated at a future date, since they are included in the remaining specimens

422

under exposure testing. Based on the autopsy performed to date, the following conclusions are drawn:

- Galvanized duct performed poorly. No plastic duct was used in the specimens of the first set of full autopsies.

- Bleed water voids were present in the ducts even after "good grouting procedures." Anti-bleed grout was not evaluated in the first set of full autopsies, but it is included in one of the remaining specimens for future autopsy.

- Voids from bleed water in grout were shown to be very detrimental to the duct.

- A clear trend was found with respect to cracking and mild steel corrosion. As cracking increased, stirrup and rebar corrosion increased. This trend was not clearly shown on strands, since strand ratings were all very low and close in value

- Mixed reinforcing (2/3 PS) beams showed the worst corrosion resistance. The best performance was obtained from 100%S PS specimens, followed by 100%U PS specimens

- Phase I beam results showed that there was a reduced risk of corrosion damage with increasing levels of prestress

- High performance concrete specimens (low permeability concrete, w/c=0.29), appear to perform better than class C fly ash concrete specimens. However, both appear to be effective in minimizing the chloride penetration through concrete

- Industry standard duct splices as well as heat shrink duct splices do not seem to provide adequate corrosion protection

- Duct splice damage did not show a direct correlation with the severity of corrosion

- No difference was found between normal and fly ash grout. Low strand corrosion ratings on all specimens after autopsy, did not allow clear identification of the effect of different types of grout

4.7.2 Load/Prestress Level versus Corrosion. The Effect of Cracking

The effect of cracking (width and number) on corrosion protection was an area of great emphasis in this experimental program. The effect of cracking was primarily investigated using standard variables and the sections that would be expected to crack under service loads. The range of crack widths investigated in this program were based on a survey of relevant literature performed by West[4.2] regarding critical crack widths for corrosion and recommended allowable crack widths. Consideration was also given to the applied moment-crack width behavior computed for the sections. Three different load levels were used: unloaded, service load, and temporary overloaded. The following conclusions are drawn:

- The specimen corrosion protection decreases as the applied load increases

- Corrosion protection decreases with increasing cracking

- An increase in transverse crack width produces a decrease in corrosion protection

- Longitudinal or splitting cracks in the concrete surface are a clear indication of very severe corrosion within the member.

- The chloride content in the concrete is significantly higher at crack locations, and increases as the crack width increases

- The specimen corrosion protection increases as the level of prestress increases

- Mixed reinforcement (2/3 PS) beams showed the worst corrosion performance. Increasing the post-tensioning level from 2/3 PS to 100% PS significantly increased the corrosion protection

424

- The corrosion protection of the 2/3 PS beam was much more similar to Non-PS beams, as opposed to 100% PS Beams
- There was not a clear difference in the corrosion resistance among the fully prestressed beams designed with the ultimate strength method as compared to those designed with allowable stress method.

4.7.3 Fly Ash in Concrete

Concrete plays an important role in corrosion protection of steel reinforcement. One of the objectives of this research program is to evaluate the effectiveness of high performance concrete as a function of cracking. Three different concrete mixes were selected for comparison. The reference mix was the standard concrete: TxDOT Class C concrete. The alternates were a TxDOT Class C concrete with 25% Class F Fly Ash and a High Performance Concrete (0.29 w/c, 25% fly ash+superplasticizer). The following conclusions are drawn:

- Both the high performance concrete and the fly ash concrete beams showed good corrosion protection by minimizing the chloride penetration through the concrete
- The high performance concrete tends to show a slightly better corrosion protection than the fly ash concrete, but the difference is not significant.
- No conclusions can be drawn on corrosion protection of the high performance concrete and the fly ash concrete with respect to the standard TxDOT concrete due to the unfortunate lack of directly comparable specimens at the time of the first autopsy.

4.7.4 Duct Splices for Galvanized Steel Duct

In most practical applications, the post-tensioning ducts must be spliced at some location. It was decided to compare industry standard (IS) splices to heat

425

shrink (HS) splices and unspliced duct. The effect of damaged splices was also examined. The IS splice consisted of a 1 ft length of oversized duct placed over the contact butt splice of the ducts. Concrete is prevented from entering the splice by wrapping the ends with duct tape. The heat shrink splice consists of a 8 inch length of heat shrink tubing placed over the contact butt splice of the ducts. The original diameter of the heat shrink tubing was 4 inches. No mechanical connection was made between the two ducts being connected. The conclusions are as follows:

- The industry standard splice allowed moisture and chlorides to enter through the sides of the splice and get trapped between the duct and the splice due to inefficiency of duct tape.

- The heat-shrink splice also allowed moisture to enter through the sides and get trapped due to insufficient adhesion between the splice and the duct. It also traps bleed water from the grout.

- Damage inflicted on the duct splices did not show a direct correlation with the severity of corrosion.

- Neither the industry standard splice nor the heat-shrink splice appears to be a satisfactory duct splice for the corrosion protection of a galvanized steel duct.

4.7.5   High Performance Fly Ash Grouts

Two high performance grouts (a fly ash grout and an antibleed grout) were selected for investigation, in comparison with TxDOT standard grout.   The fly ash grout specimen was autopsied, and results are reported herein.   The antibleed grout specimen will be autopsied at a future date. Antibleed grout had a water-cement ratio of 0.33 with 2% cement weight of antibleed admixture. Based on the information to date, the following conclusions are drawn:

426

- The fly ash grout aided in the corrosion protection of the galvanized steel ducts

- The fly ash grout, in comparison to TxDOT standard grout, did not show an increase in corrosion protection of the prestressing strand. This result may be due to the strand ratings being very low and close in value. Several more years of exposure testing may be required to yield more conclusive results

4.7.6 Exposure Testing Results

Half-cell potential readings were measured using a saturated calomel reference electrode at the end of each wet cycle (once every four weeks). All measurements were performed according to ASTM C876.[4.12] In general, half-cell potential readings are inadequate in determining the severity of corrosion activity, but prove to be successful for relative comparison of specimens. The conclusions are as follows:

- There is an exact correlation in specimen performance between the greatest negative potential at the end of testing for autopsy beams and the time to corrosion

- Both half cell potential readings and corrosion rating graphs show the loaded Non-PS and 2/3 PS beams were the most corroded.

- Half-cell potential readings did not show a distinct correlation in high performance and fly ash concrete specimens with the corresponding corrosion ratings.

Corrosion rate measurements were taken four times during the exposure duration. Two types of equipment were used in this experimental program: the Pr Monitor and the 3LP. Measurements of the Phase I beams were taken after seven, twelve, fifteen and forty-seven months of exposure. Measurements of the Phase II beams were taken after 37 months of exposure. A final attempt to take

427

corrosion rate measurements of all beams was made immediately prior to the forensic examination. This attempt was unsuccessful due to complications with the 3LP equipment. Corrosion rate readings did not show good correlation with forensic examination results. The presence of zinc in the galvanized steel ducts may have played a role in the erroneous results.

Chloride content was found to be a useful method in determining the onset of corrosion. However, there was not a direct relationship between the acid soluble chloride content at the bar/duct level and the severity of corrosion at time of autopsy.

4.8 RECOMMENDATIONS FOR FUTURE TESTING

The following recommendations are given for consideration in similar experimental programs:

- A smaller concrete cover may be used to accelerate the time to initiation of corrosion.
- Epoxy coated mild steel could be used to clearly separate and accelerate the corrosion of the post-tensioning system.
- Connection wires used to take half-cell potential readings and corrosion rate measurements should be protected against the outdoor environment, to avoid possible deterioration and corrosion that would increase resistivity.
- Add more control specimens or examine fewer variables.

4.9 IMPLEMENTATION OF RESULTS

After final autopsies of twelve out of twenty-seven beam specimens and partial autopsies of two beam specimens, research results generated the following findings. Final autopsies of the remaining beam specimens will be more conclusive for strand duct and grout types, and also for the use of encapsulated anchorage systems.

Post-tensioning Ducts

- Galvanized ducts should not be used in aggressive exposures.

Level of Prestress

- Mixed reinforcement members should not be used in aggressive exposures unless special provisions are made to effectively seal cracks and concrete cover from exposure to chlorides.

- Fully prestressed members are recommended in aggressive environments to delay moisture and chloride ingress.

- Post-tensioning systems need additional protection above the current typical practice when in aggressive environments. In particular the use of galvanized duct appears unwise. The use of plastic ducts and encapsulated anchorage protection systems appear promising but while plastic duct was clearly superior in the macrocell specimens the use in the beam specimens cannot be conclusively evaluated until after final autopsies of the remaining beam specimens.

Duct Splices for Galvanized Ducts

- Neither the standard industry practice of duct taped sleeves nor heat shrink splices should be considered as watertight

- Better systems than industry standard or heat-shrink splices for galvanized steel ducts should be investigated and developed if galvanized duct continues to be used in non-aggressive environments.

High Performance Fly Ash Grout

- Standard Class C grout with fly ash is not recommended.

- The use of antibleed admixture appear promising but cannot be conclusively evaluated until after final autopsies of the remaining beam specimens.

429

Concrete type

- High Performance Concrete is recommended in aggressive environments due to the significantly reduced permeability and crack control. Fly ash (Class C) concrete may also be considered when the environment is less aggressive.

Grouting Procedure

- Stringent grouting procedures should be enforced during construction.

Plastic Chairs

- Fully plastic chairs are recommended for use throughout the substructure to eliminate corrosion damage. Chairs or bolster strips that contain any steel should be avoided.

CHAPTER 5

Large Scale Column Corrosion Tests

Post-tensioned concrete piers or columns may be exposed to very severe environments affecting their long-term durability. Two main exposure conditions are of special interest: partially submerged structures in sea water and structures exposed to deicing salts. The durability study of post-tensioned columns or vertical concrete elements under these conditions have unique characteristics that require different tests, than the macrocell and beam tests described in the previous chapters. This chapter reports the procedures and results from long-term corrosion tests of large scale column elements.

5.1 BACKGROUND AND OBJECTIVES

Columns or piers in sea water are exposed to a very severe environment. This is especially the case for columns in the tidal zone (region between low and high tides) with periodic wetting and drying. In addition, above the high tide zone, the "wicking effect" (or capillary rise) may take place, which combined with periodic splashing, provide the conditions for aggressive chloride exposure (see Figure 5.1) and subsequent corrosion damage (see Figure 5.2).

Bridge piers on columns and like members in parking garages or other structures, may be subject to deicing salts that are applied to roadways in cold (ice and snow) environments. Depending on the ability of the drainage systems to evacuate run off from the top slabs and decks, these chlorides combined with water may trickle down the structures along the concrete faces, providing unfavorable conditions of intermittent moisture and chlorides.
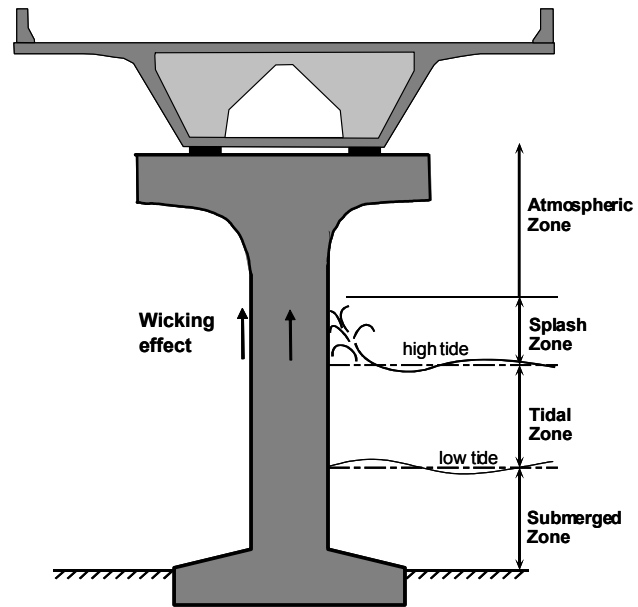
Figure 5.1 Exposure of Partially Submerged Column in Sea Water.

(a) Deicing Chemical Exposure
"Attack from Above"

(b) Coastal Saltwater Exposure
"Attack from Below"

Figure 5.2 Typical Corrosion Damage in Bridge Substructures.[5.1]

432

In order to provide detailed observations to improve the durability design of columns under these exposure conditions, a research study was started with the dual intent to evaluate how to use post-tensioning to improve corrosion protection and how to protect the post-tensioning systems from corrosion damage.

The column durability study was originally developed by West.[5.1] The specific objectives for this portion of the research were to investigate:

1. The effect of post-tensioning on concrete pier and column durability (corrosion protection) through precompression of the concrete and precompression of construction joints, and

2. The relative performance of various aspects of corrosion protection for post-tensioning, including concrete type, duct type, post-tensioning bar coatings and loading.

A total of ten large-scale column specimens were designed, constructed and placed under exposure testing by West and Larosche.[5.3] Exposure testing began in July 1996 and was performed by West, Larosche and Schokker until April 1999. Exposure testing was maintained by other graduate research assistants until August 2000, when the author took over responsibility for the exposure testing. Continued exposure testing was carried out until the author performed full autopsies, which began in January 2003, after six and a half years of accelerated exposure.

Test concept, variables, specimen types, materials, experimental set up, construction and exposure testing details were reported by West et al.[5.1, 5.3] In the following discussion, Section 5.2 include a summary of the most important aspects from West et al. report[5.3]. Sections 5.3 through 5.6 include the author's contribution to the research series with the final exposure testing results, autopsy findings, conclusions and recommendations.

5.2   EXPERIMENTAL PROGRAM

5.2.1   Test Specimen

Test specimens are circular cast-in place columns. The columns were patterned after standard Texas Department of Transportation (TxDOT) multicolumn substructures (see Figure 5.3).   The column dimensions and details were selected such that covers, reinforcement sizes and post-tensioning hardware were of similar order of magnitude as in practical applications, with consideration for construction and loading of the specimens.   A reduced nominal column diameter of 18 in. and reduced height of 6 ft were selected for the actual test specimens.

5.2.1.1   Design Loading

Typical bridge column reinforcement is based on minimum reinforcement requirements, and the nominal capacity of the column is usually well in excess of the design loading dictated by analysis of the bridge. Thus, it was decided to obtain design loading for a typical TxDOT multicolumn bridge substructure (see Figure 5.3), proportion the test specimen to meet minimum requirements and compare the column capacity against the design loading.   During testing, the columns would be subjected to the design loading, which would provide a more realistic representation of the typical case.

The prototype bridge substructure carried two lanes of traffic and one shoulder. The bent was skewed to the roadway alignment at 45 degrees. The superstructure consisted of five Type C precast, pretensioned bridge girders with a 75 ft span and a 8 in. thick cast-in-place concrete deck.

The three-column frame bent was analyzed using a plane frame analysis program. AASHTO LRFD was used for design loading on the bridge.

434
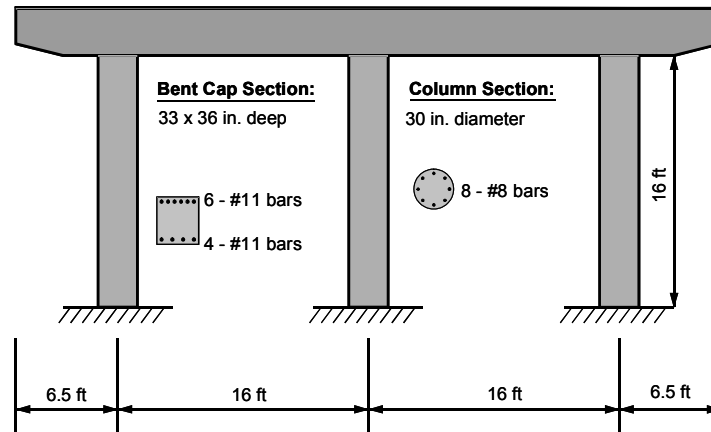
Figure 5.3 Prototype Multicolumn Substructure.[5.1]

The bent cap was divided into several segments and the analysis was performed to refine the end moments of inertia, either using the gross transformed moment of inertia or elastic cracked section moment of inertia (positive or negative bending). The frame was re-analyzed and the various combinations of axial load and moment for the columns were determined. The calculated forces for the outside columns are shown in Table 5.1. Loading on the substructure was not symmetric due to the shoulder. The critical combination was taken at the top of column 3, with the largest eccentricity.

Table 5.1 Calculated column forces for Prototype Substructure (unfactored).[5.1]

Location	Data	Column 1		Column 3	
Column Base	N_{max}	1781 kN	(400.4 kips)	994 kN	(223.4 kips)
	M_{max}	55.8 kN-m	(494.4 k-in.)	74.6 kN-m	(660.0 k-in.)
	e = M/N	30.5 mm	(1.2 in.)	76.2 mm	(3.0 in.)
Column Top	N_{max}	1716 kN	(385.7 kips)	**928 kN**	**(208.7 kips)**
	M_{max}	144.8 kN-m	(1281.6 k-in.)	**118.0 kN-m**	**(1044.0 k-in.)**
	e = M/N	83.8 mm	(3.3 in.)	**127 mm**	**(5.0 in.)**

The design loading from the prototype analysis was scaled for use with the column specimens. Axial forces are scaled by the square of the ratio of column diameters, following Equation 5.1. Bending moments are scaled by the cube of the ratio of column diameters, following Equation 5.2.

$$N_{specimen} = \left(\frac{D_{specimen}}{D_{prototype}}\right)^2 \times N_{prototype} = 75.2 \text{ kips}$$

Eq. 5.1

$$M_{specimen} = \left(\frac{D_{specimen}}{D_{prototype}}\right)^3 \times M_{prototype} = 225 \text{ kip in.}$$

Eq. 5.2

Assuming an average load factor of 1.5, the factored design forces are:

$$N_f = 112.6 \text{ kips}, \quad M_f = 338.6 \text{ kip in}$$

5.2.1.2   Reinforced Concrete Design

The smallest circular column used by TxDOT is 18 in. diameter. This column was selected as the nonprestressed or reinforced concrete design in the research program. The reinforced concrete section is shown in Figure 5.4.
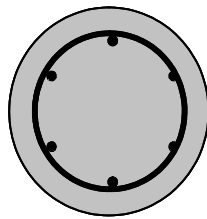
Main Reinforcement:
6 - #6 bars
Spiral:
#3 at 6 in. pitch
Column Diameter: 18 in.
Clear Cover to Spiral: 2 in.

Figure 5.4 Reinforced Concrete Column Section Details.[5.1]

The reinforced concrete (3600 psi) section was analyzed using a layer-by-layer strain compatibility section analysis technique to produce axial force-moment interaction diagrams, as shown in Figure 5.5. The factored resistance is well in excess of the factored loading.
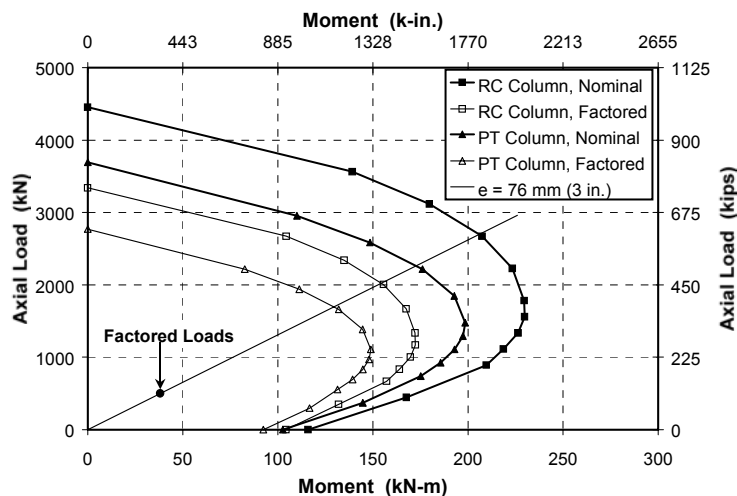
Figure 5.5 Column Interaction Diagrams[5.1]

The elastic decompression moment for the column was calculated for the design service loading, and was equal to 169 kip in. The service load moment of 225 kip in. exceeded the decompression moment.

5.2.1.3 Post-Tensioned Column Design

The design of the post-tensioned columns kept the same mild steel reinforcement (due to the need for confinement and concerns for creep) as the reinforced column design, and added four threaded prestressing bars (bars are often used instead of strands in columns). The four PT bars would provide continuity between the column and foundation, effectively developing the flexural capacity about more than one axis, and would increase the decompression moment, which could improve durability at construction joints.

437

A minimum effective prestress of 60% of ultimate (fpe =0.6 fpu) was used for design and analysis purposes.   The column section details are shown in Figure 5.6.
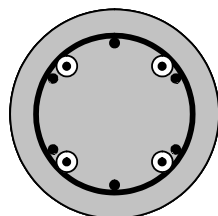
Main Reinforcement:
6 - #6 bars
4 – 5/8 in. PT bars
$f_{pe} = 0.6f_{pu}$

Spiral:
#3 at 6 in. pitch

Column Diameter: 18 in.
Clear Cover to Spiral: 2 in.

** Only PT bars provide continuity to foundation

Figure 5.6 Post-Tensioned Column Section Details.[5.1]

The decompression moment was calculated as 406 kip in. which exceeded the applied service moment of 225 kip in. by a considerable margin.

The post-tensioned column section was analyzed using the layer-by-layer strain compatibility analysis technique. A detailed description of the procedure is included in Reference 5.1. The calculated moment diagrams are also shown in Figure 5.5. The lower nominal capacity of the post-tensioned columns illustrates the effect of post-tensioning on the axial load carrying capacity of these elements. However, even with this reduction, the factored resistance of the post-tensioned columns far exceeded the factored loads.

Long-term prestress losses were calculated for periods of 500, 1000 and 1500 days, see details in Reference 5.1. Table 5.2 summarizes the results. Losses are not uniform in the loaded case due to the eccentric loading.   The calculated losses indicate that with an initial prestress of 0.68 fpu the effective prestress in the columns will meet or exceed the design value for an experiment duration longer than 1500 days.   The average initial prestress in the gross column section was about 500 psi.

438

Table 5.2 Long-Term Prestress Losses.[5.1]

Time Period (days)	Prestress Loss ΔF_{p1}	ΔF_{p2}
Case 1: Loaded, $f_{pi} = 0.68f_{pu}$		
500	10.7%	8.8%
1000	11.5%	9.6%
1500	11.9%	9.9%
Case 2: Unloaded, $f_{pi} = 0.68f_{pu}$		
500	7.8%	7.8%
1000	8.4%	8.4%
1500	8.8%	8.8%
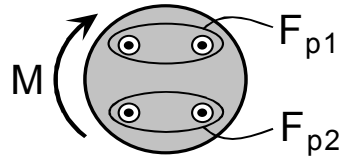
5.2.2 Variables

Variables selected for exploration fall into five main categories: Column to foundation joint, loading, concrete type, post-tensioning duct types and prestressing bar coatings.

5.2.2.1 Control Variables

Standard variables based on typical current TxDOT practice were defined to represent control cases. Table 5.3 summarizes the control variables used for the research study.

Table 5.3 Control variables based on TxDOT practice. [5.1]

Variable	Typical mix or material used.
Concrete	Based on TxDOT Specification Item 421, Tx DOT Class C concrete for bridge substructures, Maximum w/c ratio = 0.533, Maximum coarse aggregate size = 3/4 in., Retarder, Rheocrete 300-R, Entrained air admixture, 2 in. clear cover to main steel.
Cement Grout	Based on TxDOT Specification Item 426.3.4a w/c ratio = 0.44 Type I cement
PT Duct	Rigid galvanized steel duct.

5.2.2.2 Column to Foundation Connection

The construction joint between the column and foundation presents a possible weak link in corrosion protection since it represents a pre-formed crack that could open under loading. This problem is aggravated by the potential exposure conditions at the column foundation interface, since the cold joint could be directly exposed to moisture and chlorides in coastal and deicing chemical exposures. Selected configurations are shown in Figure 5.7. In this figure, reinforcing cages (mild steel) consisting on 6#6 longitudinal bars and #3 bar spiral at 6 in. pitch are shown. A two-inch cover was left at the base of the column and the reinforcing cage. Only dowels or post-tensioned bars crossed the joint.
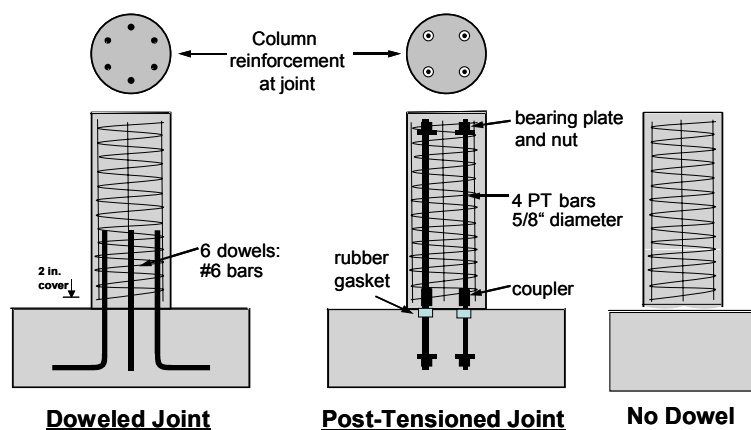
Figure 5.7 Column-Foundation Joint Configurations.[5.1]

5.2.2.3 Loading

Two loading conditions were considered: unloaded and service load. The columns were subjected to the combined axial load and moment conditions obtained from the prototype substructure analysis for the service load condition:

$$N_{service} = 75.2 \text{ kips}, \quad M_{service} = 225 \text{ kip in.}$$

The unloaded case was included since it could represent a worse case condition for allowing moisture and chloride penetration at the construction joint.

5.2.2.4   Concrete Type

TxDOT standard concrete mix was used in eight specimens. In two columns, 35% of cement by volume (31% replacement by weight) was replaced with fly ash (ASTM Class C), with no other significant changes to the concrete mix.

5.2.2.5   Post-Tensioning Ducts

Impermeable plastic ducts are compared directly within individual specimens to standard galvanized steel ducts, without duct splices, as shown in Figure 5.8. Uncoated post-tensioning bars were used in columns where duct type was evaluated.
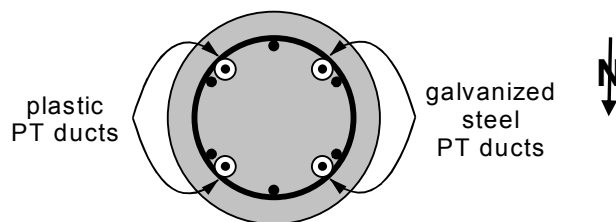
Note: PT bars are uncoated

***Figure 5.8 Comparison of Ducts Types for Post-Tensioning.*[5.1]**

A rubber gasket was placed around the protruding PT-bars in the top of the foundation to seal the dead ends of the ducts as shown in Figure 5.16. As it is discussed in Section 5.5 it was a serious error in the specimen definition not to splice ducts at this location.

5.2.2.6   *Prestressing Bar Coating*

Two prestressing bar coatings are investigated: Epoxy coated (according to ASTM A775-97) and zinc galvanized prestressing bars. The coated bars were compared directly to uncoated bars within individual specimens (see Figure 5.9). In both cases, anchorage hardware was either epoxy coated or galvanized. Nuts and couplers are proportioned to limit damage in epoxy coating or zinc coating.
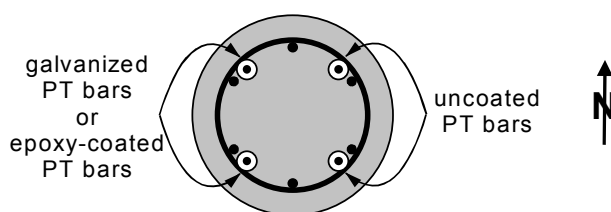
Note: all ducts are galvanized steel

Figure 5.9 Comparison of Prestressing Bar Coatings.[5.1]

5.2.3   Specimen Types

Ten specimens were used to address all selected variables, using the notation shown in Table 5.4. The complete experimental program is listed in Table 5.5.

Table 5.4 Specimen Notation.[5.1]

Connection Type	Loading	Concrete type	PT Protection
DJ: **Doweled Joint**	**N:** No Load	**TC:** TxDOT Class C	**PD:** Plastic Duct
PT: **Post-Tensioned Joint**			**EB:** Epoxy-Coated PT Bar**
NJ: **No dowel**	**S:**Service Load	**FA:** 35% Fly Ash	**GB:** Galvanized PT Bar**
			Blank: Not applicable (i.e., no PT)
Example: PT-TC-S-PD			

* plastic ducts used for bars 1 and 2, galvanized steel ducts used for bars 3 and 4

** epoxy-coated or galvanized bars used for bars 3 and 4, uncoated bars used for bars 1 and 2

Table 5.5 Column Specimen Types and Variables.[5.1]

Specimen	Foundation Connection	Concrete Type	Loading	PT Protection
1 DJ-TC-N	Doweled	Class C	Unloaded	n/a
2 PT-TC-N-PD	Post-tensioned	Class C	Unloaded	Plastic Duct
3 NJ-TC-N	No dowel	Class C	Unloaded	n/a
4 DJ-TC-S	Doweled	Class C	Service	n/a
5 PT-TC-S-PD	Post-tensioned	Class C	Service	Plastic Duct
6 NJ-TC-S	No dowel	Class C	Service	n/a
7 PT-TC-S-EB	Post-tensioned	Class C	Service	Epoxy-coated PT Bar
8 PT-TC-S-GB	Post-tensioned	Class C	Service	Galvanized PT Bar
9 DJ-FA-S	Doweled	35% Fly Ash	Service	n/a
10 PT-FA-S-PD	Post-tensioned	35% Fly Ash	Service	Plastic Duct

5.2.4   Materials

The materials used in the column corrosion tests are summarized in Table 5.6.

Table 5.6 Column Construction Material Details.[5.1]

Item	Description

Column Concrete: Texas DOT Class C Concrete for Bridge Substructures	• w/c = 0.45 (based on slump, max. allowable w/c = 0.53)
	• f'c = 3600 psi minimum allowable
	• batch proportions: (per 1 yd³)
	     Coarse Aggregate (3/4 in.) 1877 lbs
	     Fine Aggregate 1186 lbs
	     Type I/II Cement 564 lbs
	     Water 254 lbs
	     Set retarder 24 oz
	     Entrained Air Admixture 4 oz
	• cylinder strengths: 7-day 4358 psi
	     (average) 14-day 5250 psi
	      28-day 5284 psi

Table 5.6 (Continued) Column Construction Material Details.[5.1]

Item	Description

Column Concrete: Texas DOT Class C Concrete with 31% Fly Ash by Weight	• w/(c +p) = 0.42
	• f'c = 3600 psi minimum allowable
	• batch proportions: (per 1 yd^3)
	    Coarse Aggregate (3/4 in.) 1855 lbs
	    Fine Aggregate 1245 lbs
	    Type I/II Cement 362 lbs
	    Class C Fly Ash 162 lbs
	    Water 220 lbs
	    Set retarder 20.0 oz
	    Entrained Air Admixture 3.5 oz
	• cylinder strengths: 7-day 4447 psi
	  (average) 28-day 6473 psi

Foundation Concrete Mix 1 (for RC Columns, Capitol Aggregates Mix 241)	• w/(c + p) = 0.39
	• f'c = 8000 psi design strength
	• batch proportions: (per 1 yd^3)
	    Coarse Aggregate (3/4 in.) 1790 lbs
	    Fine Aggregate 1131 lbs
	    Type I/II Cement 525 lbs
	    Class C Fly Ash 225 lbs
	    Water 295 lbs
	    Set Retarder 22.5 oz
	• avg. cylinder strengths: 28-day 6220 psi

Foundation Concrete Mix 2 (for PT Columns, Capitol Aggregates Mix 246)	• w/(c + p) = 0.25
	• f'c = 14,000 psi design strength
	• batch proportions: (per 0.764 m^3 (1 yd^3))
	    Coarse Aggregate (0.5 in.) 1665 lbs
	    Fine Aggregate 1371 lbs
	    Type I/II Cement 714 lbs
	    Class C Fly Ash 254 lbs
	    Water 240 lbs
	    Superplasticizer 160 oz
	• cylinder strengths: 7-day 5102 psi
	  (average) 14-day 7536 psi
	            28-day 8478 psi

TxDOT Grout for Post-Tensioning	• w/c = 0.44
	• batch proportions: (per 1 ft^3)
	    Type I Cement 82.4 lbs
	    Water 36.2 lbs

Threaded Prestressing Bars	• 5/8 in. diameter high strength threaded prestressing bar • Grade 157 (157 ksi) • Supplier: Dywidag Systems, Inc.
Mild Steel Reinforcement	• ASTM A615, Grade 60 (60 ksi)

444

Table 5.6 (Continued) Column Construction Material Details.[5.1]

Item	Description
Steel Duct	• Corrugated, semi-rigid, galvanized steel duct • 1.575 in. outside diameter • Supplier: Dywidag Systems, Inc.
Plastic Duct	• Corrugated, flexible plastic duct • 2 in. outside diameter • Supplier: Dywidag Systems, Inc.
Epoxy Bonding Agent	• Sikadur 32 High-Mod - Epoxy Bonding Adhesive • Supplier: Sika

Cylinder compressive strengths are included in Tables 5.7 and 5.8. Foundation concrete strengths did not reach their design values, but were deemed sufficient. Grout for post-tensioning was not sampled for strength testing, as such testing is not required by TxDOT specifications.

Table 5.7 TxDOT Class C Concrete Cylinder Strengths.[5.1]

Column Numbers	Average Cylinder Strength		
	7 Day	**14 Day**	**28 Day**
1, 3, 4, 6	33.0 MPa (4791 psi)	42.6 MPa (6177 psi)	42.0 MPa (6091 psi)
2, 5, 9, 10	27.0 MPa (3924 psi)	29.8 MPa (4324 psi)	30.9 MPa (4478 psi)
Averages	30.0 MPa (4358 psi)	36.2 MPa (5250 psi)	36.4 MPa (5284 psi)

Table 5.8 FlyAsh (35%) Concrete Cylinder Strengths.[5.1]

Column Numbers	Average Cylinder Strength		
	7 Day	**14 Day**	**28 Day**
7	35.2 MPa (5107 psi)	41.6 MPa (6028 psi)	46.2 MPa (6706 psi)
8	26.1 MPa (3788 psi)	n/a	43.0 MPa (6240 psi)
Averages	30.7 MPa (4447 psi)	n/a	44.6 MPa (6473 psi)

5.2.5 Experimental Setup

The experimental setup was designed to meet the following requirements:

- Provide a realistic simulated foundation for the column specimens
- Permit loading of the columns
- Accommodate exposure conditions consisting of salt water continuously ponded around column base and regular application of saltwater to one face of columns (dripper system)

The experimental setup is shown in Figures 5.10 and 5.11. The dripper system is shown in Figure 5.12.
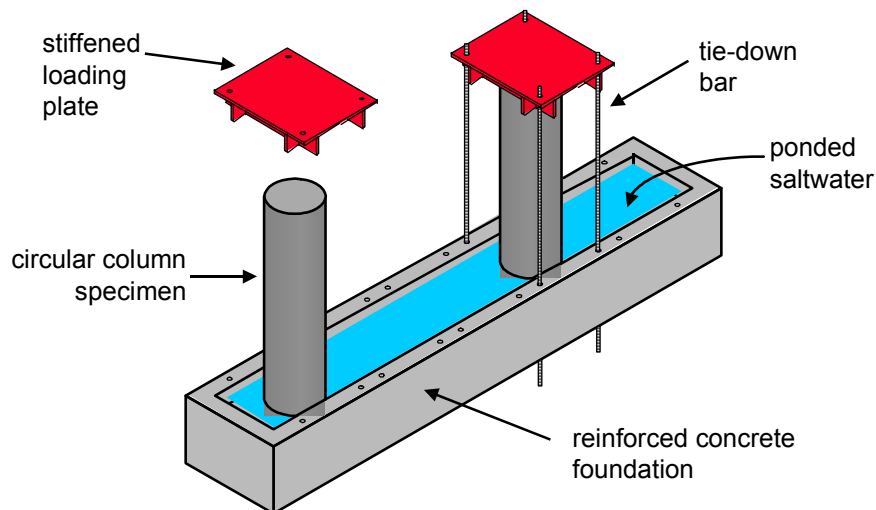
Figure 5.10 Column Corrosion Test Setup – Schematic.[5.1]

The dimensions of the reinforced concrete foundation (designed using a strut and tie model) were 15.33 ft long, 36 in. wide and 18 in. high, with a 6 x 6 in. curb along the perimeter of the top surface to contain ponded saltwater. Loading was applied on the columns using a stiffened loading plate on top of the column and four-one inch threaded prestressing bars. The forces in the bars were adjusted to apply the desired moment and axial force.

446

Figure 5.11 Column Corrosion Test Setup.[5.1]

All foundation reinforcement was epoxy-coated to prolong the life of the foundation. The top surface and curbs of the foundation were painted with swimming pool paint to improve water –tightness of the ponded area. Details of the foundation reinforcement and loading plates are included in Reference 5.1.

The loading system was treated as external prestressing in the column calculations, and loading force losses were estimated for various time periods. Loading force losses were small, 6.6% for post-tensioned columns and 3.6% for reinforced concrete columns, in the period of 500 days from first loading. For this reason, it was decided to simplify the loading system and not use springs, readjusting periodically the loading forces on the columns.

5.2.5.1 Exposure Conditions

Exposure testing consisted of saltwater based on ASTM G109 (3.5% NaCl in tap water), continuously ponded around the base of the columns to simulate a

447

coastal exposure.   To simulate deicing salts dripping from the superstructure or saltwater spray, a dripper system was placed on one face of each column, as shown in Figure 5.12.   Saltwater was pumped for a period of six to eight hours every two weeks, controlling equal flow rates to each column.
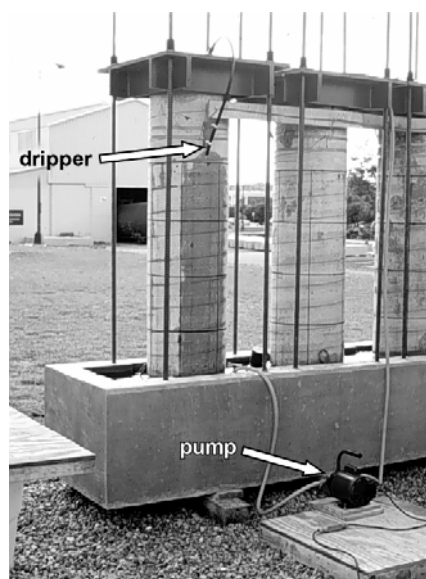
Figure 5.12 Column Dripper System. [5.1]
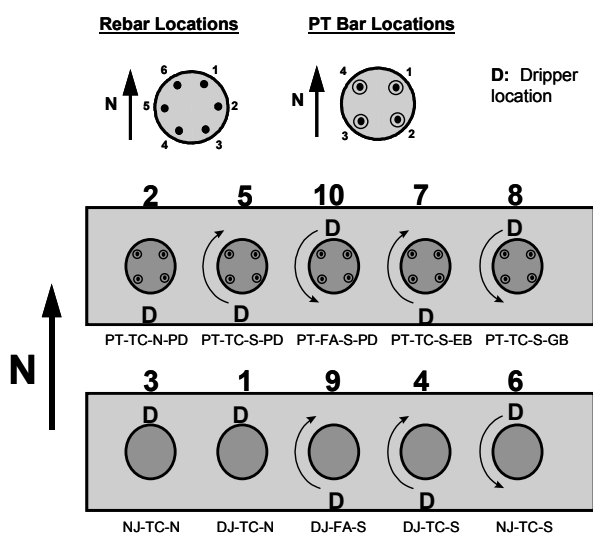
Figure 5.13 Specimen Location Specimen Details. [5.1]

5.2.5.2   Specimen Location

The specimen location on two foundations is shown in Figure 5.13.   The mild steel bars and post-tensioning bars were numbered according to the scheme shown.   The curved arrows in the figure indicate the direction of applied moment on each column. Columns without arrows were not loaded. The dripper was located on the tension side for the loaded columns.

5.2.6 Specimen Fabrication

Column foundations were constructed inside the Ferguson Laboratory. Once the foundations had been cast, column reinforcement and post-tensioning hardware was assembled. Each foundation was then transported and placed in the final location and the columns were cast in place, post-tensioned and loaded. A detailed description of the construction process is included in Reference 5.3. Photos of foundation and column fabrication are shown in Figures 5.14 and 5.15.

Top View   *End view*
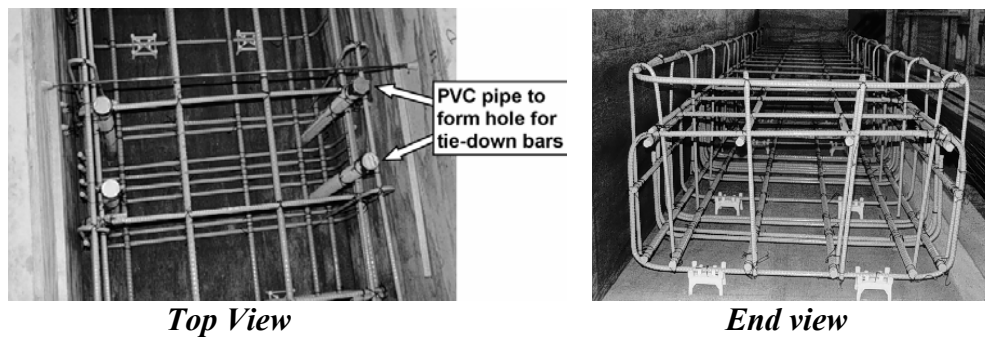
Figure 5.14 Foundation Reinforcement.[5.2]

Column Reinforcement on Foundation   *Pouring Column Concrete*
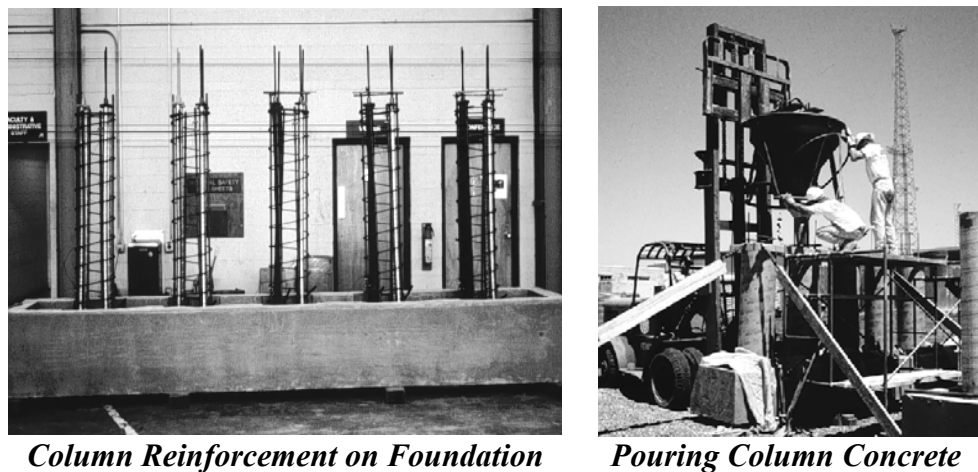
Figure 5.15 Column Construction.[5.2]

As shown in Figure 5.16, short lengths of post-tensioning bar were cast into the foundation to provide anchorage for the column post-tensioning bars. Shallow, square pockets were formed around each bar to accommodate rubber gaskets to seal the "dead end" of the post-tensioning ducts. The column post-tensioning bars were coupled to the protruding bars prior to placement of the ducts. Ground clamps were used to attach ground wires for measurements of potentials to the post-tensioning bar ends prior to capping.
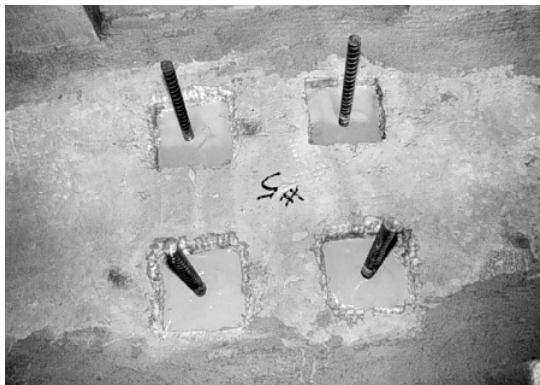
PT Bars Protruding from Foundation
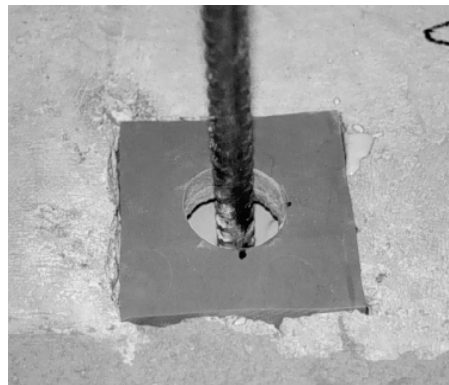
Gasket Around Post-Tensioning Bar
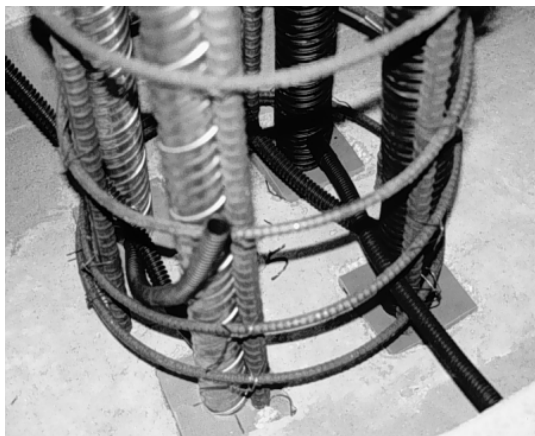
Reinforcement, Ducts and Grout Tubes

Top of Column Prior to Capping

Figure 5.16 Column Post-Tensioning Details.[5.2]

Losses during stressing were negligible. The post-tensioning jacking force, F_{pj}, was taken equal to the initial prestress force, F_{pi} ($0.68f_{pu}A_{pbar}$=30 kips). Each bar was post-tensioned individually, monitoring the post-tensioning force during stressing with a load cell and by a pressure gauge on the hydraulic pump (see Figure 5.17).

Grouting was done immediately after post-tensioning, all according to TxDOT Specifications. Grouts were mixed in large buckets using a paddle mixer mounted on a large hand held drill, and pumped immediately using an electric grout pump, until a continuous flow of grout was exiting the vent. Figure 5.18 shows the inlet and vent for grouting.
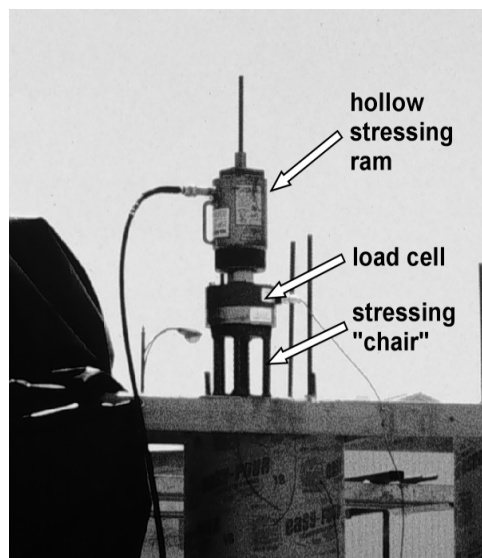
Figure 5.17 Column Post-Tensioning.[5.1]
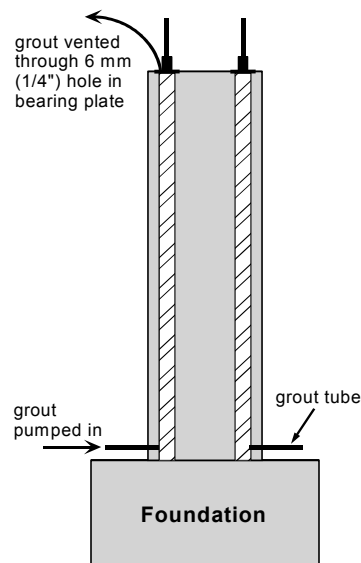
Figure 5.18 Inlet and Vent for Grouting.[5.1]

An important caution was suggested by West et al.[5.1] after grouting: "..after the column grouting had been completed, the possibility of an error in the post-tensioning grout came to light. It is possible that incorrectly labeled cement barrels may have resulted in partial or complete cement replacement with Class F

fly ash. The amount of fly ash, if any, is not certain. If the fly ash content is high, very little hydration will have occurred. The effect of this uncertainty on the experimental results is not certain. Persons performing invasive inspections or autopsies on the columns should be aware of the possibility of fly ash in the grout. The most likely columns to contain fly ash grout are PT-TC-S-EB and PT-TC-S-GB."

5.2.7   Specimen Loading

Column loading was performed using the loading system shown in Figure 5.19. The applied forces are shown in Figure 5.20. A separate hydraulic pump was used for each ram, and the forces T1 and T2 were applied simultaneously in four increments of 22% and a final increment of 12%. Tie-down bar nuts were tightened to refusal using a large wrench once the desired forces had been attained.
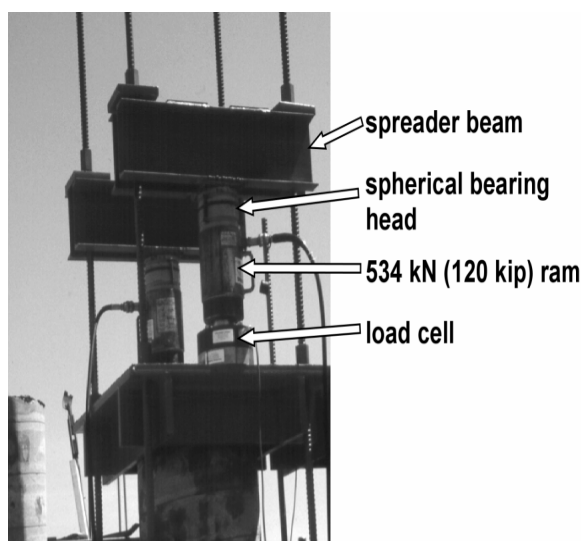
Figure 5.19 Loading System.[5.1]   Figure 5.20 Column Loading Forces. [5.1]
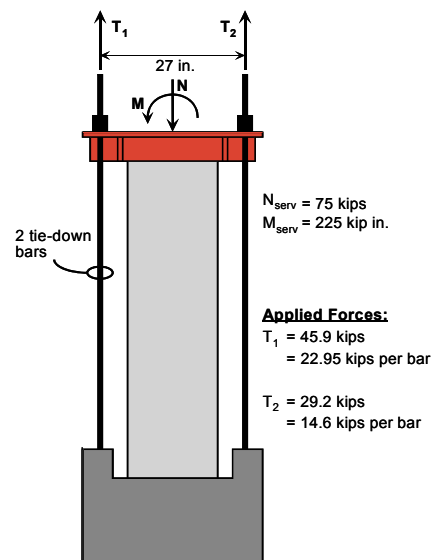
5.2.8   Measurements during Exposure Testing

Specimen monitoring during exposure testing included half-cell potential measurements every four weeks, periodic visual inspection for signs of corrosion and distress, and chloride samples taken occasionally to monitor chloride ingress at various depths and heights.

5.2.8.1   Half-Cell Potential Readings

Half-Cell (HC) potentials were measured against a Saturated Calomel Electrode (SCE), once a month, according to ASTM C876.[5.4] The numerical significance of the HC potential readings for normal reinforcing is shown in Table 5.9. The voltmeter was connected to the reinforcing cage using a wire that was left attached to the reinforcing cage prior to concrete casting.   Figure 5.21 shows the reinforcement placement, and level numbering for HC readings. The readings were taken on three out of six reinforcing bars (labeled 1, 3 and 6) and on all four post-tensioning bars at three different heights (labeled levels 1, 3 and 5) in the column.

Standard ASTM C876 was developed for uncoated reinforcement steel, and therefore, the values reported in Table 5.9 may not necessarily be appropriate for grouted prestressing bars (coated or uncoated) in concrete.

Table 5.9 Interpretation of Half Cell Potentials for
Uncoated Reinforcing Steel [5.4]

Measured Potential (vs SCE)	Probability of Corrosion
more positive than –130 mV	less than 10% probability of corrosion
Between -130 mV and –280 mV	corrosion activity uncertain
more negative than –280 mV	greater than 90% probability of corrosion

453

5.2.8.2   Chloride Penetration

Chloride samples were taken periodically from specimens representing each concrete type, joint type, and load level. Powder samples were taken at three depths: 0.5 in, 1 in., and 2 in. The two-inch depth data represent the chloride concentration at the bar level. The chloride samples are also taken at three heights to investigate possible "wicking" effects: 3 in., 9 in., and 15 in., as shown in Figure 5.21. The three-inch height represents the constantly submerged concrete. Each sample is taken from two locations and the powder is combined to give a representative sample.
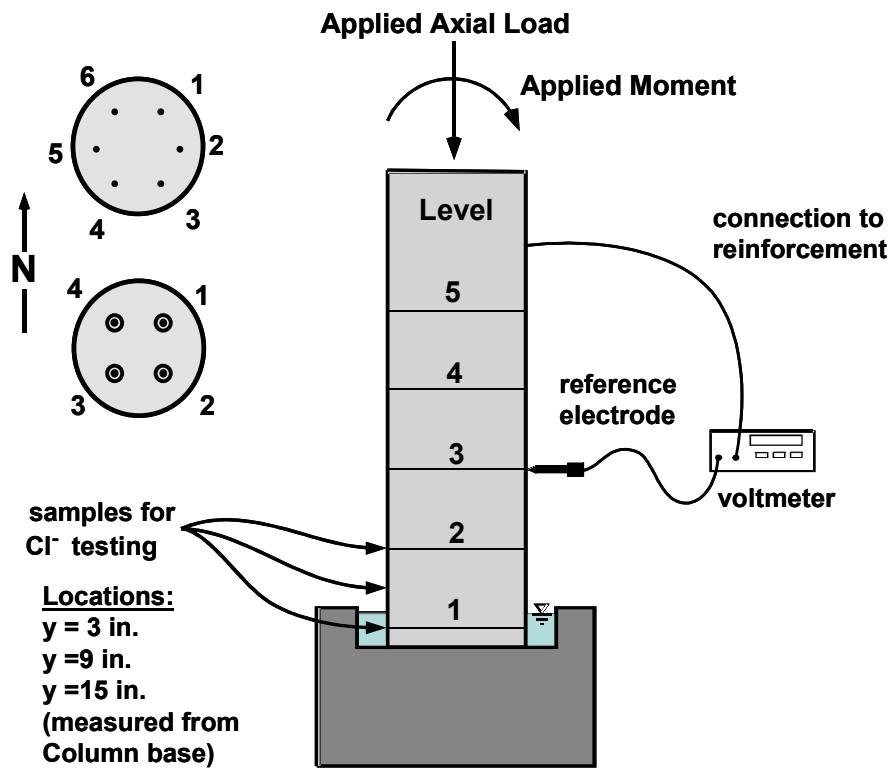
Figure 5.21 Numbering and Locations for Half-Cell Potential Measurements and Chloride Samples (adapted from ref. 1 and 2).

5.3   EXPOSURE TEST RESULTS

Exposure testing started in July 1996 and ended in January 2003, after 2367 days (six and a half years).   During this period, half-cell potential measurements and chloride samples were taken periodically, except between 1361 days and 1648 days of testing when half-cell readings were interrupted. During this interruption, specimens remained continuously ponded around the column base, without the application of saltwater to the face of the columns (dripper system).

5.3.1   Half-Cell Potential Readings

Half-Cell (HC) potential plots were developed for all specimens. Two types of data are plotted for each non-prestressed specimen:

- All Half-Cell Potentials: Potentials measured for each reinforcing bar at each level (level 1 – bottom, level 2 – mid-height, level 3 – top). Figure 5.22 and Figure 5.23 show "all" Half-Cell Potentials for specimens NJ-TC-N and DJ-TC-N. Plots for the other non-prestressed specimens are included in Appendix C.
- Average Half-Cell Potentials: Average potentials for all bars at each level (level 1 – bottom, level 2 – mid-height, level 3 – top). "Average" half cell potentials are included in Appendix C.

For post-tensioned specimens, four types of data were plotted:

- All Half-Cell Potentials (**Rebar**): Potentials measured for each reinforcing bar at each level (level 1 – bottom, level 2 – mid-height, level 3 – top). Figure 5.24 shows "all" Half-Cell potentials for specimen PT-TC-N-PD.   HC-Plots for other post-tensioned specimens are included in Appendix C.

455

- Average Half-Cell Potentials (**Rebar**): Average potentials for all reinforcing bars at each level (level 1 – bottom, level 2 – mid-height, level 3 – top). See HC Potential plots in Appendix C.

- All Half-Cell Potentials (**PT-Bars**): Potentials measured for each PT-Bar at each level (level 1 – bottom, level 2 – mid-height, level 3 – top). Figure 5.25 shows "all" Half-Cell Potentials for post-tensioning bars in specimen PT-TC-N-PD. Plots for all other post-tensioning specimens are included in Appendix C.

- Average Half-Cell Potentials (**PT-Bars**): Average potentials for PT-Bars #1 and #2, and Average potentials for PT-Bars #3 and #4. See plots in Appendix C.

Each post-tensioned specimen has two plain post-tensioning bars or ducts and two bars or ducts that investigate a protection variable. For these reason, average values were obtain in pairs (ducts #1 and #2, and ducts #3 and #4; or, PT-bar #1 and #2, and PT-bar #3 and #4). Each variable is clearly separated for each specimen in the plots.

Specimens are also compared relatively to each other on the same plot. Three types of comparison plots were constructed:

- Average Half-Cell Potentials (**Rebar**) at Level 1, Level 3 and Level 5 in Non-Prestressed Columns. See Figure 5.26 through Figure 5.28.

- Average Half-Cell Potentials (**Rebar**) at Level 1, Level 3 and Level 5 in Post-Tensioned Columns. See Figure 5.29 through Figure 5.31.

- Average Half-Cell Potentials (**PT Bars**) (grouped in pairs #1,#2 and #3,#4), at Level 1, Level 3 and Level 5 in Post-Tensioned Columns. See Figure 5.32 through Figure 5.34.

456

In these plots, ASTM C876[5.4] corrosion threshold values are shown for reference.

Table 5.10 shows a summary of the probability of corrosion for reinforcing bars in non-prestressed columns, at levels 1, 2 and 3. In a similar manner, Table 5.11 shows a summary of the probability of corrosion for reinforcing bars and post-tensioned bars in PT-columns, at the same three levels 1, 3 and 5.
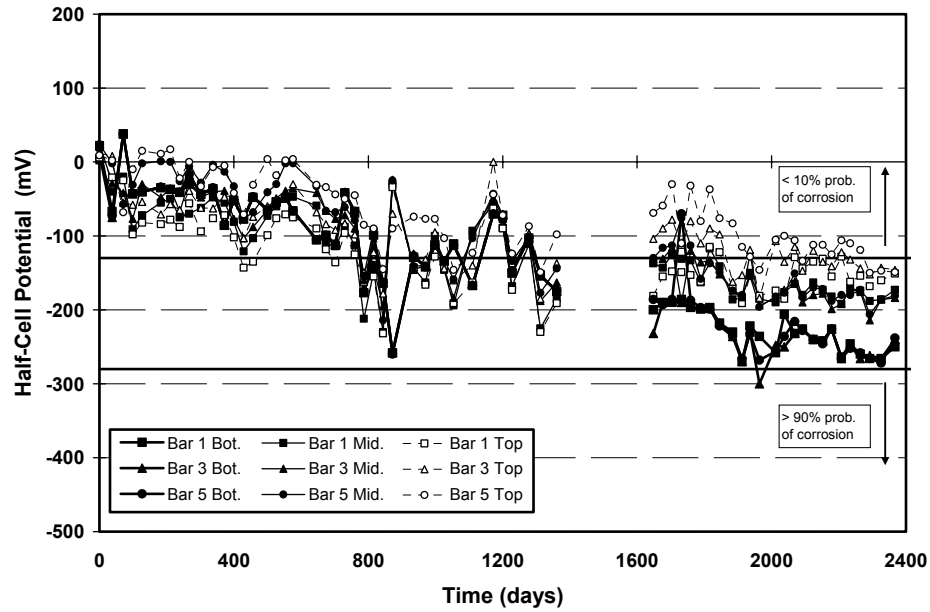
Figure 5.22 All Half-Cell Potential Readings: Column NJ-TC-N
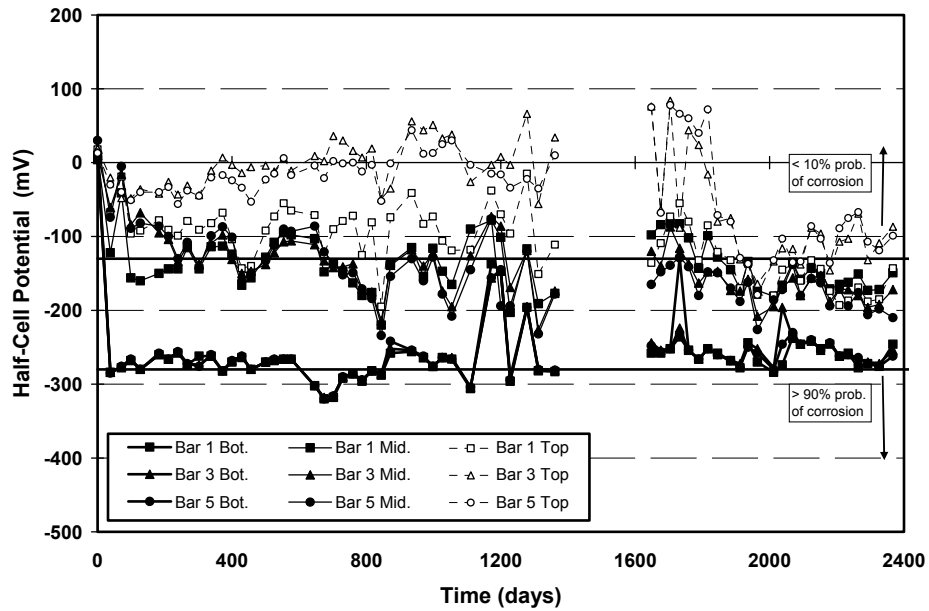
Figure 5.23 All Half-Cell Potential Readings: Column DJ-TC-N
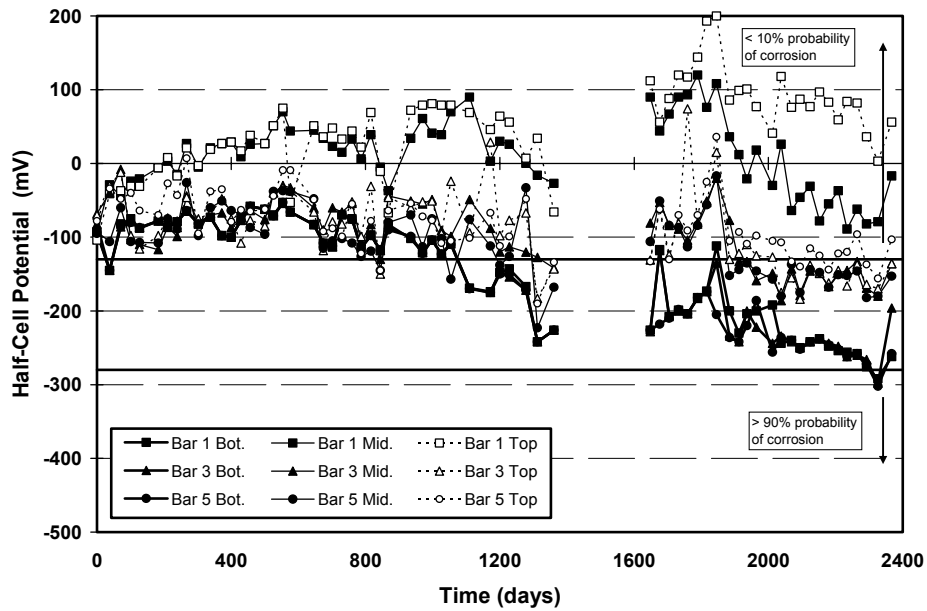
Figure 5.24 All Half-Cell Potential Readings: Column PT-TC-N-PD – Rebar

458
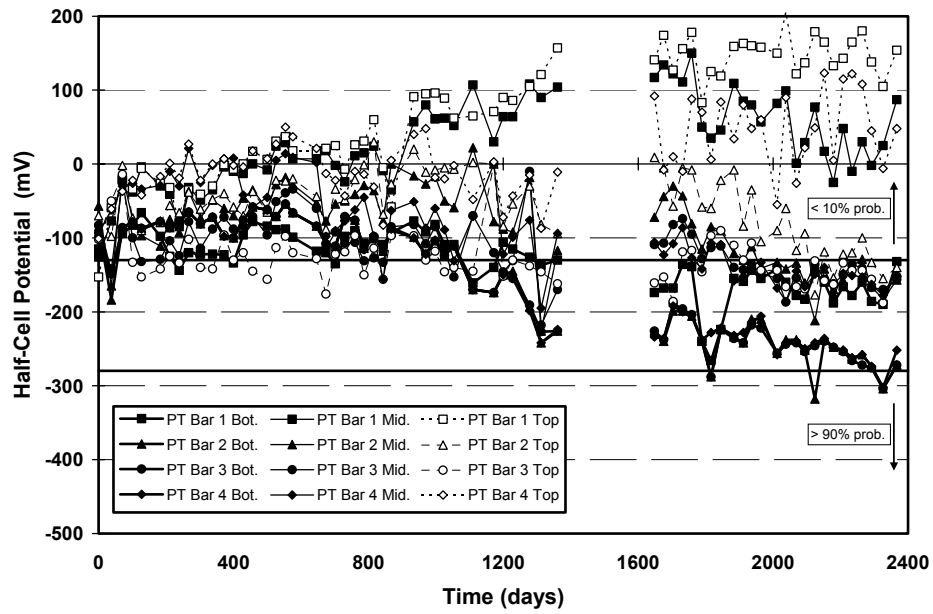
Figure 5.25 All Half-Cell Potential Readings: Column PT-TC-N-PD – PT Bars
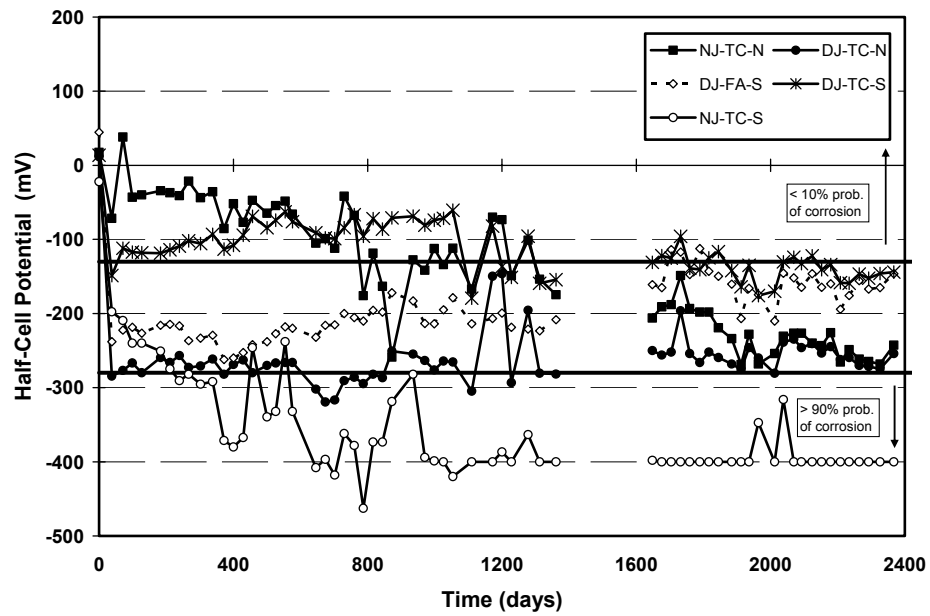
Figure 5.26 Average Half-Cell Potential Readings at Column Base (Level 1): Non-Prestressed Columns

459
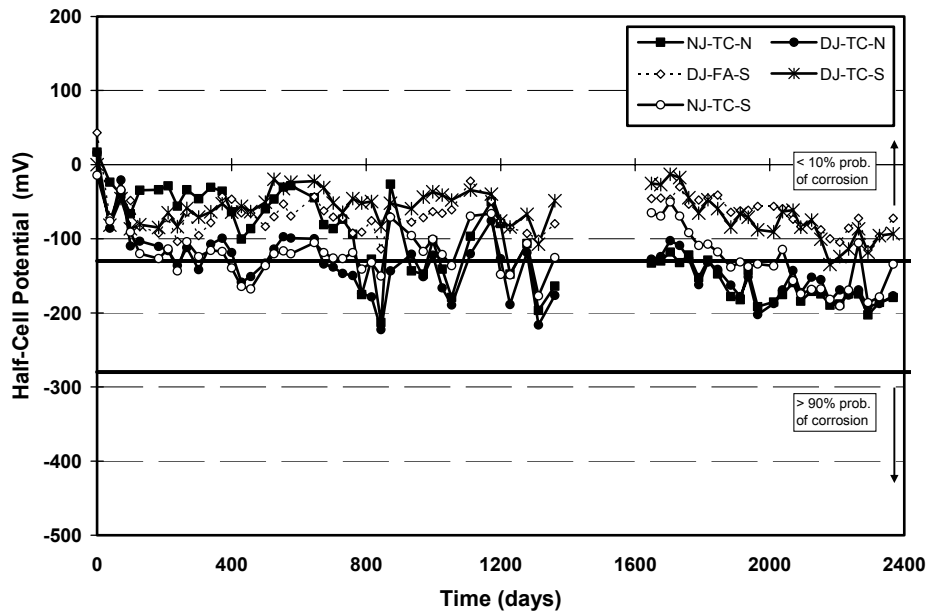
Figure 5.27 Average Half-Cell Potential Readings at
Column Mid-height (Level 3): Non-Prestressed Columns
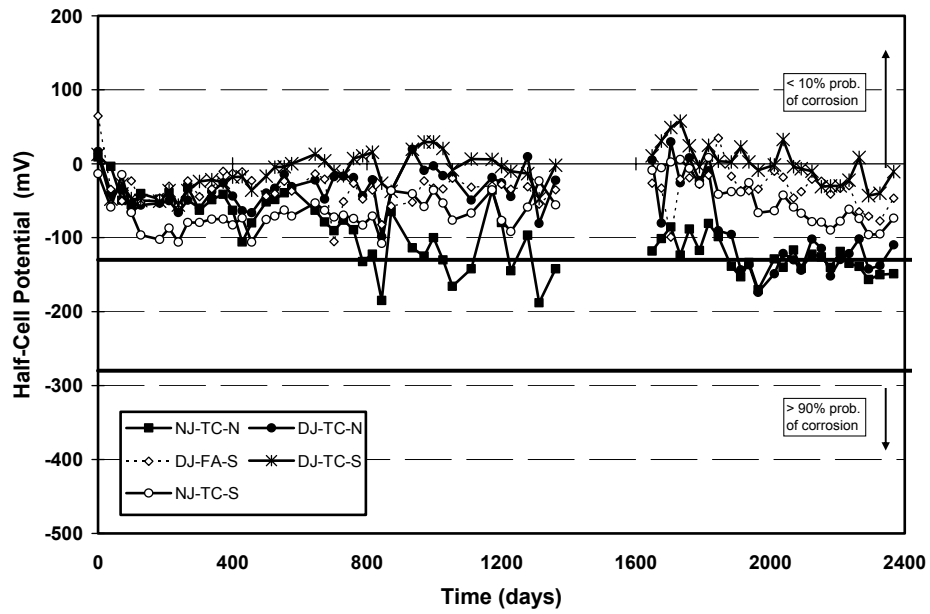
Figure 5.28 Average Half-Cell Potential Readings at
Top of Column (Level 5): Non-Prestressed Columns
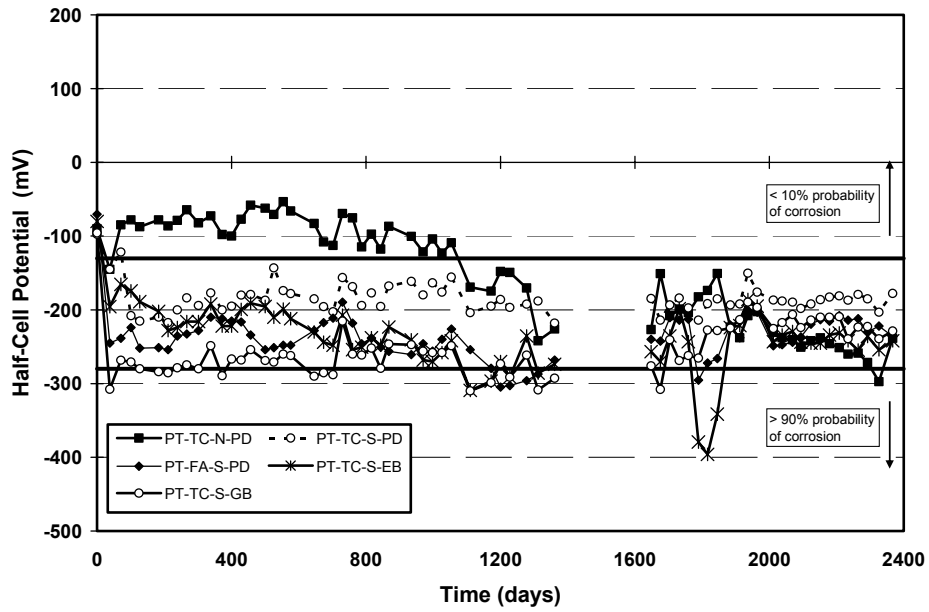
***Figure 5.29 Average Half-Cell Potential Readings at
Column Base (Level 1): PT Columns – Rebar***
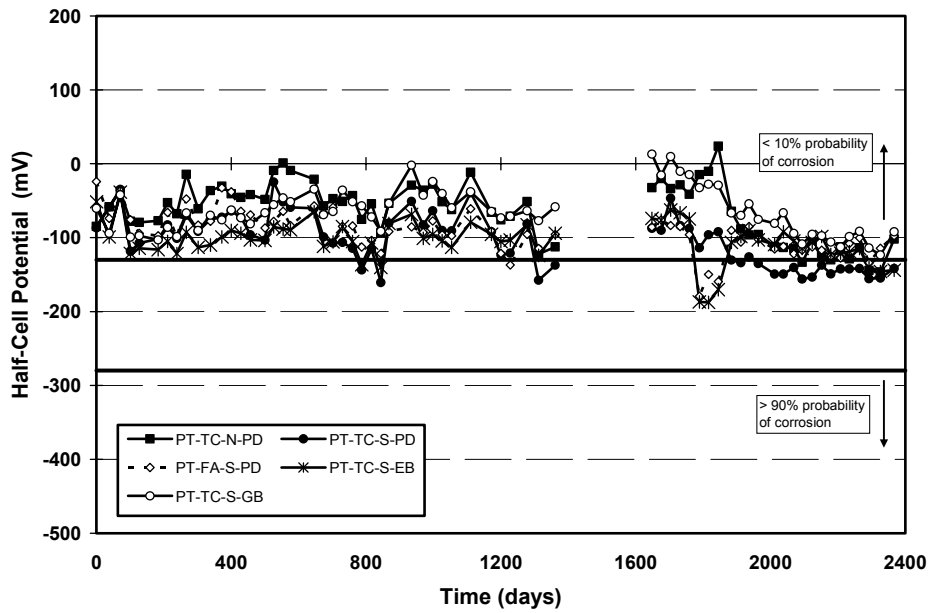
***Figure 5.30 Average Half-Cell Potential Readings at
Column Mid-Height (Level 3): PT Columns – Rebar***

461
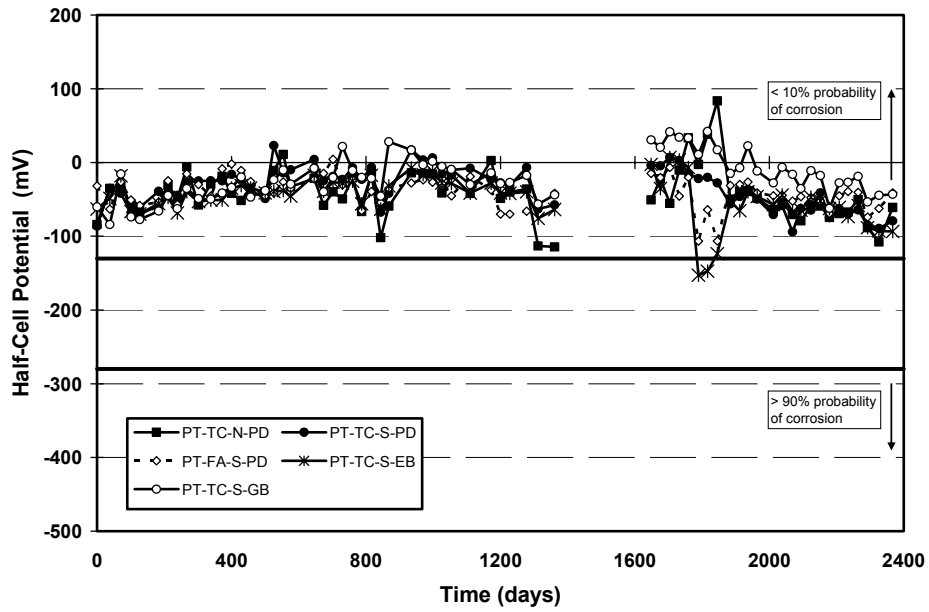
***Figure 5.31 Average Half-Cell Potential Readings at
Top of Column (Level 5): PT Columns – Rebar***
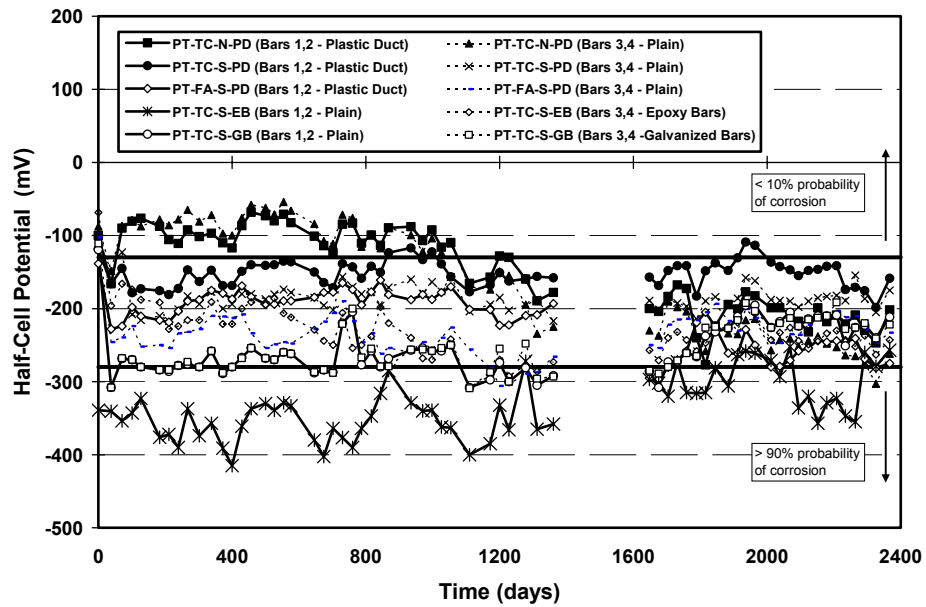
***Figure 5.32 Average Half-Cell Potential Readings at
Column Base (Level 1): PT Columns – PT Bars***

462
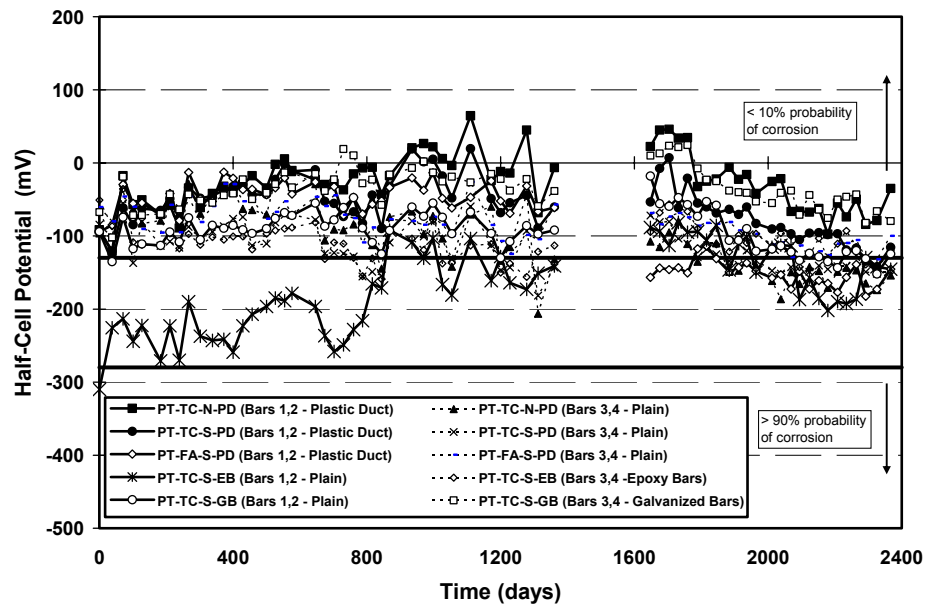
Figure 5.33 Average Half-Cell Potential Readings at Column Mid-Height (Level 3): PT Columns – PT Bars
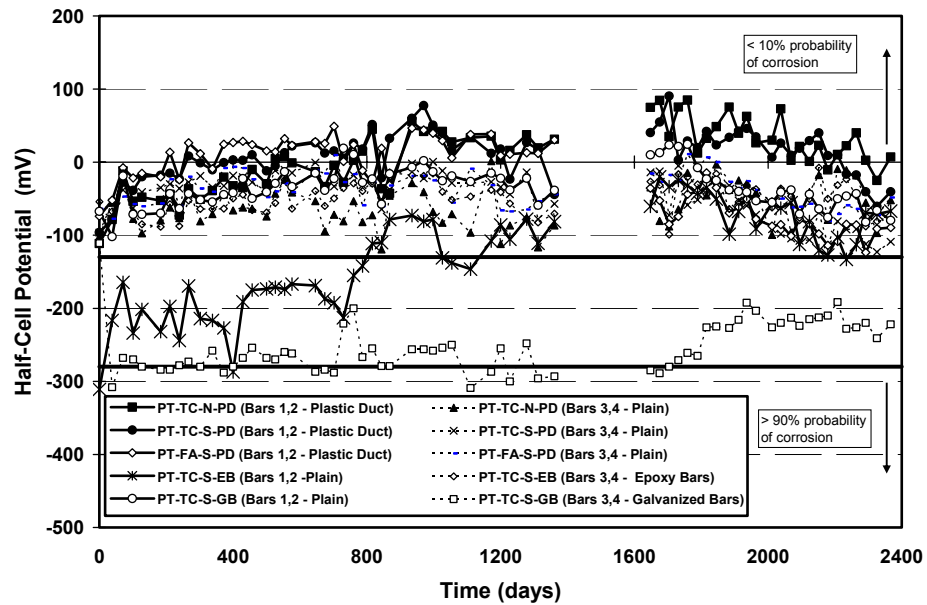
Figure 5.34 Average Half-Cell Potential Readings at Top of Column (Level 5): PT Columns – PT Bars

463

Table 5.10 Nonprestressed Column Average Half-Cell Readings Summary

Specimen	Level	Probability of Corrosion
NJ-TC-N	5	uncertain
	3	uncertain
	1	uncertain
DJ-TC-N	5	low
	3	uncertain
	1	uncertain
DJ-FA-S	5	low
	3	low
	1	uncertain
DJ-TC-S	5	low
	3	low
	1	uncertain
NJ-TC-S	5	low
	3	uncertain
	1	high

Table 5.11 Post-Tensioned Column Average Half-Cell Readings Summary.

Specimen	Level	Rebar	Reading PT Bars (Plain)	PT Bars (Protected)
PT-TC-N-PD	5	low	low	low
	3	low	low	low
	1	high	uncertain	uncertain
PT-TC-S-PD	5	low	low	low
	3	uncertain	low	low
	1	uncertain	uncertain	uncertain
PT-FA-S-PD	5	low	low	low
	3	low	low	low
	1	uncertain	uncertain	uncertain
PT-TC-S-EB	5	low	low	low
	3	low	uncertain	low
	1	uncertain	high	uncertain
PT-TC-S-GB	5	low	low	low
	3	low	low	low
	1	uncertain	uncertain	uncertain

Analysis of the non-prestressed specimen plots, indicates that higher HC potentials are observed at Level 1 corresponding to the continuously submerged zone. In general, the HC potential at this level was in the range between -130 mV and -280 mV (uncertain probability of corrosion as described in Table 5.9). The only specimen showing higher average HC-potentials at this level was specimen NJ-TC-S (No dowel - normal Type C concrete - service load), with readings more negative than -400 mV (>90% probability region). At Level 3 (column mid-height) three specimens showed potential values in the uncertain range (between 10% and 90% probability of corrosion): NJ-TC-N (No dowel – type C Concrete - unloaded), DJ-TC-N (doweled – type C concrete - unloaded) and NJ-TC-S (No dowel – type C concrete - service load). Specimens DJ-TC-S (doweled – Type C concrete - service load) and DJ-FA-S (doweled – fly ash concrete - service load) showed average potentials more positive than -130 mV, suggesting a very low probability of corrosion (<10%). At Level 5 (top level) all specimens showed low probability of corrosion, with slightly higher probability of corrosion in specimen NJ-TC-N (No dowel – type C concrete, unloaded), which showed values in the Low to Uncertain probability ranges (around -130 mV).

For post-tensioned specimens, a higher probability of rebar corrosion was found at the bottom level (Level 1). At this level specimen PT-TC-N-PD (type C concrete – unloaded – plastic ducts) showed the higher probability of corrosion, with readings in the order of -300 mV. Other post-tensioning specimens showed readings at Level 1 in the uncertain probability range, with readings between -130 mV and -280 mV. At levels 3 and 5, all post-tensioned specimens showed low probability of rebar corrosion (values more positive than -130 mV), with a slightly higher probability of corrosion at level 3 in specimen PT-TC-S-PD (type C concrete – service load – plastic duct).

The probability of corrosion for post-tensioned bars at level 1 was found in the uncertain probability range (between -130 mV and -280 mV) for all specimens, except for specimen PT-T-S-EB (type C concrete – service load – epoxy coated bars) that showed a high probability of corrosion (above 90% probability) for the two non-protected PT-bars. At Levels 3 and 5, all specimens showed low probability of corrosion (below 10%), except again for specimen PT-TC-S-EB where a slightly higher probability of corrosion was found on the plain (non protected) PT-bars.

Very negative Half-Cell potentials at the three inch level (Level 1) may not be the result of very high corrosion rates or severity; therefore, the results presented above must be evaluated with care. As explained by West,[5.2] "…When the oxygen supply is restricted, as in the case of submerged concrete, the rate of cathodic reaction is reduced and the corroding system is said to be under diffusion control. A system under diffusion control is illustrated by mixed potential theory in Figure 5.35. Because the slope of the cathodic reaction becomes very steep, the corrosion potential at equilibrium is very negative and the corrosion rate is small. Thus, very negative half-cell potentials in submerged concrete should not necessarily be interpreted as an indication of significant corrosion activity."
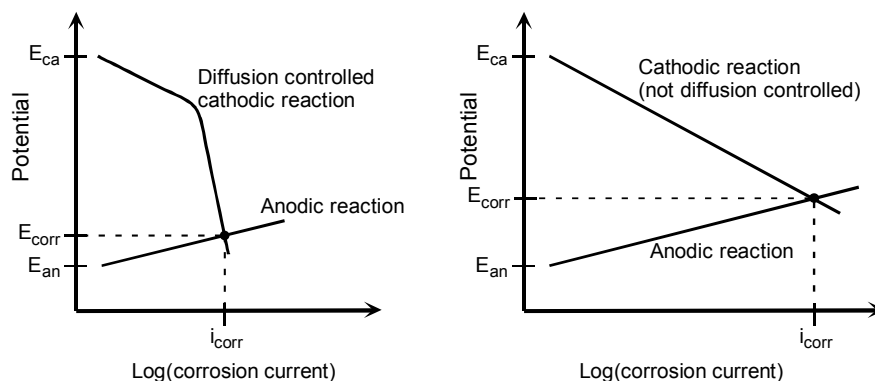
Figure 5.35 Effect of Diffusion Controlled Cathodic Polarization (Lack of Oxygen) on Corrosion Potential and Current[5.2]

Half-Cell potentials may also be misleading if absolute values at specific dates are used, instead of trends or changes of these values over time. Commonly, a well defined transition between stable readings to more negative readings would define the onset of corrosion. Also, a continuing trend of more negative readings could be the indication of corrosion activity. However, if half-cell potential readings have been consistent with no significant deviations, this may be the indication that corrosion is not occurring in the element under consideration. With this concept, specimens NJ-TC-N, NJ-TC-S, PT-TC-N-PD (Rebar and PT Bars), PT-FA-S-PD (PT Bars), and PT-TC-S-EB (Rebar) showed some indication of corrosion activity over time; however, specimens DJ-TC-N, DJ-TC-N, DJ-FA-S, DJ-TC-S, PT-TC-S-PD (Rebar and PT Bars), PT-FA-S-PD (Rebar), PT-TC-S-EB (PT Bars), PT-TC-S-GB (Rebar and PT Bars), showed steady potentials, and therefore uncertain corrosion activity.

5.3.2   Chloride Content in Concrete

Concrete chloride samples were taken directly from the column specimens after 20 months, 32 months and 78 months (end of testing). Acid-soluble chloride content results at 20 months and at 32 months were reported in reference 5.1. After 78 months (at the end of testing) powder samples were collected from the column specimens at 3 inches, 9 inches and 15 inches from the base of the specimens, on both the dripper and the non-dripper side. At each location, samples were taken at three different depths: 0.5 inches, 1.0 inch and 2.0 inches.

Figure 5.36 and Figure 5.37 show chloride penetration plots for column NJ-TC-N. Figure 5.38 and Figure 5.39 show chloride penetration plots for column PT-TC-N-PD. Plots for other specimens are included in Appendix C.

The relative specimen performance with respect to chloride penetration is compared in Figures 5.40 through 5.45. These plots have been constructed for all specimens at each depth in all sample locations, for both the dripper and non-dripper sides.

Chloride threshold value is indicated in the figures at 0.033%. This value, intended as a guide only, is based on the widely accepted chloride threshold value of 0.2% of the weight of cement.[5.5]

As can be observed from the figures, acid soluble chloride contents at a height of 3 inches (submerged zone) and at 9 inches, are in most specimens well in excess of the threshold value for corrosion. However, at 15 inches, most specimens show low chloride contents, below the threshold value, at all depths. Exceptions are fly ash specimens (DJ-FA-S and PT-FA-S-PD) that show chloride contents below the threshold value at 9 inches on the non-dripper side (at all depths), and on the dripper side (at 0.5 in. and 2 in.).

Typically, chloride contents at 2 in. depth are 20% to 80% lower than those chloride contents at 1 in. depth, with few exceptions (NJ-TC-N dripper side, DJ-TC-N non-dripper side, DJ-TC-S dripper side, PT-TC-S-PD non dripper side, PT-TC-S-EB dripper side). Additionally, all post-tensioned specimens, and non-prestressed specimens with fly ash concrete, show less chloride penetration than non-prestressed specimens with normal Type C concrete.

From these results, the wicking effect or upward migration of chlorides in the specimens is evident. Significant chloride contents were found at 9 inches from the column base, and much lower contents were found at 15 inches, suggesting that the chloride content is due to the wicking effect, and not to the trickle water coming from above.
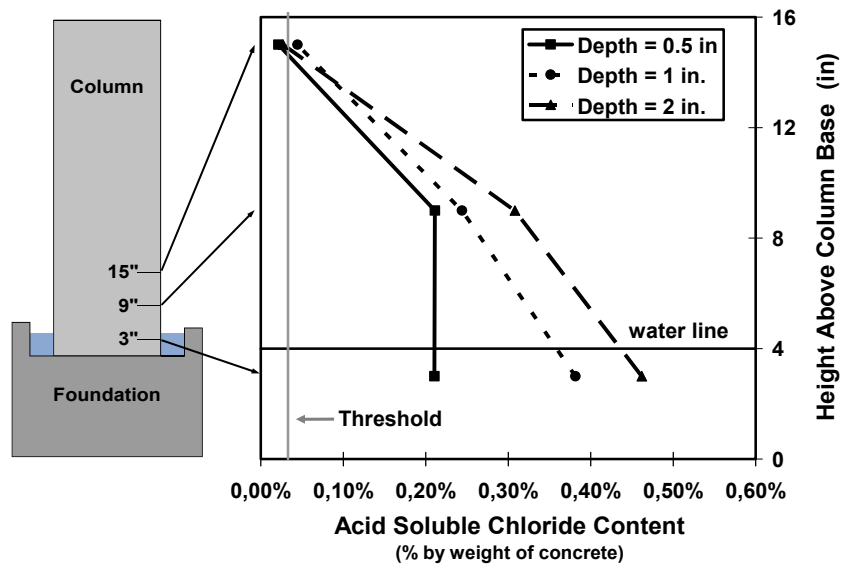
Figure 5.36 Concrete Chloride Penetration for Column NJ-TC-N in Non-Dripper Side at End of Testing
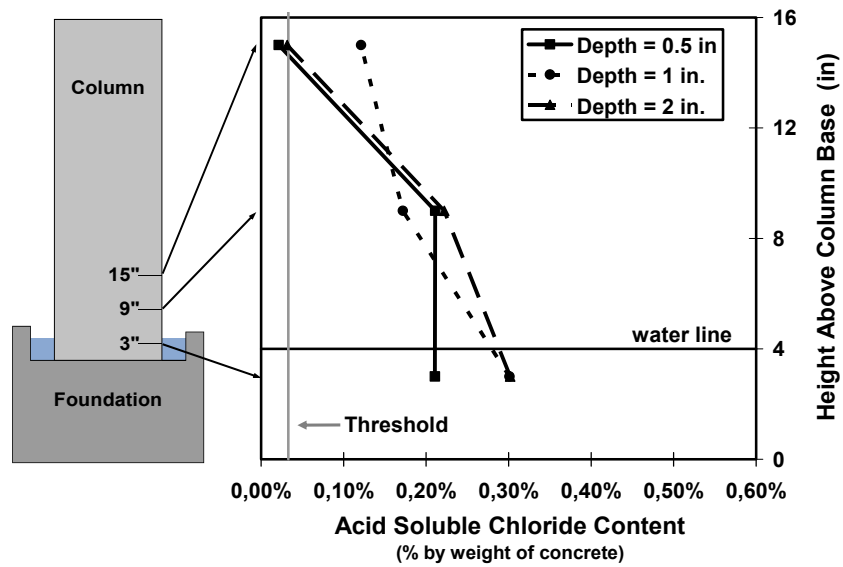
Figure 5.37 Concrete Chloride Penetration for Column NJ-TC-N in Dripper Side at End of Testing

469
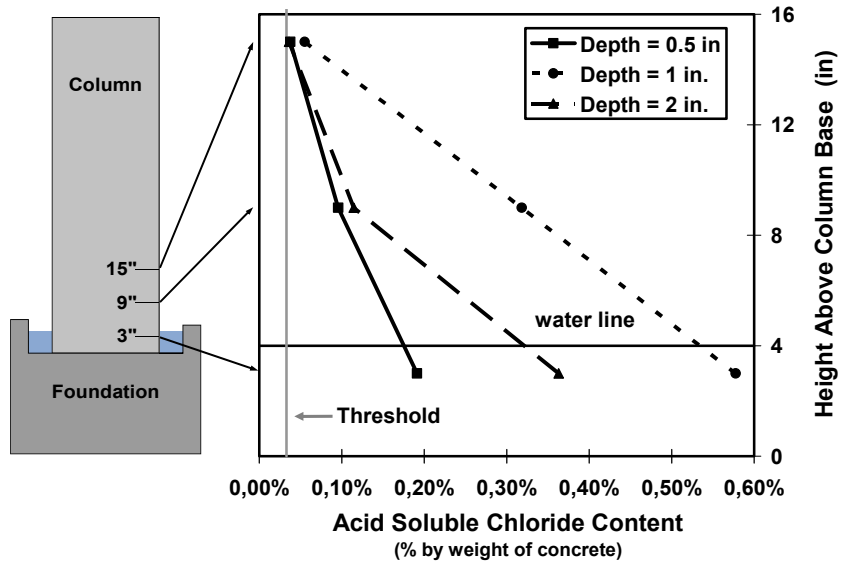
Figure 5.38 Concrete Chloride Penetration for Column PT-TC-N-PD in Non-Dripper side at End of Testing
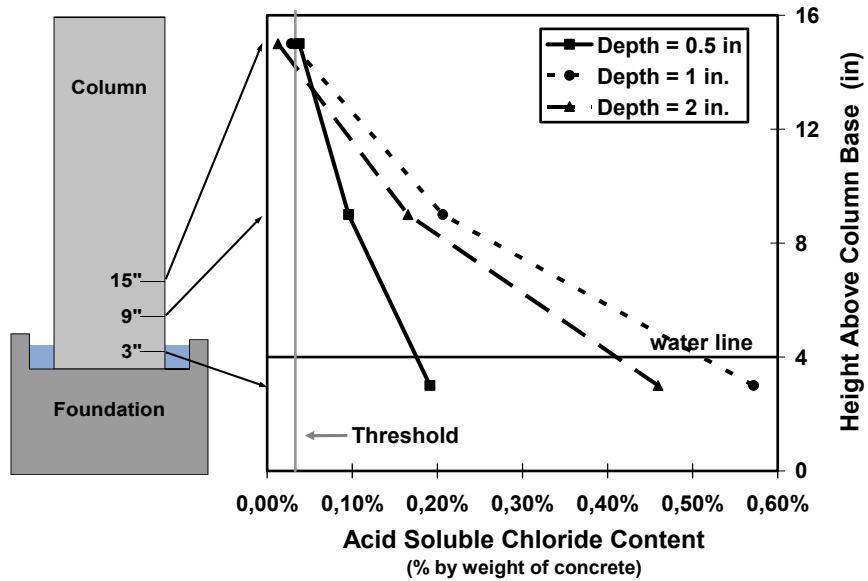
Figure 5.39 Concrete Chloride Penetration for Column PT-TC-N-PD in Dripper Side at End of Testing

470
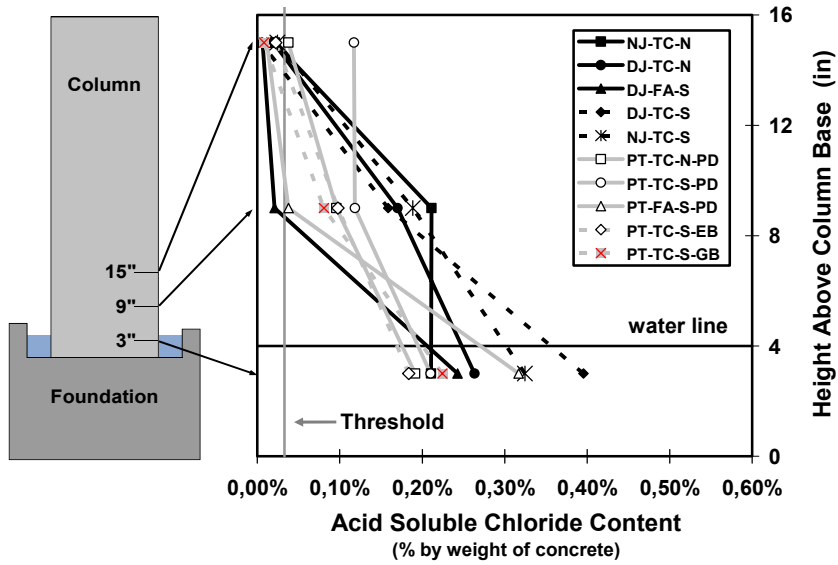
Figure 5.40 Concrete Chloride Penetration at 0.5 inches for All Columns in Non-Dripper Side at End of Testing
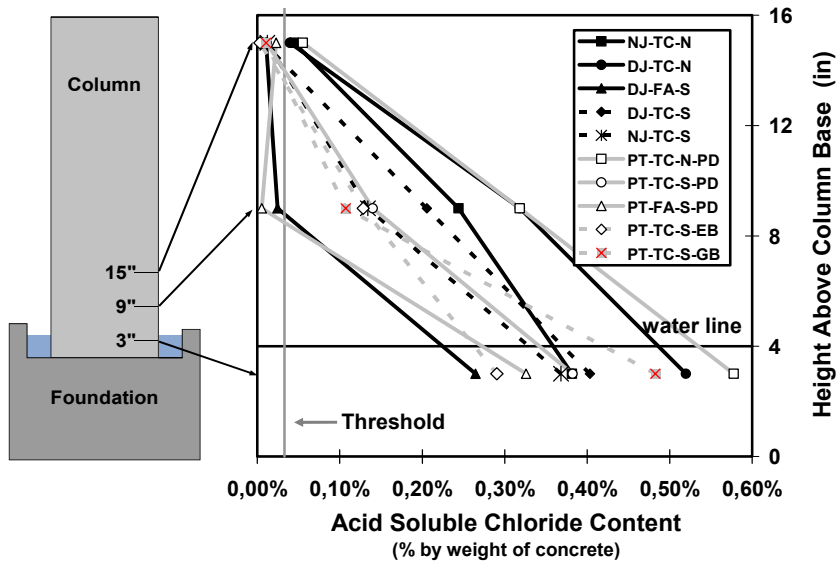
Figure 5.41 Concrete Chloride Penetration at 1.0 inches for All Columns in Non-Dripper Side at End of Testing

471
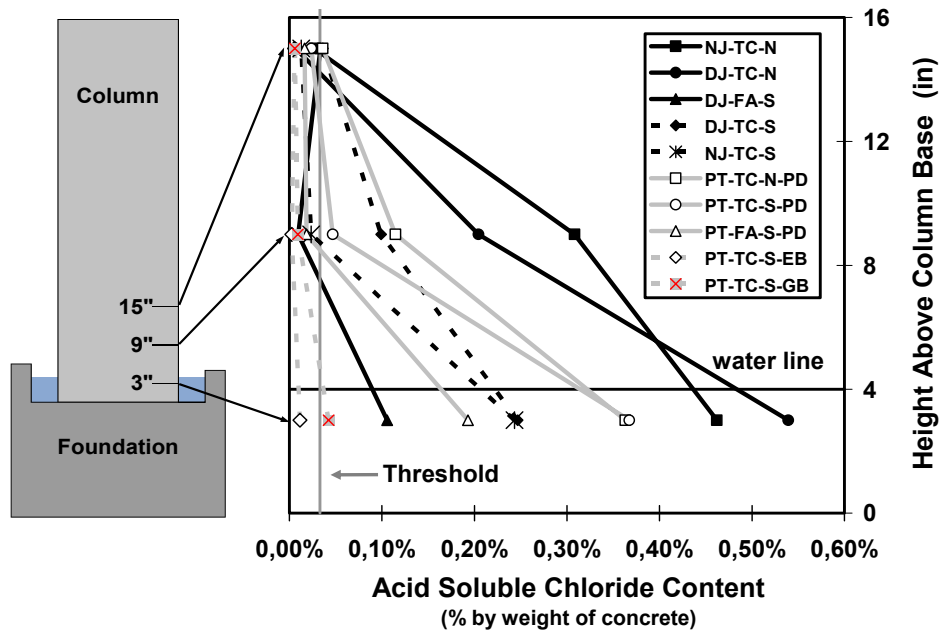
Figure 5.42 Concrete Chloride Penetration at 2.0 inches for All Columns in Non-Dripper Side at End of Testing
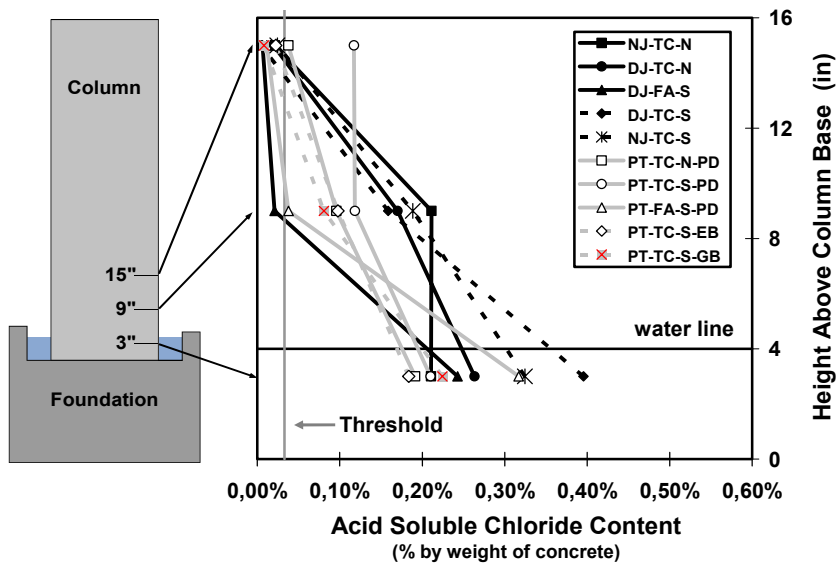
Figure 5.43 Concrete Chloride Penetration at 0.5 inches for All Columns in Dripper Side at End of Testing

472
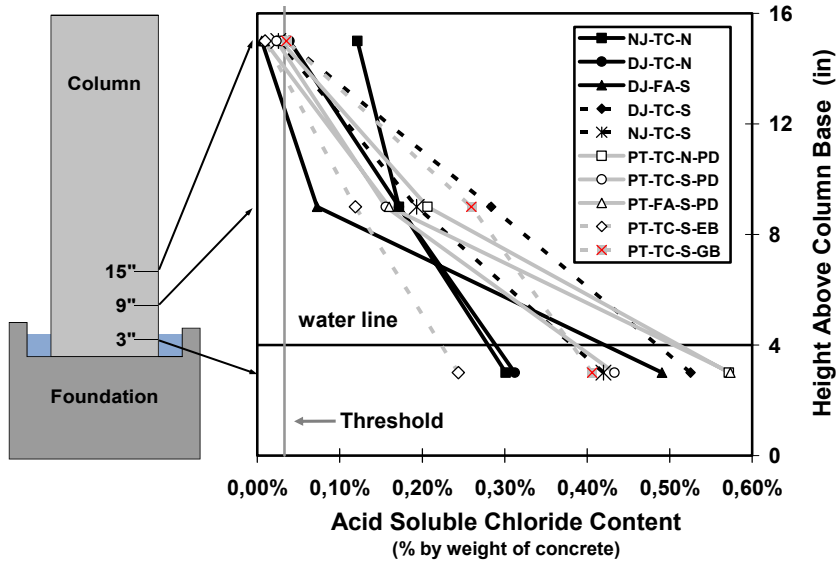
Figure 5.44 Concrete Chloride Penetration at 1.0 inches for All Columns in Dripper Side at End of Testing
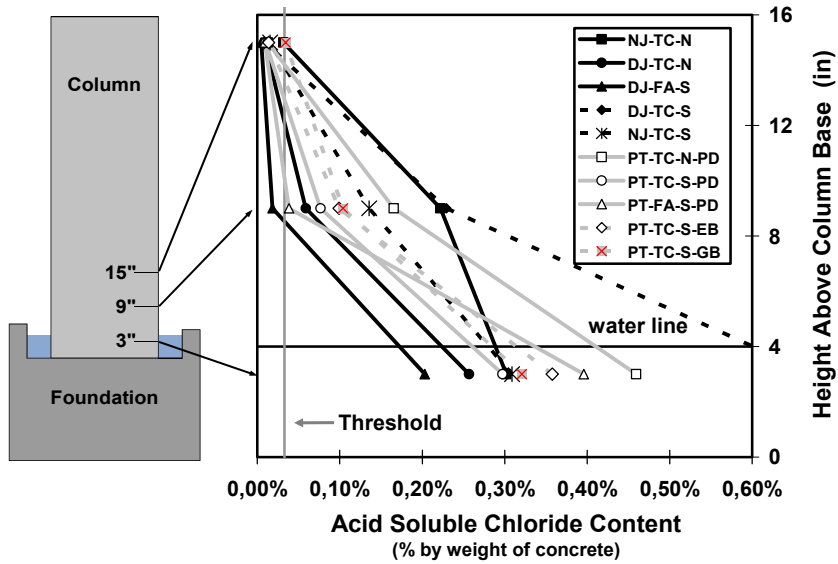
Figure 5.45 Concrete Chloride Penetration at 2.0 inches for All Columns in Dripper Side at End of Testing

473

5.3.3 Prediction of specimen Performance using Half-Cell Potential Data

The higher probability of corrosion using half-cell potential readings was found at the base of the column specimens. There was not a distinct trend with respect to dripper and non – dripper sides. The poorest performance was found for unloaded non-prestressed specimens and specimens with no-joint.

There was not a distinct trend between post-tensioned and non-prestressed columns. Only specimen NJ-TC-S showed slightly higher probability of corrosion than other specimens, when analyzing absolute values.

Only specimens NJ-TC-N, NJ-TC-S, PT-TC-N-PD (Rebar and PT Bars), PT-FA-S-PD (PT Bars), and PT-TC-S-EB (Rebar) showed some indication of corrosion activity over time, when analyzing trends over the total exposure period.

There was not a distinct trend with respect to post-tensioned bars in plastic ducts or galvanized ducts. Neither, was there any distinction between Galvanized or Epoxy coated bars, compared to plain PT-Bars.

5.4 FORENSIC EXAMINATION

5.4.1 Procedure

5.4.1.1 Specimen Condition at End of Testing

Specimens were evaluated at the end of testing for signs of cracking or distress and corrosion stains.

474

5.4.1.2 Foundation Saw Cuts

Prior to concrete removal, column specimens sharing the same foundation were separated by saw cutting as shown in Figure 5.46. Due to special saw cutting equipment requirements, saw cutting had to be contracted with an external concrete demolition company.

Figure 5.46 Saw Cutting of Column Foundation.

5.4.1.3 Concrete Removal

Concrete in column specimens was carefully removed using pneumatic equipment, as shown in Figure 5.47. Care was exercised to ensure total exposure and removal of spiral and longitudinal mild steel reinforcement and post-tensioning duct/PT bar systems. Reinforcement was immediately inspected for any color changes due to drying of the corroded steel surfaces, if any. Reinforcement cages were dismantled for careful reinforcement inspection and rating.

Figure 5.47 Concrete Removal and Reinforcement Dismantling.

5.4.2   Autopsy Program

All specimens (ten in total) were autopsied at the end of six and a half years of continuous exposure testing.   After concrete was removed from each column, mild steel reinforcement, post-tensioning ducts and high-strength post-tensioning bars were carefully inspected and rated according to the corrosion

rating scheme explained in the following section.   During autopsy, ducts were cut open in half longitudinally, and grout samples were taken at different locations to investigate chloride ingress to the post-tensioning bar level. Anchorages and bar splices were also inspected for signs of corrosion in the areas exposed to concrete and at the crevices, where steel pieces in the post-tensioning system were in contact.

5.4.3   Evaluation and Corrosion Rating used during Forensic Examination

To maintain consistency in the corrosion ratings among the different series in the durability project, the same generalized evaluation and rating system previously used in the macrocell and beam corrosion tests, was used in the column series with only minor changes due to the specific specimen characteristics.   The length of reinforcing bar, post-tensioning bar and post-tensioning duct in the column was subdivided into 34 two-inch increments.   In addition, the post-tensioning bar length within the foundation was subdivided into seven two-inch increments.   Dowels were subdivided into 26 two-inch increments and spirals were subdivided into 11 two-inch increments for every spiral step in the column North side and 11 two-inch increments for every step in the column South side. At each increment, the steel was examined and a rating was assigned to describe the corrosion severity within that increment. The ratings for all increments were summed to give a total corrosion rating for the element that could be compared for different specimens.   This method allowed evaluation of corrosion extent and severity.

5.4.3.1   *Mild Steel Reinforcement (Spirals, longitudinal Steel and dowels)*

Mild steel reinforcement was examined at the intervals described above, which is also illustrated in Figure 5.48.

Dowel distribution
at joint

Rebar location
(no rebar at joint)

6 dowels:
#6 bars

17 two-inch
increments

Column Joint

6 two-inch
increments

3 two-inch
increments

(A)

6 longitutinal
6 bars:

34 two-inch
increments

Column Joint

(B)

North

#3 spiral at
6 in. pitch

286 two-inch
increments

Column Joint

(C)
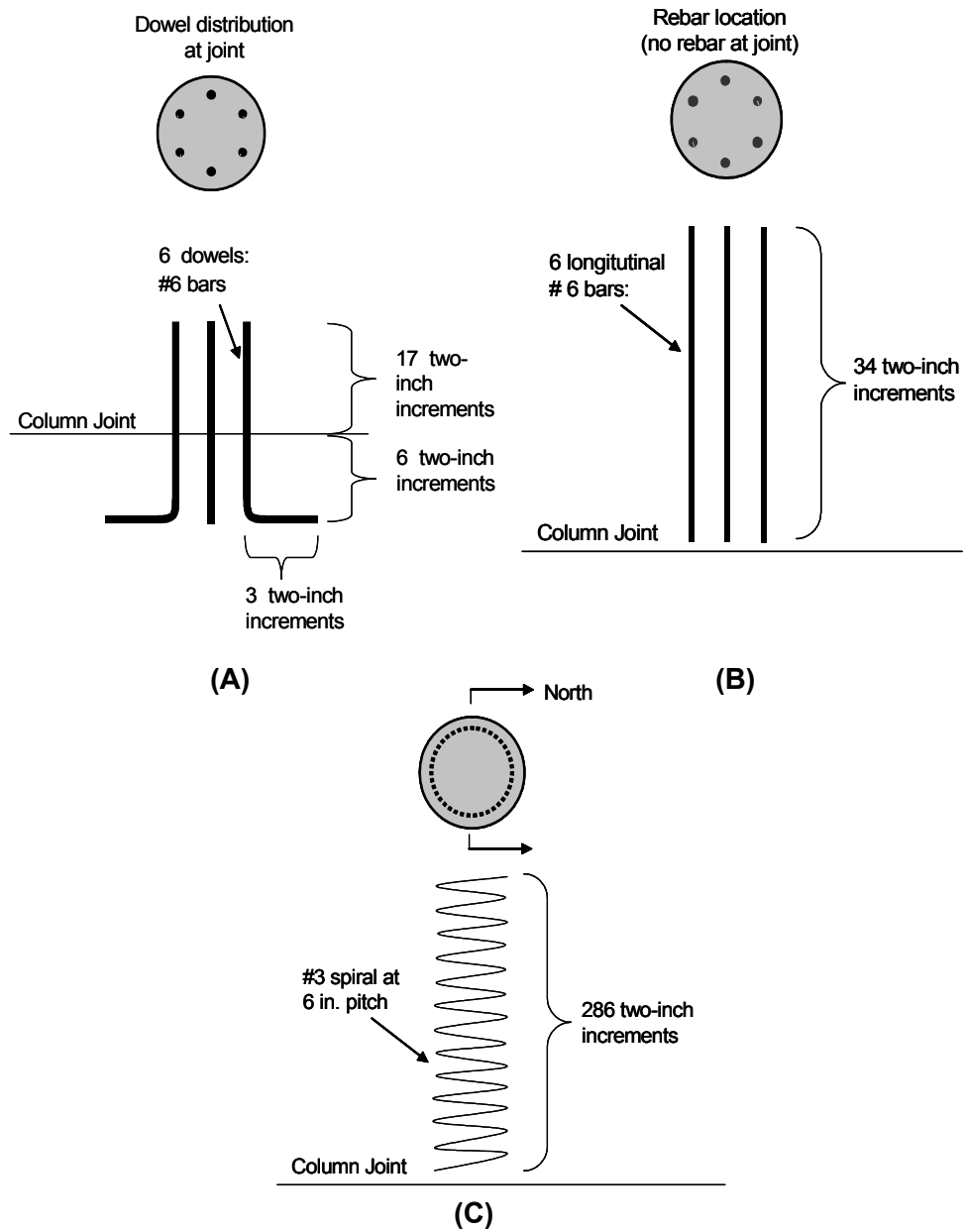
Figure 5.48 Intervals for Corrosion Ratings on (A) dowels,
(B) mild steel longitudinal bars, and (C) spiral

478

Corrosion ratings were assigned to indicate corrosion severity for each interval (considering top and bottom surfaces in the same corrosion rating). This procedure differs from that used in the beam and macrocell corrosion series, where the horizontal rebar top and bottom surfaces were rated separately. However, it was found that one corrosion rating was enough to adequately determine extent and severity of corrosion in these vertical bars. The total bar corrosion rating was calculated as indicated in the following equations.

Mild steel longitudinal bars:

$$\text{Bar Corrosion Rating} = \sum_{i=1}^{34}\sum_{j=1}^{6} R_{Bar_j, Segment_i} \qquad \textit{Eq. 5.3}$$

Mild steel dowels:

$$\text{Dowel Corrosion Rating} = \sum_{i=1}^{26}\sum_{j=1}^{6} R_{Dowel_j, Segment_i} \qquad \textit{Eq. 5.4}$$

Spiral reinforcement:

$$\text{Spiral Corrosion Rating} = \sum_{i=1}^{13}\sum_{j=1}^{11} R_{North\ Segment_j, Spiral\ Step_i} + \sum_{i=1}^{13}\sum_{j=1}^{11} R_{Sourth\ Segment_j, Spiral\ Step_i}$$
$$\textit{Eq. 5.5}$$

The reason for having distinctive totals for the North and South spiral sides was intended to identify any difference in spiral corrosion condition between the dripper and the non-dripper sides.

The corrosion rating system used is described in Table 5.12.

Table 5.12 Evaluation and Rating System for Corrosion Found on Mild Steel Bars [5.6]

Code	Meaning	Description	Rating
NC	No Corrosion	No evidence of corrosion	0
D	Discoloration	No evidence of corrosion, but some discoloration from original color	1
L	Light	Surface corrosion on less than one half of the interval, no pitting. Surface corrosion can be removed using cleaning pad.	2
M	Moderate	Surface corrosion on more than one half of the interval, no pitting. **and/or** Corrosion can not be completely removed using cleaning pad.	4
P	Pitting	Pits visible to unaided eye.	8
AR	Area Reduction	Measurable reduction in bar cross-sectional area due to corrosion	R^2

R = Estimated cross-sectional area reduction in percent.

5.4.3.2 Post-Tensioning Ducts

Post-Tensioning ducts were examined over 34 two-inch intervals, as indicated in Figure 5.49. At each location, corrosion ratings are assigned to indicate the severity of corrosion on the top and bottom surfaces of the inside and outside of each duct to reflect the possibility of different corrosion severity and extent. The corrosion rating system is described in Table 5.13. The total duct corrosion rating was calculated as follows:

$$\text{Duct Corrosion Rating} = \sum_{i=1}^{34} \left(R_{TopOuter,i} + R_{BotOuter,i} + R_{TopInner,i} + R_{BotInner,i} \right) \quad \textbf{\textit{Eq.5.6}}$$

where,

$R_{TopOuter,i}$ = top outer surface corrosion rating, interval i

$R_{BotOuter,i}$ = bottom outer surface corrosion rating, interval i

$R_{TopInner,i}$ = top inner surface corrosion rating, interval i

$R_{BotInner,i}$ = bottom inner surface corrosion rating, interval i.

480

Duct location

Rubber
gaskets to
seal dead
end of PT
ducts.

34 two-inch
increments

Column joint
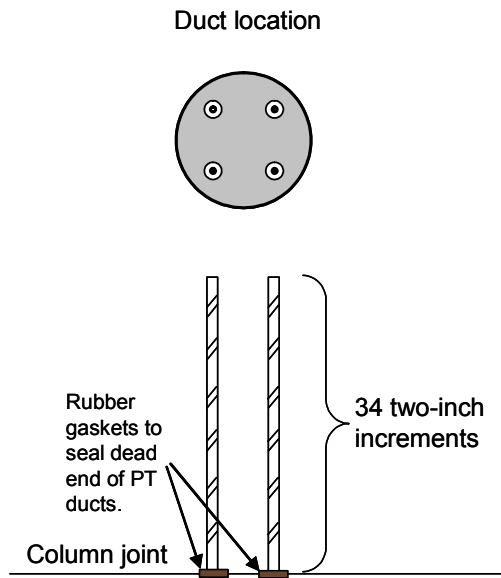
Figure 5.49 Intervals for Corrosion Ratings on PT Ducts

Table 5.13 Evaluation and Rating System for Corrosion Found on Post-Tensioning Duct[5.6]

Code	Meaning	Description	Rating
NC	No Corrosion	No evidence of corrosion	0
D	Discoloration	No evidence of corrosion, but some discoloration from original color	1
L	Light	Surface corrosion on less than one half of the interval, no pitting.	2
M	Moderate	Surface corrosion on more than one half of the interval, no pitting.	4
S	Severe	Corrosion completely covers the interval. **and/or** Presence of pitting.	8
H	Hole Through Duct	Hole corroded through duct. Used in conjunction with ratings D, L, M and S.	$32 + A_h$

A_h =   Area of hole(s) in mm^2

481

5.4.3.3   Post-tensioning Bars

Post-tensioning bars were examined at 34 intervals inside the column element and at seven two-inch increments in the short length of bar embedded in the foundation with bearing plate and nut as shown in Figure 5.50.
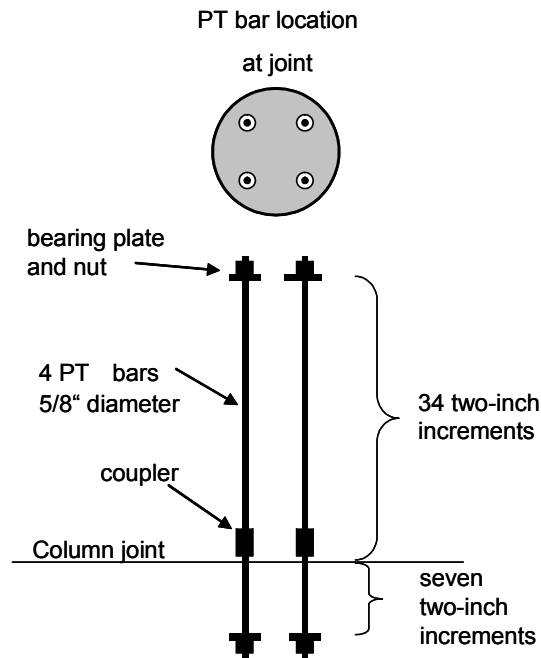
Figure 5.50 Intervals for Corrosion Ratings on PT Bars

The total corrosion rating was calculated as follows:

$$\text{PT Bar Corrosion Rating} = \sum_{i=1}^{34}\sum_{j=1}^{4} R_{\text{PT Barj, Segment i}} + \sum_{k=1}^{7}\sum_{j=1}^{4} R_{\text{PT Barj, Segment k}} \qquad \textbf{\textit{Eq. 5.7}}$$

where, $R_{\text{PT Bar j, Segment i}}$ = PT Bar j corrosion rating, interval i

(PT bar portion located inside column element).

$R_{\text{PT Bar j, Segment k}}$ = PT Bar j Corrosion rating, interval k

(PT bar portion inside foundation).

482

The evaluation and rating system used for PT bars was the same system used for mild steel bars, as shown in Table 5.12.

5.4.4   Forensic Examination Results

5.4.4.1   Detailed Visual Inspection

A brief summary of forensic examination results after six and a half years of exposure is provided for each column specimen in the following sections. In general, at the end of testing rust stains were only visible in the base of the columns, in the bottom12 inches.   No signs of cracking were observed in the column surfaces.   Figure 5.51 shows the condition of the specimens after unloading and tie down bar cutting.

Tie down bars had uniform corrosion at the column base level, which stained the foundation, but no severe pitting was observed on these high-strength bars.

Figure 5.51 Specimen Condition at the End of Testing.

5.4.4.1.1 Specimen NJ-TC-N (No dowel, Class C Concrete, No load)

No signs of cracking were visible in the column surfaces and no corrosion stains were present at the column base, as observed in Figure 5.52.

Corrosion in the spiral was mostly concentrated at the spiral base (first 18 inches). In this region light corrosion was observed in a few segments with only two two-inch segments in the North side (dripper side) showing severe corrosion and pitting. The rest of the spiral had some discoloration from the original bar color with no signs of corrosion. See Figure 5.53.

Corrosion Rating:

Specimen	NJ-TC-N
Autopsy after 6.5 years	
Spiral	532
Rebar	2
Dowel	NA
Duct #1	NA
Duct #2	NA
Duct #3	NA
Duct #4	NA
PT-Bar	NA

Figure 5.52 Condition of Specimen NJ-TC-N at the End of Testing

Reinforcing bars were in excellent condition. Only rebar #2 showed light corrosion in one of the two inch segments as shown in Figure 5.53.

Complete Cage

Spiral

Rebar #2
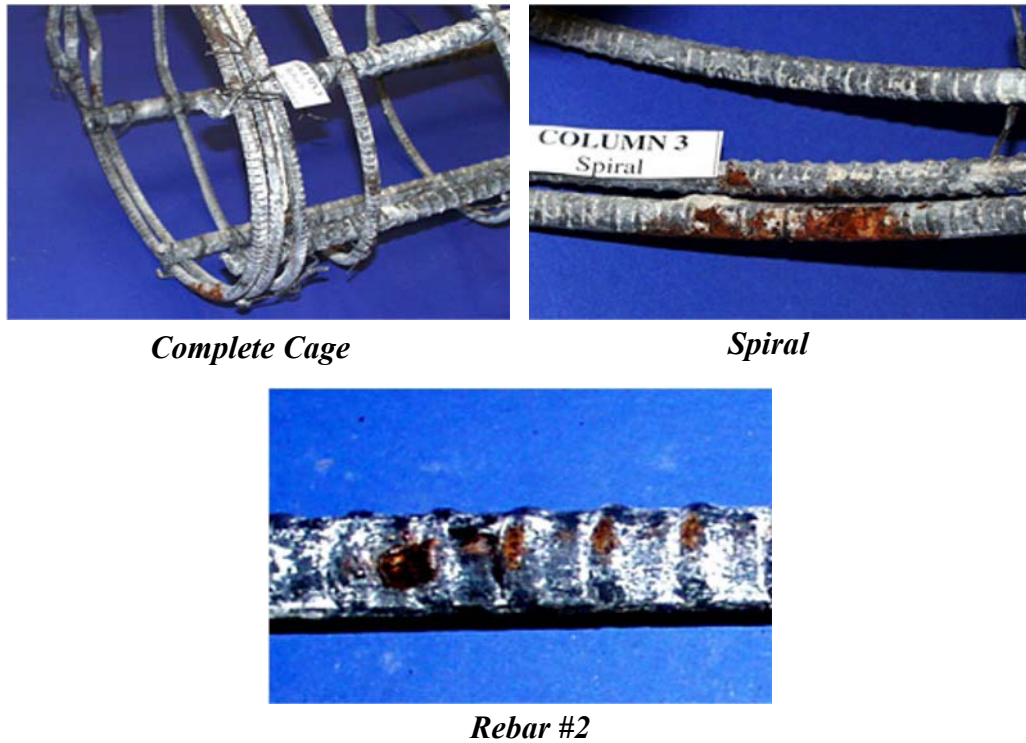
Figure 5.53 Reinforcement Condition for Specimen NJ-TC-N

5.4.4.1.2 Specimen DJ-TC-N (Doweled Joint, Class C Concrete, No Load)

Only very few corrosion stains were visible at the base of the column. The rest of the specimen had no signs of cracking or corrosion stains.

Spiral reinforcement had pitting in the North side at the base of the column in the center three two-inch segments, as shown in Figure 5.54. Light to moderate corrosion extended up to a height of 14 inches from the column base, in

Corrosion Rating:

Specimen	DJ-TC-N
Autopsy after 6.5 years	
Spiral	595
Rebar	35
Dowel	2704
Duct #1	NA
Duct #2	NA
Duct #3	NA
Duct #4	NA
PT-Bar	NA

485

both the North and the South sides. In the dripper side, light corrosion was concentrated in the center six inches of the total height of the spiral. In the non-dripper side, only discoloration and few areas of light corrosion were visible in the total spiral height.

Figure 5.54 Condition of Specimen DJ-TC-N at the End of Testing

The six reinforcing bars showed only light corrosion and discoloration in the first eight inches from the column base. The rest of the bar lengths were in excellent condition.

All six dowels showed severe corrosion and pitting at the column base (column-foundation interface). As shown in Figure 5.55, area reduction in the dowel bars was concentrated and severe, especially in Dowel #4 and Dowel #5.

Complete Cage   *Spiral*

Rebar #3   *Dowel #4*
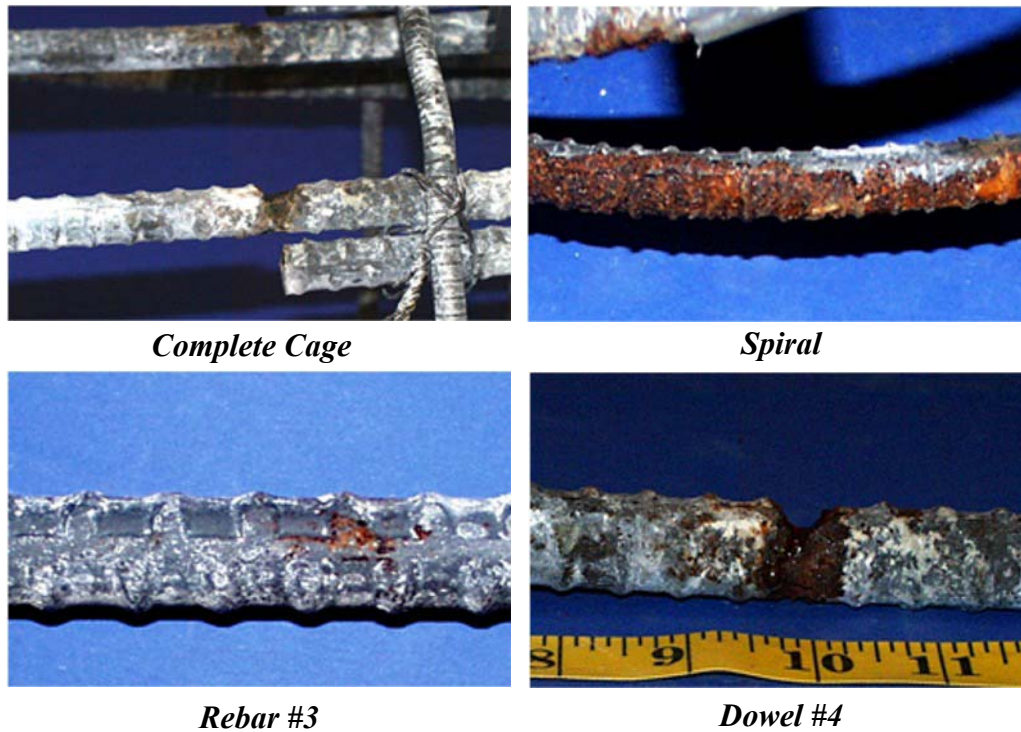
Figure 5.55 Reinforcement Condition for Specimen DJ-TC-N

5.4.4.1.3 Specimen DJ-FA-S (Doweled Joint, Fly Ash Concrete, Service Load)

The specimen surface had no signs of corrosion stains or cracking.   Concrete was in excellent condition at the end of testing.   See Figure 5.56.

Spiral reinforcement had moderate corrosion in the North side (non-dripper side) at the four-inch level from the column base.   Light corrosion was also concentrated in the spiral North side in the center four two-inch segments from the four-inch height up to a height of 30 inches.

Corrosion Rating:

Specimen	DJ-FA-S
Autopsy after 6.5 years	
Spiral	360
Rebar	19
Dowel	619
Duct #1	NA
Duct #2	NA
Duct #3	NA
Duct #4	NA
PT-Bar	NA

487

Figure 5.56 Condition of Specimen DJ-FA-S at the End of Testing.

The rest of the spiral in the North and South sides had from light corrosion to only discoloration.

Mild steel longitudinal reinforcement showed very few areas of light corrosion. Rebar #2 had light corrosion between the heights of 36 to 52 inches from the column base (with respect to the rebar analysis length of 68 inches). This bar was located in the dripper side.

Dowels showed in general light to moderate corrosion in the two-inch segment at the column base (joint location). Dowel #1 showed the heaviest corrosion and area loss in this region, as shown in Figure 5.57.

Complete Cage   *Spiral*

Rebar #1   *Dowel #1*
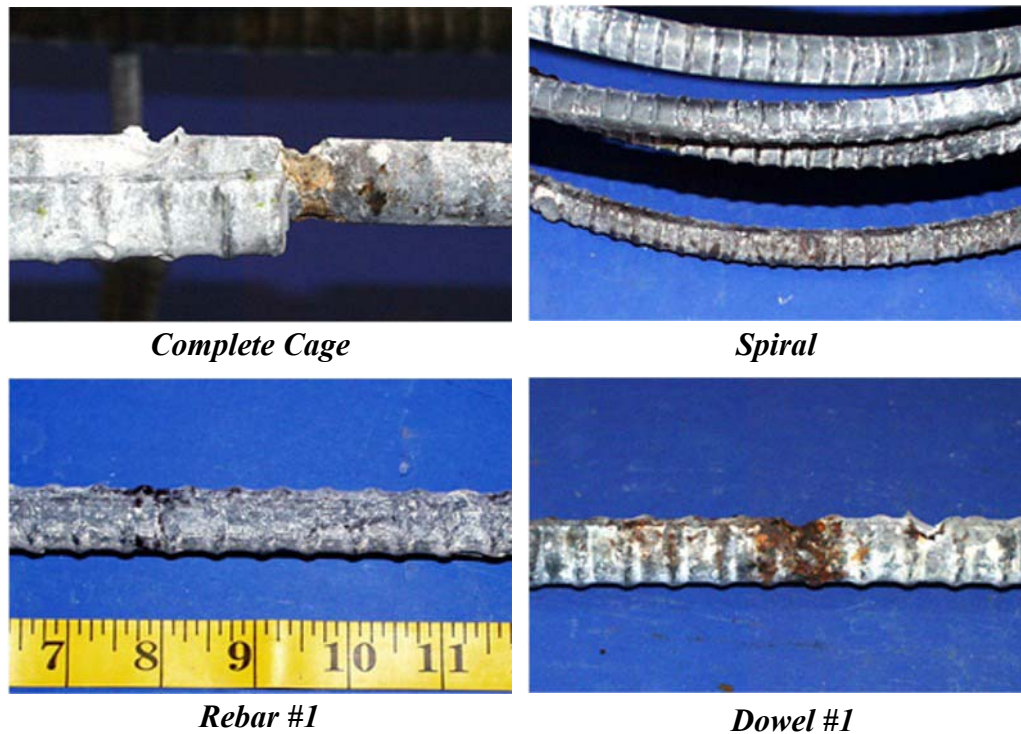
Figure 5.57 Reinforcement Condition for Specimen DJ-FA-S

5.4.4.1.4 Specimen DJ-TC-S (Doweled Joint, Class C Concrete, Service Load)

No signs of corrosion were observed in the column surfaces at the end of testing. Concrete was in excellent condition.

Spiral reinforcement showed very similar corrosion ratings in the non-dripper and dripper sides. Light to moderate corrosion was concentrated in the first 22 inches from the column base; and, also some areas of moderate corrosion were observed in a few segments at the 46-inch and 53-inch levels.

Corrosion Rating:

Specimen	DJ-TC-S
Autopsy after 6.5 years	
Spiral	458
Rebar	26
Dowel	86
Duct #1	NA
Duct #2	NA
Duct #3	NA
Duct #4	NA
PT-Bar	NA

489

Figure 5.58 Condition of Specimen DJ-TC-S at the End of Testing

Rebar corrosion in all cases was reduced to only light corrosion and bar discoloration in the first six segments.   Moderate corrosion was very localized as observed in Rebar #3 in Figure 5.59.

Dowels showed light pitting and moderate corrosion in the vicinity of the column joint. Section loss was not significant, as observed in Figure 5.59.
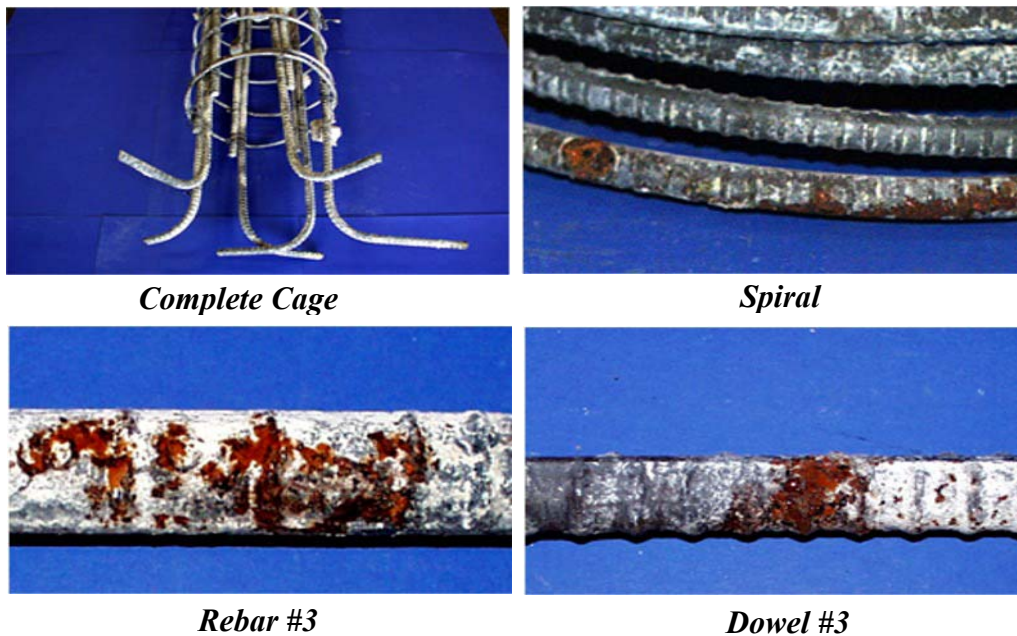

Complete Cage

Spiral

Rebar #3

Dowel #3

Figure 5.59 Reinforcement Condition for Specimen DJ-TC-S

5.4.4.1.5 Specimen NJ-TC-S (No dowel, Class C Concrete, Service load)

No signs of cracking or spalling were visible on the column surfaces. Rust stains extended the first 5 inches, from the column base, as shown in Figure 5.60. No other signs of corrosion were visible in the specimen.

Extremely severe spiral corrosion was mostly located at the base, in the North side (Dripper side) in the first three spiral steps (see Figure 5.61).

Rebar corrosion was concentrated in the first four inches from the column base. Rebar #1 showed the most severe corrosion with light pitting, while the other bars only had light to moderate corrosion . See Figure 5.61.

The specimen did not have dowels.

Corrosion Rating:

Specimen	NJ-TC-S
Autopsy after 6.5 years	
Spiral	10266
Rebar	32
Dowel	NA
Duct #1	NA
Duct #2	NA
Duct #3	NA
Duct #4	NA
PT-Bar	NA

Figure 5.60 Condition of Specimen NJ-TC-S at the End of Testing

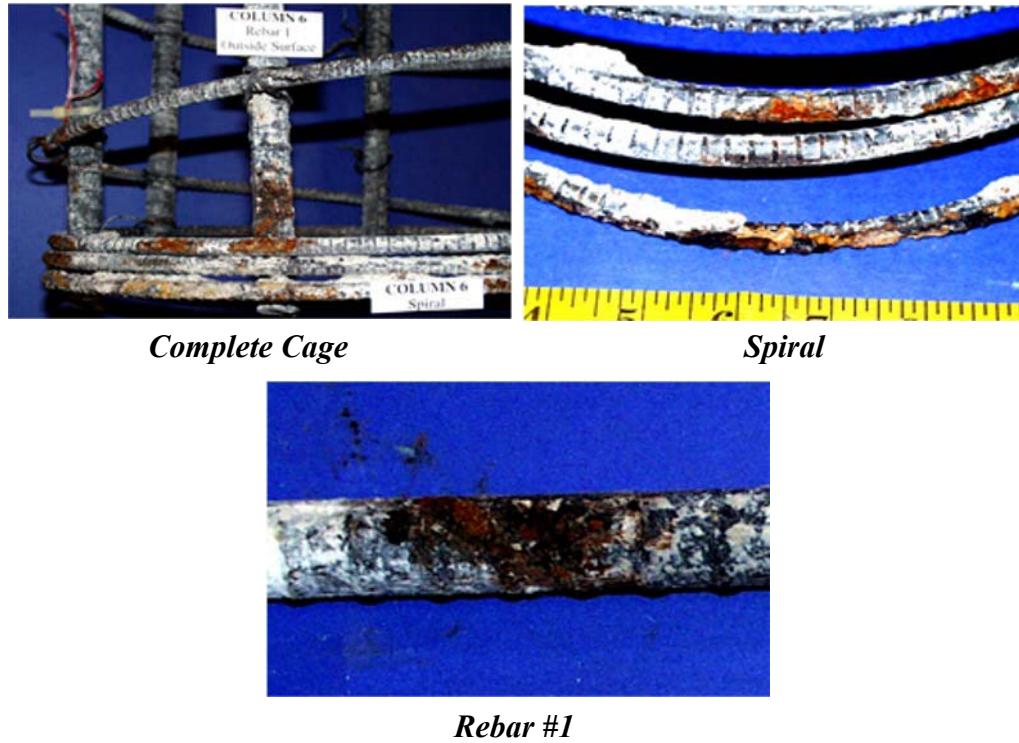**Complete Cage**   **Spiral**

Rebar #1

Figure 5.61 Reinforcement Condition for Specimen NJ-TC-S

5.4.4.1.6 Specimen PT-TC-N-PD (Post-Tensioned, Class C Concrete, No Load, Plastic Duct)

As shown in Figure 5.62, the concrete surface was in excellent condition at the end of testing. No signs of corrosion stains or cracking were visible.

As shown in Figure 5.63, the spiral reinforcement showed light to moderate uniform corrosion in the first two steps (up to a height of nine inches).   From this level to the top of the

492

Corrosion Rating:	
Specimen	PT-TC-N-PD
Autopsy after 6.5 years	
Spiral	351
Rebar	9
Dowel	NA
Duct #1	Plastic
Duct #2	Plastic
Duct #3	276
Duct #4	4
PT-Bar	673

spiral (corresponding to the top of the column), the reinforcement only showed discoloration.

Figure 5.62 Condition of Specimen PT-TC-N-PD at the End of Testing

Complete Cage

Spiral

Rebar #1

Figure 5.63 Reinforcement Condition for Specimen PT-TC-N-PD

Rebar corrosion was negligible .

As shown in Figure 5.65, plastic ducts were in good condition with no signs of damage.   One galvanized steel duct (Duct #3) showed moderate corrosion in the first 10 inches from the column base. This duct was located in the dripper side. Severe corrosion was found on this duct in the first two inches, in the area were the rubber gasket was located. Duct #4 in the non-dripper side showed negligible corrosion at the base.

The anchorage plate in the top of the column, below the pour-back, was found with moderate to severe corrosion, as shown in Figure 5.64.   This finding was typical for all Post-Tensioned specimens.

Post-tensioned bars showed severe corrosion and section loss at the column-foundation joint section, as shown in Figure 5.65.   PT bar localized corrosion was observed in both post-tensioned bars in the dripper side, in both plastic and galvanized steel duct.

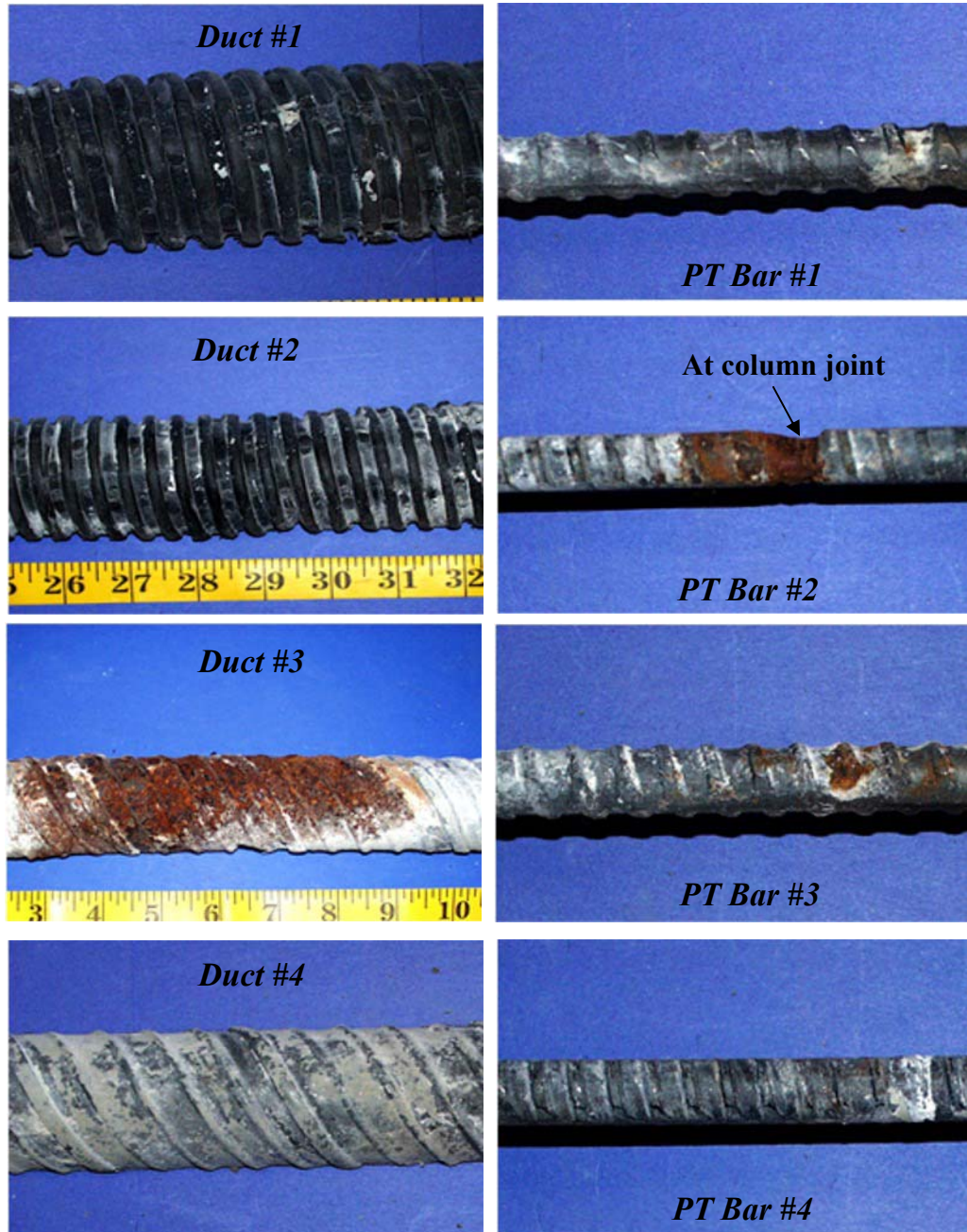*Figure 5.64 PT Bar Top Anchorage Condition for Specimen PT-TC-N-PD*

494

Figure 5.65 Reinforcement Condition for Specimen PT-TC-N-PD

495

5.4.4.1.7 Specimen PT-TC-S-PD (Post-Tensioned, Class C Concrete, Service Load, Plastic Duct)

As shown in Figure 5.66, no signs of corrosion or cracking were present in the concrete surfaces at the end of testing.

As shown in Figure 5.67, spiral reinforcement was found in very good condition at the end of testing. There was light corrosion up to a level of 9 inches in both dripper and non-dripper sides.

Rebar corrosion was negligible.

Figure 5.68 indicates that plastic ducts were in good condition, while galvanized steel ducts showed substantial area loss (approximately 260 mm^2 for Duct #3 and 1400 m^2 for Duct #4) in the first two inches from the column base, behind the rubber gasket. Post-tensioned bars showed moderate corrosion in the vicinity of the joint section and light to negligible corrosion in the other areas.

Corrosion Rating:

Specimen	PT-TC-S-PD
Autopsy after 6.5 years	
Spiral	339
Rebar	3
Dowel	NA
Duct #1	Plastic
Duct #2	Plastic
Duct #3	312
Duct #4	1461
PT-Bar	146

Figure 5.66 Condition of Specimen PT-TC-S-PD at the End of Testing

Complete Cage   *Spiral*

Rebar #4

Figure 5.67 Reinforcement Condition for Specimen PT-TC-S-PD

Duct #1   *Duct #4*

At column joint
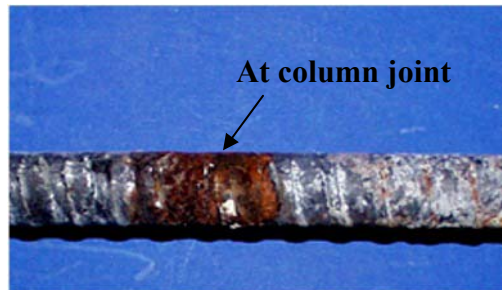
PT Bar #1

Figure 5.68 Duct and PT Bar Condition for Specimen PT-TC-S-PD

5.4.4.1.8 Specimen PT-FA-S-PD (Post-Tensioned, Fly Ash Concrete, Service Load, Plastic Duct)

The concrete surface was in excellent condition at the end of testing as shown in Figure 5.69.

Figure 5.70 indicates that spiral reinforcement showed light corrosion and discoloration in approximately the first 23 inches from the column base level. No distinction was observed between the dripper and non-dripper sides. Rebar reinforcement corrosion was negligible.

Corrosion Rating:

Specimen	PT-FA-S-PD
Autopsy after 6.5 years	
Spiral	337
Rebar	12
Dowel	NA
Duct #1	Plastic
Duct #2	Plastic
Duct #3	12
Duct #4	12
PT-Bar	95

Plastic ducts were in good condition and galvanized steel ducts showed moderate to severe corrosion in the first two inches from the column base level, in the rubber gasket location, as shown in Figure 5.71. Post-tensioned bars also showed moderated corrosion concentrated around the column-foundation joint section.

Figure 5.69 Condition of Specimen PT-FA-S-PD at the End of Testing
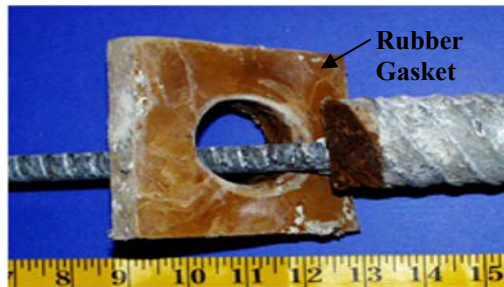
Complete Cage   *Spiral*

Rebar #6

Figure 5.70 Reinforcement Condition for Specimen PT-FA-S-PD.

Duct #1   *PT Bar #2 and Duct #2*

PT Bar #3 and Duct #3

Figure 5.71 Duct and PT Bar Condition for Specimen PT-FA-S-PD

5.4.4.1.9 Specimen PT-TC-S-EB (Post-Tensioned, Class C Concrete, Service Load, Epoxy –Coated PT Bar)

Few corrosion stains were visible at the end of testing in the base of the column, as shown in Figure 5.72.

Figure 5.73 shows that spiral reinforcement corrosion was limited to discoloration in the whole spiral length and mild steel longitudinal reinforcement had negligible corrosion.

Figure 5.74 showed ducts had very severe corrosion and extensive area loss in the first two to three inches from the column base level, behind the rubber gasket location.

Corrosion Rating:

Specimen	PT-TC-S-EB
Autopsy after 6.5 years	
Spiral	291
Rebar	6
Dowel	NA
Duct #1	1740
Duct #2	16
Duct #3	2590
Duct #4	440
PT-Bar #1,#2	42
PT-Bar #3,#4	10

Epoxy-coated post-tensioning bars (PT Bars #3 and #4) showed localized corrosion at the column-foundation joint section.   The other areas of bar were in excellent condition. Regular black steel bars (PT Bars #1 and #2) had light to moderate corrosion in the vicinity (+/- 10 inches) of the column base.
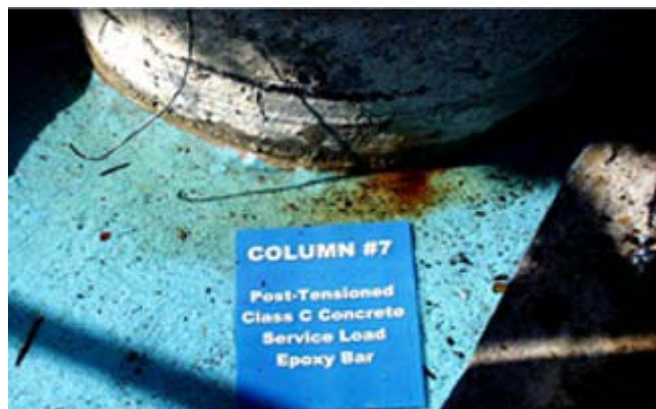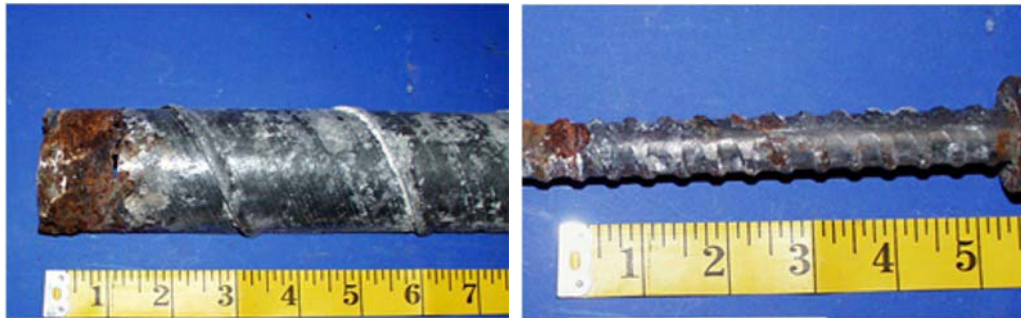

Figure 5.72 Condition of Specimen PT-TC-S-EB at the End of Testing

Spiral

Rebar #3

Figure 5.73 Reinforcement Condition for Specimen PT-TC-S-EB

Duct #4

PT Bar #1

PT Bar #3

Figure 5.74 Duct and PT Bar Condition for Specimen PT-TC-S-EB

5.4.4.1.10 Specimen PT-TC-S-GB (Post-Tensioned, Class C Concrete, Service Load, Galvanized PT Bar)

Figure 5.75 showed that at the end of testing, no cracking or other signs of distress were observed.

Figure 5.76 indicates that the spiral reinforcement in the dripper side had only light corrosion at a level of three inches from the column base, and light corrosion in the center region from a height of 53 inches to 64 inches. In the non-dripper side, no corrosion was found in the spiral steel. No corrosion was found on mild steel longitudinal reinforcement .

Corrosion Rating:

Specimen	PT-TC-S-GB
Autopsy after 6.5 years	
Spiral	331
Rebar	0
Dowel	NA
Duct #1	2174
Duct #2	1810
Duct #3	2664
Duct #4	2665
PT-Bar #1,#2	39
PT-Bar #3,#3	21

Figure 5.77 shows that ducts were corroded with extensive area loss in the first two inches from the column base level, at the rubber gasket location.

Figure 5.75 Condition of Specimen PT-TC-S-GB at the End of Testing

Galvanized PT bars (PT Bars #3 and #4) showed localized corrosion and pitting at the column base level. Black steel bars showed a more uniform corrosion in the vicinity of the joint section (the region defined between 12 inches at each side of the joint).

Complete Cage

Spiral

Rebar #3

Figure 5.76 Reinforcement Condition for Specimen PT-TC-S-GB

Duct

PT Bar #4

Figure 5.77 Reinforcement Condition for Specimen PT-TC-S-GB

5.4.4.2 Corrosion Rating Summary

Spiral, longitudinal mild steel, dowel, duct and post-tensioning bar ratings are listed in Tables 5.14 through 5.24, and plotted in Figure 5.78 through Figure 5.87. Average, standard deviation and median values are listed at the bottom of the total corrosion tables. All these results correspond to the autopsy performed at six and a half years of exposure testing.

Data is presented in two analysis scenarios:

- Maximum corrosion rating in any two-inch increment
- Total corrosion rating in the complete element, adding corrosion rating for all increments

Specimen notation from Table 5.4 is repeated herein, in Table 5.14, to assist the reader:

Table 5.14 Specimen Notation[5.1]

Connection Type	Loading	Concrete type	PT Protection
DJ: **Doweled Joint**	**N:** No Load	**TC:** TxDOT Class C	**PD:** Plastic Duct
PT: **Post-Tensioned Joint**			**EB:** Epoxy-Coated PT Bar**
NJ: **No dowel**	**S:** Service Load	**FA:** 35% Fly Ash	**GB:** Galvanized PT Bar**
			Blank: Not applicable (i.e., no PT)
Example: PT-TC-S-PD			

* plastic ducts used for bars 1 and 2, galvanized steel ducts used for bars 3 and 4

** epoxy-coated or galvanized bars used for bars 3 and 4, uncoated bars used for bars 1 and 2

Table 5.15 Maximum Spiral Corrosion Rating
in any two-inch increment for All Specimens

Specimen	Maximum Spiral Corrosion Rating	
Name	Dripper side	Non-Dripper side
NJ-TC-N	100	2
DJ-TC-N	62	4
DJ-FA-S	8	4
DJ-TC-S	8	4
NJ-TC-S	3470	1
PT-TC-N-PD	8	4
PT-TC-S-PD	2	2
PT-FA-S-PD	2	2
PT-TC-S-EB	1	1
PT-TC-S-GB	2	2

Table 5.16 Total Spiral Corrosion Rating for All Specimens

Specimen	Total Spiral Corrosion Rating		
Name	Dripper side	Non-Dripper side	Total
NJ-TC-N	322	210	532
DJ-TC-N	367	228	595
DJ-FA-S	175	185	360
DJ-TC-S	216	242	458
NJ-TC-S	10123	143	10266
PT-TC-N-PD	177	174	351
PT-TC-S-PD	169	170	339
PT-FA-S-PD	159	178	337
PT-TC-S-EB	148	143	291
PT-TC-S-GB	177	154	331
Average	1203.3	182.7	1386
Std. Dev.	2974.1	32.5	2961.5
Median	177	176	355.5

505

***Table 5.17 Maximum Rebar Corrosion Rating
in any two-inch Increment for All Specimens.***

Specimen Name	Maximum Rebar Corrosion Rating
NJ-TC-N	2
DJ-TC-N	2
DJ-FA-S	1
DJ-TC-S	2
NJ-TC-S	8
PT-TC-N-PD	2
PT-TC-S-PD	2
PT-FA-S-PD	2
PT-TC-S-EB	2
PT-TC-S-GB	0

Table 5.18 Total Rebar Corrosion Rating for All Specimens

Specimen Name	Total Rebar Corrosion Rating						
	Bar #1	Bar #2	Bar #3	Bar #4	Bar #5	Bar #6	Total
NJ-TC-N	0	2	0	0	0	0	2
DJ-TC-N	3	7	4	8	9	4	35
DJ-FA-S	4	13	0	0	2	0	19
DJ-TC-S	9	2	9	3	0	3	26
NJ-TC-S	16	10	0	0	0	6	32
PT-TC-N-PD	0	0	6	0	0	3	9
PT-TC-S-PD	0	0	0	0	3	0	3
PT-FA-S-PD	0	0	0	3	3	6	12
PT-TC-S-EB	2	4	0	0	0	0	6
PT-TC-S-GB	0	0	0	0	0	0	0
Average	3.4	3.8	1.9	1.4	1.7	2.2	14.4
Std. Dev.	5.0	4.4	3.1	2.5	2.7	2.4	12.2
Median	1	2	0	0	0	1.5	10.5

**Table 5.19 Maximum Dowel Corrosion Rating
in any two-inch Increment for All Specimens**

Specimen Name	Maximum Dowel Corrosion Rating
NJ-TC-N	NA
DJ-TC-N	2276
DJ-FA-S	591
DJ-TC-S	8
NJ-TC-S	NA
PT-TC-N-PD	NA
PT-TC-S-PD	NA
PT-FA-S-PD	NA
PT-TC-S-EB	NA
PT-TC-S-GB	NA

NA: NON APPLICABLE

Table 5.20 Total Dowel Corrosion Rating for All Specimens

Specimen Name	Total Dowel Corrosion Rating						
	Dowel #1	Dowel #2	Dowel #3	Dowel #4	Dowel #5	Dowel #6	Total
NJ-TC-N	NA	NA	NA	NA	NA	NA	NA
DJ-TC-N	24	8	15	2284	365	8	2704
DJ-FA-S	603	4	0	4	4	4	619
DJ-TC-S	20	26	25	1	6	8	86
NJ-TC-S	NA	NA	NA	NA	NA	NA	NA
PT-TC-N-PD	NA	NA	NA	NA	NA	NA	NA
PT-TC-S-PD	NA	NA	NA	NA	NA	NA	NA
PT-FA-S-PD	NA	NA	NA	NA	NA	NA	NA
PT-TC-S-EB	NA	NA	NA	NA	NA	NA	NA
PT-TC-S-GB	NA	NA	NA	NA	NA	NA	NA
Average	216	13	13	763	125	7	1136
Std. Dev.	273.9	9.6	10.3	1075.5	169.7	1.9	1129.7
Median	24	8	15	4	6	8	619

NA: NON APPLICABLE

Table 5.21 Maximum Duct Corrosion Rating in any two-inch Increment for All Specimens

Specimen Name	Maximum Duct Corrosion Rating			
	Duct #1	Duct #2	Duct #3	Duct #4
NJ-TC-N	NA	NA	NA	NA
DJ-TC-N	NA	NA	NA	NA
DJ-FA-S	NA	NA	NA	NA
DJ-TC-S	NA	NA	NA	NA
NJ-TC-S	NA	NA	NA	NA
PT-TC-N-PD	Plastic	Plastic	232	2
PT-TC-S-PD	Plastic	Plastic	292	1446
PT-FA-S-PD	Plastic	Plastic	8	8
PT-TC-S-EB	1732	8	2582	432
PT-TC-S-GB	2166	1802	2656	2657

NA: NON APPLICABLE

Table 5.22 Total Duct Corrosion Rating for All Specimens

Specimen Name	Total Duct Corrosion Rating			
	Duct #1	Duct #2	Duct #3	Duct #4
NJ-TC-N	NA	NA	NA	NA
DJ-TC-N	NA	NA	NA	NA
DJ-FA-S	NA	NA	NA	NA
DJ-TC-S	NA	NA	NA	NA
NJ-TC-S	NA	NA	NA	NA
PT-TC-N-PD	Plastic	Plastic	276	4
PT-TC-S-PD	Plastic	Plastic	312	1461
PT-FA-S-PD	Plastic	Plastic	12	12
PT-TC-S-EB	1740	16	2590	440
PT-TC-S-GB	2174	1810	2664	2665
Average	1957	913	1171	916
Std. Dev.	217.0	897.0	1193.7	1022.9
Median	1957	913	312	440

NA: NON APPLICABLE

Table 5.23 Maximum PT-Bar Corrosion Rating in any two-inch Increment for All Specimens

Specimen Name	Maximum PT-Bar Corrosion Rating
NJ-TC-N	NA
DJ-TC-N	NA
DJ-FA-S	NA
DJ-TC-S	NA
NJ-TC-S	NA
PT-TC-N-PD	608
PT-TC-S-PD	4
PT-FA-S-PD	4
PT-TC-S-EB	4
PT-TC-S-GB	4

NA: NON APPLICABLE

Table 5.24 Total PT-Bar Corrosion Rating for All Specimens

Specimen Name	Total PT-Bar Corrosion Rating				
	Bar #1	Bar #2	Bar #3	Bar #4	Total
NJ-TC-N	NA	NA	NA	NA	NA
DJ-TC-N	NA	NA	NA	NA	NA
DJ-FA-S	NA	NA	NA	NA	NA
DJ-TC-S	NA	NA	NA	NA	NA
NJ-TC-S	NA	NA	NA	NA	NA
PT-TC-N-PD	15	626	16	16	673
PT-TC-S-PD	16	22	27	81	146
PT-FA-S-PD	37	15	12	31	95
PT-TC-S-EB	27	15	4	6	52
PT-TC-S-GB	18	21	12	9	60
Average	23	140	14	29	205
Std. Dev.	8.4	243.1	7.5	27.6	236.2
Median	18	21	12	16	95

NA: NON APPLICABLE
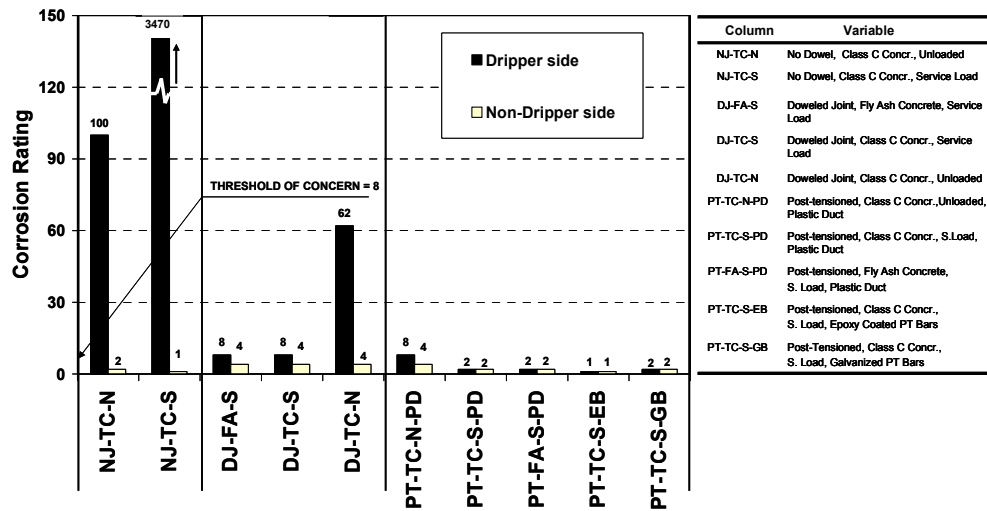
Figure 5.78 Maximum Spiral Corrosion Rating in any two-inch Increment for All Specimens.
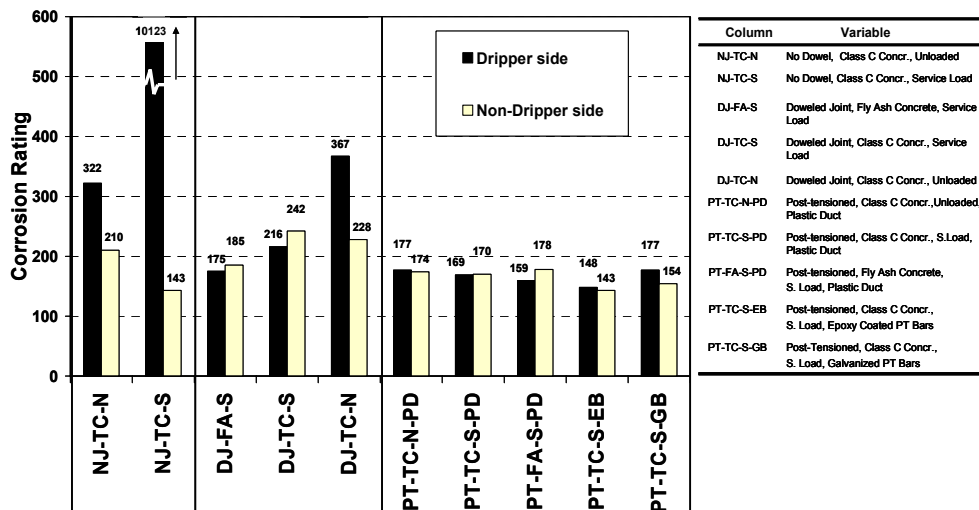
Figure 5.79 Total Spiral Corrosion Rating for All Specimens.

510
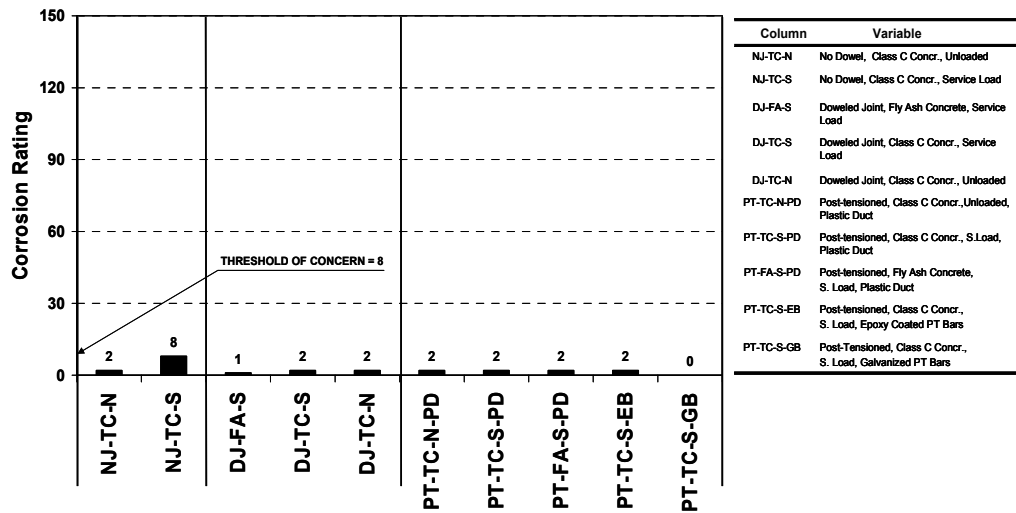
*Figure 5.80 Maximum Rebar Corrosion Rating
in any two-inch Increment for All Specimens.*
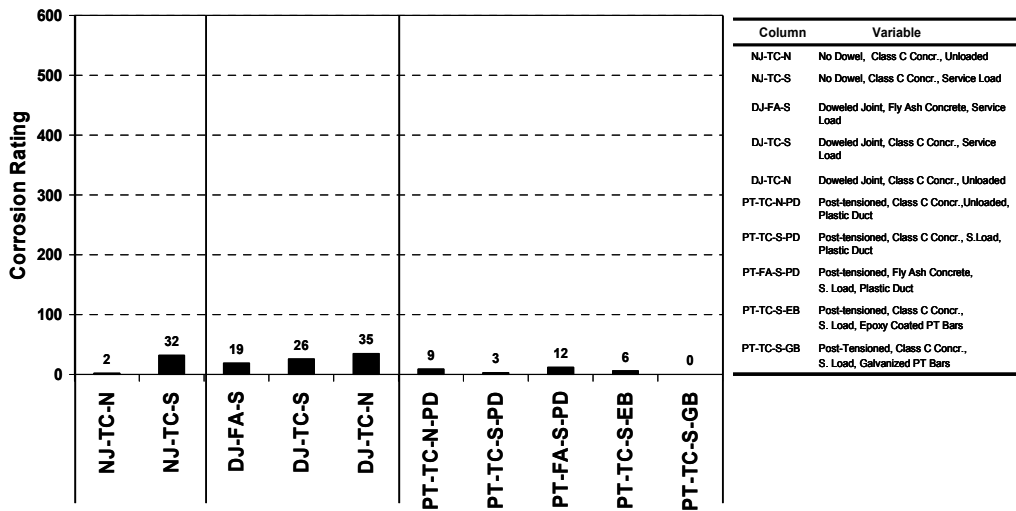
Figure 5.81 Total Rebar Corrosion Rating for All Specimens.

511
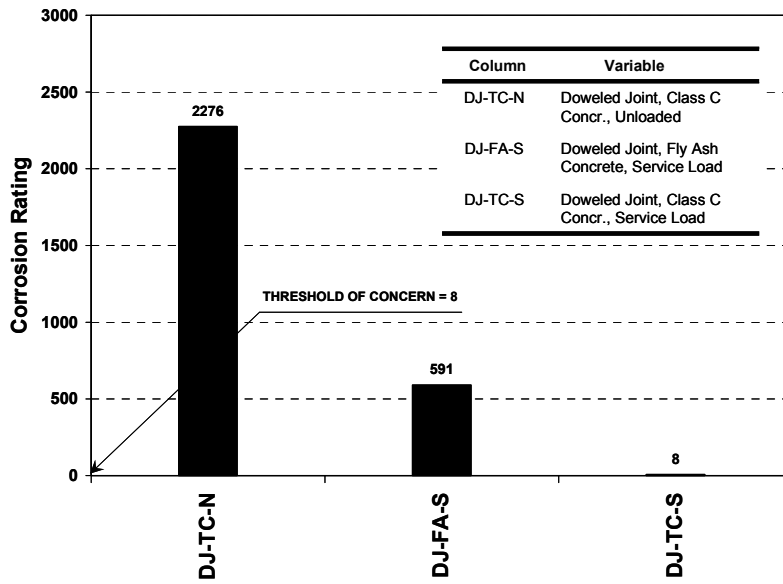
*Figure 5.82 Maximum Dowel Corrosion Rating
in any two-inch Increment for All Specimens.*
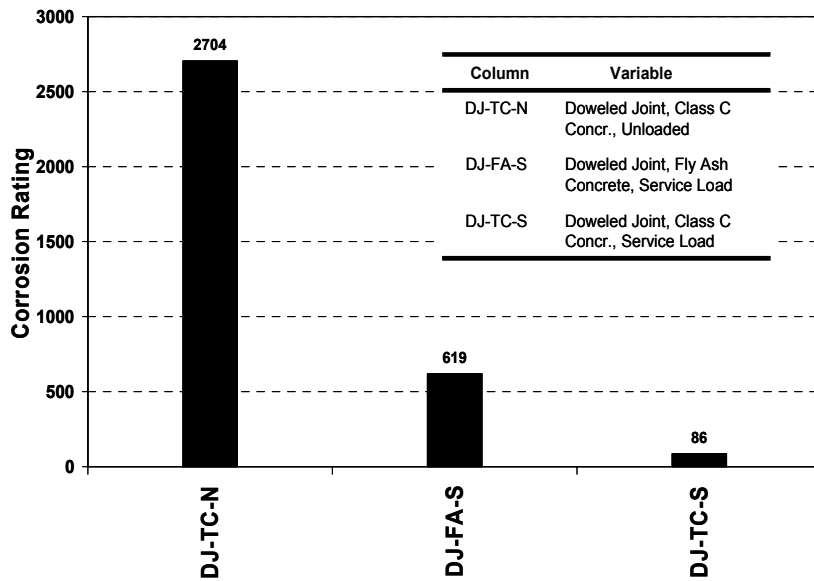
Figure 5.83 Total Dowel Corrosion Rating for All Specimens.

512
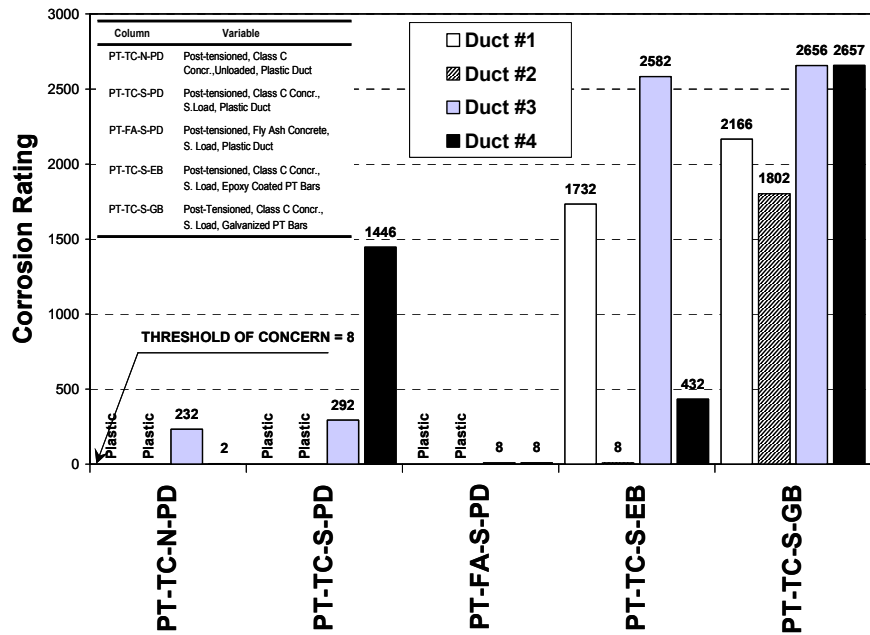
Figure 5.84 Maximum Duct Corrosion Rating in any two-inch Increment for All Specimens.
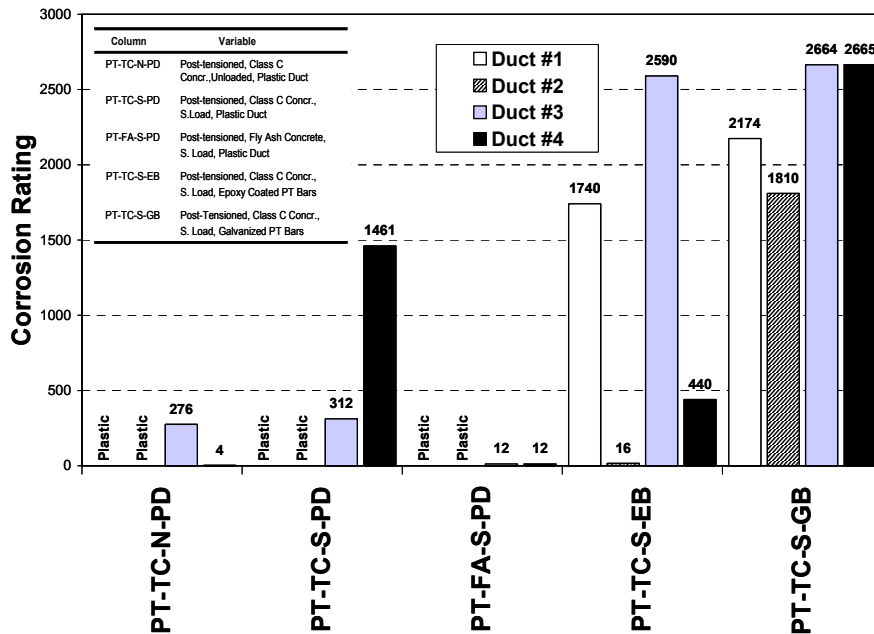
Figure 5.85 Total Duct Corrosion Rating for All Specimens.

513
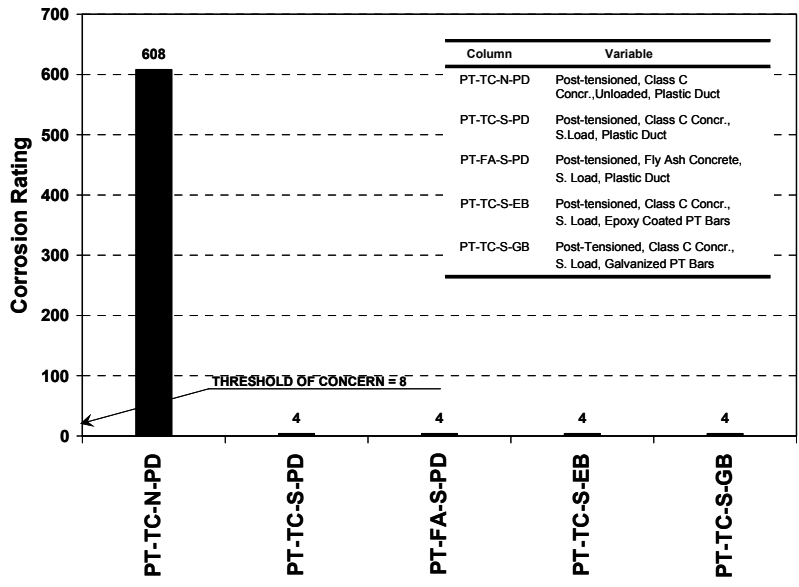
Figure 5.86 Maximum PT-Bar Corrosion Rating in any two-inch Increment for All Specimens.
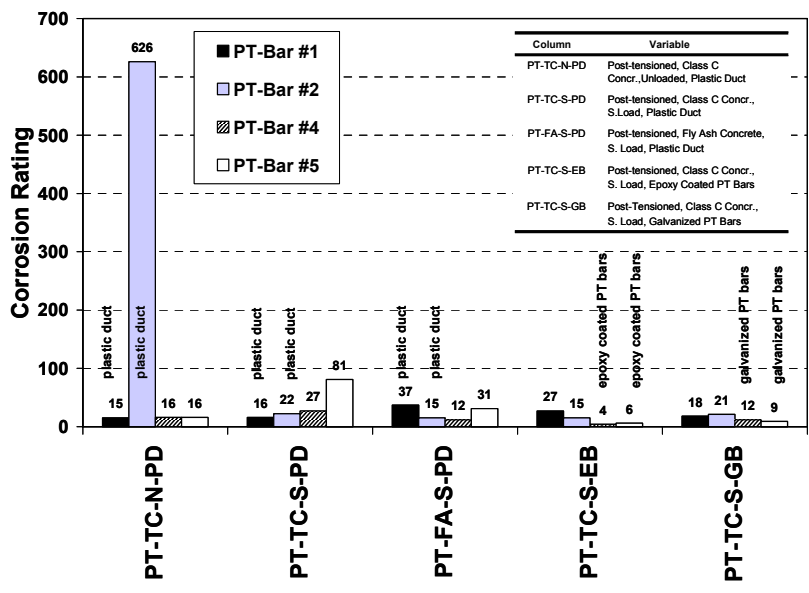
Figure 5.87 Total PT-Bar Corrosion Rating for All Specimens.

514

Based on the pitting values of Tables 5.12 and 5.13, and to put corrosion ratings in perspective, a "threshold value of concern" was assigned at the corrosion rating of 8, for the maximum (rebar, PT bars, and duct) corrosion rating found in any two-inch interval. A corrosion rating of 8 corresponds to pitting visible to the unaided eye in rebar or PT bars and pitting and severe corrosion found on the duct surface. Above this threshold value, severe pitting, and section loss is expected.

A threshold value is not indicated in the total corrosion ratings, since it could be misleading. However, by comparing maximum corrosion ratings with total corrosion rating, it is possible to gain a sense of corrosion severity and extent in the element.

After six and a half years of exposure, Figure 5.78 shows that in the dripper side, specimen NJ-TC-S (No dowel, type C concrete, service load) showed extremely severe spiral corrosion rating, over 400 times the threshold value. With applied loading the epoxy joint used in non-joint specimens could have opened up in the North side (refer to applied moment direction in Figure 5.13) and moisture and chlorides could have been able to penetrate the joint (see Figure 5.60). In addition, it appears that the concrete cover was between half to one inch at the base of the column, instead of the design value of two inches, and therefore moisture could have penetrated rapidly to the spiral level.

Specimen NJ-TC-N and DJ-TC-N also showed very high maximum spiral corrosion ratings. Specimens DJ-FA-S, DJ-TC-S, and all post-tensioned specimens showed essentially negligible maximum spiral corrosion ratings at or below the threshold value. In the non-dripper side, all specimens showed maximum corrosion ratings below the threshold value.

Spiral corrosion in all specimens was mostly concentrated in the bottom 18 inches. Total spiral corrosion was higher in specimen NJ-TC-S, the same

515

specimen that showed maximum spiral corrosion in any two-inch increment. The worst performance of this specimen was followed by moderately elevated readings for specimens NT-TC-N and DJ-TC-N. For all other specimens, (DJ-FA-S, DJ-TC-S, and all PT specimens) total spiral corrosion rating is similar and there is not a clear distinction between the dripper and the non dripper sides.

Maximum rebar corrosion rating as shows in Figure 5.80 was in all cases below the threshold value, at levels of very light corrosion, except specimen NJ-TC-S that had a rating of 8, just at the threshold value, meaning some pitting visible with the unaided eye. Using maximum corrosion ratings no clear distinction exists, between post-tensioned and non post-tensioned specimens, and between specimens with Fly Ash concrete and Class C concrete.

Total rebar corrosion ratings of Figure 5.81 suggest a better performance of PT specimens. However, the exception was specimen NJ-TC-N (No dowel, class C concrete, no load), which showed very low total corrosion rating, only surpassed by specimen PT-TC-S-GB.

Dowel corrosion was mostly concentrated at the column-foundation interface. At this cold joint localized corrosion was extremely severe. Figure 5.82 indicated that specimens DJ-TC-N and DJ-FA-S showed very large dowel section loss. Specimens DJ-TC-S showed a maximum corrosion rating equal to the threshold value, representing some pitting in the bar surface. Total dowel corrosion ratings were very similar to the maximum dowel corrosion ratings since corrosion was localized. Dowel joints did not have an epoxy bonding agent at the joint, as with the no-joint specimens, and therefore, moisture and chlorides found an easy path towards the dowel location. The loaded specimen with Standard Concrete may have been benefited from the precompression applied to the joint. It is not clear the reason why Specimen DJ-FA-S showed more dowel corrosion than Specimen DJ-TC-S. One possibility is to consider that loading

was able to open up a larger opening at the joint in the South side, allowing for moisture to penetrate more easily.

Figure 5.84 showed that specimen PT-TC-S-GB had the most extensive maximum duct corrosion rating; however this corrosion was mostly concentrated in the first two-inch increment, and was mostly due to the negative conditions given by the use of the rubber gasket at the column-foundation interface. The rubber gaskets were found to be detrimental for the performance of galvanized ducts, since moisture was trapped in the inner gasket faces and corrosion was accelerated. This result shows that a better splicing method is required. For the same reasons, specimens PT-TC-S-EB and PT-TC-S-PD showed high duct corrosion ratings in the first and second two-inch increments. Specimen PT-FA-S-PD showed maximum duct corrosion ratings equal to the threshold value; however this specimen was also starting to have severe localized corrosion due to the use of the gasket. Figure 5.71 (PT bar #3 and duct #3) clearly shows this situation.

Since corrosion of galvanized steel ducts was mostly concentrated underneath the rubber gasket, total duct corrosion ratings are very similar to maximum duct corrosion rating.

Figure 5.86 shows that PT bar maximum corrosion rating was generally below the threshold value of concern, meaning only moderate surface corrosion in the most damaged two-inch increment. The only exception was specimen PT-TC-N-PD (post-tensioned, class C concrete, no load, plastic duct) that showed very severe pitting in PT bar #2, as was shown in Figure 5.65. This PT bar showed this high corrosion at the column-foundation interface, where the plastic duct was interrupted. This shows the serious error made at the specimen definition, not adequately spliceing ducts to the foundation.

517

Corrosion on PT bars extended a few inches up from the column base section, resulting in the total corrosion ratings shown in Figure 5.87. However, the corrosion was low in most specimens.

Epoxy coated and galvanized PT bars showed somewhat lower total corrosion rating than plain bars, and corrosion on these bars was more concentrated around the column-foundation interface.

5.4.4.3 *Chloride Content in Grout*

Grout chloride content profiles are shown in Figure 5.88 through Figure 5.92. Grout samples were taken at 3, 15, 30 and 50 inches from the column base.

The acid soluble chloride threshold value of concern is shown in the figures at 0.14% assuming chloride threshold of 0.2% by weight of cement and a water cement ratio of 0.44.

As observed in the figures, grout chloride contents at 30 and 50 inches are in all cases lower than the threshold value. At 15 inches, only the grout for PT bar #3 (galvanized) in specimen PT-TC-S-GB showed chloride contents in excess of the threshold value. It exceeded the threshold by 80%. At 3 inches (submerged zone) specimens showed grout acid soluble-chloride contents higher than the threshold value in five PT bars: PT bar #1 and #3 in specimen PT-TC-N-PD, PT bar #1 in specimen PT-TC-S-PD, PT bar #1 in specimen PT-TC-S-EB; and, PT bar #3 in specimen PT-TC-S-GB.

After autopsy very high porosity was observed in grouts for specimens PT-TC-S-EB and PT-TC-S-GB. As explained in Section 5.2.6 the constructors of the specimens were concerned that during construction and grout injection, it was possible that incorrectly labeled cement barrels may have resulted in partial or complete cement replacement with Class F Fly Ash, with the most likely columns affected by this error being specimens PT-TC-S-EB and PT-TC-S-GB. The

resulting porosity could be the reason for the high chloride content observed at 15 inches.
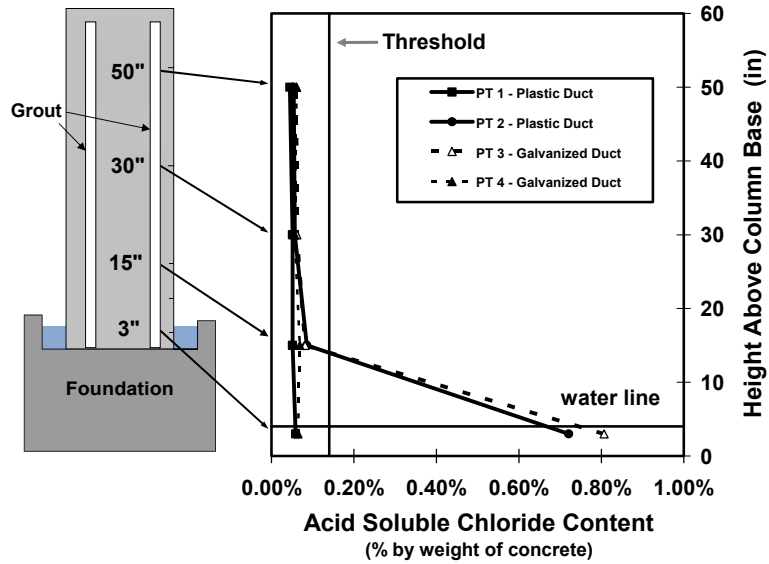
Figure 5.88 Grout Chloride Penetration for Column PT-TC-N-PD at End of Testing
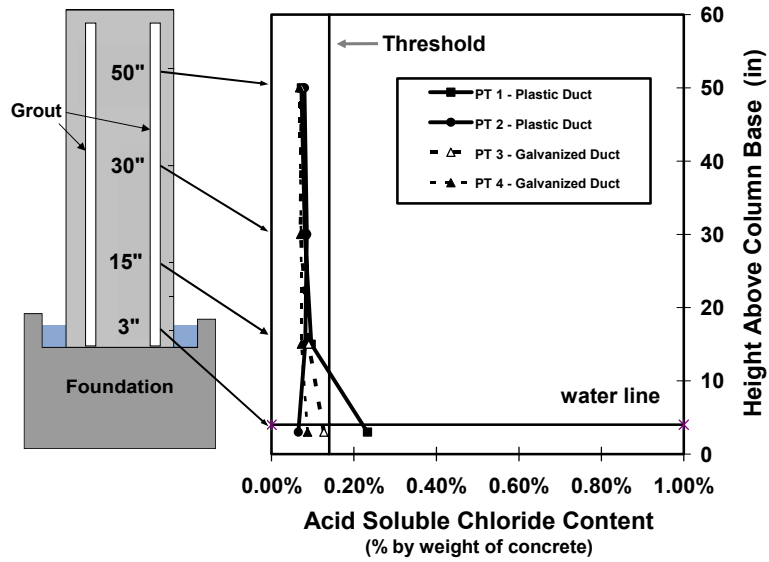
***Figure 5.89 Grout Chloride Penetration for Column PT-TC-S-PD
at End of Testing***
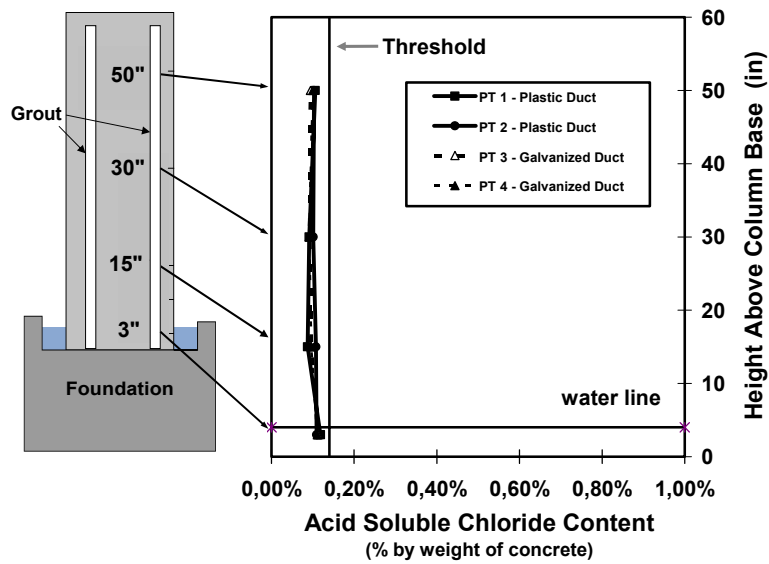
***Figure 5.90 Grout Chloride Penetration for Column PT-FA-S-PD
at End of Testing***

520
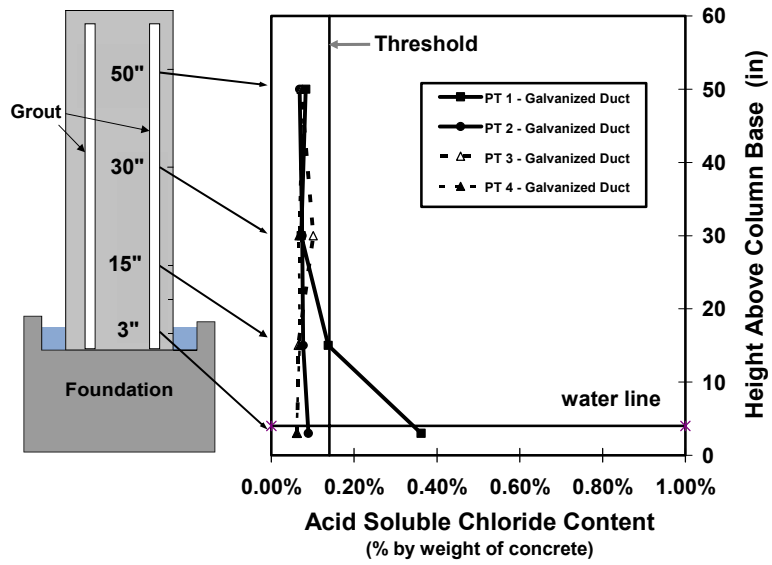
*Figure 5.91 Grout Chloride Penetration for Column PT-TC-S-EB
at End of Testing*
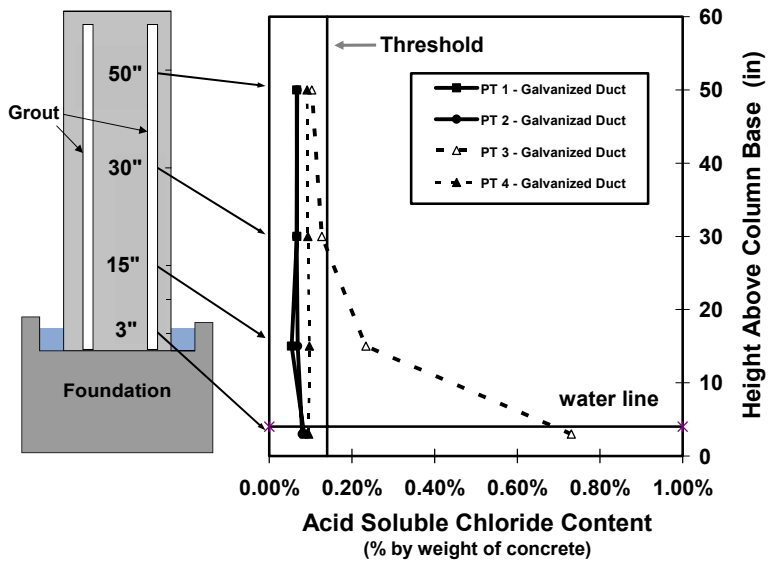
*Figure 5.92 Grout Chloride Penetration for Column PT-TC-S-GB
at End of Testing*

521

5.5   ANALYSIS AND DISCUSSION OF RESULTS

After full autopsy has been performed on the column specimens at six and a half years of accelerated exposure testing, the effect of all variables involved in this testing program can be analyzed and compared.   Limited autopsy results performed at the end of 1998 for specimens DJ-TC-N (doweled joint - Class C concrete - unloaded) and PT-TC-S-PD (post-tensioned – Class C concrete – service load – plastic duct) were described in Reference 5.1.

5.5.1   Overall Performance

One of the objectives for this research program was to investigate the effect of typical the cold joint between foundation and columns on chloride ion movement and corrosion activity.   After autopsy, corrosion in dowels, ducts and post-tensioning bars was mostly found concentrated at the column-foundation interface.   The joint acted as a weak link in corrosion protection, behaving as a pre-formed crack, which could have opened under loading.   Specimen NJ-TC-N (No dowel-Class C concrete – unloaded) showed very low spiral and rebar corrosion with respect to the other specimens, which could be explained by the epoxy bonding agent used to prepare the foundation surface on no-joint specimens prior to casting.   Figure 5.93 shows the severe section loss due to corrosion in a dowel crossing the joint location.

The wicking effect (migration of chlorides upward in the concrete from ponded base) was typically observed in the first 18 inches from the base of the columns.   Spiral, rebar, duct dowel and post-tensioned bar corrosion was very severe at or near the column-foundation interface and decreased with increasing column height.

*Figure 5.93 Typical corrosion and section loss found on dowels
at the column-foundation interface*

As shown in Figure 5.94, galvanized steel ducts were found severely corroded inside the rubber gaskets that were supposed to seal the "dead end" of these ducts. The use of these gaskets was found to be detrimental for the performance of galvanized ducts, since moisture was trapped and corrosion was accelerated. A better spliceing method is required.
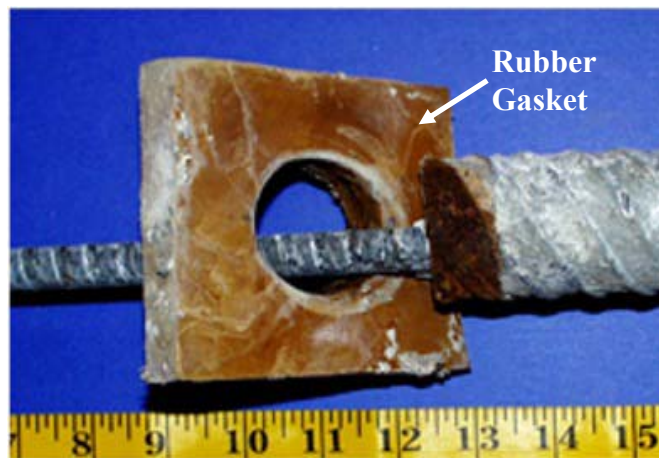
Figure 5.94 Duct corrosion found inside rubber gaskets

Epoxy coated bars and galvanized post-tensioned bars showed localized corrosion at the column-foundation interface, but negligible occurrence of corrosion away from the interface.

The relative performance of the column specimens is better described by organizing the corrosion ratings according to performance. Figure 5.95 through Figure 5.98 show the results for spiral, rebar, dowel and PT-bars. Ducts have not been included, since some specimens have plastic ducts and others only galvanized ducts, which makes it difficult to compare the specimens with average values. Duct performance can be analyzed with the use of Figure 5.84 and Figure 5.85.

Specimen NJ-TC-S shows the worst spiral corrosion rating. The reason appears to be the effect of loading on the epoxy joint on this specimen, slightly opening the North joint side and allowing moisture and chlorides to penetrate the joint. In addition, concrete cover on spiral at the bottom of the column seems to have been somewhat smaller than the 2-inch design cover, allowing for moisture and chlorides to easily penetrate the concrete up to the spiral level. Post-tensioned columns show the lesser spiral corrosion, showing the positive effect of concrete and joint precompression.

The better rebar performance was shown for post-tensioned columns, except for Specimen NJ-TC-N. This no-joint specimen was unloaded and epoxy jointed. The worst rebar performance was shown on Specimen DJ-TC-N, since this specimen did not have any epoxy bonding agent between the column and the foundation, which allowed the joint to act as a preset crack. This specimen was unloaded, which could have played an important role. There was not a distinct trend among specimens with fly ash and standard concrete. Fly ash non-post-tensioned specimen DJ-FA-S (doweled, fly ash concrete, service load) showed

only a slight decrease in rebar corrosion with respect to Specimen DJ-TC-S (doweled specimen with standard concrete and service load).

Corrosion Rating

Column	Variable
NJ-TC-N	No Dowel, Class C Concr., Unloaded
NJ-TC-S	No Dowel, Class C Concr., Service Load
DJ-FA-S	Doweled Joint, Fly Ash Concrete, Service Load
DJ-TC-S	Doweled Joint, Class C Concr., Service Load
DJ-TC-N	Doweled Joint, Class C Concr., Unloaded
PT-TC-N-PD	Post-tensioned, Class C Concr.,Unloaded, Plastic Duct
PT-TC-S-PD	Post-tensioned, Class C Concr., S.Load, Plastic Duct
PT-FA-S-PD	Post-tensioned, Fly Ash Concrete, S. Load, Plastic Duct
PT-TC-S-EB	Post-tensioned, Class C Concr., S. Load, Epoxy Coated PT Bars
PT-TC-S-GB	Post-Tensioned, Class C Concr., S. Load, Galvanized PT Bars

Spiral decreasing performance after six and a half years of exposure

PT-TC-S-EB 291
PT-TC-S-GB 331
PT-FA-S-PD 337
PT-TC-S-PD 339
PT-TC-N-PD 351
DJ-FA-S 360
DJ-TC-S 458
NJ-TC-N 532
DJ-TC-N 595
NJ-TC-S 10266

Figure 5.95 Total Spiral Corrosion Rating Ordered According to Performance

Corrosion Rating

Column	Variable
NJ-TC-N	No Dowel, Class C Concr., Unloaded
NJ-TC-S	No Dowel, Class C Concr., Service Load
DJ-FA-S	Doweled Joint, Fly Ash Concrete, Service Load
DJ-TC-S	Doweled Joint, Class C Concr., Service Load
DJ-TC-N	Doweled Joint, Class C Concr., Unloaded
PT-TC-N-PD	Post-tensioned, Class C Concr.,Unloaded, Plastic Duct
PT-TC-S-PD	Post-tensioned, Class C Concr., S.Load, Plastic Duct
PT-FA-S-PD	Post-tensioned, Fly Ash Concrete, S. Load, Plastic Duct
PT-TC-S-EB	Post-tensioned, Class C Concr., S. Load, Epoxy Coated PT Bars
PT-TC-S-GB	Post-Tensioned, Class C Concr., S. Load, Galvanized PT Bars

Rebar decreasing performance after six and a half years of exposure

PT-TC-S-GB 0
NJ-TC-N 2
PT-TC-S-PD 3
PT-TC-S-EB 6
PT-TC-N-PD 9
PT-FA-S-PD 12
DJ-FA-S 19
DJ-TC-S 26
NJ-TC-S 32
DJ-TC-N 35

Figure 5.96 Total Rebar Corrosion Rating Ordered According to Performance

Specimen DJ-TC-N (doweled joint, standard concrete, unloaded) showed the worst dowel performance. The reason is associated with the joint not being epoxy sealed, serving as a preset crack. The dowel performance of fly ash concrete specimen DJ-FA-S was worst than Specimen DJ-TC-S. This result is explained by the fact that corrosion mostly occurred at the column-foundation interface, and therefore the concrete in the column did not play an important role.
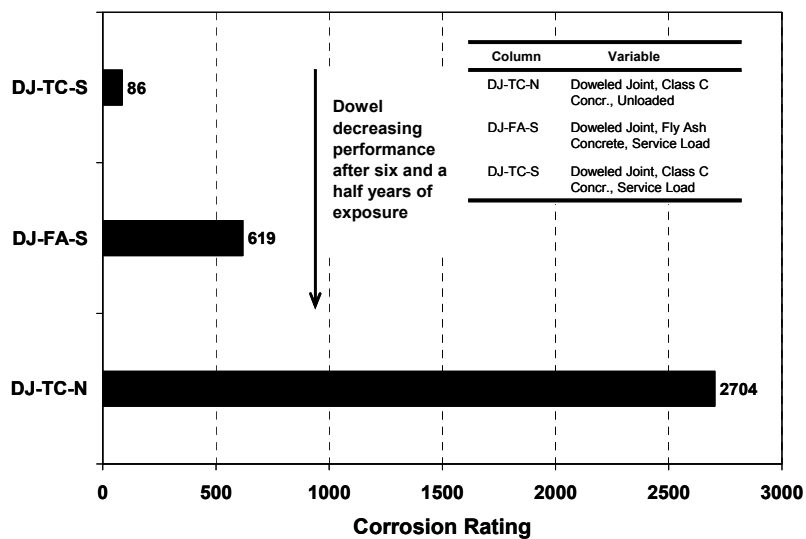
Figure 5.97 Total Dowel Corrosion Rating Ordered According to Performance

Post-tensioned bar corrosion was mostly concentrated at the column-foundation interface, as in the previous case for the dowels. For this reason, concrete type did not play an important role. The worst performance was observed in Specimen PT-TC-N-PD (post-tensioned column, standard Class C concrete, unloaded, plastic duct). However it is not clear why this performance is worst than Specimen PT-TC-S-PD (post-tensioned column , standard Class C concrete, service load, plastic duct). The best performance was observed in

526

galvanized and epoxy coated post-tensioning bars, although in both cases corrosion had started.
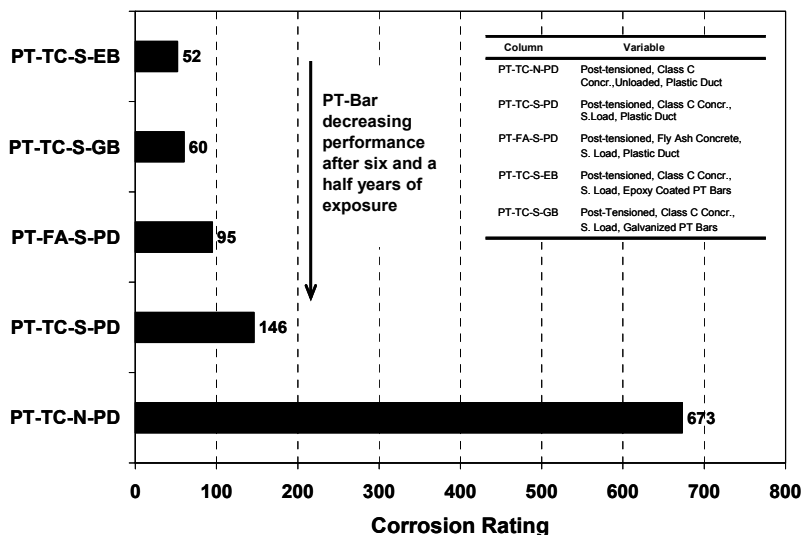
Figure 5.98 Total PT-Bar Corrosion Rating
Ordered According to Performance

5.5.2   Comparison between Half-Cell Potentials and Corrosion Ratings

At the end of testing, half-cell potential readings were compared with corrosion found during autopsies on specimen reinforcement.   In general, half-cell potentials were able to detect the higher probability of corrosion occurring at the base of the column, and low to negligible probability of corrosion above column mid-height.   However, since dowel bars, post-tensioning bars and ducts all showed severe corrosion at the joint area, it is difficult to determine which source of corrosion potential was being detected by the half-cell readings.   The post-tensioning bar may have been in electrical contact with the mild steel reinforcement, and therefore, half-cell potential measurements may have been a combination of active corrosion sources.

527

5.5.3 Effect of Loading

The effect of loading on spiral corrosion is not clear when looking at the non-prestressed specimen corrosion rating data, Figure 5.95. Specimen NJ-TC-S (No dowel-Class C concrete – service load) showed very high corrosion ratings when compared to specimen NJ-TC-N (No dowel-Class C concrete-no load); however, the trend was reversed for specimen DJ-TC-S (doweled – Class C concrete – service load) that showed less corrosion rating than specimen DJ-TC-N (doweled – Class C concrete – no load). A more clear distinction was found on post-tensioned specimens, where spiral corrosion rating was higher in the non-loaded specimen than in the specimens continuously subjected to service load. Similar results were obtained for rebar corrosion, see Figure 5.96.

Dowels and post-tensioned bars (see Figures 5.97 and Figure 5.98) were found to corrode more at the column-foundation interface in non-loaded specimens; in contrast to galvanized ducts, which corroded more in specimens under service loading. Service loading may have caused the joints to open. However, the contradiction between dowel and duct corrosion, makes it difficult to draw any definite conclusions.

5.5.4 Effect of Trickle Saltwater

The trickle system on one face of the columns did produce a clear increase in spiral corrosion in non-prestressed specimens, as shown in Table 5.15. The trend was not shown in post-tensioned specimens, where spiral corrosion ratings were very similar in both column faces. Rebar, duct or post-tensioned bars did not show any distinct corrosion trend with respect to dripper and non-dripper sides (see Figure 5.13 for dripper and element location, and corrosion rating data on Tables 5.18, 5.22 and 5.24).

5.5.5 Effect of Joint Type

Corrosion was mostly concentrated at the column-foundation interface, see examples in Figures 5.53 and 5.57 (complete cage) At this section, doweled and post-tensioned specimens showed very severe section loss, with less corrosion observed in galvanized and epoxy coated PT-bars, as shown in Figure 5.98.

There was not a distinct trend with respect to the use of post-tensioned joints versus doweled joints.   The doweled joint would be expected to provide the least corrosion protection since the joint is not precompressed. However, this behavior was not clearly shown after autopsy.

As shown in Figure 5.95 and 5.96, the use of post-tensioning did provide enhanced spiral and rebar corrosion protection, compared to non-post-tensioned specimens.   In the case of the spirals, the effect of post-tensioning was dramatic, since very severe section loss and pitting in the stirrup in non-prestressed specimens was reduced to light to moderate surface corrosion in post-tensioned specimens.

The use of post-tensioned joints also provided better resistance to the wicking effect, when acid-soluble chloride contents were compared to doweled and no-joint specimens, see Figure 5.42.

5.5.6 Effect of Concrete Type

As shown in Figure 5.97 and Figure 5.98, the effect of concrete type was not clearly shown in dowel and PT-bar performance since the corrosion in these specimens was mainly at the column-foundation interface, and therefore, chloride penetration through concrete had little effect.   On the contrary, as shown in Figures 5.84 and 5.85, duct corrosion –even when it was mostly concentrated at the column base – was lower in Fly Ash specimens.

As shown in Figures 5.95 and 5.96, spiral and rebar corrosion in non-prestressed specimens showed a better performance in Fly Ash concrete than in Class C concrete specimens. This trend was not clearly shown in post-tensioned specimens.

5.5.7 Effect of Duct Type

Since post-tensioning bar corrosion was mostly concentrated at the column-foundation interface, where ducts were interrupted, the duct type had little influence on PT-bar performance. However, advanced galvanized steel duct corrosion inside the rubber gasket, suggested a significant superiority of plastic duct. The use of the rubber gaskets was a serious error. Instead of gaskets, the ducts must have been adequately spliced at the column-foundation interface to avoid moisture and chlorides to penetrate at the joint section.

5.5.8 Effect of Post-Tensioning Bar Coatings

As shown in Figure 5.98, PT bar coatings, either epoxy or galvanized (which showed very similar results) improved the performance of post-tensioning bars, when compared to plain post-tensioning bars. From Figures 5.74 and 5.77 it is shown that the PT-bar coatings were not sufficient to stop corrosion from occurring at the column-foundation interface, but corrosion was limited to moderate surface corrosion in a few inches around the joint area.

When drawing conclusions from these observations, care must be exercised, since localized corrosion in the black steel, once it has started, could grow rapidly underneath the coatings and bar capacity could be threatened, specially when corrosion is not extended in a large bar area.

5.6 **S**UMMARY AND **C**ONCLUSIONS

Five non-prestressed and five post-tensioned columns specimens were used to investigate corrosion mechanisms and chloride ion transport ("wicking effect) in various column connection configurations and to evaluate column corrosion protection measures.   Variables included column to foundation connection (no dowel joint, doweled joint and post-tensioned joint), loading (no loading and service load – with combined moment and axial load), concrete type (TxDOT Class C concrete, and Class C Fly Ash concrete – 35% replacement by volume), prestressing bar coatings (uncoated, galvanized PT-bars, and epoxy coated PT-bars), and post-tensioning ducts (plastic and galvanized steel). Trickle water was used on one face of each column to determine the effect of salt water spray or dripping. Test specimen exposure started in July of 1996 and ended in January of 2003, after six and a half years.   Full autopsies were performed at the end of testing, and conclusions are as follows.

5.6.1 **Post-Tensioning to Improve Corrosion Protection**

The possible weak link in corrosion protection at the column-foundation interface was studied with three different configurations: no dowel joint, doweled joint and post-tensioning joint.   Determination of the effect of post-tensioning on durability through precompression of the concrete and precompression of construction joints was one of the main objectives of this research series.   The conclusions are as follows:

- Post-tensioned specimens did not show any distinct improvement in specimen performance at the column foundation interface, when compared to doweled specimens.

- Post-tensioning dramatically reduced the corrosion found on spiral reinforcement in the first 18 inches from the column base.

- Post-tensioned specimens under loading showed an increase in spiral and mild steel reinforcement corrosion protection when compared to non-loaded specimens.

- Post-tensioning reduced the risk of spiral corrosion due to saltwater dripping.

- Post-tensioning provided better resistance to the wicking effect, when acid-soluble chloride contents were compared to doweled and no-dowel specimens.

5.6.2 Fly Ash as Partial Cement Replacement in Concrete

TxDOT standard concrete mix Class C concrete was used in eight specimens (w/c = 0.45, type I/II Cement, f´c=3600). In two columns, 35% of cement by volume (31% by weight) was replaced with Class C Fly Ash, with no other significant changes to the concrete mix. After autopsy, the following conclusions are drawn:

- Fly ash concrete did seem to provide enhanced corrosion protection to galvanized steel ducts.

- Spiral and mild steel reinforcement corrosion in non-prestressed specimens showed a better performance in Fly Ash concrete than in Class C concrete specimens. This trend was not clearly shown in post-tensioned specimens.

- Post-tensioned bar corrosion did not show any distinct trend with respect to the type of concrete in the specimen.

5.6.3 Plastic Ducts for Post-Tensioning

Standard galvanized steel ducts were compared to impermeable plastic ducts in three post-tensioned specimens: Class C concrete (unloaded and service load) and Fly Ash concrete under service load. In all cases uncoated post-tensioning bars were used. The conclusions are as follows:

- Although results are very limited, advanced galvanized steel duct corrosion at the column base, inside the rubber gasket, show the superiority of using plastic ducts.

- Corrosion in post-tensioned bars in plastic ducts and galvanized ducts was always at the column-foundation interface, where the plastic or galvanized duct was interrupted. Therefore, conclusions regarding duct performance based on post-tensioning bar corrosion are not possible. The ducts need an effective splice seal at all joints.

5.6.4 Post-Tensioning Bar Coatings

Two prestressing bar coatings were investigated: epoxy coated (according to ASTM A775-97) and zinc galvanized prestressing bars. The coated bars were compared directly to uncoated bars within individual specimens. In both cases, anchorage hardware was either epoxy coated or galvanized. The following conclusions are drawn:

- Epoxy coating or galvanized post-tensioning bars showed enhanced corrosion protection, with respect to plain post-tensioning bars.

- Coatings were not sufficient to stop corrosion from occurring at the column-foundation interface. Corrosion was very localized.

- Superiority of coated bars should not be concluded, since localized corrosion may accelerate deterioration at the local level, which in turn may result in unexpected failure.

5.7   IMPLEMENTATION OF RESULTS

After full autopsy of all ten column specimens, research results generated the following findings to be implemented for partially submerged columns or columns exposed to saltwater runoff:

<u>Substructure Prestressing</u>

- Column elements should be prestressed, to improve spiral and rebar corrosion protection. However, designers should not rely entirely on post-tensioning to provide adequate corrosion protection at the cold joint. Other protection measures should be investigated.

<u>Concrete Type</u>

- Fly Ash concrete may be used to provide enhanced spiral, rebar and duct corrosion protection.

<u>Duct Types</u>

- Plastic ducts may be used to better protect post-tensioning bars. However, better sealing materials or splices should be used or developed, to seal the duct "dead" ends and protect the post-tensioning bar.

<u>Gaskets</u>

- Rubber gaskets are not effective to seal the duct "dead" ends and should not be used.

<u>Post-tensioning Bar Coatings</u>

- Galvanized steel bars or epoxy coated bars provide enhanced protection against uniform corrosion, but are susceptible to severe localized corrosion.

CHAPTER 6

Durability Design Guidelines
to Reduce Corrosion Risk

Durability design guidelines for durable bonded post-tensioned concrete tendons are the most important implementation directed aspect of the research program. Results are based on specimens that were purposely placed under a very aggressive environment. By applying salt water in continuing two week wet and dry cycles, a condition simulating a harsh and extended service application was introduced. It cannot be directly related to any specific real life exposure age.

Interim design guidelines to reduce risk from various forms of attack, including corrosion risk, were developed and published as explained in Section 1.2.3., based on research results up to 1999. After full forensic examinations of all remaining specimens in the macrocell corrosion test series, all specimens in the large scale column corrosion tests series and approximately half of the specimens from the large scale beam corrosion test series, the following items are recommended for immediate implementation. These items were included previously as they pertained to each chapter. They are repeated here as a summary of all the implementation measures found after conclusions were drawn.

6.1 MEASURES FOR IMPLEMENTATION FROM MACROCELL CORROSION TESTS

Macrocell test results generated the following findings for immediate implementation to improve corrosion protection for precast segmental construction.

Duct type

- Plastic ducts for post-tensioning should be used in all situations where aggressive exposure may occur.

Joint Type

- Epoxy joints should always be used with internal prestressing tendons.

- Dry joints should be avoided with external prestressing tendons in aggressive exposures, to protect segment mild steel reinforcement at joints and to block entry of chlorides that might be transported to locations of flaws in external tendon sheaths or anchors.

- Stringent inspection and construction practices must be exercised to guarantee good epoxy filling at the joints and complete grouting.

- Gaskets in epoxy joints should be avoided since there is a potential for incomplete epoxy coverage of the joint. Preferred practice with epoxy joints is to utilize a thorough swabbing of tendon ducts immediately after initial segment placement and stressing to seal the duct edges at the joint. Tightness of the joint should be checked by air pressure testing. Carefully coupled ducts are an alternative as long as a positive seal is obtained.

Grout type

- Calcium Nitrite Corrosion inhibitor added to the grout had little effect on the onset of corrosion but did seem to provide enhanced long-term strand corrosion protection.

6.2 MEASURES FOR IMPLEMENTATION FROM BEAM CORROSION TESTS

After final autopsies of twelve out of twenty-seven beam specimens and partial autopsies of two beam specimens, research results generated the following findings. Final autopsies of the remaining beam specimens will be more

conclusive for strand, duct and grout types, and also for the use of encapsulated anchorage systems.

Level of Prestress

- Mixed reinforcement members should not be used in aggressive exposures unless special provisions are made to effectively seal cracks and concrete cover from exposure to chlorides.

- Fully prestressed members are recommended in aggressive environments to delay moisture and chloride ingress.

- Post-tensioning systems need additional protection above the current typical practice when in aggressive environments. In particular the use of galvanized duct appears unwise. The use of plastic ducts and encapsulated anchorage protection systems appear promising but while plastic duct was clearly superior in the macrocell specimens the use in the beam specimens cannot be conclusively evaluated until after final autopsies of the remaining beam specimens.

Concrete type

- High Performance Concrete (low permeability concrete, w/c = 0.29) is recommended in aggressive environments due to the significantly reduced permeability and crack control.

- Fly ash (Class C) concrete with a higher water cement ratio (w/c = 0.44) may also be considered when the environment is less aggressive.

Duct Splices for Galvanized Ducts

- Neither the standard industry practice of duct taped sleeves nor heat shrink splices should be considered as watertight

- Better systems than industry standard or heat-shrink splices for galvanized steel ducts should be investigated and developed if galvanized duct continues to be used in non-aggressive environments.

High Performance Fly Ash Grout

- Standard Class C grout with fly ash is not recommended.

- The use of antibleed admixture appears promising but cannot be conclusively evaluated until after final autopsies of the remaining beam specimens.

Grouting Procedure

- Stringent grouting procedures should be enforced during construction.

Plastic Chairs

- Fully plastic chairs are recommended for use throughout the substructure to eliminate corrosion damage. Chairs or bolster strips that contain any steel should be avoided.

6.3 MEASURES FOR IMPLEMENTATION FROM COLUMN CORROSION TESTS

After full autopsy of all ten column specimens, research results generated the following findings to be implemented for partially submerged columns or columns exposed to saltwater dripping:

Duct Types

- Plastic ducts may be used to better protect post-tensioning bars. However, better sealing materials or splices should be used or developed, to seal the duct "dead" ends and protect the post-tensioning bar.

Substructure Prestressing

- Column elements should be prestressed, to improve spiral and rebar corrosion protection. However, designers should not rely entirely on post-tensioning to provide adequate corrosion protection at the cold joint. Other protection measures should be investigated.

Concrete Type

- Non of the column specimens had high performance concrete, so no conclusions can be made about this material.

- Fly Ash concrete (w/c = 0.42) may be used to provide enhanced spiral, rebar and duct corrosion protection.

Gaskets

- Rubber gaskets are not effective to seal the duct "dead" ends and should not be used.

Post-tensioning Bar Coatings

- Galvanized steel bars or epoxy coated bars provide enhanced protection against uniform corrosion, but are susceptible to severe localized corrosion.

(Page left blank intentionally)

CHAPTER 7

Summary and Conclusions

The research presented in this dissertation was part of the University of Texas at Austin, Center for Transportation Research Project 0-1405: "Durability Design of Post-Tensioned Bridge Substructure Elements." The project sponsored by the Texas Department of Transportation, involves two main components:

- Durability of Bridge Substructures, and
- Post-Tensioned Bridge Substructures.

The substructure emphasis is in response to the deteriorating condition of bridge substructures in some areas of Texas. The second aspect is included since there are many possible applications where post-tensioning can provide structural and economical benefits, and can possibly improve durability.

The main problem that bridge engineers faced was that there were few comprehensive durability design guidelines for post-tensioned concrete structures, especially those expose to very severe environments.

The overall project objectives for TxDOT Project 0-1405 are the following:

- To examine the use of post-tensioning in bridge substructures,
- To identify durability concerns for bridge substructures in Texas,
- To identify existing technology to ensure durability or improve durability,
- To develop experimental testing programs to evaluate protection measures for improving the durability of post-tensioned bridge substructures, and

541

- To develop durability design guidelines and recommendations for post-tensioned bridge substructures.

The author's involvement in Project 0-1405 started in August 2000, after exposure testing had begun in the macrocell, beam and column series. This dissertation's scope included the following:

- Continuation of exposure testing of the remaining macrocell specimens,

- Continuation of exposure testing of all beam and column specimens,

- Performance of comprehensive autopsies and examinations of second half of macrocell specimens,

- Performance of comprehensive autopsies and examinations of approximately half of Phase I and Phase II beams, after four and a half and three and a half years of exposure, respectively,

- Performance of comprehensive autopsies and examinations of all column specimens after six and a half years of exposure testing, and

- Updating of durability design guidelines to reduce post-tensioning system corrosion risk based on exposure testing and autopsy results

In the following sections the final results and findings from this dissertation contribution to the above mentioned project, are described in detail. Sections 7.1, 7.2 and 7.3 include the results from the macrocell corrosion tests, large scale beam corrosion tests, and large scale column corrosion tests, respectively. These results had been presented before at the end of Chapters 3, 4 and 5, and are repeated herein with minor changes as a summary of all conclusions and findings.

Once all distinct series have been described and findings have been presented, major overall conclusions are summarized in Section 7.4, for general application in the design of bonded post-tensioning concrete systems.

542

Section 7.5 includes recommendations and directions for future research.

7.1   SUMMARY AND CONCLUSIONS FROM MACROCELL CORROSION TESTS

Thirty eight macrocell specimens were used to investigate the corrosion protection of internal tendons at segmental joints. Half of the specimens were autopsied after approximately four and a half years of highly aggressive exposure and preliminary conclusions were reported.[7.1] The variables analyzed during the testing program included: joint type (dry or epoxy), duct type (galvanized steel or plastic), grout type (3 grouts with differing additives) and level of joint compression (3 different levels).   The second half of the specimens was autopsied with over eight years of very aggressive exposure. Numerous conclusions can be drawn.

7.1.1   Overall Performance

- Superiority of plastic ducts was evident. Specimens with plastic duct had the best overall performance (quantified in terms of strand, mild steel and duct corrosion).

- All galvanized steel duct specimens showed some degree of duct corrosion, from moderate uniform corrosion up to severe duct destruction.

- Thin epoxy joints provided substantially improved corrosion protection when compared to dry joints. Incompletely filled epoxy joint performance was very similar to that of a dry joint.

- Post-tensioning strands were corroded in all specimens, from light uniform corrosion to moderate pitting.

- Mild steel bars were corroded in seventeen out of the nineteen specimens. One third of those had from moderate corrosion to severe pitting.

- In many instances, the epoxy coverage, provided on the strand and mild steel bars to limit the exposed length of the anode and cathode, failed to provide complete corrosion protection to these areas. Epoxy paint peeled off in many instances allowing for moisture and chloride ingress. Corrosion under the epoxy paint was in many cases comparable to the corrosion condition in the exposed lengths. Among other effects, this affected the current density calculations.
- Metal loss calculations based on current density calculations failed to indicate the amount of corrosion in the specimens.

7.1.2 Assessing Corrosion Activity Using Half-Cell Potential Measurements

Half-Cell Potentials were taken at two week intervals at the start of the wet period and at the start of the dry period. All measurements were performed according to ASTM C876[7.2] using a saturated calomel electrode (SCE). In all cases the prestressing tendon was not in contact with the galvanized duct, and it was considered that the segmental joint allowed for ion movement. However, while HC-Potentials in dry joint specimens had a good correlation with forensic examination results, they failed to detect corrosion activity in six out of nine epoxy joint specimens, and in one epoxy joint specimen with gasket.

With respect to testing variables, the following conclusions are drawn based on Half-Cell Potential Data:
- Epoxy joint specimens showed less probability of strand corrosion than dry joint specimens.
- Macrocell specimens with plastic ducts (discontinuous) at the joint showed less probability of strand corrosion than similar specimens with galvanized steel ducts.

544

- Dry joint specimen data indicated less probability of strand corrosion with increasing levels of joint precompression. This trend was not clearly shown in epoxy joint specimens.

- Dry Joint specimens with Corrosion Inhibitor (Calcium Nitrite) showed less probability of strand corrosion with respect to specimens with Normal Grout.

7.1.3   Segmental Joints

To address typical North American practice, dry joints and epoxy joints, with and without gaskets, were selected for investigation in this testing program. All joint types were match-cast.   The AASHTO Guide Specifications for Segmental Bridges[7.3] does not permit the use of dry joints with internal tendons. However, dry joints were included as a worst case scenario for comparison purposes.   The thin epoxy-jointed specimens were assembled according to the standard practice.   In the epoxy/gasket joint, a foam gasket was glued to the face of one segment around the duct opening prior to application of the epoxy. Forensic examination after eight years of exposure included: seven specimens with dry joints, nine specimens with epoxy joints and three specimens with epoxy joints with gasket.   The conclusions are as follows:

- All galvanized steel ducts and prestressing strands in the nineteen specimens showed some degree of corrosion. The higher corrosion ratings were obtained from dry joint specimens with galvanized steel ducts and normal grout. Ducts in these specimens were extremely corroded, with corrosion centered at the joint, and with concrete cracking in the top of the specimen.   In general, dry joint specimens showed increased chloride penetration and increased corrosion of galvanized steel duct, prestressing strand and mild steel reinforcement.   These results show that dry joints do not provide adequate corrosion protection for internal tendons in aggressive environments.

- Sound epoxy joint specimens with galvanized steel ducts showed moderate to very severe duct corrosion centered away from the joint. Clear cover for specimens was small (five eights to three quarters of an inch), significantly lower than would be allowed by specifications. However, the test results indicate the potential corrosion problems when using galvanized ducts in aggressive environments if chlorides penetrate the concrete cover away from the epoxy joint.

- Thin epoxy joints provided substantially improved corrosion protection when compared to dry joints. However, test results showed that poor epoxy filling at the joint is extremely detrimental to the performance of the duct, the prestressing strand and the mild steel reinforcement. Incomplete filled epoxy joint performance was very similar to that of a dry joint.

- Corrosion of mild steel in some epoxy joint specimens was found to be the result of an external source of moisture and chlorides rather than from penetration at the epoxy joint or through the concrete. This conclusion was reinforced with chloride levels measured at the joint and away from the joint. These findings reinforce the need to provide adequate clear cover over the ends of longitudinal bars in the segments, even if external post-tensioning is used.

- In some cases, the use of gaskets in epoxy jointed specimens prevented a complete epoxy coverage of the joint. This condition could worsen under field conditions.

7.1.4   Ducts for Internal Post-Tensioning

Two duct types were investigated; standard galvanized steel duct and plastic duct. Due to size limitations, PVC pipe was used for the plastic duct. Test results indicated:

546

- Superiority of plastic ducts was evident. Strand encased in plastic ducts showed only light corrosion and discoloration. Specimens with plastic duct had the best overall performance (quantified in terms of strand, mild steel and duct corrosion).

- Galvanized steel duct was corroded in all specimens. Severe corrosion and large duct destruction was observed in dry joint specimens. Such corrosion was often centered on the dry joint. Epoxy joint specimens showed moderate to severe duct corrosion. The corrosion was often centered away from the joint.

- Concrete cover in specimens was lower than allowed by specifications. However, test results indicate that these are potential corrosion problems when using galvanized steel ducts in aggressive exposures if chlorides penetrate the cover. Plastic ducts performed well in spite of the small cover.

7.1.5 Joint Precompression

Due to the small specimen size, the strand could not be post-tensioned effectively. To simulate precompression across the joint due to post-tensioning, the pairs of match –cast segments were stressed together using external loading frames. Three levels of precompression were selected; 5 psi, 50 psi and $3\sqrt{f'c}$ psi. The lowest level of 5 psi could represent the level of precompression encountered in a precast segmental column under self weight. The precompression of 50 psi is based on AASHTO Guide Specifications.[7.3] The highest precompression value corresponded to 190 psi for this testing program. Eight out of the nineteen specimens (at eight years of exposure) had low precompression, seven medium precompression and four high precompression. Conclusions are as follows:

- Test results did not show a clear trend with respect to joint precompression when analyzing time to corrosion initiation and rate of corrosion in

prestressing strands and mild steel bars. An isolated result for dry joint specimens with galvanized steel ducts and normal grout showed that at very high levels of precompression, there is an increased level of strand and mild steel protection. This result is not clearly shown for epoxy joint specimens with and without gasket.

- Galvanized steel duct corrosion in dry joint specimens also showed better performance with a higher level of precompression. However again, this result is not clearly shown in epoxy joint specimens. Precompression level is much important in dry joint specimens.

7.1.6   Grouts for Bonded Post-Tensioning

Three cement grout types were selected for evaluation; normal grout (plain cement grout, no admixtures, w/c = 0.40), grout with silica fume (13% cement replacement by weight, w/c = 0.32, superplasticizer added) and grout with a commercial calcium nitrite corrosion inhibitor (w/c = 0.40). The dosage of corrosion inhibitor used in this testing program was the same dosage normally used for concrete (aprox. 20 liters/m^3 concrete). The Calcium Nitrite dosage was not adjusted to account for the higher cement content in grout. The testing program for the nineteen remaining specimens at eight years of exposure included thirteen specimens with normal grout, five with corrosion inhibitor and one with silica fume. Conclusions are as follows:

- Grout voids, due to entrapped air, bleed water, incomplete grout filling or lack of grout fluidity were detrimental not only to the prestressing strand, but also to the galvanized steel duct.
- Dry joint Specimens with Corrosion Inhibitor (Calcium Nitrite) added to the grout showed a lower strand corrosion rating (less strand corrosion severity) at

eight years of exposure, than specimens with normal grout (in the order of seven times smaller). This trend was not clearly shown in epoxy joint specimens. This result contradicts those obtained at four and a half years of exposure where the most severe corrosion of the prestressing tendon was found where calcium nitrite corrosion inhibitor was used.

- Epoxy joint specimens with silica fume, corrosion inhibitor and normal grout had very similar performances. No clear distinction was evident.

7.2   SUMMARY AND CONCLUSIONS FROM BEAM CORROSION TESTS

Twelve out of the twenty-seven large scale beam specimens were fully autopsied to evaluate the effect of post-tensioning on durability and to evaluate the relative performance of a large number of corrosion protection variables. Two additional specimens were partially autopsied. Full autopsies for the remaining specimens will be performed at a future date. Beams were fabricated in two phases in order to begin exposure testing on a portion of the specimens while the remaining specimens were being fabricated. In Phase I (16 beams), which started exposure testing in December 1997, researchers investigated the effect of prestress level and crack width and also included one of the high performance grout specimens. In Phase II (11 beams), which started exposure testing in December 1998, researchers investigated duct splices, grout type, concrete type, strand type, duct type, and end anchorage protection. After the first full autopsy performed at four and a half years for six Phase I beams, and three and a half years for six Phase II beams, and partial autopsies performed to two Phase I beams, preliminary conclusions were drawn.

7.2.1   Overall Performance

The variables selected for evaluation in this beam testing program fall into four main categories: level of prestress and crack width, concrete type,

prestressing strand coatings and post-tensioning hardware protection. In addition, different post-tensioning duct splices were also evaluated. After the initial autopsies of the fourteen beams, the use of large scale beam specimens was found to be a very good method for determining the effect of most of these variables. Prestressing strand coatings and post-tensioned hardware protection will be evaluated at a future date, since they are included in the remaining specimens under exposure testing. Based on the autopsies performed to date, the following conclusions are drawn:

- Galvanized duct performed poorly. No plastic duct was used in the specimens of the first set of full autopsies.

- Bleed water voids were present in the ducts even after "good grouting procedures." Anti-bleed grout was not evaluated in the first set of full autopsies, but it is included in one of the remaining specimens for future autopsy.

- Voids from bleed water in grout were shown to be very detrimental to the duct

- A clear trend was found with respect to cracking and mild steel corrosion. As cracking increased, stirrup and rebar corrosion increased. This trend was not clearly shown on strands, since strand ratings were all very low and close in value

- Mixed reinforcing (2/3 PS) beams showed the worst corrosion resistance. The best performance was obtained from 100%S PS specimens, followed by 100%U PS specimens

- Phase I beam results showed that there was a reduced risk of corrosion damage with increasing levels of prestress

- High performance concrete specimens (low permeability, w/c=0.29) appear to perform better than class C fly ash concrete specimens. However, both appear to be effective in minimizing the chloride penetration through concrete

550

- Industry standard duct splices as well as heat shrink duct splices do not seem to provide adequate corrosion protection

- Duct splice damage did not show a direct correlation with the severity of corrosion

- No difference was found between normal and fly ash grout. Low strand corrosion ratings on all specimens after autopsy, did not allow clear identification of the effect of different types of grout

7.2.2 Load/Prestress Level versus Corrosion. The Effect of Cracking

The effect of cracking (width and number) on corrosion protection was an area of great emphasis in this experimental program. The effect of cracking was primarily investigated using standard variables and the sections that would be expected to crack under service loads. The range of crack widths investigated in this program were based on a survey of relevant literature performed by West[7.4] regarding critical crack widths for corrosion and recommended allowable crack widths. Consideration was also given to the applied moment-crack width behavior computed for the sections. Three different load levels were used: unloaded, service load, and temporary overloaded. The following conclusions are drawn:

- The specimen corrosion protection decreases as the applied load increases

- Corrosion protection decreases with increasing cracking

- An increase in transverse crack width produces a decrease in corrosion protection

- Longitudinal or splitting cracks in the concrete surface are a clear indication of very severe corrosion within the member.

- The chloride content in the concrete is significantly higher at crack locations, and increases as the crack width increases

551

- The specimen corrosion protection increases as the level of prestress increases
- Mixed reinforcement (2/3 PS) beams showed the worst corrosion performance. Increasing the post-tensioning level from 2/3 PS to 100% PS significantly increased the corrosion protection
- The corrosion protection of the 2/3 PS beam was much more similar to Non-PS beams, as opposed to 100% PS Beams
- There was not a clear difference in the corrosion resistance among the fully prestressed beams designed with the ultimate strength method as compared to those designed with allowable stress method.

7.2.3   Fly Ash in Concrete

Concrete plays an important role in corrosion protection of steel reinforcement. One of the objectives of this research program is to evaluate the effectiveness of high performance concrete as a function of cracking. Three different concrete mixes were selected for comparison. The reference mix was the standard concrete: TxDOT Class C concrete. The alternates were a TxDOT Class C concrete with 25% Class F Fly Ash and a High Performance Concrete (0.29 w/c, 25% fly ash+superplasticizer). The following conclusions are drawn:

- Both the high performance concrete and the fly ash concrete beams showed good corrosion protection by minimizing the chloride penetration through the concrete
- The high performance concrete tends to show a slightly better corrosion protection than the fly ash concrete, but the difference is not significant.
- No conclusions can be drawn on corrosion protection of the high performance concrete and the fly ash concrete with respect to the standard TxDOT concrete due to the unfortunate lack of directly comparable specimens at the time of the first autopsy.

7.2.4 Duct Splices for Galvanized Steel Duct

In most practical applications, the post-tensioning ducts must be spliced at some location. It was decided to compare industry standard (IS) splices to heat shrink (HS) splices and unspliced duct. The effect of damaged splices was also examined. The IS splice consisted of a 1 ft length of oversized duct placed over the contact butt splice of the ducts. Concrete is prevented from entering the splice by wrapping the ends with duct tape. The heat shrink splice consists of a 8 inch length of heat shrink tubing placed over the contact butt splice of the ducts. The original diameter of the heat shrink tubing was 4 inches. No mechanical connection was made between the two ducts being connected. The conclusions are as follows:

- The industry standard splice allowed moisture and chlorides to enter through the sides of the splice and get trapped between the duct and the splice due to inefficiency of duct tape.

- The heat-shrink splice also allowed moisture to enter through the sides and get trapped due to insufficient adhesion between the splice and the duct. It also traps bleed water from the grout.

- Damage inflicted on the duct splices did not show a direct correlation with the severity of corrosion.

- Neither the industry standard splice nor the heat-shrink splice appears to be a satisfactory duct splice for the corrosion protection of a galvanized steel duct.

7.2.5 High Performance Fly Ash Grouts

Two high performance grouts (a fly ash grout and an antibleed grout) were selected for investigation, in comparison with TxDOT standard grout. The fly ash grout specimen was autopsied, and results are reported herein. The antibleed grout specimen will be autopsied at a future date. Antibleed grout had a water-

553

cement ratio of 0.33 with 2% cement weight of antibleed admixture. Based on the information to date, the following conclusions are drawn:

- The fly ash grout aided in the corrosion protection of the galvanized steel ducts

- The fly ash grout, in comparison to TxDOT standard grout, did not show an increase in corrosion protection of the prestressing strand.   This result may be due to the strand ratings being very low and close in value. Several more years of exposure testing may be require to yield more conclusive results

7.2.6   Exposure Testing Results

Half-cell potential readings were measured using a saturated calomel reference electrode at the end of each wet cycle (once every four weeks).   All measurements were performed according to ASTM C876.[7.2] In general, half-cell potential readings are inadequate in determining the severity of corrosion activity, but prove to be successful for relative comparison of specimens. The conclusions are as follows:

- There is an exact correlation in specimen performance between the greatest negative potential at the end of testing for autopsy beams and the time to corrosion

- Both half cell potential readings and corrosion rating graphs show the loaded Non-PS and 2/3 PS beams were the most corroded.

- Half-cell potential readings did not show a distinct correlation in high performance and fly ash concrete specimens with the corresponding corrosion ratings.

Corrosion rate measurements were taken four times during the exposure duration. Two types of equipment were used in this experimental program: the Pr Monitor and the 3LP. Measurements of the Phase I beams were taken after

554

seven, twelve, fifteen and forty-seven months of exposure. Measurements of the Phase II beams were taken after 37 months of exposure. A final attempt to take corrosion rate measurements of all beams was made immediately prior to the forensic examination. This attempt was unsuccessful due to complications with the 3LP equipment. Corrosion rate readings did not show good correlation with forensic examination results. The presence of zinc in the galvanized steel ducts may have played a role in the erroneous results.

Chloride content was found to be a useful method in determining the onset of corrosion. However, there was not a direct relationship between the acid soluble chloride content at the bar/duct level and the severity of corrosion at time of autopsy.

7.3 SUMMARY AND CONCLUSIONS FROM COLUMN CORROSION TESTS

Five non-prestressed and five post-tensioned columns specimens were used to investigate corrosion mechanisms and chloride ion transport ("wicking effect) in various column connection configurations and to evaluate column corrosion protection measures. Variables included column to foundation connection (no dowel joint, doweled joint and post-tensioned joint), loading (no loading and service load – with combined moment and axial load), concrete type (TxDOT Class C concrete, and Class C Fly Ash concrete – 35% replacement by volume), prestressing bar coatings (uncoated, galvanized PT-bars, and epoxy coated PT-bars), and post-tensioning ducts (plastic and galvanized steel). Trickle water was used on one face of each column to determine the effect of salt water spray or dripping. Test specimen exposure started in July of 1996 and ended in January of 2003, after six and a half years. Full autopsies were performed at the end of testing, and conclusions are as follows.

555

7.3.1 Post-Tensioning to Improve Corrosion Protection

The possible weak link in corrosion protection at the column-foundation interface was studied with three different configurations: no dowel joint, doweled joint and post-tensioning joint. Determination of the effect of post-tensioning on durability through precompression of the concrete and precompression of construction joints was one of the main objectives of this research series. The conclusions are as follows:

- Post-tensioned specimens did not show any distinct improvement in specimen performance at the column foundation interface, when compared to doweled specimens.

- Post-tensioning dramatically reduced the corrosion found on spiral reinforcement in the first 18 inches from the column base.

- Post-tensioned specimens under loading showed an increase in spiral and mild steel reinforcement corrosion protection when compared to non-loaded specimens.

- Post-tensioning reduced the risk of spiral corrosion due to saltwater dripping.

- Post-tensioning provided better resistance to the wicking effect, when acid-soluble chloride contents were compared to doweled and no-dowel specimens.

7.3.2 Fly Ash as Partial Cement Replacement in Concrete

TxDOT standard concrete mix Class C concrete was used in eight specimens (w/c = 0.45, type I/II Cement, f′c=3600). In two columns, 35% of cement by volume (31% by weight) was replaced with Class C Fly Ash, with no other significant changes to the concrete mix. After autopsy, the following conclusions are drawn:

- Fly ash concrete did seem to provide enhanced corrosion protection to galvanized steel ducts.

556

- Spiral and mild steel reinforcement corrosion in non-prestressed specimens showed a better performance in Fly Ash concrete than in Class C concrete specimens. This trend was not clearly shown in post-tensioned specimens.

- Post-tensioned bar corrosion did not show any distinct trend with respect to the type of concrete in the specimen.

7.3.3 Plastic Ducts for Post-Tensioning

Standard galvanized steel ducts were compared to impermeable plastic ducts in three post-tensioned specimens: Class C concrete (unloaded and service load) and Fly Ash concrete under service load. In all cases uncoated post-tensioning bars were used. The conclusions are as follows:

- Although results are very limited, advanced galvanized steel duct corrosion at the column base, inside the rubber gasket, show the superiority of using plastic ducts.

- Corrosion in post-tensioned bars in plastic ducts and galvanized ducts was always at the column-foundation interface, where the plastic or galvanized duct was interrupted. Therefore, conclusions regarding duct performance based on post-tensioning bar corrosion are not possible. The ducts need an effective splice seal at all joints.

7.3.4 Post-Tensioning Bar Coatings

Two prestressing bar coatings were investigated: epoxy coated (according to ASTM A775-97) and zinc galvanized prestressing bars. The coated bars were compared directly to uncoated bars within individual specimens. In both cases, anchorage hardware was either epoxy coated or galvanized. The following conclusions are drawn:

- Epoxy coating or galvanized post-tensioning bars showed enhanced corrosion protection, with respect to plain post-tensioning bars.

- Coatings were not sufficient to stop corrosion from occurring at the column-foundation interface. Corrosion was very localized.

- Superiority of coated bars should not be concluded, since localized corrosion may accelerate deterioration at the local level, which in turn may result in unexpected failure.

7.4 MAJOR OVERALL CONCLUSIONS

Based on the results from the macrocell, beam and column corrosion test series, the following major overall conclusions are drawn:

Ducts for Internal Post-Tensioning

- The use of galvanized steel ducts appears unwise. Severe duct destruction and pitting was found in most specimens with this type of duct. From macrocell and column corrosion test results the superiority of plastic ducts was evident. The use of plastic ducts and encapsulated anchorage protection systems appear promising but cannot be conclusively evaluated until after final autopsies of the remaining beam specimens.

- Unspliced plastic ducts, such as those used in the macrocell and column series, showed better protection of the strands or bars when compared to galvanized steel ducts. However, the need for better splicing systems to avoid any moisture and chloride penetration and the corresponding localized strand or bar corrosion was evident.

558

Cracking and Joints

- Cracking due to loading, had a definite effect on corrosion damage. As cracking increased, reinforcement corrosion increased. Larger crack widths and crack density were found to be the cause of very severe localized and uniform reinforcement corrosion activity.

- Sound epoxy joint filling is mandatory to prevent moisture and chloride ingress. Dry joints and incompletely filled epoxy joints in the macrocell specimens showed very poor performance. Similar results were observed in the column tests at the column bases for the non-doweled specimens. Dry joints performed as preset cracks.

Concrete Type

- High performance concrete appears to be effective in minimizing the chloride penetration through concrete.

Concrete Cover

- Small concrete cover was clearly shown to be detrimental to reinforcement performance. When segmental joints allowed for moisture and chloride ingress, the smaller cover typical at the joint faces increased the corrosion activity in the reinforcement. Similar results were obtained at the base of the column specimens when analyzing spiral performance.

Levels of Post-Tensioning

- As the level of post-tensioning or concrete precompression increased, the corrosion protection increased. Mixed reinforced beams showed substantially more corrosion than fully prestressed members. Crack control and concrete precompression are definite factors in reducing corrosion risk. Lower permeability due to

559

increased precompression also provided better resistance to wicking effects.

Galvanized Ducts Splices

- Neither the industry standard splice nor the heat-shrink splice appear to be a satisfactory duct splice to prevent moisture and chloride ingress to the grout for the corrosion protection of a galvanized steel duct.

Gaskets for Post-Tensioning

- The use of supplementary gaskets in the joints to avoid epoxy filling of the ducts, in the case of the macrocell specimens; or the use of rubber gaskets to seal the duct ends, in the case of the column specimens, were detrimental to the performance of the specimens. Both gaskets allowed for moisture and chloride ingress. Gaskets used at the duct ends trapped moisture and produce crevice corrosion in the galvanized steel ducts.

Grouts for Post-Tensioning

- The standard TxDOT Class C grout performed poorly in all specimens under evaluation. Better results were obtained with corrosion inhibitor added to the grout, and the use of fly ash. However, grout voids were not avoided with these grout mixes. The use of antibleed grouts appear promising but result cannot be conclusive until final autopsies of the remaining beam specimens.

- Grout voids, due to entrapped air, bleed water, incomplete grout filling or lack of grout fluidity showed to be detrimental not only to the prestressing strand, but also to the galvanized duct. In addition, bleed water was found to be detrimental to the galvanized

560

ducts when using heat-shrink or industry standard splices. Antibleed and better thixotropic grouts should be considered.

- Stringent grouting procedures must be enforced.

Post-Tensioning Bars or Strands

- Post-tensioning bar coatings (epoxy or galvanized) showed enhanced general corrosion protection, with respect to plain post-tensioning bars. However, under very severe localized attack, as in a crack or joint location, corrosion activity is severe, which in turn may result in unexpected failure.

- The use of epoxy-coated and galvanized strands will be more conclusive after final evaluation of the remaining beam specimens.

Exposure Testing

- Of the exposure testing methods used: half-cell Potential readings, chloride content determinations and corrosion current readings, only the first two showed some degree of correlation with forensic examination results.

7.5 RECOMMENDED CHANGES AND PROCEDURES

The following recommendations are given for consideration in similar experimental programs:

- When using the modified ASTM G-109 macrocell specimens, a few standard ASTM G-109 specimens should be constructed for comparison.

- Where possible, when analyzing several variables in similar experimental programs, at least three specimens should be considered for each variable to clearly validate the results.

561

- Connection wires used for non-destructive measurements should be protected against the outdoor environment to avoid possible deterioration and corrosion that would increase resistivity. Also, wiring systems should be protected against salt water contact while filling up the Plexiglas containers for the aggressive exposure of the corrosion specimens.

7.6   DIRECTIONS FOR FUTURE RESEARCH

After the research results had been summarized, it is concluded that post-tensioning in concrete structures can provide enhanced durability, besides the well known structural and economical benefits. However, to ensure that the post-tensioning system is well protected against corrosion or deterioration, further research is needed in some specific areas. The author recommends additional testing in the following fields:

- Use of encapsulated and electrically isolated systems
- Use of improved grouts for post-tensioning and better grouting procedures
- Use of post-tensioning duct couplers
- Development of better splice systems for galvanized ducts that might be used in non-aggressive environments.
- Use of impermeable surface membranes
- Development of better non-destructive methods for determining corrosion activity within post-tensioned concrete members.
- Use of improved concrete mix designs
- Use of improved strand or bar materials

Appendix A
Macrocell Corrosion Tests
Supplementary Material

A.1   CORROSION CURRENT PLOTS

The following corrosion current plots complement those contained in Figures 3.6 through Figure 3.9. Main variables can be evaluated by inspection of the following figures per variable type: Joint Type (Figures A.1, A.2, A.3, A.4 and 3.6), Duct Type (Figures A.5 and 3.7), Joint Precompression (Figures A.6, A.7, A.8, A.9 and 3.8), and Grout Type (Figures A.10, A.11, A.12, A.13 and 3.9).
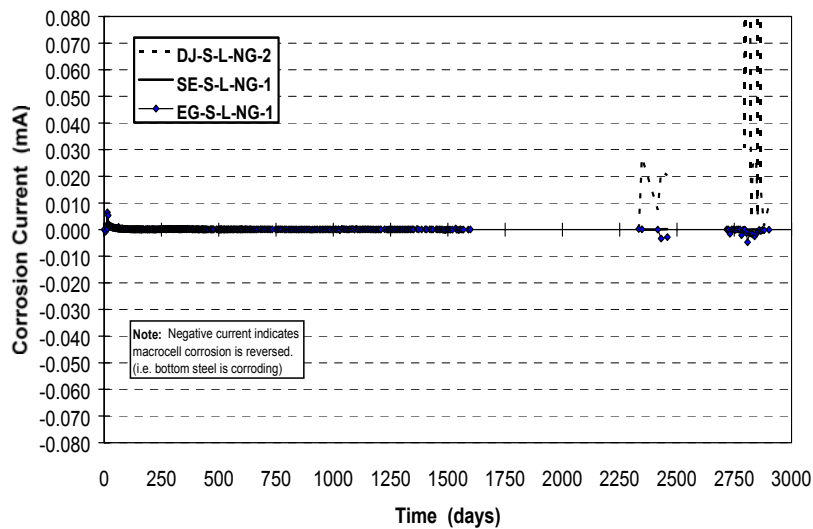
Figure A.1 Macrocell Corrosion Current: Dry, Epoxy and Epoxy with Gasket Joint, Steel Duct, Low Precompression and Normal Grout
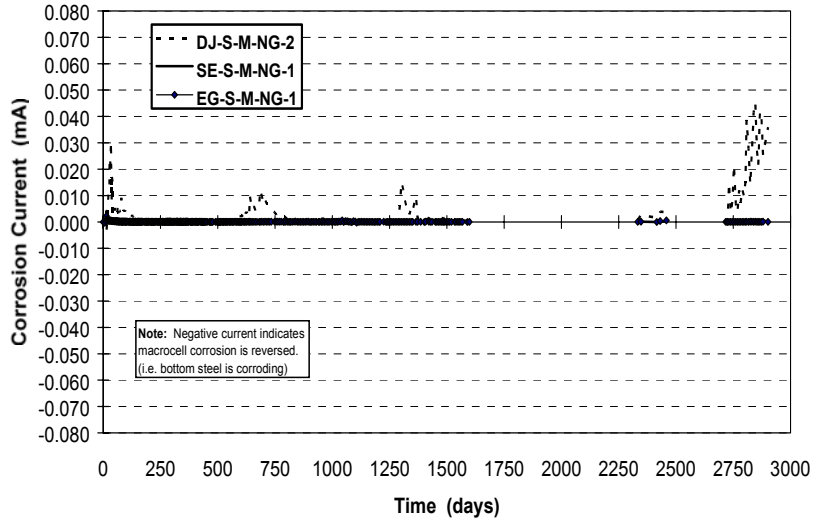
*Figure A.2 Macrocell Corrosion Current: Dry, Epoxy and Epoxy with Gasket Joint,
Steel Duct, Medium Precompression and Normal Grout*
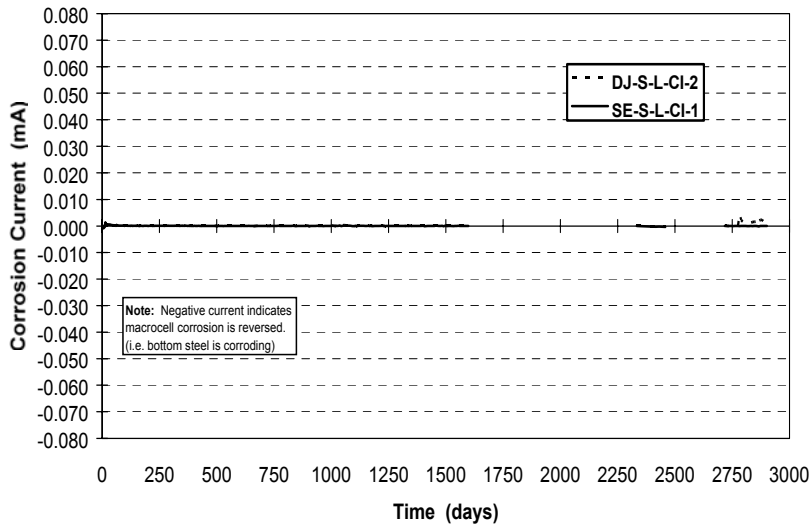
*Figure A.3 Macrocell Corrosion Current: Dry and Epoxy Joint, Steel Duct,
Low Precompression and Corrosion Inhibitor in Grout*

564
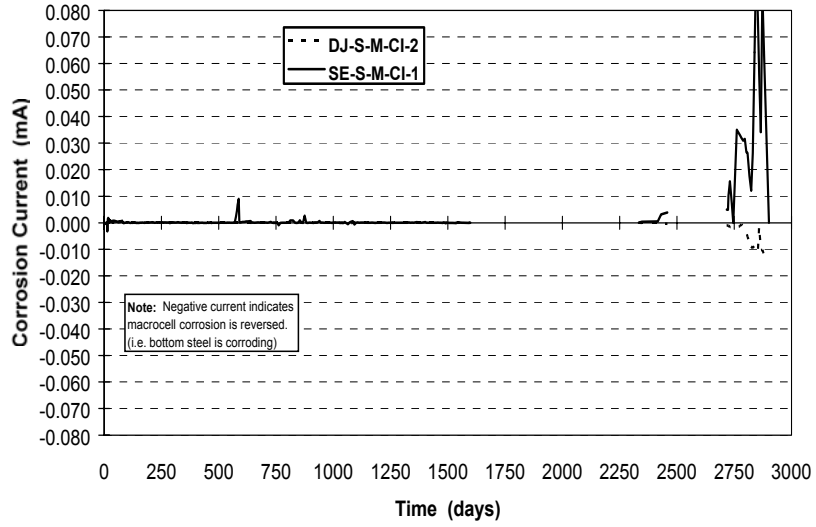
***Figure A.4 Macrocell Corrosion Current: Dry and Epoxy Joint, Steel Duct,
Medium Precompression and Corrosion Inhibitor in Grout***
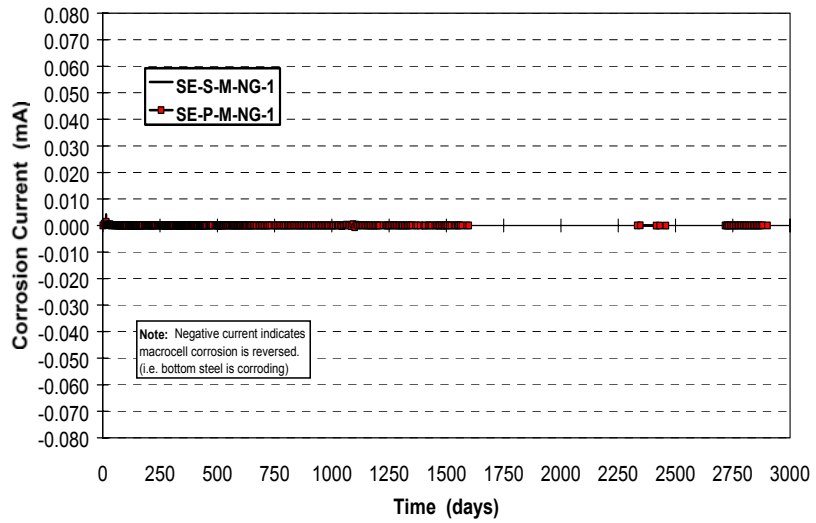
***Figure A.5 Macrocell Corrosion Current: Epoxy Joint, Steel and Plastic Duct,
Medium Precompression, and Normal Grout***

565
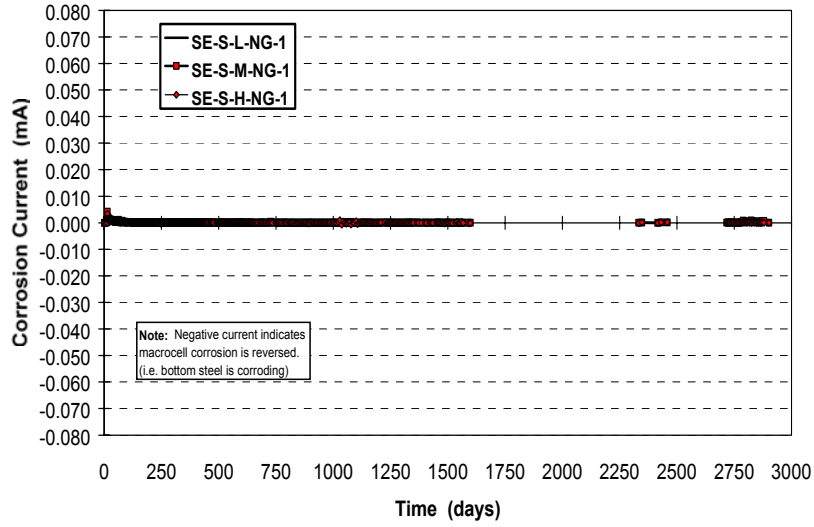
*Figure A.6 Macrocell Corrosion Current: Epoxy Joint, Steel Duct,
Low, Medium and High Precompression, and Normal Grout*
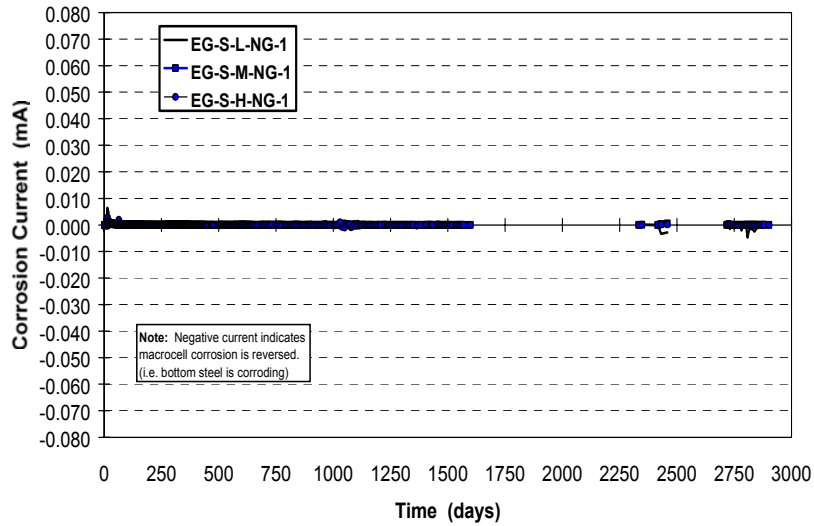
*Figure A.7 Macrocell Corrosion Current: Epoxy with Gasket Joint, Steel
Duct, Low, Medium and High Precompression, and Normal Grout*

566
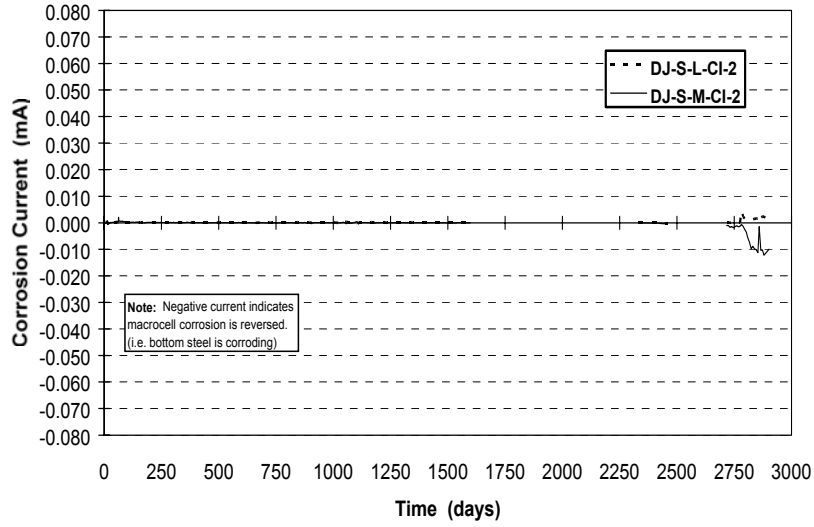
***Figure A.8 Macrocell Corrosion Current: Dry Joint, Steel Duct,
Low and Medium Precompression, and Corrosion Inhibitor in Grout***
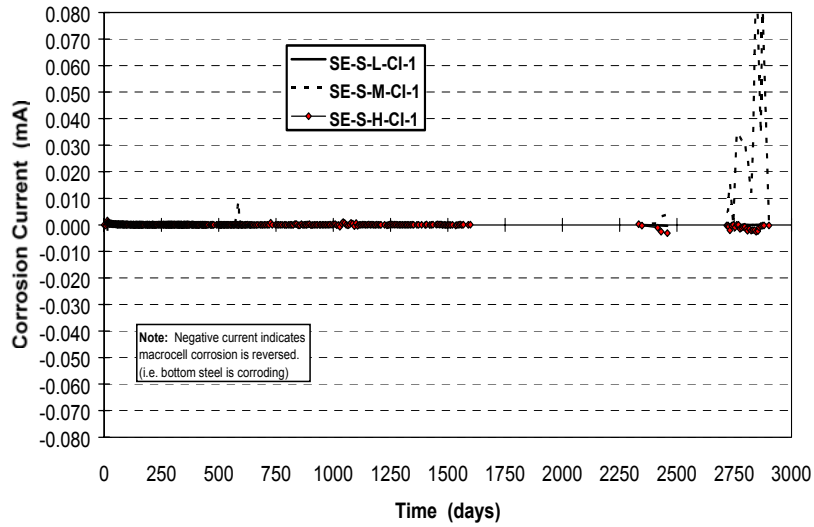
***Figure A.9 Macrocell Corrosion Current: Epoxy Joint, Steel Duct, Low,
Medium and High Precompression, and Corrosion Inhibitor in Grout***

567
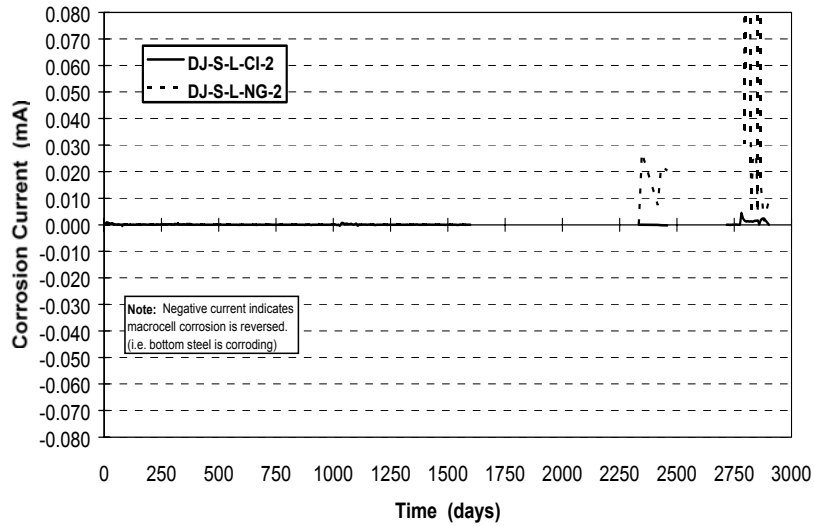
Figure A.10 Macrocell Corrosion Current: Dry Joint, Steel Duct, Low Precompression, and Different Grouts (Normal and with Corrosion Inhibitor Added)
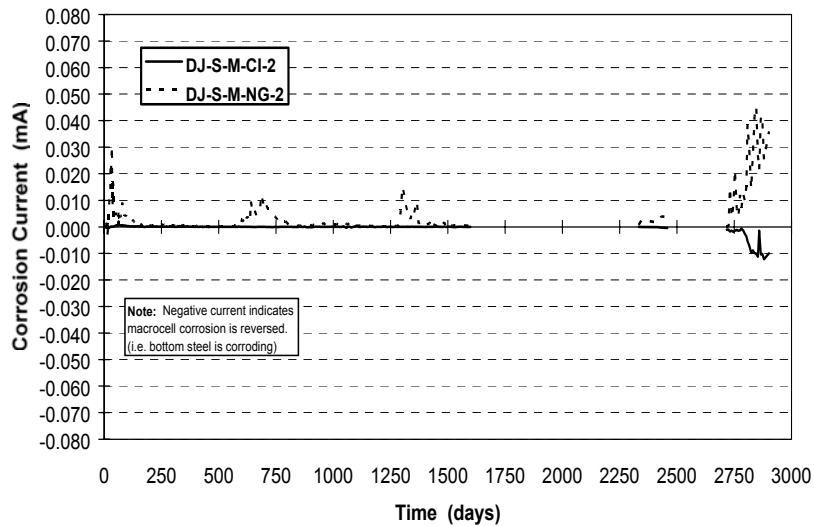
Figure A.11 Macrocell Corrosion Current: Dry Joint, Steel Duct, Medium Precompresion, and Different Grouts (Normal and with Corrosion Inhibitor Added)

568
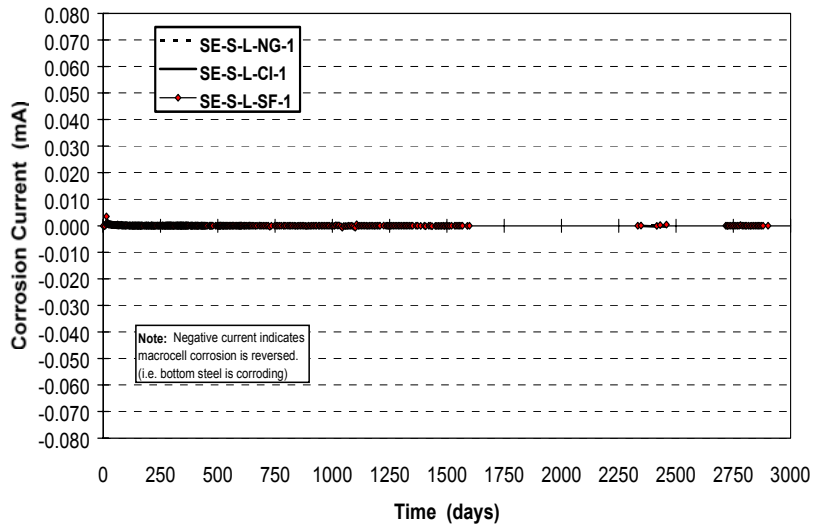
***Figure A.12 Macrocell Corrosion Current: Epoxy Joint, Steel Duct, Low
Precompression and Different Grouts (Normal, Corrosion Inhibitor, Silica
Fume)***
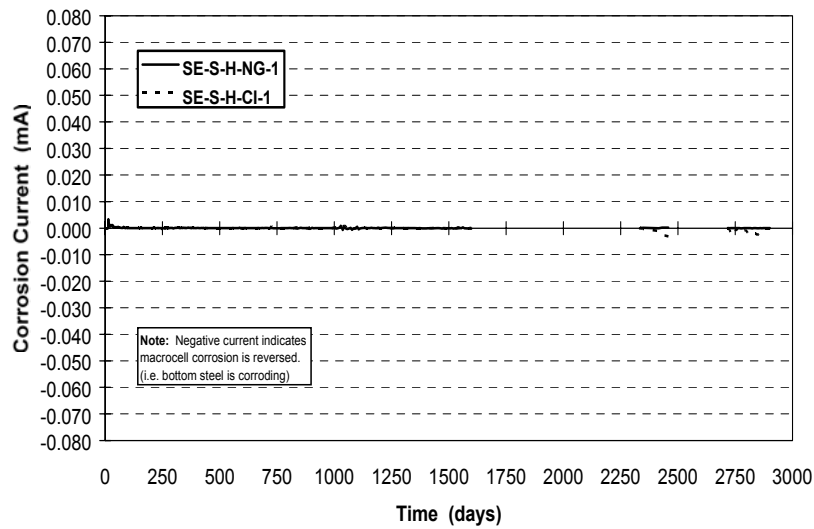
***Figure A.13 Macrocell Corrosion Current: Epoxy Joint, Steel Duct, High
Precompression, and Different Grouts (Normal and with Corrosion Inhibitor
Added)***

569

A.2   HALF CELL PLOTS

As with the corrosion current plots, the following Half-Cell reading plots complement those contained in Figures 3.10 through Figure 3.13.   The main variables can be evaluated by inspection of the following figures per variable type: Joint Type (Figures A.14, A.15, A.16, A.17 and 3.10), Duct Type (Figures A.18 and 3.11), Joint Precompression (Figures A.19, A.20, A.21, A.22 and 3.12), and Grout Type (Figures A.23, A.24, A.25, A.26 and 3.13).
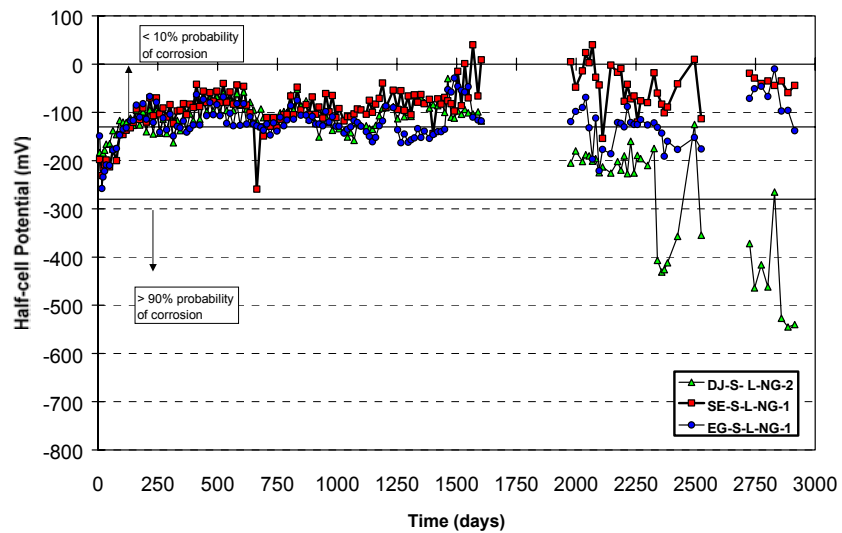
Figure A.14 Half-Cell Potentials: Dry , Epoxy and Epoxy with Gasket Joints, Steel Duct, Low Precompression, and Normal Grout
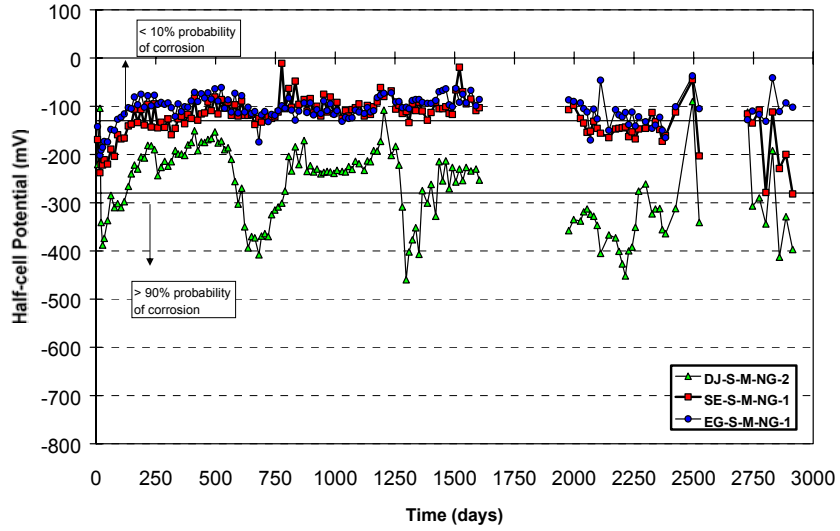
Figure A.15 Half-Cell Potentials: Dry, Epoxy and Epoxy with Gasket Joints, Steel Duct, Medium Precompression and Normal Grout
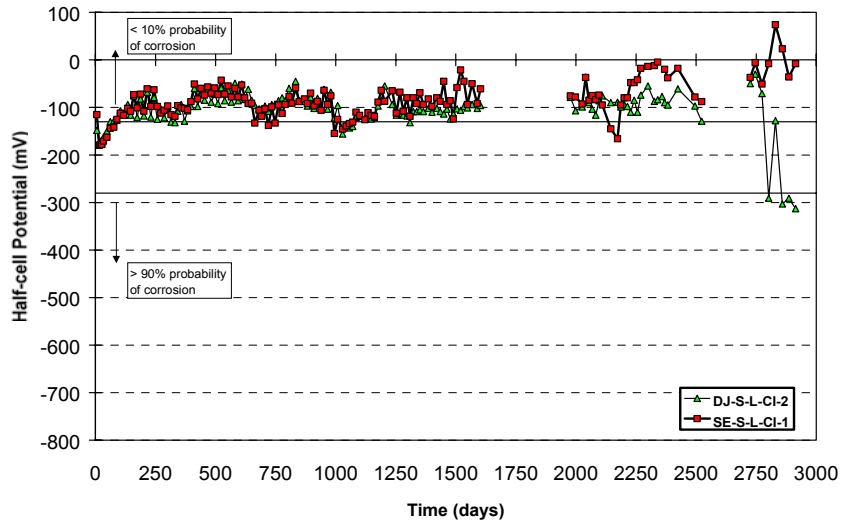
Figure A.16 Half-Cell Potentials: Dry and Epoxy Joint, Steel Duct, Low Precompression, and Corrosion Inhibitor in Grout

571
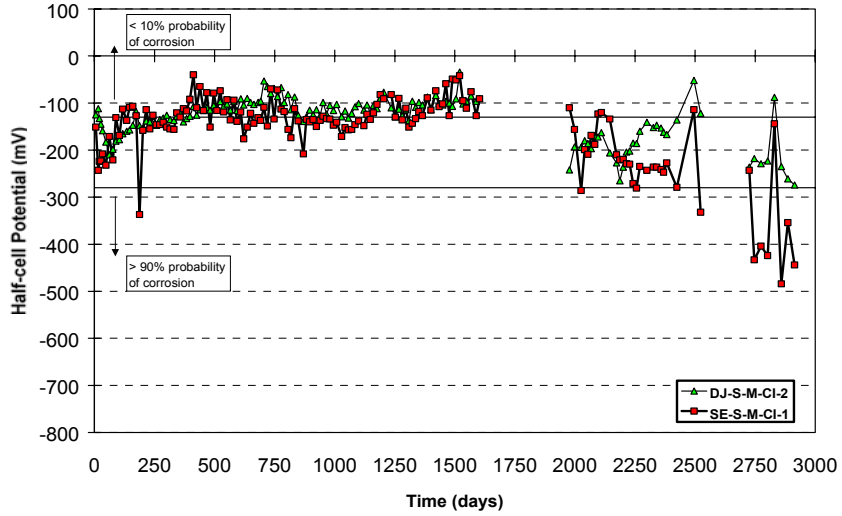
*Figure A.17 Half-Cell Potentials: Dry and Epoxy Joint, Steel Duct,
Medium Precompression, and Corrosion Inhibitor in Grout*
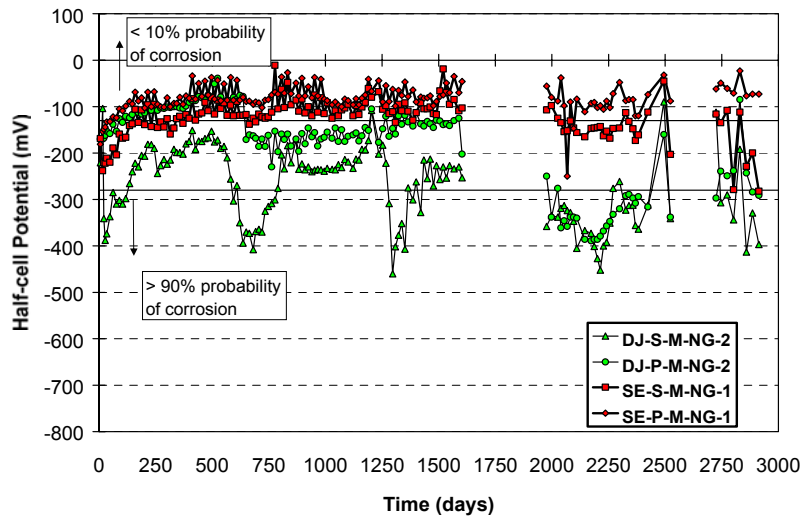
*Figure A.18 Half Cell Potentials: Dry and Epoxy Joint, Steel and Plastic Duct,
Medium Precompression, and Normal Grout*
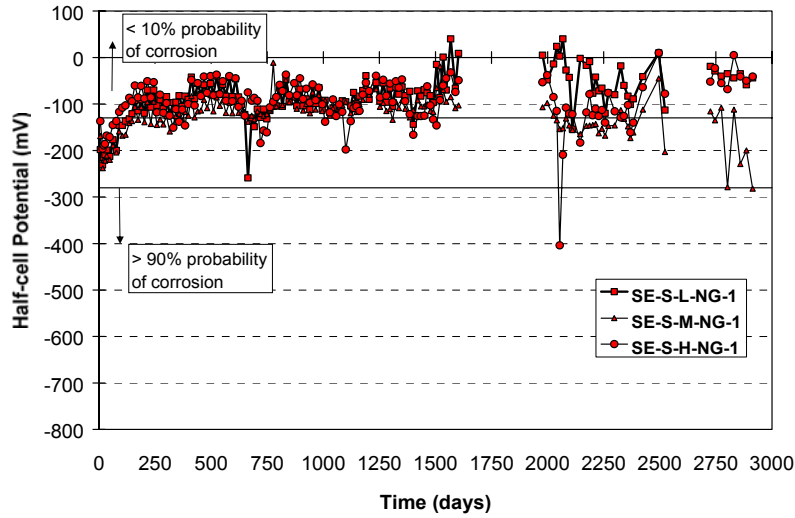
Figure A.19 Half-Cell Potentials: Epoxy Joint, Steel Duct,
Low, Medium and High Precompression, and Normal Grout
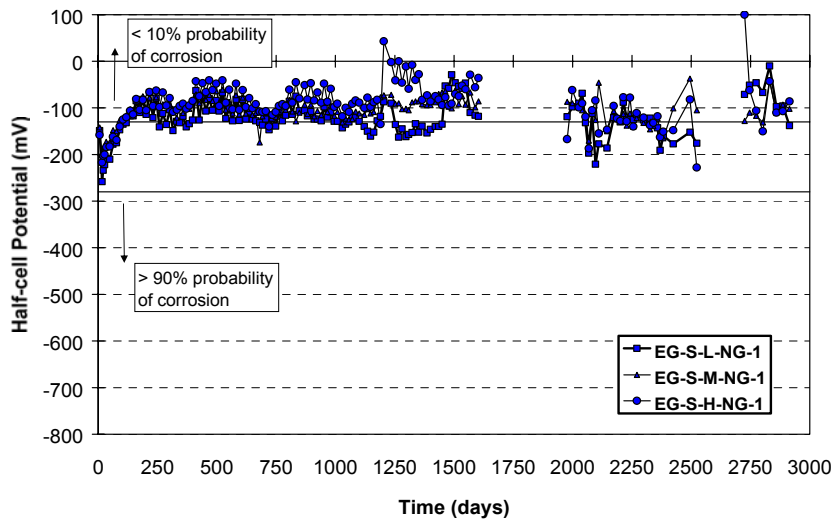
Figure A.20 Half Cell Potentials: Epoxy Joint with Gasket, Steel Duct,
Low, Medium and High Precompression, and Normal Grout

573
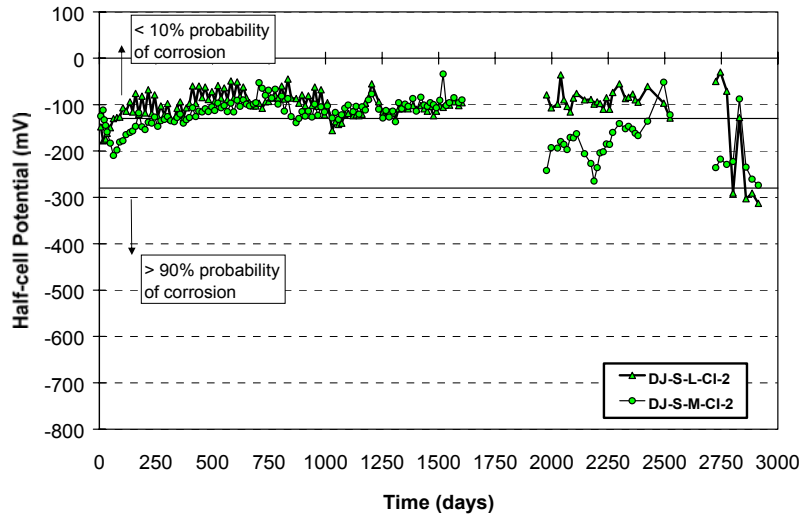
Figure A.21 Half-Cell Potentials: Dry Joint, Steel Duct,
Low and Medium Precompression, and Corrosion Inhibitor in Grout
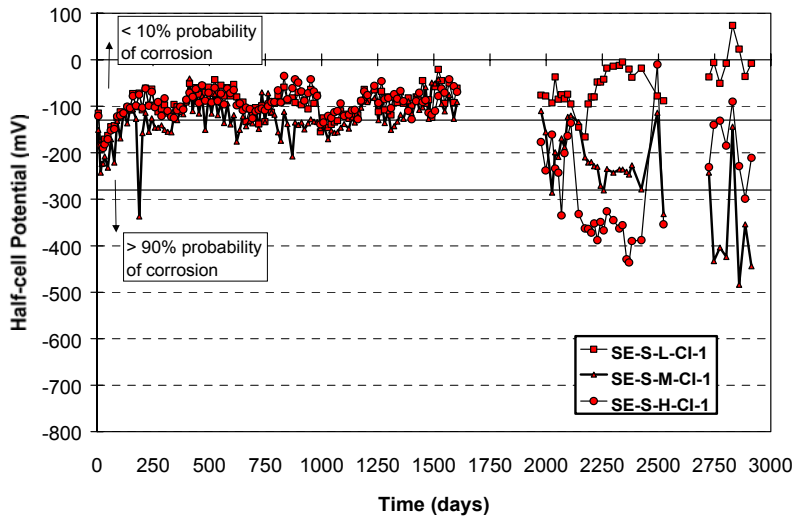
Figure A.22 Half-Cell Potentials: Epoxy Joint, Steel Duct, Low, Medium and
High Precompression, and Corrosion Inhibitor in Grout

574
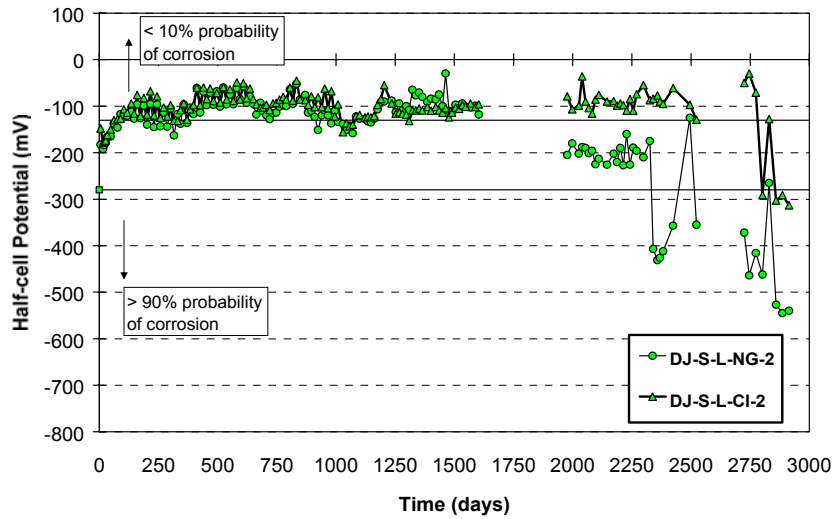
Figure A.23 Half-Cell Potentials: Dry Joint, Steel Duct,
Low Precompression, Normal Grout and Grout with Corrosion Inhibitor Added
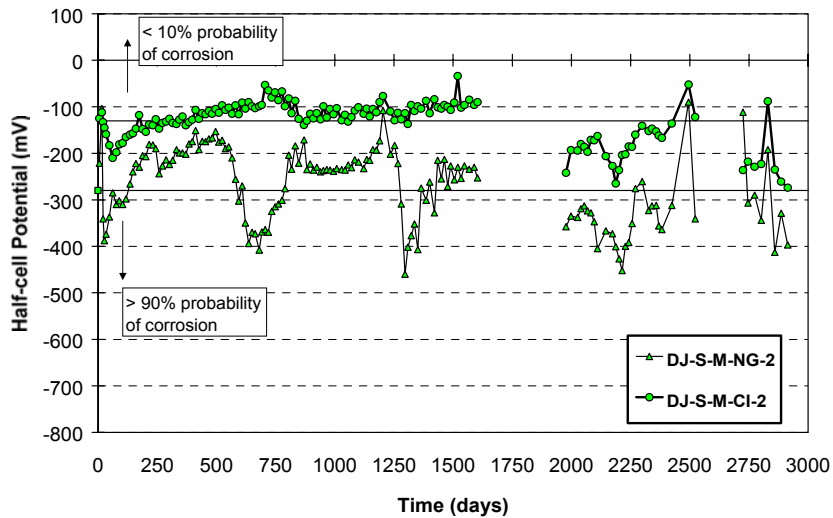
Figure A.24 Half-Cell Potentials: Dry Joint, Steel Duct, Medium
Precompression, and Different Grouts (Normal and Corrosion Inhibitor Added)

575
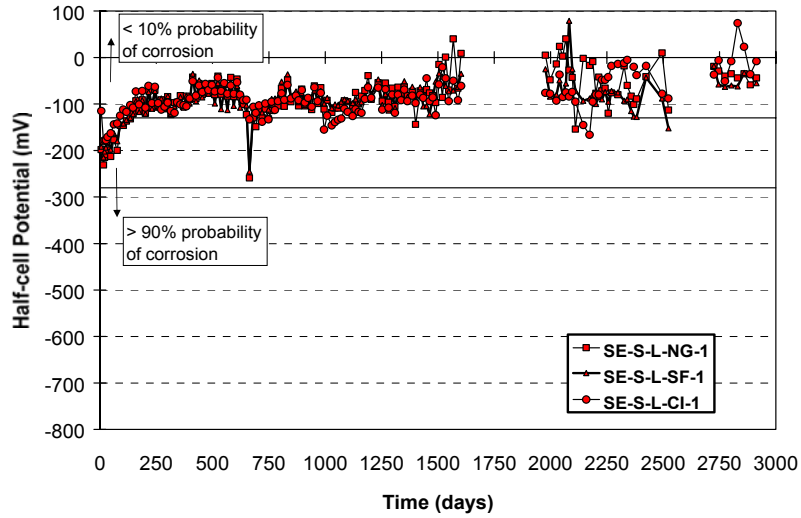
Figure A.25 Half-Cell Potentials: Epoxy Joint, Steel Duct, Low Precompression, and Different Grouts (Normal, Silica Fume and Corrosion Inhibitor Added)
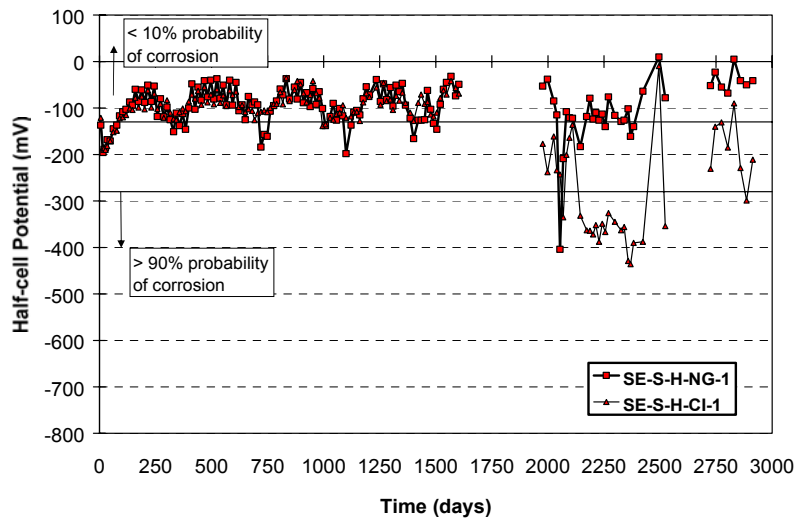
Figure A.26 Half-Cell Potentials: Epoxy Joint, Steel Duct, High Precompression, and Different Grouts (Normal and Corrosion Inhibitor Added)

576

A.3   SPECIMEN PERFORMANCE REPRODUCIBILITY

The following half-cell potential plots complement those included in Section 3.2.3.
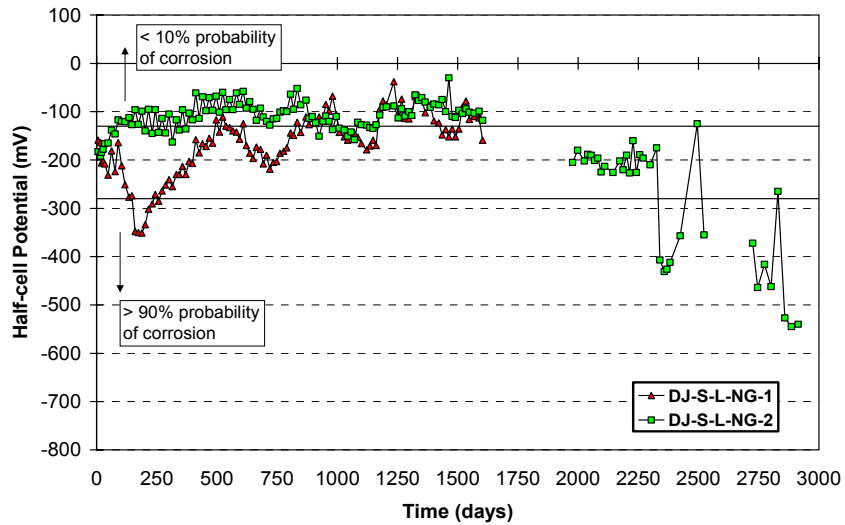
Figure A.27 Half-Cell Potentials for Duplicated Specimens with Dry Joint, Steel Duct, Low Precompression and Normal Grout
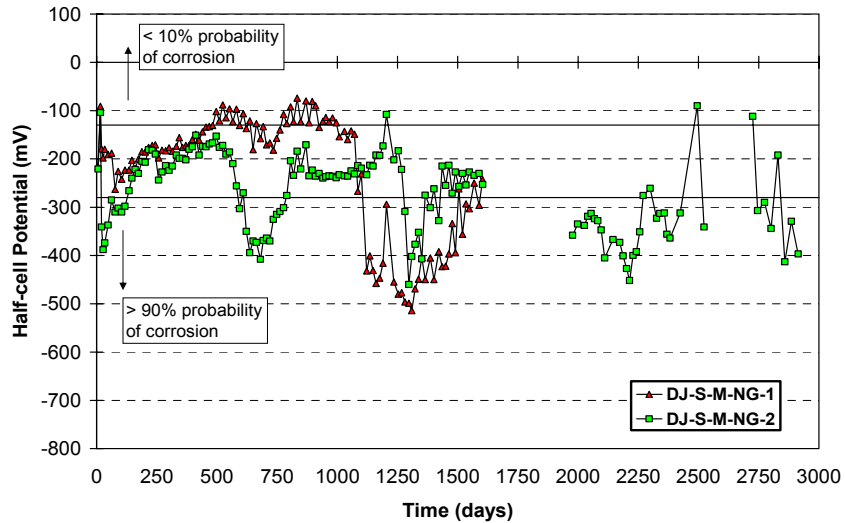
Figure A.28 Half-Cell Potentials for Duplicated Specimens with Dry Joint, Steel Duct, Medium Precompression and Normal Grout

577
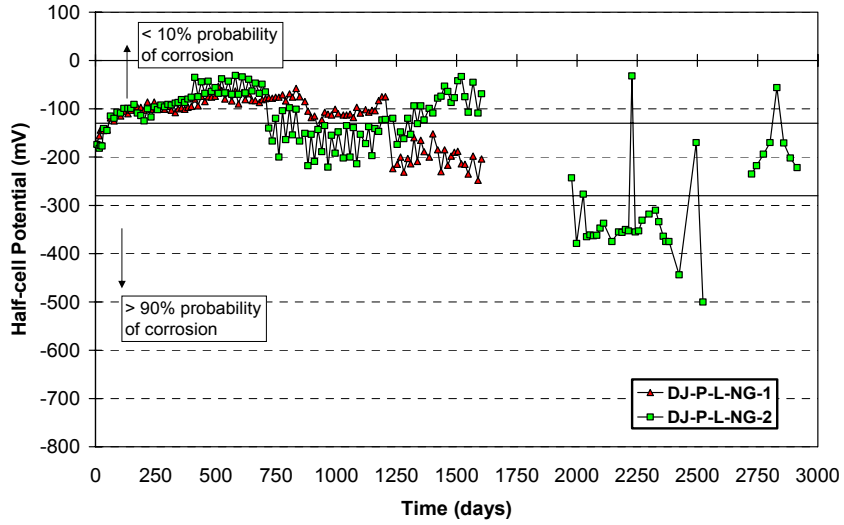
Figure A.29 Half-Cell Potentials for Duplicated Specimens with Dry Joint, Plastic Duct, Low Precompression, and Normal Grout
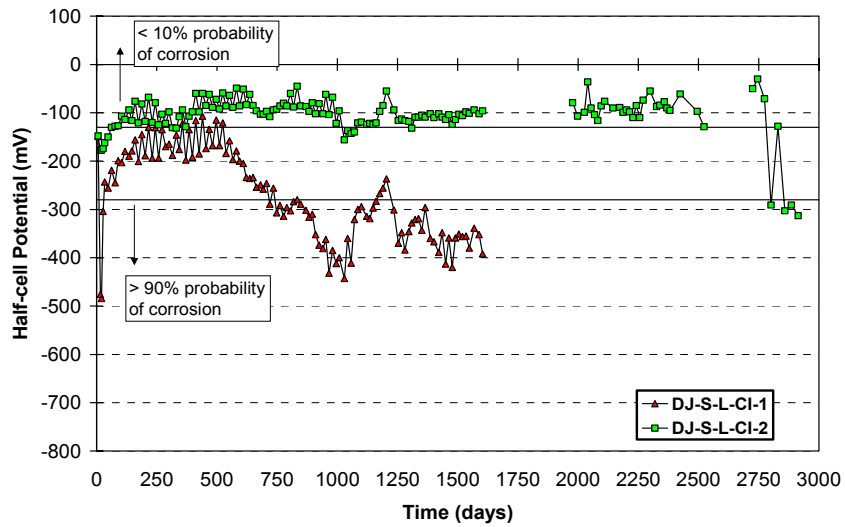
Figure A.30 Half-Cell Potentials for Duplicated Specimens with Dry Joint, Steel Duct, Low Precompression, and Grout with Corrosion Inhibitor Added

578
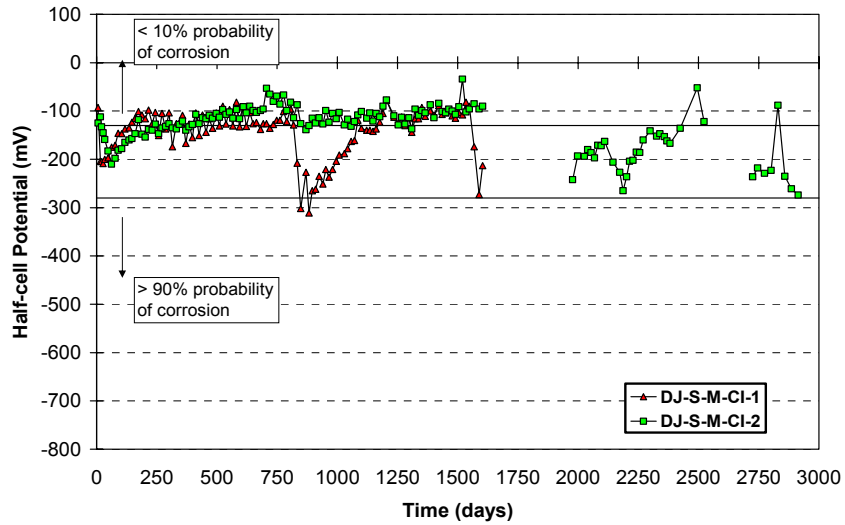
Figure A.31 Half-Cell Potentials for Duplicated Specimens with Dry Joint, Steel Duct, Medium Precompression and Grout with Corrosion Inhibitor Added
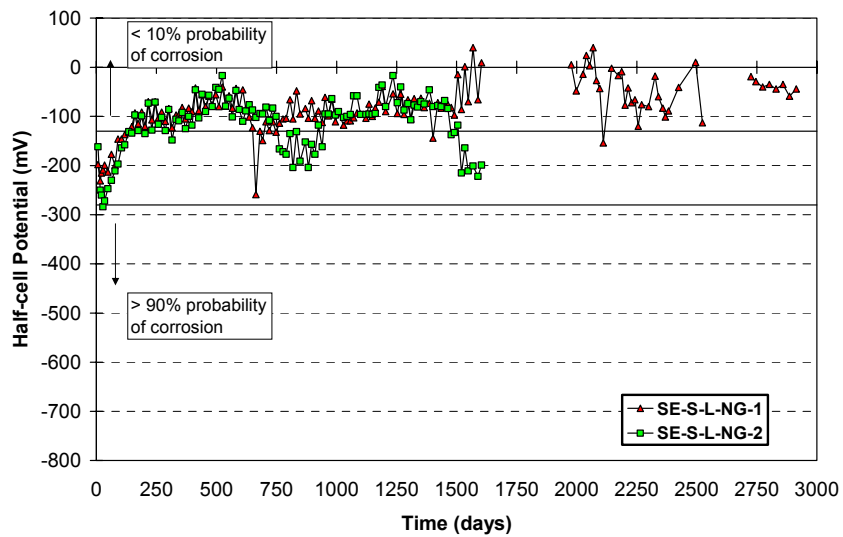
Figure A.32 Half-Cell Potentials for Duplicated Specimens with Epoxy Joint, Steel Duct, Low Precompression, and Normal Grout

579
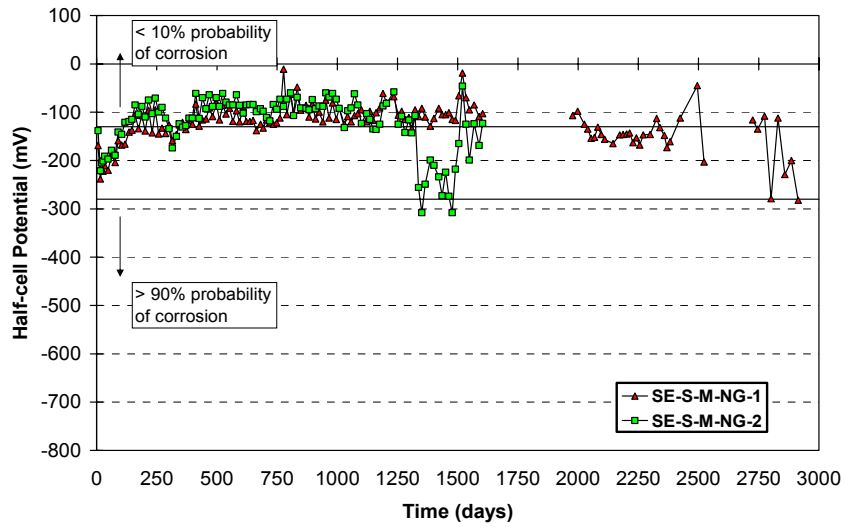
Figure A.33 Half-Cell Potentials for Duplicated Specimens with
Epoxy Joint, Steel Duct, Medium Precompression, and Normal Grout
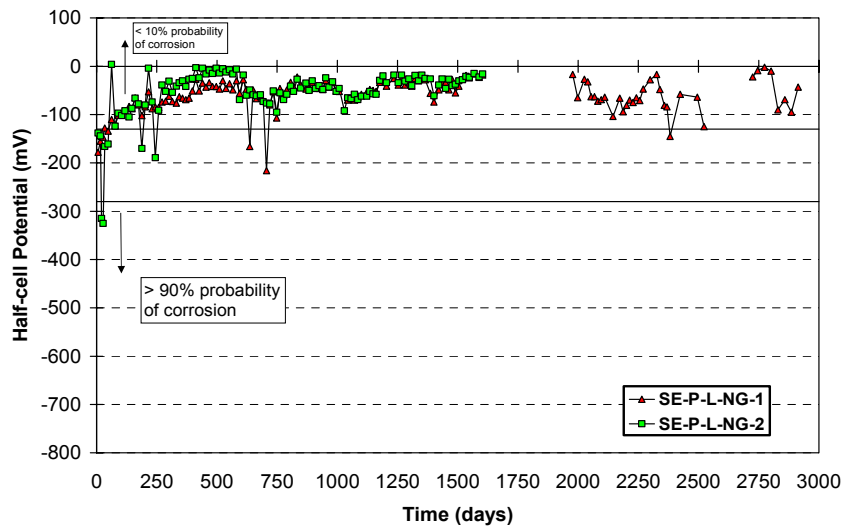
Figure A.34 Half-Cell Potentials for Duplicated Specimens with
Epoxy Joint, Plastic Duct, Low Precompression, and Normal Grout
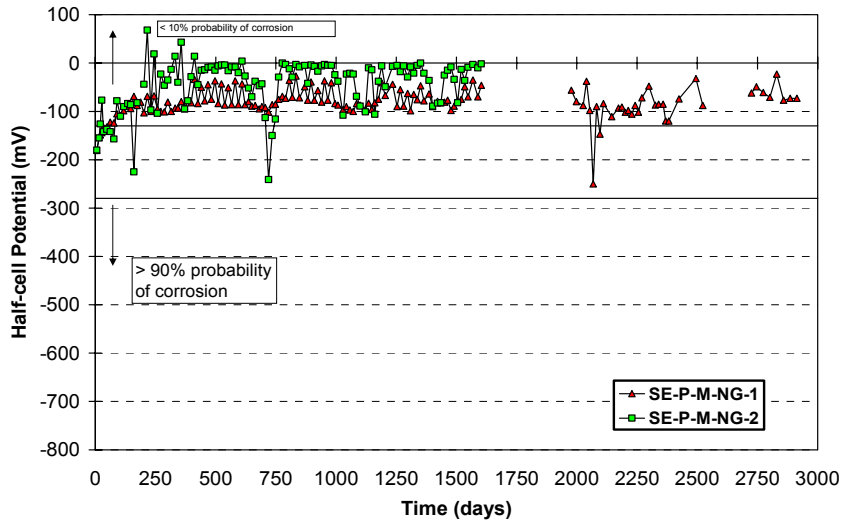
***Figure A.35 Half-Cell Potentials for Duplicated Specimens with
Epoxy Joint, Plastic Duct, Medium Precompression, and Normal Grout***
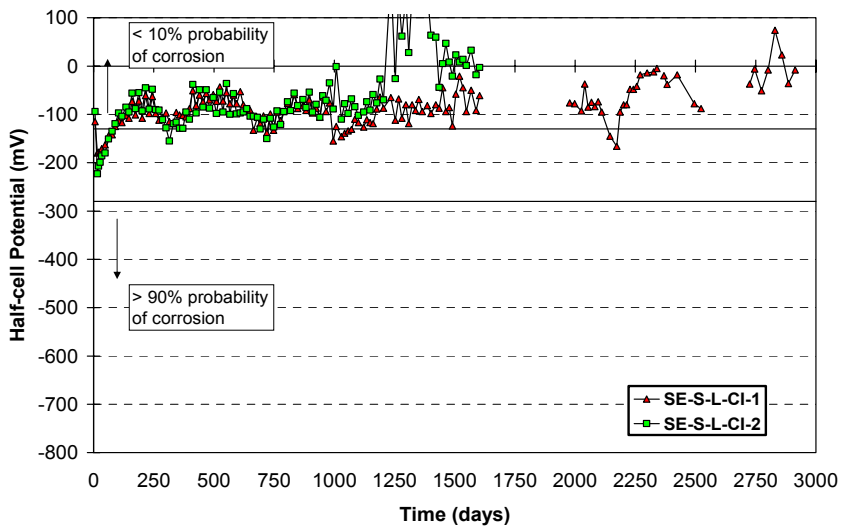
***Figure A.36 Half-Cell Potentials for Duplicated Specimens with
Epoxy Joint, Steel Duct, Low Precompression, and
Grout with Corrosion Inhibitor Added***

581
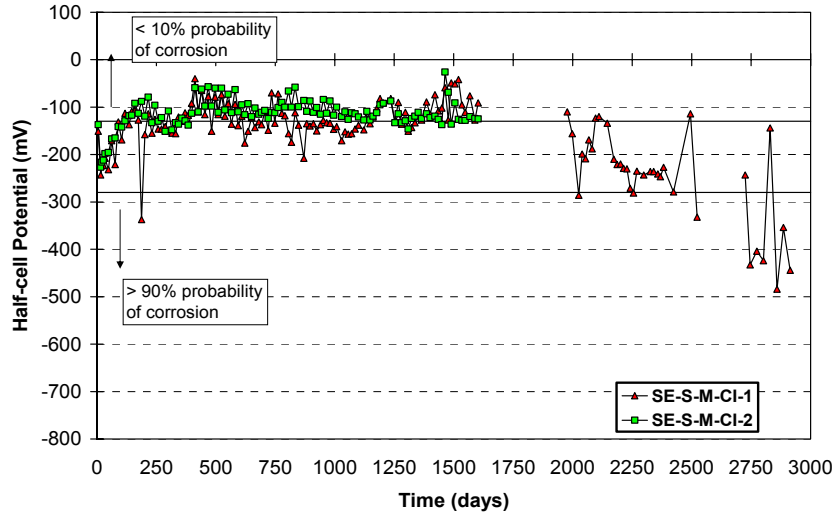
Figure A.37 Half-Cell Potentials for Duplicated Specimens with Epoxy Joint, Steel Duct, Medium Precompression, and Grout with Corrosion Inhibitor Added
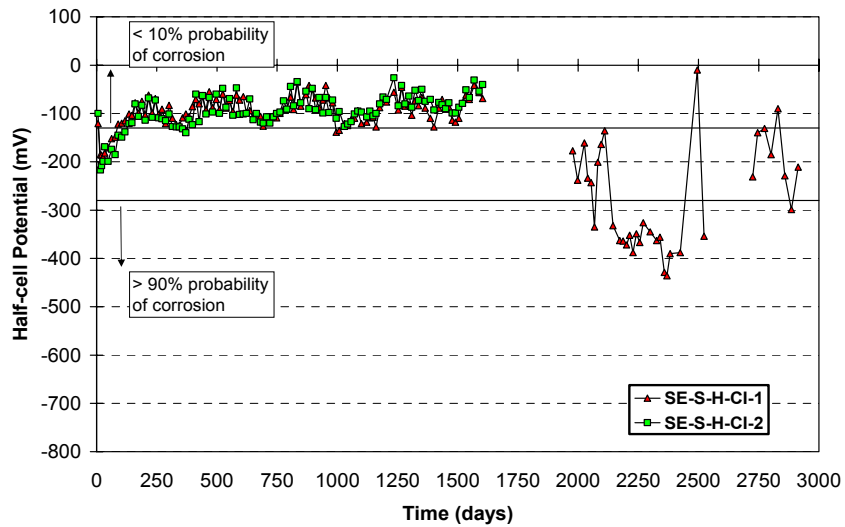
Figure A.38 Half-Cell Potentials for Duplicated Specimens with Epoxy Joint, Steel Duct, High Precompression, and Grout with Corrosion Inhibitor Added

582
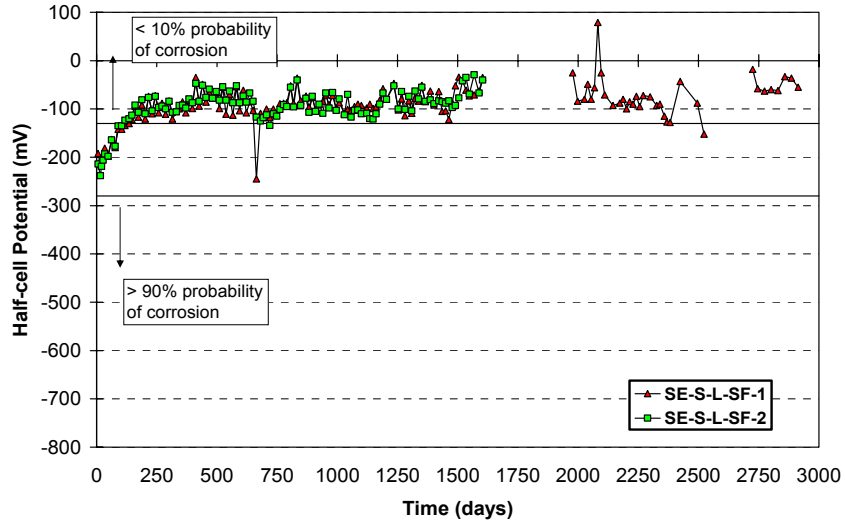
Figure A.39 Half-Cell Potentials for Duplicated Specimens with Epoxy Joint, Steel Duct, Low Precompression, and Grout with Silica Fume Added
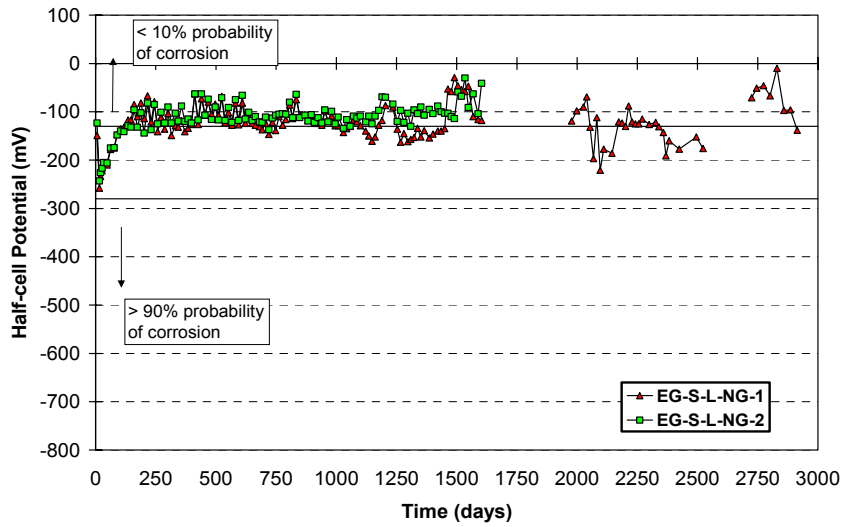
Figure A.40 Half-Cell Potentials for Duplicated Specimens with Epoxy Joint with Gasket, Steel Duct, Low Precompression, and Normal Grout

583
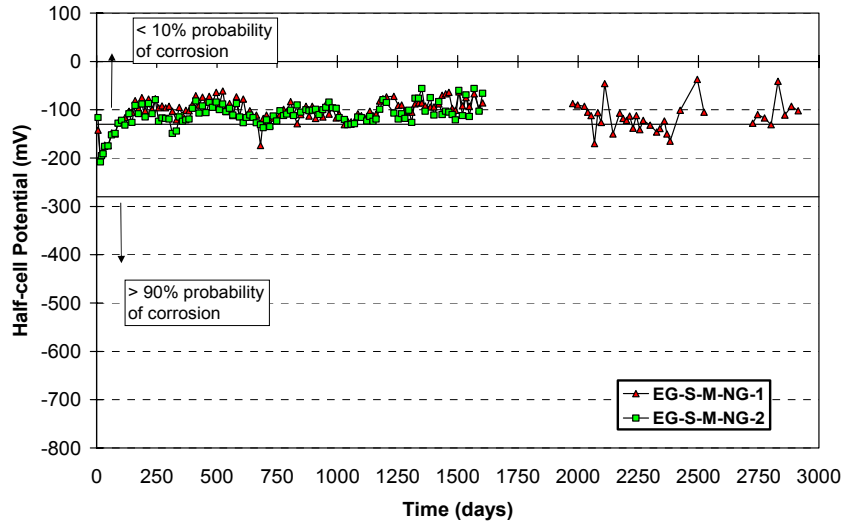
Figure A.41 Half-Cell Potentials for Duplicated Specimens with Epoxy Joint with Gasket, Steel Duct, Medium Precompression, and Normal Grout
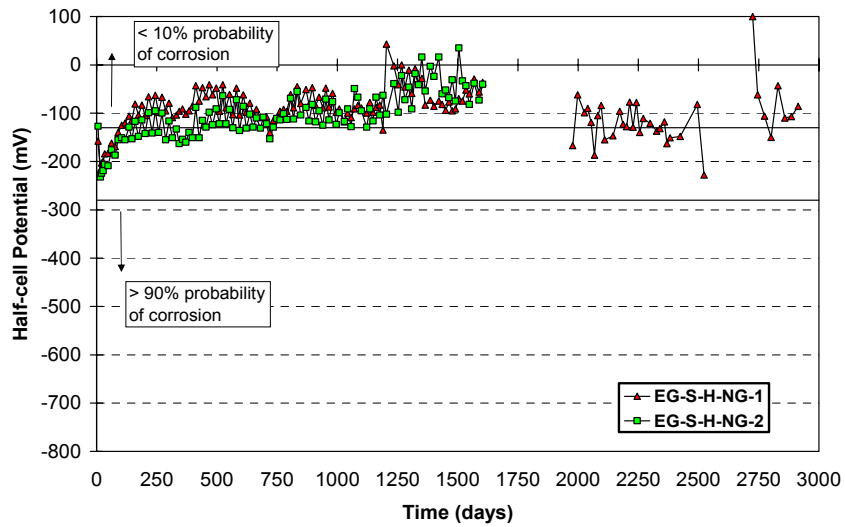
Figure A.42 Half-Cell Potentials for Duplicated Specimens with Epoxy Joint with Gasket, Steel Duct, High Precompression, and Normal Grout

584

Appendix B
Beam Corrosion Tests
Supplementary Material

B.1 DETAIL BEAM CONSTRUCTION DRAWINGS

Complete construction details of the four sections (Non-PS,2/3 PS, 100%U PS and 100%S PS) are shown in the following detailed drawings.

Long Term Exposure Test — Linear Flexural Elements

Sheet:	Title:		Sheet:	Title:
S1	Non-PS — Section		S11	2/3 PS — Section
S2	Non-PS — Stirrup Layout		S12	2/3 PS — Stirrup Layout
S3	100%S — Section		S13	2/3 PS — Anchorage Zone
S4	100%S — Stirrup Layout		S14	2/3 PS — End Detail
S5	100%S — Anchorage Zone		S15	Reaction Beam — Section
S6	100%S — End Detail		S16	Reaction Beam — Stirrup Layout
S7	100%U — Section			
S8	100%U — Stirrup Layout		D1	Bar Details
S9	100%U — Anchorage Zone		D2	Anchorage Hardware
S10	100%U — End Detail		D3	PT Duct and Splice Details

Durability of P/T
Bridge Substructures

Drawing List

JSW   n/a

9-Jun-97   0

Figure B.1 Sheet 0: Drawing List[4.2]

585
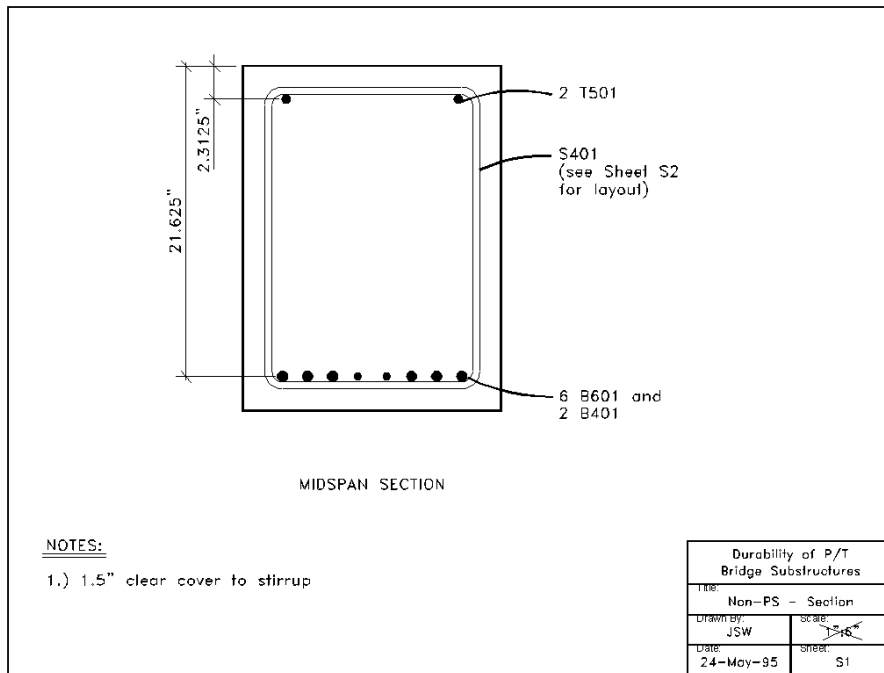
Figure B.2 Sheet S1: Non-PS Section [4.2]
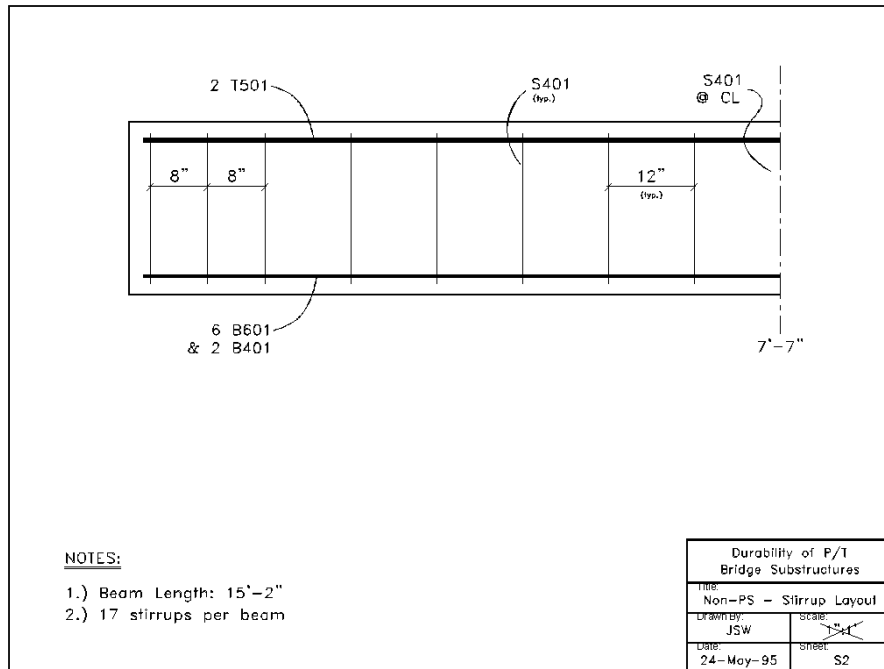
Figure B.3 Sheet S2: Non-PS Stirrup Layout[4.2]

586
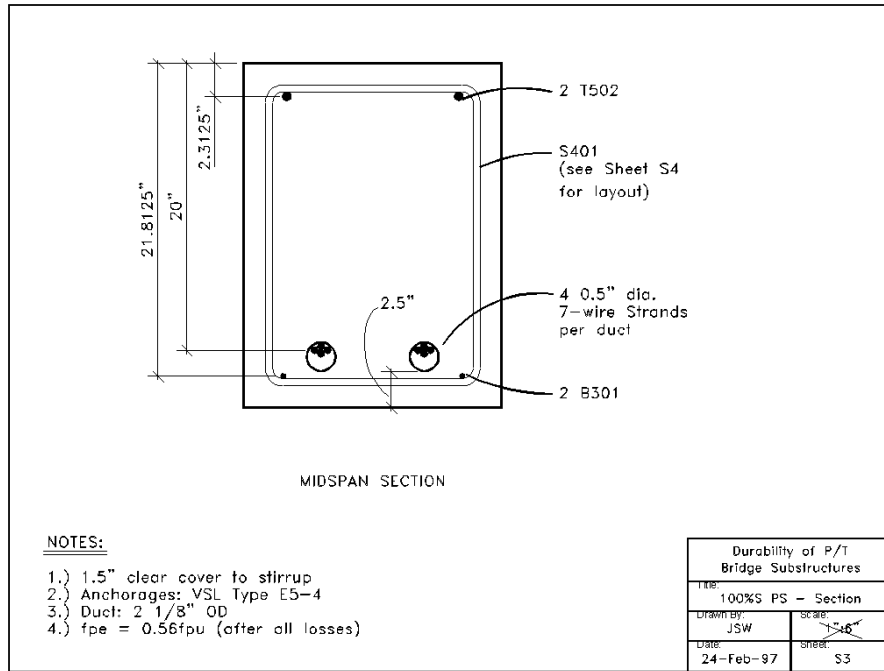
Figure B.4 Sheet S3: 100%S PS Section[4.2]
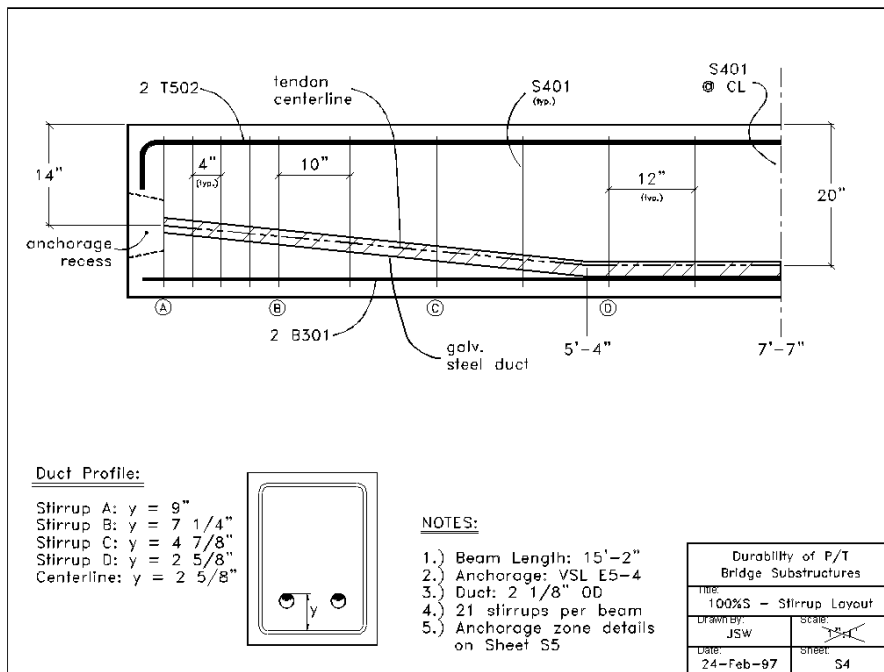
Figure B.5 Sheet S4: 100%S Stirrup Layout [4.2]

587
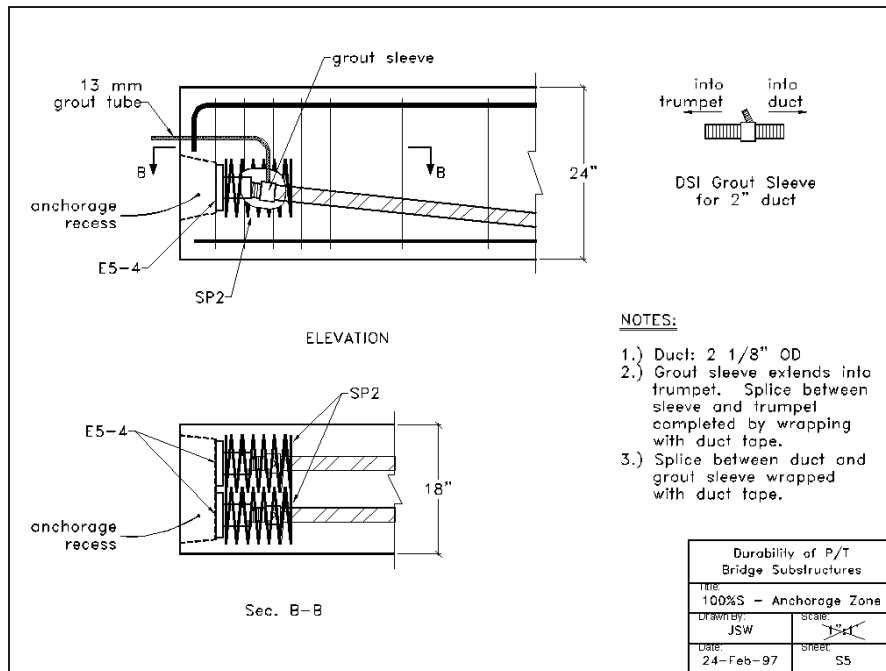
Figure B.6 Sheet S5: 100%S Anchorage Zone [4.2]
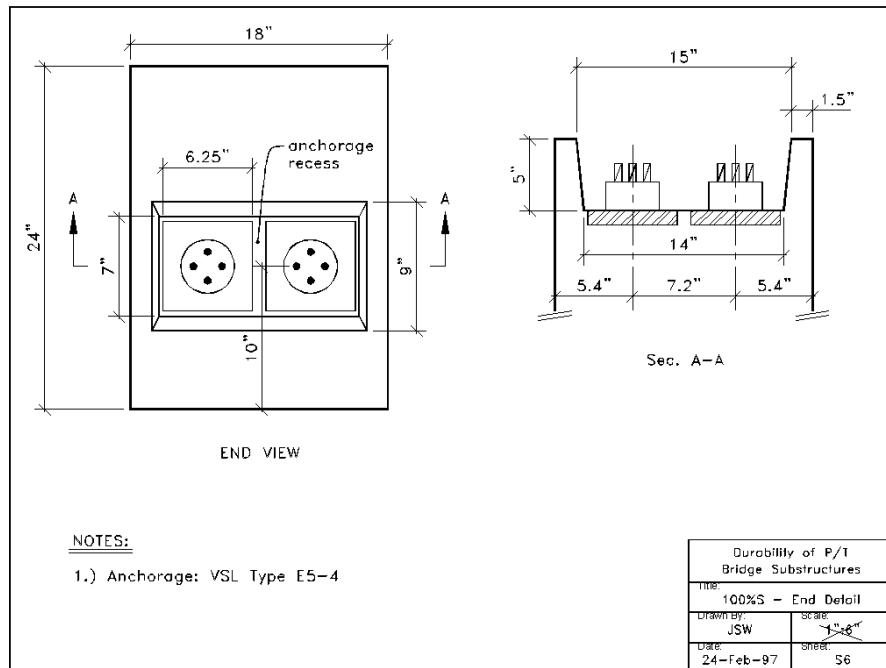
Figure B.7 Sheet S6: 100%S End Detail [4.2]

588
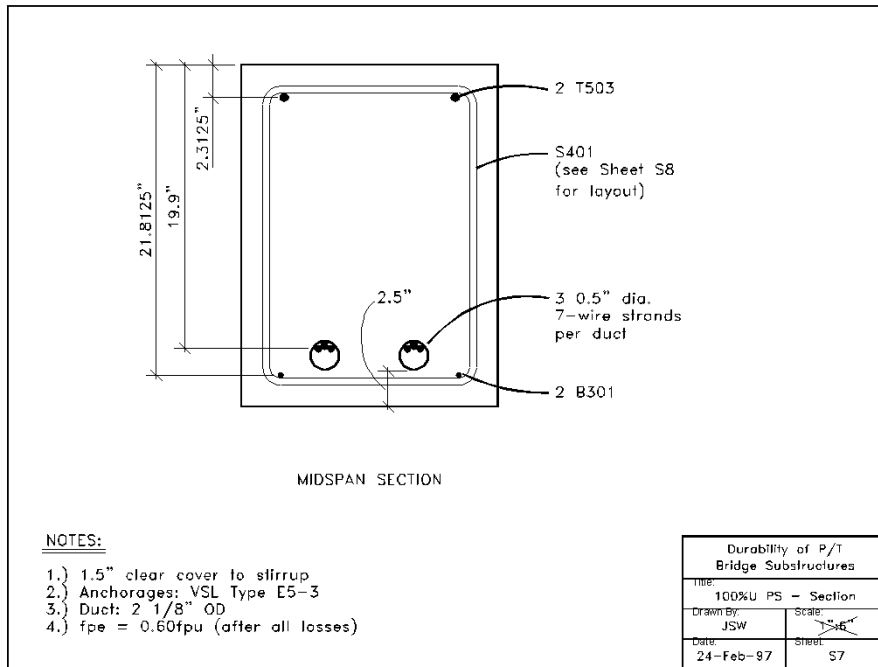
Figure B.8 Sheet S7: 100%U PS Section [4.2]
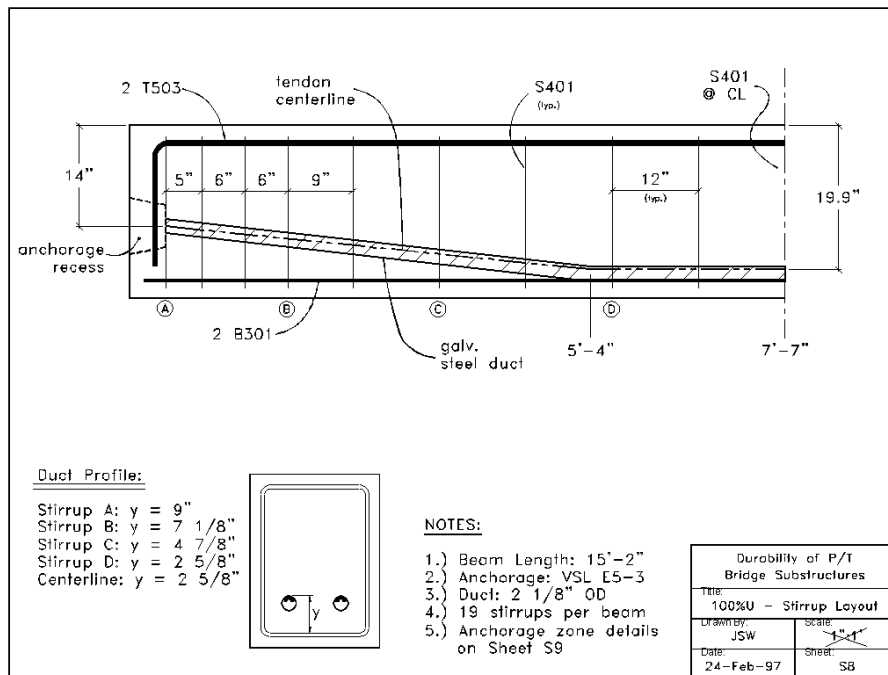
Figure B.9 Sheet S8: 100%U Stirrup Layout [4.2]

589
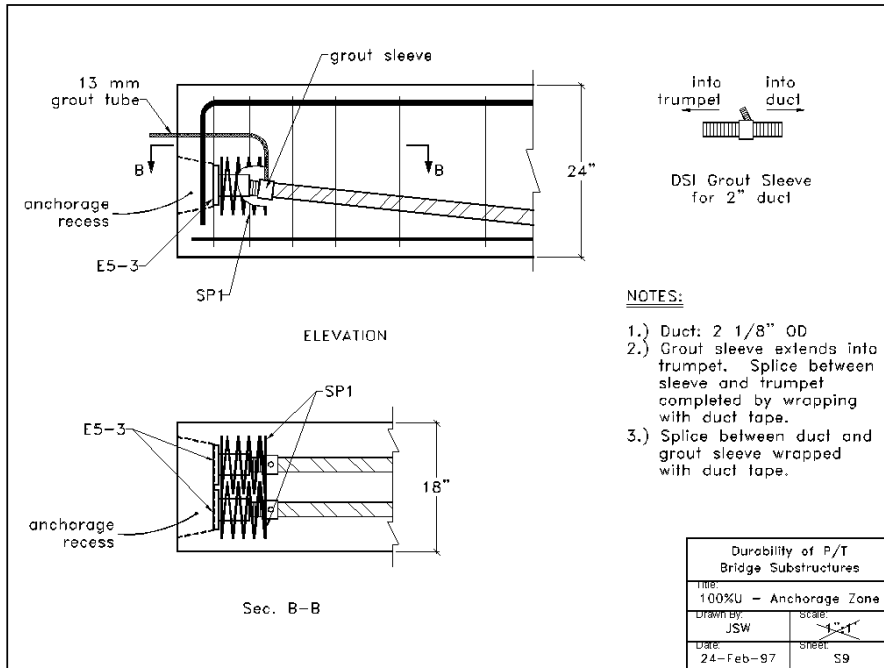
Figure B.10 Sheet S9: 100%U Anchorage Zone[4.2]
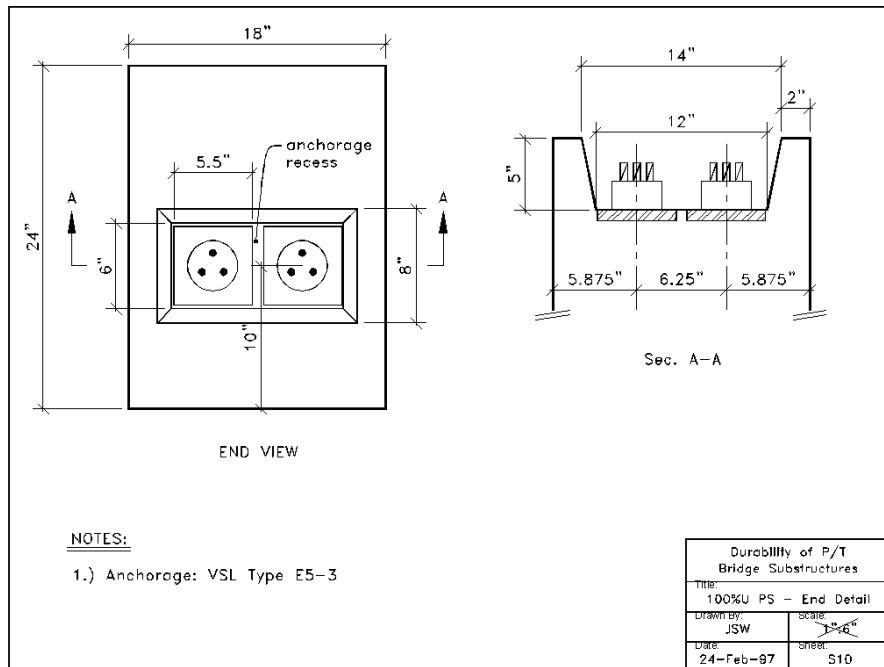
Figure B.11 Sheet S10: 100%U End Detail [4.2]

590

NOTES:

1.) 1.5" clear cover to stirrup
2.) Anchorages: VSL Type E5-3
3.) Duct: 2 1/8" OD
4.) fpe = 0.60fpu (after all losses)

MIDSPAN SECTION

Durability of P/T Bridge Substructures	
Title: 2/3 PS – Section	
Drawn By: JSW	Scale: 1:6
Date: 24-Feb-97	Sheet: S11
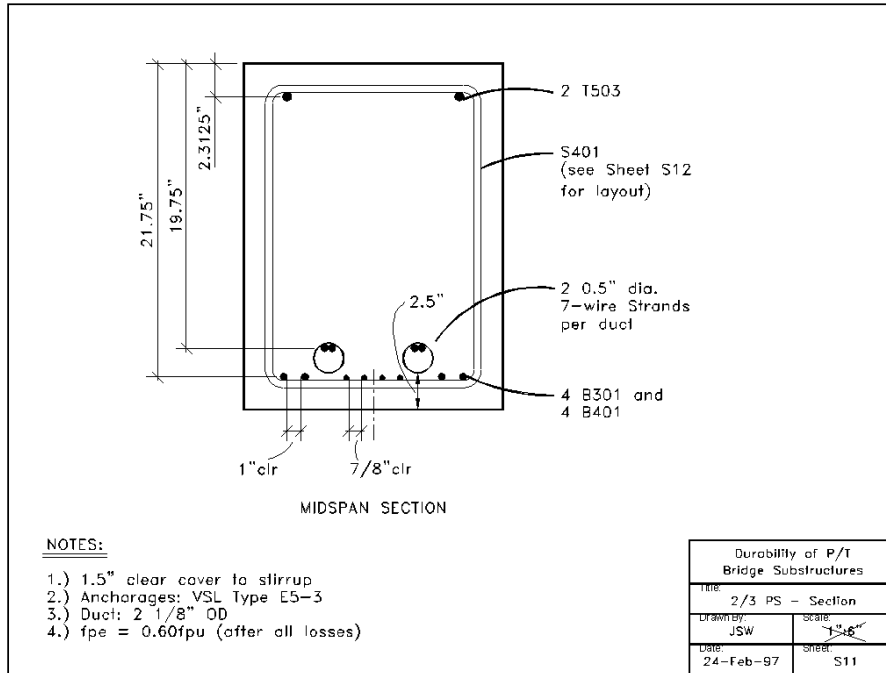
Figure B.12 Sheet S11: 100%S End Detail[4.2]

Duct Profile:

Stirrup A: y = 9"
Stirrup B: y = 7 3/8"
Stirrup C: y = 4 7/8"
Stirrup D: y = 2 5/8"
Centerline: y = 2 5/8"

NOTES:

1.) Beam Length: 15'-2"
2.) Anchorage: VSL E5-3
3.) Duct: 2 1/8" OD
4.) 17 stirrups per beam
5.) Anchorage zone details on Sheet S13

Durability of P/T Bridge Substructures	
Title: 2/3 PS – Stirrup Layout	
Drawn By: JSW	Scale: 1:4
Date: 24-Feb-97	Sheet: S12
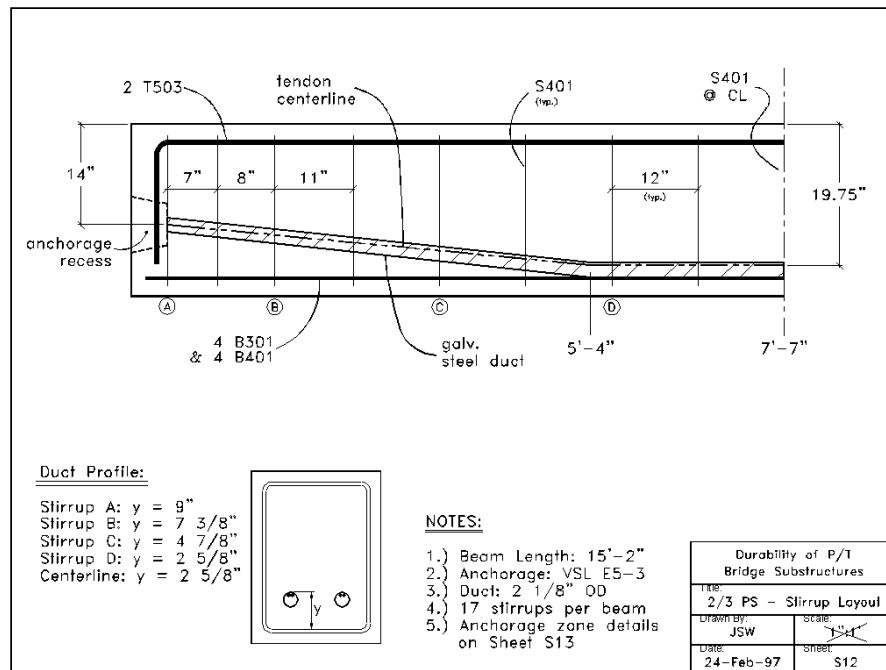
Figure B.13 Sheet S12: 2/3 PS Stirrup Layout [4.2]

591
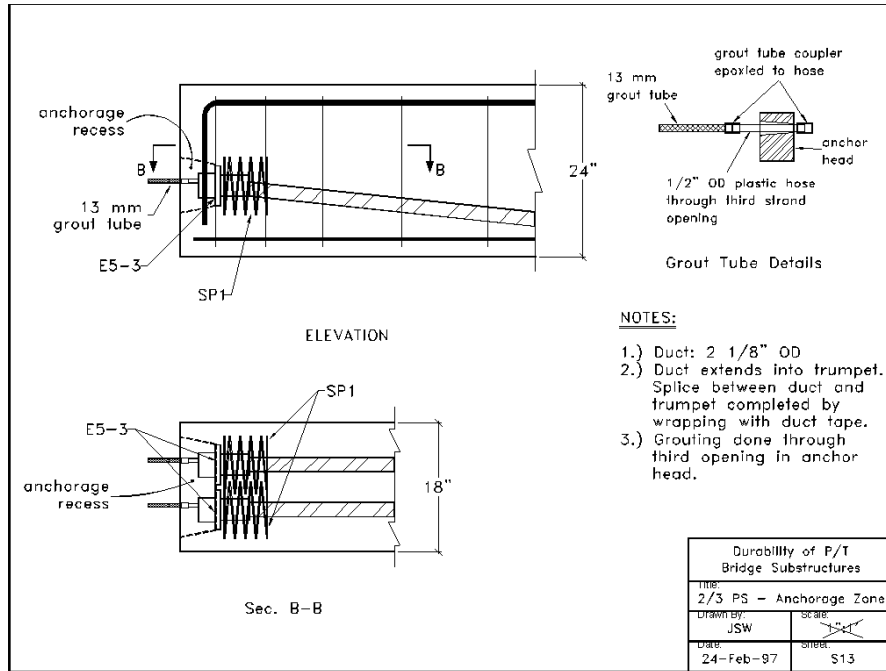
Figure B.14 Sheet S13: 2/3 PS Anchorage Zone[4.2]
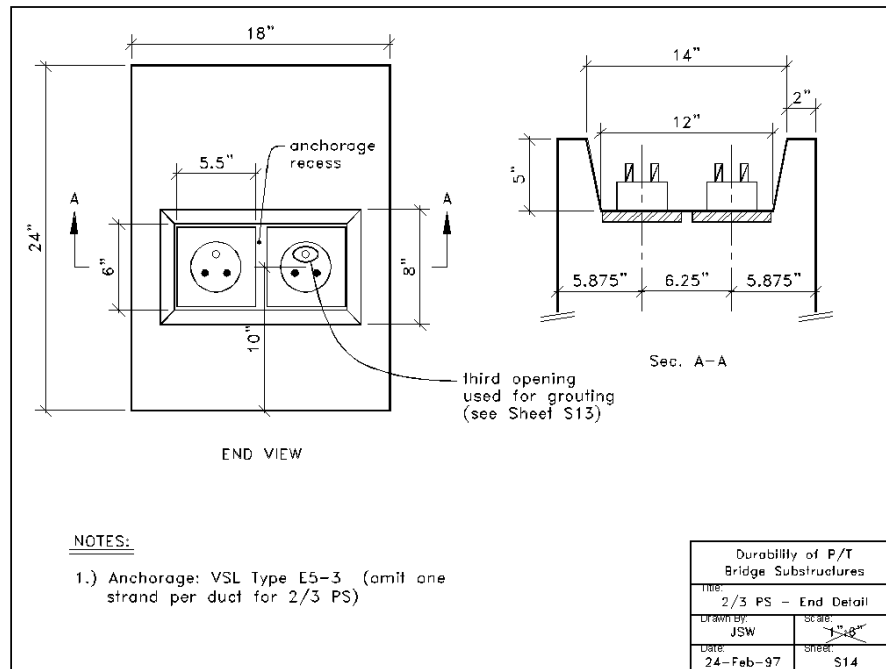
Figure B.15 Sheet S14: 2/3 PS End Detail [4.2]

592
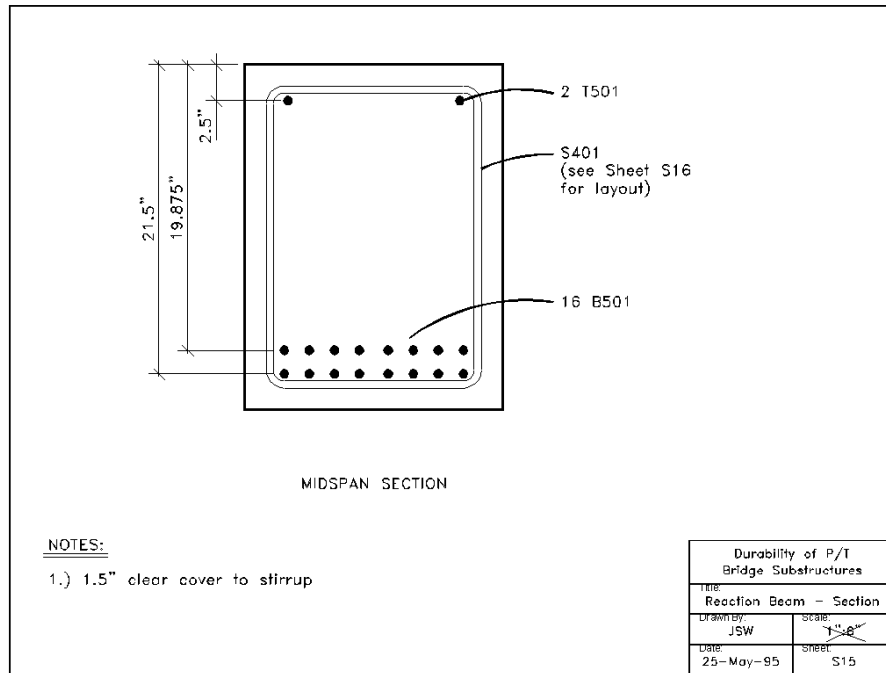
Figure B.16 Sheet S15: Reaction Beam Section [4.2]
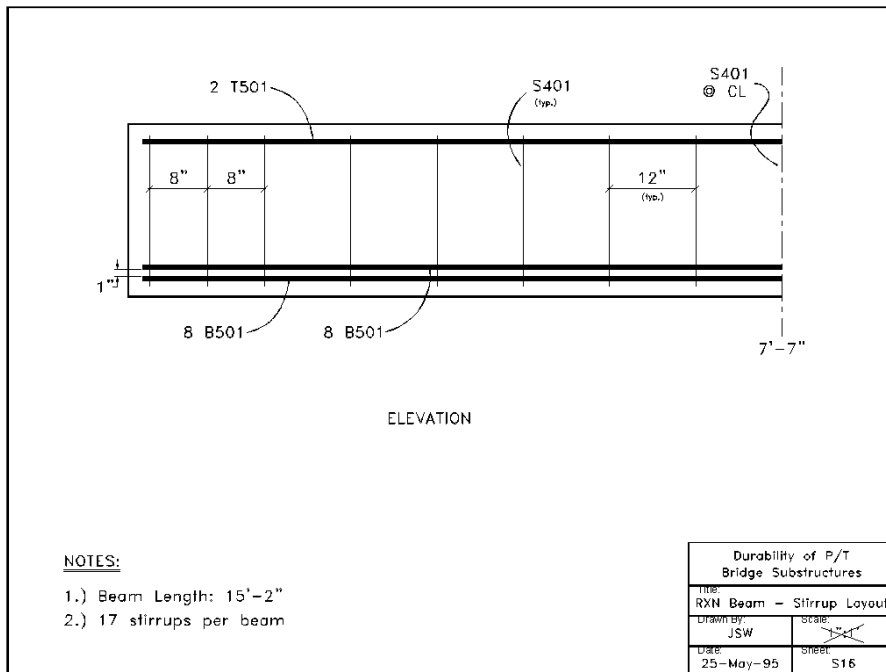
Figure B.17 Sheet S16: Reaction Beam Stirrup Layout[4.2]

593
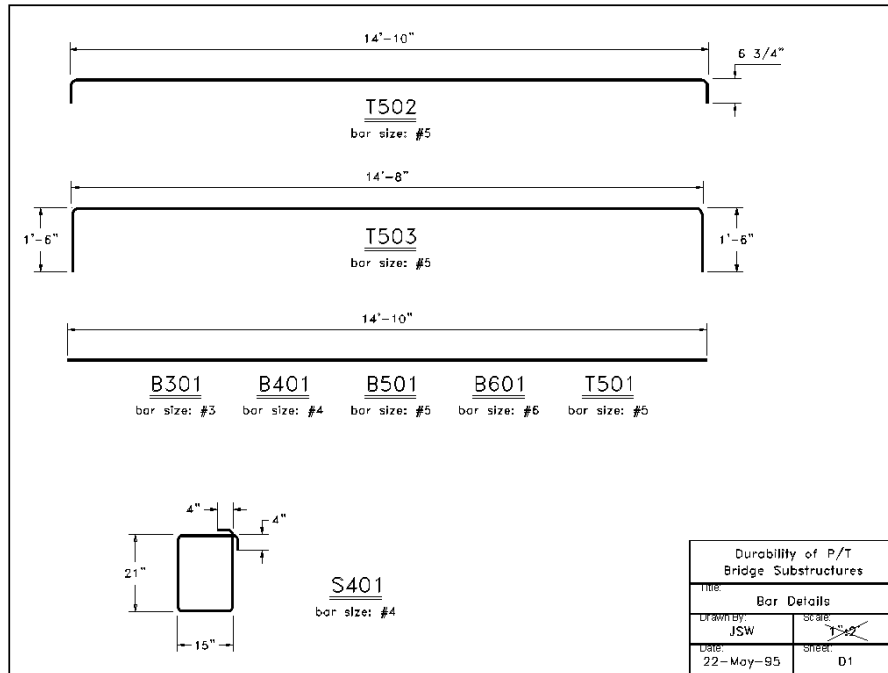
Figure B.18 Sheet D1: Bar Details [4.2]
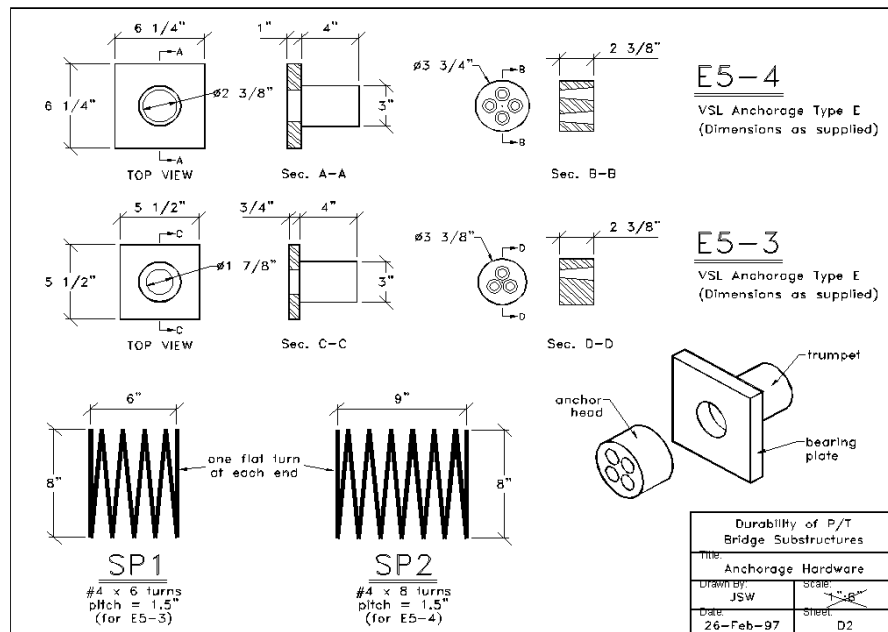
Figure B.19 Sheet D2: Anchorage Hardware [4.2]

594
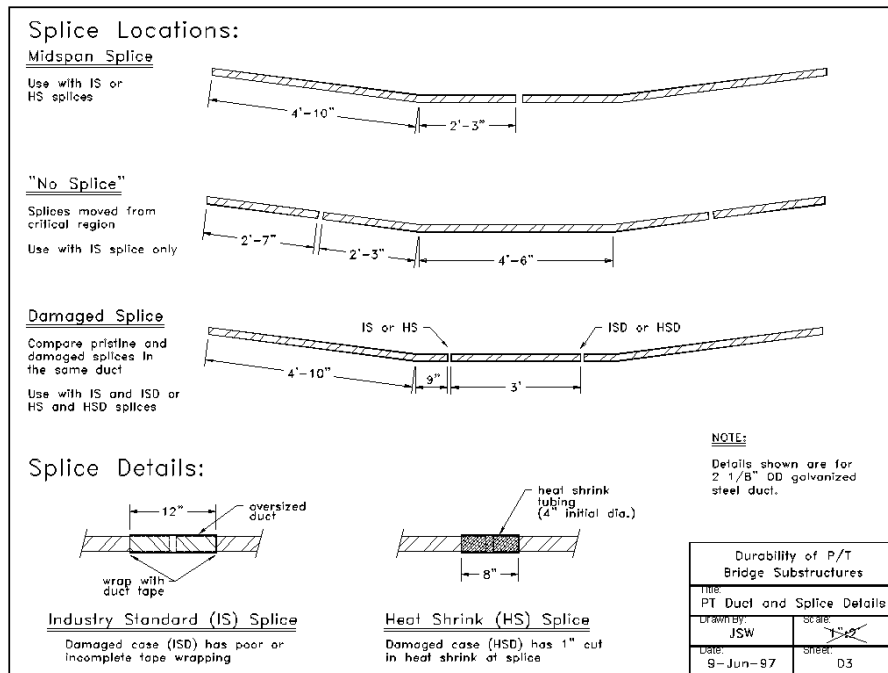
Figure B.20 Sheet D3: Post-Tensioning Duct and Splice Details [4.2]

B.2   SURFACE CRACK PATTERNS AND WIDTHS PRIOR TO AUTOPSY

Crack patterns and widths for all Autopsy specimens immediately prior to concrete demolition and reinforcement removal, are shown in Figures B.21 through Figure B.32.

Beam 1.3: Non-PS - Constant Service Load
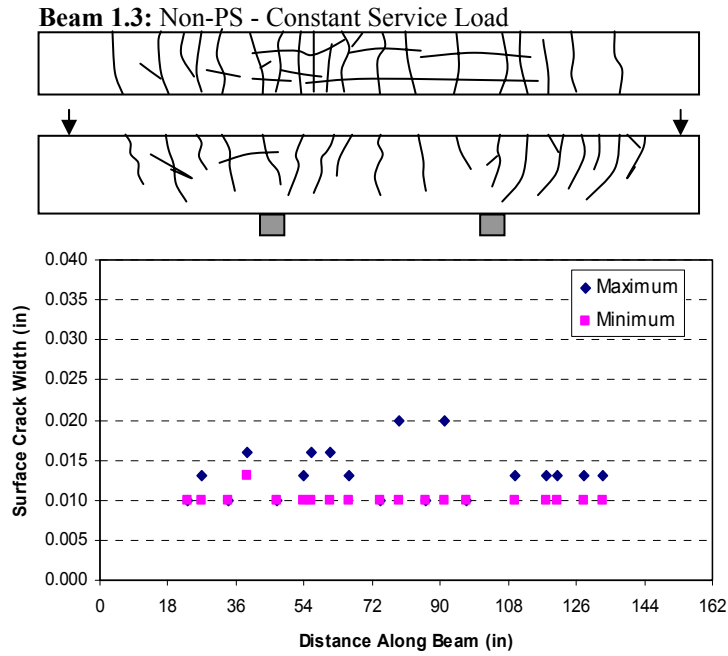
Figure B.21 Final Crack Pattern and Measurements – Beam 1.3

Beam 2.3: 2/3 PS - Constant Service Load
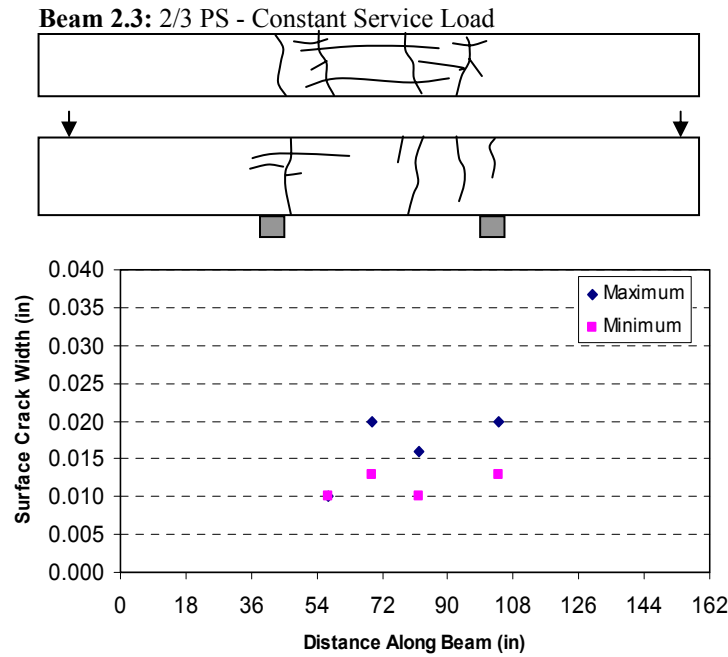
Figure B.22 Final Crack Pattern and Measurements – Beam 2.3

596

Beam 2.11: 2/3 PS - Constant Service Load
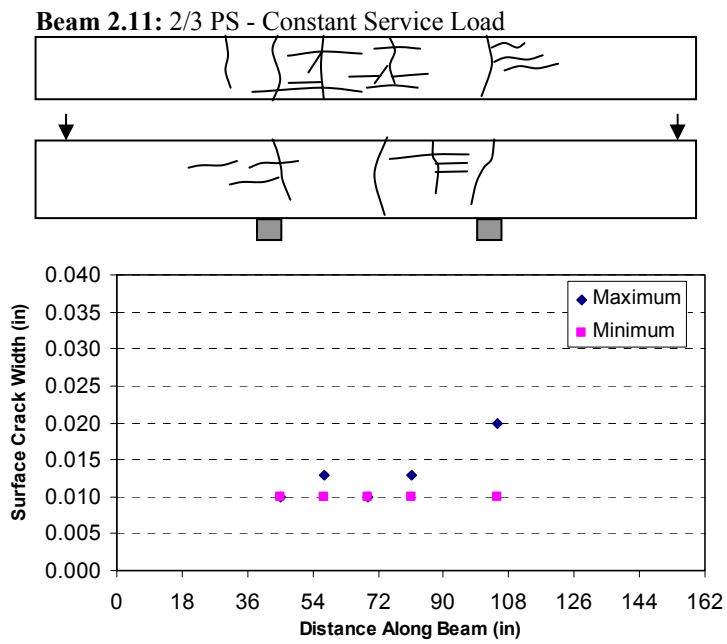
Figure B.23 Final Crack Pattern and Measurements – Beam 2.11

Beam 3.2: 100%U PS - Constant Service Load
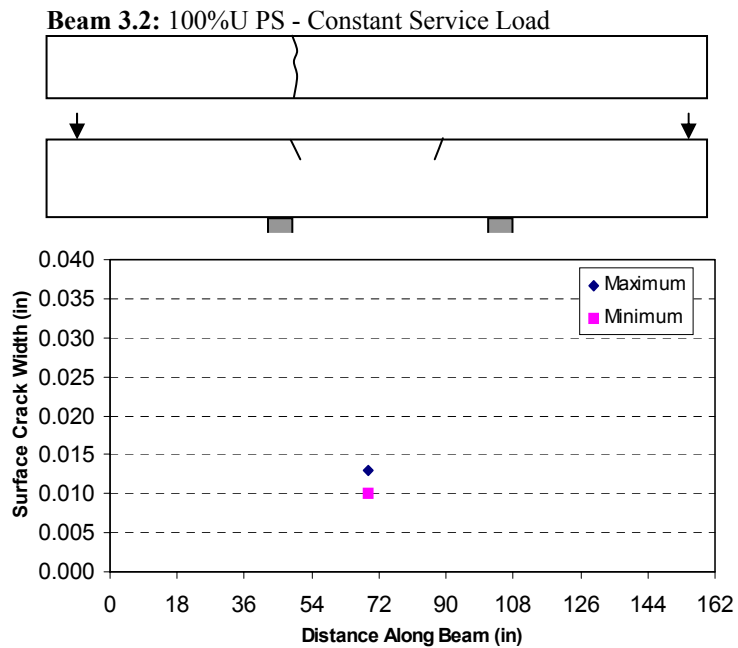
Figure B.24 Final Crack Pattern and Measurements – Beam 3.2

597

Beam 3.3: 100%U PS - 124% Overload
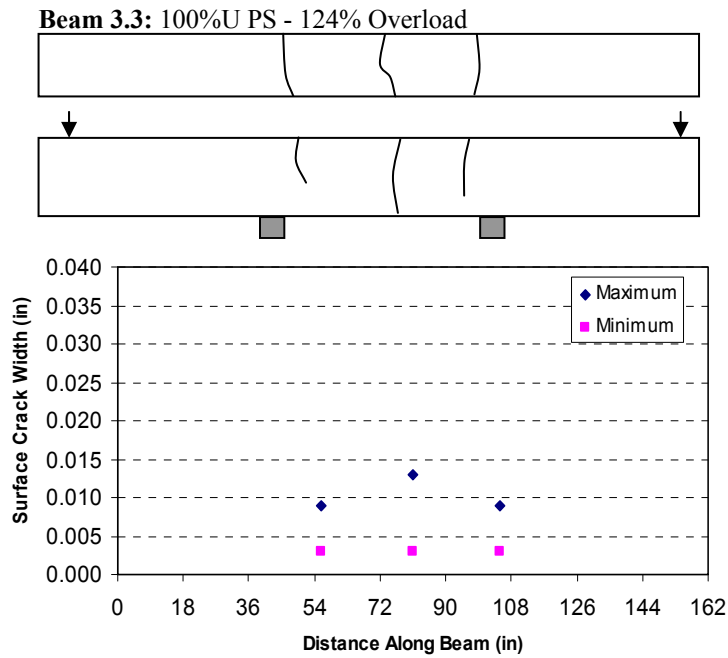
Figure B.25 Final Crack Pattern and Measurements – Beam 3.3

Beam 4.2: 100%S PS - Constant Service Load
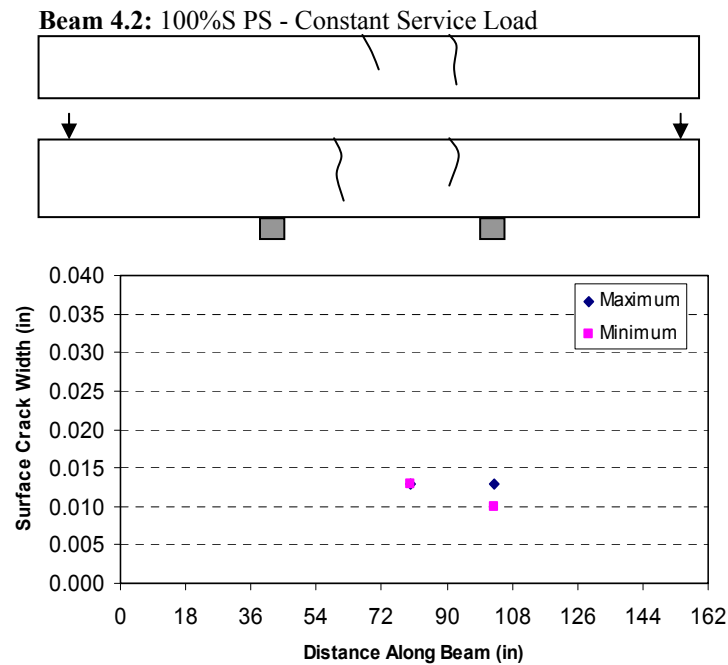
Figure B.26 Final Crack Pattern and Measurements – Beam 4.2

598

Beam 1.5: Non-PS - Constant Service Load
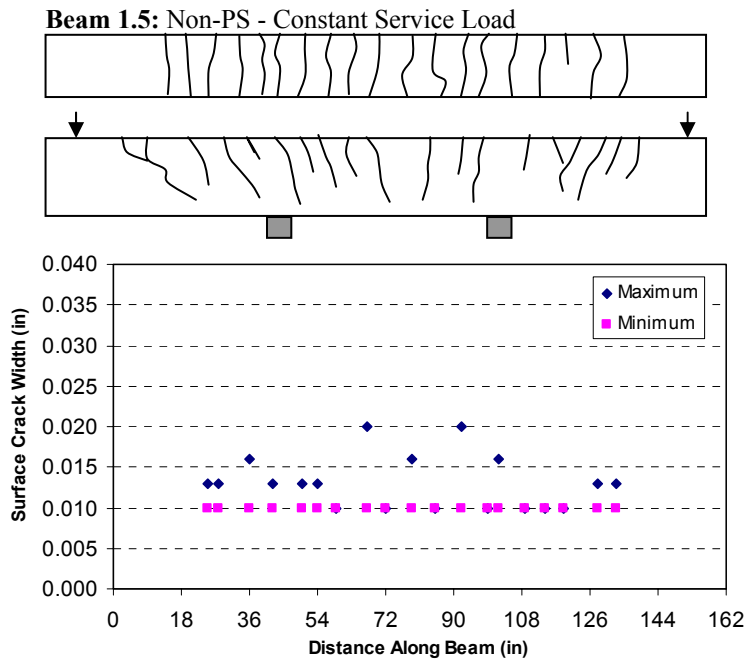
Figure B.27 Final Crack Pattern and Measurements – Beam 1.5

Beam 1.6: Non-PS - Constant Service
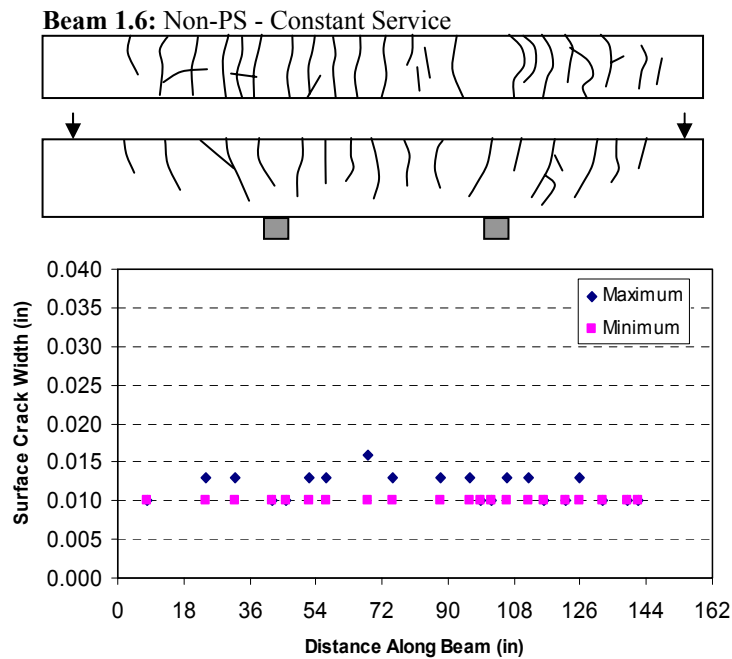
Figure B.28 Final Crack Pattern and Measurements – Beam 1.6

599

Beam 2.5: 2/3 PS - Constant Service Load
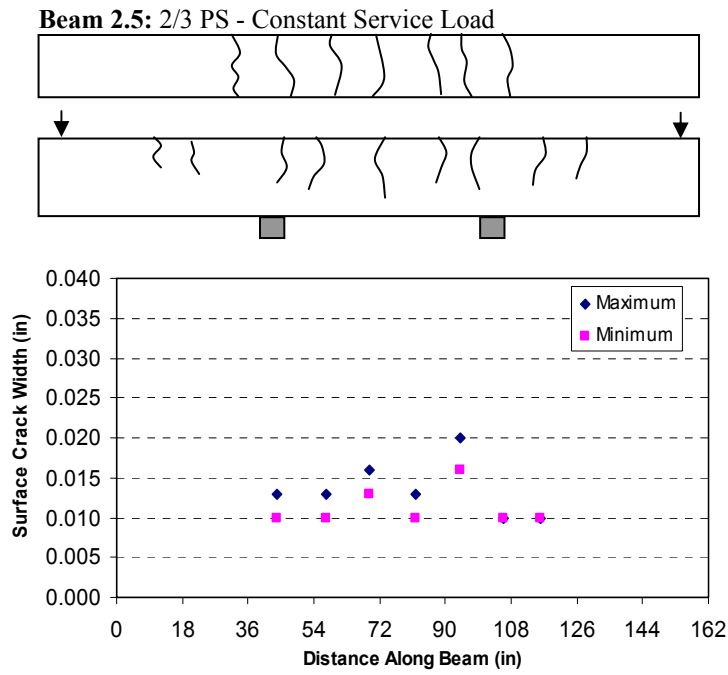
Figure B.29 Final Crack Pattern and Measurements – Beam 2.5

Beam 2.6: 2/3 PS - Constant Service Load
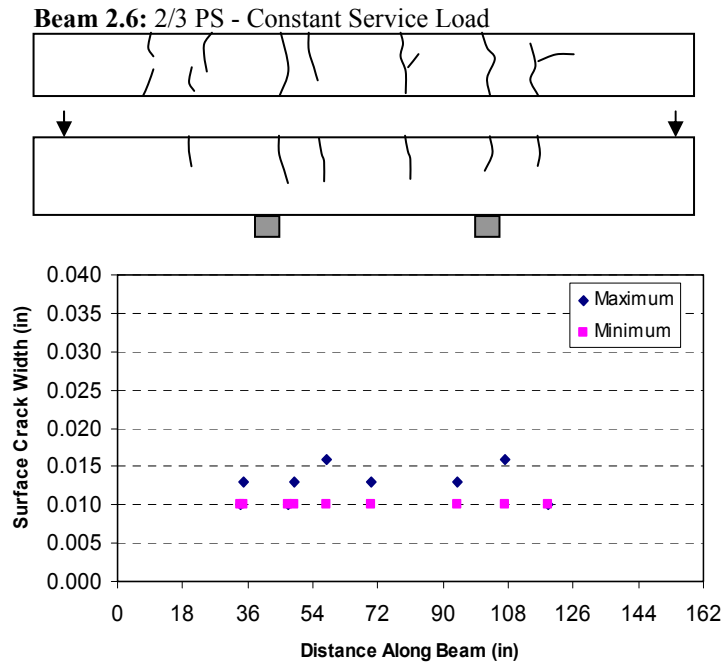
Figure B.30 Final Crack Pattern and Measurements – Beam 2.6

Beam 3.6: 100%U PS - Constant Service Load
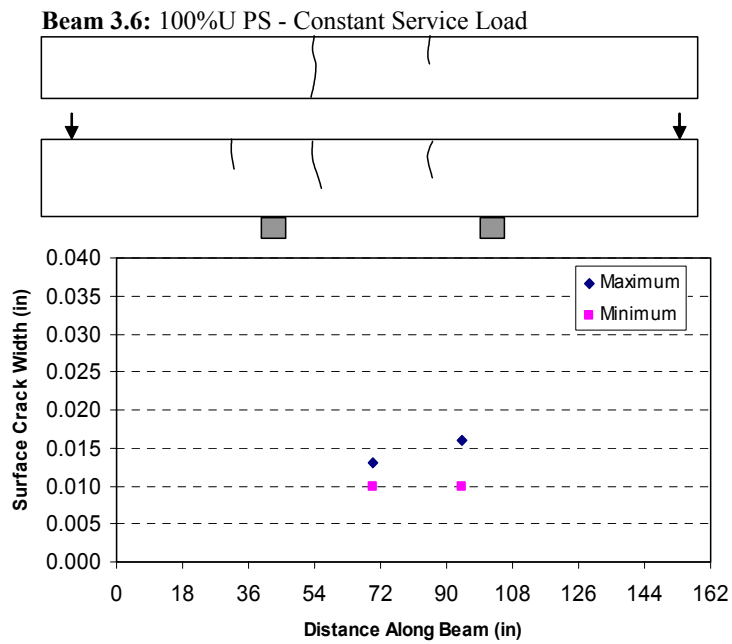
Figure B.31 Final Crack Pattern and Measurements – Beam 3.6

Beam 3.7: 100%U PS - Constant Service
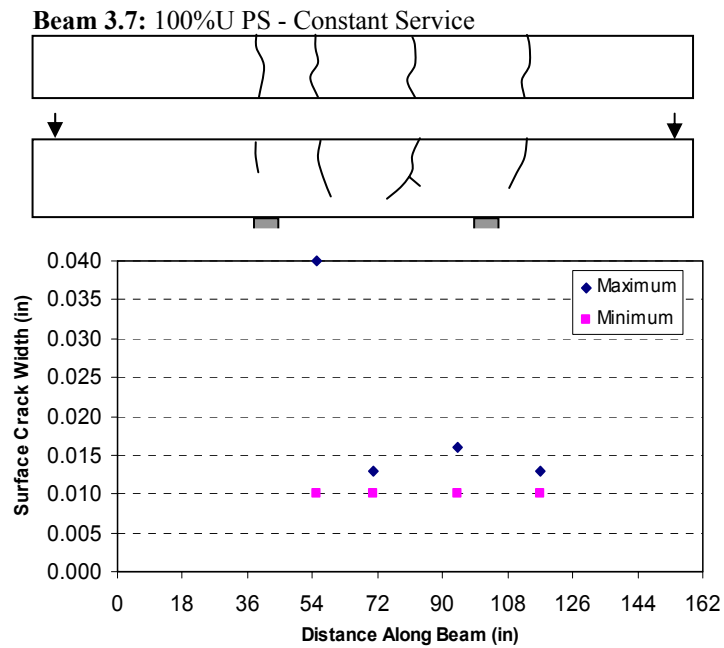
Figure B.32 Final Crack Pattern and Measurements – Beam 3.7

601

B.3   HALF-CELL POTENTIALS (LINE GRAPHS)
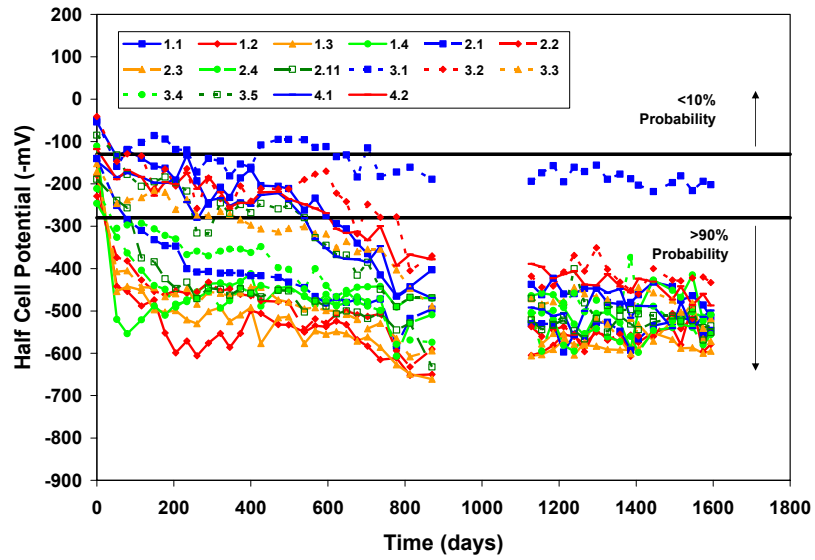
Figure B.33 Half-Cell Potential Readings for All Phase I Beams
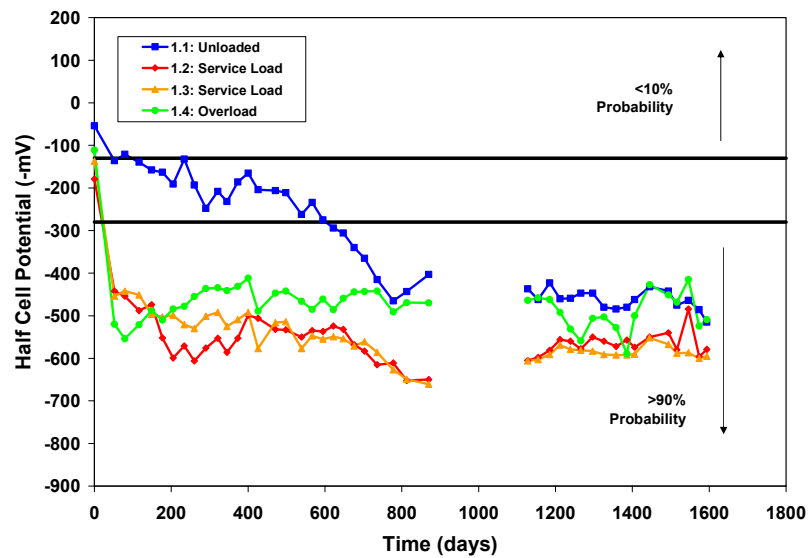
Figure B.34 Half-Cell Potential Readings for All Non-PS Phase I Beams
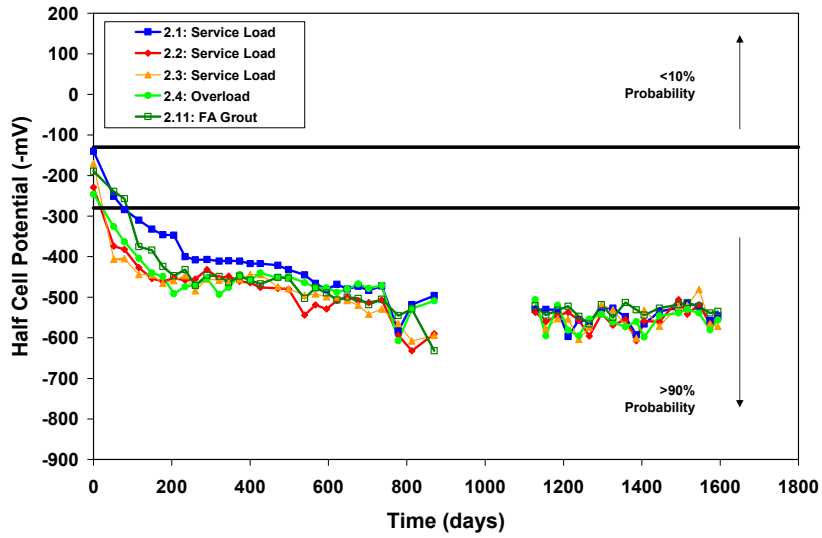
Figure B.35 Half-Cell Potential Readings for All 2/3 PS Phase I Beams
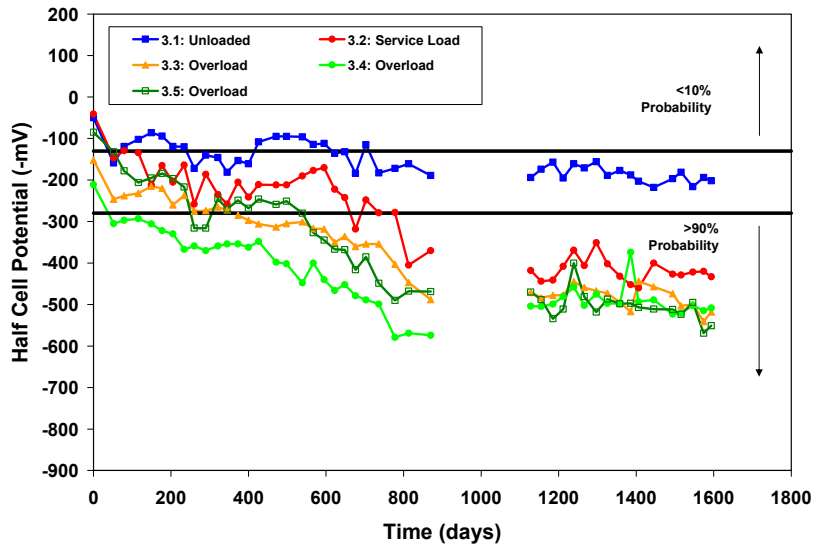
Figure B.36 Half-Cell Potential Readings for All 100%U PS Phase I Beams

603
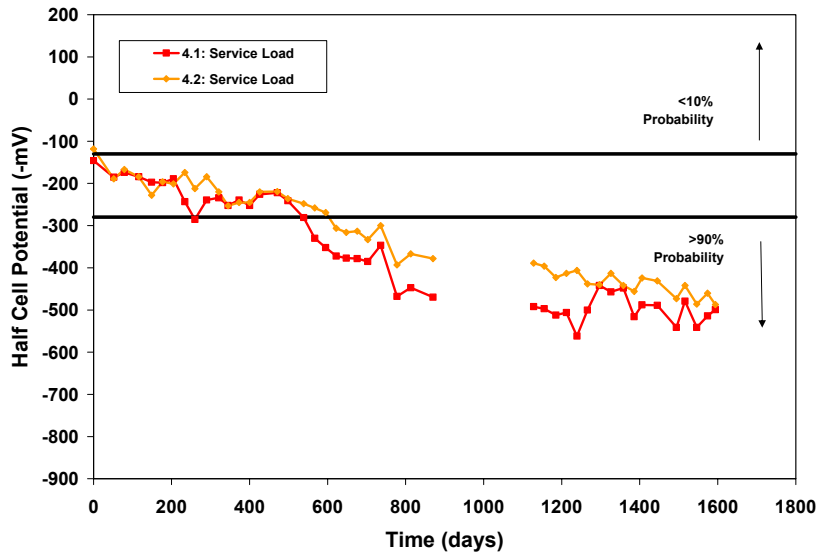
Figure B.37 Half-Cell Potential Readings for All 100%S PS Phase I Beams
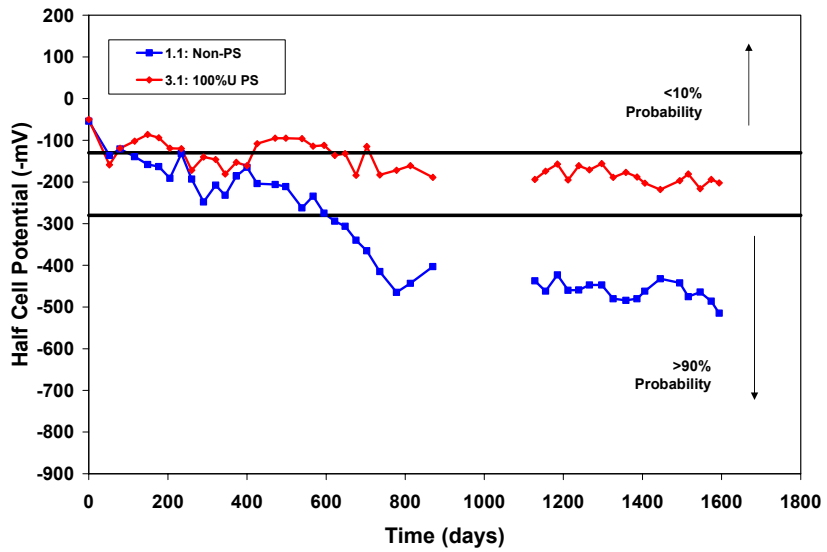
Figure B.38 Half-Cell Potential Readings for All Unloaded Phase I Beams

604
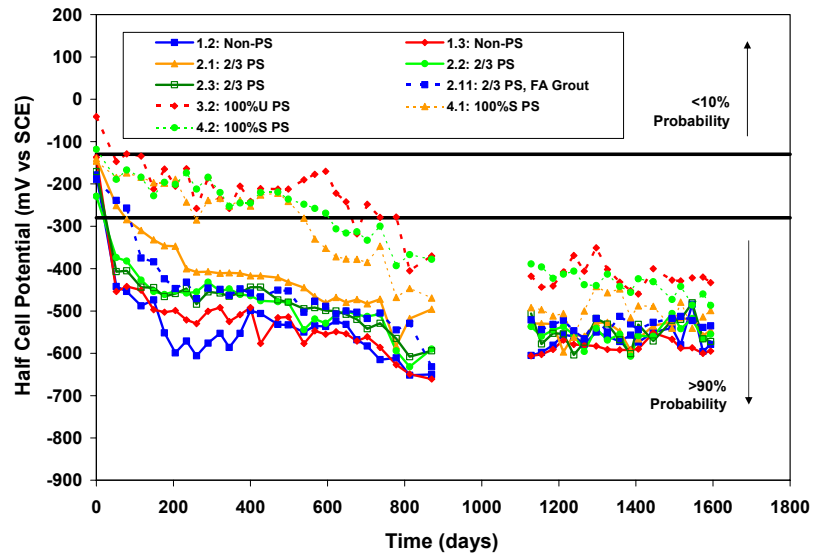
***Figure B.39 Half-Cell Potential Readings for All 100%
Service Load Phase I Beams***
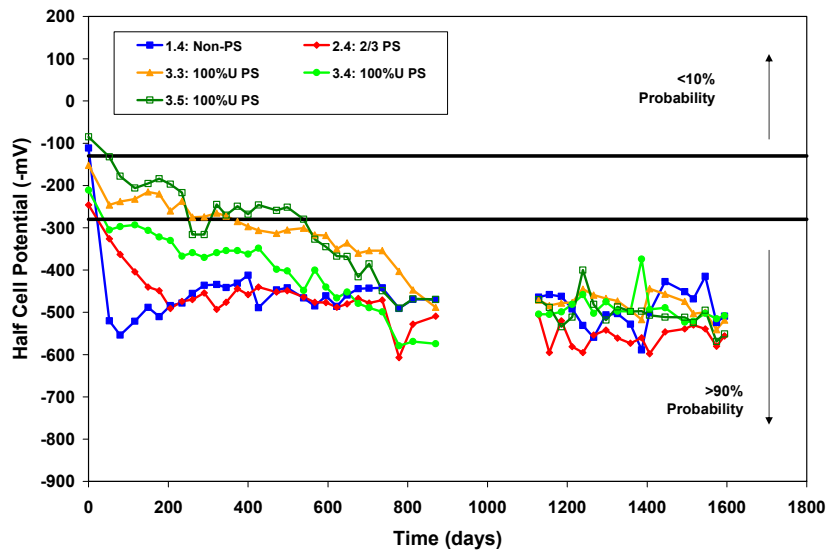
Figure B.40 Half-Cell Potential Readings for All Overloaded Phase I Beams

605
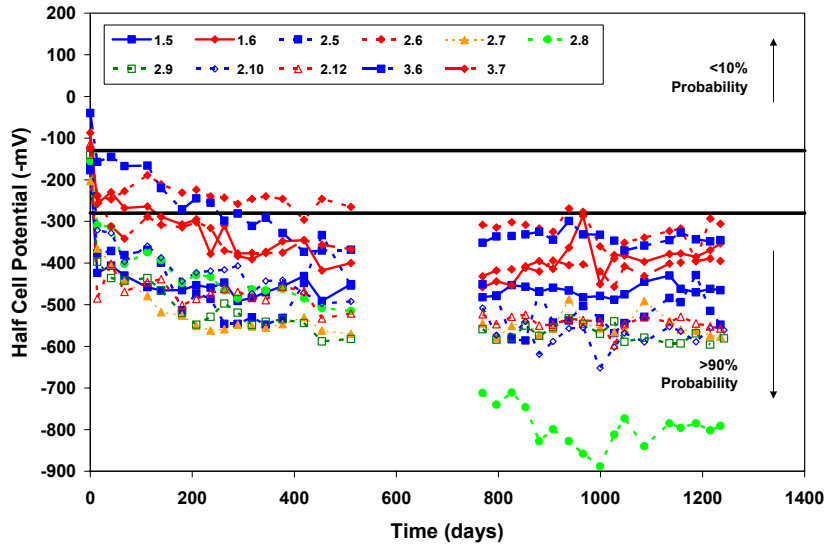
Figure B.41 Half-Cell Potential Readings for All Phase II Beams
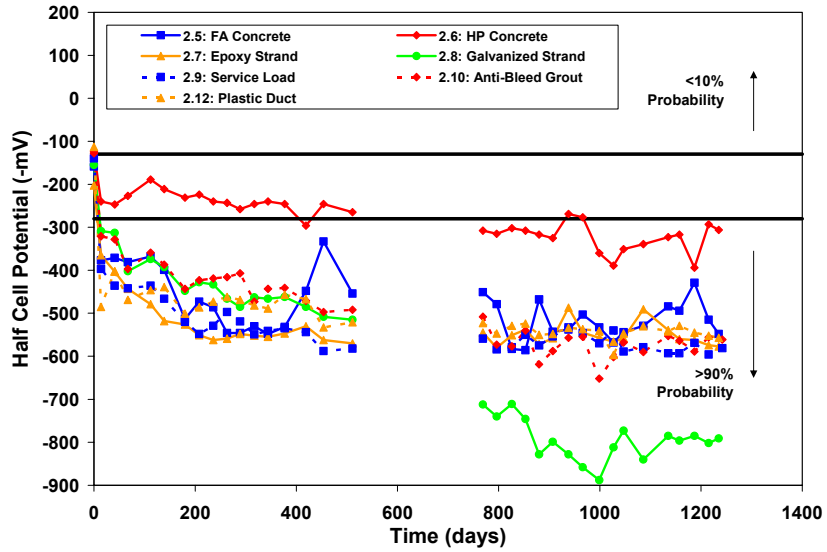
Figure B.42 Half-Cell Potential Readings for All 2/3 PS Phase II Beams
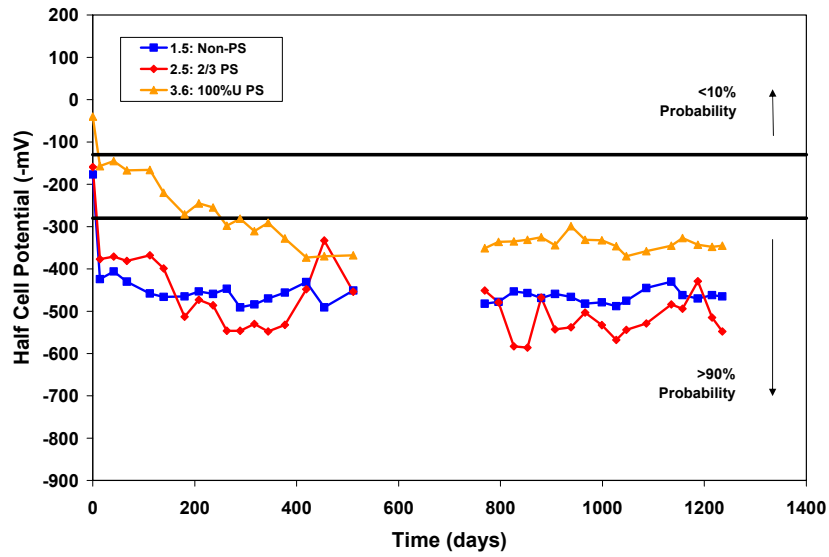
Figure B.43 Half-Cell Potential Readings for
All Fly Ash Concrete Phase II Beams
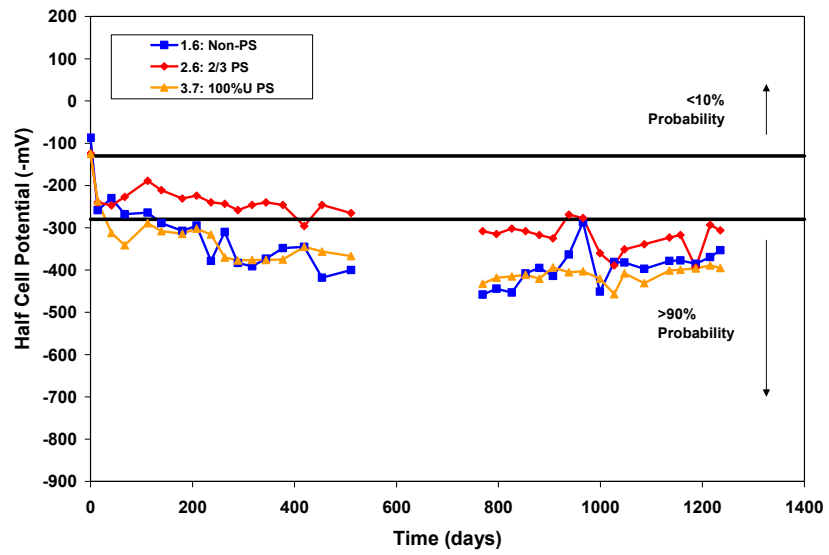
Figure B.44 Half-Cell Potential Readings for
All High Performance Concrete Phase II Beams

607
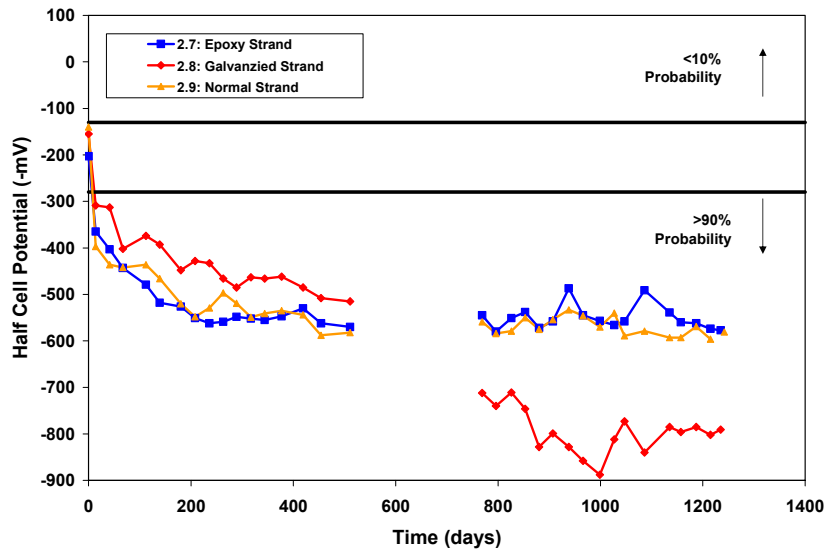
***Figure B.45 Half-Cell Potential Readings for
All Varying Strand Type Phase II Beams***
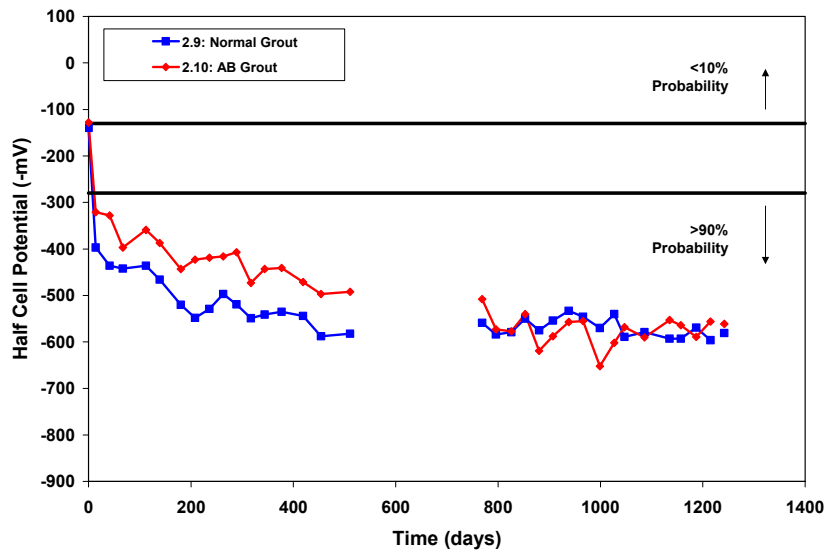
***Figure B.46 Half-Cell Potential Readings for
All Varying Grout Type Phase II Beams***

608
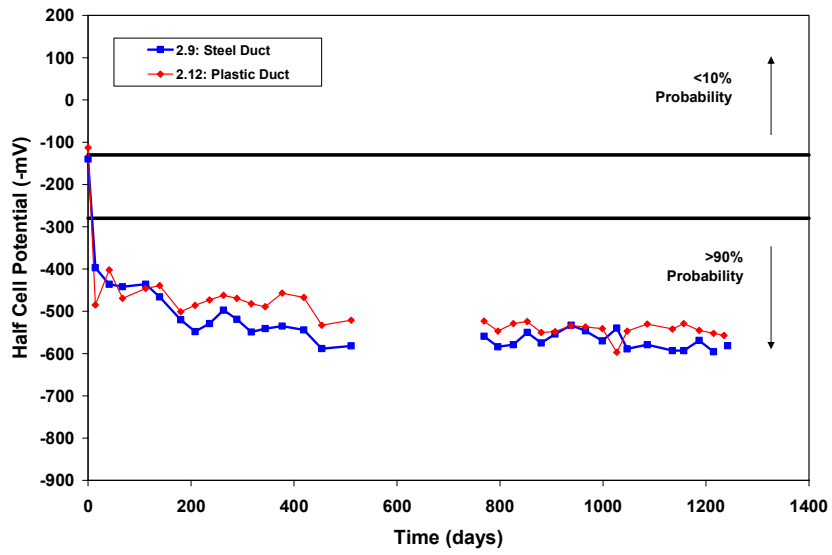
***Figure B.47 Half-Cell Potential Readings for
All Varying Duct Type Phase II Beams***

B.4 HALF-CELL POTENTIALS (CONTOUR MAPS)

1.1 - Unloaded (uncracked)

2.11 - Service (cracked)

1.2 - Service (cracked)

3.1 - Unloaded (uncracked)

1.3 - Service (cracked)

3.2 - Service (uncracked)

1.4 - Overload (cracked)

3.3 - Overload (cracked)

2.1 - Very Small Cracks

3.4 - Overload (cracked)

2.2 - Service (cracked)

3.5 - Overload (cracked)

2.3 - Service (cracked)

4.1 - Service (uncracked)

2.4 - Overload (cracked)

4.2 - Service (uncracked)

-430 to -580 V_{SCE}

-280 to -430 V_{SCE}

-130 to -280 V_{SCE}

$+20$ to -130 V_{SCE}

Figure B.48 Contour Maps of Half-Cell Potential Readings at 498 Days[4.3]

610

B.5 HALF-CELL POTENTIALS (OUTLIERS)

Table B.1 Half-Cell Outliers – Phase I Beams

Beam	Day of Reading	Initial Reading	Altered Reading
1.1	736	-269	-415
	1297	-199	-447
	1326	-171	-480
1.2	1297	-255	-550
	1326	-261	-560
	1445	-312	-550
2.2	212	-304	-537
3.1	778	-403	-172
3.2	1297	-205	-351
	1326	-173	-402
4.1	1546	-791	-541

Table B.2 Half-Cell Outliers – Phase II Beams

Beam	Day of Reading	Initial Reading	Altered Reading
2.8	938	-402	-828
	966	-389	-858
3.6	454	-262	-370
	1086	-515	-358
3.7	344	-470	-376

B.6   CORROSION RATE READINGS
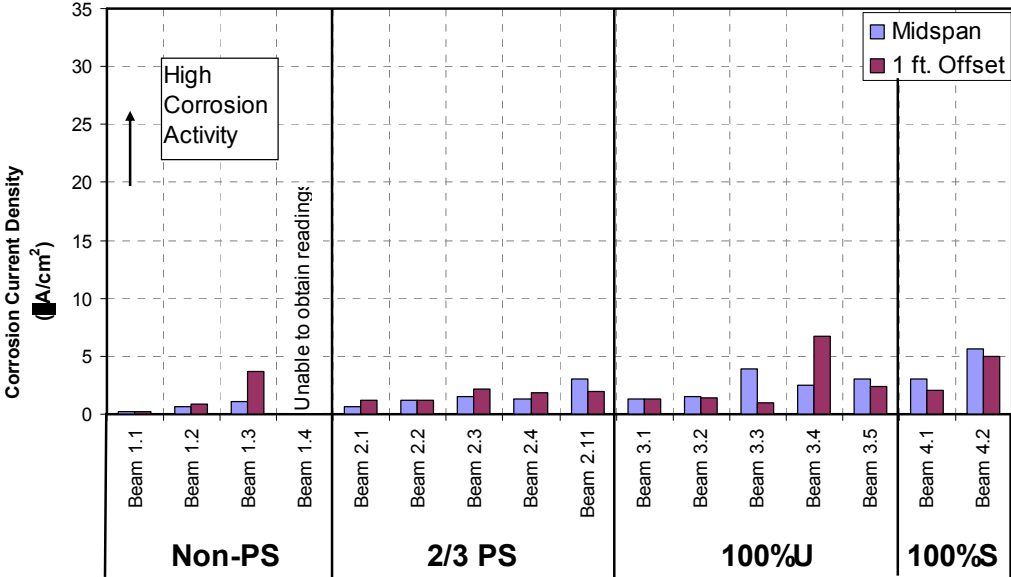
Figure B.49 Phase I Beams - Measured Corrosion Rates
(Seven Month Exposure Duration - PR Monitor Equipment)
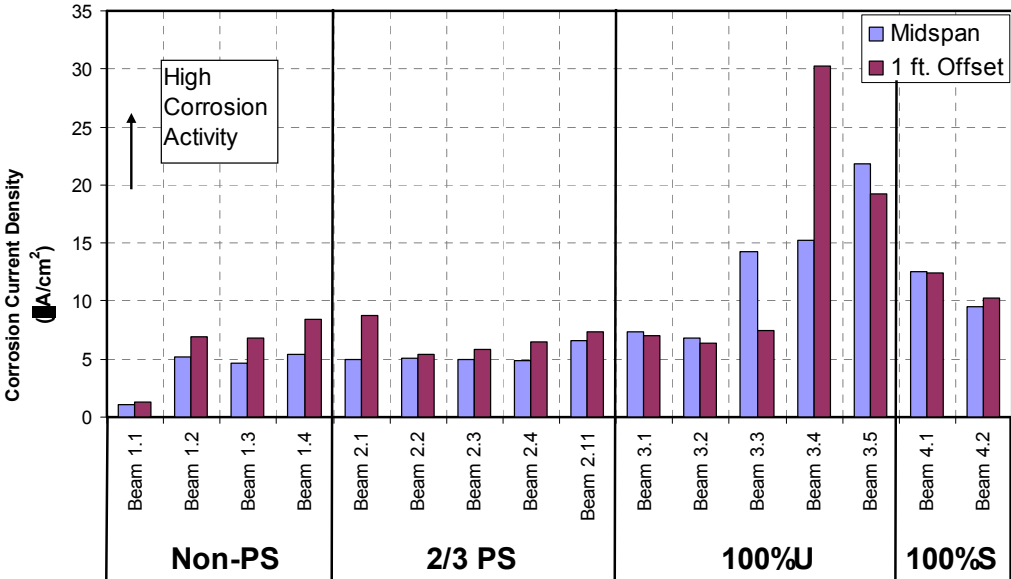
Figure B.50 Phase I Beams - Measured Corrosion Rates
(Twelve Month Exposure Duration – 3LP Equipment)
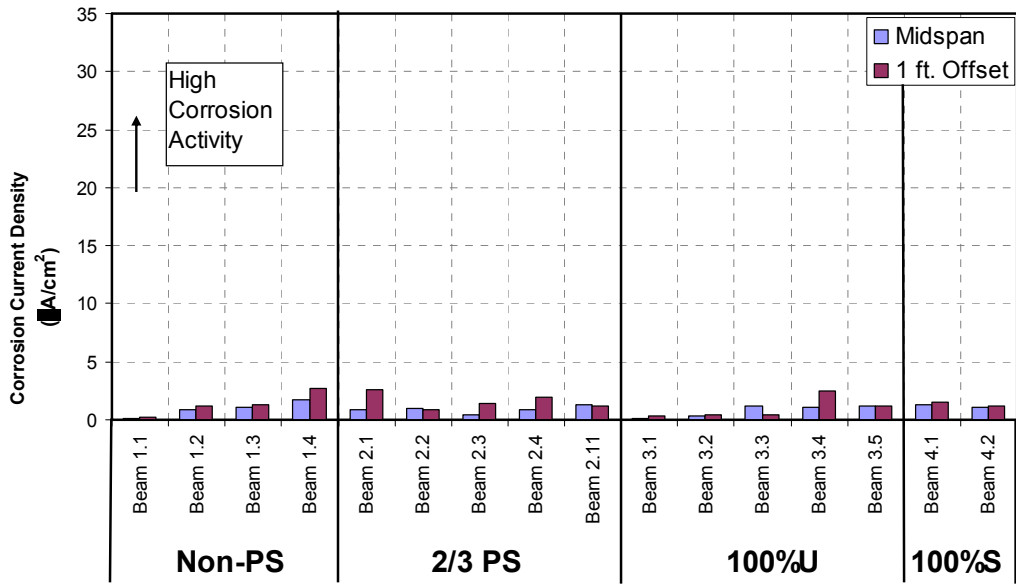
***Figure B.51 Phase I Beams - Measured Corrosion Rates
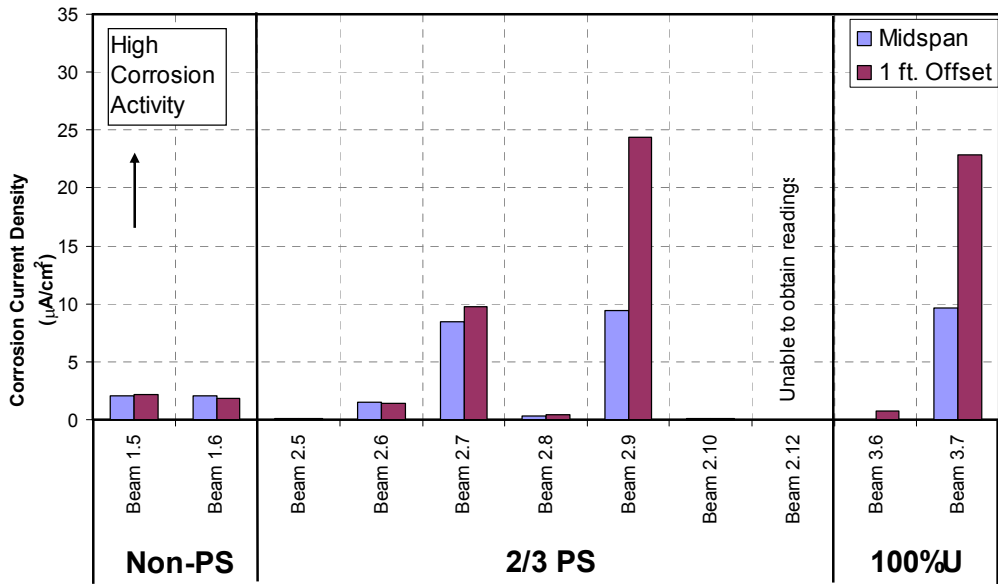(Fifteen Month Exposure Duration - PR Monitor Equipment)***
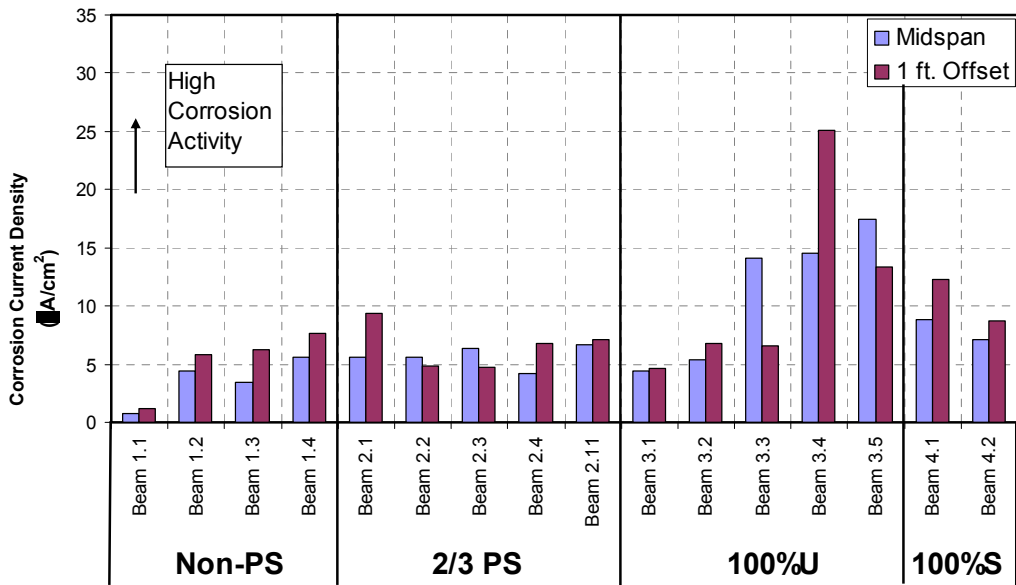
***Figure B.52 Phase I Beams - Measured Corrosion Rates
(Fifteen Month Exposure Duration – 3LP Equipment)***

613
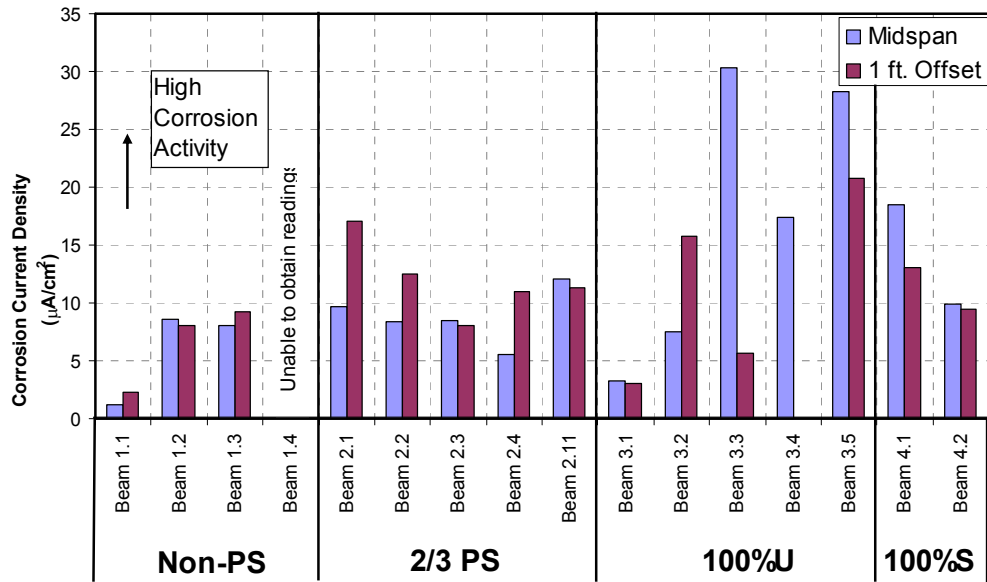
Figure B.53 Phase I Beams - Measured Corrosion Rates
(47 Month Exposure Duration – 3LP Equipment)

Figure B.54 Phase II Beams - Measured Corrosion Rates
(35 Month Exposure Duration – 3LP Equipment)

614

B.7   BLOCK CHLORIDE PENETRATION GRAPHS

**Acid Soluble Chloride Content
(% by weight of concrete)**
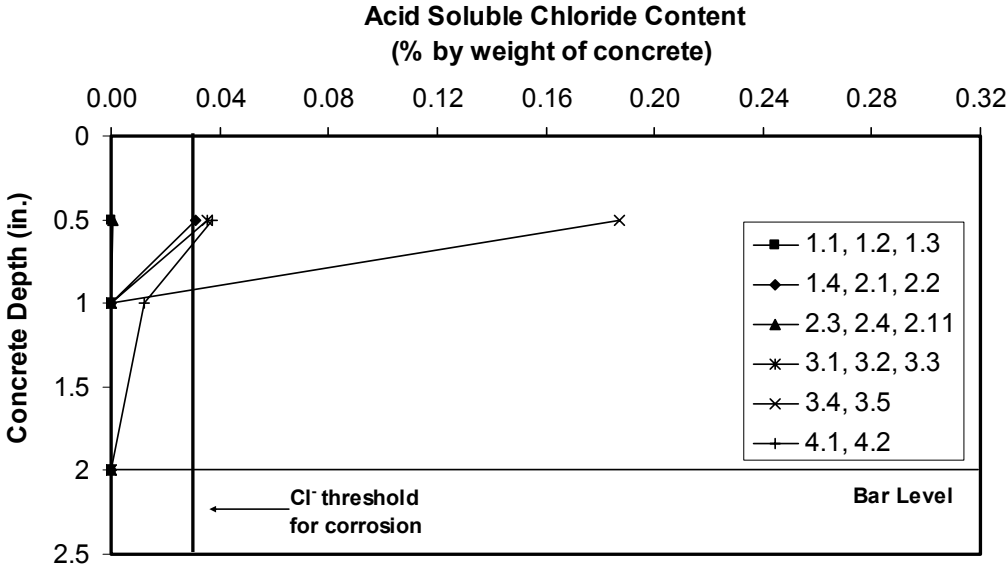
***Figure B.55 Block Chloride Penetration at 7 Months
(Phase I Ponded Block Specimens)***

**Acid Soluble Chloride Content
(% by weight of concrete)**
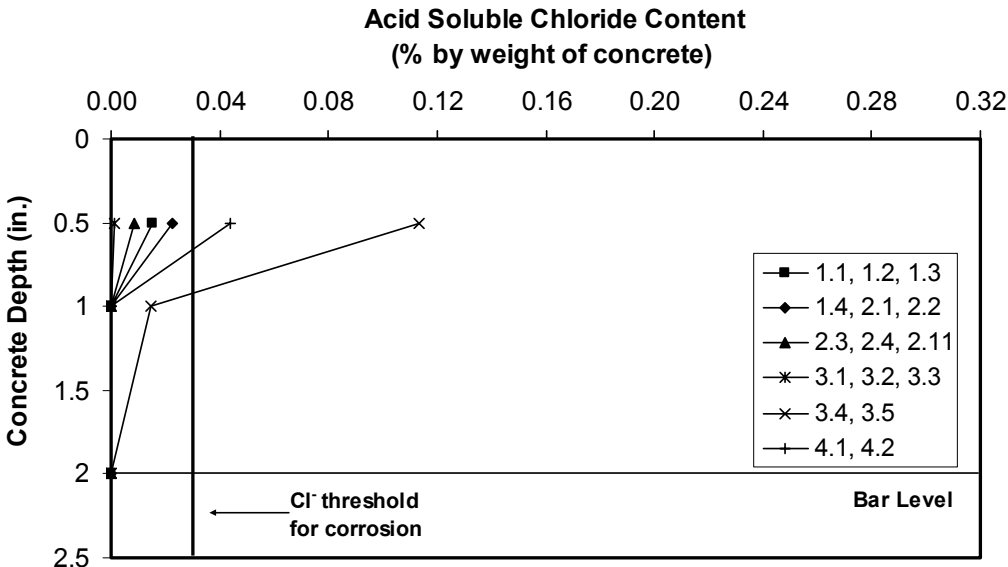
***Figure B.56 Block Chloride Penetration at 14 Months
(Phase I Ponded Block Specimens)***

615
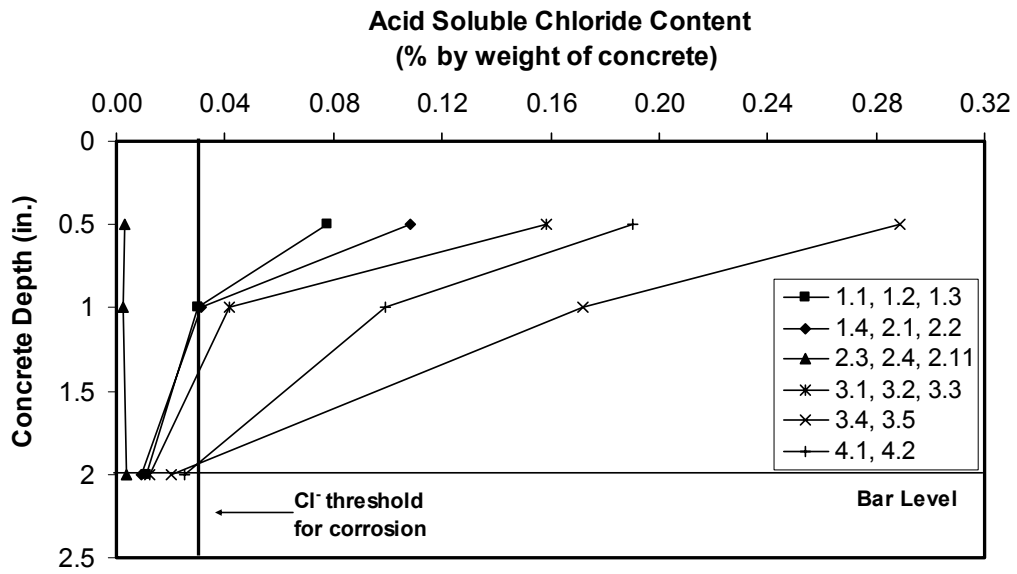
Figure B.57 Block Chloride Penetration at 41 Months
(Phase I Ponded Block Specimens)
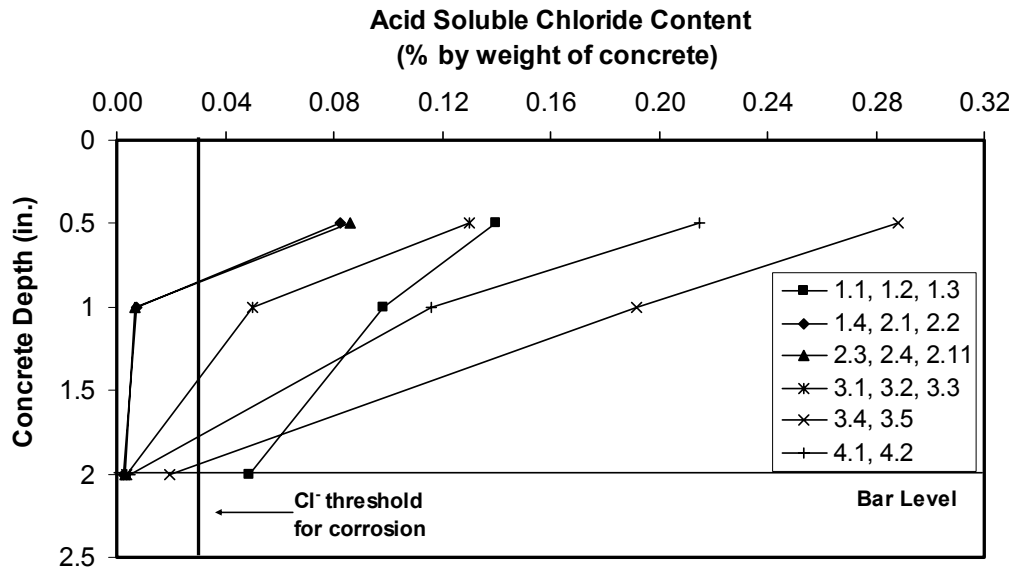
Figure B.58 Block Chloride Penetration at 54 Months

(Phase I Ponded Block Specimens)

616
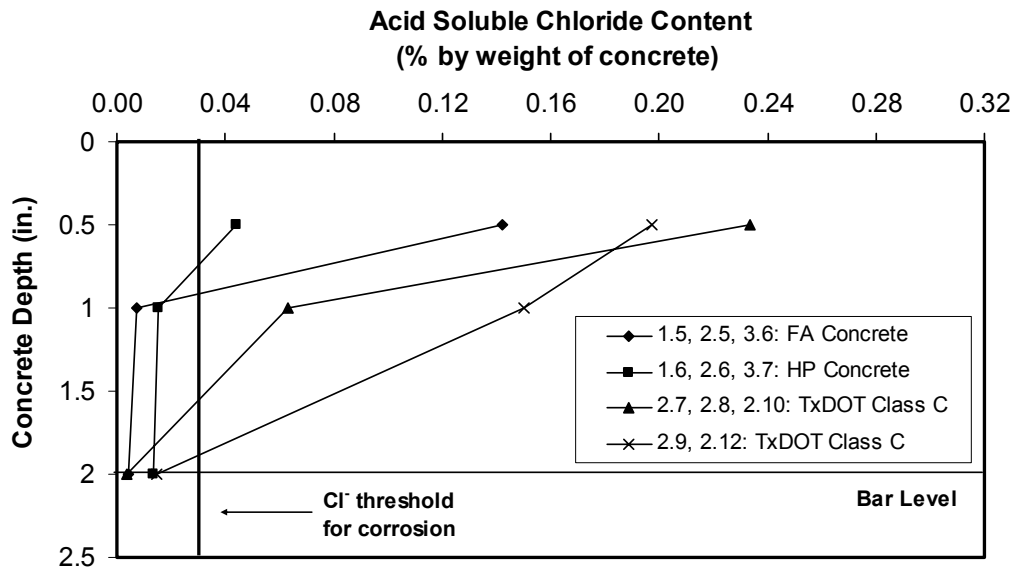
Figure B.59 Block Chloride Penetration at 29 Months
(Phase II Ponded Block Specimens)
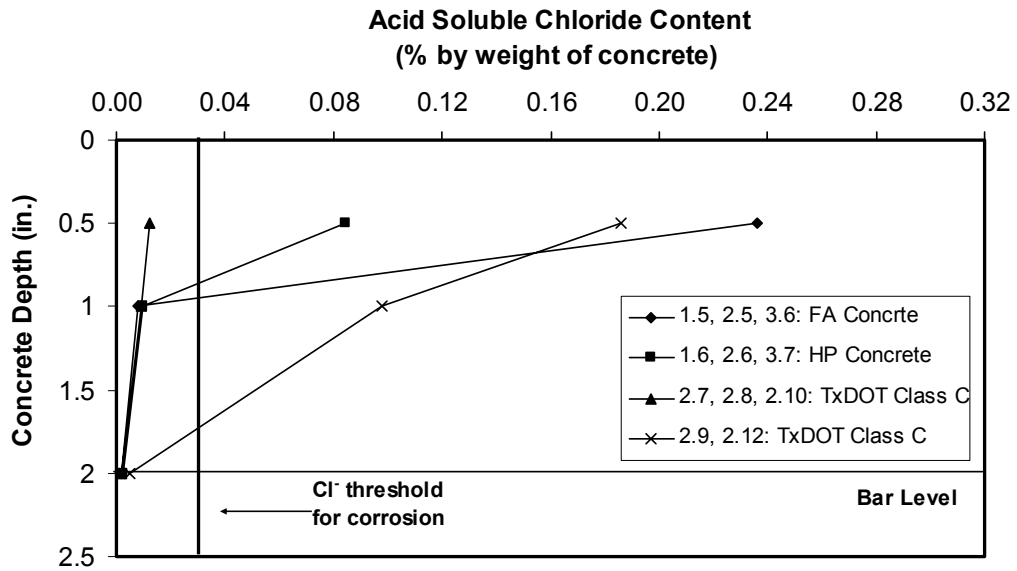
Figure B.60 Block Chloride Penetration at 42 Months
(Phase II Ponded Block Specimens)
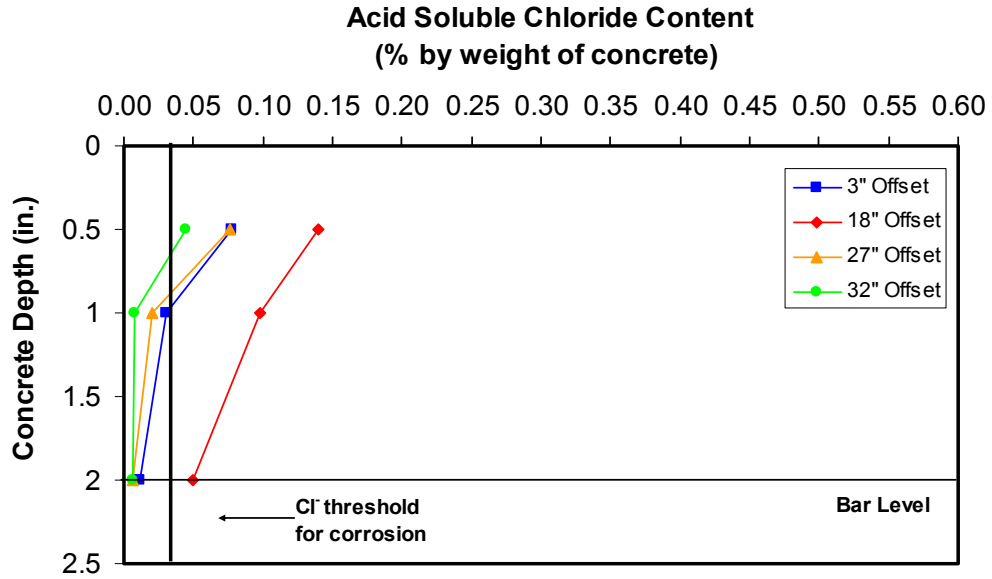
617

B.8 BEAM CHLORIDE PENETRATION GRAPHS

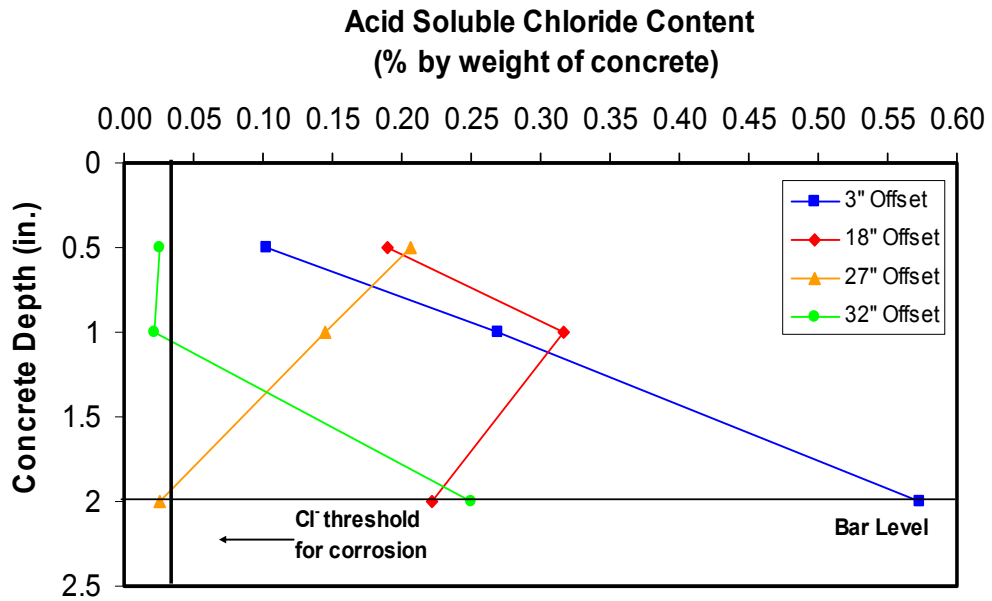*Figure B.61 Chloride Penetration at 54 Months – Beam 1.1*

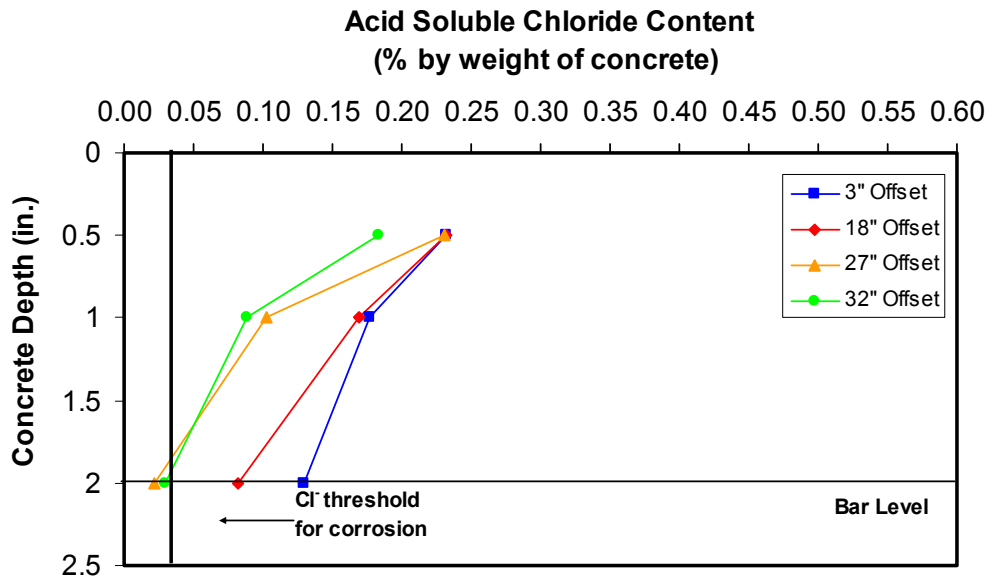*Figure B.62 Chloride Penetration at 54 Months – Beam 1.3*

618
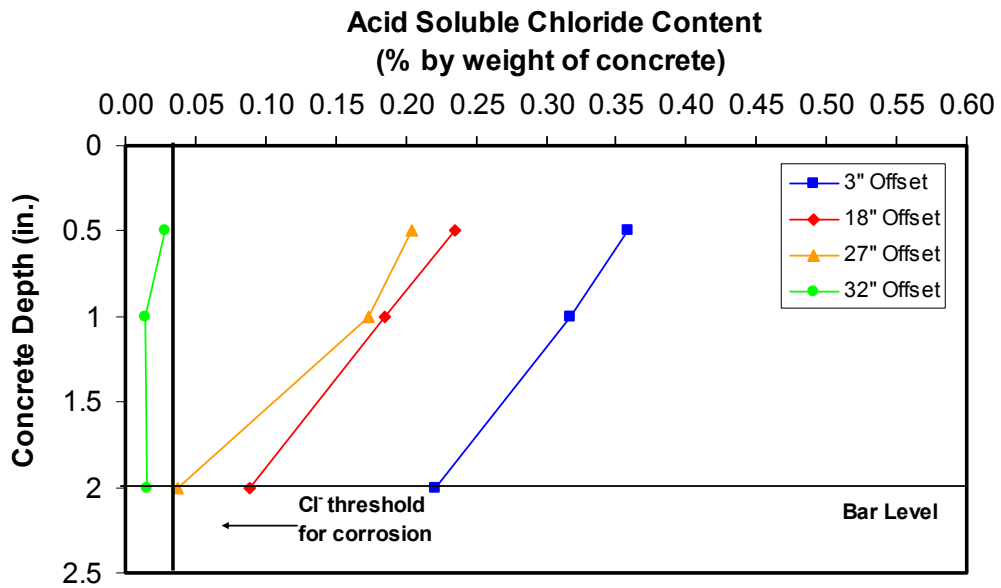
Figure B.63 Chloride Penetration at 54 Months – Beam 2.3

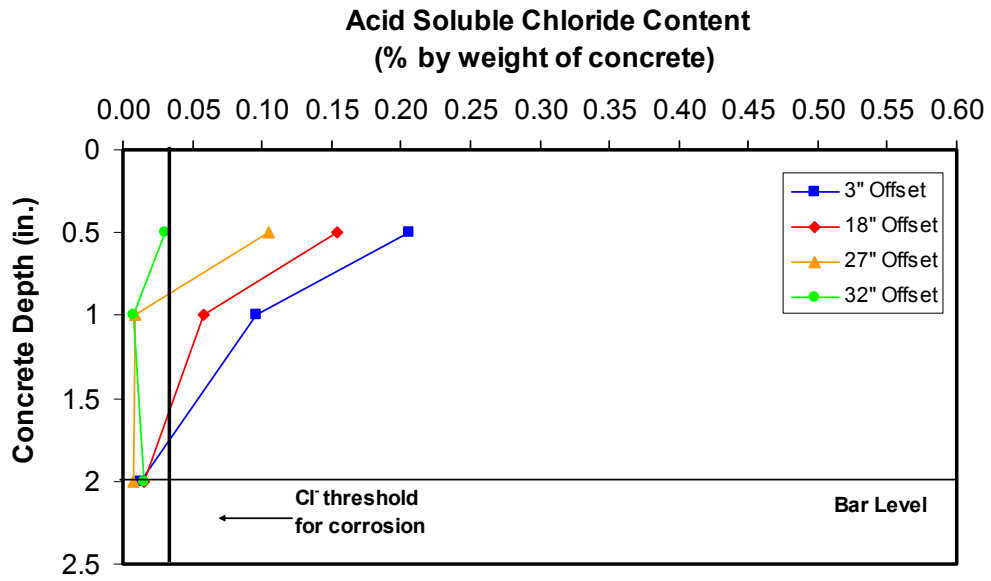**Figure B.64 Chloride Penetration at 54 Months – Beam 2.11**

Figure B.65 Chloride Penetration at 54 Months – Beam 3.1
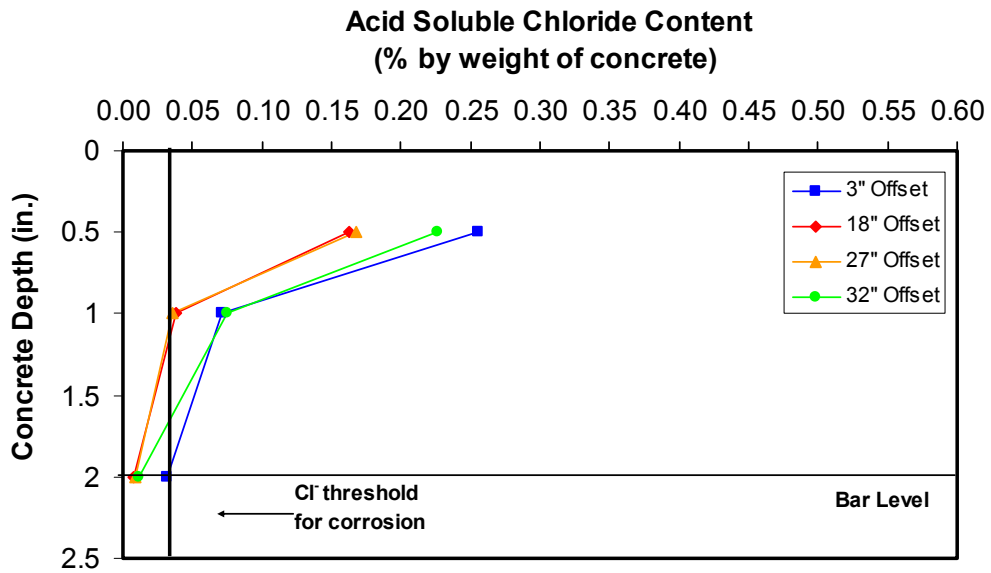

Figure B.66 Chloride Penetration at 54 Months – Beam 3.2
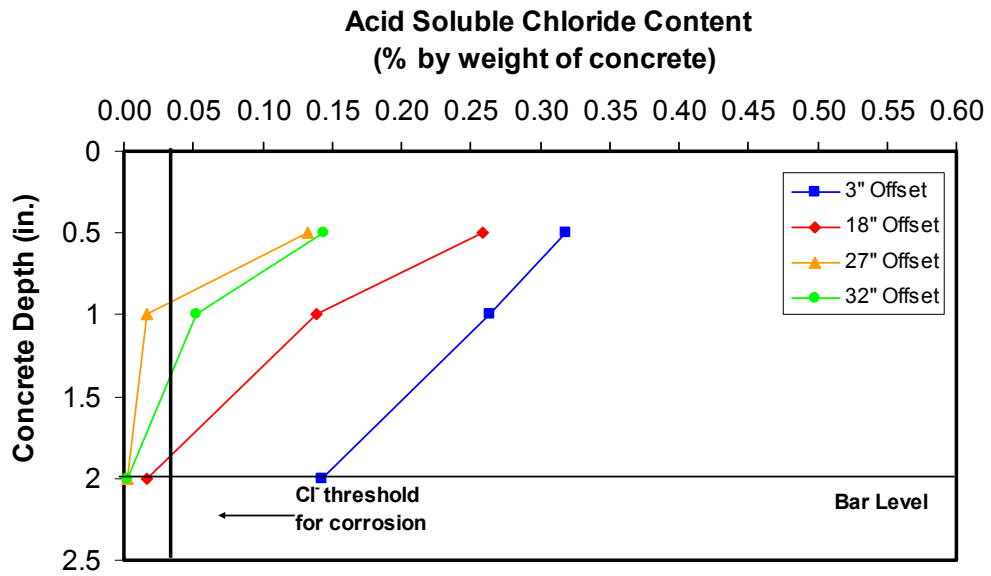
Figure B.67 Chloride Penetration at 54 Months – Beam 3.3
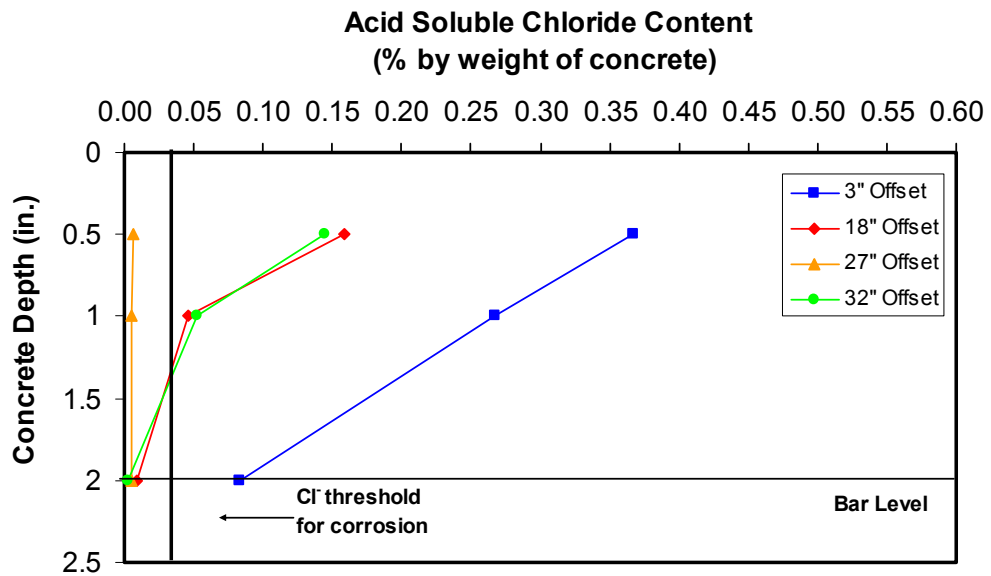

Figure B.68 Chloride Penetration at 54 Months – Beam 4.2

621

Figure B.69 Chloride Penetration at 42 Months – Beam 1.5

Figure B.70 Chloride Penetration at 42 Months – Beam 1.6

622
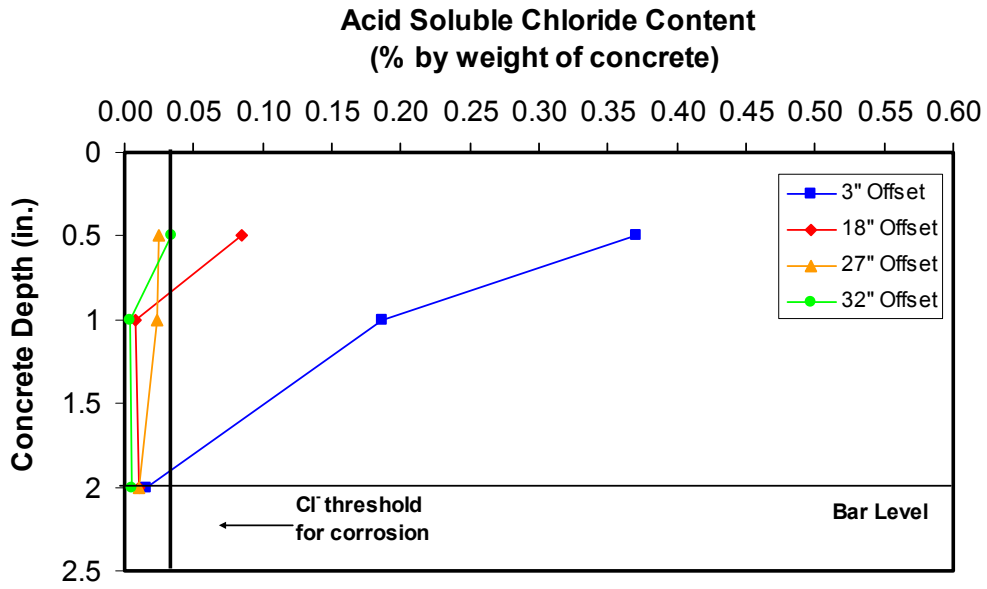
Figure B.71 Chloride Penetration at 42 Months – Beam 2.5

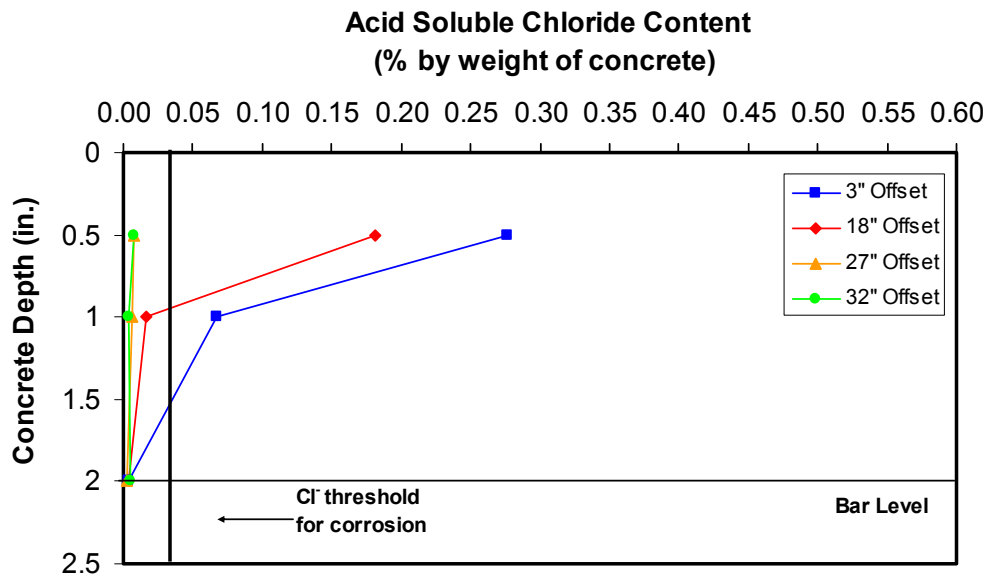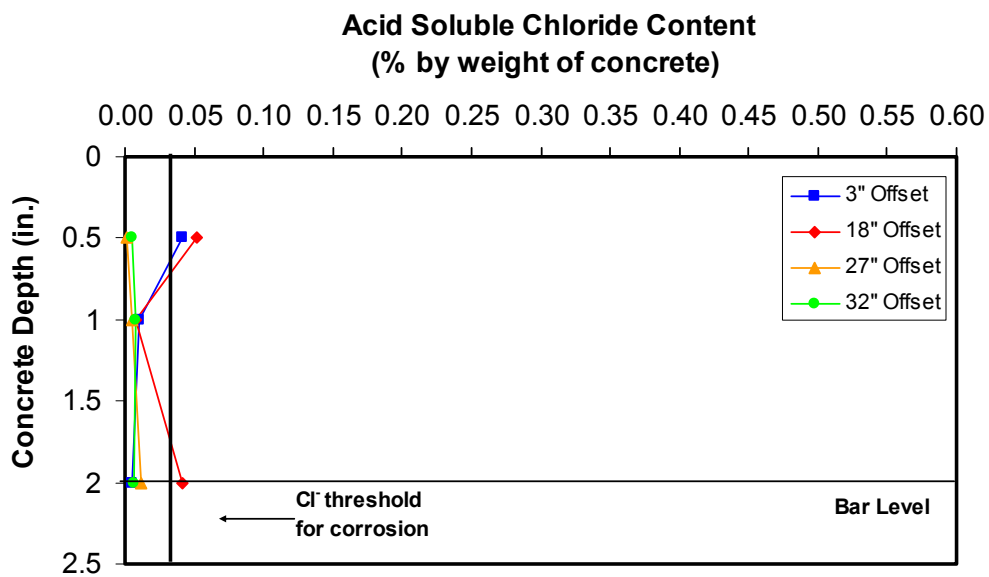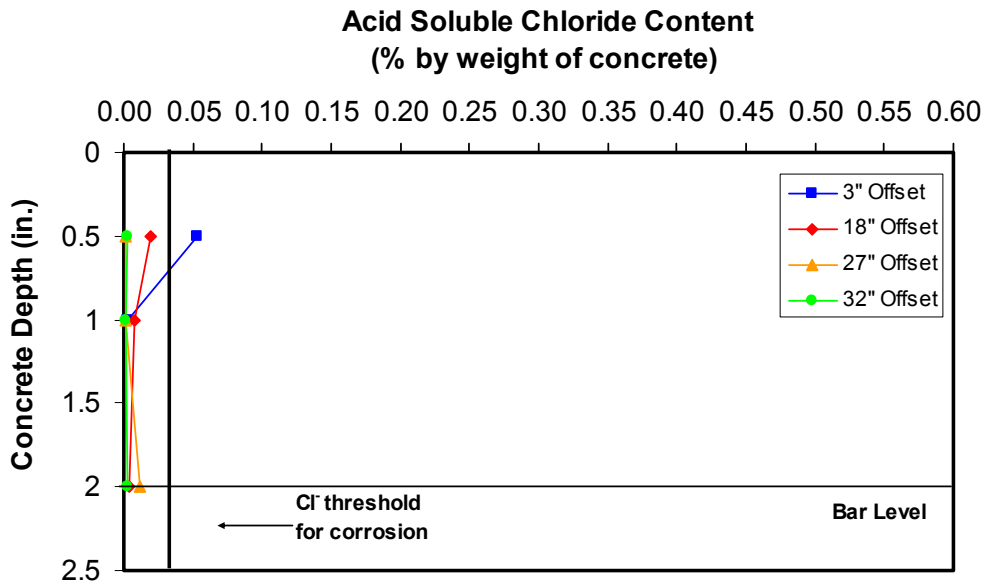
Figure B.72 Chloride Penetration at 42 Months – Beam 2.6
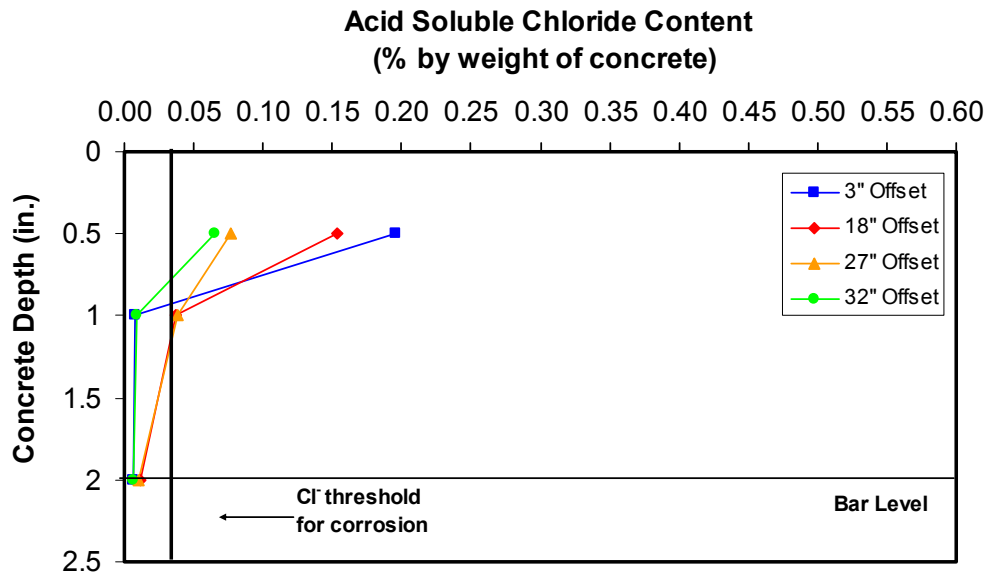
Figure B.73 Chloride Penetration at 42 Months – Beam 3.6
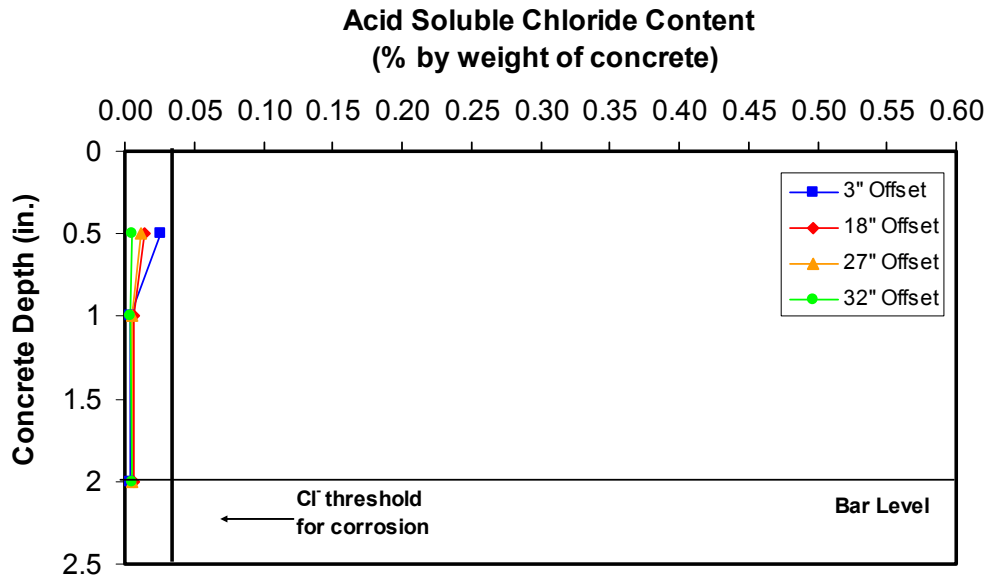
Figure B.74 Chloride Penetration at 42 Months – Beam 3.7

624

Appendix C
Column Corrosion Tests
Supplementary Material

C.1 HALF-CELL POTENTIAL PLOTS

The following Half-Cell potential plots complement those contained in Figure 5.22 through Figure 5.25. "All" Half-Cell Potential Readings are followed by "Average" Half-Cell Potential readings.
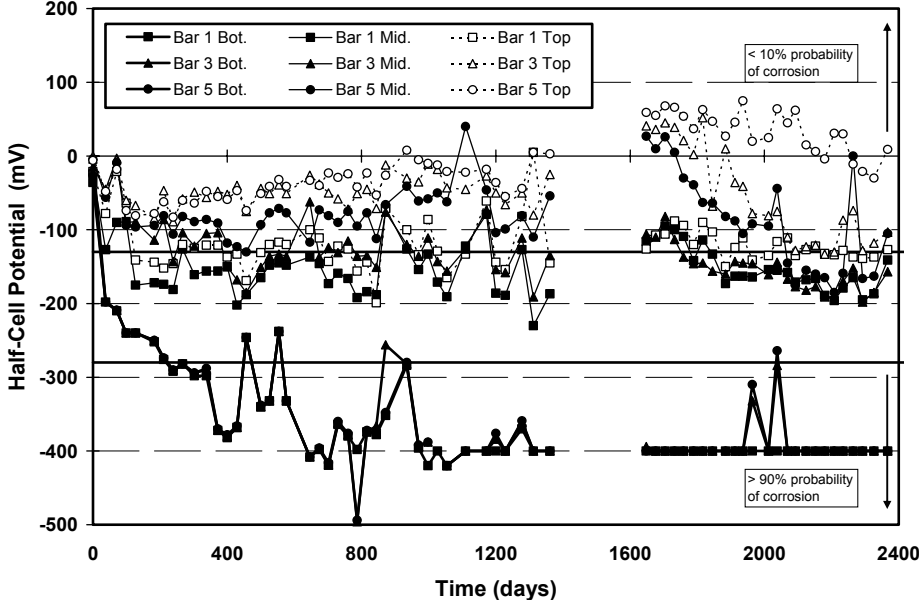
Figure C.1 All Half-Cell Potential Readings for Column NJ-TC-S

Figure C.2 All Half-Cell Potential Readings for Column DJ-TC-S

Figure C.3 All Half-Cell Potential Readings for
Column PT-TC-S-PD – Rebar

626
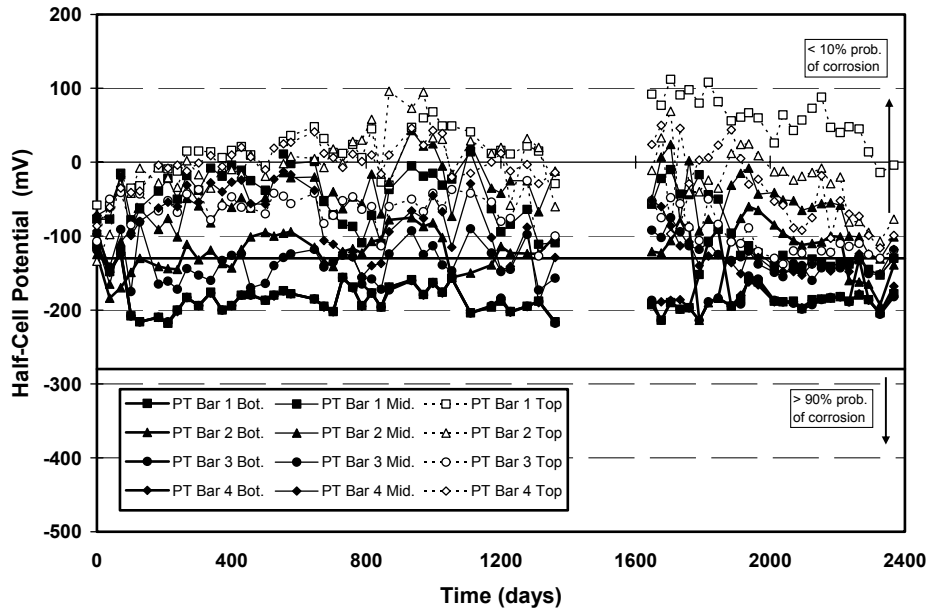
Figure C.4 All Half-Cell Potential Readings for
Column PT-TC-S-PD – PT Bars
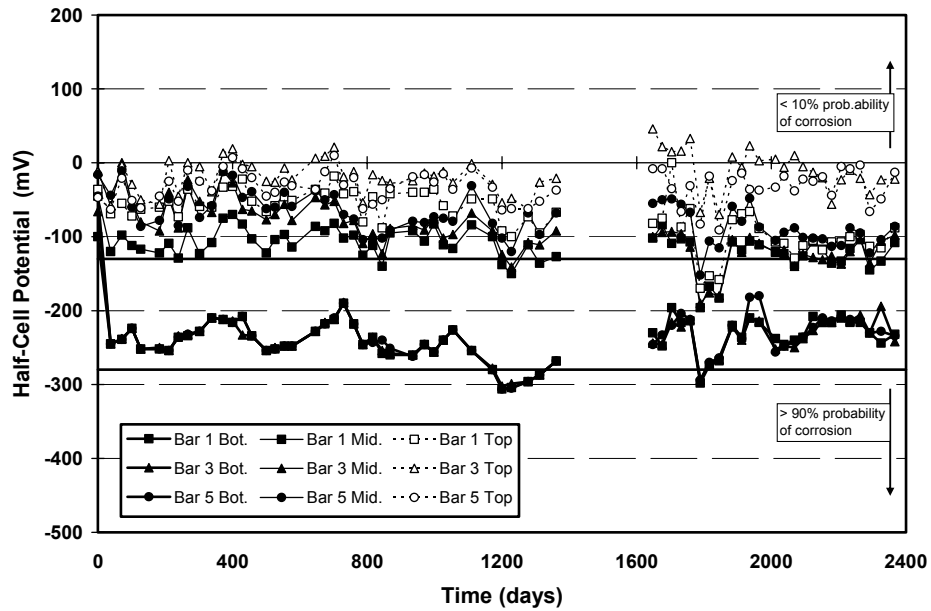
Figure C.5 All Half-Cell Potential Readings for
Column PT-FA-S-PD – Rebar

627
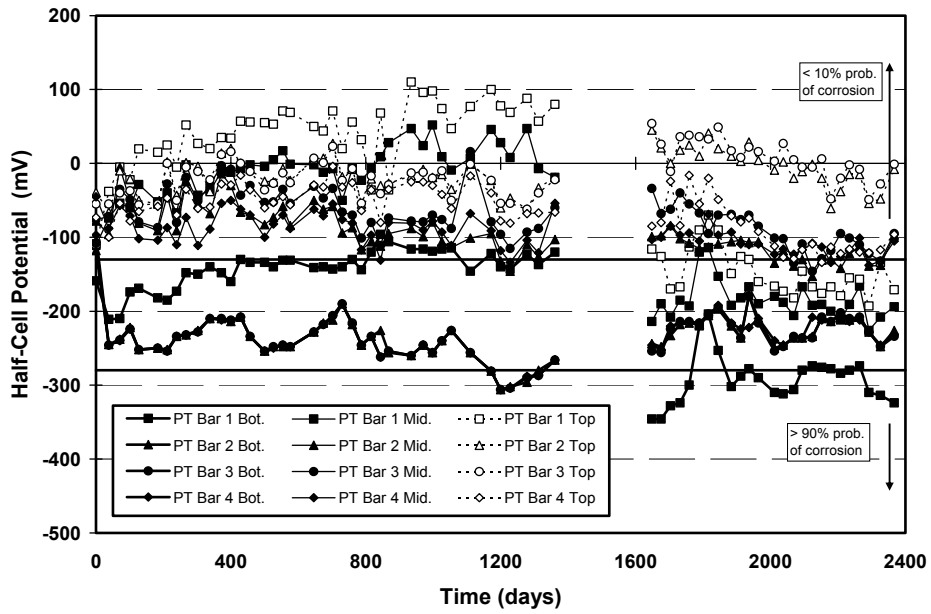
Figure C.6 All Half-Cell Potential Readings for
Column PT-FA-S-PD – PT Bars
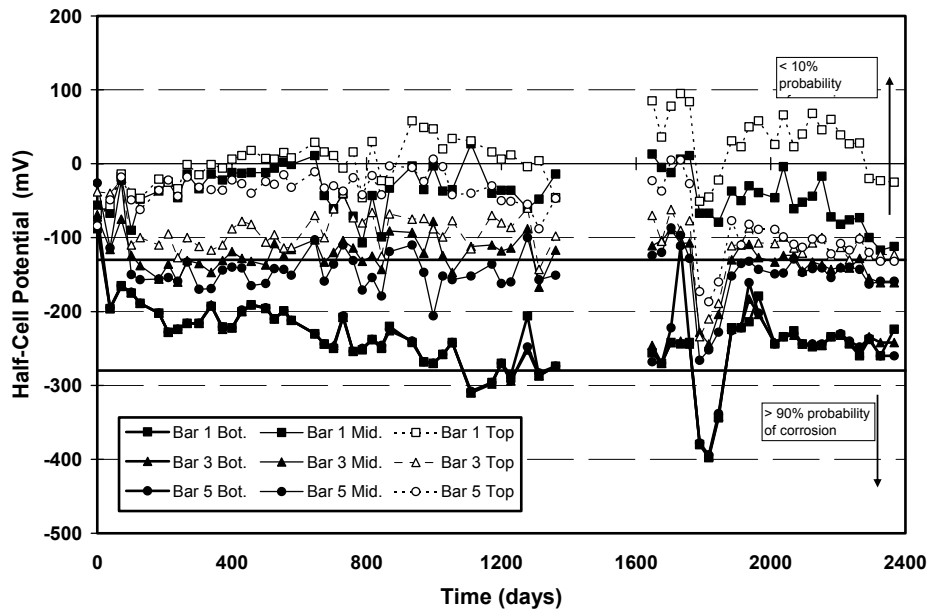
Figure C.7 All Half-Cell Potential Readings for
Column PT-TC-S-EB – Rebar
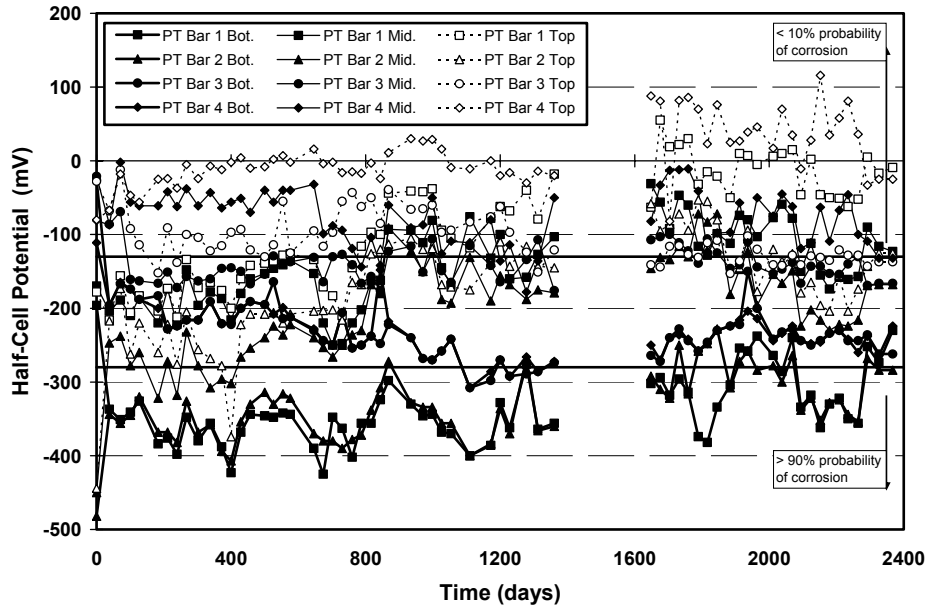
Figure C.8 All Half-Cell Potential Readings for
Column PT-TC-S-EB – PT Bars
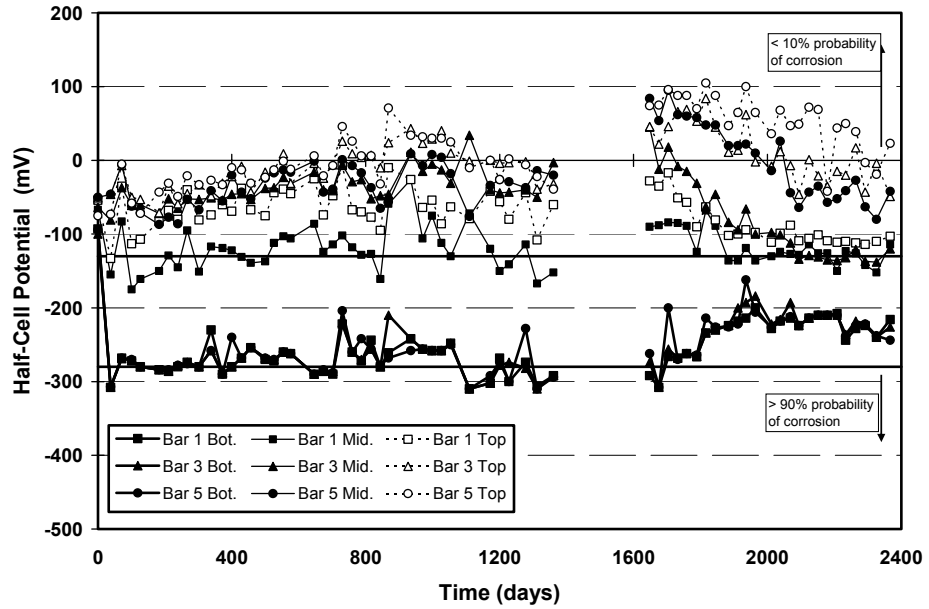
Figure C.9 All Half-Cell Potential Readings for
Column PT-TC-S-GB – Rebar

629
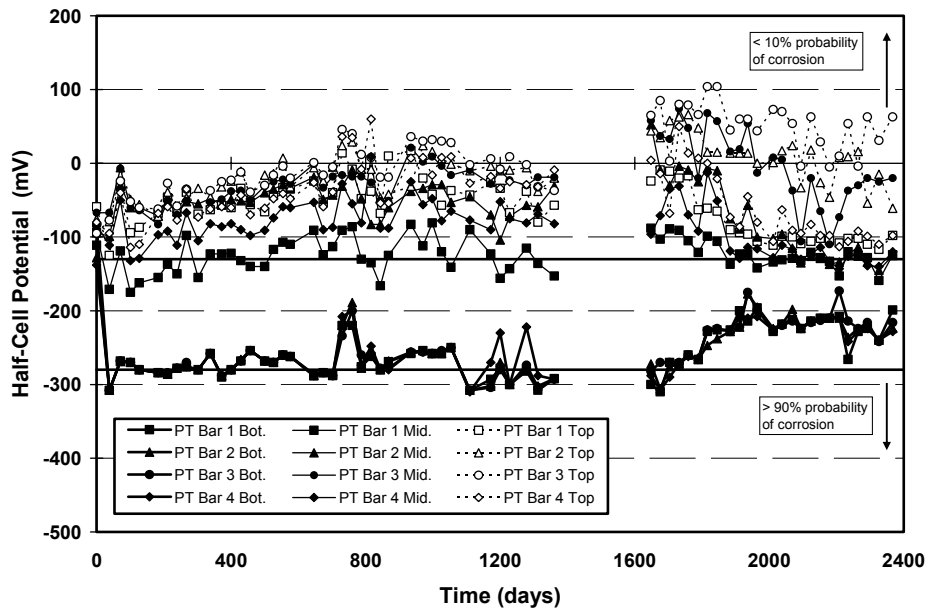
Figure C.10 All Half-Cell Potential Readings for
Column PT-TC-S-GB – PT Bars
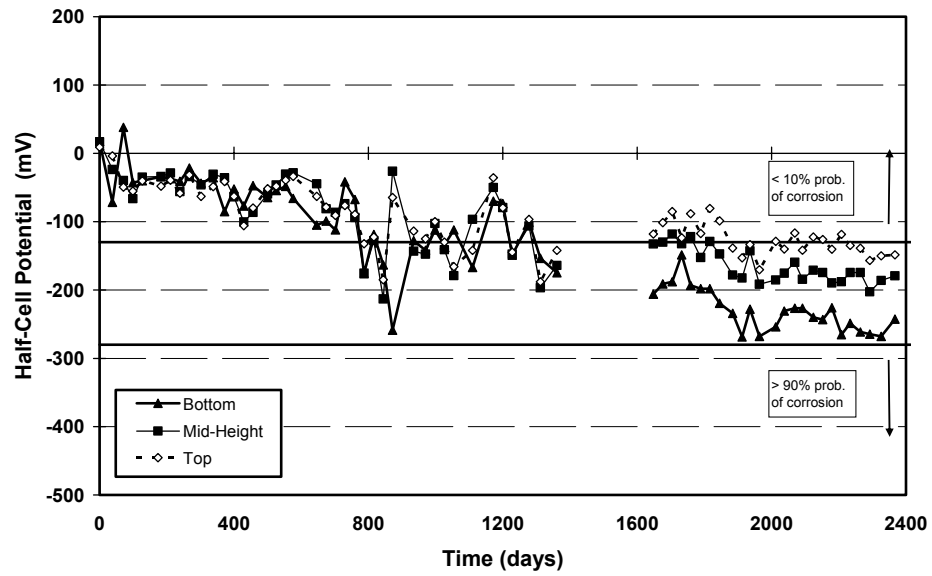
Figure C.11 Average Half-Cell Potential Readings for Column NJ-TC-N

630
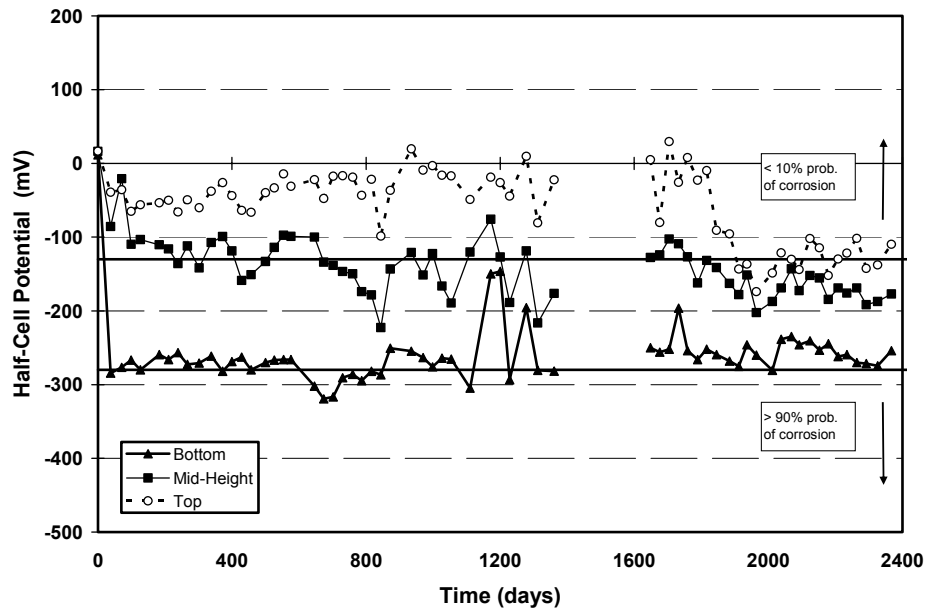
Figure C.12 Average Half-Cell Potential Readings for Column DJ-TC-N
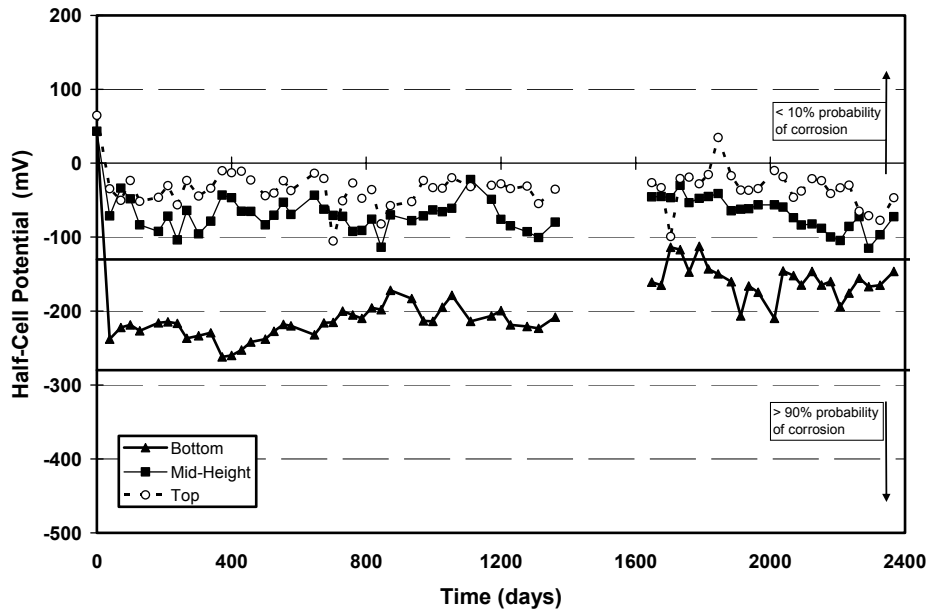
Figure C.13 Average Half-Cell Potential Readings for Column DJ-FA-S

631
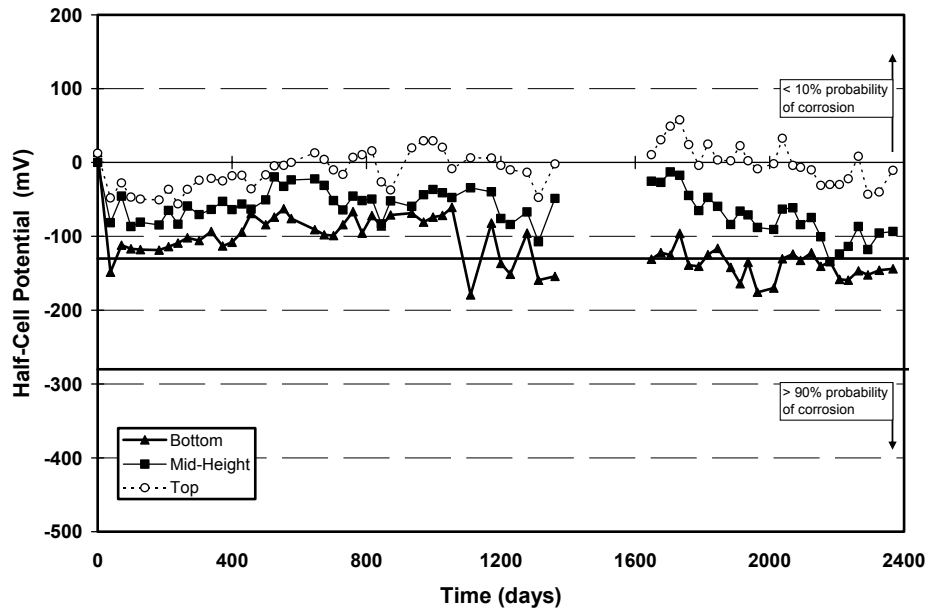
Figure C.14 Average Half-Cell Potential Readings for Column DJ-TC-S
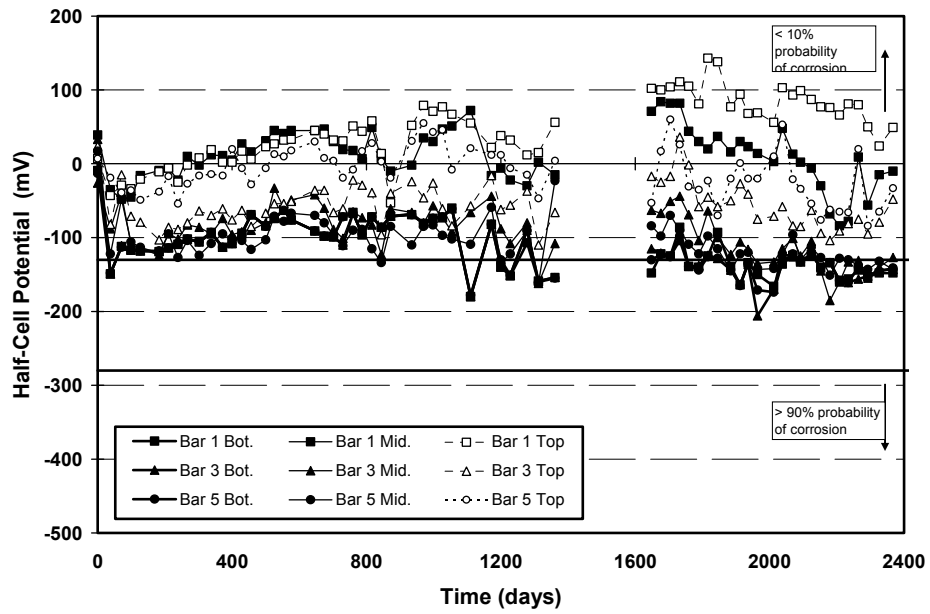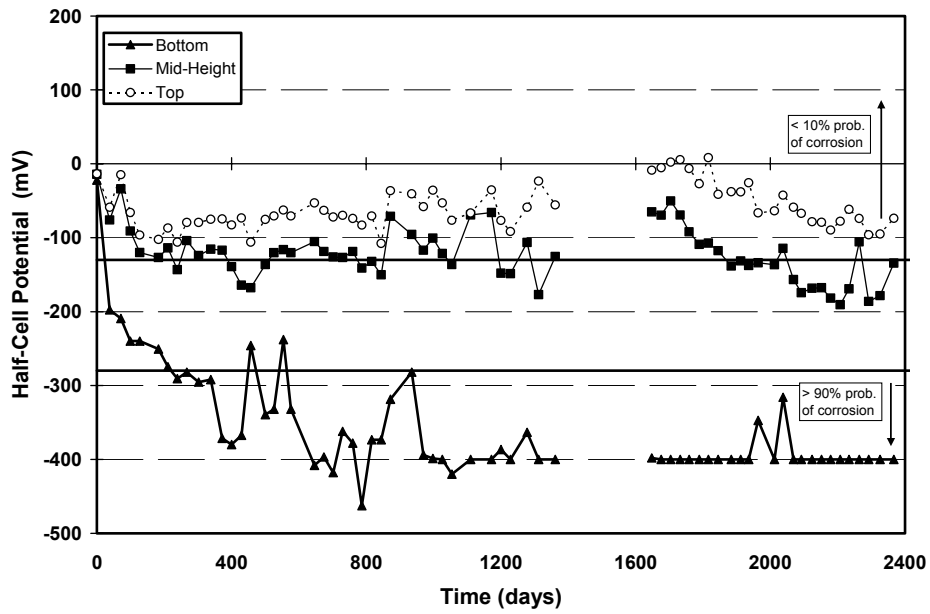

Figure C.15 Average Half-Cell Potential Readings for Column NJ-TC-S
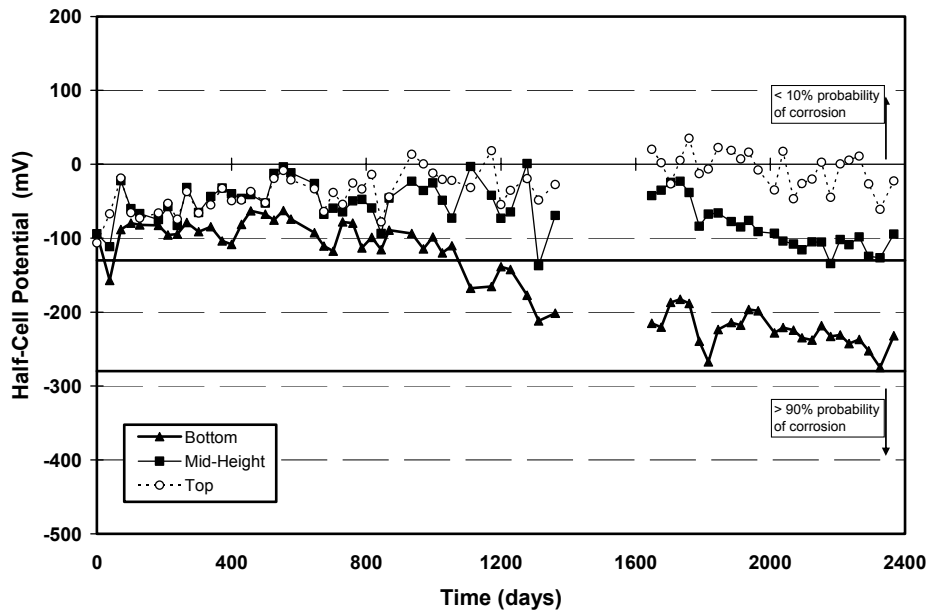
632
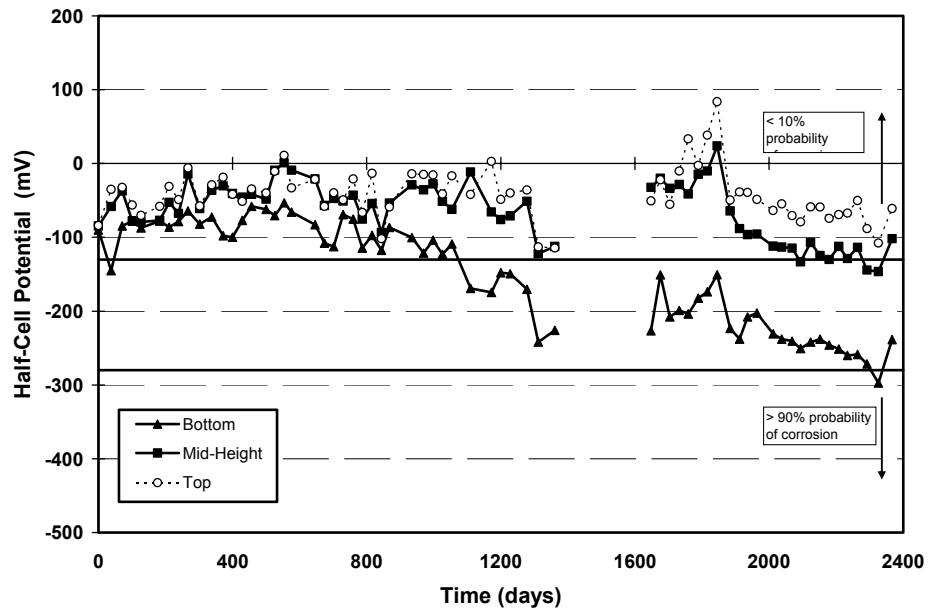
Figure C.16 Average Half-Cell Potential Readings for
Column PT-TC-N-PD – Rebar
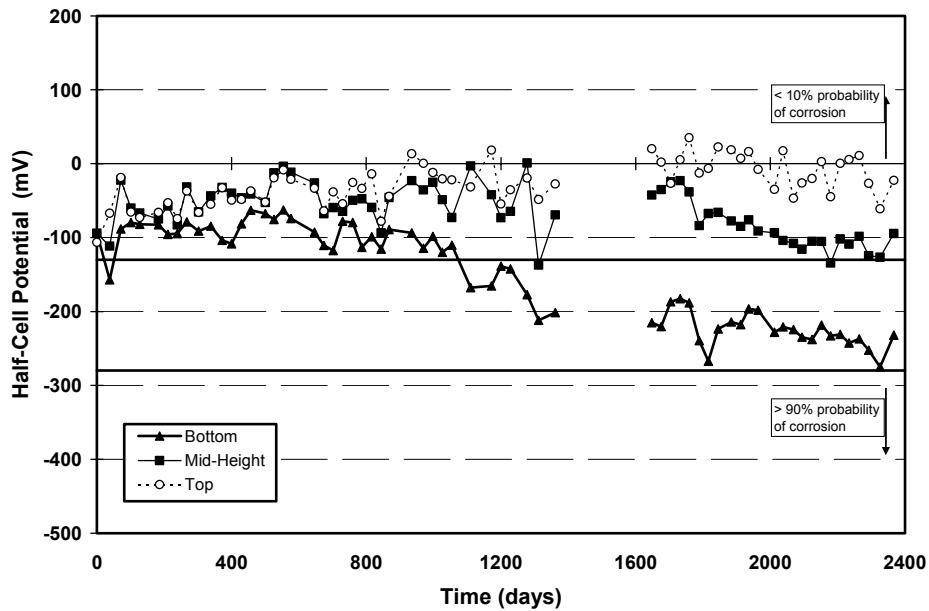
Figure C.17 Average Half-Cell Potential Readings for
Column PT-TC-N-PD – PT Bars

C.2 Concrete Chloride Content Plots

The following Acid-Soluble Chloride Content Plots complement those contained in Figure 5.36 through Figure 5.45. Chloride Threshold value is indicated in the figures at 0.033%. This value, intended only as a guide, is based on the widely accepted chloride threshold value of 0.2% of the weight of cement.[5.5]
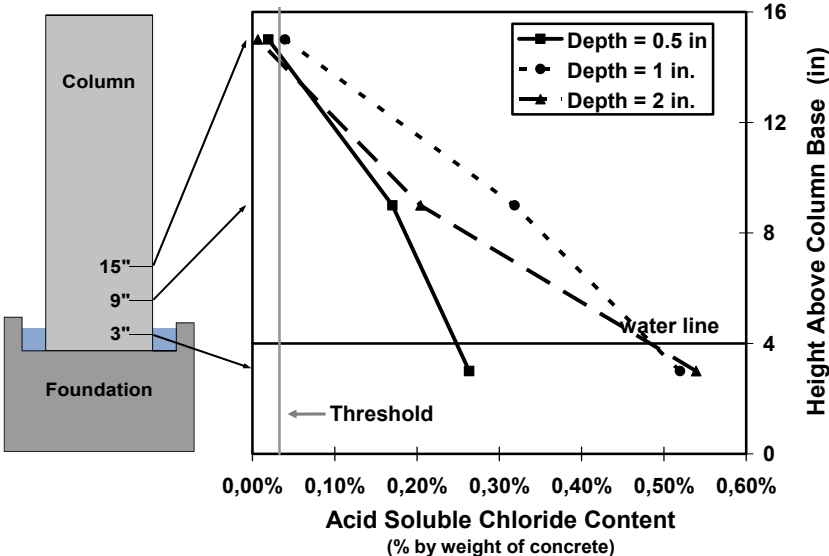
***Figure C.18 Concrete Chloride Penetration for Column DJ-TC-N
in Non-Dripper Side at End of Testing***
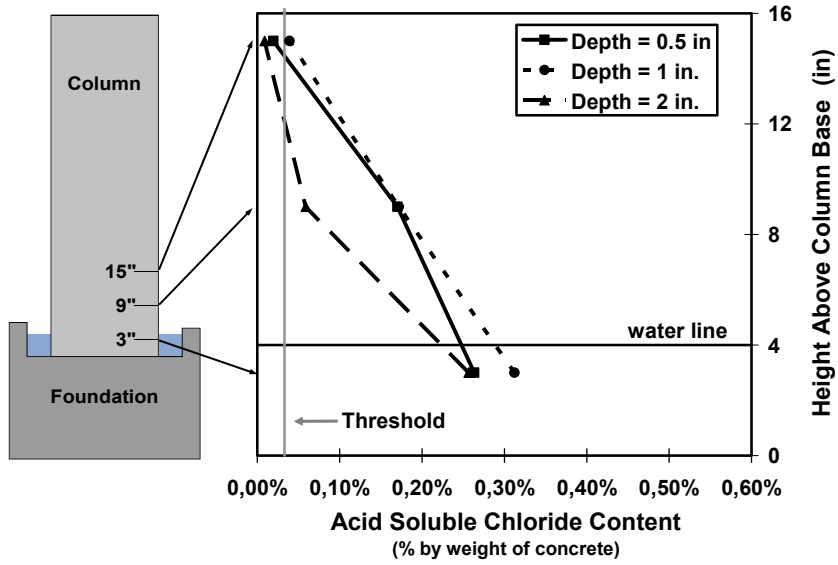
*Figure C.19 Concrete Chloride Penetration for Column DJ-TC-N
in Dripper Side at End of Testing*
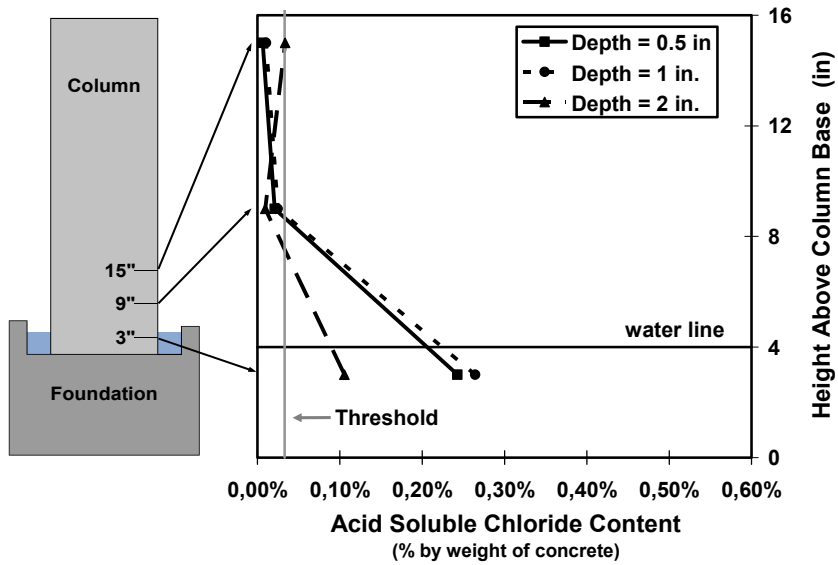
*Figure C.20 Concrete Chloride Penetration for Column DJ-FA-S
in Non-Dripper Side at End of Testing*

635
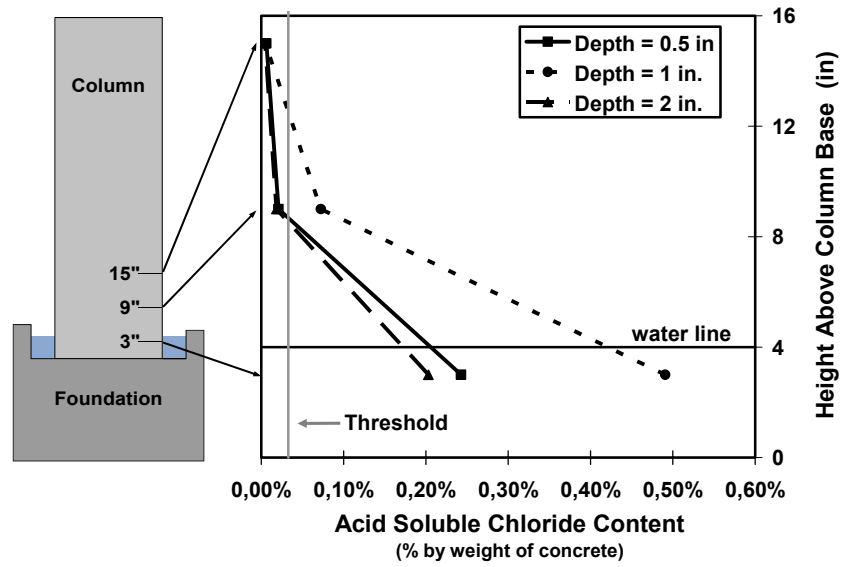
Figure C.21 Concrete Chloride Penetration for Column DJ-FA-S in Dripper Side at End of Testing
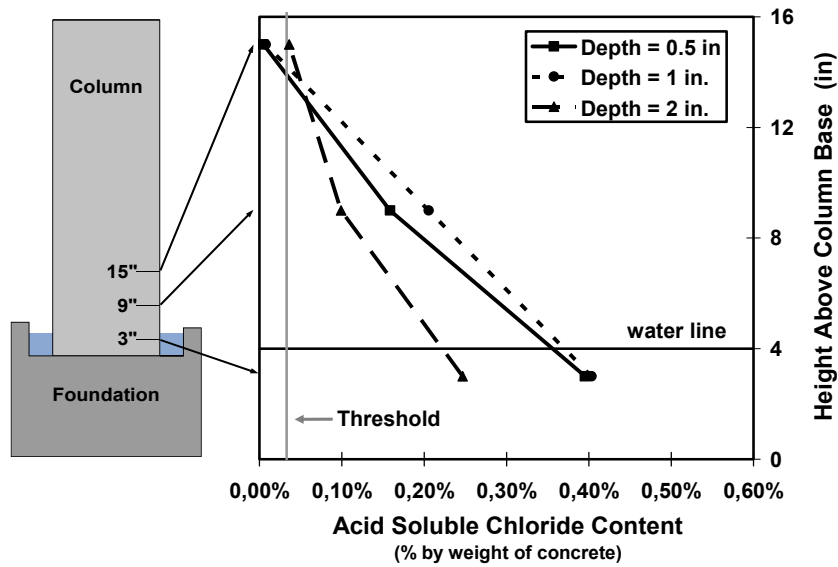
Figure C.22 Concrete Chloride Penetration for Column DJ-TC-S in Non-Dripper Side at End of Testing

636
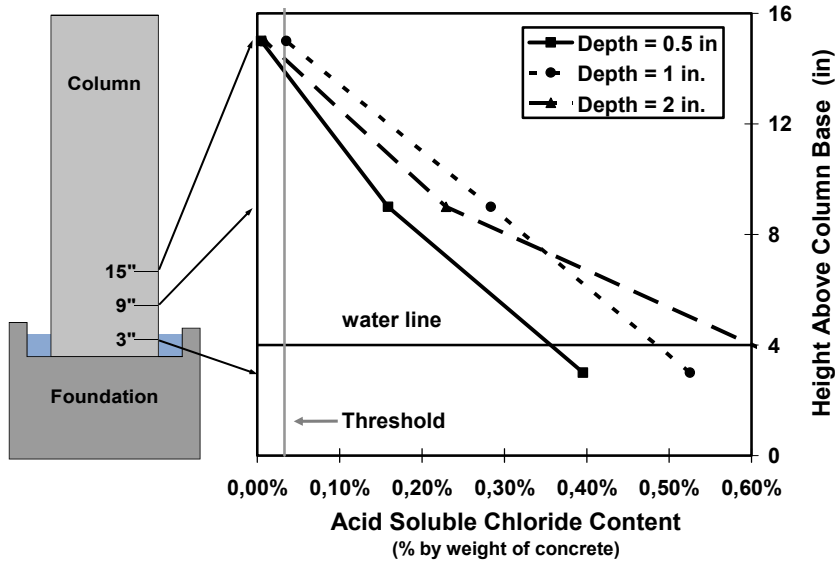
Figure C.23 Concrete Chloride Penetration for Column DJ-TC-S in Dripper Side at End of Testing

.
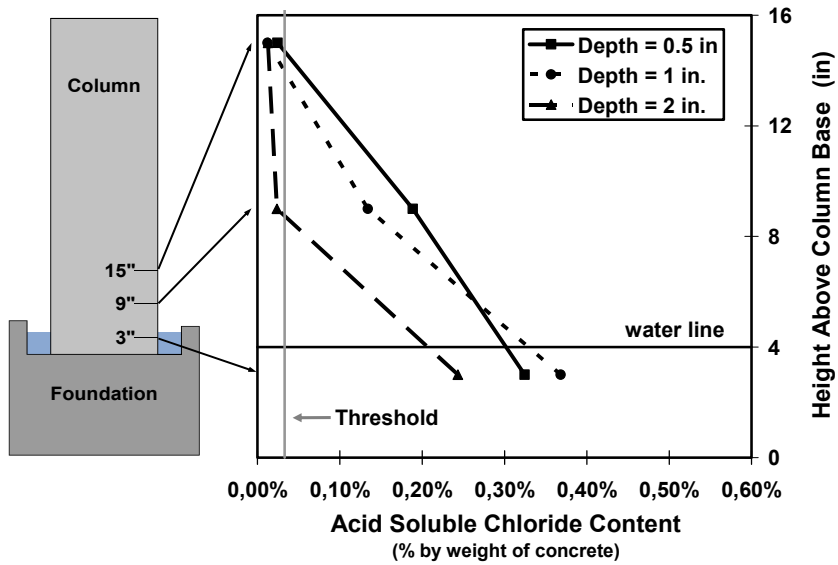
Figure C.24 Concrete Chloride Penetration for Column NJ-TC-S in Non-Dripper Side at End of Testing

637
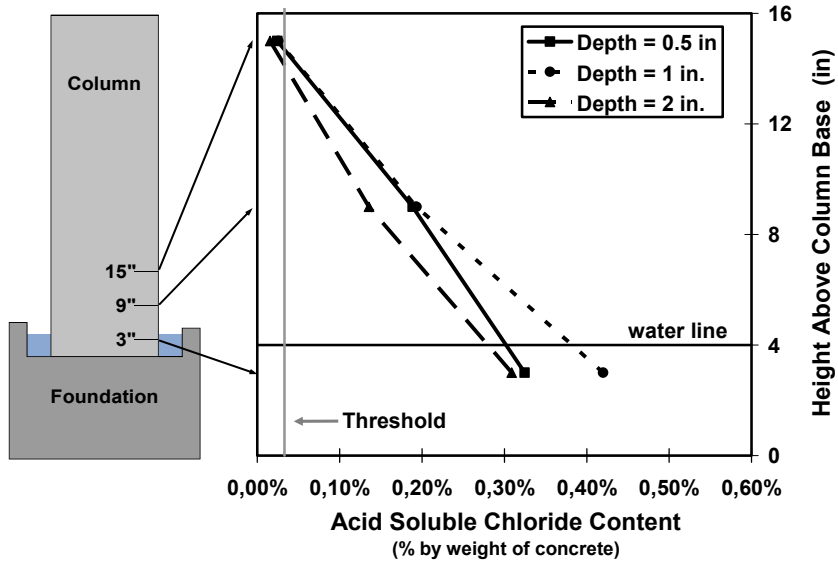
Figure C.25 Concrete Chloride Penetration for Column NJ-TC-S in Dripper Side at End of Testing
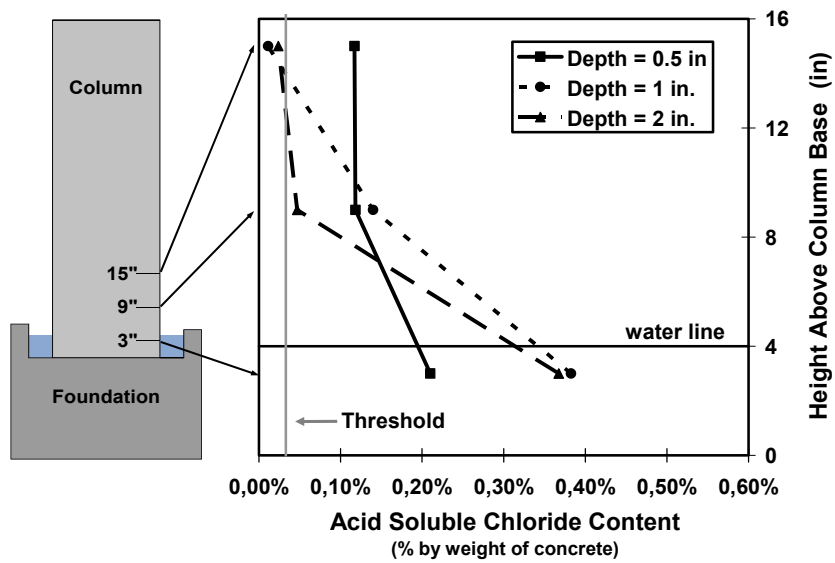
Figure C.26 Concrete Chloride Penetration for Column PT-TC-S-PD in Non-Dripper Side at End of Testing

638
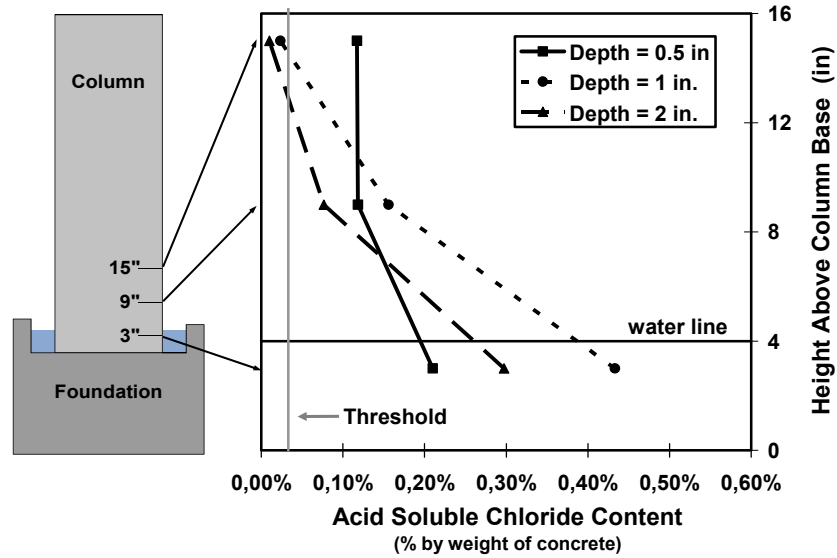
***Figure C.27 Concrete Chloride Penetration for Column PT-TC-S-PD
in Dripper Side at End of Testing***
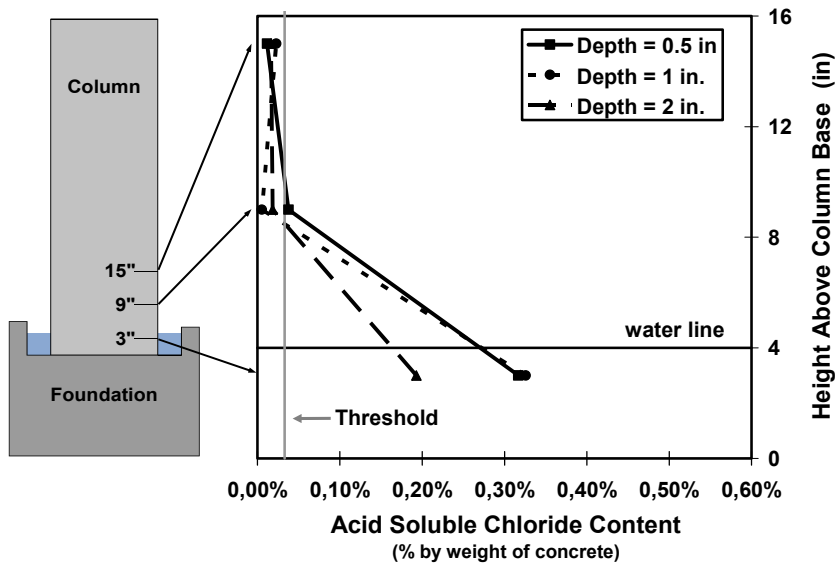
***Figure C.28 Concrete Chloride Penetration for Column PT-FA-S-PD
in Non-Dripper Side at End of Testing***

639
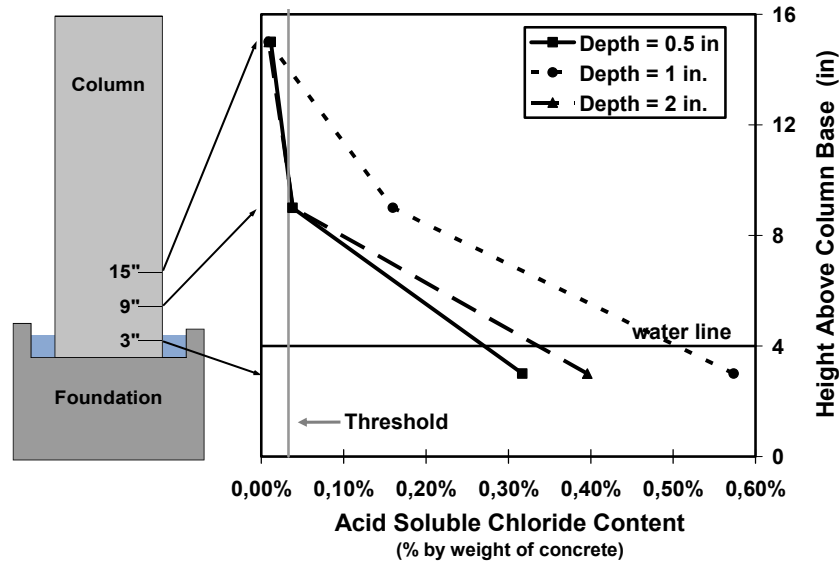
Figure C.29 Concrete Chloride Penetration for Column PT-FA-S-PD in Dripper Side at End of Testing
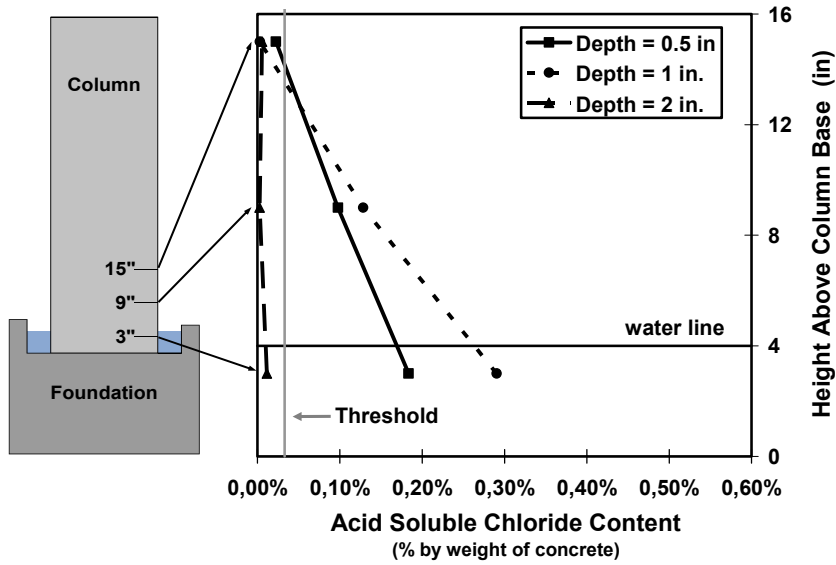
Figure C.30 Concrete Chloride Penetration for Column PT-TC-S-EB in Non-Dripper Side at End of Testing

640
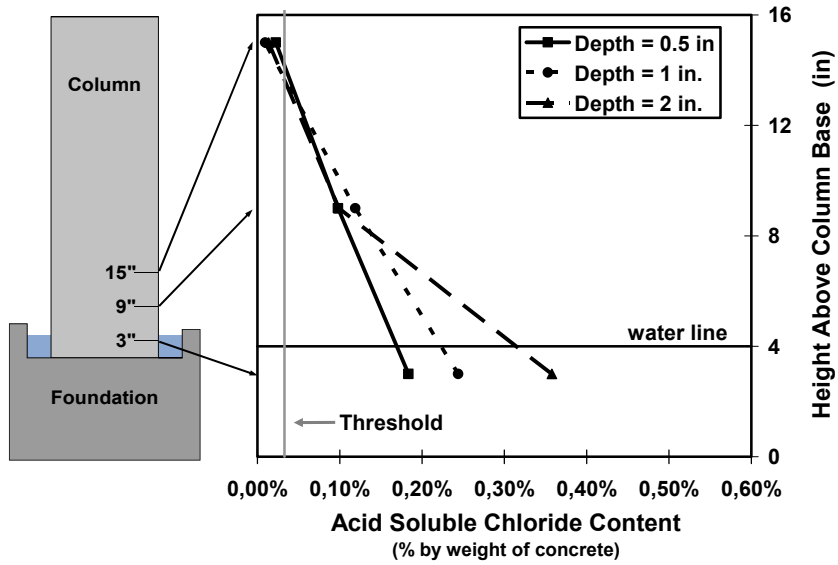
***Figure C.31 Concrete Chloride Penetration for Column PT-TC-S-EB
in Dripper Side at End of Testing***
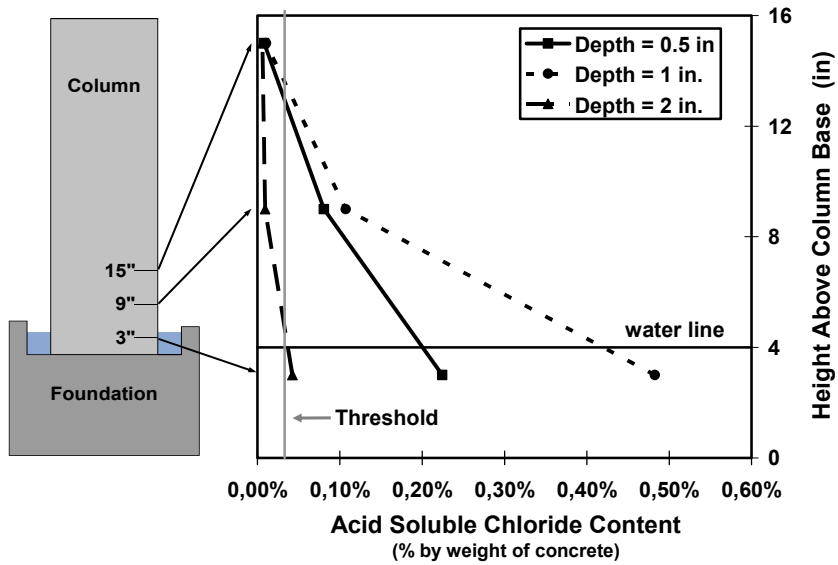
***Figure C.32 Concrete Chloride Penetration for Column PT-TC-S-GB
in Non-Dripper Side at End of Testing***

641
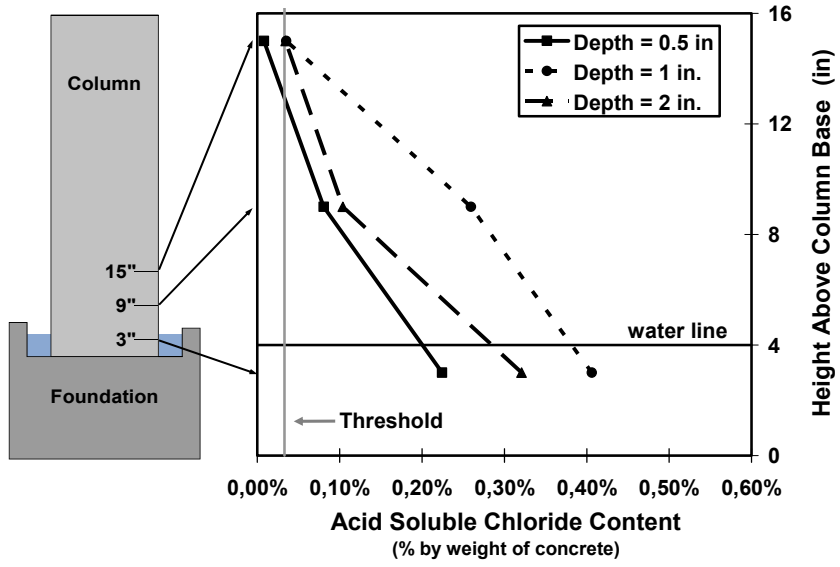
Figure C.33 Concrete Chloride Penetration for Column PT-TC-S-GB in Dripper Side at End of Testing

References

Chapter 1 References

1.1 **Matt, P. et al. (2000)**, "Durability of Prestressed Concrete Bridges in Switzerland", 16th Congress of IABSE, September 2000, Congress Report, 2000.

1.2 **Woodward, R. (2001),** "Durability of Post-tensioned tendons on road bridges in the UK." Durability of Post-tensioning tendons. *fib-IABSE Technical Report, Bulletin 15*. Workshop 15-16 November 2001, Ghent (Belgium), 2001, pp.1-10.

1.3 **Godart, B. (2001),** "Status of durability of post-tensioned tendons in France." Durability of Post-tensioning tendons. *fib-IABSE Technical Report, Bulletin 15*. Workshop 15-16 November 2001, Ghent (Belgium), 2001, pp.25-42.

1.4 **Mutsuyoshi, H (2001),** "Present Situation of Durability of Post-Tensioned PC Bridges in Japan." Durability of Post-tensioning tendons. *fib-IABSE Technical Report, Bulletin 15*. Workshop 15-16 November 2001, Ghent (Belgium), 2001, pp.75-88.

1.5 **Bertgagnoli, G., Carbone, V.I., Giordano, L., Mancini, G. (2001),** "Repair and strengthening of damaged prestressed structures." Durability of Post-tensioning tendons. *fib-IABSE Technical Report, Bulletin 15*. Workshop 15-16 November 2001, Ghent (Belgium), 2001, pp.139-153.

1.6   **Freyermuth, C.L. (2001),** "Status of the durability of post-tensioning tendons in the United States." Durability of Post-tensioning tendons. *fib-IABSE Technical Report, Bulletin 15*. Workshop 15-16 November 2001, Ghent (Belgium), 2001, pp. 43-50.

1.7   **Moreton, A. (2001)** "Performance of Segmental and Post-Tensioned Bridges in Europe," Journal of Bridge Engineering, ASCE, Vol. 6, No. 6, November/December 2001.

1.8   **Jungwirth, D. (2001),** "Problems, Solutions and Developments at Pot-Tensioning Tendons from the German Point of View," Durability of Post-tensioning tendons. *fib-IABSE Technical Report, Bulletin 15*. Workshop 15-16 November 2001, Ghent (Belgium), 2001, pp.11-24.

1.9   **Eibl, J. (2001),** "External prestressing of German bridges and its further development." Durability of Post-tensioning tendons. *fib-IABSE Technical Report, Bulletin 15*. November 2001, Ghent (Belgium), 2001, pp.227-234.

1.10   **Virlogeux, M.,** "Advocationg for quality in prestressed concrete."

1.11   *fib* **Bulletin No. 15 (2001),** "Durability of Post-Tentensioning Tendons." Proceedings of Workshop, Ghent, Belgium, November 2001.

1.12   **Poston, R.W., West, J.S. (2001),** "North American Strategies for Improving Bonded Post-tensioned Concrete Construction." Durability of Post-tensioning tendons. *fib-IABSE Technical Report, Bulletin 15*. Workshop 15-16 November 2001, Ghent (Belgium), 2001, pp.245-255.

1.13   **Chandra, V. (2002),** "A Review of Post-Tensioning Tendons in the Boston Central Artery/Tunnel Project", 1st Annual Concrete Bridge Conference, FHWA, NCBC, PCI. Nashville, TN, Octobre 9, 2002.

1.14   **Potter, J.L. (2002)**,"National Status of Post-Tensioning Condition Evaluations and Enhancements." 1st Annual Concrete Bridge Conference, FHWA, NCBC, PCI. Nashville, TN, October 9, 2002.

644

1.15   **DeHaven, T.A. (2002),** "Overview of Recent Developments in Grouting of Post-Tensioning Tendons" 1st Annual Concrete Bridge Conference, FHWA, NCBC, PCI. Nashville, TN, October 9, 2002.

1.16   **FLDOT (2002),** New Directions for Florida Post-Tensioned Bridges. Florida Department of Transportation.   Post-Tensioning in Florida Bridges. By Corven Engineering, Inc. Tallahassee, Florida, February 2002

1.17   **Theryo, T., García, P., Nickas, W. (2002)** " Lessons Learned from the Vertical Tendon Corrosion Investigation of the Sunshine Skyway Bridge High Level Approach Piers," Proceedings of the first fib Congress: Concrete Structures in the 21st Century, Session 8, Osaka, Japan, 2002.

1.18   **ASBI (2002),** "2002 Grouting Certification Training Manual," American Segmental Bridge Institute, Phoenix, Arizona, 2002.

1.19   **PTI (2001),** "Specification for Grouting of Post-Tensioned Structures," Post-Tensioning Institute (PTI), February 2001, First edition.

1.20   **ASBI (2001),** "Interim Statement on Grouting Practices," American Segmental Bridge Institute (ASBI), December 2000.

1.21   **ASBI (2002),** "2002 Grouting Certification Training Manual," ASBI, 2002.

1.22   **The Concrete Society (1996),** "Durable Bonded Post-Tensioned Concrete Bridges," The Concrete Society Technical Report TR47. Crowthorne, United Kingdom, 1996.

1.23   **VSL (2002),** "Grouting of Post-Tensioning Tendons," VSL Report Series. VSL International Ltd. Lyssach, Switzerland, May 2002.

1.24   **FIP (1996),** "Corrosion protection of Prestressing Steels," Fédération Internationale de la Précontrainte (FIP), London, 1996.

1.25 *fib* **(2000)**, "Corrugated Plastic Ducts for Internal Bonded Post-Tensioning," Fédération Internationale du béton (*fib*) Technical Report Bulletin No. 7, January, 2000.

1.26 *fib* **(2000),** "Grouting of tendons in prestressed concrete," Fédération Internationale du béton (*fib*) Technical Report Bulletin No. 20, July, 2000.

1.27 **Hamada, Y. et al. (2001)** "Maintenance of Prestressed Concrete Bridges." Fib-IABSE Technical Report, Bulletin 15. Workshop 15-16 November 2001, Ghent (Belgium), 2001, pp. 109-120.

1.28 **Kitazono, H. et al. (2002)** "Manual for Maintenance of Durable Prestressed Concrete Bridges," Proceedings of the first fib Congress: Concrete Structures in the 21st Century, Session 12, Osaka, Japan, 2002.

1.29 **Matt, P. (2001)** "Non-destructive Evaluation and Monitoring of Post-Tensioning Tendons," Fib-IABSE Technical Report, Bulletin 15. Workshop 15-16 November 2001, Ghent (Belgium), 2001, pp. 103-108.

1.30 **West, J.S., Vignos, R.P.,Breen,J.E., and Kreger, M.E. (1999)** "Corrosion Protection for Bonded Internal Tendons in Precast Segmental Construction," Research Report 1405-4, Center for Transportation Research, Bureau of Engineering Research, The University of Texas at Austin, October 1999.

1.31 **Ganz, H.R. (2002)** "Recent Developments in the Protection of Prestressing Steels," Proceedings of the first fib Congress: Concrete Structures in the 21st Century, Session 7, Osaka, Japan, 2002.

1.32 **Schokker, A.J., Koester, B.D, Breen, J.E., and Kreger, M.E. (1999)** "Development of High Performance Grouts for Bonded Post-Tensioned Structures," Research Report 1405-2, Center for Transportation Research, Bureau of Engineering Research, The University of Texas at Austin, December 1999.

646

1.33   **West, J.S. (1999)** "Durability Design of Post-Tensioned Bridge Substructures," Ph.D. Dissertation, The University of Texas at Austin, May 1999.

1.34   **Schokker, A.J. (1999),** "Improving Corrosion Resistance of Post-Tensioned Substructures Emphasizing High Performance Grouts," Ph.D. Dissertation, The University of Texas at Austin, May 1999.

1.35   **Koester, B.D. (1995),** "Evaluation of Cement Grouts for Strand Protection Using Accelerated Corrosion Tests," Master of Science Thesis, The University of Texas at Austin, December 1995.

1.36   **Larosche, C.J. (1999),** "Test Method for Evaluating Corrosion Mechanisms in Standard Bridge Columns," Master of Science Thesis, The University of Texas at Austin, August 1999.

1.37   **Kotys, A.L. (2003)** "Durability Examination of Bonded Tendons in Concrete Beams under Aggressive Corrosive Environment." Unpublished Master of Science Thesis, The University of Texas at Austin. (under preparation), 2003.

1.38   **Vignos, R.P. (1994)**, "Test Method for Evaluating the Corrosion Protection of Internal Tendons Across Segmental Bridge Joints." Master of Science Thesis, The University of Texas at Austin, May 1994.

1.39   **Hamilton, H.R. (1995),** "Investigation of Corrosion Protection Systems for Bridge Stay Cables," Ph.D. Dissertation, The University of Texas at Austin, 1995.

647

1.40   **Schokker, A.J., West, J.S., Breen, J.E., and Kreger, M.E. (1999)**, "Interim Conclusions, Recommendations, and Design Guidelines for Durability of Post-Tensioned Bridge Substructures," Research Report 1405-5, Center for Transportation Research. The University of Texas at Austin, October 1999.

Chapter 2 References

2.1   **Schupack, M. (2001).** "Prestressing Reinforcement in the New Millennium," *Concrete International*, Vol 23, No. 12, December 2001.

2.2   **Godart, B. (2001).** "Status of durability of post-tensioned tendons in France." *Durability of Post-tensioning tendons*. *fib*-IABSE Technical Report, Bulletin 15. Workshop 15-16 November, Ghent (Belgium), 25-42, 2001.

2.3   **Yunovich, M., Thompson,N.G. (2003).** "Corrosion of Highway Bridges: Economic Impact and Control Methodologies," *Concrete International*, January 2003, pp.52-57.

2.4   **Manning, D.(1988).** "*Durability of Prestressed Concrete Highway Structures*," NCHRP 140. Transportation Research Board. National Research Council. Washington, DC., 1988.

2.5   **Freyermuth, C.L. (2001).** "Status of the durability of post-tensioning tendons in the United States." *Durability of Post-tensioning tendons*. *fib*-IABSE Technical Report, Bulletin 15. Workshop 15-16 November, Ghent (Belgium), 2001, pp.43-50.

2.6   **Schokker, A.J. (1999),** "Improving Corrosion Resistance of Post-Tensioned Substructures Emphasizing High Performance Grouts," Ph.D. Dissertation, The University of Texas at Austin, May 1999.

2.7   **Jungwirth, D. and Gehlen, B. (2002).** "Problems, Solutions, Developments and Applications at Different Kinds of Post-Tensioning Tendons from the European Point of View," Proceedings of the first fib Congress: *Concrete Structures in the 21st Century*, Session 2, Osaka, Japan.

2.8   **Virlogeux, M. (1999).** "Message from the President," *Structural Concrete*, *fib*, Vol. P1, No.1, March 1999.

2.9   **Chaussin R., Chabert, A. (2001).** "Strategies for improvement – Approach in France-" *Durability of Post-tensioning tendons*. *fib*-IABSE Technical Report, Bulletin 15. Workshop 15-16 November, Ghent (Belgium), 2001, pp.235-244.

2.10 **FLDOT (2002)**. "*New Direction for Florida Post-Tensioned Bridges*," Corven Engineering Inc. Volume 1 of 5, Tallahassee, Florida, February 15.

2.11 **AASHTO, LRFD (1998)**. *Bridge Design Specifications*, 2nd Edition, American Association of State Highway and Transportation Officials, Washington, D.C., 1998.

2.12 **West, J.S. (1999).** "Durability Design of Post-Tensioned Bridge Substructures," Ph.D. Dissertation, The University of Texas at Austin, May 1999.

2.13 **Kuesel, Th. R. (1990).** "Whatever Happened to Long –Term Bridge Design?," *Civil Engineering*, February, 57-60

2.14 *fib* **–IABSE (2001).** "*Durability of Post-Tensioned Tendons*" Technical Report. Bulletin 15. Workshop 15-16 November, Ghent, Belgium, 2001.

2.15 **Zivanovic, I.,Lecinq,B.,Fuzier,JP.(2002).** "Durability Specifics for Prestressing," Proceedings of the first fib Congress: *Concrete Structures in the 21st Century*, Session 8, Osaka, Japan, 2002.

649

2.16 **Mutsuyoshi, H. (2001).** "Present Situation of Durability of Post-Tensioned PC Bridges in Japan." *Durability of Post-tensioning tendons. fib*-IABSE Technical Report, Bulletin 15. Workshop 15-16 November, Ghent (Belgium), 2001, pp.75-88.

2.17 **M**iller, M.D. (2000). "Durability Survey of Segmental Concrete Bridges," American Segmental Bridge Institute, ASBI, Second Edition, September 2000.

2.18 **Theryo, T., García, P., Nickas, W. (2002).** " Lessons Learned from the Vertical Tendon Corrosion Investigation of the Sunshine Skyway Bridge High Level Approach Piers," Proceedings of the first fib Congress: *Concrete Structures in the 21st Century*, Session 8, Osaka, Japan, 2002.

2.19 **ASBI (2002).** "*2002 Grouting Certification Training Manual*," American Segmental Bridge Institute, Phoenix, Arizona, 2002.

2.20 **ACI 222.R-96 (1997)** Corrosion of Metals in Concrete. American concrete Institute. March 1997.

2.21 **Qing Li, Ch. (2002)**. "Initiation of Chloride-Induce Reinforcement Corrosion in Concrete Structural Members – Prediction," *ACI Structural Journal*, Vol 99 No.2, March-April 2002, pp.133-141.

2.22 **Hamada, Y. Ishikawa, Y., Mizoe, M., Miyagawa, T. (2001)**. "Maintenance of Prestressed Concrete Bridges." *Durability of Post-Tensioning Tendons*. fib-IABSE Technical Report, Bulletin 15. Workshop 15-16 November, Ghent, Belgium, 2001, pp.109-120.

2.23 **Domone, P.L. and Jefferis, S.A. (1994)** *Structural Grouts*, Blackie Academic & Professional, London, 1994.

2.24 **Schupack,M. (1971)**. "Grouting Tests on Large Post-Tensioning Tendons for Secondary Nuclear Containment Structures," Journal *of the Prestressed Concrete Institute*, March-April 1971, pp.85-97.

2.25   **Shupack, M., (1974)**. "Admixture for Controlling Bleed in Cement Grout Used in Post-Tensioning," *Journal of the Prestressed Concrete Institute*, November-December 1974.

2.26   **Pielstick, B.H. (2002).** "Grouting of Segmental Post-Tensioned Bridges in America," Proceedings of the first fib Congress: Concrete *Structures in the 21ˢᵗ Century*, Session 8, Osaka, Japan, 2002.

2.27   **Hamilton, H.R. (1995)** "Investigation of Corrosion Protection Systems for Bridge Stay Cables," Doctor of Philosophy Dissertation, The University of Texas at Austin, September 1995.

2.28   **Jones, D.A. (1992).** *"Principles and Prevention of Corrosion,"* Mac Millan Publishing Company, New York, 1992.

2.29   **Rosenberg, A., Hansson, C.M., and Andrade, C., (1989).** "Mechanisms of Corrosion of Steel in Concrete," *Materials Science of Concrete I*, The American Ceramic Society, 1989, pp.285-313.

2.30   **Fontana, M.G. (1986).** *Corrosion Engineeering*, McGraw-Hill Book Company, New York, 1986.

2.31   **Violetta, B. (2002)** "Life-365 Service Life Prediction Model," *Concrete International*, Vol 24, No. 12, December 2002, pp.53-57.

2.32   **Ganz, H.R. (2001)**. "Evolution of Prestressing Systems." *Durability of Post-Tensioning Tendons. fib*-IABSE Technical Report, Bulletin 15. Workshop 15-16 November. Ghent, Belgium, 2001, pp.155-171.

2.33   **Shupack,M. and Suarez, M.G. (1982)** "Some Recent Corrosion Embrittlement Failures of Prestressing Sytems in the United States," *Journal of the Prestressed Concrete Institute*, March-April 1982.

2.34 **Ikawa,K.,Ishii,K.,Fukute,T. and Seki,H. (1996).** "Behavior and Protection of Hydrogen Embrittlement on Tendons of PC Members," Concrete in marine Environment: Proceedings of the Third CANMET/ACI International Conference, St. Andrews by-the-Sea, Canada, SP-163, V.M. Malhotra, Ed., 1996, pp.253-273.

2.35 **Yamaoka, Y., Hideyoshi, T. and Kurauchi, M. (1988)**. "Effect of Galvanizing on Hydrogen Embrittlement of Prestressing Wire," Journal of the Prestressed Concrete Institute, July-August 1988.

2.36 **Woodward, R. (2001),** "Durability of Post-tensioned tendons on road bridges in the UK." Durability of Post-tensioning tendons. *fib-IABSE Technical Report, Bulletin 15*. Workshop 15-16 November 2001, Ghent (Belgium), 2001, pp.1-10.

2.37 **The Concrete Society (1996),** "Durable Bonded Post-Tensioned Concrete Bridges," The Concrete Society Technical Report TR47. Crowthorne, United Kingdom, 1996.

2.38 **Ganz, H.R. (2002).** "Recent Developments in the Protection of Prestressing Steels," Proceedings of the first fib Congress: *Concrete Structures in the 21ˢᵗ Century*, Session 7, Osaka, Japan, 2002.

2.39 **Matt, P. (2000).** "Performance of Post-Tensioned Bridges in Switzerland and Practical Experience with a New Generation of Tendons," ASBI Annual Convention , Brookling, USA, 2000, pp.7-8.

2.40 **Schupack, M.(2001).** "Prestressing Reinforcement in the New Millennium," *Concrete International*, Vol. 23, No. 12, December 2001, pp.38-45.

2.41 **Neville, A.M.,(1997).** *Properties of Concrete*, 4ᵗʰ Edition, John Wiley & Sons, New York, NY.1997.

2.42 **Mindess, S., and Young, J.F. (1981).** *Concrete*, Prentice-Hall Inc., Englewood Cliffs, New Jersey, 1981.

2.43 **CEB (1989)**, *Durable Concrete Structures* – CEB Design Guide, Bulletin D'information No. 182, Comité Euro-International du Béton, Laussanne, June 1989.

2.44 **Nmai, C.K. (1995).** "Corrosion-Inhibiting Admixtures: Passive, Passive-Active versus Active Systems," *Advances in Concrete Technology*: Proceedings of the Second CANMET/ACI International Symposium, Las Vegas, Nevada, SP-154, V.M. Malhontra, Ed., 1995, pp.565-585.

2.45 **Shaw,M. (1997).** "Migrating Corrosion Inhibitors for Reinforced Concrete Protection," Proceedings of the seventh International Conference on Structural Faults and Repair, Volume 2, Edinburgh, Scotland, 1997, pp.317-324.

2.46 **Wollman, G.P., Yates, D.L., and Breen, J.E, (1988)**. "Freeting Fatigue in Post-Tensioned Concrete," Research Report 465-2F, Center for Transportation Research, The University of Texas at Austin, November, 1988.

2.47 **PTI (2001).** "*Guide Specification for Grouting of Post-Tensioned Structures*," Post-Tensioning Institute (PTI), February 2001, First edition, 2001.

2.48 *fib* **(2000).** "*Grouting of tendons in prestressed concrete*," Fédération Internationale du béton. Technical Report Bulletin No. 20, Laussane, Switzerland, July 2000.

2.49 **VSL (2002).** "*Grouting of Post-Tensioning Tendons*," VSL Report Series. VSL International Ltd. Lyssach, Switzerland, May 2002.

2.50 **Tourneur, S. (2002).** "Prestressing: 60 years of innovation," Proceedings of the first fib Congress: *Concrete Structures in the 21ˢᵗ Century*, Osaka, Japan, 2002.

2.51 *fib* **(2000)**, "Corrugated Plastic Ducts for Internal Bonded Post-Tensioning," Fédération Internationale du béton (*fib*) Technical Report Bulletin No. 7, Laussane, Switzerland, 2000.

2.52 **Moreton, A. (2001).** "Performance of Segmental and Post-Tensioned Bridges in Europe," *Journal of Bridge Engineering*, ASCE, Vol. 6, No.6, November/December 2001.

2.53 **Clark, G. (2001).** "Strategies for improvement – Approach in Europe – The UK strategy and fib developments," *Durability of Post-Tensioned Tendons*. Fib-IABSE Technical Report, Bulletin 15. Workshop 15-16 November, Ghent, Belgium, 2001, pp.221-226.

2.54 **ACI 222.3R.** Unpublished ACI Committee Report 222. (under preparation)

2.55 **McCraven, S.C. (2001).** "New Generation of Reinforcement for Transportation Instrastructure," Concrete Construction, September 2001, pp.41-47.

2.56 **(2001)** "Will new generation reinforcing materials solve our corrosion problems?," Concrete Perspectives, *Concrete Construction*. September 2001, pp.51-54.

2.57 **Gaubinger, B., Bahr,G, Hampel,G, Kollegger,J. (2002).** "Innovative Anchorage System for CFRP-Tendons," Proceedings of the first fib Congress: *Concrete Structures in the 21ˢᵗ Century*, Session 7, Osaka, Japan, 2002.

2.58   **Matt, P. (2001).** "Non-destructive Evaluation and Monitoring of Post-Tensioning Tendons," *Durability of Post-Tensioned Tendons*. Fib-IABSE Technical Report, Bulletin 15. Workshop 15-16 November, Ghent, Belgium, 2001, pp.103-108.

2.59   **Raiss, M.E. (2001).** "Appropriate detailing in the design process for durable post-tensioned bridges," *Durability of Post-Tensioned Tendons*. Fib-IABSE Technical Report, Bulletin 15. Workshop 15-16 November, Ghent, Belgium, 2001, pp.203-220.

Chapter 3 References

3.1   **Freyermuth, C.L. (2001).** "Status of the durability of post-tensioning tendons in the United States." *Durability of Post-tensioning tendons*. *fib*-IABSE Technical Report, Bulletin 15. Workshop 15-16 November, Ghent (Belgium), 2001, pp.43-50.

3.2   **AASHTO (1989***), Guide Specifications for Design and Construction of Segmental Concrete Bridges* , American Association of State Highway and Transportation Officials, Washington, D.C., 1989.

3.3   **West, J.S. (1999).** "Durability Design of Post-Tensioned Bridge Substructures," Ph.D. Dissertation, The University of Texas at Austin, May 1999.

3.4   **Vignos, R.P. (1994)**, "Test Method for Evaluating the Corrosion Protection of Internal Tendons Across Segmental Bridge Joints." Master of Science Thesis, The University of Texas at Austin, May 1994.

3.5   **ASTM (1992)**, "Standard Test Method for Determining the Effects of Chemical Admixtures on the Corrosion of Embedded Steel Reinforcement in Concrete Exposed to Chloride Environments," ASTM G109-92, American Society for Testing and Materials, Philadelphia, PA., 1992.

3.6   **AASHTO (1999)**, *Guide Specifications for Design and Construction of Segmental Concrete Bridges*, American Association of State Highway and Transportation Officials, Washington, D.C. 2nd Edition, 1999.

3.7   **ASTM (1991)**, "Standard Test Method for Half-Cell Potentials of Uncoated Reinforcing Steel in Concrete," ASTM C876-91, American Society for Testing and Materials, Philadelphia, Pa., 1991.

3.8   **West, J.S., Vignos, R.P., Breen, J.E., and Kreger, M.E. (1999)**, "Corrosion Protection for Bonded Internal Tendons in Precast Segmental Construction," Research Report 1405-4,Center for Transportation Research, The University of Texas at Austin, Austin, Texas, October 1999.

3.9   **Broomfield, J.P., Rodriguez, J., Ortega, L.M., and Garcia, A.M. (1993)**, "Corrosion Rate Measurement and Life Prediction for Reinforced Concrete Structures," Proceedings of the 5th International Conference on Structural Faults and Repair held on June 29, Vol. 2, Venue, University of Edinburgh, 1993, pp.155-163.

3.10   **Al-Qadi, I.L., Peterson, J.E., and Weyers, R.E. (1993)**, "A Time to Cracking Model for Critically Contaminated Reinforced Concrete Structures," Proceedings of the 5th International Conference on Structural Faults and Repair held on June 29. Vol. 3, Venue, University of Edinburgh, 1993, pp.91-99.

3.11 **Concrete Reinforcing Steel Institute (1992)**, "CRSI Performance Research: Epoxy-Coated Reinforcing Steel," Interim Report, CRSI, Schaumburg, Ill, January 1992.

3.12 **Virmani, Y.P., Clear, K.C., and Pasko, T.J. (1983)**, "Time-to-Corrosion of Reinforcing Steel in Concrete Slabs, Vol. 5,: Calcium Nitrite Admixture or Epoxy-Coated Reinforcing Bars as Corrosion Protection Systems," Report No. FHWA/RD-83/012, Federal Highway Administration, Washington, D.C., September 1983, pp.71.

3.13 **AASHTO (1994),** "Sampling and Testing for Chloride Ion in Concrete and Concrete Raw Materials," AASHTO T 260-94, American Association of State Highway and Transportation Officials, Washington, D.C., 1994.

3.14 **Poston, R.W. (1984),** "Improving Durability of Bridge Decks by Transverse Prestressing," Doctor of Philosophy Dissertation, The University of Texas at Austin, 1984.

3.15 **Hamilton, H.R. (1995),** "Investigation of Corrosion Protection Systems for Bridge Stay Cables," Doctor of Philosophy Dissertation, The University of Texas at Austin, 1995.

3.16 **Sason, A.S. (1992),** "Evaluation of Degree of Rusting on Prestressed Concrete Strand," *PCI Journal*, Vol. 37, No. 3, May-June 1992, pp.25-30.

3.17 **Wouters, J.P. (1998),** Personal Communication, Whitlock Dalrymple Poston and Associates, Inc., Manassas, Virginia, July 1998..

3.18 **ACI Committee 222, (1996), "**Corrosion of Metals in Concrete," ACI 222R-96, American Concrete Institute, Detroit, Michigan, 1996.

3.19 **Koester, B.D. (1995)**, "Evaluation of Cement Grouts for Strand Protection Using Accelerated Corrosion Tests," Master of Science Thesis, the University of Texas at Austin, December 1995.

Chapter 4 References

4.1 **Armstrong, S.D., Salas, R.M., Wood, B.A., Breen, J.E. and Kreger, M.E., (1997)** *"Behavior and Design of Large Structural Bridge Pier Overhangs,"* Research Report 1364-1, Center of Transportation Research, University of Texas at Austin, 1997.

4.2 **West, J.S., (1999)** *"Durability Design of Post-Tensioned Bridge Substructures,"* Doctor of Philosophy Dissertation, The University of Texas at Austin, May 1999.

4.3 **Schokker, A.J., (1999)** *"Improving Corrosion Resistance of Post-Tensioned Substructures Emphasizing High Performance Grouts,"* Doctor of Philosophy Dissertation, The University of Texas at Austin, May 1999.

4.4 **West, J.S., Schokker, A.J., Larosche,C.J., Breen, J.E., Kreger, M.E. (1999)** *"Long-Term Post-Tensioned Beam and Column Exposure Test Specimens: Experimental Program,"* Center for Transportation Research, Report 1405-3. The University of Texas at Austin, October 1999.

4.5 **Kotys, A.L., (2003)** *"Durability Examination of Bonded Tendons in Concrete Beams Under Aggressive Corrosive Environment,"* Master of Science in Engineering Thesis, The University of Texas at Austin, May 2003.

4.6 **AASHTO**, **(1998)** *"LRFD Bridge Design Specifications,"* 2nd Edition, American Association of State Highway and Transportation Officials, Washington, D.C., 1998.

4.7 **ACI Committee 318, (1995)** *"Building Code Requirements for Structural Concrete,"* ACI 318-95, American Concrete Institute, Detroit, MI, 1995.

4.8 **Breen, J.E., Burdet, O., Roberts, C., Sanders, D. and Woollman, G.**, **(1994)** *"Anchorage Zone Reinforcement for Post-Tensioned Concrete Girders,"* NCHRP Report 356, Transportation Research Board, Washington, D.C., 1994, 204 pp.

4.9 **ASTM G109, (1992)** *"Standard Test Method for Determining the Effects of Chemical Admixtures on the Corrosion of Embedded Steel Reinforcement in Concrete Exposed to Chloride Environments,"* ASTM G109-92, American Society for Testing and Materials, Philadelphia, PA., 1992.

4.10 **AASHTO T259, (1980)** *"Standard Method of Test for Resistance of Concrete to Chloride Ion Penetration,"* AASHTO Designation T 259-80, American Association of State Highway and Transportation Officials, Washington, D.C., 1980.

4.11 **Jones, D.A., (1992)** *"Principles and Prevention of Corrosion,"* Mac Millan Publishing Company, New York, 1992.

4.12 **ASTM C876, (1991)** *"Standard Test Method for Half-Cell Potentials of Uncoated Reinforcing Steel in Concrete,"* ASTM C876-91, American Society for Testing and Materials, Philadelphia, PA., 1991.

4.13 **Fontana, M.G., (1986)** "Corrosion Engineering," 3rd Edition, McGraw-Hill, INC., New York, New York, 1986.

4.14 **Jones, D.A., (1996)** *"Principles and Prevention of Corrosion,"* 2nd Edition, Prentice Hall, Inc., Upper Saddle River, NJ, 1996.

4.15 **Flis, J., Sehal, A., Li, D., Kho, Y., Sabol, S., Pickering, H., Osseo-Asare, K., and Cady, P.D., (1992***) "Condition Evaluationof Concrete Bridges Relative to Reinforcement Corrosion, Volume 2: Method for Measuring the Corrosion Rate of Reinforcing Steel,"* SHRP-S/FR-92-104, Strategic Highway Research Program, Washington, D.C., 1992.

4.16 **Andrade, C., Castelo, V., Alonso, C. and Gonzalez J.A., (1986)** "The Determination of Corrosion Rate of Steel Embedded in Concrete by the Polarization Resistance and AC Impedance Methods," Corrosion Effect of Stray Currents and the Techniques for Evaluation Corrosion of Rebars in Concrete, ASTM STP 906, V. Chaker, Editor, American Society for Testing and Materials, Philadelphia, PA., 1986.

4.17 **CONCORR, Inc., (1996)** *"FHWA-SHRP Showcase: Assessment of Physical Condition of Concrete Bridge Components,"* Federal Highway Administration, Washington, D.C., 1996.

4.18 **Cady, P., and Gannon, E., (1992)** *"Condition Evaluation of Concrete Bridges Relative to Reinforcement Corrosion, Volume 8: Procedure Manual,"* SHRP-S/FR-92-330, Strategic Highway Research Program, Washington, D.C., 1992

4.19 **AASHTO T260, (1994)** *"Standard Method of Test for Sampling and Testing for Chloride Ion in Concrete Ram Materials,"* AASHTO Designation T 260-94, American Association of State Highway and Transportation Officials, Washington, D.C., 1994.

4.20 **ACI Committee 222, (1996)** "*Corrosion of Metals in Concrete,*" ACI 222 R-96, American Concrete Institute, Detroit, Michigan, 1996.

4.21 **West, J.S., Vignos, R.P., Breen, J.E., and Kreger, M.E. (1999),** "Corrosion Protection for Bonded Internal Tendons in Precast Segmental Construction," Research Report 1405-4,Center for Transportation Research, The University of Texas at Austin, Austin, Texas, October, 1999.

4.22 **Poston, R.W., (1984)** "Improving Durability of Bridge Decks by Transverse Prestressing," Doctor of Philosophy Dissertation, The University of Texas at Austin, 1984.

4.23   **Hamilton, H.R., (1995)** *"Investigation of Corrosion Protection Systems for Bridge Stay Cables,"* Doctor of Philosophy Dissertation, The University of Texas at Austin, 1995.

4.24   **Sanson, A.S., (1992)** *"Evaluation of Degree of Rusting on Prestressed Concrete Strand,"* PCI Journal, Vol. 37, No. 3, May-June 1992.

Chapter 5 References

5.1   **West, J.S., (1999)** *"Durability Design of Post-Tensioned Bridge Substructures,"* Doctor of Philosophy Dissertation, The University of Texas at Austin, May 1999.

5.2   **Schokker, A.J., (1999)** *"Improving Corrosion Resistance of Post-Tensioned Substructures Emphasizing High Performance Grouts,"* Doctor of Philosophy Dissertation, The University of Texas at Austin, May 1999.

5.3   **West, J.S., Schokker, A.J., Larosche,C.J., Breen, J.E., Kreger, M.E. (1999)** *"Long-Term Post-Tensioned Beam and Column Exposure Test Specimens: Experimental Program,"* Center for Transportation Research, Report 1405-3. The University of Texas at Austin, October 1999.

5.4   **ASTM**, **(1991)** "Standard Test Method for Half-Cell Potentials of Uncoated Reinforcing Steel in Concrete," ASTM C876-91, American Society for Testing and Materials, Philadelphia, Pa., 1991.

5.5   **ACI Committee 222 (1996),** "Corrosion of Metals in Concrete," ACI 222 R-96, American Concrete Institute, Detroit, Michigan, 1996.

5.6   **West, J.S., Vignos, R.P., Breen, J.E., and Kreger, M.E. (1999),**
"Corrosion Protection for Bonded Internal Tendons in Precast Segmental
Construction," Research Report 1405-4,Center for Transportation
Research, The University of Texas at Austin, Austin, Texas, October
1999.

Chapter 7 References

7.1   **West, J.S., Vignos, R.P., Breen, J.E., and Kreger, M.E. (1999),**
"Corrosion Protection for Bonded Internal Tendons in Precast Segmental
Construction," Research Report 1405-4,Center for Transportation
Research, The University of Texas at Austin, Austin, Texas, October
1999.

7.2   **ASTM (1991)**, "Standard Test Method for Half-Cell Potentials of
Uncoated Reinforcing Steel in Concrete," ASTM C876-91, American
Society for Testing and Materials, Philadelphia, Pa., 1991.

7.3   **AASHTO (1999)**, *Guide Specifications for Design and Construction of
Segmental Concrete Bridges*, American Association of State Highway and
Transportation Officials, Washington, D.C. 2nd Edition, 1999.

7.4   **West, J.S., (1999)** *"Durability Design of Post-Tensioned Bridge
Substructures,"* Doctor of Philosophy Dissertation, The University of
Texas at Austin, May 1999.

Vita

Rubén Mario Salas Pereira was born on June 20, 1968 in San José, Costa Rica, and is the son of Rubén Salas Granados and María Teresa Pereira García. After graduating with honors from the Lice Laboratorio (High School), San José, Costa Rica, in 1985, he entered the Universidad de Costa Rica, in San José, where he received the degree of "Licenciado en Ingeniería Civil" with Distinction in April, 1991, he was awarded "Graduación de Honor." During the summers of 1987 to 1989, and the year of 1990, he was employed as an Engineering Assistant at CARREZ S.A. Construction Company, San José, Costa Rica. In 1991, he worked part time in the Engineering Division of SALPER S.A. Construction Company, San José, Costa Rica. In the same year he joined the team that subsequently developed the Great Metropolitan Area Transportation Master Plan for the Costa Rican Ministry of Public Works and Transportation. In June of 1991, he became a Professor in the Civil Engineering Department, Universidad de Costa Rica, where he was later awarded "profesor adjunto." In January of 1992, he worked at the Pan American Institute of Highways, Federal Highway Administration, McLean Virginia, and became International Instructor for Federal Highway Administration teaching short courses in Latin America in the field of Scour at Highway Bridges. He enrolled in the Master of Science program at The University of Texas at Austin, where he received his Master's Degree in May 1994. Back in Costa Rica, he worked at Francisco Mas & Asociados S.A., a consulting firm, and in 1996 he was employed at Franz Sauter & Asociados S.A., an engineering and architecture consulting firm, where he is now a partner and serves as Project Manager and Structural Engineer. In September 2000 he entered the Graduate School at The University of Texas at Austin to pursue a Ph.D. in structural engineering.

Permanent Address: P.O. Box 582-2070

San José, COSTA RICA

This dissertation was typed by the author